Final Report

INVESTIGATION IN AND RESEARCH OF AEROSPACE RELATED MICROWAVE TECHNOLOGY

A report of work in the period

1 January 1965 to 31 October 1966

Under Grant

NGR 39-010-030

from

National Aeronautics and Space Administration

Washington, D. C. 20546

FACILITY FORM 602

N67-33083
(ACCESSION NUMBER)

(THRU)

533
(PAGES)

1
(CODE)

CR-87055
(NASA CR OR TMX OR AD NUMBER)

07
(CATEGORY)

THE MOORE SCHOOL OF ELECTRICAL ENGINEERING

UNIVERSITY OF PENNSYLVANIA

PHILADELPHIA, PENNSYLVANIA 19104

28 February 1967

Moore School Report No. 67-20

FINAL REPORT

INVESTIGATION IN AND RESEARCH OF AEROSPACE RELATED MICROWAVE TECHNOLOGY

A report of work in the period
1 January 1965 to 31 October 1966

Under Grant
NGR 39-010-030
from
National Aeronautics and Space Administration
Washington, D. C. 20546

The Moore School of Electrical Engineering
University of Pennsylvania
Philadelphia, Pennsylvania 19104

28 February 1967

Moore School Report No. 67-20

ACKNOWLEDGEMENT

The work reported herein is the result of a cooperative effort by a number of persons on the Moore School staff. Those who participated in the investigation and their areas of particular interest are listed below:

E. J. Denlinger	Quantum Generators and Amplifiers
N. Farhat	Systems Considerations Detection Modulation
A. A. Gundjian	Quantum Generators and Amplifiers
P. P. Lombardini	Propagation Environmental Considerations
O. M. Salati	Antennas Electromagnetic Radiation Hazards Radio Interference
R. F. Schwartz	Transmission Lines and Components Millimeter and Submillimeter Wave Measurements
R. M. Showers	Systems Considerations Radio Interference
L. W. Zelby	Generators, Electron Beam Type

In addition, Dr. P. L. Bargellini contributed to the systems work. All of the above listed authors contributed to the editing of the entire report.

R. M. Showers

R. M. Showers
Principal Investigator

TABLE OF CONTENTS

		Page No.
Acknowledgement		ii
Abstract		ix
Chapter I.	INTRODUCTION	1
	1.1 Sources of Information	4
	1.2 References	7
Chapter II.	SYSTEMS CONSIDERATIONS	8
	2.1 Introduction	8
	2.2 System Classification	10
	2.2.1 Point-to-Point	13
	2.2.2 Active Radar	29
	2.2.3 Radiometry	33
	2.2.4 Plasma Reentry Communications	38
	2.3 References	38
Chapter III.	SUGGESTIONS FOR RESEARCH	40
	3.1 Introduction	40
	3.2 Investigation of Materials	43
	3.2.1 Dielectrics	43
	3.2.2 Ferrites	44
	3.2.3 Semiconducting Materials	44
	3.2.4 Maser Materials	45
	3.3 Generators, Electron Beam Type	46
	3.3.1 Specific Devices	46
	3.3.2 Harmonic Mixing	47
	3.3.3 Cerenkov Radiation	48
	3.3.4 Backward Wave Devices	48
	3.4 Quantum Generators and Amplifiers	49
	3.4.1 Submillimeter Molecular Masers	49
	3.4.2 Pressure Tuned Submillimeter Diode Lasers	49
	3.4.3 Photoelectric Difference Frequency Generation	50
	3.4.4 Bulk Semiconductor Phenomena	51
	3.4.5 Amplification by Stimulated Emission	54
	3.4.6 Radiation Helped Tunneling Diode	57
	3.4.7 Amplification by Resonance Saturation in Gases	61

continued

Page No.

3.5 Modulation..... 61
3.5.1 The Effect of High Electric Fields on the Absorption in Germanium of MM Waves--as a Pulse Modulator..... 62
3.5.2 Electromechanical Modulators..... 62
3.5.3 Modulation by Rotation of the Polarization Plane..... 63
3.6 Transmission Lines and Components..... 64
3.6.1 Circular Waveguide..... 64
3.6.2 Beam Waveguide..... 65
3.6.3 Comparative Waveguide Study..... 66
3.6.4 Cladded Dielectric Guide..... 67
3.7 Propagation Investigation of the Spectrum of Air Absorption Using Coherent Sources..... 67
3.8 Detection..... 69
3.8.1 Superheterodyne and Homodyne Detection. 69
3.8.2 Hot Carrier Diode..... 70
3.8.3 1000 GHz Superheterodyne Receiver..... 70
3.8.4 Non-Heterodyne Down Conversion..... 71
3.8.5 Reflection Cavity Detector..... 72
3.8.6 Mixing in Bulk Semiconductors..... 72
3.8.7 Glow Discharge Detector..... 72
3.9 Phased Arrays..... 73
3.10 References..... 74

Chapter IV. GENERATORS, ELECTRON BEAM TYPE..... 77

4.1 Introduction..... 77
4.2 Device Characteristics..... 79
4.2.1 Tornadotron..... 84
4.2.2 Electromagnetic Amplifying Lens (EAL).. 86
4.2.3 Dematron..... 88
4.2.4 Ubitron..... 91
4.2.5 Cycloidotron..... 93
4.2.6 Laddertron..... 95
4.2.7 Bermutron..... 96
4.2.8 Miscellaneous..... 98
4.3 Discussion..... 102
4.4 Conclusions..... 108
4.5 Recommendations..... 110
4.6 References..... 113

Chapter V. QUANTUM GENERATORS AND AMPLIFIERS..... 118

5.1 Introduction..... 118
5.2 Generation Using the Maser Principle..... 118

continued

Page No.

5.2.1 The Resonant Cavity..... 118
5.2.2 Available Radiative Transition Frequencies..... 119
5.3 Bremsstrahlung Radiation from Solids..... 129
5.4 The Gunn Effect..... 130
5.4.1 Characteristics of the Oscillation..... 131
5.4.2 Limitations of the Gunn Oscillator..... 134
5.5 Solid State Plasma Instabilities..... 135
5.6 Negative Effective Masses in Semiconductors.... 137
5.7 The Read Diode..... 138
5.8 Amplification of Submillimeter Waves..... 141
5.8.1 Negative Resistance Amplifiers..... 141
5.8.2 Varactor Diodes..... 143
5.8.3 Amplification by Maser Action in Solids..... 144
5.8.4 Amplification in Gases..... 156
5.9 Some Nonlinear Phenomena in the Millimeter-Submillimeter Range of Frequencies..... 157
5.9.1 General Remarks..... 157
5.9.2 Hot Electron Devices..... 158
5.9.3 Photoelectric Effects..... 160
5.9.4 Gas Plasma Generation..... 165
5.10 The Josephson Effect..... 166
5.11 Conclusions..... 168
5.12 References..... 169

Chapter VI. MODULATION..... 175

6.1 Introduction..... 175
6.2 Internal Modulation Methods..... 175
6.3 External Modulation..... 176
6.3.1 Free Carrier Absorption Modulators..... 176
6.3.2 The Point Contact Diode Modulator..... 181
6.3.3 Ferrite Modulators..... 182
6.3.4 Electromechanical Modulator..... 184
6.4 Conclusions and Recommendations..... 185
6.5 References..... 187
6.6 Selected References on Optical Modulation..... 190

Chapter VII. TRANSMISSION LINES AND COMPONENTS..... 193

7.0 Introduction..... 193
7.1 Objectives and Requirements..... 195
7.1.1 Attenuation..... 195
7.1.2 Impedance..... 195
7.1.3 Mechanical Requirements..... 197

continued

Page No.

7.1.4 Power Levels and Voltage Breakdown..... 197
7.1.5 Mechanical Tolerances..... 198
7.2 Characteristics of Various Transmission Systems..... 199
7.2.1 Hollow Metallic Waveguides..... 199
7.2.2 Helical Waveguide..... 208
7.2.3 Dielectric Rods and Tubes..... 211
7.2.4 Dielectric Coated Wires..... 214
7.2.5 Dielectric Image Lines..... 214
7.2.6 H-Lines..... 216
7.2.7 The Groove Waveguide..... 219
7.2.8 Beam Waveguides..... 219
7.3 Transmission Line and Waveguide Components..... 222
7.3.1 General Comments..... 222
7.3.2 Mode Launchers..... 223
7.3.3 Mode Suppressors..... 224
7.3.4 Tuners and Transformers..... 225
7.3.5 Loads..... 226
7.3.6 Attenuators..... 228
7.3.7 Slotted Sections, Impedance Meters, and Directional Couplers..... 229
7.3.8 Hybrid Structures..... 230
7.3.9 Resonant Structures..... 230
7.3.10 Ferrite and Antiferrimagnetic Devices.. 231
7.3.11 Commercially Available Components in the Millimeter Wavelength Region..... 234
7.4 Conclusions and Recommendations..... 236
7.5 References..... 238

Chapter VIII. PROPAGATION
8.1 Introduction..... 243
8.2 Summary of Underlying Theory..... 244
8.2.1 Spectra of Rarefied Gases..... 244
8.2.2 Pressure Broadening..... 248
8.3 Constituents of the Earth's Atmosphere..... 250
8.4 Effects of Atmospheric Oxygen..... 257
8.5 Effects of Water Vapor..... 263
8.6 Remarks on Propagation in the Earth's Atmosphere..... 266
8.7 Effects of Atmospheric Precipitation on Propagation..... 282
8.8 Tropospheric Scintillation..... 289
8.9 Summary and Review of Recommendations..... 290
8.10 References..... 291

continued

Page No.

Chapter IX. DETECTION 299

9.1 Introduction 299
9.2 Thermal Detectors 300
9.2.1 The Golay Cell 301
9.2.2 Special Bolometers 302
9.3 Photoelectric Detectors 309
9.3.1 Photoconductive Detectors 309
9.4 Semiconductor Diode Detectors and Mixers 317
9.4.1 Point Contact Diode Detectors 318
9.4.2 Hot Carrier Diode Detectors 340
9.5 Bulk Semiconductor Detectors 343
9.5.1 Heterodyne Down Converters 343
9.5.2 Non-Heterodyne Down Conversion 345
9.6 Other Types of Detectors 350
9.7 Comparison and Evaluation of Millimeter and Submillimeter Wave Detectors 352
9.8 Millimeter and Submillimeter Detectors, Applications and Future Development 362
Appendix 9.1: Relation between Noise Figure, Noise Equivalent Power, and Effective Noise Temperature 366
9.9 References 370

Chapter X. ANTENNAS 379

10.0 Introduction 379
10.1 Antenna Applications 380
10.2 Limitations on Antenna Gain 382
10.3 Fresnel Region Phenomena 406
10.4 Antenna Temperature 407
10.5 Antenna Types 408
10.6 Conclusions 411
10.7 References 412

Chapter XI. ENVIRONMENTAL CONSIDERATIONS 414

11.1 Introduction 414
11.2 Terrestrial Radiometry 414
11.3 Propagation Considerations 423
11.3.1 Re-entry Plasma 423
11.3.2 Interplanetary Dust 424
11.3.3 Interplanetary Plasma 426
11.4 Extra-Terrestrial Radiometry 427
11.5 Summary and Recommendations 438
Appendix XI.A: Fundamentals of Radiometry 440
References 454

continued

Page No.

Chapter XII. MILLIMETER AND SUBMILLIMETER WAVE MEASUREMENTS..... 461

12.1 Introduction..... 461
12.2 Quantities to be Measured..... 462
12.3 Limitations of Existing Techniques in General..... 462
12.4 Objectives in Measurement..... 464
12.5 Power Measurement..... 465
12.6 Frequency and Wavelength Measurement..... 474
12.7 Materials Measurements..... 477
12.8 Conclusions..... 484
12.9 References..... 485

Chapter XIII. ELECTROMAGNETIC RADIATION HAZARDS..... 491

13.1 Definition of Hazards..... 491
13.2 Biological Hazards..... 491
13.3 Flamable Materials..... 499
13.4 Electroexplosive Devices..... 504
13.5 Components..... 506
13.6 Conclusions and Recommendations..... 507
13.7 References..... 509

Chapter XIV. RADIO INTERFERENCE..... 513

14.0 Introduction..... 513
14.1 Characteristics of Components..... 515
14.2 Intersystem Compatibility..... 516
14.3 Conclusions..... 520
14.4 References..... 520

ABSTRACT

The state of the art of technology related to aerospace applications of millimeter and submillimeter waves has been reviewed. The work performed is meant to be a supplement to previous reviews, and covers the approximate time period 1962 to 1966. Detailed chapters cover the following topics: generation, detection, transmission, propagation, modulation, environment, antennas, measurements, radio interference, and radiation hazards.

Charts have been prepared which provide a convenient summary of the state of the art for the purpose of estimating the present capability of point-to-point communication systems, radar, and radiometry. The presentation is such as to enable a relatively simple procedure for estimating the benefits to be derived from future improvement in component capabilities.

A classification is presented which indicates the relative importance of research in specific technical and applications areas with respect to their potential for improving the capabilities of future aerospace systems operating in the pertinent wavelength range.

Chapter I

INTRODUCTION

In recent years developments in the frequency spectrum between microwaves and visible light can be considered to have closed the gap which once existed. The availability of devices to perform almost all electrical or electronic functions of equipment on either side of the "gap" has stimulated interest in their possible use and also encouraged further component development. One of the purposes of this work is to bring up to date previous literature surveys[1, 4] of the range from 10 GHz to 3000 GHz, with major emphasis above 100 GHz.

In a recent signal density study a preliminary state of the art survey of the electromagnetic spectrum from zero to 10^{25} cycles per second was given. The main interest of that report was in defining terminology and problem areas in electromagnetic interference. A descriptive diagram of the spectrum and the nomenclatures used for different portions of it were given. The region above 100 MHz is of interest for space operations although, to date, only the region from 100 MHz to 10 GHz has been exploited to any significant extent. Most of the experimental work has been conducted only up to 100 GHz; however, more or less standard components are available to 300 GHz. The literature on space communications covers primarily the range from 1 or 2 GHz to 10 GHz. Below 1 GHz, atmospheric, man-made, and cosmic noise are considered to be a major limitation, and above 10 GHz, absorption by oxygen and water vapor is high. "Windows" at 15 GHz, 35 GHz, and 94 GHz are currently receiving attention.

The major objective of this work is to determine those areas of research which are likely to provide the greatest payoff for aerospace applications. These applications may be in communications, guidance, geophysical sensing, telemetering, tracking, data processing, etc. Since research in this frequency range is, in many cases, in early stages, many of the applications of this work may be considered to be quite remote. It was decided that the absence of an immediate application was not justification for omitting a particular line of investigation. Thus, the approach used is to examine on a high technical level the present state of the art to determine what physical principles are available for exploitation in this frequency range in the development of methods for generating, modulating, transmitting, receiving and detecting electrical signals. In view of the aerospace applications, some consideration is given implicitly to size and weight requirements associated with each of the techniques; however, large physical size or weight associated with a particular development was not, per se, considered as justifying omission of further work, since pertinent components could be used on ground based terminals of electronic systems.

Generally, the attempt has been made to include in this report all technical areas in which substantial work has been done. In order to place the various technical areas in their proper perspective with respect to applications, a brief discussion of some of the basic millimeter and submillimeter wave systems is given in Chapter II, along with charts which provide a succinct summary of the state of the art. One of the purposes of this chapter is to provide a common reference on

the relation between the various parts of such systems. Chapter III gives, in one sense of the word, a summary of the report. In particular, it lists a number of areas in which it is considered that additional research would provide advances in the state of the art with the greatest probability of success. Data supporting these suggestions are given in the subsequent chapters.

For the purposes of this report (in accordance with common usage) the submillimeter region of the electromagnetic spectrum is defined to extend from 300 GHz to 3 THz in frequency, or from 1 mm (1000 μm) to 0.1 mm (100 μm) in wavelength, whereas the millimeter region is defined to extend from 30 GHz to 300 GHz in frequency or from 10 mm (10,000 μm) to 1 mm (1000 μm) in wavelength.

The term "ultramicrowave" is found in the literature and generally includes both the millimeter and submillimeter range.

With regard to techniques, until recently the work in the millimeter range has been carried out by attempting to extend microwave (classical) techniques, and in the submillimeter range by extending optical (quantum) techniques. The results of these approaches are clearly evident in this report. However, the distinction is probably only one of convenience, since recent developments have produced a clear overlapping in frequency of these techniques with the result that the understanding of particular phenomena may depend upon matching both conceptual points of view.

1.1 SOURCES OF INFORMATION

A very substantial review of technology of the region between 10 GHz and 300 GHz was reported in 1962[4] representing work up to 1961. Separate report sections were issued on generation; components, transmission techniques and materials; propagation and absorption; plasma effects in aerospace communications; system considerations and applications. It is a very complete document in the frequency range covered, and by extension serves as one of the basic sources of such information in the frequency range from 300 GHz to 3 THz. The report described the state of the art as far as frequencies, power levels, attenuations and sensitivities are concerned. Applications were described as such. No attempt was made to indicate what type of device was best suited for a particular purpose, nor were particularly promising avenues of research mentioned.

References 2, 3, 4, and 6 survey the border region between the far infrared and submillimeter waves.

Interest in optical techniques has been tremendously revived in recent years by the advent of the optical maser (laser) and the promise of high quality (e.g., broadband and coherent) optical communication. Fiber optics opened another area of interest.[7,8] Infrared technology as a low frequency extension of optical techniques has received a fair amount of attention and is the subject of several books.[9,10]

Propagation of millimeter and submillimeter waves has been studied by Long and others (Refs. 11, 12, 3, 4, 14, 15). High atmospheric attenuation is experienced at sea level over most of the range of 1 mm to 0.1 mm.

The NASA Information Center supplied about 1400 references based upon a vocabulary submitted for machine search of their literature. Also, NASA STAR has been manually searched.

The assistance of the following organizations, which were personally visited during the course of this program, is gratefully acknowledged:

Advanced Technology, Inc., Timonium, Md.

Aeroneutronics, New Port Beach, Calif.

Aerospace Corporation, El Segundo, Calif.

Airborne Instrument Laboratories, Deer Park, L.I., N.Y.

Autonetics, Anaheim, Calif.

Bell Telephone Labs., Holmdel, N. J.

CSF, Corbeville, France

Duke University, Durham, N. C.

Frankford Arsenal, Phila, Pa.

General Electric, Schenectady, N. Y.

General Motors, Def. Res. Lab., Santa Barbara, Calif.

Hughes Research Labs., Malibu, Calif.

Jet Propulsion Lab., Pasadena, Calif.

Johns Hopkins University, Baltimore, Md.

Martin Co., Orlando, Florida

National Air Development Center, Johnsville, Pa.

NASA Technical Services Branch, Wash., D. C.

NBS, Boulder, Colorado

NESCO, Pasadena, Calif.

North Carolina University, Chapel Hill, N. C.

Ohio State University, Columbus, Ohio (Antenna Lab.)

Raytheon, Galeta, Calif.

RPI, Troy, N.Y.

Rohr Corp., Chula Vista, Calif.

Services Electronic Research Lab., Baldock, England

Space General Corp., El Monte, Calif.

Stanford Research Institute, Stanford, Calif.

Stanford University, Stanford, Calif.

TRG, Inc., Melville, N.Y.; Boston, Mass.

U.S. Army Electronics Command, Ford Monmouth, N.J.

University College, Gower St., England

University of Illinois, Urbana (Conference on Electron Device Research, June 23, 1965)

University of Michigan, Ann Arbor, Mich.

University of Sheffield, England

Varian Associates, Palo Alto, Calif.

Watkins-Johnson, Palo Alto, Calif.

Wheeler Laboratories, Smithtown, N. Y.

White Sands Missile Range Electr. Res. and Dev. Activity, N.M.

Finally, while every attempt was made to have this work complete, it is acknowledged that time did not permit devotion of as much effort to some areas as would have been desirable. The authors also hope the reader will be sympathetic with their problem of keeping up with current developments. Considerable interest has recently been demonstrated in this field and new items worthy of inclusion appear in the literature each month.

1.2 REFERENCES TO CHAPTER I

1. P.D. Coleman and C. Enderby, "Megavolt Electronics Cerenkov Couplèr for the Production of Millimeter and Submillimeter Waves," J. Appl. Phys., 31, pp. 1695-1696, Sept. 1960.

2. P.D. Coleman, "Spanning the Microwave Infrared Gap," Proc. IRE, 50, pp. 1219-1224, May, 1962.

3. I., Kaufman, "The Band between Microwave and Infrared Regions," 47, Proc. IRE, pp. 381-396, March, 1959.

4. RCA Victor Co., Ltd., "The Radio Spectrum from 10 GHz to 300 GHz in Aerospace Communications," Contract AF 33(616)-7868, 7 Volumes, Jan. 1962.

5. O. M. Salati, "The Applicability of Signal Density Studies in Interference Prediction," Ph.D. Dissertation, Univ. of Pa., Dec. 63.

6. P. D. Coleman, "Electron Devices for the Millimeter Infrared Gap," 1961 IRE Conv. Record, pt. 3, pp. 54-63.

7. I. Luneburg, and E. Snitzer, "Characteristics of Dielectric Waveguide Modes," AFCRL-63-304, July 1963.

8. O. M. Salati, "Handling Light with Fiber Optics," Electronic Industries, 20, pp. 102-108, Dec. 1961.

9. R. Borchert, and W. Jubitz, Infrarottechnik, Veb Verlag Technik Berlin, 1958.

10. P. W. Kruse, L. D. Mc Glauchlin, and R. B. McQuistan, "Elements of Infrared Technology," John Wiley and Sons, New York, 1962.

11. N. G. Iaroslavskii, and A. E. Stanevich, "Rotational Spactrum of Water Vapor and the Absorption of Humid Air in the 40-2500 μ Wavelength Region," Optics and Spectroscopy, 6, pp. 521-522, June 1959.

12. M. W. Long, and W. K. Rivers, "Submillimeter Wave Radiometry," Proc. IRE, 49, June 1961, pp. 1024-1027.

13. G. R. Nicoll, "The Measurement of Thermal and Similar Radiations at Millimeter Wavelengths," Proc. IEE, 104, pp. 519-527, Sept. 1957.

14. E. S. Rosenblum, "Atmospheric Absorption of 10-400 GHz Radiation: Summary and Bibliography to 1961, Microwave Journal, 4, pp. 91-96, March, 1961.

15. H. H. Thessing, and P. J. Caplan, "Atmospheric Attenuation of Solar Millimeter Wave Radiation," J. Appl. Phys, 27, pp. 538-543, May 1956.

Chapter II

SYSTEMS CONSIDERATIONS

2.1 INTRODUCTION

Possible scientific and technical uses of the region of the electromagnetic spectrum between 30 GHz and 1000 GHz have been presented in various past publications.[1,2,3]

It is not the purpose of this presentation to provide a complete listing of all possibilities; however, it can be stated that millimeter and submillimeter waves are especially attractive in the following fields:

a) interaction with matter (spectroscopy, propagation phenomena, investigations of planetary atmospheres, and planetary and lunar surfaces, etc.)

b) passive and active radio astronomy (radiometry)

c) communications

d) radar

e) navigation

In the field of radiospectroscopy, molecular absorption in gases and vapors, resonance effects, nonlinear effects and other related phenomena dictate by their own nature the frequency at which the investigations have to be carried out. In radio and radar astronomy the theoretical resolution achievable with antennas of relatively modest size is obvious. In communications two major factors suggest the use of millimeter wave frequencies. The first is the bandwidth availability which is far in excess of anything obtainable at lower frequencies; the second is the high antenna gain obtainable with apertures of modest size. Additional

factors are the saturation of the lower parts of the spectrum and the possibility of choosing millimeter and submillimeter wavelengths which would provide sufficient attenuation to give effective protection against electromagnetic countermeasures, jamming, etc., while at the same time permitting the required communication capability.

In radar work the antenna size-beamwidth relationship and available bandwidth allow range and angle resolutions higher than anything obtainable at lower frequencies. Although the applications of millimeter waves to navigation systems in air or in space have been rather limited so far, it is possible to conceive new concepts and techniques which should permit obtaining superior results. There may well be cases where millimeter and submillimeter waves could provide the answer to not yet entirely solved problems (e.g., all electronic zero weather landing systems, terrain clearance indicators, collision avoidance systems, altimeter for use on earth or on other planets or satellites, station keeping systems when a large number of aircraft must operate in close flight formation, rendezvous and docking operations in space, etc.).

There have been essentially two major factors against the wide-spread use of millimeter and submillimeter wave systems:

1) the difficulty of generating adequate amounts of power, and
2) the difficulty of obtaining low noise amplifiers and detectors.

Atmospheric absorption, which traditionally has been held as another factor against millimeter and submillimeter waves, although certainly an obstacle in systems operating on or near the earth's surface, is not encountered in space and falls off rapidly at higher altitudes.

Millimeter wave development, which had been handicapped by the two above-mentioned factors, was delayed around 1960 as a result of the development of the first laser because of its promise to revolutionize the communication field. Today, after six years of intense work on lasers resulting in only limited advances in the field of communication and indications of certain serious technical limitations, activity on millimeter waves is continuing at a fairly steady pace.

This chapter is not intended to analyze either (1) or (2) above or to investigate the details of specific techniques. It is mainly directed toward the identification and clarification of possible systems in general forms. It is further intended to define significant operational parameters for each system category.

Once such parameters are identified, it should be possible to determine whether or not the present state of the art provides a possibility of implementing a certain system. Similarly, it should help to identify areas where additional efforts should be concentrated in order to advance the state of the art.

2.2 SYSTEM CLASSIFICATION

For the purpose of evaluation, it seems appropriate to try to divide the many possible applications of millimeter and submillimeter waves into a limited number of general categories. After discussion of the properties of these general categories and the ability of present technology to meet requirements, specific applications can be evaluated with reference to the given data, provided they are such that their principal characteristics are covered in the main categories. For this

purpose, we arbitrarily choose the following three general classifications:

1. point-to-point communication
2. active radar
3. radiometry.

The point-to-point system is chosen as being most representative of the application of communications for aerospace use primarily because it is one of the simplest communication systems one can conceive. Communication systems using millimeter waves do not now exist in any form other than as experimental models in laboratories. More complex communication systems are usually assemblages of point-to-point systems (if the word point is used rather loosely). One of the most pressing problems is communications from an earth-based station with a satellite far off in space. Requirements for bit rates up to 10^8 per second have been expressed as being realistic at some time in the next five years or so. These bit rates should be available from transmitters in the satellite or space vehicle and should be directly receivable either on the surface of the earth or by a satellite orbiting the earth. Shorter range missions, having reduced requirements, are of course also conceivable. Examples of such systems are contained in refs. 1, 4, and 5 and are classed as ground-to-air, air-to-ground, air-to-air, ground-to-reentry vehicle, ground-to-satellite, satellite-to-satellite, moon relay, etc.

It is convenient to divide millimeter wave point-to-point systems according to the following:

1) whether they are long range or short range
2) whether transmission is through the atmosphere.

For transmission at long ranges through the atmosphere, the possible frequencies are severely limited. On the other hand, short-range communication (such as at airports) might be feasible over a substantial portion of the millimeter and submillimeter spectrum.

Another type of point-to-point communication is that in which a solid link is imposed. Such links are conceivable at millimeter waves for transmission from one point on the surface to the other. Indeed, very interesting technologies are available for consideration and exploitation of such systems. No further discussion of such systems is given here because it is considered to be of relatively little importance at the present time.

Various types of radar can be included under the category of radar systems. Radar can be used for object identification and location, for navigation by means of sights on objects whose locations are accurately known, for vehicle docking maneuvers, and for planetary or lunar surface examination. Although radar systems come in many types and varieties, we shall consider here primarily the conventional system which emits and detects pulses of radio-frequency energy spaced at regular intervals. Consideration should also be given to FM-type systems.

Radiometer systems are so called because essentially they are used to detect the presence of "hot" objects. Usually, these objects emit energy in accordance with the black-body radiation law. However, the word is also used to describe techniques used for the measurement of objects which emit by other than a black-body process. For example, one can detect solar radiation reflected from the surface of the moon,

and one can also detect sources of random radio noise of cosmic origin which, basically, are other than thermal in their character. Radiometers can be used to detect objects both near and far, and can be used to explore the surface of a planet or a moon in order to obtain scientific or technological information of interest in connection with space flight.

Systems to which explicit consideration is not given here are: altimeters, instruments for cloud and ceiling height measurements, clear air turbulence detection, lunar communications satellites, molecular spectroscopy, radio astronomy, and such laboratory studies as the measurement of properties of materials, and exploration of propagation characteristics of various atmospheres. Persons concerned with these applications should be able to obtain the information on the state of the art pertaining to their particular use from the information presented in connection with the above main three system classes and data supplied in later sections of the report.

2.2.1 Point-to-Point

For the purpose of comparing point-to-point systems, we adopt the relationship given below[5] for the ratio of signal power to noise power in the receiver:

$$\frac{S}{N} = \frac{G_T \, G_R \, P_T \, \lambda^2}{r^2 (4\pi)^2 \, hf \left[1 + (e^{hf/kT} - 1)^{-1} \right] B \, L_o} \qquad (2.1)$$

In this formula r is the range, λ is wavelength, f the frequency, P_T the transmitter power output, G_T the effective transmitter antenna gain, G_R the effective receiver antenna gain, B the bandwidth, and the quantity in brackets takes into account both thermal and quantum noise. The quantum noise $h\nu B$ has been included merely in order to demonstrate the departure of the noise performance of actual millimeter and submillimeter receiving systems from the ideal limit (see Fig. 2.2). L_o (≥ 1) is a factor to take into account losses in transmission other than free space propagation such as those due to atmospheric attenuation. Now, the information rate (R) is limited by the Shannon formula

$$R \leqq B \log_2 \left(1 + \frac{S}{N}\right)$$

and for $\frac{S}{N}$ small

$$R \approx B \frac{S}{N} (1.44)$$

Hence, we may write

$$r^2 R \simeq \frac{G_T\, G_R\, P_T\, \lambda^2\, (1.44)}{(4\pi)^2\, hf \left[1 + (e^{hf/kT} - 1)^{-1}\right] L_o} \qquad (2.2)$$

Substituting for the antenna gain an equivalent expression in terms of effective antenna aperture $A \simeq A_{eff} = \frac{G\lambda^2}{4\pi}$ we have

$$r^2 R = \frac{A_T\, A_R\, P_T\, (1.44)}{hf \left[1 + (e^{hf/kT} - 1)^{-1}\right] \lambda^2\, L_o} = \frac{v\, A_T\, A_R\, P_T}{L_o} \qquad (2.3)$$

where

$$v = \frac{1.44}{h\lambda C\left[1 + (e^{hf/kT} - 1)^{-1}\right]} = M\frac{1.44}{h\lambda Cf} = \frac{M\,1.44}{hC^2} = 2.4 \times 10^{16} M$$

where M has been previously defined[4] as used in the above expression. Hence, we have finally

$$\frac{L_o r^2 R}{v} = A_T\, A_R\, P_T \qquad (2.4)$$

In this equation, the numerator of the left-hand side describes the ability of the system to transmit information. The right-hand side contains the most significant design parameters which can be mutually varied to provide the desired performance. The parameter in the denominator of the left-hand side is to some extent controllable, and to some extent uncontrollable. L_o is, of course, dependent on a basic decision on the geographical layout of the system. There is an upper limit on v which is determined in an "ideal" system by quantum noise. Otherwise the value of v is a function of the effective temperature (T in eq. (2.1)) of the receiving system (receiver and receiving antenna) and it is this quantity which can be controlled to some extent in system design. The quantity L_o can only be controlled by choosing particular geographic transmission and receiving paths, and operating frequency.

The equivalent receiving noise temperature $T = T_{RS}$, the equivalent noise temperature of the system (receiver + antenna), is given by

$$T_{RS} = T_R + T_A$$

where T_R is the equivalent noise temperature of the receiver related to the receiver noise figure F_R by

$$T_R = T_o(F_R - 1) \quad , \quad T_o = 290^o$$

The quantity T_A is the equivalent noise temperature of the antenna used with the receiver. (a technical discussion of this quantity appears in Chapter X). Many factors affect it; in particular atmospheric absorption is to be taken into account when the communication system is operating through the earth's atmosphere at mm or submm wavelength. In that case the equivalent antenna noise temperature is given by

$$T_A = (1 - \frac{1}{L_o}) T_B + \frac{1}{L_o} T_{sky} + T_{SL} + T_{BL}$$

where T_{BL} is the contribution of the antenna backlobes, and T_B is the average brightness temperature of the atmosphere. A value of $T_B \approx 290^oK$ is normally assumed. T_{SL} is the contribution of the ohmic losses in the antenna and in the associated structures. This quantity can be reduced by proper design to a value of tens of degrees. The sky temperature T_{sky} includes the contribution of the moon, the sun, or any radio sources viewed by the main beam of the antenna. Very little information about T_{sky} is available above 10 GHz. However, radio maps of sky temperature at 10 GHz indicate maximum values of T_{sky} of a few tens of degrees in prescribed regions of the sky. At this frequency $L_o^{-1} \simeq 1$; thus the contribution $L_o^{-1} T_{sky}$ is at most a few tens of degrees.

At the higher frequencies L_o^{-1} decreases; for instance, at 400 GHz, $L_o^{-1} \simeq 10^{-6}$ (see Fig. 2.5) which makes the total contribution $L_o^{-1}\, T_{sky}$ negligible for all $T_{sky} \lesssim 10^{6}\,^{o}K$.

If the antenna is operating outside the earth's atmosphere and is not viewing any radio noise source, the antenna temperature will be

$$T_A = T_{sky} + T_{SL}$$

When the antenna is outside the earth's atmosphere and is viewing the earth

$$T_A = \left(1 - \frac{1}{L_o}\right) T_B + \frac{1}{L_o}\, T_{earth} + T_{SL}$$

Since $T_{earth} \simeq T_B = 290^{o}$

$$T_A = \left(290 + T_{SL}\right) \left[{}^{o}K\right]$$

On the basis of the above considerations and the fact that $0 < L_o^{-1} < 1$, we may conclude that over the entire frequency range of 10-1000 GHz, when the antenna is not viewing a radio source, the total equivalent noise temperature of the antenna is less than a few hundred degrees. When the receiver equivalent noise temperature is considerably larger than T_A, the system equivalent noise temperature is determined by the receiver. Receivers have been constructed up to 600 GHz with noise equivalent temperatures ranging from 10^3 to $10^{6}\,^{o}K$ (see Fig. 2.2).

It should be noted in passing that if the values of the parameters P_t, the power output and the antenna apertures, A_T, A_R, and L_o are all assumed equal to 1 in eq. 2.4, then the quantity v is the so-called "range rate" (r^2R). In actual practice, the effectiveness of various communication systems can vary quite widely from the ideal which has been assumed. The theory of such systems is adequately discussed in the literature and will not be pursued further here. It must be remembered, however, that values of the performance of a given system obtained in this analysis are idealistic. The order of magnitude figures obtained, however, should be practically realizable with an appropriate amount of development work.

Hence, utilizing these relationships, if one specifies the transmitted power, effective antenna gain, frequency, transmission loss, noise figure and reference temperature (usually 290°K), one can obtain the maximum possible system capability. Values of the pertinent parameters as a function of frequency are given in Figs. 2.1 through 2.5. The curves shown represent the approximate best state of the art of each of these parameters at a given frequency. On a number of curves the performance of certain presently available components is indicated as a documentation for the curves. However, the actual state of the art is reflected in more detail in similar data given in appropriate chapters which follow in this report. Additional data are also given in references 4-8.

The curves of Figs. 2.1 through 2.4 are derived by taking 10 times the logarithm of both sides of equation 2.4 yielding

$$10 \log r^2 R - 10 \log v + 10 \log L_o = 10 \log P_T + 10 \log A_T + 10 \log A_R \tag{2.6}$$

In this form each term can be plotted as an equivalent number of decibels (or decilogs) as appropriate. Then the performance of any given system can be readily estimated by simple addition (or subtraction) of appropriate coordinates.

Figure 2.1 gives the value of the first term on the left of eq. 2.6 as a function of the required performance in range and rate.

Figure 2.2 gives the value of the second term as a function of frequency and receiver equivalent temperature. This curve also shows some representative points indicating some of the better performing detectors available at the present time.

Figure 2.3(a) shows output capabilities or representative CW transmitter generators (tube and solid state types). The present state of the art is shown by the dotted curve. Equivalent data for pulsed sources are shown in Fig. 2.3(b).

Figure 2.4 shows the effective antenna aperture in dG (decilog) with respect to 1 m^2 as a function of frequency for various available antennas. Above 200 GHz the curve has been arbitrarily extended horizontally at the size of the 200" Mount Palomar telescope. Figure 2.4 shows also the limit on antenna size as a result of atmospheric scintillation.[11]

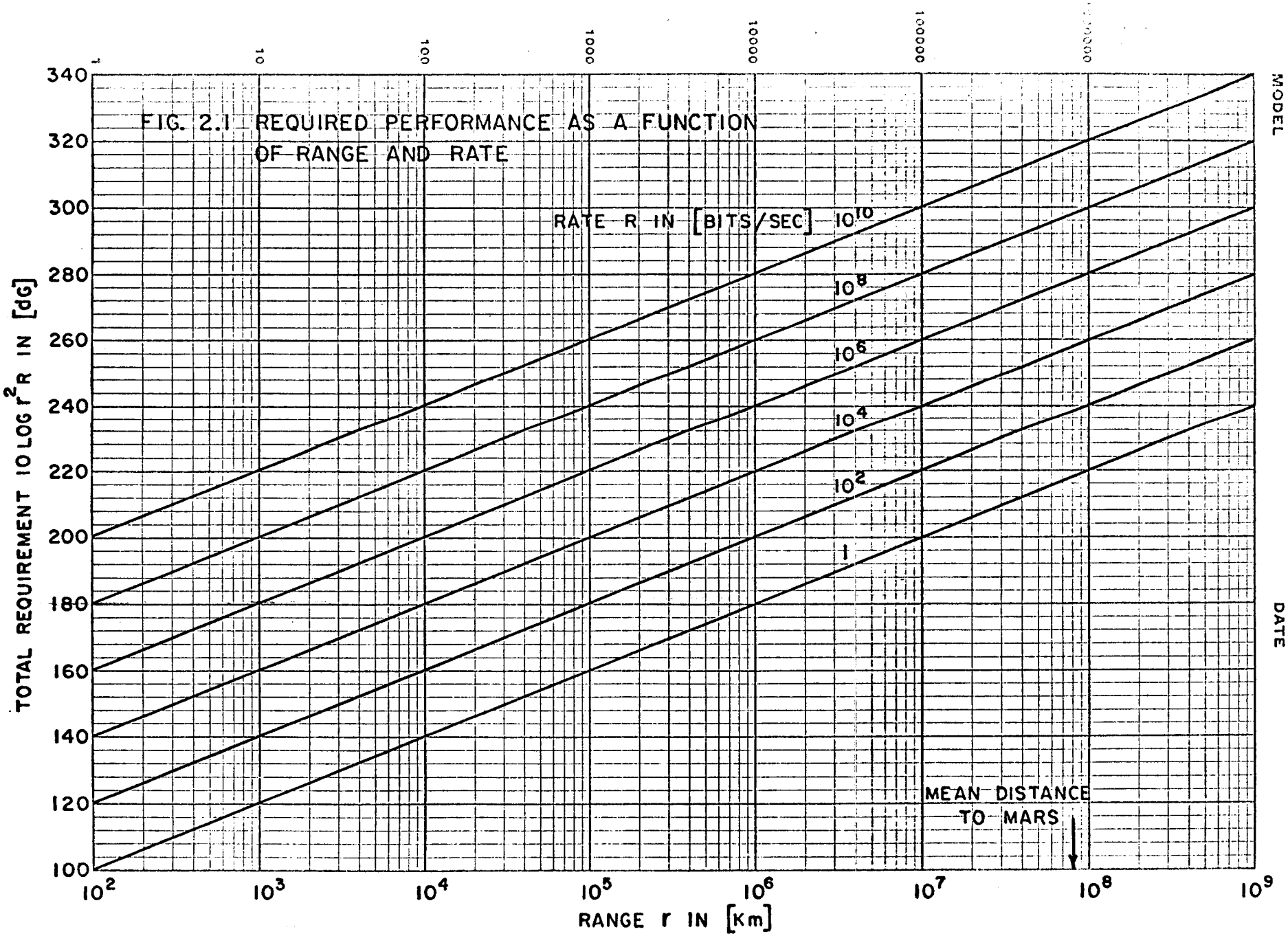

FIG. 2.1 REQUIRED PERFORMANCE AS A FUNCTION OF RANGE AND RATE

MODEL

DATE

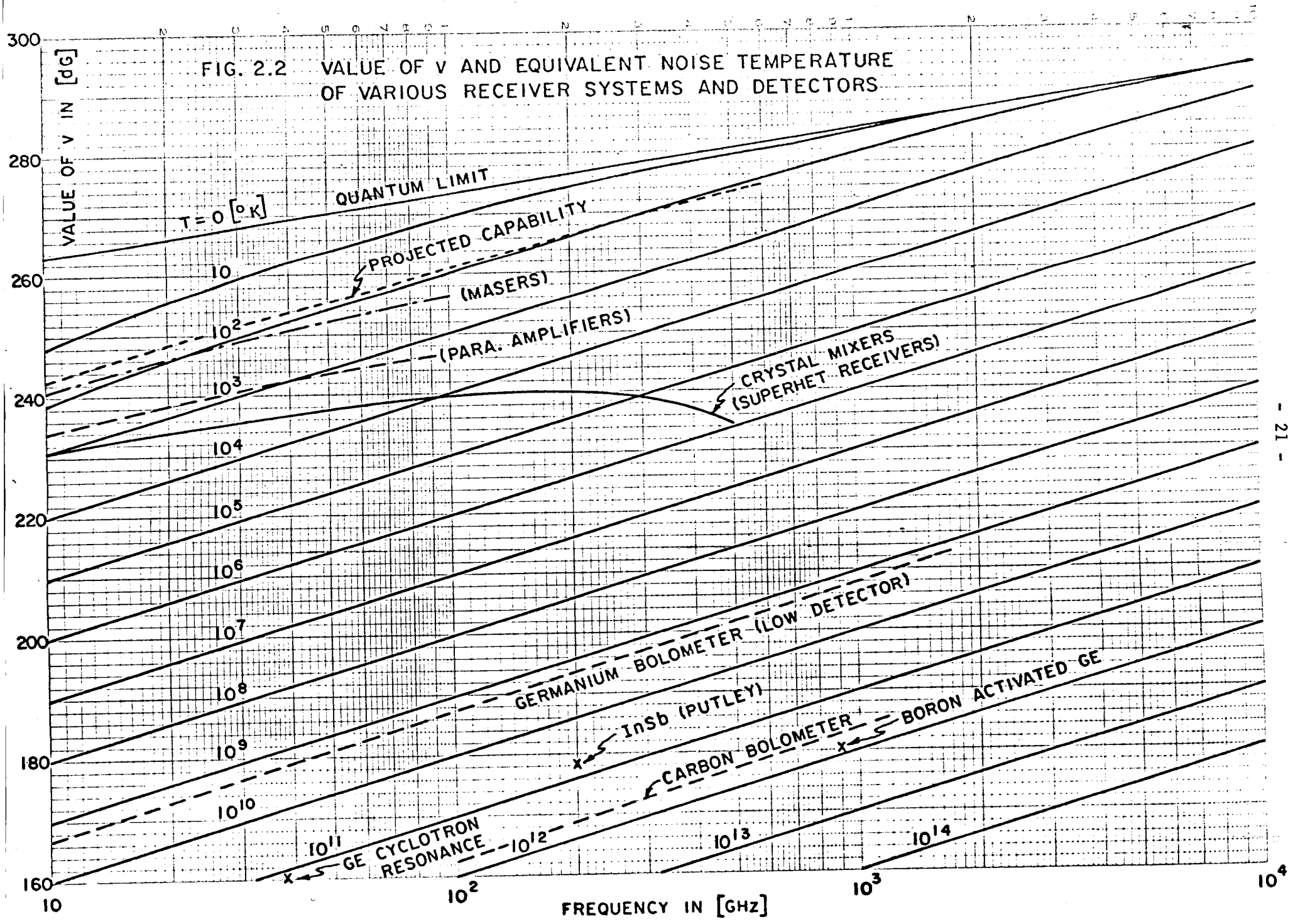

FIG. 2.2 VALUE OF V AND EQUIVALENT NOISE TEMPERATURE OF VARIOUS RECEIVER SYSTEMS AND DETECTORS

NO. 340-L310 DIETZGEN GRAPH PAPER
SEMI-LOGARITHMIC
3 CYCLES X 10 DIVISIONS PER INCH
EUGENE DIETZGEN CO.
MADE IN U. S. A.

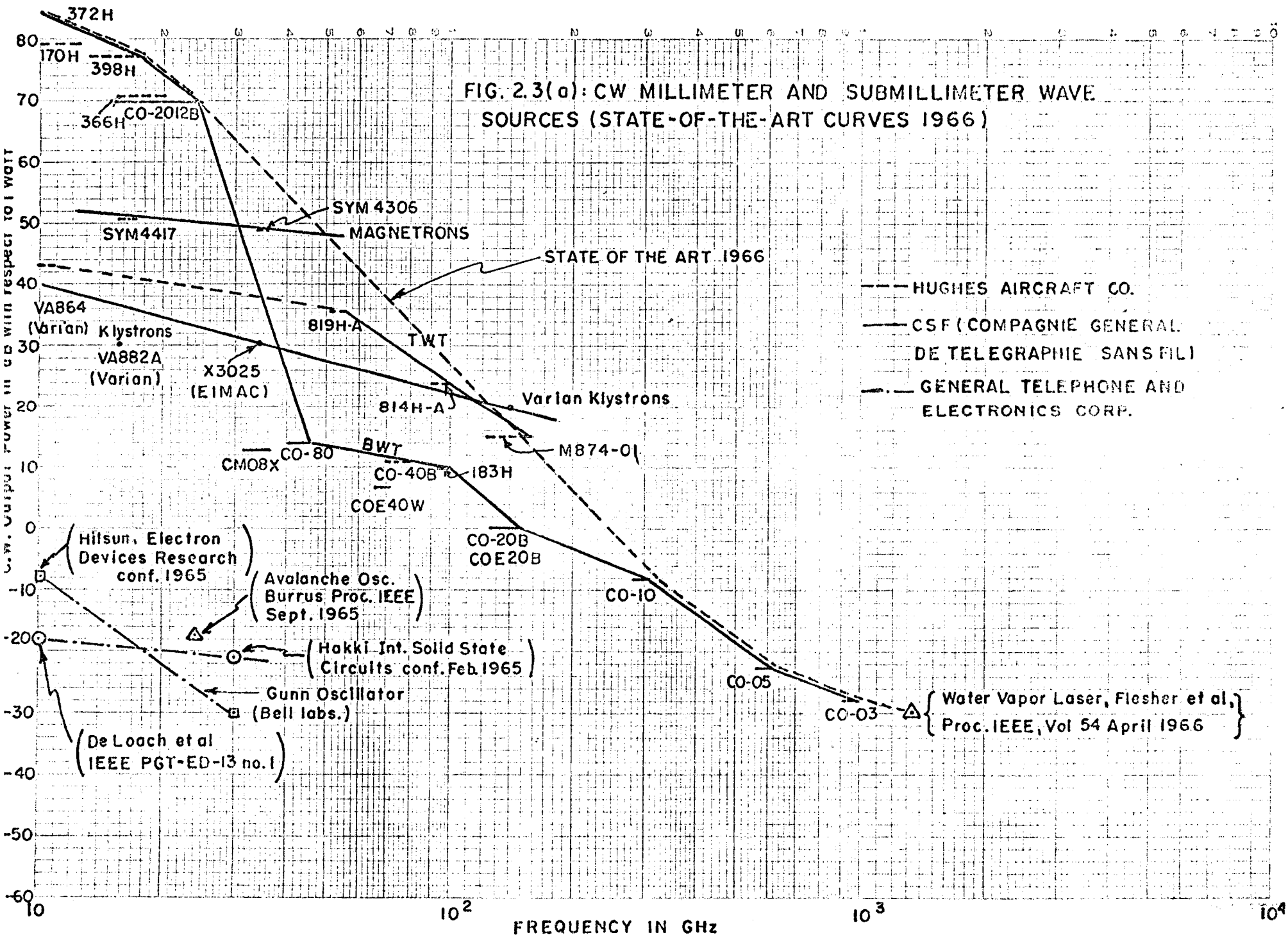

NO. 340-L310 DIETZGEN GRAPH PAPER
SEMI-LOGARITHMIC
3 CYCLES X 10 DIVISIONS PER INCH

EUGENE DIETZGEN CO.
MADE IN U.S.A.

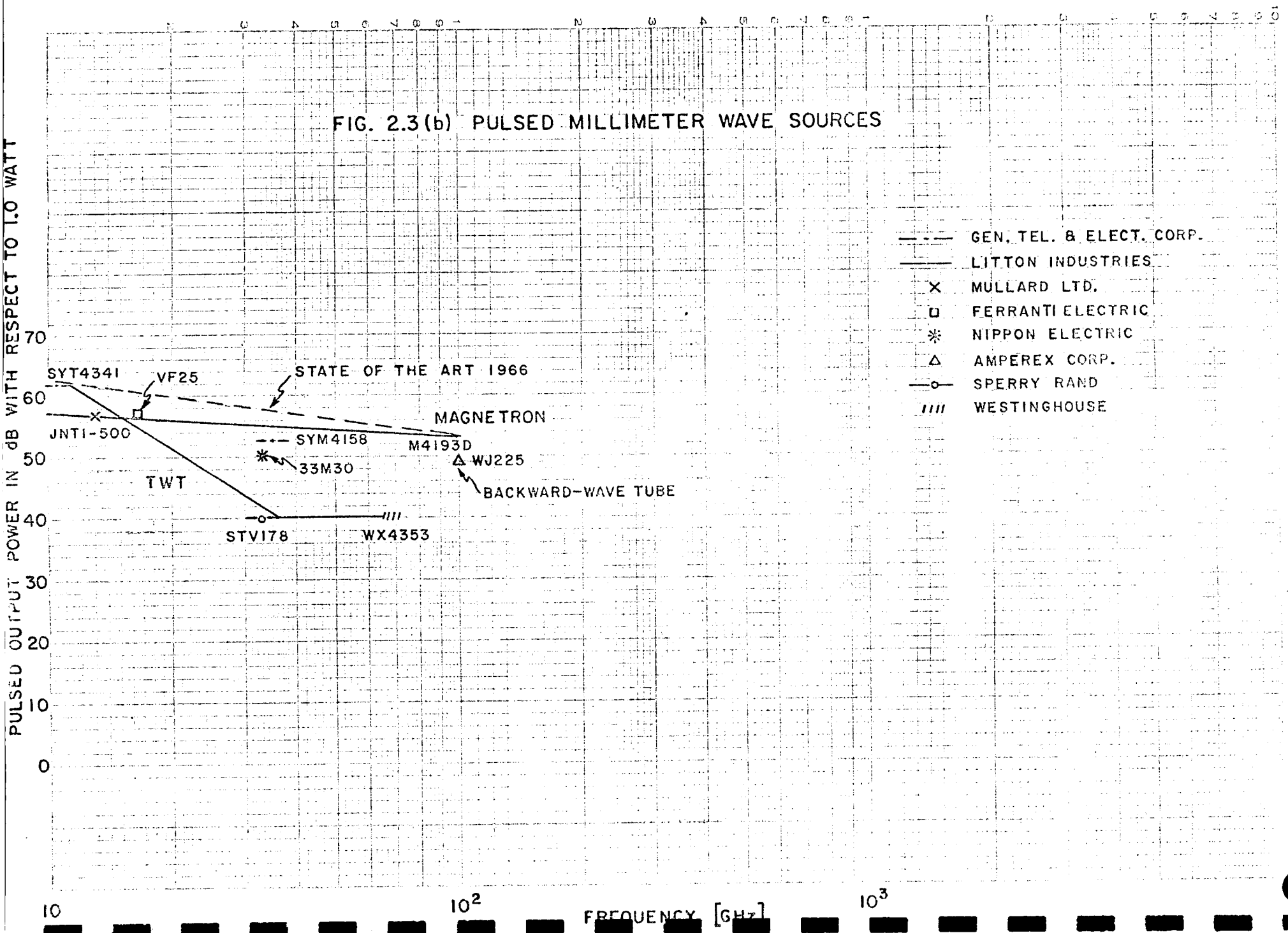

FIG. 2.3(b) PULSED MILLIMETER WAVE SOURCES

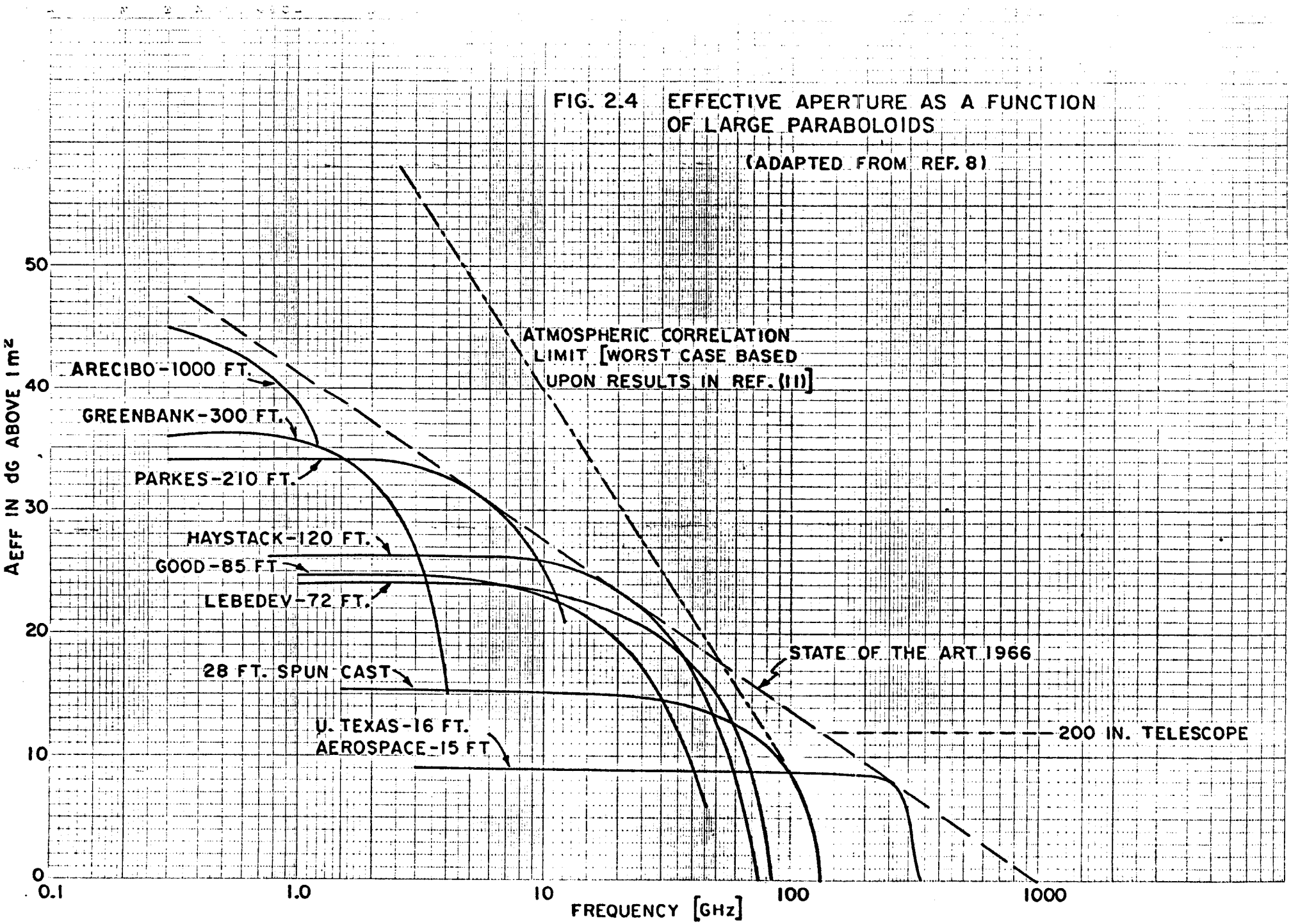

FIG. 2.4 EFFECTIVE APERTURE AS A FUNCTION OF LARGE PARABOLOIDS

(ADAPTED FROM REF. 8)

For transmission based on the earth, atmospheric losses must be taken into account. These losses (in dB) are shown in general form in Fig. 2.5.

In the following we shall determine the capabilities of a number of communication systems with the aid of the general state-of-the-art curves given in Figs. 2.2, 2.3, 2.4, and 2.5. The following cases are considered:

1. space vehicle to space vehicle
2. space vehicle to ground station.

Practical considerations lead to the following assumptions concerning the components of the systems considered.

a) Space vehicle antenna size is limited by booster capability and space vehicle weight allocation. Antennas with aperture areas up to 10 m^2 are representative of current capability.

b) Antenna size at the ground station is assumed to be given by the state-of-the-art data of Fig. 2.4.

c) Millimeter and submm sources on board space vehicles and at the ground station are assumed to be given by state-of-the-art curve of Fig. 2.5.

d) Receivers on board space vehicles are crystal mixer superheterodyne, while the ground station can employ masers, superheterodyne (crystal mixer) or parametric amplifier receiver systems.

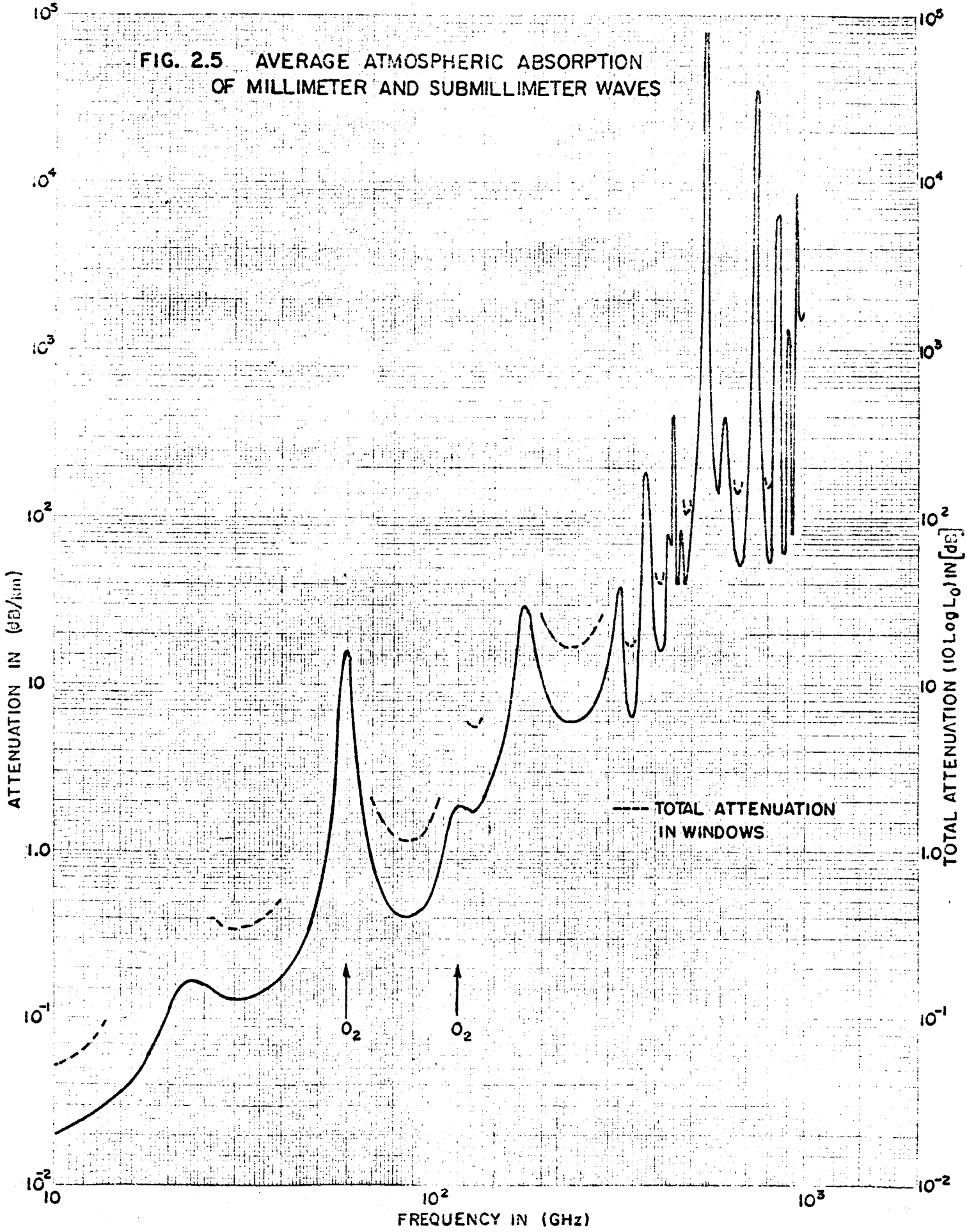
FIG. 2.5 AVERAGE ATMOSPHERIC ABSORPTION OF MILLIMETER AND SUBMILLIMETER WAVES
ATTENUATION IN (dB/km)
TOTAL ATTENUATION (10 Log L₀/IN [dB])
FREQUENCY IN (GHz)
TOTAL ATTENUATION IN WINDOWS
O₂
O₂
10⁵
10⁴
10³
10²
10
1.0
10⁻¹
10⁻²
10
10²
10³

2.2.1.1 Space Vehicle to Space Vehicle

In this case $L_o = 1$, since no losses other than free space loss are present,

$$A_T = A_r = 10 \text{ m}^2$$

and the logarithmic form of the range rate equation reduces to

$$r^2R \left[dG\right] = 10 \log v + 10 \log P_T + 20$$

Using Figs. 2.2 and 2.4 which give the dependence of the first two terms on the right-hand side of the equation above on frequency, one obtains the result shown in Fig. 2.6 for the maximum capability of this system. Figure 2.6 shows $r^2R = 280$ dG at 100 GHz; Fig. 2.1 shows that this capability will indicate, for instance, a communication rate of 10^6 bits/sec over a range of 10^8 km, which is of the order of the mean range to Mars ($\sim 8\ 10^7$ km).

2.2.1.2 Ground Station to Space Vehicle

In this case the effect of the atmospheric attenuation presented in Fig. 2.5 is to be taken into account. The effect of this attenuation appears twice in the rate-range equation; once directly due to the term ($10 \log L_o$) and once indirectly through ($10 \log v$), since v represents the receiving system capability and can be expressed as shown in Fig. 2.2 by the equivalent receiver noise temperature.

NO. 340-L210 DIETZGEN GRAPH PAPER
SEMI-LOGARITHMIC
2 CYCLES X 10 DIVISIONS PER INCH

EUGENE DIETZGEN CO.
MADE IN U. S. A.

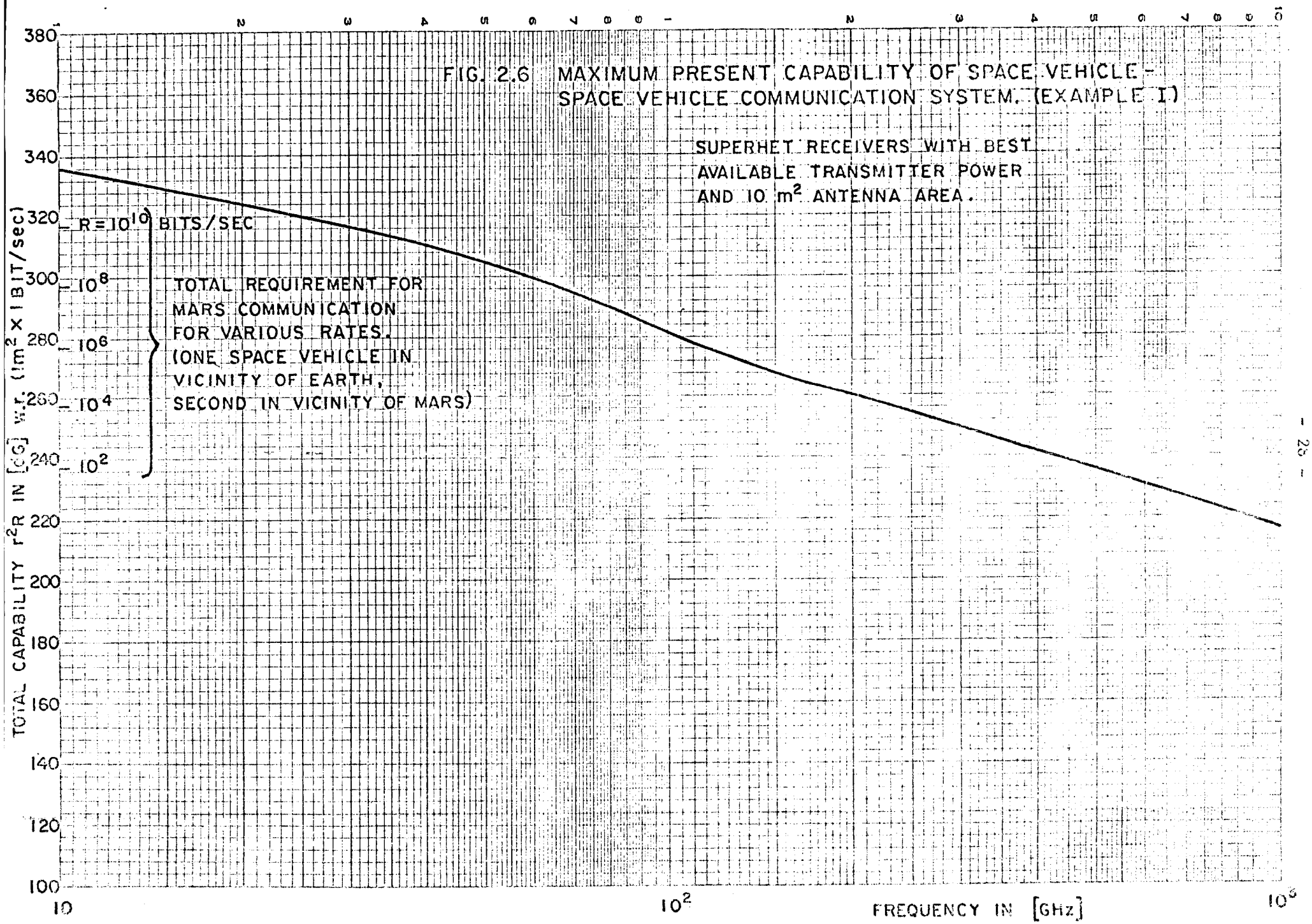

FIG. 2.6 MAXIMUM PRESENT CAPABILITY OF SPACE VEHICLE - SPACE VEHICLE COMMUNICATION SYSTEM. (EXAMPLE I)

If we assume that the receiving system equivalent noise temperature T_S is approximately equal to the T_R, the equivalent noise temperature of the receiver, and use the value of v shown in Fig. 2.2, we will have for the range-rate equation

$$r^2_R\ (dG) = 10 \log v + 10 \log P_T + 10 \log A_T + 10 \log A_R - 10 \log L_o$$

where the first term is given by Fig. 2.2, the second term by the state-of-the-art curve of Fig. 2.4, the fourth term is taken to be 10 dG since the space vehicle antenna is assumed to have $A_T = 10\ m^2$. The fourth term is given by Fig. 2.4 (state-of-the-art curve) and the fifth term is given by Fig. 2.5. The result which is the maximum capability of this system is shown in Fig. 2.7, which also shows clearly the degradation in the range-rate due to atmospheric absorption in the atmospheric windows.

2.2.2 Active Radar

The performance of a radar system can be given in terms of the following equation, [obtained from equations 2.1 and 2.3 of ref. 10 and the relation $A_{eff} = (\frac{G\lambda^2}{4\pi})$; σ = target cross-sectional area.]

$$\frac{r^4_{max}}{\sigma} = \frac{P_t\ A_{eff}^2}{4\pi\ \lambda^2\ hfB \left[1 + \left(e^{\frac{hf}{kT}} - 1\right)^{-1}\right] L_o^2}$$

$$= \frac{P_t\ A_{eff}^2}{4\pi\ (1.44)\ B} \quad \frac{v}{L_o^2} \qquad (2.7)$$

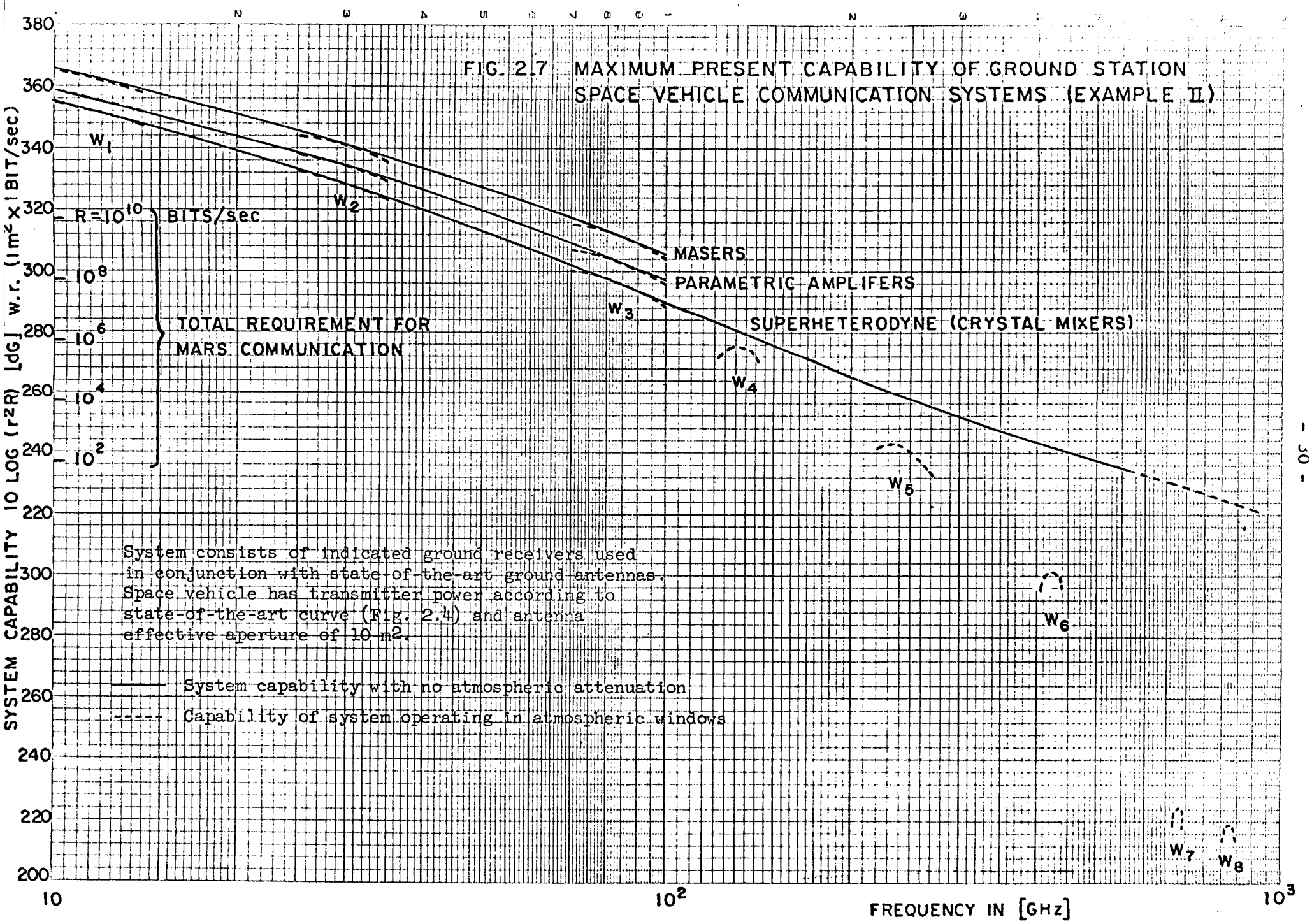

FIG. 2.7 MAXIMUM PRESENT CAPABILITY OF GROUND STATION SPACE VEHICLE COMMUNICATION SYSTEMS (EXAMPLE II)

Here, the signal-to-noise ratio has been arbitrarily placed equal to unity at the maximum range, the receiving and transmitting antennas have been assumed to be identical, B is the bandwidth and v the same quantity previously defined. It should also be noted that the more general form of the noise relation, which takes into account the quantum limit, has been inserted.

Where pulse integration is used, it is customary to use the energy ratio (ratio of total energy received per observation time to the noise power density). The minimum value of this quantity will also be assumed to be unity at maximum range; hence

$$\frac{r^4_{max}}{\sigma} = \frac{P_t A_{eff}^2}{4\pi (1.44)} \frac{v}{L_o^2} \tau f_o t_o \qquad (2.8)$$

where τ and f_o are respectively the pulse length and pulse repetition frequency, t_o is thus observation time. Now let $\tau f_o t_o = T_p$ = the total time in an observation period in which power is transmitted. Then eq. 2.8 becomes

$$\frac{r^4_{max}}{\sigma} \frac{L_o^2}{T_p} = \frac{v P_t A_{eff}^2}{[4\pi\ 1.44]} \qquad (2.9)$$

Previous figures can be used in evaluating this relation for v (Fig. 2.2), L_o (Fig. 2.5), P_t (Fig. 2.3) and A_{eff} (Fig. 2.4). With specific values for any given system inserted as previously, the range can be obtained from Fig. 2.8. With present state-of-the-art

K&E SEMI-LOGARITHMIC 359-96
KEUFFEL & ESSER CO. MADE IN U.S.A.
7 CYCLES X 60 DIVISIONS

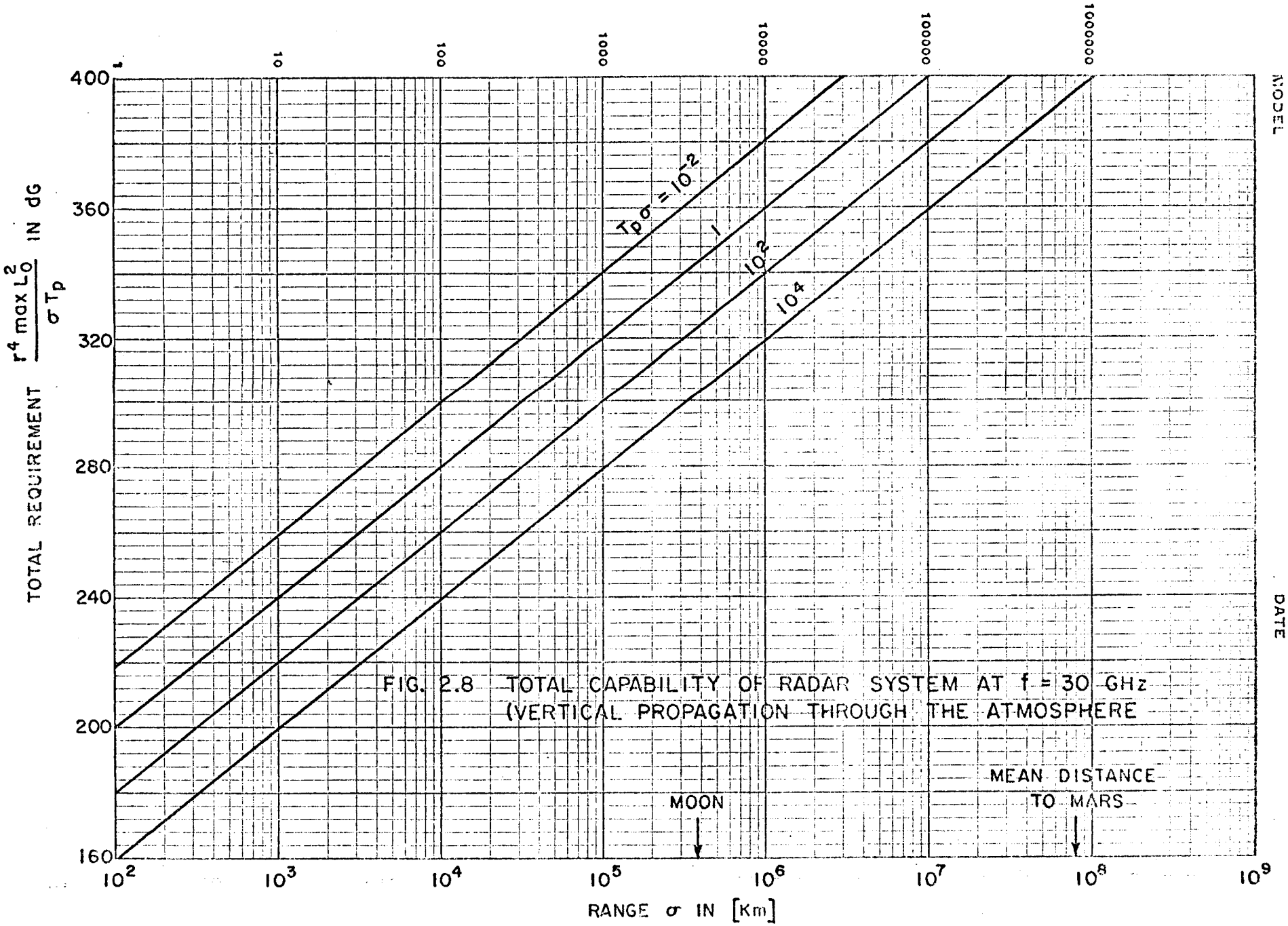

FIG. 2.8 TOTAL CAPABILITY OF RADAR SYSTEM AT f = 30 GHz (VERTICAL PROPAGATION THROUGH THE ATMOSPHERE

MODEL

DATE

components, the maximum radar performance is given in Fig. 2.9, which performance is the value of $\frac{r_{max}^4 L_o^2}{\sigma T_p}$. This capability is shown for both CW and pulsed sources.

2.2.3 Radiometry

A radiometer is essentially a power detector. It is primarily used in connection with incoherent radiation sources.

The minimum detectable temperature change ΔT is given by

$$\Delta T = \frac{T_{RS}}{\sqrt{B\tau}} \tag{2.10}$$

where T_{RS} is the equivalent receiving system noise temperature

B is the effective bandwidth of the radiometer

and τ is the integration time.

T_{RS} is given as follows:

$$T_{RS} = T_o(F_R-1) + T_{BL} + \left(1 - \frac{\Omega_s}{\Omega_a}\right) T_{sky} + \left(1 + \frac{1}{L_o}\right) T_B + \frac{1}{L_o} \frac{\Omega_s}{\Omega_a} T_s + T_{SL} \tag{2.11}$$

where

T_{SL} = contribution of ohmic losses in antenna and associated structure

T_o = reference temperature (usually 290°K)

F_R = noise figure of receiver; for superheterodyne receivers

$= L_c(F_{IF} + NR - 1)$

L_c = conversion loss

NR = noise ratio

NO. 340-L310 DIETZGEN GRAPH PAPER
SEMI LOGARITHMIC
3 CYCLES X 10 DIVISIONS PER INCH
EUGENE DIETZGEN CO.
MADE IN U.S.A.

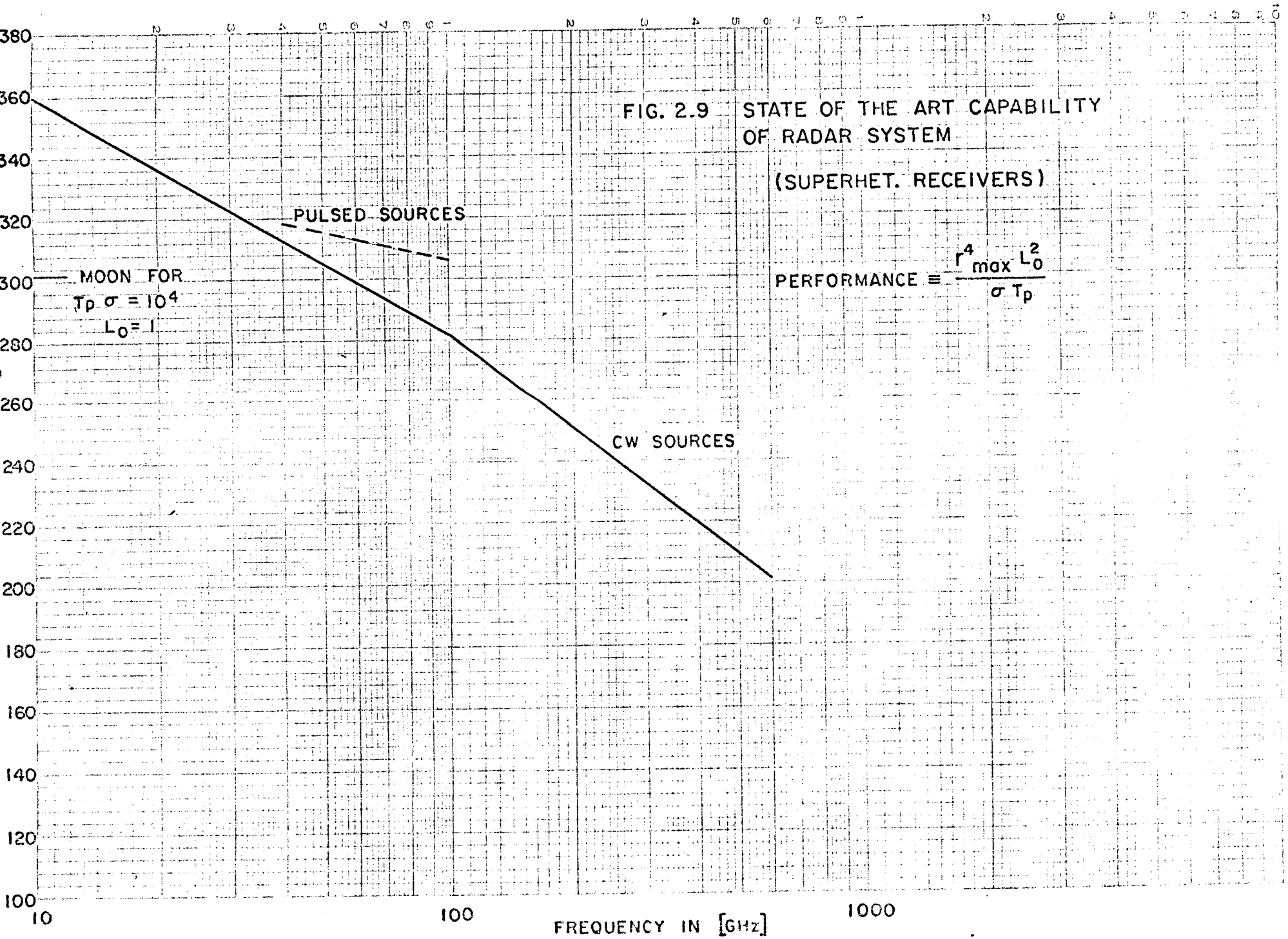

FIG. 2.9 STATE OF THE ART CAPABILITY OF RADAR SYSTEM (SUPERHET. RECEIVERS)

F_{IF} = noise figure of IF amplifier

T_{BL} = back lobes temperature

T_{sky} = sky temperature

$\frac{1}{L_o}$ = loss factor of propagation = $\exp\left(\int_o^\infty \alpha(h)\, dh \sec\theta\right)$

$\alpha(h)$ = attenuation constant, function of altitude

θ = slant angle of ray

T_B = $\int_{L_p}^{o} T(h)\, d(L_o)$ is the brightness temperature of absorbing medium

L_p = the loss factor of propagation at the ground level

$\frac{\Omega_s}{\Omega_a}$ = ratio of source solid angle to antenna beam solid angle

T_S = brightness temperature of the source

Assume that the source of radiation which is to be determined has an effective temperature difference from that of the receiver (T_{RS}) of ΔT_S. If the solid angle subtended by the source (Ω_s) is smaller than the solid angle of the main lobe of the antenna (Ω_a), then the temperature difference observed by the receiver due to ΔT_S will be (if atmospheric losses are neglected)

$$\frac{\Omega_s}{\Omega_a}\ \Delta T_S \tag{2.12}$$

Hence, we may write (using (2.10) and the relation $\Omega_a = \frac{\lambda^2}{A_{eff}}$)

$$\frac{1}{\sqrt{\tau}\ \Omega_s\ \Delta T_{S(min)}} = \frac{\sqrt{B}}{\Omega_a\ T_{RS}} = \frac{\sqrt{B}\ A_{eff}}{\lambda^2\ T_{RS}}$$

Now, replacing the effective receiver temperature by an equivalent expression, taking into account the quantum noise, ie.

$$\frac{T_{RS}k}{hf} \approx \left[1 + \left(e^{\frac{hf}{kT_{RS}}} - 1\right)^{-1}\right]$$

we have

$$\frac{1}{\sqrt{\tau}\,\Omega_s\,\Delta T_{S(min)}} = \frac{k}{1.44}\sqrt{B}\;v\,A_{eff}$$

where v is as previously defined. Utilizing decilogs, one can calculate the sensitivity of any system utilizing a state-of-the-art ground-based antenna and any of the specified detectors. The results are shown on Fig. 2.10. Note again, however, that atmospheric losses have been neglected. They can be serious except at those frequencies corresponding to very low loss windows.

Note that in Fig. 2.10 the relative performance of coherent and incoherent detectors is readily determined. Attention is drawn to the trend in incoherent detector performance to become superior to the superheterodyne receiver at higher frequencies.

In the case where the antenna main lobe solid angle is narrower than that of the object being viewed, then ΔT in (2.10) is equal to ΔT_S, and we have

$$\frac{1}{\sqrt{\tau}\,\Delta T_S} = \frac{\sqrt{B}}{T_{RS}}$$

This relation is independent of antenna size.

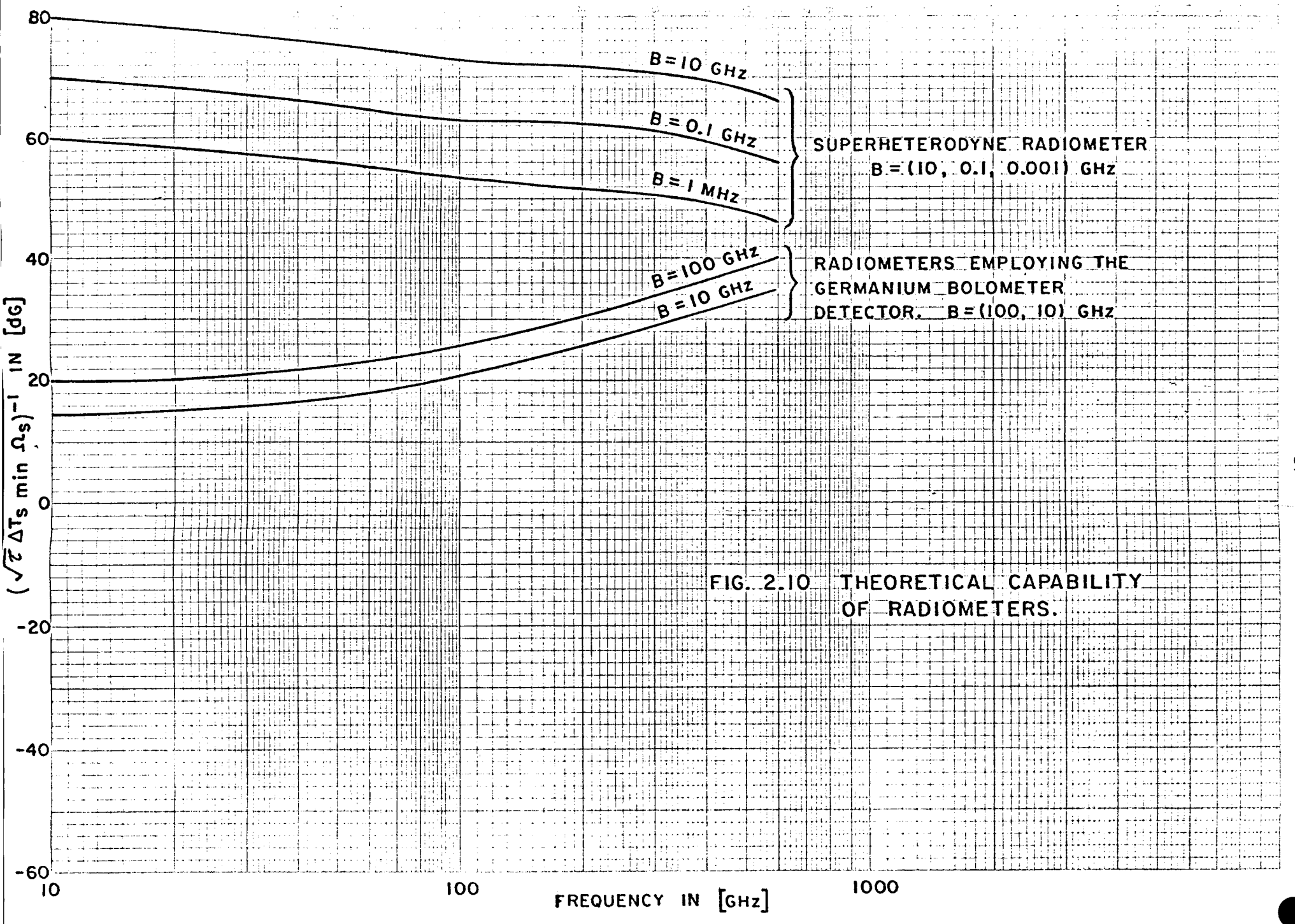

FIG. 2.10 THEORETICAL CAPABILITY OF RADIOMETERS.

2.2.4 Plasma Reentry Communications

A system problem not included in the above discussion is that concerned with the radio blackout experienced by a space vehicle reentering the earth's atmosphere. Although at one time it had been assumed that communications could be maintained at 93 GHz, recent evidence indicates otherwise. A fairly detailed analysis of this problem in the case of lifting reentry vehicle has been published recently;[12] however, it does not provide quantitative data at frequencies above 10 GHz. In this work no particular effort was made to evaluate this phenomenon because of the rather extensive programs underway elsewhere.

2.3 REFERENCES TO CHAPTER II

1. "The Radio Spectrum from 10 Gc to 300 Gc in Aerospace Communications," Vols. I-VII, RCA Victor Co., Ltd., Montreal, Canada, 1962, (Electromagnetic Warfare and Communications Laboratory).

2. A. G. Fox, "The Communications Frontier between Classical and Quantum Physics," IRE Trans. on Microwave Theory and Technique, Vol. MTT 7, p. 401, Oct. 1959.

3. D. D. King, Editorial (scanning the Issue), Proc. IEEE, April 1966, Vol. 54, No. 4.

4. S. K. L. Brinkman and L. S. Stokes, "Deep Space Communication: System Trade-off Parameters," Conference Record, 1966 Winter Convention on Aerospace and Electronic Systems, IEEE, pp. IB-1 to IB-11.

5. "Parametric Analysis of Microwave and Laser Systems for Communication and Tracking," 3rd Quarterly Report, Contract No. NAS 5--9637, June 1966, Hughes Aircraft Co.

6. "Special List of Microwave Tubes," Office of the Director of Defense Research and Engineering Advisory Group on Electron Devices, GED 200.2/31

7. D. C. Forster, "High power sources of mm-wavelengths," Proc. IEEE, Vol. 54, pp. 532-39, April 1966.

8. J. Ruze, "Antenna tolerance theory--a review," Proc. IEEE, Vol. 54, pp. 636, April 1966.

9. Defense Communications Agency, DCS Research and Development Guide, Millimeter Waves Communications, D No. 460977.

10. R. S. Berkowitz, (ed) "Modern Radar," J. Wiley, 1965.

11. K. A. Norton, et al, "An Experimental Study of Phase Variations in Line-of-Sight Microwave Transmission," NBS, Monograph 33, Nov. 1961.

12. "Lifting Reentry Communications, Vol. I, A Comparative Evaluation of Potential Systems," Aerospace Corporation, Report TR 669 (6220-10)3, May 1966.

CHAPTER III

SUGGESTIONS FOR RESEARCH

3.1 INTRODUCTION

We can look upon research as contributing to:

1. the fund of knowledge
2. the development of techniques applicable to immediate or other problems
3. the revelation of the existence of effects other than the one being investigated which are of importance.

The recommendations given in this chapter are based upon a possible payoff in any of these categories. They are, of course, restricted to those which relate to the extension of our knowledge of, and ability to apply, techniques of millimeter and submillimeter waves in aerospace applications. These applications can be considered to be of a rather broad nature, as has been discussed already in Chapter II.

With regard to physical limitations on the use of devices in aerospace applications such as size, weight, necessity for operating at cryogenic temperatures, etc; it is recognized that certain of these techniques may be severely limited at the present time. However, for many of the techniques, it may be expected that new developments may overcome such limitations. Furthermore, in some applications, some of the equipment may be located on the surface of the earth where such limitations do not apply. For these reasons, such limitations have not been considered as justifying elimination of further work.

Table 3.1

STRENGTH OF RECOMMENDATIONS FOR FURTHER RESEARCH IN AEROSPACE APPLICATIONS

HIGH	MEDIUM	MARGINAL	NOT EVALUATED
GENERATION (3.4.1) Gas Maser (3.2) Solid State Maser Materials (3.2.4) a. > 100 GHz (3.4.5) b. tuning methods (3.4.4.1) Gunn Effect (3.2.3) a. materials	(3.3.1) Theoretical study of limitations on efficiency and max. freq. (3.3.1) Development of Bermutron (3.4.2) Injection lasers a. materials b. pressure tuning (3.3.1) Teaser (3.4.4.3) Josephson effect	(3.3.4) Analysis of electron beam efficiency (3.3.3) Cerenkov and other radiation coupler studies (3.3.2) Multi-stream interaction studies (3.4.3) Photoelectric diff-freq. generation (3.4.4) Bremsstrahling negative effective mass	Harmonic generation mixing
AMPLIFICATION (3.4.5) Gas maser (3.4.5) T.W. Solid State Maser (3.4.7) Saturated Gas Amplifier			Parametric Amplifier
MODULATION AND DETECTION (3.8.2) Dev. of improved hot electron mixers (3.8.3) and local oscillators	(3.5) Gen'l. investivation of modulation techniques (3.8.1) Homodyne detection techniques (3.8.4) Non-heterodyne down conversion	(3.8.7) Glow discharge detector. (see chapter on detectors) (3.5.3.1) Faraday effect (3.5.3.2) Pockels effect (3.4.6) Radiation helped tunnel diode	

continued

TABLE 3.1 (Continued)

STRENGTH OF RECOMMENDATIONS FOR FURTHER RESEARCH IN AEROSPACE APPLICATIONS

HIGH	MEDIUM	MARGINAL	NOT EVALUATED
MODULATION AND DETECTION			
(3.5.1) Dev. of high speed modulators based upon saturation of electron drift velocity in germanium in the presence of high fields	(3.8.5) Reflection cavity detector (3.8.1) Dev. of high gain, broadband IF amplifiers (3.8.6) Investigation of simultaneous generation, mixing and amp. of IF in semiconductors		
ANTENNAS AND PROPAGATION			
(3.7a,d) Exp. study of propagation characteristics at atmospheric windows	(3.9) Materials and techniques for constructing phased arrays (3.7b) Computer calculation of atmospheric attenuation vs frequency as function of altitude		Arrays of dipoles or slots Surface wave structures Travelling wave antenna
COMPONENTS			
	(3.6.1) Overmoded transmission (3.6.4) line (circular) (3.2.2) Ferrites	(3.6.2) Beam waveguide (3.6.3) Comparative study of waveguides	
MISCELLANEOUS			
(3.2) Collection of data on properties of materials (10 GHz to 3 Tc)	(3.2) Experimental measurements of properties of materials 10 GHz to 3 Tc (3.7c) Radiometry of the sun with airborne receivers		

3.1.1 Summary of Recommendations

Table 3.1 gives a summary of areas recommended for further research, classified according to technical area and according to their promise for useful results. A brief discussion of each of these recommendations is given in succeeding subparagraphs of this chapter as identified by the number next to the listing in the table. For more detailed discussion of each of these areas, subsequent chapters of this report should be consulted.

3.2 INVESTIGATION OF MATERIALS

Because of the lack of instrumentation in the millimeter and submillimeter wavelength range, knowledge of many of the important properties of materials has been limited. Admittedly, there are some data on materials in this frequency range, but they are considered inadequate for researchers and development engineers who have need of them. Hence, it is recommended that the following careful investigations of material properties be carried out. Along with this work, investigations should be made of the possibilities of synthesizing new materials with properties that are particularly desirable for the purposes at hand. A description of areas of interest follows.

3.2.1 Dielectrics

Values of dielectric constant and conductivity in the submillimeter range are needed in the development of various types of transmission lines. In addition, the development of Fabry-Perot type filters is dependent upon knowledge of these parameters.

3.2.2 Ferrites

Ferrite materials have a variety of applications. These include waveguide components, modulators, amplifiers, and reverse isolators in masers. As discussed in Chapter VII, a relatively large number of materials is available for consideration, and data on their characteristics are critically needed.

3.2.3 Semiconducting Materials

It appears from our study (see Chapters V, VI and IX) of new phenomena and effects in semiconductors, which are relevant to submillimeter techniques, that the study of a number of somewhat unconventional properties of semiconductors is very important and promising for the proper development of new, and the extension of existing, techniques to the submillimeter region.

Thus, the modulation scheme based on the electric field dependent mobility property of germanium requires the study of this phenomenon (usually called "hot electron conductivity") from the point of view of sensitivity and frequency response (probably limited by the reciprocal of the electron relaxation time). The hot electron thermoelectric detection scheme requires the development of semiconducting materials with very short dielectric and electronic relaxation times. The details of the electron energy band structure in some semiconductors such as GaAs, InSb, etc. is of primary interest in the development of Gunn generators; specifically, it is desirable to have materials with small energy spacing between the conduction

band and satellite high effective mass energy bands, high saturation velocities, and short electron relaxation times. The pressure tuned and composition dependent injection diode lasers require a detailed knowledge of the dependence of the energy gap width on pressure (deformation potential) and natural composition.

In summary, it is considered that a study of this type may be one of the most effective methods of advancing the technical state of the art in the utilization of semiconductors with millimeter and submillimeter waves.

3.2.4 Maser Materials

Paramagnetic materials are needed for maser operation above 100 GHz, which is the limiting frequency to today's most commonly used maser material--iron doped TiO_2. The latter has a spin 5/2 with a zero field splitting of 43.3 and 81.1 GHz. Gerritsen and Sabisky[1] investigated the paramagnetic resonance of trivalent manganese in rutile and concluded that this material may be appropriate for submm masers. It has a large outer zero field splitting of 412 GHz, fairly long relaxation times, and narrow resonance lines. Another material that looks favorable as a possible maser material for the submm range is MgO[2]. It is an especially good transmitter when cooled to $90^{\circ}K$, or below.

New materials suitable for an optically pumped maser are needed. The requirements are that it have a long spin lattice relaxation time at elevated temperatures for microwave frequencies

and a short radiative lifetime for the optical pump transition. Pump power dissipation and pump coupling efficiency must also be considered.

3.3 GENERATORS, ELECTRON BEAM TYPE

It is inevitable that in the development of millimeter and submillimeter wave generators of the classical variety attention should be centered about phenomena which do not require mechanical structures with stringent tolerance requirements. A number of phenomena such as Bremsstrahlung, cyclotron transition, radiation, Cerenkov radiation, and multi-stream interaction have been considered. Bremsstrahlung,[3] and transition radiation[3,4] have been shown to produce intensities substantially below that of Cerenkov radiation, although the interaction impedance of the latter was shown to be small, as well,[5] in the case of isotropic media. Even though this, in itself, would not preclude consideration of these phenomena as potential generators, it is believed that those which are expected to yield higher output intensities should be considered first.

3.3.1 Specific Devices

There is little doubt that the most suitable devices for extending the frequency range are those of the distributed interaction variety. In the study of these, the principle of the bermutron appears most promising. With respect to other devices of this class, a study of maximum frequency and efficiency limitations of electron beam-distributed circuit interaction seems

almost imperative in order to avoid unnecessary and costly delays in attempts to develop devices outside the range of their usefulness.

The Teaser has shown harmonic outputs at submillimeter frequencies and is based on a principle that is promising because of its simplicity, as well as some successful experimental results. This device seems to have received inadequate attention to date.

3.3.2 Harmonic Mixing

The dispersion relation for beams traversing the same space (one dimensional analysis) is given by

$$1 = \sum_{i=1}^{n} \frac{\omega_{pi}^{2}}{(\omega - ku_{oi})^{2}} \text{ or } 1 = \int_{-\infty}^{\infty} \frac{\omega_{p}^{2} f(u)du}{(\omega - ku)^{2}}$$

depending upon whether there are n discrete beams with discrete velocities u_{oi}, and plasma frequency ω_{pi}, or whether there is a continuous velocity distribution f(u). k is the propagation vector. Oscillation at various harmonics is possible for complex values of ω for real values of k. Such harmonic radiation generated by an electron beam in a plasma has been observed[6,7] below 10 GHz.

This scheme is free of the limitations imposed by mechanical tolerances. Instead, it is restricted by rather poor RF coupling mechanisms. Analytical studies (more than one dimension) of multi-stream interaction are recommended to determine ultimate frequency limits, with particular attention centered about efficient coupling methods.

3.3.3 Cerenkov Radiation

A substantial controversy continues with respect to the effectiveness of this phenomenon as a potential RF generator. Even though the interaction impedance is low (~ 200Ω), Coleman[8] has observed 0.8 watts at 39 GHz[5] with a relatively simple coupler. Periodic metallic couplers have been used. Consideration should be given to introduction of a periodic dielectric coupler which may have two advantages: (1) Because of its periodicity, and the resulting effective anisotropy, the interaction impedance may be increased; and (2) Because of the periodicity of both the beam and the structure, substantial power may be available in high order harmonics. It is recommended, therefore, that utilization of Cerenkov radiation in dielectric periodic structures be considered for the determination of interaction impedances and output frequency spectra.

3.3.4 Backward Wave Devices

Backward wave oscillators have been developed to frequencies in the neighborhood of 720 GHz. Their size is presently considered to be a serious limiting factor. However, the device has by no means been optimized in this respect. Since it has been indicated that the size of such devices can be reduced, at least in the lower range of frequencies of interest, a basic study should be made indicating theoretical as well as practical limitations on this size. The electron efficiency must be maximized to obtain optimum results.

Five watts have been obtained at 5 mm with a two pound device. Power supply may be the major weight problem. It is recommended that a basic study be made of the relation between electron efficiency and beam geometry and focusing techniques. The possible availability of exotic magnetic materials may be a major factor in the success of this study.

3.4 QUANTUM GENERATORS AND AMPLIFIERS

3.4.1 Submillimeter Molecular Masers

These devices, which have been in development for only about two years, have produced stimulated emissions at wavelengths from 20 to 350μ (sec. 5.2.2.2(3)) using electric discharge excitations of different gas molecules such as water vapor and CN radical compounds. The high power levels (of the order of watts), operation at room temperature, and the multiplicity of emission wavelengths in the submillimeter range obtained by this method, make the latter a very promising and useful generation scheme. Three goals should be achieved: (a) to extend our knowledge of how these devices operate (some of them are not now completely understood), (b) to find new emission lines in the yet uncovered gaps of the submillimeter band, and (c) to optimize their size and efficiency.

3.4.2 Pressure Tuned Submillimeter Diode Lasers (see also Sec. 3.2)

A narrow energy gap semiconductor, PbSe ($E_G = 0.165$ eV) was recently used with success in a diode laser (5.2.2.2(4)) by a group at the Lincoln Laboratory, MIT. The natural lasing wavelength is 8.5μ.

The possibility of increasing this wavelength continuously up to a few hundred microns by applying a pressure to the semiconductor is a very attractive possibility. The drawback of this scheme is the necessity of auxiliary bulky equipment in order to provide cooling and high pressures. More recently, $Pb_xSn_{1-x}Te$ alloy junction lasers were studied (5.2.2.2(4)) at the Lincoln Laboratory, and coherent emission at 16μ was observed. Furthermore, since the band gap is found to be an increasing function of x, it is thought possible to reach very small values of energy gap width by choosing the proper x. An intensive study of such alloys seems to be very promising.

3.4.3 Photoelectric Difference Frequency Generation

The availability of optical lasers with substantial power outputs, and the possibility of continuously shifting the lasing wavelength substantially, makes mixing of these beams an attractive way of generating mm and submm wave energy of continuously variable frequency. Photomixers of various types have been under investigation. One of these is a photoemissive mixing scheme being investigated at the University of Sheffield. Here, two ruby laser beams impinge on the photoemissive surface of a strip transmission line. With proper adjustments of the angles of incidence of the two beams the photoemissively generated difference frequency will possess the proper propagation constants in the transmission line and therefore will be received at the output of the latter. No experimental results are available however. Another is a scheme developed by

Microwave Associates, Inc. which uses a high speed heterojunction (Sec. 5.9).

Two investigations are proposed. One of these is primarily theoretical, aimed at a thorough theoretical evaluation of the photomixing techniques. In the other, a variation of the heterojunction scheme should be studied. In this the space charge junction region of the p-n heterojunction $GaAs_xP_{1-x} \longrightarrow GaAs$ is used as a waveguide to guide the difference frequency directly to a radiating antenna. The construction of such a device should not represent major difficulties since the epitaxial layer growing as well as masking with close tolerances are well-developed techniques (see Fig. 3.1).

Another possible scheme may result from the use of the high speed point-contact photodiodes described in 5.9.3.2. It is, indeed, possible to visualize a scheme such as that shown in Fig. 3.2, where the point contact lead which carries the photoconductively generated difference frequency signal launches the latter in a particular waveguide (oversized or regular).

3.4.4 Bulk Semiconductor Phenomena

3.4.4.1 The Gunn Generator (see 5.4)

It is felt that research efforts should be fruitfully concentrated on further work on the Gunn effect in the immediate future since:

1. The operation mechanism is reasonably well understood.

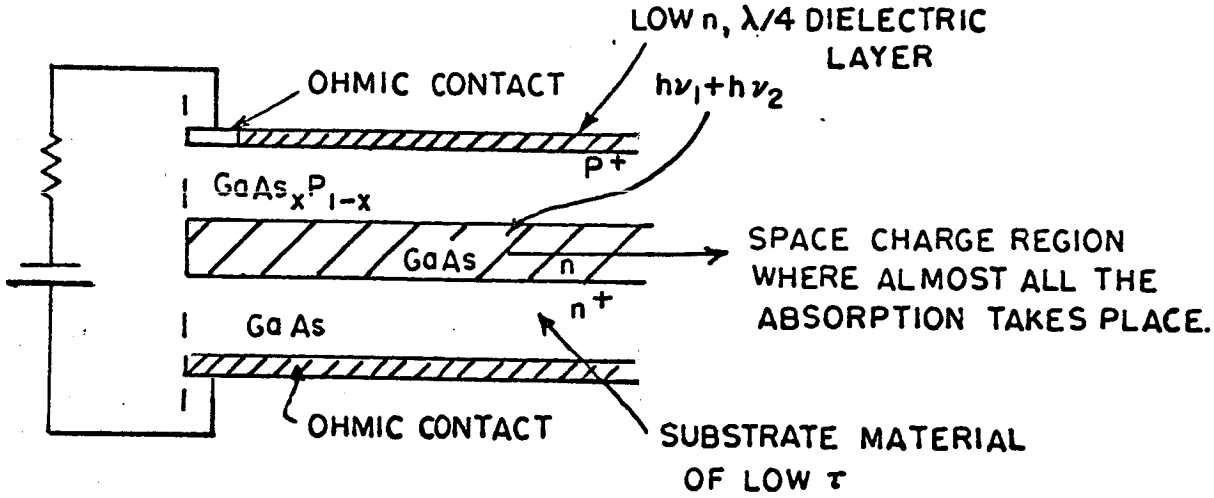

FIG. 3.1 HETEROJUNCTION PHOTOMIXING

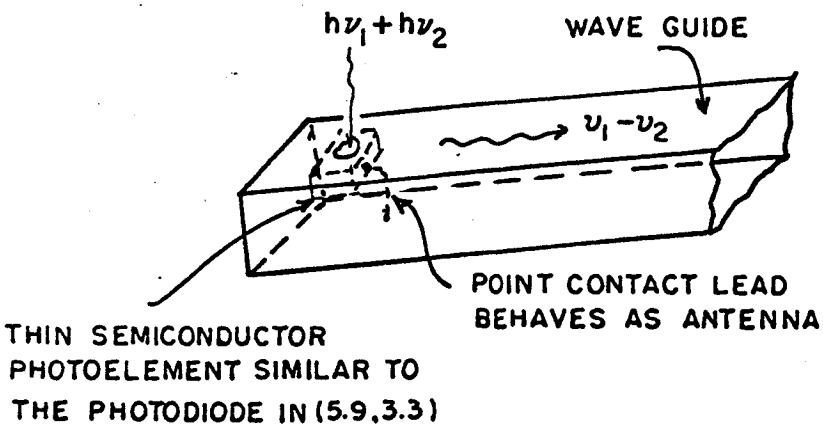

FIG. 3.2 POINT CONTACT PHOTOMIXING

2. No other phenomenon or device known at present can compete with the simplicity, the small size, and by now high efficiency (6%) of the Gunn oscillator.

3. Operation is at room temperature.

4. Higher output powers might be obtained by phase locking several Gunn generators.

Research in this area should be oriented toward the investigation of new materials (other than GaAs) rather than trying to generate higher frequencies from thinner and thinner GaAs wafers. It is fairly well established (see Chapter V) that the upper limit of generated oscillation frequencies in GaAs is a few-hundred GHz for a 1μ thick wafer.

An important breakthrough in obtaining higher oscillation frequencies can only be achieved by the discovery of materials with sensibly larger saturation velocities v_s and smaller scattering times τ_s, than in GaAs, together with small energy separation ΔE between the main conduction band and the satellite high effective mass minima.

Finally, considerable improvement in the efficiency of the device appears to be possible by changes in geometry[9, 10].

3.4.4.2 Negative Mass and Bremsstrahlung Amplifier-Generator Schemes

These two schemes are still in the theoretical stage (Sec. 5.3, 5.6 and 5.8); however, they offer very attractive possibilities, both in terms of generation and amplification of submillimeter radiation. Even though an immediate result may not be expected from an investigation in these areas, such efforts would certainly be worthwhile

for a long-range program. In particular, it is strongly recommended that research efforts be made similar to those at the University of Michigan, described in Section 5.3.

3.4.4.3 Josephson Effect

The Josephson effect has recently received enthusiastic attention for application to a number of devices because of its theoretical efficiency and voltage tuning characteristics. Experiments to date have been disappointing, but further work is certainly justified.

3.4.5 Amplification by Stimulated Emission

We refer here to the schemes described in Section 5.8.3. With the advent of the submillimeter masers (5.2.2.2(3)) it should be possible to develop, with little difficulty, a scheme identical to the He-Ne amplifier (5.8.3.1) in the submillimeter region making use of the recently discovered active gases. Such amplification (although of small magnitude) has been reported very recently.[11]

Also, solid state maser amplifiers such as the chromium doped titanium dioxide (TiO_2) 8 mm traveling wave amplifier, described in Section 5.8.3.2, can very likely be developed for any frequency range provided a search for the proper material is made. The most interesting features of such an amplifier are: (1) a wide tuning range, (2) a reasonable bandwidth for most applications, (3) operation on a continuous basis, (4) a very low noise figure, and (5) high gain stability. Another feature of solid state

amplifiers is the possibility of generating or amplifying a signal at a higher frequency than the pump frequency. Such an operation was achieved first by J. M. Minkowski of Johns Hopkins University with $f_p = 5.6$ GHz and $f_s = 9.8$ GHz. It was recently demonstrated in the mm wave region by W. Hughes of Westinghouse[12] with $f_p = 65.2$ GHz and $f_s = 96.7$ GHz. Higher frequency operation is predicted to be possible with Cr^{+3} impurities in tungstates ($f_s \approx 200$ GHz) and in calcium fluoride and strontium chloride (60-300 GHz)[13] with manganese-doped rutile ($f_s \approx 300$-350 GHz)[1] and with optically pumped maser materials ($f_s \leq 2000$ GHz at $4.2^{o}K$ for ruby).[14] The latter two materials can possibly be used at liquid nitrogen temperature operation.

Since M_n^{+3}-doped rutile has a large zero field splitting (412 GHz), the number of spins in the uppermost level at $4.2^{o}K$ is small. By raising the temperature to $77^{o}K$, the number of spins will increase and stronger interactions will result. In addition, the material has a large pump to signal frequency ratio (6:1). These two characteristics should give maser gain at elevated temperatures. Also, by pumping a maser at frequencies in the optical spectrum, amplification should be possible at $77^{o}K$ with nearly the same noise and gain-bandwidth characteristics as conventional helium-cooled masers. If active materials having the proper relaxation time ratio for optical pumping could be found, they might lead to extremely simplified masers. Furthermore, the development of nitrogen-cooled masers would be desirable

for remote field operations, since nitrogen is more abundant and more easily handled than helium.

To this date, no traveling wave masers above 40 GHz have been built. They have a much greater tuning range and instantaneous bandwidth and a much lower noise temperature than does a cavity maser. The difficulties associated with high frequency operation are: (1) obtaining a ferrite to provide reverse isolation for keeping the amplifier stable, (2) mechanical problems associated with the small sizes of the active samples and the slow-wave structures, and (3) obtaining pump sources with adequate power to saturate the amplifier. The first and most serious problem may be solved by investigating the use of ferrites as discussed in Section 3.2.2.

If a traveling wave maser cannot be built at these high frequencies, then the cavity maser's amplifier characteristics can approach those expected from a TWM by coupling several cavities together to give a large instantaneous bandwidth. This was demonstrated by G. Broussaud and L. Malnar of Paris, France, with an X-band cavity maser using ruby.[15] Two groupings of three symmetrical cavities were coupled together on one transmission line to give a three-peaked response curve having a 60 MHz bandwidth and 22 dB gain. In comparison, a single cavity maser had only a 5 MHz bandwidth and 23 dB gain.

A very important consideration associated with a practical maser amplifier to be used in the field is that of easing complex

operational problems with the use of light-weight helium-recycling systems. A 96 MHz cavity maser was operated in a closed cycle liquid helium refrigerator (CCR) by Jet Propulsion Laboratory for 10 consecutive days without adjustments.[16] The maser-CCR was installed on an 85 foot diameter paraboloid antenna. Both a maser and a superconducting magnet have been operated in a CCR.[17] The maser, magnet, and CCR combination can perform in any orientation and can be moved (as in a scanning antenna) without affecting its operation.

3.4.6 Radiation Helped Tunneling Diode

A physical and qualitative description is given here of a novel scheme. The mathematical treatment of it is possible but lengthy and not trivial; it should be carried out, however, in the near future. This scheme results basically from the following reasoning: in order to be able to use the phenomenon of photo-conductivity in the detection of electromagnetic radiation it is necessary to provide, within the photoconductor, energy levels situated just below (or just above) the conduction band (or valence band) and separated from the latter by not more than $\Delta E = hf$, where f is the frequency of the radiation to be detected as shown in Fig. 3.3. Such energy levels can be provided by different types of impurities; however, it is difficult, if not impossible, to find impurities providing exactly or approximately any required $\Delta E = hf$.

The scheme presented here does provide exactly any amount of ΔE; however, it is a priori expected to be less sensitive than an ordinary photoconductor.

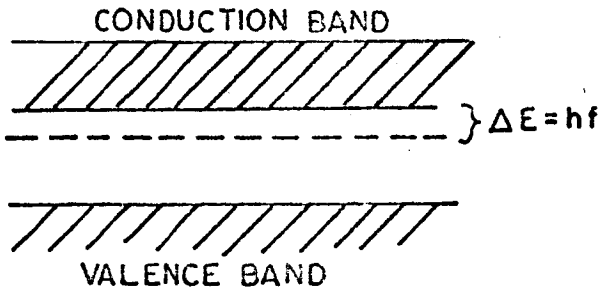

FIG. 3.3 SEMICONDUCTOR ENERGY LEVEL STRUCTURE

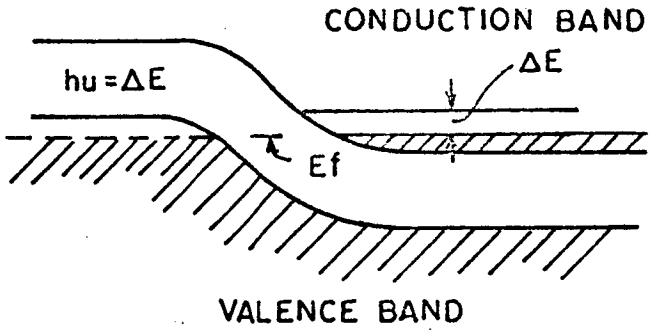

FIG. 3.4 TUNNEL DIODE ENERGY LEVEL STRUCTURE

Consider the relative positions of the Fermi level and the energy bands in a tunnel diode structure of $0^{\circ}K$. In Fig. 3.4, the electron occupation of the bands is as shown by the hatched lines. It is clear that in order to conserve energy, no electron is allowed to tunnel from the right to the left-hand side or vice versa, since equi-energy levels are fully occupied. However, when radiation of frequency hf impinges on the left-hand face of the tunnel diode and is almost completely absorbed by the left-hand side p-type degenerate semiconductor, there will be a finite transition probability between the uppermost levels of the left and the empty levels $\Delta E = hf$ above the Fermi level on the right. Because of the very narrow junction (< 100 Å) width and the high electric field in the junction, a substantial photoelectric effect can be expected to result from the application of the electromagnetic field. It may be noticed that the above scheme would work at any frequency f since at $0^{\circ}K$ the levels on the right are empty for any ΔE. At liquid helium temperature, $KT = \Delta E = 0.00035$ eV while

$$hf\ (1000\ \text{GHz}) = 0.004\ \text{eV}$$

Therefore, this scheme should operate at liquid helium temperatures and for frequencies close to 3 THz or more.

Finally, if the p-type half of the tunnel diode is made "just-degenerate" i.e., E_f coincident with the edge of the valence band (see Fig. 3.5), it is possible to "tune" the detector by

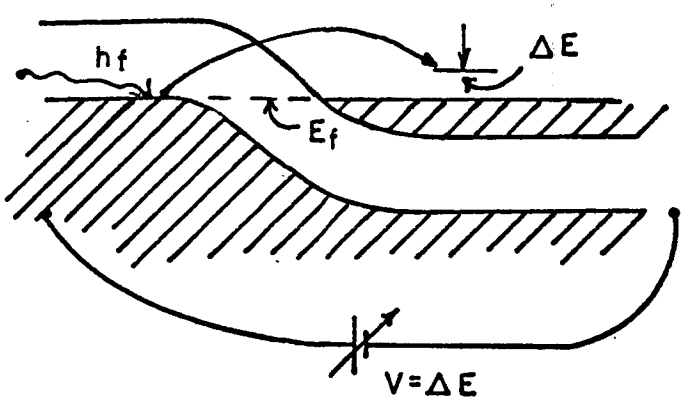

FIG. 3.5 RADIATION ASSISTED TUNNELING

adjusting the forward bias V to $\Delta E/e$; thus only signals of frequency f such that $hf > \Delta E = V$ will be detected.

3.4.7 Amplification by Resonance Saturation in Gases

The scheme of amplification of millimeter waves in a gas which is resonance saturated by a local oscillator of a slightly different frequency is described in section 5.8.4.1. It is felt that further research in this area is worthwhile since this scheme is a particularly simple one and provides amplification at room temperature. Also, it appears that the novel CN radical laser materials have good prospects of being used in this scheme since their lasing frequencies are exactly in the fractional millimeter range.

3.5 MODULATION

Methods of modulation can be classified as to whether they are internal (i.e. can be achieved by varying a parameter of the generation device) or external (can be achieved by controlling transmission or absorption properties of media separate from the generation device). Here we are concerned only with external modulation methods; hence the problem of finding suitable "materials" is of paramount importance. Identification and measurement of the properties of materials that exhibit effects useful for construction of modulators are generally recommended. A number of specific suggestions for areas worth pursuing are made below.

3.5.1 The Effect of High Electric Fields on the Absorption in Germanium of MM Waves -- as a Pulse Modulator.

It has been shown by Arthur and co-workers[18] that the absorption coefficient of n-type (4 or 5 Ohm) germanium at $\lambda = 8$mm is decreased when the germanium is subjected to high external electric fields. The effect is caused by the tendency of the electron drift velocity to saturate at high electric fields. This is equivalent to a decrease in the electron mobility at high electric fields, since the absorption coefficient is proportional to the slope of mobility ($\frac{dv}{dE}$). Significant departures from Ohm's law occur at electric fields as low as 10 V/cm; furthermore, the change in attenuation is approximately proportional to the square of the electric field.

This effect can be used to construct pulsed microwave and millimeter wave modulators with a theoretical response time of the order of 10^{-12} sec. The power requirements should not be high and the operation is simple. Furthermore, it would be of interest to determine at what wavelength below 8 mm the effect will not be negligible.

3.5.2 Electromechanical Modulators

Small electrically controlled mechanical displacement can be produced in various materials such as solid solutions of barium zironate and barium stannate in barium titanate by application of external electric fields. This effect can be used to produce amplitude modulation at mm wavelengths by control of waveguide

dimensions. The small and accurately controlled displacements possible are consistent with the small size of the waveguides at those wavelengths. Time constants of the order of 10^{-6} sec are predicted[19]. This and the small power requirements make the development of such a modulator for operation at mm and submm wavelengths attractive.

3.5.3 Modulation by Rotation of the Polarization Plane (see Sec. 3.2)

3.5.3.1 The Faraday Effect

Here, the primary effort required is for the identification and testing of ferrite materials suitable for operation at mm wavelengths and high modulating frequencies without appreciable heating. Hexagonal crystal materials such as cobalt-barium, magnesium-barium and nickel ferrites have been identified by Jonker et al[20] to be suitable for modulation frequencies in the 100 MHz range. Their practicality as mm wave modulators is yet to be demonstrated.

3.5.3.2 The Pockels Effect

This is related to the change of the dielectric constant of a crystal with respect to the electric field of the modulating signal. It occurs in crystals without a center of symmetry and is useful in hexagonal, tetragonal, and trigonal crystals where the unperturbed indicatrix is an ellipsoid of revolution. The application of an electric field destroys the rotational symmetry of the indicatrix and thus causes a rotation of the polarization plane of the carrier.

In both of the above cases an investigation should be made to determine if materials with these properties are available which are sufficiently non-absorbing at the frequencies of interest.

3.6 TRANSMISSION LINES AND COMPONENTS

There has been and is substantial activity in investigating transmission media which may be applicable to submillimetric wavelengths (see Chapter VII). These may be divided into two categories:

1) methods applicable for long distance guided transmission (overmoded circular waveguide, helical waveguide, and beam waveguide)

2) methods particularly applicable for short distance transmission and component development (H-guide, groove guide, overmoded rectangular waveguide, dielectric guide in its various forms).

Circular and helical guides (Secs. 7.2.1.3 and 7.2.2) have been under study for years and the fundamental problems have been largely solved. There remain technological problems in extending these techniques to the submillimeter region. These concern the choice of suitable materials and methods of fabrication, and the study of their effects on overall performance.

3.6.1 Circular Waveguide

In the case of circular waveguides operating in the TE_{01} mode, good results have been obtained by utilizing a lossy dielectric coating to effectively attenuate the unwanted modes. As the frequency is increased and as the diameter is decreased,

it is expected that difficulty will be experienced in properly coating the inside of the guide. New techniques and/or new materials may have to be sought to adapt this form of waveguide to ultramicrowave transmission. For example, one technique that might be investigated for this purpose is the metallic waveguide with an internal oxide layer, e.g., aluminum/aluminum oxide.

Helical waveguides, on the other hand, would seem to be too complicated a structure to contemplate reducing the size greatly over the present arrangement. For good performance a tightly wound helix is required. At the frequencies already investigated, a wire size of AWG 30 to 40 was used. If the wire size should be scaled in accordance with the wavelength, this would make the resultant choice prohibitively small in size at 300 GHz and above. In addition to this, the helical waveguide as developed by Bell Telephone Laboratories has a multiple layered dielectric between the helix and other wall. It is felt that fabrication of this would be increasingly difficult as the size is reduced. For these reasons the somewhat simpler lined circular waveguide is favored for development as a transmission medium in the 300-3000 GHz range.

3.6.2 Beam Waveguide

The beam waveguide (Sec. 7.2.8) is favored by many investigators as representing a technique better adapted to standard optical procedures and more or less independent of wall properties. Very low attenuation values can be obtained and bends and corners can

be fabricated. In beam waveguide development, the principal concern is with developing criteria for selecting the optimum technique from the three mentioned herein, i.e., lens type, aperture type, or mirror type. This is not only a theoretical problem, but considerable experimental work is required as well. Careful evaluation of materials at the frequencies of interest is required. There is, however, little doubt that satisfactory beam waveguides can be made for the submillimeter region.

3.6.3 Comparative Waveguide Study

From among the short-haul and component-type waveguides named (Secs. 7.2.1.2, 7.2.3, 7.2.5, 7.2.6, 7.2.7), there is at the moment no clear-cut comparative evaluation by means of which one can positively state that a certain type is the best for a certain requirement. Comparison on some basis other than attenuation alone is required. For example, a figure of merit which includes physical size, attenuation, and mode purity would be desirable since these qualities seem to be inseparably linked. Other qualities to be compared are potential for component design, ease of fabrication, need for evacuation (at submillimeter wavelengths), adaptability to antenna feeds and/or generation devices, and ease of mode launching.

A comparative study of all presently reported guiding systems should be done at a frequency where instruments already exist, say 100 GHz. When all of the features of the various systems have been

catalogued, then the path for fruitful further work will be indicated.

3.6.4 Cladded Dielectric Guide

It is noted that the concept of using cladded dielectric guides (Sec. 7.2.3) in the submillimeter wavelength region has received no attention as yet, and it would be appropriate to investigate this technique to some extent aside from the above-mentioned comparative evaluation. The work at optical frequencies has shown that single mode operation can be achieved provided that the right values of dielectric constants can be secured. In a sense, this technique is related to that of the dielectric lined circular waveguide, and it would be appropriate to show this interrelationship in a formal way. Work on cladded dielectric waveguides could not only be of scientific interest, but could result in techniques applicable to component development.

3.7 PROPAGATION INVESTIGATION OF THE SPECTRUM OF AIR ABSORPTION USING COHERENT SOURCES

Work is needed to consolidate the knowledge of the spectrum of air absorption in the frequency range 100 GHz to 3000 GHz. The suggested steps are:

a) A laboratory study of the lines of water vapor absorption using a mixture of N_2 and H_2O at various pressures, and a coherent source of millimeter waves. The range of frequencies to be covered depends upon the availability of the sources. It would

be convenient, if possible, to proceed gradually from the presently available band toward higher frequencies, starting from the nearest H_2O lines, i.e. 180 and 320 GHz approximately.

The absorption line around 180 GHz has very recently been analyzed using a Fabry-Perot interferometer technique.[15] While this technique allows a considerable economy in cell length, nevertheless, it leaves some doubt about the amount of intermolecular interaction.[21] It seems, therefore, advisable to repeat the measurements using a standard propagation cell.

b) A careful recomputation of the atmospheric absorption for various distributions of humidity versus height using the values obtained from measurements (a), keeping in mind that the new data may improve the agreement between theory and experiment in the lower region of the millimeter band.

c) A systematic check of the actual propagation characteristics through the atmosphere by monitoring an extraterrestrial source in the range of frequencies considered in item (b). Since a satellite-borne coherent source is not presently available, the thermal radiation of the sun may be used. The sun radiation has already been observed[22] in the millimeter range, but systematic data are not available.

d) A study of propagation of waves in the above frequency range under controlled environmental conditions on a given path. This study should give an evaluation of the magnitude of the effect of the various atmospheric parameters which limit the precision of the propagation measurements performed on open links.

For example, the absorption on a path of 100,000 wavelengths in a closed room could be measured at various temperatures and humidities as a check of item (a). The same facility could also be used to study the absorption of water droplets of controlled dimensions, which simulate typical rainfalls. Analogously, one could use it to study the effect of refraction on signal scintillation in the presence of space and time controlled inhomogeneities of temperature, density or humidity along the path.

3.8 DETECTION

3.8.1 Superheterodyne and Homodyne Detection

The use of superheterodyne detection (which has been shown to be feasible and practical at a wavelength as short as 2 mm[23] at submillimeter wavelengths seems straightforward (see Chap. IX). The development of such systems is closely related to the development of point contact diodes (mixers), sources (local oscillators), IF amplifiers and other components for this range of wavelengths. Since the three basic components listed above are being developed today for operation at wavelengths less than 1 mm, there is no reason why superheterodyning could not be achieved at these wavelengths. The problem here seems to be a technological one.

The use of homodyne detection at submm wavelengths has advantages over the superheterodyne in that intermediate frequency amplifiers are not required, and frequency instability does not limit the amplifier bandwidth. The main problem here is the phase locking of the local oscillator with the detected carrier.

Since this has been recently achieved at optical frequencies, there is reason to expect it can be achieved at the longer submm wavelengths. Furthermore, the local oscillator must be the same type as the transmitter; in fact, for two-way transmission, the same oscillator can function in both receiving and transmitting.

3.8.2 Hot Carrier Diode

These diodes have the following attractive characteristics:

1) electrically and mechanically rugged
2) room temperature operation as video and heterodyne detectors
3) low noise figure
4) almost perfect square law characteristic over wide dynamic range.

All these properties point to the desirability of extending the technique of detection by the thermoelectric effect of hot electrons to higher operating frequency ranges, i.e., above 100 GHz. This is basically a materials problem. Semiconductors with lower relaxation time and lower electron scattering time are to be investigated. This diode is particularly suitable for use in mm wave mixers.

3.8.3 1000 GHz Superheterodyne Receiver

Great need for such a receiver exists today for the purpose of radiometric observation of the sun in addition to its apparent usefulness in outer space high-speed communications. The effect of atmospheric absorption at this frequency can be reduced drastically by installation of such a receiver (radiometer) on-board an aeroplane cruising at the easily attainable altitude of 30,000 feet.

It is proposed that work be done on the development of a sensitive superheterodyne receiver operating at about 1000 GHz using a crystal mixer in conjunction with a CW water vapor laser as a local oscillator. Such a development should point the way for extension of the highly sensitive superheterodyne detection scheme beyond the .3 mm wavelength region.

1000 GHz mixers with reasonable conversion loss are within the reach of the state of the art.[24] Harmonic mixing has been demonstrated at 1160 GHz and 1800 GHz by Strauch et al[25] and Woods, et al[26] respectively. The latter mixed the output of a 300 GHz carcinotron with a 150 GHz klystron using a cross guide mixer.

3.8.4 Non-Heterodyne Down Conversion

Materials such as those employed in the construction of masers could provide a system of quantum energy levels that can be utilized to down convert mm and submm incident signals to microwave frequencies where sensitive measuring equipment is available. Detailed calculations of such a detection scheme have been presented by Krumm and Haddad.[27] Several materials could be utilized in this scheme (see Table 9-VIII). Their performance, however, has not been actually evaluated. This, in addition to the possibility of using gases with appropriate energy levels, should be investigated.

3.8.5 Reflection Cavity Detector

The principle of a reflection cavity detector involves detecting the change in the reflection of microwaves from a cavity containing a cooled semiconductor slab when the latter is subjected to mm/submm radiation.[28] It is the change in the slab conductivity due to mm/submm wave absorption that gives rise to the effect. The availability of sensitive microwave equipment for reflection measurements and the simplicity of the scheme make its development attractive.

3.8.6 Mixing in Bulk Semiconductors

Mixing in bulk semiconductors utilizes the nonlinear character of photoconductivity. The practicality of this detector at mm wavelengths has been demonstrated by a number of workers. Further development of these schemes to bring them out of the laboratory realm is desirable. This is especially so in view of the recent demonstration by Hakki[29] of simultaneous generation (Gunn effect), mixing, and IF amplification in a single n-type GaAs wafer. Although the external signal was about 6 GHz, the extension of this attractive scheme to higher frequencies should be evaluated.

3.8.7 Glow Discharge Detector

Due to the attractive properties of the glow discharge detector such as ruggedness, overload capacity, simplicity, and extended frequency range (Severin[30] predicts sensitivity comparable

to crystal detectors at 2 mm), a closer look at the practical merits of this detector seems worth while.

3.9 PHASED ARRAYS

Mechanical steering of antennas is probably adequate for most applications in the millimeter and submillimeter regions since relatively small apertures will provide the high gains required.

For sophisticated radars and other similar applications, high speed scanning, perhaps on a pulse to pulse basis, may be required. Such high speed scanning can only be carried out by electronic means at this time. Electronically steered antennas are usually phased arrays. The steering is accomplished by phase shifting of the energy to individual dipoles, slots or to sub-radiators such as horns.

Present methods of phase shifting rely on ferrites. These have been used successfully up to 75 GHz; the most successful application being a slab of ferrite in the mouth of an exponential horn. Further extension of this technique will require new materials. Thus, research on materials which can provide electronic phase shifting at millimeter and submillimeter wavelengths is needed.

3.10 REFERENCES TO CHAPTER III

1. H. J. Gerritsen, E. S. Sabisky, "Paramagnetic resonance of trivalent manganese in rutile (TiO_2)," Physical Review, Vol. 132, No. 4, pp. 1507-1512, Nov. 15, 1963.

2. R. F. Rowntree, and W.S.C. Chang, "Measurement of the Properties of Laser Crystals at Submillimeter Wavelengths," Rept. 1093-11 NASA Grant NSG-74-60, Dec. 31, 1962, and W.S.C. Chang, R. F. Rowntree, "Properties of Materials for Submillimeter Masers," Proc. of the International Conf. on Quantum Electronics, Paris, 1963, pp. 677-684.

3. L. G. Lamize, "Comparison of the characteristics of Cerenkov, transition, and Bremsstrahlung radiation in the microwave region," ZW, Teckh. Fiz., Vol. 31, pp. 301-310, 1961.

4. L. W. Zelby, "Some Aspects of Transition Radiation," RCA Internal Memorandum, 1963.

5. P. E. Coleman, et al, "Megavolts Electronics, Submillimeter Wave Research," Contract No. AF 33(657)-10224, Repts., Dept. of Electrical Engineering, University of Illinois, 1961-63.

6. M. A. Allen, and G. S. Kino, "Interaction of an electron beam with a fully ionized plasma," Phys. Rev. Ltrs., Vol. 6, No. 4, pp. 163-165, Feb. 1961.

7. R. E. Skinner and J. Vollmer, "Coherent radiation by plasma oscillation," Phys. Fluids, Vol. 7, No. 1, pp. 148-150, Jan. 1964.

8. P. D. Coleman and C. Enderley,"Megavolt electronic Cerenkov coupler for the production of millimeter and submillimeter waves," J. Appl. Phys., Vol. 31, No. 9, pp. 1695-1696, Sept. 1960.

9. P. Das, P. W. Staecker, "Upper frequency limit for Gunn oscillations imposed by carrier energy-relaxation time," Electronic Letters, July 1966, Vol. 2, No. 7, p. 258.

10. R. A. Giblin, "Improvement in efficiency of a Gunn-effect oscillator with change of geometry," Electronic Letters, July, 1966, Vol. 2, No. 7, p. 236.

11. H. A. Gebbie, "Submillimeter maser amplification and continuous wave emission," Nature, 2 July 1966, p. 62.

12. W. Hughes, "Maser operations at 96 Gc with Pump at 65 Gc," Proc. of IRE, Vol. 50, No. 7, p. 1691, July 1962.

13. This scheme suggested by A. Gundjian.

14. H. Hsu, F. K. Tittel, "Optical pumping of microwave masers," Proc. of IEEE, pp. 185-189, January 1963.

15. G. Broussaud, L. Malnar, Influence Des Circuits Hyperfrequences Sur Les Performances D'un Maser a Cavites Couplees, Low Noise Electronics, Macmillan Co., New Jersey, p. 200, 1962.

16. W. Higa, E. Wiebe, "Operation of masers in closed cycle helium refrigerators," Proc. of IEEE, p. 851, May, 1963.

17. J. McEvoy, L. Moris, J. Panas, "Conduction Cooling of a Traveling Wave Maser Superconducting Magnet in a Closed Cycle Refrigerator," Paper presented at 1964 Cryogenic Engineering Conference, Phila., Pa., August 19, 1964.

18. J. B. Arthur, A. F. Gibson, and J. W. Granville, "The effect of high electric fields on the absorption of germanium," Jour. of Electronics, Ser. 1, V2, pp. 145-153, Sept. 1965.

19. M. M. Nekrasov and Yu. M. Poplavko, "Possible use of electrostriction in waveguide techniques," Radio Engineering and Electronic Physics, Vol. 9, Feb. 1964, pp. 276-278 (English ed.)

20. G. H. Jonker, H. P. J. Wijn, and P. B. Braun, "A new class of oxide ferromagnetic materials with hexagonal crystal structure," Proc. Inst. Elect. Eng., Vol. 104, part B., supplement s, pp. 249-254, 1957.

21. C. H. Townes, A. L. Shawlow, Microwave Spectroscopy, McGraw-Hill, New York, 1955.

22. V. Y. Ryadov, N. F. Furashov, G. A. Sharanov, "Measurement of atmospheric transparency to .87 mm waves," Radio Engineering and Electron Physics (translation), Vol. 9, No. 6, 1964, p. 989.

23. R. Meredith and F. L. Warner, "Superheterodyne Radiometers for Use at 70 Gc/sec and 140 Gc/sec," presented at the IRE Orlando Millimeter and Submillimeter Conf., Orlando, Fla., Jan. 1963.

24. Private communications with R. Bauer, ADTEC, Timonium, Md.

25. R. G. Strauch, R. A. Miesch, and R. E. Cupp, "Submillimeter wave harmonic mixing," IEEE Trans. on Microwave Theory and Techniques (Correspondence), Vol. MTT-13, p. 873, Nov. 1965.

26. D. R. Woods, and R. G. Strauch, "Submillimeter wave harmonic mixing," Proc. of IEEE, April, 1966.

27. C. F. Krumm and G. I. Haddad, "Millimeter and submillimeter wave quantum detectors," Proc. IEEE, Vol. 54, pp. 627-632, April 1966.

28. G. I. Haddad, Private Communication.

29. B. W. Hakki, "GaAs post-threshold microwave amplifier mixer and oscillator," Proc. IEEE (letters), Vol. 54, pp. 299-300, Feb. 1966.

30. P. J. W. Severin, "The interaction of microwaves with the cathode fall and negative glow in a glow discharge," Supplement, 1965, No. 2, p. 73, Philips Research Reports.

Chapter IV

GENERATORS, ELECTRON BEAM TYPE

4.1 INTRODUCTION

The demand for increasing efficiency of utilization of the electromagnetic spectrum has been hampered to a large extent by lack of devices producing usable amounts of power in the millimeter and submillimeter range. A number of studies of generators in this range,[1] as well as review and state-of-the-art reports and articles,[2-8] indicate that one may divide the possible devices into two broad classes: (1) classical, or wave producing devices, and (2) quantum or photon producing devices. Admittedly, this division is quite arbitrary with respect to the frequency produced, since there is a substantial overlap. The mechanism of generation, however, makes the distinction quite valid. The wave generator is based on interaction of moving charges with electromagnetic waves supported by some sort of structure; the photon generator utilizes transitions between atomic energy levels.

The extension of tubes using velocity or density modulated electron beams to higher frequencies has been accomplished primarily by advances in manufacturing techniques with respect to miniaturization rather than by development of new concepts (cf. ref. 2). This process is slow and limited because with scaling, the power output is reduced to unusable levels and the problem of coupling

the energy out of the structure becomes quite severe.* Additional problems due to frequency scaling are demonstrated by the following: To scale a typical TWT or BWO in frequency by a factor n, keeping the voltages and currents constant, the linear dimensions of the circuit must be reduced by n, so that the cross-sectional area of the beam is reduced by n^2 which increases the current density by n^2, and the volume of the device is decreased by n^3.+ The confining magnetic induction must be increased by n.

The slow rate of frequency extension by scaling demonstrates the severity of these problems, because since 1950[9] the range of wave generators has been extended by less than a factor of three. The initial success in scaling may have been responsible for the rather optimistic prediction (Fig. 1.33, p. 152, ref. 1), which has already (within three years of the estimate) fallen more than two years behind the predicted values.

This chapter will be concerned with wave generators. General characteristics of various classes of such devices will be described, their advantages and limitations discussed, and possible extensions in frequency suggested. Thus, the tenor of this report will be substantially different from a previous work on the

---

* Pierce[9] points out some of the problems connected with scaling, particularly those related to heat dissipation.

\+ The reduction of volume by n^3, the heat dissipation problems, and about 100 amp/cm^2 of emission current density required, account for the fact that the magnetron family tubes have not been developed at frequencies comparable to those of TWT's and BWO's; although 100 kW above 90 GHz,[10] and about 30 kW above 10 GHz[2] have been reported.

subject,[1] in that here we will present primarily a critical evaluation of present-day devices, and possible utilization of various phenomena. Exhaustive enumeration and cataloging of devices available either as stock items or reported in the technical literature will not be attempted. Some first-order estimates of possible frequency extension of several of the described devices and recommendations for further investigations will be made.

The emphasis has been placed on devices reported in the open literature, although some covered by other reports have also been discussed. This choice has been made primarily because most of the devices reported in the open literature have been tested, whereas those covered by other reports were very frequently in various stages of design and development. Furthermore, it was felt that with the great interest of the technological community in millimeter and submillimeter waves, it was unlikely that a successful device in this frequency range would not be immediately reported.

The following will discuss first several recently developed, or proposed, tubes; second, a consideration of some phenomena which may be suitable for development as tubes; and finally, a brief discussion of some aspects of frequency limitation.

4.2 DEVICE CHARACTERISTICS

The last 15 years witnessed a proliferation of RF amplifiers and generators with various exotic prefixes to "tron," a number of

which are listed in Table 4.I. All of these devices utilize the interaction between charged particles, generally electrons, and a structure supporting electromagnetic waves. In the first part of the table, klystron-like devices using one or a few cavities have been listed. These progress through devices using combinations of cavities and distributed interaction circuits to distributed interaction devices. Several devices at the end of the table represent "coupling devices" based on Cerenkov type interaction; the last two, the tornadotron and EAL, which are different in principle from the others, have not been tested.

The devices differ from each other primarily in detail rather than in general characteristics. (This may be borne out by the fact that the capabilities of such devices differ only to the extent of manufacturing ingenuity applied to specific variations). The characteristics of any of these represent some combination of the following:

Table 4.I Classes of Tubes:

I Cavity Interaction
II Distributed Interaction
III Miscellaneous Interaction

I	Fields	Energy Exchange	Beam Path	Wave	RF Circuit
Klystron *	P	O	R	S	RE
Reflex Klystron*	P	O	K	S	RE
Mixed Field Reflex Klystron*	P	O	R	S	RE
Retarded Field Oscillator*	P	O	K	S	RE
Barkhausen-Kurz Oscillator*	P	O	K	S	RE
Multi-Cavity Klystron*	P	O	R	S	RE
Floating Drift Tube Klystron*	P	O	R	S	RE
Monotron*	P	O	R	S	RE
Hybrid Klystron*	P	O	R	S+T	SL
Anti-Klystron*	P	O	K	S	RE
Laddertron*	P	O	R	T	SL
Reflectron	P	O	R	S	SL
Strophotron	C	O	R	S	RE
O-BWO*	P	O	R	T	SL
TWT*	P	O	R	T	SL
II					
Microtron*	C	O	K	T	SL
Rotatron*	P	O	K	S	RA
Spiratron*	P	O	R	T	SL
Helitron*	P	O	R	T	FA
Amplitron*	C	M	K	T	SL
Platinotron*	C	M	K	T	SL
Stabilitron*	C	M	K	T	SL
M-BWO*	C	M	K/R	T	SL
Torotron (Axiatron)*	C	M	R	T	SL
Magnetron*	C	M	K	S	RE
Waveguide Magnetron	C	M	K	S	RE
Mitron*	C	M	K	T	SL

continued

Table 4.I Classes of Tubes (cont'd)

III	Fields	Energy Exchange	Beam Path	Wave	RF Circuit	Freq. (GHz)	Power Output (Watts)
Ubitron	C	O	K	T	FA	54	150 K
Bermutron	P	O	K/R	S+T	FA,RE	34	2
Dematron	C	M	K	T	SL	9.3	400 K ED-9
Cycloidotron	C	M	K	T	FA	N O	D A T A
Teaser	C	O-M	K	T	FA	300	10 m
Easitron	P	O	R	T	SL,RE	N O	D A T A
Dromotron	C	M	K	S	RE	N O	D A T A
Crestatron	P	O	R	T	SL	N O	D A T A
Twystron	P	O	R	T+S	SL,RE	N O	D A T A
Phreatron	P	O	R	T	SL	93	25
Harmodotron*	P	O	R	S	RE		
Undulator*	C	M	K	T	FA		
X Tornadotron*	C	O	K	T	RE		
X EAL	C	O	R/K	T	RA	N O	D A T A

P - Parallel E and B Fields

C - Crossed E and B Fields

O - Kinetic Energy Exchange

M - Potential Energy Exchange

R - Rectilinear

K - Curved

T - Traveling

F - Forward

B - Backward

S - Standing

FA - Fast

SL - Slow

RE - Resonant

* Discussed in reference 1.

X No experimental model available.

1. With respect to the beam and/or structure:

   a) periodic or not

   b) re-entrant or not

   c) straight or curved

2. With respect to the structure:

   a) slow or fast wave

   b) traveling or standing wave

   c) forward or backward wave.

Whatever the device, however, either a periodic beam with a "smooth" structure, or a "smooth" beam with a periodic structure, is required for RF generation in one form or another.

It has been attempted to separate various classes of the devices in the arrangement, although some overlap was unavoidable. The first part of Table 4.I represents a progression from "resonant" generators (klystron) to "distributed interaction" generators (TWT). The devices between the monotron and strophotron, however, represent hybrid devices in that they utilize both resonant and distributed circuits. The second set represents various types of crossed field devices closely related to the magnetron. Devices representing other concepts have been listed in the third part. These are tubes representing particular variations of the types previously mentioned, and employing fast wave circuits and periodic beams, or such phenomena as Bremsstrahlung, Cerenkov and cyclotron radiation, or harmonic generation.

Some other aspects of these devices, such as confined or Brillouin flow, magnetostatic or electrostatic beam focusing, distributed cathode, etc., have not been included in this classification.

All of the wave generating devices utilize some combination of the above characteristics. Consequently, the upper frequency limit of these devices will be that determined by those constructional and electronic features which can be adapted to highest frequencies. Since in the last 15 years the, apparently, best combination resulted in extending the spectrum of such devices from about 300 GHz[9] only by a factor of three,[11] one might safely assume that 1 THz represents a reasonable limit for this class. This will be discussed more extensively later, particularly with respect to some of the work by Elliott[12] and Senitzky[13] on limitations of electron beam devices. The implications of this work were mentioned[1] but with inadequate emphasis on its consequences, i.e., its effect on the direction of subsequent research.

To avoid duplication, with few possible exceptions, devices covered by reference 1 will not be discussed.

4.2.1 Tornadotron

The tornadotron[14] was proposed in 1958 as a scheme for millimeter wave production. The device essentially consists of a cylindrical cavity whose end-plates are at lower potentials than the cylinder in order to contain an electron cloud within the

cavity. Because of the superposed magnetic induction parallel to the axis of the cavity, and a pump RF field, the electron cloud executes two circular motions: a rotation about its axis, and a spiraling outward of its axis about the axis of the cavity. Radiation is generated by increasing the magnetic induction which forces the cloud to spiral inward. In this radiation phase, the power radiated by one electron is

$$P_e = \frac{e^2 \omega_c^4 r^2}{6\pi \epsilon_o} = \frac{e^2 \omega_c^2 v^2}{6\pi \epsilon_o c^3}$$

Calculations indicated a power output of 160 W (1.6×10^{-4} joules) at 1.1 mm with the induction pulsed from 0.1 to 10 Tesla in 1 μsec; and 16 kW (0.016 joules) at 0.11 mm with induction pulse from 1 to 100 Tesla in 1 μsec. These figures seem to indicate that higher power can be obtained at shorter wavelengths. This is only due to higher pump energy, current, voltage, and electron density used in the latter case.

The fact that to date no successful attempt has been made to generate radiation using the tornadotron principle speaks against it. It may also be noted that some of the assumptions used in calculation of the performance data are not quite valid. First, multiplication of the coherent power output due to one electron by the square of the number of electrons in the beam leads to grossly inflated values because of the shielding effect; secondly,

the finite size of the cloud will contribute to the reduction of the radiated power because of phase interference; finally, the calculations were based on the assumption of adiabatic changes, i.e.,assuming that the ratio of kinetic energy, associated with transverse velocity, to the induction is an adiabatic invariant. Since the condition $\dot{B}/B^2 << 1$ is not necessarily satisfied, the assumption is not necessarily valid.* Further, the requirements for high voltages and high magnetic induction indicate that this may not be a suitable scheme for millimeter wave generation.

4.2.2 Electromagnetic Amplifying Lens (EAL)

The EAL[15] is another of the many devices belonging to the magnetron family, but, unlike many others, it has not been built and tested.[16] The suggested device utilizes an external cathode and an axial magnetic field producing a scalloped, rotating, hollow electron beam. The RF structure comprises a number of waveguides as shown in Fig. 4.1. It can be seen that the structure resembles an inverted magnetron with an external cathode and internal anode. Its mode of operation differs from that of a magnetron, or amplitron, in that it is above cutoff (wave propagates) in the axial direction. As a result, isolation between input and output can be obtained, and the device acts essentially as an amplifier.

---

* Spitzer, ("Physics of Fully Ionized Gases," 2nd Ed., Interscience Publishers, N. Y., 1962, p. 11) points out that the magnetic moment--if redefined-- is constant to all orders of $\dot{B}/B^2$ when investigated in terms of asymptotic expansion; but it is not a constant rigorously.

The EAL is fed by a wave from an open ended circular cylindrical waveguide in the TE_{01} mode, impinging on one end of the tube. Before the wave reaches the interaction space, it is processed in such a manner that a pi-mode potential distribution in the circumferential direction is established on the tips of the vanes. The vanes are formed by cutting down the full-width waveguide to half-width. Between the output end of the interaction region and the output face of the tube, the 180-degree phase relationship between adjacent channels is converted back to a zero-degree phase relationship at the output face. The calculated gain for the tube is about 25 db for $\theta = 2\beta\ell > 45$. Here, $\beta - 2\pi/\lambda$ is the axial propagation constant, and ℓ = the length of interaction. Since the RF and beam currents enter the calculation of the gain, the expected results are not so optimistic as indicated.

As in the case of the tornadotron, a device incorporating the EAL principle has not been tested. The rather stringent requirements on the beam size and its axial and azimuthal motion, as well as scalloping, make it an extremely unlikely candidate for a generator at any frequency; e.g., in the lower frequency range, say up to about 100 GHz, the beam diameter would have to be of the order of centimeters; at higher frequencies the waveguide dimensions would have to be of the order of tenths of millimeters for beam diameters below a centimeter. At this stage, therefore, the EAL principle does not seem to be a strong contender as a wave generator.

4.2.3 Dematron

The dematron[17] (see Fig. 4.2) belongs to the magnetron family, and represents a distributed emission variant of the amplitron. The beam is not re-entrant and it interacts with a forward wave. The fundamental difference between the dematron and other devices in its class is that the dematron uses a velocity taper, either for the wave or the beam. The reason for the use of the taper is to compensate for the decrease of the effective dc electric field strength as a result of local increase of space charge due to bunching. When bunching occurs, the beam slows down, falls out of synchronism, and absorbs energy from the wave. Consequently, in order to maintain synchronism, and useful interaction over the length of the device, either the wave must be slowed by tapering the slow-wave structure, or the beam velocity must be maintained by increasing the electric field or decreasing the magnetic induction. When the circuit velocity is kept constant, the interaction is of the same type as in magnetrons. Consequently, the operation of the dematron with a beam velocity taper can be analyzed in terms of a series of connected equivalent magnetrons for which the interaction impedance is kept constant.

The fundamental relation, using the Hartree magnetron starting equation, is

$$V = a \lambda_s fB - \frac{(\lambda_s f)^2}{2(e/m)}$$

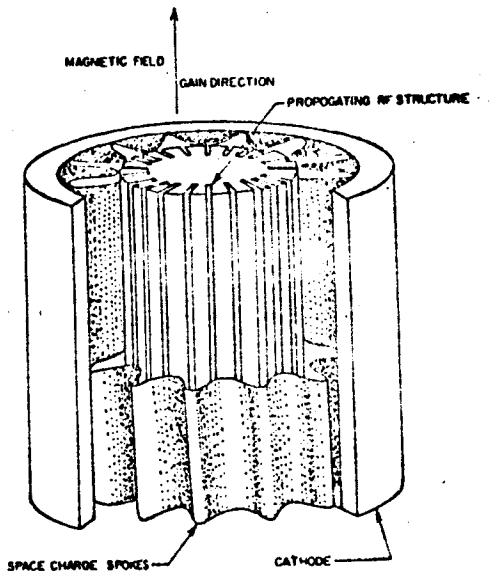

Fig. 4.1 Diagrammatic Sketch of EAL
(Taken from Ref. 15)

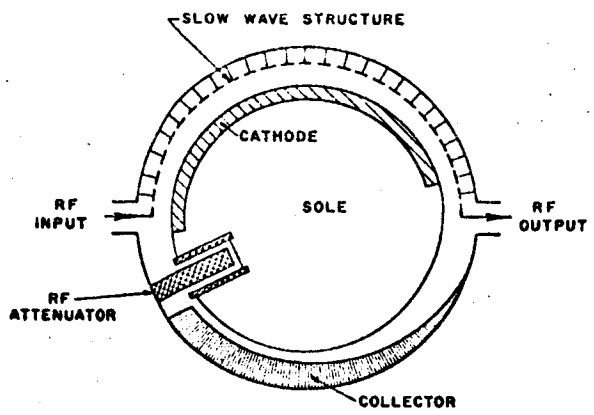

Fig. 4.2 Diagrammatic Sketch of DEMATRON
(Taken from Ref. 17)

where $\underline{a}$ is anode to cathode spacing, and λ_s is the spatial harmonic wavelength. For a constant phase velocity circuit, $\lambda_s f$ is constant. The beam velocity can be maintained by changing V, i.e. either $\underline{a}$, B, or both.

The experiments on this tube were performed in the X-band, with dc anode voltages less than 30 kV and corresponding B fields. To consider the requirements at about 1 THz, consider a circuit with phase velocity of about 0.1 c, i.e., $\lambda_s \cong 3 \times 10^{-5}$ m/sec. With $\underline{a} = (1/3) \times 10^{-2}$ m, and B = 1T, V is about 100 kV. Now

$$\frac{1}{\lambda_s} = \frac{1}{\lambda_o} + \frac{n}{P}$$

where P is the period of the structure. With $P \cong 10^{-4}$m, operation at the third spatial harmonic would be required, and with $P \cong 3 \times 10^{-4}$m, operation at the ninth harmonic would be required. On this basis, the dematron principle seems suitable for extension to higher frequencies. The numbers used above were extreme, and it is not suggested that this device could be extended to 1 THz, since other considerations (such as dissipation, rate of decay at higher spatial harmonics with distance from the structure, etc.) were not included in the calculations. The device seems to hold greater promise than conventional magnetrons and amplitrons for extending the operating region to higher frequencies because of the extended

synchronism between the beam and wave. Since the dematron is essentially an amplifier, modifications (possibly a re-entrant circuit) would be needed to convert it to a generator.

4.2.4 Ubitron

The ubitron[18,19] is a traveling wave tube in which a periodic, undulating beam interacts with a TE_{01} mode in a waveguide. The average axial beam velocity must have such a value that when the beam moves axially a distance P, the wave moves a distance $P + \lambda_g$, where λ_g is the guide wavelength, and P is the period of the transverse velocity. With this slip between the beam and the waves, the most favorably phased electron always sees a decelerating field.

The periodicity of the transverse velocity is due to a periodic magnetic field. When the waveguide supports a TE_{01} mode, as shown in Fig. 4.3, the beam can be made to undulate in the x-z plane, due to the magnetic field in the y-z plane, and to interact with the strongest E-field. Bunching of the electrons is due to the effects of the RF and magnetic fields. The average axial velocity of the beam, combined with the periodicity of the magnetic field, must be such that a net energy exchange from the beam to the wave takes place. This occurs when

$$f = \frac{v_o v_p}{v_p - v_o} \left(\frac{2n+1}{2P}\right)$$

where v_o, v_p are the average beam, and RF phase velocities, respectively; and P is the period of the magnetic field (the same as the period of transverse velocity).

Assuming a 70 kV beam, and $v_p \cong 1.3$ c, with $P \cong 10^{-3}$ m, $f \cong (2n+1) \times 10^{11}$. This might indicate that the ubitron may well work in the 100 GHz, and higher region. However, the requirements of high beam energy (dc voltages), high magnetic field and its periodicity detract from the apparently attractive picture. Although the tube does have an advantage of an unloaded waveguide (with its relative ease of manufacture and heat dissipation), and is capable of producing high power, the highest frequency thus far obtained is 64 GHz, with a B-field of 1 T. It seems, therefore, that the upper operating frequency is limited by the beam periodicity, and high beam energy requirements. At 3 GHz, about 100 kV accelerating voltage is required, and at 30 GHz, about 1 MV. This high beam energy requirement at high frequencies makes the device unsuitable for millimeter wave generation. Extension of this principle to loaded waveguides has been suggested. This may result in lower beam energy requirement, and higher frequency output, as a result of the combination of beam and circuit periodicity. On the other hand, introduction of a periodic circuit may complicate the manufacturing process due to the tolerance requirements. The use of devices like the rebatron[20] for pre-bunching of the beam does not seem feasible because the very high beam energies would require excessive B-field strengths and periodicity to produce beam undulation.

4.2.5 Cycloidotron

The cycloidotron,[21] like the ubitron, belongs to that type of electron beam tube which utilizes a fast wave circuit and a periodic beam. It is claimed that this method is more suitable for extending the frequency range of electron beam devices. The problem in these tubes is the production of beams with suitable periodicities. In order to obtain amplification, bunching of the beam is required. This is accomplished by the interaction of the beam, in crossed dc E_o and B_o fields, with the TE_{02} mode in a rectangular waveguide.

The beam enters the waveguide and executes cycloidal motion, due to E_0 and B_0, in the plane in which the ac electric field is zero, and the ac magnetic field is maximum. The latter exerts a force on the electrons moving in a direction transverse to it, and produces an ac motion as in the plane indicated in Fig. 4.4. This ac motion, superposed on the cycloidal motion due to the dc fields, leads to transfer of power to the RF field when the wave is in synchronism with one of the beam harmonics. Calculations indicate that at 1 mm wavelength, B_o of the order of 10 T, and $E_o \sim 10^6$ Volts/cm are required, with a beam drift velocity of 0.02 c.

This tube is subject to criticism similar to that for the ubitron, because for high frequencies the intensity requirements for the induction and electric field intensities are excessive,

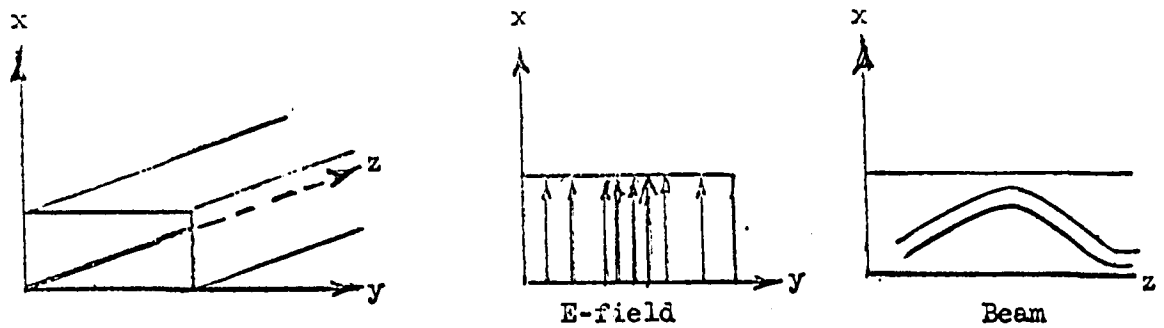

Figure 4.3 Diagram of a Ubitron (from Ref. 18)

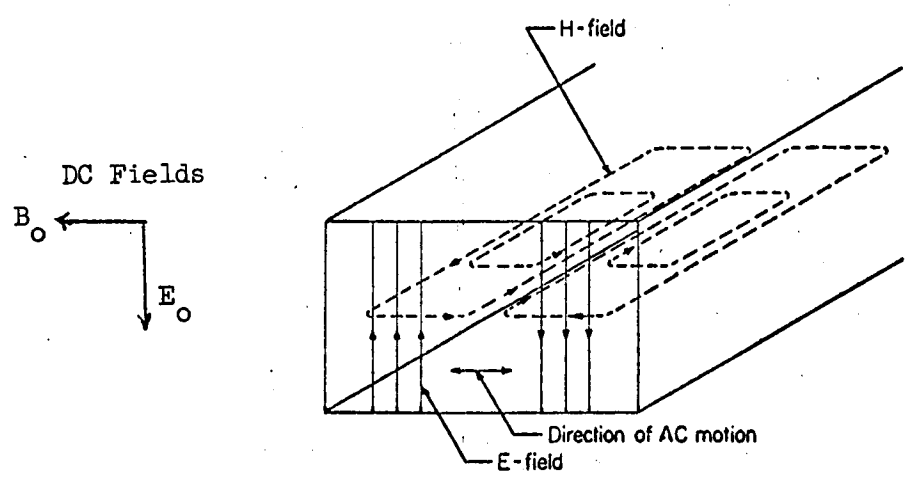

Figure 4.4 Diagram of a Cycloidotron with Field Lines for TE_{02} Mode in Rectangular Waveguide

although beam energy requirements are reasonable. Furthermore, no experimental data are available to indicate the feasibility of this tube.

4.2.6 Laddertron

The laddertron[22] is a variation of a multigap klystron. It comprises, basically, two cavities adjacent to a ribbon electron beam, as shown in Fig. 4.5. Sides of the cavity adjacent to the beam are slotted and constitute a slow wave structure. The "output" cavity is fitted with a microwave window; the other, with a tuning plunger. The size and spacing of the slots depend on the desired mode of operation. In the 0-type Laddertron, the slots are all of the same size, and in the dominant mode the fields are the same in each slot, with maximum in the center of each slot. In the pi-mode the slots alternate in length, and in the dominant mode the fields are out of phase in adjacent slots. A ribbon beam passing between the slots excites the cavity. The wave thus excited modulates the beam, with the structure and cavity providing the feedback path. In both modes, the electric field parallel to the beam is maximum at the beam, but the pi-mode device has a broader electronic tuning range. The operating frequency for either mode lies in the region

$$\frac{1}{4a^2} < \frac{f^2}{c^2} < \frac{1}{4}\left(\frac{1}{a^2} + \frac{1}{h^2}\right)$$

and is governed by the size of the cavity. The power output at 50 GHz is of the order of watts (less than 10). The cavity size is 5.2×10^{-3} m by 3.4×10^{-3} m, with 10 slots. Operation up to about 150 GHz is expected, with cavity dimensions scaled linearly. Thus, at 300 GHz, the cavity size would be about 10^{-3} m by 0.5×10^{-3}m, and at 1 THz about 0.3×10^{-3}m by 0.15×10^{-3}m. The power supply demands for this tube are modest: accelerating voltages less than 3 kV, and beam current densities less than 200×10^{3} A/m^2 (20 A/cm^2).

This feature of low power requirement would make the laddertron attractive. The cavity size in the millimeter and submillimeter range could be made. Heat dissipation problems, however, and attenuation at such frequencies may be excessive. On the basis of these considerations, it appears that the laddertron operation might be extended somewhat above 150 GHz by technological improvements. The principle, however, does not appear too attractive for extension to higher frequencies.

4.2.7 Bermutron

The bermutron[23] is a modified version of the rotatron.[1] The device can be operated either with a resonant, or non-resonant circuit. The beam couples to the circuit wave through slots through which the beam is swept periodically, as shown in Fig. 4.6.

As in other types of electronic tubes, synchronism between the beam and the circuit wave must be established. The synchronism factor is of the form $(\sin x)/x$, where $x = v_e/v_p - 1$; v_e is the

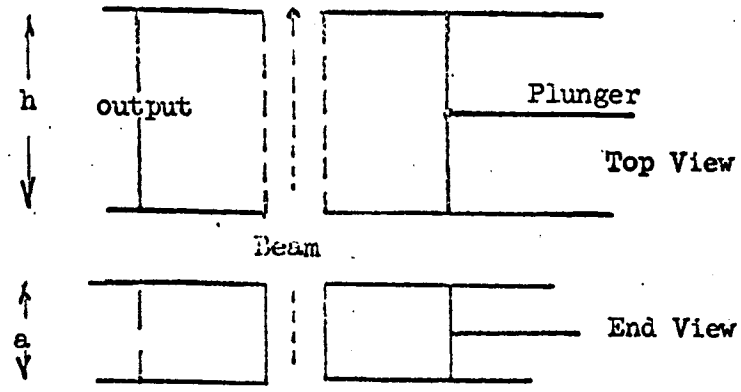

Figure 4.5 Diagram of a Laddertron (from Ref. 22)

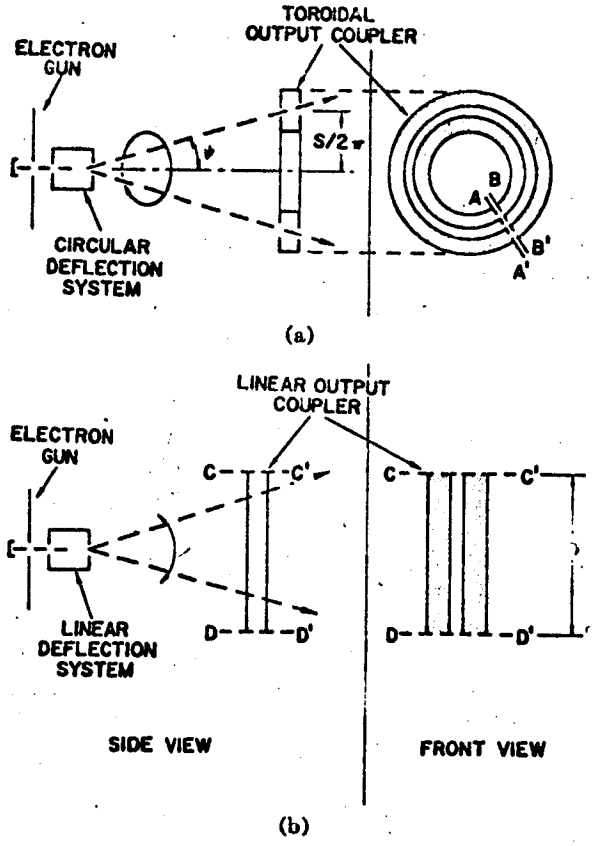

Figure 4.6 Sweeping electron beam harmonic multipliers. (a) Circular sweep. (b) Linear sweep. In actual practice, the slots would be screened in order to contain the fields (from Ref. 23)

velocity with which the beam sweeps along the slot, and v_p, the phase velocity of the wave. The power output is reduced by the synchronism factor, as well as the transit time factor, analogous to that in klystrons. Another important aspect of the design is the electron beam diameter which should be less than one-half guide wavelength of the desired harmonic at the output to prevent destructive interference. With a ridge deflection cavity, with the input at f = 8.5 GHz, an output of 2W was obtained at 34 GHz. Deflection power was 3.1 kW and beam current 150 mA.

With reduction of the deflection power requirement, by selection of a more suitable cavity, the principle on which this device is based might be applied in a high frequency generator. A multiplication factor of 4 is apparently quite readily obtainable, and sources in the 300 GHz range are available as well.

4.2.8 Miscellaneous

In addition to the devices reported above, which incorporate fairly standard variations of the basic principles of electron beam-wave interactions, there are a few others based either on wave polarization, or changes in circuit structure. These will be discussed briefly below.

4.2.8.1 Synchronous-Wave Amplifier

The schematic diagram of the synchronous-wave amplifier[24] is shown in Fig. 4.7. The basic difference between this device and an extended interaction klystron is that here the degree of coupling

is optimized by the relative polarization between the input and output. As a consequence of this, the structure can be made long enough to yield almost any desired gain. Theoretical estimates lead to gain values of the order of 30 dB for structures five wavelengths long. The experimental device at 3 GHz had rods 0.318 cm in diameter with a period of 1.080 cm. Scaling these dimensions by a factor of 30 seems feasible (e.g. 0.001 cm diameter and 0.036 cm period) so that this device might be useful near the 100 GHz band. With these dimensions, however, the heat dissipation problem may be very severe. The device exhibits a tendency toward oscillations which may be utilized for wave generation near those frequencies.

4.2.8.2 Ring-Plane Traveling-Wave Amplifier

The ring-plane traveling-wave amplifier[25] is a traveling-wave device utilizing a two-plane ring circuit shown in Fig. 4.8. The tube is capable of producing high power output (0.1 to 50 kW in the frequency range 33 to 36 GHz) with reasonable operating parameters: 30 kV, 1A electron beam. Unfortunately, the upper cutoff frequency for this device occurs approximately when the ring circumference equals one free-space wavelength. Considering a 0.5 mm diameter beam, and 0.7 mm ID of the ring, $\lambda \cong 4.3$ mm, the upper frequency limit would be about 80 GHz. With a four-plane structure, the upper frequency cutoff could possibly be doubled.

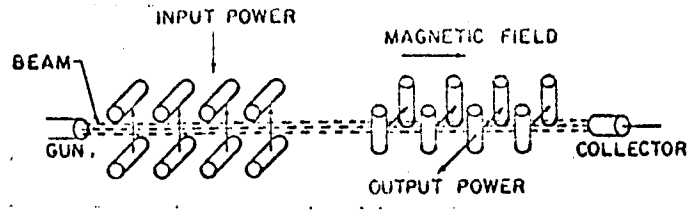

Figure 4.7 Schematic representation of the synchronous-wave amplifier; the structures of rods shown indicate periodic resonant circuits that support a transverse electric field with the polarization indicated by the arrows. (from Ref. 24).

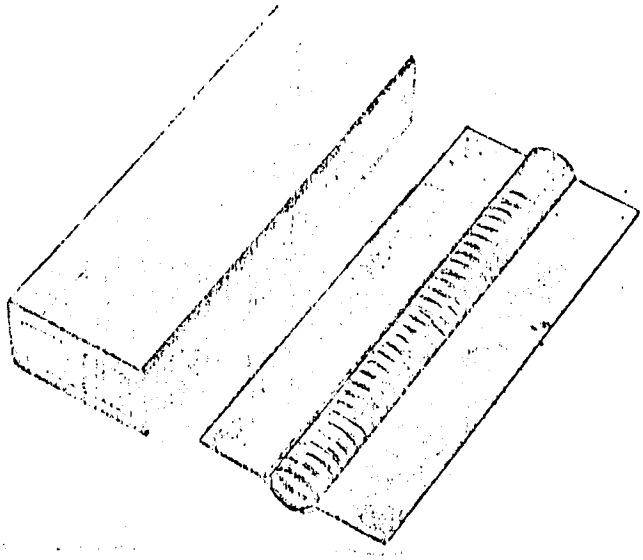

Figure 4.8 Diagram of a Ring-Plane Traveling-Wave Amplifier (from Ref. 25)

4.2.8.3 Waveguide-Magnetron

The waveguide magnetron[26] is another of the devices utilizing crossed fields for the production of microwaves. Operations above 100 GHz, with power outputs at about 5 W, have been reported. Dimensions of the anode are in fractions of millimeters, and the induction required is in Teslas, so that it does not seem likely that this would be a practical device at much higher frequencies.*

4.2.8.4 Teaser (Bott's Bottle)

The teaser[27-28] utilizes the helical motion of an electron beam (about 4 mm in diameter) due to magnetic induction to induce oscillations in a circular cylindrical cavity. This is done as follows: a "corkscrew" shaped magnetic induction induces helical motion of the electron beam. The radius of the beam is then constructed by the increasing intensity of the magnetic induction. This, in turn increases the transverse energy of the electrons by the same amount, assuming that the process is adiabatic (since in this case, the magnetic moment $\vec{m} = \omega_T \vec{B}/B^2$ is constant; ω_T is the transverse energy). The beam, then, enters a suitable circuit and generates a signal through cyclotron radiation.

About 2W of generated power at the fundamental (between 75-150 GHz) and more than 10 W at the second harmonic (300 GHz) were reported for a 20 kV beam in a field of 5T. Predictions for

* It is difficult to assess the future of this device on the basis of the reported data.

extending the frequency of operation of this device are optimistic. However, the requirements of high magnetic induction, and problems associated with coupling out of the generated radiation (see also Conclusions and Recommendations) mitigate this optimism substantially.

4.3 DISCUSSION

Electron transit time, which led to undesirable effects in some vacuum tubes (triodes, pentodes, etc.), has been utilized to advantage in another class of tubes: klystrons, magnetrons, and traveling wave tubes. This exploitation of the transit time for velocity of density modulation of the electron beam led to the development of relatively efficient oscillators at frequencies several orders of magnitude higher than was possible with the older type tubes. The general characteristics of such tubes, based on the interaction of an electron beam with an electromagnetic wave supported by a resonant or traveling wave structure, can be discussed in terms of coupling schemes utilizing the uncoupled dispersion diagrams of the two systems. Figure 4.9-A shows a dispersion diagram of a typical slow wave structure and of Hahn-Ramo lines of two electron beams with two different average velocities, $v_1 > v_2$.

The characteristics of the coupled system can be easily deduced on the basis of kinematics of waves,[29-30] and the resulting coupled system is shown in Fig. 4.9-B. The intersection of the characteristics of the beam-wave and the circuit wave represents the point of synchronism.

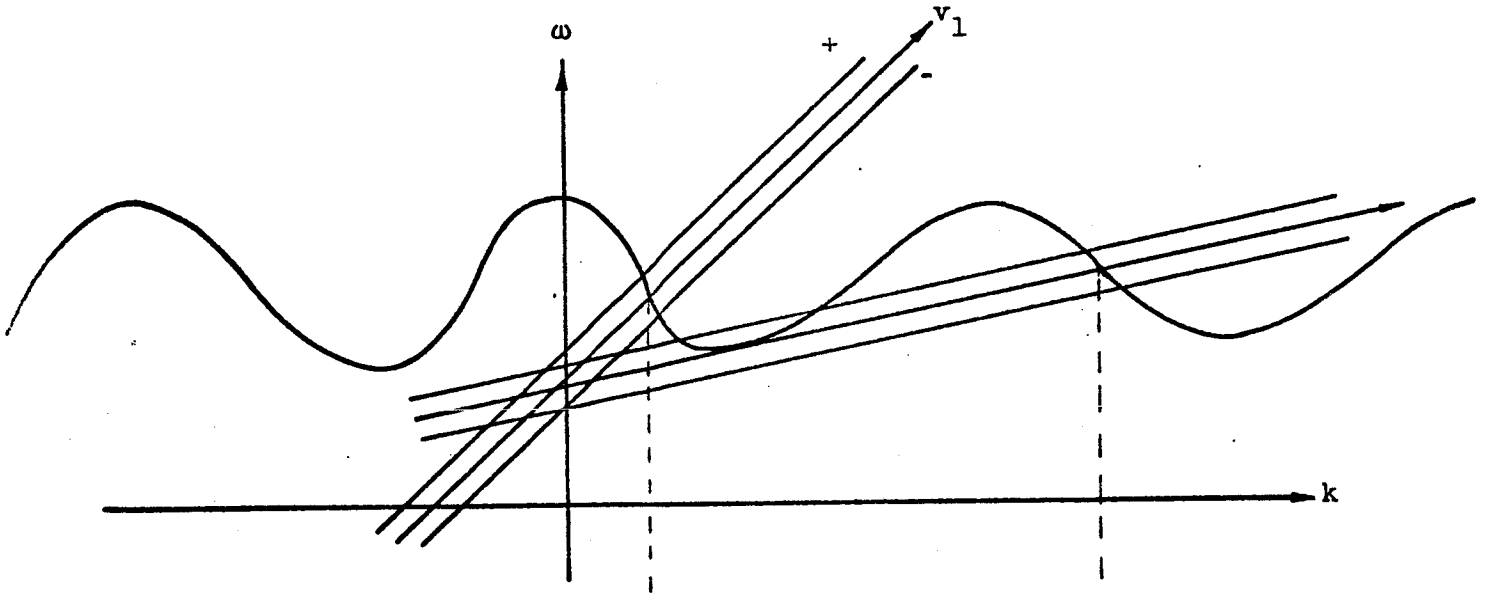

Fig. 4.9-A Dispersion Diagram of a Typical Slow Wave Structure

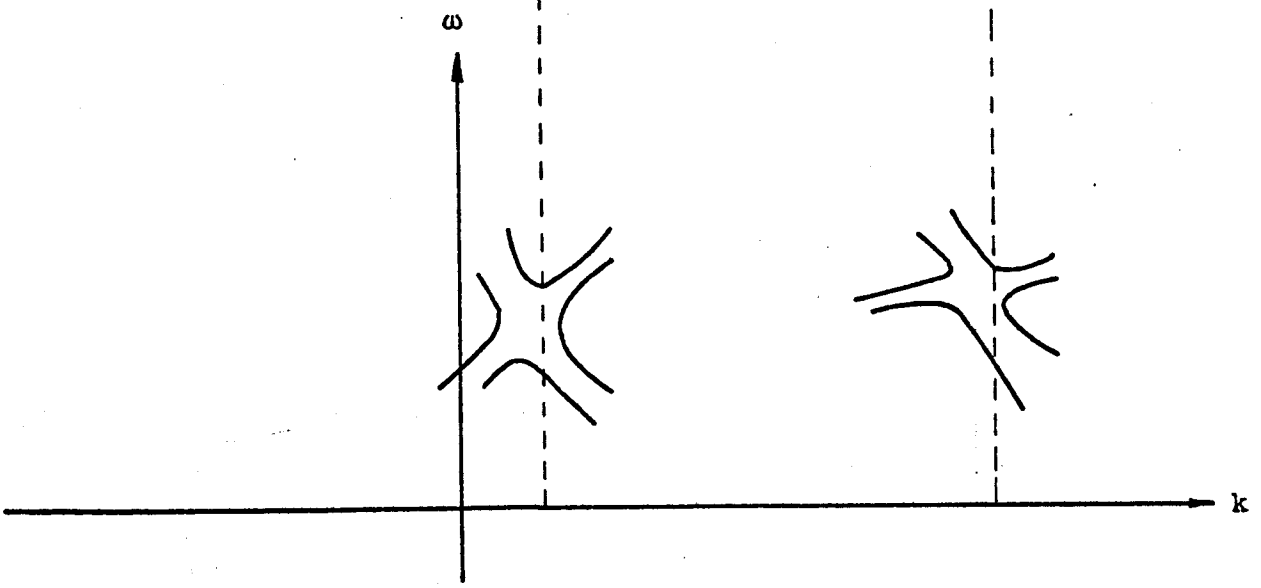

Fig. 4.9-B Dispersion Diagram of a Coupled System

Strong interaction obtains near or at synchronism between the beam and the wave. Thus, in order that the device operate at high frequencies in low order modes, high beam energies are required (e.g. near v_1); at the same high frequencies low beam energies are required (e.g. near v_2) if interaction with spatial harmonics is satisfactory. At high order spatial harmonics, however, the electromagnetic field decays extremely rapidly from the supporting structure reducing the strength of the interaction. To maintain the same interaction strength, therefore, the electron beam must be brought closer to the structure. This creates mechanical tolerance, secondary electron emission, and heat dissipation problems.

It has been pointed out before that scaling has its limitations. This is borne out by the fact that, to date, no successful operation above 800 GHz has been reported even though predictions[31] called for 0.01 W output at 3 THz by 1963. Senitzky[13] points out the existence of noise on electron beams due to quantum mechanical effects. The minimum of this noise energy is comparable to that of a 3 THz signal. Further, Elliot[12] has derived a criterion for the limit of the operating point of oscillators requiring resonant structures,

$$I_o^2 \geq \frac{2\,\omega^2\,\epsilon}{Q^2\bar{V}}\,\bar{U}$$

where I_o is the "average" ac beam current density; Q, the quality factor of the structure; $\overline{V}$, the volume of the region of beam-wave interaction; and $\overline{U}$, the average signal energy stored in the resonant field. Unfortunately, this criterion does not seem realistic when Figs. 2 to 4 of reference 12 are considered. The current densities at the demanded frequencies are readily obtainable, and yet, klystron operation has not substantially exceeded 100 GHz.

In view of this, it may well be that for operation near and above 1 THz, it will be necessary to resort to "structureless" devices.[32] The tenor of a recent paper,[33] which describes only a very limited group of devices, certainly does not lead to an optimistic conclusion with respect to millimeter and submillimeter wave generation in spite of the high power tubes near 100 GHz; nor are the limitations of various devices indicated there.

In the frequency range below 1 THz, it seems that modifications of the bermutron, by selecting a more suitable scheme for beam deflection, may lead to a suitable wave generator. Carcinotrons near this frequency range have been reported,[11] but extension of their range is contingent upon the increase of gun perveances and beam area convergence ratios because of the effect of the beam current on the maximum frequency.[34]

In the frequency range near 1 THz, it would seem desirable to depart from manufactured slow wave structures because of the high precision, and close tolerance requirements coupled with small

sizes.[2] This point of view has been reflected in attempts to utilize Cerenkov couplers for microwave generation. A reasonably complete set of data has been obtained by Coleman's group[35] at the University of Illinois for isotropic and anisotropic Cerenkov couplers of a form proposed by Getting. The group utilized nearly delta function type bunches of electrons with velocities about 0.9 c. They concluded that the interaction resistance of isotropic couplers is too low to make this type of system useful for RF generation.

Work of a similar nature has been continuing at RCA[36] where dc beam acceleration techniques have been used, as well as couplers of various shapes. Reasonably high interaction resistances have been measured (in excess of 1 kΩ). Because of experimental difficulties, however, these require further verification. The Cerenkov effect has been also used in the development of the phreatron.[37] In this case, it was used for the purpose of density modulation of the beam; i.e.,the coupler was used as a slow-wave structure for high energy beams. The Cerenkov effect was also considered by Durney and Grow,[38] as well as by many others. Thus far, however, no practical device has been produced.

The advantage in utilizing the Cerenkov effect lies in the fact that the periodicity of the structure is essentially that of the lattice of the medium and that a periodic beam is not required. It is possible that utilization of a periodic dielectric structure

may increase the interaction resistance over that of a smooth coupler.

A number of other schemes have been suggested for the production of millimeter and submillimeter waves. Among those is the cyclotron frequency multiplier,[39] in which one takes advantage of the beam harmonics in a static magnetic induction. With the input at 10 GHz, an output of 28 W at 100 GHz has been calculated. Another scheme for the use of cyclotron waves has also been proposed[40] in which the output frequency would consist of the sum of the beam wave and a harmonic of the circuit wave, i.e., $f_b + nf_c$, not unlike the multiplication scheme using the Doppler effect.[41,42] In the Doppler case the high output frequency is obtained by the Doppler shift resulting from reflections of the input wave from relativistic electron bunches. Specifically, $f_{out} = f_1 + nf_o$, where f_1 is the input frequency, and f_o is the fundamental rebatron frequency.[20] Neither of the last two schemes has been reduced to practice.

Still other schemes, utilizing the principle of cyclotron radiation, have been under development, e.g. the orbitron amplifier and the cyclotron-synchronous wave amplifier,[43] as well as the "teaser."[28] The former two have been described primarily in DDC reports, and not enough data are available to assess the possibilities offered by them. The "teaser" appears promising on the basis of the data reported, but even in this case, much more information

would be desirable. Other schemes falling into the category of "structureless" devices have also been suggested. Among these are Bremsstrahlung,[44] excitation of plasma oscillations,[45] and harmonic generation in plasmas.[46] The disadvantage of these schemes appears to lie in the low levels of detected radiation, primarily due to the low coupling efficiency (see Conclusions and Recommendations).

4.4 CONCLUSIONS

The literature review indicates that scaling of many types of devices for millimeter and submillimeter wave generation has just reached its limit. This is in spite of the very high current densities reported,[47] (about 800 A/cm^2) and large area convergence ratios[48] (1300:1).

The only successfully operating devices are those using either a periodic or resonant circuit, or a periodic beam. Substantial amounts of power are available up to 100 GHz; devices in higher frequency ranges, particularly above 300 GHz, are still in experimental stages although some outputs at 780 GHz were observed.

The periodic circuits utilize variations of the helix, meander line, and Karp structures. Periodic beams use static fields (e.g. ubitron) or a combination of static and RF fields

(e.g. cycloidotron, orbitron),[43] with the M-type devices having potentially higher efficiencies.*[49]

The problem of obtaining high interaction impedance in the millimeter and submillimeter range has not been solved, nor has the problem of efficient coupling out of the generated radiation, although this is still a matter of controversy. The two problems are connected and remain the most important.[32] Unfortunately, study of these two problems would have no means of guaranteeing palpable results within a given research period; consequently, prospects for support are negligible. It seems that new coupling schemes will be developed only haphazardly as they happen to occur in conjunction with other studies. This approach is favored by a large number of people concerned with these problems. It is quite evident that the support of "concrete" projects like scaling in size and available tubes, or utilizing variations of known schemes for high frequency generation, has not led to many efficient devices in the desired frequency range. On the other hand, the development of an efficient coupling scheme would open the doors for the utilization of such "structureless" phenomena as Cerenkov radiation, transition radiation, cyclotron radiation, Bremsstrahlung beam plasma interaction, and others.

---

* Briefly this is due to the fact that in M-type devices synchronism between the electron beam and wave can theoretically be maintained longer than in O-type devices.

These phenomena are very closely related and many can be explained in terms of Cerenkov radiation, whether the electron beam path is rectilinear or curved.[50-51] Under certain dynamic and geometric conditions, however, such systems either cease radiating completely,[52,54] or the amount of radiated power is substantially diminished. This again points up the need for coupling schemes more efficient than those presently in use.

4.5 RECOMMENDATIONS

Recommendations can be split into two categories: immediate and long range.

4.5.1 Short-term Recommendations

To make short-term recommendations, it is convenient to refer to Table 4.1. Of the devices listed in parts I and II, most have been well-established, and if they have not reached their upper frequency limit, they certainly appear to have approached it. Further advances in this category can be made only by technological improvements with respect to machining, cooling, spurious and high-field emission, and production of higher current density beams.

The devices listed in part III of the table, (all of the distributed interaction variety) are relatively new and, with the exception of the ubitron, not too well developed. Some of those, however, utilize some novel features which seem attractive for extension in frequency.

The principle of operation of the bermutron appears to offer such possibilities of frequency extension. To overcome the frequency limitations due to the sweeping speed of one electron beam, it is recommended that the feasibility of using several synchronized beams as, for instance, in a multiple beam klystron,[55] swept alternately in a bermutron-like device, be determined. Second, an investigation should be made of the feasibility of sweeping a rebatron beam in a bermutron; and third, investigation of a device using concentration modulation[56] is recommended.

Further, the ubitron and cycloidotron principle seem more attractive than the remaining devices in this table (4.1.III) because they utilize smooth structures (as does the bermutron) with periodic beams. The reason that they appear somewhat less attractive than the bermutron is that in the ubitron the required strength and periodicity of the static magnetic induction may become excessive at higher frequencies. In the cycloidotron the power output may become too small to be useful because of the bunching, which is due to the time varying induction, and is thus limited by the power density limit of the waveguide.

Finally, it is recommended that the feasibility of using synthesized-plasma hollow cathodes[57] in carcinotrons be studied to extend their frequency range because of the very high current densities available from such cathodes.

The dematron is an attractive device in the X-band, but because it belongs to the magnetron family, scaling in frequency requires scaling in volume, so that it does not seem suitable for frequency extension. The teaser, orbitron, and other devices based on Cerenkov, or cyclotron, radiation require additional theoretical considerations with respect to generation under symmetry conditions, etc. (cf. refs. 50-52). The utilization of such, and similar devices, however, is contingent upon the development of efficient couplers, a point mentioned before, but because of its importance worth repeating.

The devices in Table 4.1.III are not recommended for further development for various reasons, e.g., the undulator power output will always be less than the corresponding ubitron, the phreatron and harmodotron, essentially Cerenkov-like devices, have very low interaction impedances since they use homogeneous, isotropic dielectrics; and there are no data available for the others. Lack of data and experience with respect to millimeter wave generation puts the cylotron-wave converter[58] in this class also (see also above).

4.5.2 Long Range Recommendations

Among the long-range recommendations, the first is an extension of the study reported here. This extension should concern itself with detailed theoretical calculations of the limits of the untried devices (cf. Table 4.1.III) including loss and heat dissipation calculations. Thus, study should include the general

consideration of inherent frequency and power limits of electron beam-circuit devices, using the work of Senitzky[13] as a starting point.

The same priority should be given to a study of some novel coupling schemes, a point which cannot be overemphasized, for possible efficient utilization of such phenomena as Cerenkov, Bremsstrahlung, and cyclotron radiation, and electron beam-plasma interaction including density modulation. Although the question of coupling is believed completely solved by many, the fact remains that unless more effective coupling schemes are developed, the phenomena mentioned above cannot be readily applied for development of practical devices, i.e., reasonable power outputs in the millimeter and submillimeter range.

4.6 REFERENCES TO CHAPTER IV

1. I. P. Shkarofsky, and E. Brannen, "The radio spectrum from 10 Gc to 300 Gc in Aerospace Communications," ASD-TR-61-589, vol. II, March 1962.

2. A. Karp, "Millimtere-wave values," Forschr. Hochfrequenztechnik, vol. 5, pp. 73-128, 1960.

3. P. D. Coleman, "Spanning the microwave infra-red gap," Proc. IRE, vol. 50, No. 5, 1219-1224, May 1962.

4. W. C. Brown, et al, Report of Electronics Research Laboratory, University of California, Berkeley, California; declassified, June, 1962.

5. J. Feinstein, R. W. Peter, A. Karp and J. Allison, URSI National Committee Report, XIV General Assembly, Tokyo, Sept. 1963. Also, Radio Science, vol. 68D, No. 5, pp. 655-59, 663-67, May 1964.

6. L. Nichols, R. Edwards and H. J. Krohn, "Millimeter wave generators," Electro-Technology, Science and Engineering Series No. 60, pp. 63-84; Sept. 1964.

7. S. N. Sen, "Millimeter wave generation," J. Science Indust. Res. (India), vol. 23, pp. 416-422; Oct. 1964.

8. J. F. Hull, "Microwave tubes of the mid-sixties," IEEE Convention Record, Part V; 22-26 March 1965.

9. J. R. Pierce, "Millimeter waves," Phys. Today, vol. 3, No. 11, pp. 24-29; Nov. 1950.

10. Private Communications

11. CSF Reports

12. R. S. Elliot, "Some limitations on the maximum frequency of coherent oscillations," J. Appl. Phys., vol. 23, No. 8, pp. 812-818; Aug. 1952.

13. Senitzky, I. R., "Quantum effects in the interaction between electrons and high frequency fields," Phys. Rev., vol. 95, No. 4, pp. 904-11; Aug. 1954.

14. G. Weibel, "High Magnetic Field Submillimeter Wave Generators with Parametric Excitation," Proc. of Symp. on Electronic Waveguides, Polytechnic Inst. of Brooklyn, pp. 389-405; April 1958.

15. W. C. Brown and G. E. Combrowski, "Analysis of a new crossed-field amplifier, the electromagnetic amplifying lens," IRE Trans on Electron Devices, vol. ED-9, pp. 221-28; March 1962.

16. W. C. Brown, "Electronic components for power engineering," Electronic Progress (Raytheon), vol. 9, No. 4, pp. 9-13; 1965.

17. G. E. Pokorny, A. E. Kushnik, and J. F. Hull, "The dematron--a new crossed field amplifier," IRE Trans. on Electron Devices, vol. ED-9, pp. 337-45; July 1962

18. R. M. Phillips, "The ubitron, a high power traveling wave tube based on periodic beam interaction in unloaded waveguide," IRE Trans. on Electron Devices, vol. ED-7, No. 4, pp. 231-241; Oct. 1960.

19. R. M. Phillips, "The ubitron, a high power millimeter-wave traveling wave tube," Proc. IEEE, vol. 53, No. 10, p. 1648;

20. P. D. Coleman, "Theory of the rebatron--a relativistic bunching accelerator for use in megavolt electronics," J. Appl. Phys., vol. 28, pp. 927-935; Sept. 1957.

21. B. L. Bobroff and H. A. Haus, "The cycloidotron, a proposed crossed-field, fast wave millimeter tube," IEEE Trans. on Electron Devices, vol. ED-10, pp. 235-242; July 1963.

22. K. Fujisawa, "The Laddertron, a new millimeter oscillator," IEEE Trans. on Electron Devices, vol. ED-11, pp. 381-391; Aug. 1964.

23. I. Kaufman, and G. Oltman, "Harmonic generation by electron beam pattern motion--the bermutron," IEEE Trans. on Electron Devices, vol. ED-12, No. 1, pp. 31-39; Jan. 1965.

24. R. E. Hayes, "A synchronous-wave amplifier," IEEE Trans. on Electron Devices, vol. ED-11, pp. 98-101; March 1964.

25. C. E. Enderby, "Ring-plane traveling wave amplifier: 40 kW at 9 mm," IEEE Trans. on Electron Devices, vol. ED-11, pp. 262-66; June 1964.

26. T. Okabe, "Waveguide-magnetrons," IEEE Trans. on Electron Devices, vol. ED-12, pp. 421-24; July 1965.

27. J. L. Hirschfield, and J. M. Wachtel, "Electron cyclotron maser," Phys. Rev. Ltrs., vol. 12, No. 19, pp. 533-536; May 1964.

28. H. A. Gebbie and I. B. Bott, "Two approaches to submillimeter waves," New Scientist, vol. 25, No. 431, pp. 426-429; Feb. 1965

29. P. A. Sturrock, "Kinematics of growing waves," Phys. Rev., vol. 112, No. 5, pp. 1488-1503; December 1958.

30. A. Bers and R. J. Briggs, "Criteria for Determining Absolute Instabilities and Distinguishing Between Amplifying and Evanescent Waves," M.I.T. Res. Lab. of Electronics, QPR No. 71, pp. 122-131; October 1963 and others, cf. G. Convert, Ann. de Radioelectricite, vol. 19, No. 78, pp. 300-320; October 1964; R. N. Sudon, Phys. Fluids, vol. 8, No. 10, pp. 189-1904, October 1965; P. Rolland, Phys. Rev., vol. 140, No. 3B, pp. 776-787, Nov. 1965.

31. Reference 1, p. 107

32. Round Table Discussion, Proc. of the Symposium on Electronic Waveguides, Polytechnic Institute of Brooklyn; April 1958, p. 147.

33. D. C. Forster, "High power sources at millimeter wavelengths," Proc. IEEE, vol. 54, No. 4, pp. 532-539; April 1966.

34. R. G. E., Hutter, Beam and Wave Electronics in Microwave Tubes, D. Van Nostrand Co., Princeton, N. J., 1960.

35. P. D. Coleman, et al, "Megavolts Electronics, Sub-millimeter Wave Research," Contract No. AF 33(657)-10224, Reports, Dept. of Elec. Eng., Univ. of Ill. 1961-1963.

36. A. Boornard, et al, "Microwave Cerenkov Generator," Contract No. AF 30(602) 30615; 1961-64.

37. M. D. Petroff, "Millimeter Wavelength Power Generation Utilizing the Phreaton Effect," Contract No. DA 36-039 AMC 02209(E); 1965.

38. C. H. Durney and R. W. Grow, "Traveling-Wave Tubes with Non-Periodic Dielectric Circuits," Contract No. Nonr-1288(05) Electrical Engineering Dept., University of Utah; 1963, 1964.

39. J. Dain, and R. R. Thompson, "A cyclotron resonance frequency multiplier," IEEE Trans on Electron Devices, vol. ED-10, pp. 195-200; May 1963.

40. K. Bloetekjaer, "A proposed harmonic generator based on cyclotron waves," IRE Trans. on Electron Devices, vol. ED-9, pp. 27-32; Jan. 1962.

41. M. D. Sirkis and C.C.T. Wang, "Generation of millimeter waves by means of the Doppler effect," IEEE Trans. on Electron Devices, vol. ED-10, p. 417; Nov. 1963.

42. C.C.T. Wang and M. D. Sirkis, "Frequency Mixing in a Relativistic Electron Beam, IEEE Trans on Electron Devices, vol. ED-11, pp. 266-276; June 1964.

43. Reports of the Electrical Engineering Department of the University of Utah, Microwave Devices Lab., 31 March 1963, 31 March 1964, 30 June 1964, 31 Dec. 1964, NASA N63-18702, AD 601869, AD 605418, AD 612954.

44. B. W. Hakki, "Bremsstrahlung as a source of microwave power," IEEE Trans. on Electron Devices, vol. ED-9, pp. 439-448; Nov. 1962

45. R. E. Skinner and J. Vollmer, "Coherent radiation by plasma oscillation," Phys. Fluids, vol. 7, No. 1, pp. 148-50; Jan. 1964.

46. B. Murphy, "Harmonic generation in a microwave discharge," Phys. Fluids, vol. 8, No. 8, pp. 1534-1540; Aug. 1965.

47. "Cesium Vapor Cathode Study," RCA Microwave Research Laboratory, April 1965, AD 614648.

48. J. W. Sedin, et al, "Applied Research on a High-Power Millimeter Wave Generator," Watkins-Johnson Co., Palo Alto, Calif., 28 Feb. 1963, NASA publ. N63-14471.

49. H. Heffner and D. A. Watkins, "The practicality of E-type traveling wave devices," Proc. IRE, vol. 43, No. 8, pp. 1007-1008; Aug. 1955.

50. J. R. Pierce, "Interaction of moving charges with circuits," J. Appl. Phys., vol. 24, No. 5, pp. 627-638; May 1965.

51. A. M. Sayied, "Cerenkov effect under the influence of an external magnetic field," Proc. Phys. Soc., vol. 79, pt. 4, No. 510, pp. 816-818; 1962.

52. R. Gajewski and J. L. Hirschfield, "Influence of coulomb interaction on the cyclotron radiation of electrons moving in a single orbit," Phys. Fluids, vol. 4, No. 4, pp. 736-739; June 1961.

53. L. W. Zelby and J. Vollmer, "Influence of source symmetry on Cerenkov radiation," J. Appl. Phys., vol. 36, No. 1, pp. 322-323; Jan. 1965.

54. T. Erber and Hsio-Chang Shih, "Cerenkov radiation from extended charge structures," Acta Physica Austriaca, vol. 19, No. 1, pp. 18-44; 1964.

55. M. R. Boyd, et al, "The multiple-beam klystron," IRE Trans. on Electron Devices, vol. Ed-9, pp. 247-252; May 1962.

56. H. Lashinsky, "Concentration modulation electron-beam devices," IRE Trans. on Electron Devices, vol. ED-8, pp. 185-191.

57. A. L. Eichenbaum, "Kilovolt extraction of dense electron beams from synthesized-plasma cathodes," Proc of IEEE, vol. 53, No. 5, pp. 478-481, May 1965.

58. D. C. Watson, et al, "A cyclotron-wave microwave power converter," Proc. IEEE, vol. 53, No. 11, pp. 1797-1798; Nov. 1965.

Chapter V

QUANTUM GENERATORS AND AMPLIFIERS

5.1 INTRODUCTION

In this section are presented the results of a search of the most recent literature concerning the amplification and generation of electromagnetic radiation by devices whose behavior is mostly attributable to quantum mechanical effects.

5.2 GENERATION USING THE MASER PRINCIPLE

The basic principle of microwave amplification by the stimulated emission of radiation is well known to consist basically of the inversion of the thermal equilibrium population between two energy eigenlevels E_2 and E_1, where $E_2 > E_1$, of the unperturbed Hamiltonian of a given physical system. Consequently, electromagnetic radiation with a frequency f such that $hf = E_2 - E_1$ acts as a perturbation of the existing Hamiltonian. The electrons in the upper levels make transitions to the lower levels, simultaneously generating photons hf which add to the existing radiation. This additive build-up of photons is "coherent." It is clear that the incident radiation is <u>amplified</u> as it propagates in the "active medium;" in order to transform this amplifier into a generator, sufficient feedback must be provided from the output to the input of the maser. Oscillations at frequency f will then be generated.

5.2.1 <u>The Resonant Cavity</u>

The problem of providing a proper resonant cavity in which growing oscillations may be contained is solved for any frequency f of

interest in this report by the use of Fabry-Perot interferometer type mirrors. W. Culshaw[1,2] has investigated thoroughly the use of the Fabry-Perot interferometer at millimeter wavelengths, and the quality factors of the order of several thousand seem to be readily obtainable at any frequency using low loss dielectric materials such as polystyrene ($\epsilon = 2.56$, $\delta = 0.001$) or, better yet, fused quartz ($\epsilon = 3.83$, $\tan \delta = 0.0001$), in the form of n parallel quarter-wave plates with $\lambda/4$ spacing in air. There is, however, a need for data describing the electrical properties of known new materials at these frequencies. Very often the Fabry-Perot mirrors are simply chosen to be flat metallic discs of brass or some other material of high conductivity.

5.2.2 Available Radiative Transition Frequencies f

It is clear that it would be possible to generate any frequency f using the maser principle as long as the proper physical system is available which provides two energy levels E_1 and E_2 such that $E_2 - E_1 = hf$ and the transition probabilities between the different energy levels allow the population inversion in E_2 with respect to E_1. Historically, radiative transitions observed in different active materials fall into two major classes--the optical and the microwave. However, recently the gap between these classes is being rapidly closed.

5.2.2.1 Optical Frequency Transitions

Here the maser is called a "laser." The frequencies in this case are in the visible light or infrared region. Typical examples are: the 6934 Å radiation from Cr^{3+} : Al_2O_3, and the 26,130 Å radiation from U^{3+} : CaF_2 (see ref. 3 for other materials).

The semiconductor injection diode lasers fall into this class since the largest generated wavelengths are of the order of 5 microns, recently reported by Lincoln Labs.[4] In this latter case a high magnetic field parallel to the current was used (first magneto-optical laser) and 1% tuning was possible by changing the intensity of the magnetic field from 20-60 kilo-Oersted.

5.2.2.2 Microwave Frequency Transitions

The principle of microwave generation by stimulated emission of radiation is the same as for lasers; however, the energy difference $E_2 - E_1$ is now so small that the active medium is very different from the optical maser. The transitions in this case are between the quantized rotational or inversion levels of the molecules.

It is clear that the problem consists now in carrying out an extensive spectroscopic program in order to determine the rotational energy levels of different molecules as well as the transition probabilities between these levels. Such studies have already been made[5] and are being pursued presently.[6]

Maser action can be obtained by four different methods.

1. Beam Maser: In this case the gas molecules populating the upper energy states of a two energy level system are separated from the molecules of the lower energy state by passing the active gas beam through either a spatially inhomogeneous electric field or magnetic field. Possible molecules for this case are:

Molecule	Transition	Wavelength
HCN	$J = 1 \leftrightarrow 0$	3.4 mm
NH_3	$J = 2 \leftrightarrow 1$	0.252 mm
CH_3F	$J = 2 \leftrightarrow 1$	2.95 mm
CH_3CN	$J = 5 \leftrightarrow 6$	2.72 mm
CH_3NC	$J = 4 \leftrightarrow 5$	3.00 mm
ND_3	$J = 2 \leftrightarrow 1$	0.485 mm
HF	$J = 1 \leftrightarrow 0$	0.24 mm

2. Radiation Pumped Masers: The difficulty here is to find materials with at least three properly spaced energy levels and convenient transition probabilities. Solid state traveling wave masers that are discussed in Section 5.8.3 can be operated as oscillators if the reverse isolator material is not used, thus causing regeneration to occur. However, the saturation power level of such devices is about one microwatt. A basic disadvantage of optically pumped microwave masers is the inherently low efficiency, typically about 0.1%,[6,51,52] because of the high value of the ratio $\frac{hf_{\text{optical}}}{hf_{\text{microwave}}}$. An optically pumped CN laser has been operated recently using the incoherent light output of a Xenon flash lamp. Thus, about 10 mW of peak power at 5.2μ has been obtained during the photolysis of cyanogen (C_2N_2).

3. Gas Masers: Gas masers have originated with the well known He-Ne laser where an electric discharge produces the necessary population inversion through the electron bombardment of atoms. A more recently developed infrared laser which also produces the largest CW laser outputs

to date (of the order of a few kilowatts) is the CO_2 laser with a wavelength of 10.6μ.

Submillimeter gas masers which have been developed in the last two years offer the most exciting possibilities in generating submillimeter wave radiations, and perhaps they will constitute one of the very small number of practical means of generating these frequencies.

Some of the results in this field are summarized in the following.

A maser using water vapor[8] at 1 mm pressure in a glass tube 4.8 meters long and 2.5 cm internal diameter has been constructed. The discharge was pulsed with a duration of 2.9 μsec. Two spectral lines were obtained; one at 23 μ with a peak power of 10 W and another at 89μ of the order of 0.1 W.

Twelve oscillation wavelengths between 23 and 119μ from water vapor, and two wavelengths (36.3μ and 72.7μ) from deuterium oxide discharges, have been obtained in a high Q optical resonator.[16] The gas pressure was about 1 Torr and the peak value of the discharge current 380 A. The highest peak output power is of the order of 0.1 W. The laser output repetition frequency was 20 c/s.

Oscillations at fourteen wavelengths[17] between 126 and 373μ were obtained in dimethylamine, ammonia and mixtures of deuterium and bromine cyanide with which four lines between 181 and 205μ were obtained.

Stimulated emission at 337 and 310μ was obtained[9] in pulsed discharges in CH_3CN at a pressure of 1 mm mercury with a peak power estimated at 10 W. The generation of 337μ radiation is of special

interest because of the observed window at 345μ in the absorption spectrum of water vapor, which implies low losses along the transmission path for communication at this wavelength.

The possibility of operating continuously these submillimeter masers has been demonstrated recently[73] for both a water vapor and a CH_3 CN laser with output powers of the order of several microwatts. It has also been shown [72,18] that these lasers can be built with reasonably small sizes (about two meters in length).

While the exact mechanism of transitions responsible for the operation of some of the submillimeter lasers is yet not established, a new mechanism was recently suggested[74] (see Fig. 5.1) which results in predicted emission wave numbers which agree with all of the observed CN laser emissions such as the 0.337 mm and the 0.310 mm lines as well as the newly observed[74] 0.676 mm wavelength from ICN which cannot be accounted for by any of the previously suggested mechanisms.[75,76]

The practical conclusion from these experiments is that with further investigation of new active media, it should be possible to generate almost any submillimeter wavelength of appreciable power.

4. <u>The Cyclotron Resonance Maser in Semiconductors</u>: When a magnetic field B_o is applied to a semiconductor, the eigenenergies of free carriers of effective mass m^* split further by $(n + \frac{1}{2})\hbar\omega_c$, where n can take integer values starting from zero and $\omega_c = \frac{eB_o}{m^*}$. The energy of electrons is then given by

$$E(n, k) = (n + \frac{1}{2})\hbar\omega_c + \hbar^2 \frac{\vec{k} \cdot \vec{k}}{2m^*} \qquad (5.1)$$

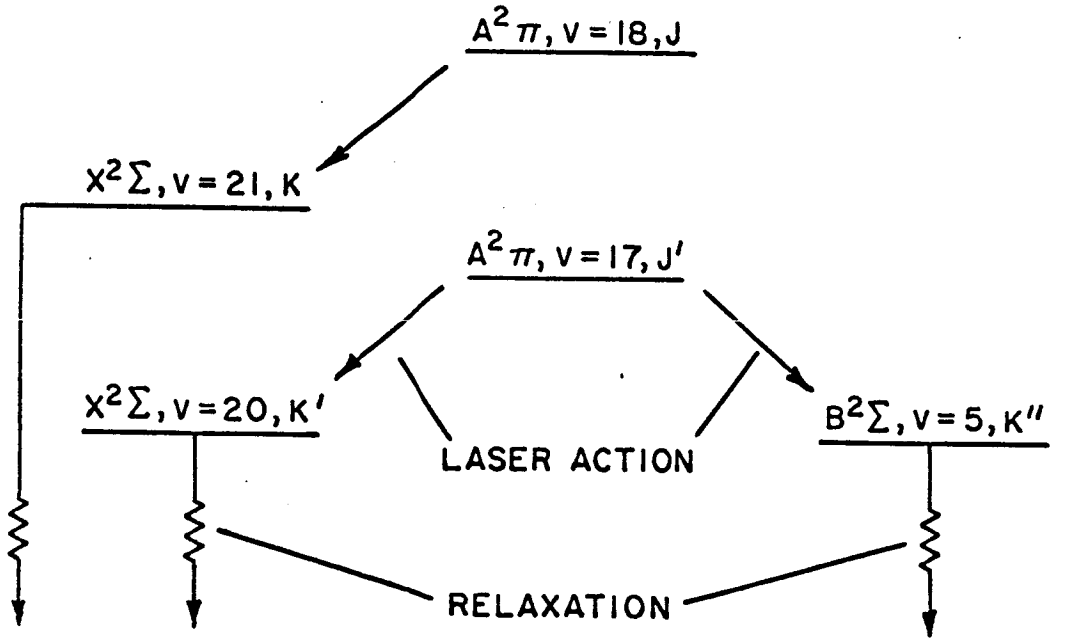

$\lambda = 0.76$ mm CORRESPONDS TO $A^2\pi_{\frac{3}{2}}\ (18, 1\frac{1}{2}) \rightarrow X^2\Sigma(21,0)$

$\lambda = 0.337$ mm AND 0.310 mm COMPARED TO $A^2\pi\ (v=17) \rightarrow B^2\Sigma(v=15)$

Figure 5.1 Postulated Mechanism of Transitions in CN Radical Lasers

Thus, to a first approximation, equally spaced Landau energy levels separated by $\hbar\omega_c$ are created in the presence of a magnetic field as shown in Fig. 5.2. In InSb, where $m^* = 0.015\ m_o$, a magnetic field of 1000 Gauss corresponds to $\hbar\omega_c = 0.0008$ eV and a frequency of 187 GHz, clearly helium temperature operation is necessary in order to reduce the thermal energy below the energy separation of Landau levels. With a magnetic field of 10 kilogauss the frequency is 1870 GHz and higher temperature operation is possible. If a technique utilizing this principle were developed it would provide the attractive possibility of continuous timing over the submillimeter band.

In a semiclassical consideration of this problem it is intuitively understood that this quantization of energy levels is effective only if the carrier scattering time is sensibly longer than the cyclotron rotational period, i.e.

$$\tau \gg \frac{1}{\omega_c} \tag{5.2}$$

But since the mobility

$$\mu = \frac{e\tau}{m^*}$$

an equivalent condition to (5.2) is

$$\mu B \gg 1 \tag{5.3}$$

Thus, equation (5.1) is effective only for high magnetic fields and high carrier mobilities.

The cyclotron resonance maser has the further interesting feature of electrical tuning adjusting the separation of the Landau energy levels by altering the magnetic field B.

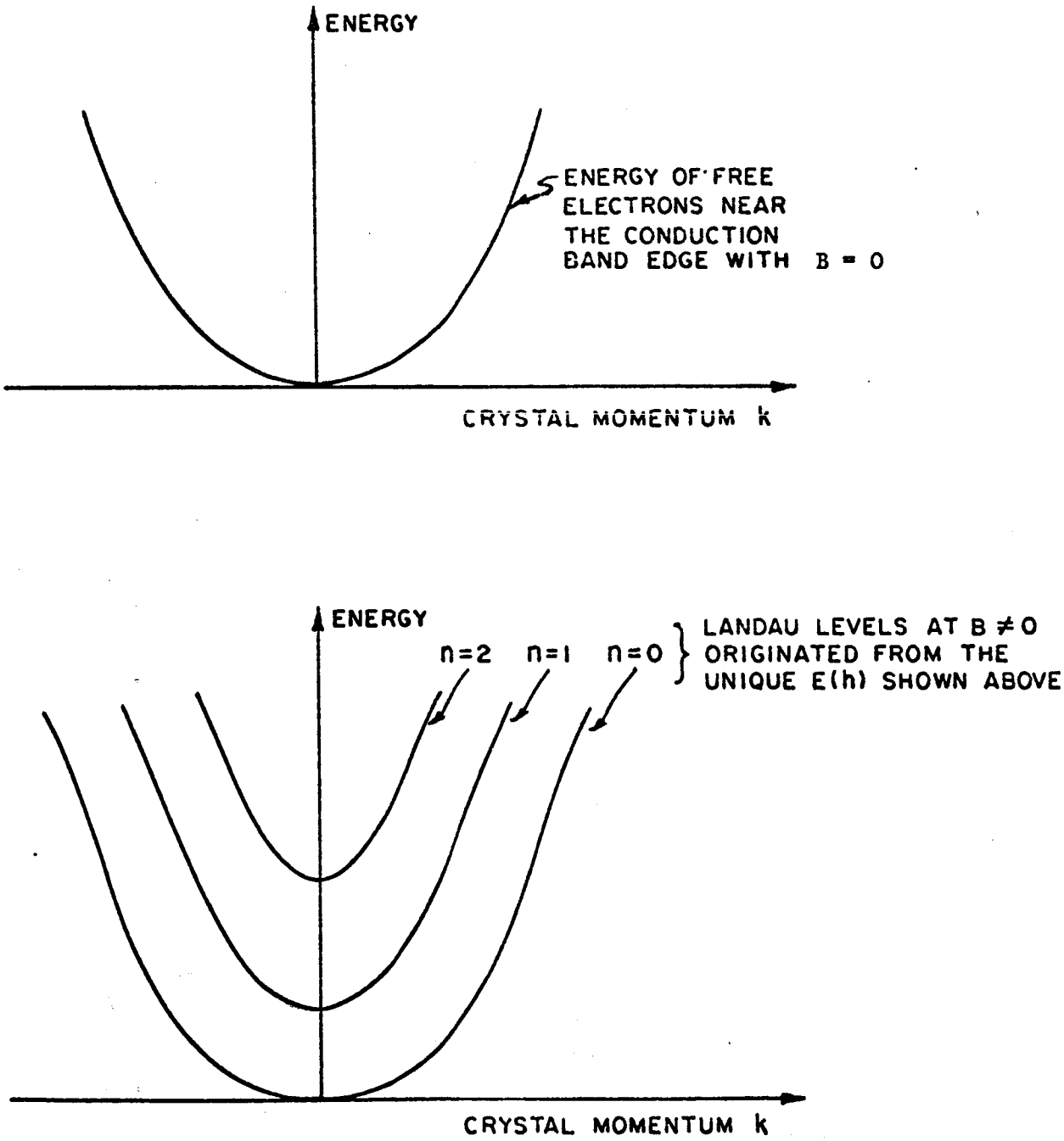

Figure 5.2 Splitting of the Conduction Band Edge into Equally Spaced Landau Levels upon the Application of a Magnetic Field

However, a major difficulty arises when an attempt is made to produce inversion of population among the Landau levels in order to utilize subsequently the stimulated emission resulting from transitions from an upper level to some lower level. Indeed, the selection rules permit only transitions where n changes by + or - 1; thus, any stimulated emission will produce a radiation of frequency f with

$$f = \frac{\Delta E}{h}$$

where the ΔE is the equal separation of Landau levels. Consequently, this stimulated emission will be immediately absorbed inside the material by stimulated up-transitions between another set of adjacent Landau levels which are separated by the same energy difference ΔE.

Possible solutions to this problem are reviewed by Jeffrey Frey.[48,68] One such solution, as suggested by B. Lax,[47] consists in utilization of Landau levels resulting from the degenerate valence band of Ge and Si where unequally spaced Landau levels are expected.

It must be recognized that extensive investigations to obtain cyclotron resonance maser action in InSb have not resulted in any positive results. However, further work in this area is attractive because of the great ease in tuning the device. On the other hand, cryogenic temperatures are necessary.

5. Mixing and Pressure Tuning of Lasers: Submillimeter signals can be obtained by mixing two optical laser outputs which differ in frequency by the desired amount. This is especially true since phase locking of two masers has been shown to be possible.[10] The nonlinear medium

could be one of the nonlinear dielectrics such as ADP or KDP, or an improved GaAsP $\longrightarrow$ GaAs heterojunction photodiode[24,25] as described below. It is clear, however, that the efficiency of such systems is very low, except possibly in the case of the semiconductor heterojunctions.

W. J. Moroney has discussed[24] and successfully implemented efficient photoelectric mixing, resulting in the generation of difference frequencies in the gigahertz frequency range. (In the above report a 40 GHz difference frequency was reported.)

On the other hand, a small-bandgap semiconductor infrared laser belonging to the family of PbSe, PbTe, SnTe and $Pb_xSn_{1-x}Te$ provides a direct source of long wavelength radiation;[57] namely, it has been possible to tune a PbSe laser from its natural lasing wavelength of 8μ to 14μ by application of external pressure. This is due to the reduction of the forbidden bandgap width. The drawback in this scheme is the necessity of a bulky pressure application equipment operating at cryogenic temperatures. The more recent work on $Pb_xSn_{1-x}Te$ lasers shows that by changing x from 0 to 1, the forbidden bandgap goes from its original small value for SnTe to zero and again a finite value for PbTe (with conduction and valence bands interchanged). It, therefore, appears that any radiation wavelength up to $\lambda = \infty$ can be obtained at a proper value of x. Clearly, it is also possible to pressure tune a $Pb_xSn_{1-x}Te$ laser to $\lambda >$ (λ with no pressure).

Besides the possibility of obtaining directly long wavelength radiation from such lasers when properly pressure tuned, an immediate possibility exists in mixing an "<u>unpressurized</u>" laser beam with the

output of a continuously "pressure tuned" laser in a "high speed" photodetector. In this way a continuously tuned submillimeter generator may be constructed. Note that Moroney's detector is usable only with GaAs lasers which have a characteristic wavelength of $\approx$ 8500 Å. In order to obtain a beat frequency of 1000 GHz a relative change of wavelength $\frac{\delta\lambda}{\lambda} = 0.003$ is required (corresponding to about 30 Å line shift). This is easily achieved by pressure tuning. It is clear that the main limitation in this scheme comes from the speed of the photoelectric mixer response.

5.3 BREMSSTRAHLUNG RADIATION FROM SOLIDS

The possibility of the stimulated emission of Bremsstrahlung and consequent amplification and generation of a broadband of frequencies extending to the submillimeter region is discussed by D. Marcuse.[11,30]

The fundamental concept can be summarized as follows: while in a conventional maser the incident electromagnetic radiation is amplified by the coherent transitions of electrons from discrete excited states to lower energy states, it is also possible that radiation be emitted from a free electron in the presence of a static electric or magnetic field (such as the coulomb field of ionized impurities in a semiconductor). This corresponds, in actual fact, to coherent transitions of the electrons between the continuum of energy levels of a free electron Hamiltonian, due to the perturbation introduced by the incident radiation. It is clear that in this case, unlike the case of the maser, there is no preferred

characteristic frequency, so that a very broadband operation is possible. Correspondingly, however, the noise due to the spontaneous emission is inherently high.

The current-carrying free electrons in a semiconductor can make transitions as described above, as a result of being scattered by the ionized impurities. Research in this specific area is described in Ref. 55, where an n-type GaAs semiconductor sample is used as the active material. Although the efforts of this group to obtain Bremsstrahlung emission have not been successful, this may have resulted from experimental conditions such as the lack of cooling.

This method of generating submillimeter radiation is basically very promising especially with the expected watts[30] of power available at frequencies near 1000 GHz. The group previously mentioned is pursuing research in this field.

5.4 THE GUNN EFFECT

A novel current instability was discovered by J. B. Gunn[12] in n-type GaAs and InP samples in 1963. The instabilities he reported were in the frequency range 0.5 to 6.5 GHz. Since then considerable efforts have been made in the field of solid state devices in order to understand and improve the operation of Gunn generators.

The device consists simply of the semiconductor sample subjected to a pulsed or dc bias electric field, and placed in a proper microwave cavity in order to monitor the generated oscillations.

5.4.1 Characteristics of the Oscillation

The main characteristics of the Gunn oscillation are as follows:

1) In order to start the oscillations the applied bias field must reach a threshold value, which is found to be very close to the electric field at which the drift velocity of the charge carriers reaches its saturation value of 10^7 cm/sec.

2) The frequency of oscillation f is approximately equal to $\frac{v_s}{\ell}$, where v_s is the saturation velocity of the charge carriers and ℓ is the length of the sample.

3) It is a bulk phenomenon existing at room temperature and unaffected by external magnetic fields.

4) The external circuit impedance affects the operation frequency only to a small extent (10% tuning range).

Various aspects of the present universally accepted theory of the Gunn effect are best discussed in a special issue[25] (see in particular ref. 44) of the Transactions on Electron Devices of the IEEE. This theory explains the existence of a dynamic negative differential mobility as a result of the formation of space-charge domains when the applied electric field bias reaches a threshold value.

The conduction bands of semiconductors such as GaAs and InP are characterized by the existence of satellite energy band minima of much higher effective mass situated a few tenths of eV above the main conduction band minimum. The dynamic negative differential mobility is the result of the excitation of the ordinary high mobility μ_1 conduction

electrons into the low mobility μ_2 satellite band. Let $\frac{\mu_2}{\mu_1} = B$. If n_1 and n_2 are respectively the number of electrons in the conduction band and the satellite band, it can be assumed that

$$\frac{n_2}{n_1} = \left(\frac{F}{F_o}\right)^K \tag{5.4}$$

where F is the local electric field

F_o is a reference field

and K is an appropriate exponent.

The average drift velocity v at a point is then

$$v = \mu_1 F_o \frac{\frac{F}{F_o} + B\left(\frac{F}{F_o}\right)^{K+1}}{1 + \left(\frac{F}{F_o}\right)^K} \tag{5.5}$$

Consequently, the differential mobility is

$$\mu = \frac{dv}{dF} = \frac{\mu_1}{(1 + E^K)^2} \left\{1 - \left[(K - 1) - B(K + 1)\right] E^K + BE^{2K}\right\}$$

where $E = \frac{F}{F_o}$.

It can be easily shown that for $K > \frac{1 + B}{1 - B}$, μ is negative for certain values of E and the v - F curve has the characteristic form shown in Fig. 5.3.

Let the applied bias voltage be such that instantaneously the electric field everywhere in the sample is equal to F_c. This is clearly an unstable situation; indeed, if at any point of the sample a slight microscopic irregularity exists (the most probable region is at the

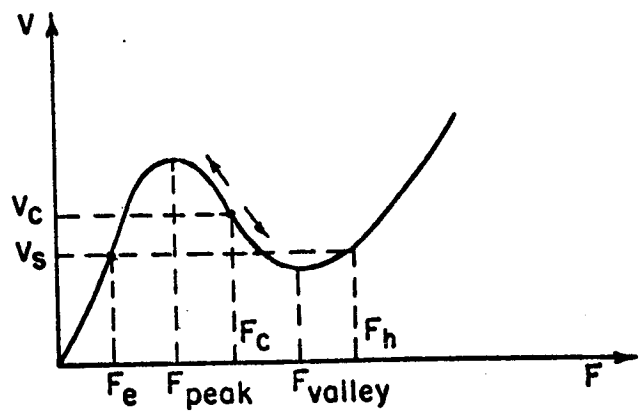

Figure 5.3 Plot of the Drift Velocity v as a Function of the Electric Field F Showing a Negative Mobility

electrodes), such that the electric field tends to become larger and smaller than F_c at the right and left respectively of this point, it is clear that electrons will accumulate suddenly at that point since more electrons will flow from the left-hand side than are drained out from the right-hand side. This accumulation will continue until the high and low electric fields reach the values F_ℓ and F_h at which the high and low field region velocities are the same v_s. As the accumulation layer moves out of the sample a new one will be formed.

This is a very general description of the phenomenon. Several kinds of operational modes are discussed in great detail in Ref. 25.

5.4.2 Limitations of the Gunn Oscillator

a) Frequency limits

It is clear that the oscillation frequency is of the order of the reciprocal of the transit time of space charge domains in the Gunn diode. Therefore, higher frequencies are expected from thinner structures or from materials which allow higher electron drift saturation velocities v_s. Since v_s for GaAs $\approx 10^7$ cm/sec, a frequency of a few GHz is expected from a 100μ thick sample.[13] It is hoped, however, that much thinner structures can be constructed using epitaxial layers; thus a reasonable limit for F may be that corresponding to a 1μ thickness, i.e., a few hundred GHz.

A fundamental limit for this phenomenon, however, is set by 1/scattering time from the satellite to the conduction bands. In the case of GaAs this time is 10^{-12} sec; therefore, an upper limit for the operation frequency is $\frac{1}{\tau} \approx 10^{12}$ Hertz, i.e., 1000 GHz. Detailed discussion is given in Ref. 45.

b) Output Power and Efficiency

The best results to date are output powers of the order of 100 mW for CW operation and 100 W peak for pulsed operation, with efficiencies typically of a few per cent and 6% for the best cases. It was shown recently[46] that the efficiency of the device can be improved by almost 100% with certain changes in the geometry of the generating semiconductor samples.

5.5 SOLID STATE PLASMA INSTABILITIES

In analogy with gaseous plasmas, the free electrons and holes in a solid, together with the ionized donors and acceptors, constitute a plasma which is expected to behave in a way similar to its gaseous counterpart. Thus, Helicon waves have been observed in sodium[58] and indium antimonide[59] while Alfven waves have been observed in bismuth.[60]

The basic differences between gaseous and solid plasmas are:

1) The plasma density n in solids is much larger than those in gases at standard temperatures.
2) The solid plasmas behave better at low temperatures where lattice scattering is reduced, while gaseous plasmas have to be operated at very high temperatures to keep the plasma density high enough.

Since a characteristic parameter is the so-called plasma frequency ω_p^2, where

$$\omega_p^2 = \frac{n e^2}{\epsilon_o m^*} \qquad \begin{cases} e = \text{electronic charge} \\ \epsilon_o = \text{dielectric constant} \\ m^* = \text{effective mass} \end{cases}$$

it is clear that high n is desirable for high frequency plasma phenomena, and therefore only solid state plasmas will be of interest in submillimeter applications.

Although much work has been done to study the possibility of different solid state plasma instabilities in a number of semiconductors or semi-metals, it has not been possible to observe experimentally any instability which could be identified with one of the theoretical predictions. The search for plasma instabilities has been carried out in indium antimonide in which electrons have, on the one hand a low effective mass which helps to provide a large ω_p, and on the other hand they have large saturation velocities, which is an important requirement for the useful interaction of an electromagnetic wave with the plasma. Indeed, for the EM wave to gain energy from the plasma wave the charged particles have to move with velocities larger than the phase velocity of the EM wave. However, even for InSb, these parameters are favorable only for a frequency of 8 GHz.[61]

More recently[63] the possibility for two-stream instabilities has been extensively studied for bismuth and graphite. It was found that bismuth can sustain a growing wave of 510 GHz along its trigonal axis at an electric field of 10 v/cm (this is a very high electric field for a semi-metal) and a wave of 2300 GHz along the binary axis with a threshold field of 15 v/cm. Experimental attempts, however, to obtain

such instabilities have been unsuccessful to this date mainly because of the difficulty in sustaining any appreciable electric field in the high conductivity host materials.

R. D. Larrabee et al[62] have reported a broadband emission of microwave radiation from 10 GHz up to 44 GHz of about 1 microwatt RF power when (pulsed) current densities of about 3×10^4 A/cm^2 were passed through n-type InSb samples which are simultaneously subjected to a longitudinal magnetic field of about 4 kilogauss. This was believed to be due to a plasma instability.

In conclusion, it may be said that the success of obtaining useful solid state plasma instabilities has been very limited in spite of substantial efforts directed towards the investigation of this field.

5.6 NEGATIVE EFFECTIVE MASSES IN SEMICONDUCTORS

Reference is made here to the article by H. Kroemer[15] which describes the possibility of the existence of regions in the crystal momentum space where the effective mass (transverse effective mass) of the charge carriers is negative. This situation arises in cubic crystals when one of the energy bands is degenerate; a typical situation is the valence band edge of p-type germanium.

A negative-mass amplifier operating on this principle would consist of a slab of the proper semiconductor placed in a waveguide, or in a general enclosure, where the signal to be amplified is located. A very strong electric field must now be applied to the crystal in such a direction that the charge carriers will be concentrated in the negative mass region of the k-space. The electric field of the signal to be amplified

must be in a direction for which the effective mass is negative. It is clear that energy will then be transferred from the crystal to the applied signal. Such a negative resistance effect would be effective up to frequencies of the order of the collision frequencies (up to 10^{12} Hertz) and would thus cover the entire microwave range.

Practically, it will be possible to populate the desired regions of k-space only if the electrons completely lose their kinetic energy between collisions, which occurs if the scattering cross-section by the optical phonons is large. Although germanium has favorable negative mass regions in k-space, its optical phonon scattering cross-section is small, and attempts to observe the negative mass effect have not yet been successful. The compound semiconductors offer better promise in this sense.

Finally, another possible way of using the negative mass is to superpose on the biasing electric field a large magnetic field in order to produce cyclotron frequency modes which would act as a source of radiation instead of absorption at the cyclotron resonance frequency. This is possible since the mass of the rotating charges is negative. It should be noted, finally, that the cyclotron frequency is tuned easily by varying the magnitude of the applied magnetic field.

5.7 THE READ DIODE[25,26]

5.7.1 Description

The Read diode, first proposed by W. T. Read, Jr. of Bell Labs., consists of a reverse biased junction where the electric field can reach the avalanche breakdown value. A typical diode structure is shown in

Fig. 5.4, together with the electric field distribution within the diode. A simplified description of the operation of this diode is as follows. When the voltage V is applied, instantaneously an electric field configuration is established. If the ac operating condition is so adjusted that during the positive portion of the ac cycle the field is above E_m and during the negative portion below it, the avalanche current I_o at the n^+p junction lags the voltage by 90°. The overall external current $I_e(t)$ lags another $\frac{\tau}{2}$ on the average with respect to I_o, where τ is the drift time of saturated velocity driven carriers through the drift region, and $\tau = \frac{W}{v}$, where v is of the order of 10^7 cm/sec in silicon. If $\frac{\tau}{2}$ corresponds to another 90° phase, the current $I_e(t)$ and voltage V (t) will be 180° out of phase. Thus, at a frequency of

$$f_c = \frac{1}{2\tau} = \frac{v}{2W}$$

the diode behaves like a negative resistance.

5.7.2 Recent Results

Read had predicted in 1958 an operation range for this diode from 1 GHz to 50 GHz with output powers of up to 20 watts at an efficiency of 30%. Today, these performance characteristics are still challenging goals for the future. Recent results, together with the highest frequency Read diode oscillator, are available in Ref. 25.

Silicon structures operating at a few tens of gigahertz have been reported often, with the possibility of tuning (up to 30%) through the variation of the avalanche current I_o (typically 10 to 20 ma). In order to increase the operation frequency, it is clear that a larger

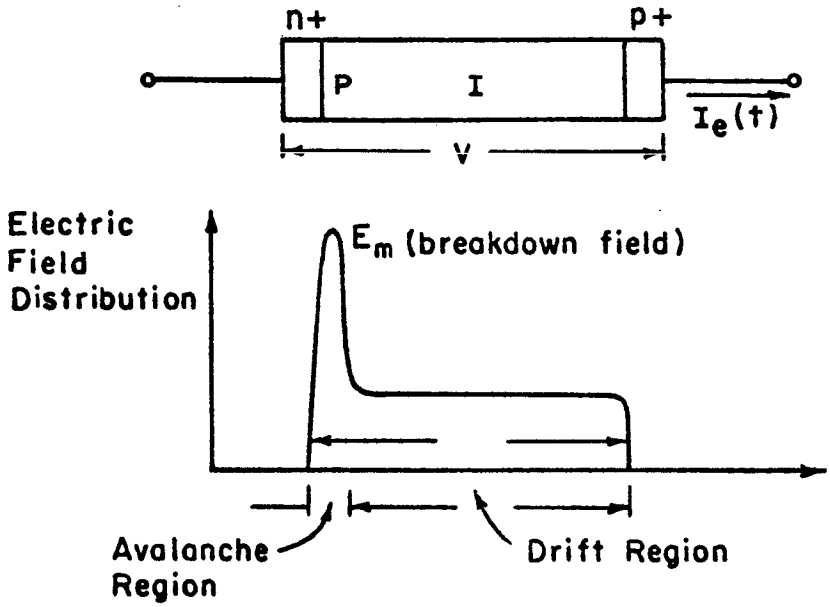

Figure 5.4 Distribution of the Electric Field in the Read Diode

velocity (v) and narrower width (w) are necessary. The most recent results [51,64] in this field show the generation of 150 mW at 70 GHz, 75 mW at 115 GHz and 6 mW at 140 GHz. One fundamental disadvantage of the Read diode scheme is its inherently high noise output because of the avalanche breakdown.

5.8 AMPLIFICATION OF SUBMILLIMETER WAVES

If low noise amplifiers are available at the signal frequency, they can be used to overcome the inherently low efficiency of available detectors.

In the frequency range up to 100 GHz, considerable effort has been devoted to maser amplifiers. It has been previously stated that a generator can be considered to be an amplifier provided with the proper amount of phase and feedback. It is thus possible to use, with slight alterations, most of the generation schemes previously described in order to amplify signals of frequencies close to the oscillation frequency.

5.8.1 Negative Resistance Amplifiers

Negative resistance amplifiers may be of the "broadband" or "narrow-band" (critically frequency-dependent) type.

a) The Negative Effective Mass

If it can be shown to be practically realizable, the negative effective mass effect described in section 5.6 could be used for the amplification of signals up to 1 Tc provided proper ways of coupling the signal in and out of the semiconductor slab are devised. One can propose the covering of the input and output faces of the slab with

dielectric layers of $\lambda/4$ thickness and small refractive index in order to reduce reflection losses.

b) The Gunn Diode

The description of the Gunn oscillator theory in section 5.4 indicates the availability of a dynamic negative resistance which would eventually be usable at frequencies (in this case, however, the negative resistance is "tuned" at the characteristic frequency $\frac{v}{L}$) limited by approximately the 1000 GHz limit of the Gunn effect.

Although Kroemer in his original explanation of the Gunn effect, which is now accepted, labeled this negative resistance as "unstabilizable," the team of B. W. Hakki at Bell Labs. reports what is believed to be a Gunn effect GaAs bulk semiconductor amplifier operated between 5 and 10 GHz (the operating frequency is determined by the dimensions). This aspect of the Gunn effect is still strongly controversial; however, it is agreed that it is not possible to obtain stabilization by mere proper external loading. It is also necessary to have the proper dimension L and carrier concentration n. One such criterion would be[25] (papers by B. W. Hakki, Bell Labs. and P. N. Butcher, Royal Radar Establishment, England)

$$10^{10}\ cm^{-2} < nL < 10^{12}\ cm^{-2}$$

c) The Read Diode

It is clear from section 5.7 that the Read diode like the Gunn effect corresponds to a tuned negative resistance which can be eventually used as an amplifier at the characteristic frequency of $\frac{1}{2\tau}$ or close to it.

The first amplifiers operating on this principle were reported by L. S. Napoli of RCA Laboratories[25] (the frequency of operation being about 8.5 GHz), and B. C. Deloach who reported an amplifier operating around 10 GHz with 30 MHz bandwidth and 20 dB gain. The drawback of the Read diode is its inherently very high noise figure which makes it useful only as a high level device.

5.8.2 Varactor Diodes

These diodes consist of a nonlinear voltage dependent capacitance. The theory of parametric amplification[19] shows that the impedance of this capacitance pumped at a frequency f_p appears to be negative real at a signal frequency f_s.

Parametric varactor diode amplifiers have been operated up to 100 GHz with silicon and GaAS junction diodes. Research is now under way on 93-94 GHz parametric amplifiers using subminiature surface-barrier varactors with etched substrate surfaces[20] and ultraminiature annular varactors.[21] The best cutoff frequencies obtained to this date are around 400 GHz with a theoretical upper limit[21] of

$$f_c = \frac{1}{2\pi R_s C_{min}} = \frac{1}{\pi \epsilon \rho}$$

where ϵ is the dielectric constant and ρ the resistivity of the particular semiconductor in use. It is interesting to note that from theoretical considerations the dielectric constant of a semiconductor is approximately proportional to $1/(E_G)^2$, while ρ is proportional to $e^{\frac{E_G}{kT}}$ where E_G is the forbidden energy gap of the semiconductor. Thus, the product $\epsilon\rho$

is a slowly varying function of E_G and a drastic improvement in f_c does not seem to be probable. It is understood of course that ρ can be changed strongly by doping, presumably without altering the dielectric constant.

The most recent effort in raising the cutoff frequency of varactor diodes as high as possible, and in generating millimeter waves by harmonic multiplication in such diodes, is illustrated by the development of n-GaAs with phosphor-bronze point contact diodes[65] and of epitaxial p-n junctions in GaAs.[66] Cutoff frequencies up to 1000 GHz are reported[67] with actual conversion from 70 GHz to 140 GHz with 20% efficiency and 15 mW output power.

5.8.3 Amplification by Maser Action in Solids

Table 5.I gives an outline of the principal characteristics of some very unique solid state maser amplifiers operating between 9.3 GHz and 96 GHz that have been built in the last five years. Their most interesting properties are described in the following paragraphs.

5.8.3.1 X-Band Ladder Line TWM[34]

This traveling wave maser utilized a Karp-type slow wave structure which is composed of a ridge waveguide with a thin copper ladder line situated in a plane midway between the ridges are shown in Fig. 5.5.

Table 5.I SOLID STATE MASER AMPLIFIERS

	X-Band Masers (9.0-12.0 GHz)					Ku-Band Maser (15.4 GHz)
References	(A)(34) Haddad and Rowe(U of Mich)	(B)(35) Ammann	(C) (36) Friedman and Nagy(J.H.Univ.)	(D) RCA (to be published)	(E) (37) Hughes Westinghouse	(F) Schmitschek, et al (38) General Dynamics/ Astronautics
Type of Maser (slow wave structure)	TWM (Karp structure Ladder Line)	Cavity	Cavity	TWM (meander line)	Cavity (powder)	reflection-type cavity (crystal covered with silver paint)
Active material	Cr^{+3} doped ruby	Cr^{+3} doped ruby (0.2%)	F^{+3} doped sapphire	Fe^{+3} doped rutile	Fe^{+3} doped aluminum nitrate	Cr^{+3} doped ruby
Signal frequency	9.65 GHz	9.3 GHz	12.04 GHz	10.0 - 11.6 GHz	9.283 GHz	15.4 GHz
Tuning range	--	--	--	1.6 GHz	150 MHz	-----
Instantaneous Bandwidth	130 MHz	7.5 MHz	5 MHz	14 MHz	4.5 MHz	3 MHz
Electronic Gain	15 dB	14.5 dB	30 dB	--	--	26 dB
Net Gain	--	--	--	25-50 dB	24 dB	-----
Pump Frequency	24 GHz	23.4 GHz	31.3 GHz	≈ 60 GHz	23.75 GHz	34.7 GHz
Magnetic field	4.1 kG	--	Zero Field	≈ 4 kG	Zero Field	-----
Type of Magnet Perm(P) Superconducting (S.C.)	P	P	(Helmholtz coils giving 5-10 g)	S.C.	P	P
Gain-bandwidth Product	Promise of 1100 MHz	--	165 MHz (250 MHz)	--	--	60 MHz
Bath Temp(K)	4.2	77°K	4.2°K	4.2°K	4.2°K	4.2°K
Noise Temp.	--	105°K	--	10-15°K	--	-----
Energy levels signal pump:						
Pump power	--	3.5 W	--	200 mW	--	several mW

Continued

Table 5.I: SOLID STATE MASER AMPLIFIERS (CONTINUED)

MILLIMETER WAVE MASER (26.0-96.0 GHz)

References	G(39)Foner and Momo	H(23)Arams AIL	I RCA(To be published	J(40) Carter	K(41)Hughes Westinghouse	L(37) Hughes	M(42) Hughes	N(42) Hughes
Type of Maser (slow wave structure)	1st CW mm wave maser cavity	1st TWM dielectrically loaded waveguide	TWM Karp-structure Ladder Line	Cavity	Cavity	1)Cavity 2)TWM (Powder)	Cavity	Cavity
Active material	Fe^{+3}-doped TiO_2	Cr^{+3} doped TiO_2	Fe^{+3} doped TiO_2	FE^{+3} doped TiO_2	Fe^{+3} TiO_2	Fe^{+3} TiO_2	Fe^{+3} TiO_2	Fe^{+3} TiO_2
Signal frequency	26.0-39.0 GHz	35.4-40.0 Gc	34.0-36.0 GHz	49.0-57.0 Gc	70 GHz	81.1 GHz	96.0 GHz	101.05GHz
Tuning Range	13.0 GHz	4.6 GHz	2.0 GHz	8.0 GHz		1)200 MHz	-----	
Instantaneous Bandwidth	--	75 MHz	≈ 100 MHz	--	10 MHz	1)10 MHz 2)75 MHz	-----	
Electronic Gain	Maser Operation	30-33 dB	--	Maser Oscillations	20 dB	1)22 dB 2)10 dB	Maser Operation	Maser Operation
Net Gain	--	17-22 dB	≈ 30 dB		--	--	-----	
Pump Frequency	≈ 70 GHz	68-79 GHz	$f_{p1} \approx 65$ GHz $f_{p2} \approx 75$ GHz	push-pull pumping at ≈ 78.2GHz	118 GHz	124.5 GHz	65.2 GHz	70.8 GHz
Magnetic Field	--	--	≈ 8 kG	$\theta=73^\circ, \theta=0$ 5.5-7.2 kG	4.6 kG	Zero Field	7.35 kG $\theta=53^\circ$ $\phi=28.5^\circ$	6.735 kG
Type of Magnet Perm(P)Superconducting (S.C)	P	P	S.C.	--	S.C.	No Magnet	P	P
Gain Bandwidth Product	--	--	--	--	--	--	-----	--
Bath Temp.	$4.2^\circ K$	$1.7^\circ K$	$4.2^\circ K$	$4.2^\circ K$	$4.2^\circ K$	$<2.2^\circ K$	$2.1^\circ K$	$2.1^\circ K$
Noise Temp.	--	$20^\circ K$	$25^\circ K$	--	--	--	-----	
Energy levels Signal: Pump:	--	3-2 1-3;2-4	4-3 1-4;3-6	5-4 3-5;4-6	5-3 3-5;4-6	--	5-2 1-3;3-5;2-4	5-2 1-3;3-5;2-6
Pump Power	--	Push-pull pumping	--	--	--	--	-----	harmonic pumping

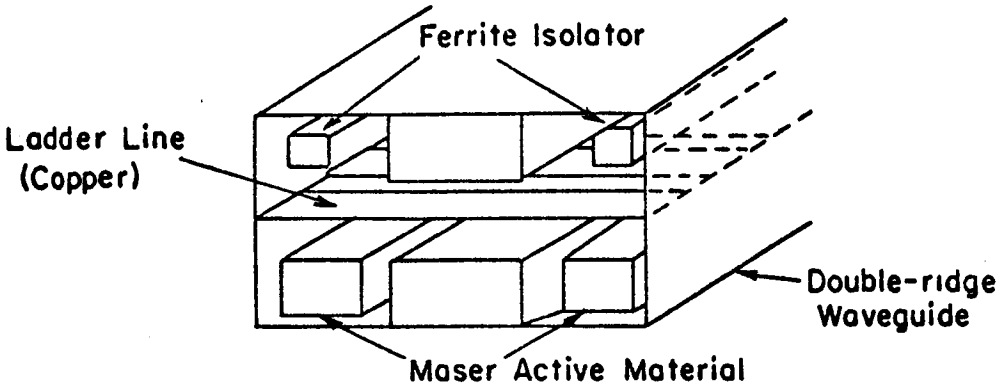

Figure 5.5 Traveling Wave Maser Structure

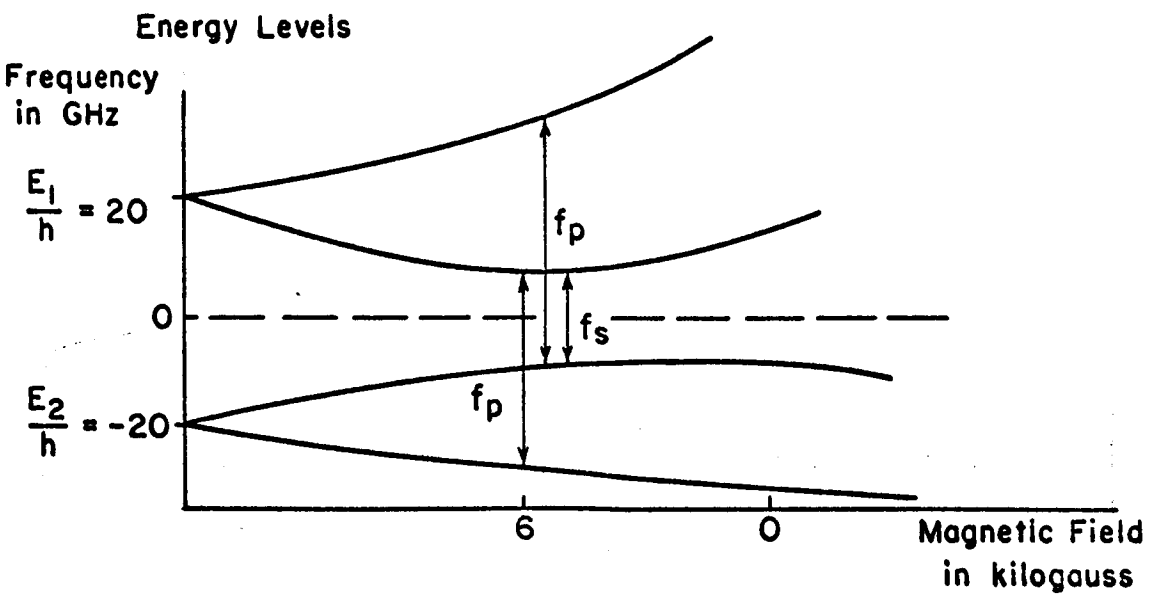

Figure 5.6 Dependence of Energy Level on Magnetic Field

It has resonant slowing of the propagating wave with definite upper and lower cutoff frequencies. The active maser material and the reverse isolator material are placed in regions having opposite senses of circular polarization.

5.8.3.2 Solid State Cavity Maser Operating at $77^{\circ}K$[35]

Nitrogen temperature maser operation was investigated using chromium doped ruby as the active material. It was found that the maser inversion ratio decreases with Cr^{+3} concentration, the paramagnetic resonance linewidth increases with concentration, and the pump power needed to saturate the amplifier increases with concentration. The optimum concentration to get the minimum value of Q_m (note: $G_{dB} = 27.3 \frac{SN}{Q_m}$) was 0.2% Cr^{+3}. Note the large amount of pump power (3.5 watts) needed to invert the maser and the high input noise temperature (105°) of the amplifier.

5.8.3.3 Iron Sapphire Maser with No Magnetic Field[36]

This was the first maser operated with crystalline field splitting only. Without a magnet, it simplifies the maser device considerably. A significant increase in the gain-bandwidth product was achieved by applying a small magnetic field of 5-10 gauss with Helmholtz coils.

5.8.3.4 X-Band Meander Line TWM

A meander line slow-wave structure which has a very broad bandwidth of high slowing was used for this traveling wave maser. It

provided a large tunable bandwidth of 1.6 GHz. The maser, operating with a superconducting magnet, is a complete field operational device to be used for a radiometer.

5.8.3.5 Zero Field Powder Maser[37]

A maser using ferric-doped aluminum nitrate in powder form was demonstrated without a magnetic field. This cavity maser had a net gain tunable over 150 MHz. A powder traveling-wave maser using a meander line slow-wave structure is being investigated.

5.8.3.6 Ku-Band Maser Using a Reflection Type Cavity[38]

A chromium-doped ruby material in the form of a rectangular block was coated with silver paint to form a completely filled cavity.

5.8.3.7 First CW Millimeter Wave Maser Using Fe^{+3} in TiO_2[39]

This cavity maser could operate over a very wide frequency range (260-390 GHz) because of the large zero field splittings of Fe^{+3}-doped rutile and the large E term in the spin Hamiltonian.

5.8.3.8 An 8mm Traveling Wave Maser[23]

Chromium doped rutile was placed in a waveguide along the path of the signal to be amplified. This purely dielectric slowing gave a very wide tunable bandwidth of 4.6 GHz. The configuration of the energy levels illustrating the push-pull pumping technique is given in Fig. 5.6.

The magnetically unbiased crystal has two doubly degenerate energy levels at E_1 and E_2. The application of a magnetic field splits these two levels into four as shown. The figure is self-explanatory for

the pump and signal energy differences. In this push-pull pumping scheme $\frac{f_s}{f_p}$ is relatively large in magnitude corresponding to a high energy conversion efficiency.

5.8.3.9 Millimeter Wave Ladder Line Traveling Wave Maser

This maser[32] used a Karp-type slow wave structure and only four inches of iron-doped rutile to obtain a net gain of more than 30 dB over 2.0 GHz. Operating at $4.2^{o}K$ a multiple pumping scheme was used to make the effective pump frequency nearly 110 GHz. A superconducting magnet was used to provide the necessary magnetic field.

5.8.3.10 A CW Solid State, Push-Pull Maser in the 5-6 Millimeter Wavelength Region[40]

Cavity maser oscillations were observed from 49 to 57 GHz with iron-doped rutile as the active material. Push-pull pumping was employed.

5.8.3.11 A 70 GHz Maser[41]

Maser amplification was obtained at a signal frequency of 70 GHz and a pump frequency of 118 GHz. The iron ion Fe^{+3} was used in a host crystal of TiO_2 (rutile).

Normally, it is assumed that in order to get amplification, the pump frequency must be at least twice the signal frequency. For equal signal and idle relaxation times the inversion ratio, which is the ratio of the inverted population difference with the pump on to the thermal equilibrium population difference with the pump off, is given by the expression[56]

$$I = \frac{f_p}{2f_s} - 1$$

However, in most maser materials, the relaxation times between levels are not equal and the inversion ratio is then given by:

$$I = \frac{f_p/f_s - \left(1 + T_1^{idle}/T_1^{sig.}\right)}{\left(1 + T_1^{idle}/T_1^{sig.}\right)}$$

For this 70 GHz maser the energy levels of the active material were as shown in Fig. 5.7.

Since $T_1^{idle}/T_1^{sig.} = T_{13}/T_{35}$ was less than one, it was found that maser amplification at 70 GHz should be possible for a pump frequency of 120 GHz. This was experimentally proven by constructing a maser in a typical reflection-type spectrometer. A gain of 20 dB has been demonstrated at a bandwidth of approximately 10 MHz.

5.8.3.12 A Zero Field Millimeter Maser[37]

Iron doped rutile was used in both single crystalline and powdered form to obtain a zero field maser operating at 81.1 GHz. Two traveling wave powder masers were constructed by inserting thin slabs of powdered rutile in a waveguide and by filling a straight piece of G-band waveguide completely with powder rutile. Only about 10 dB of electronic gain was observed.

5.8.3.13 Maser Operation at 96 GHz with Pump at 65 GHz[42]

A cavity maser using Fe^{+3}-doped rutile was operated with a signal frequency considerably greater than the pump frequency. The orientation of the dc magnetic field with the crystal axes was chosen so that the energy level configuration was obtained as shown in Fig. 5.8.

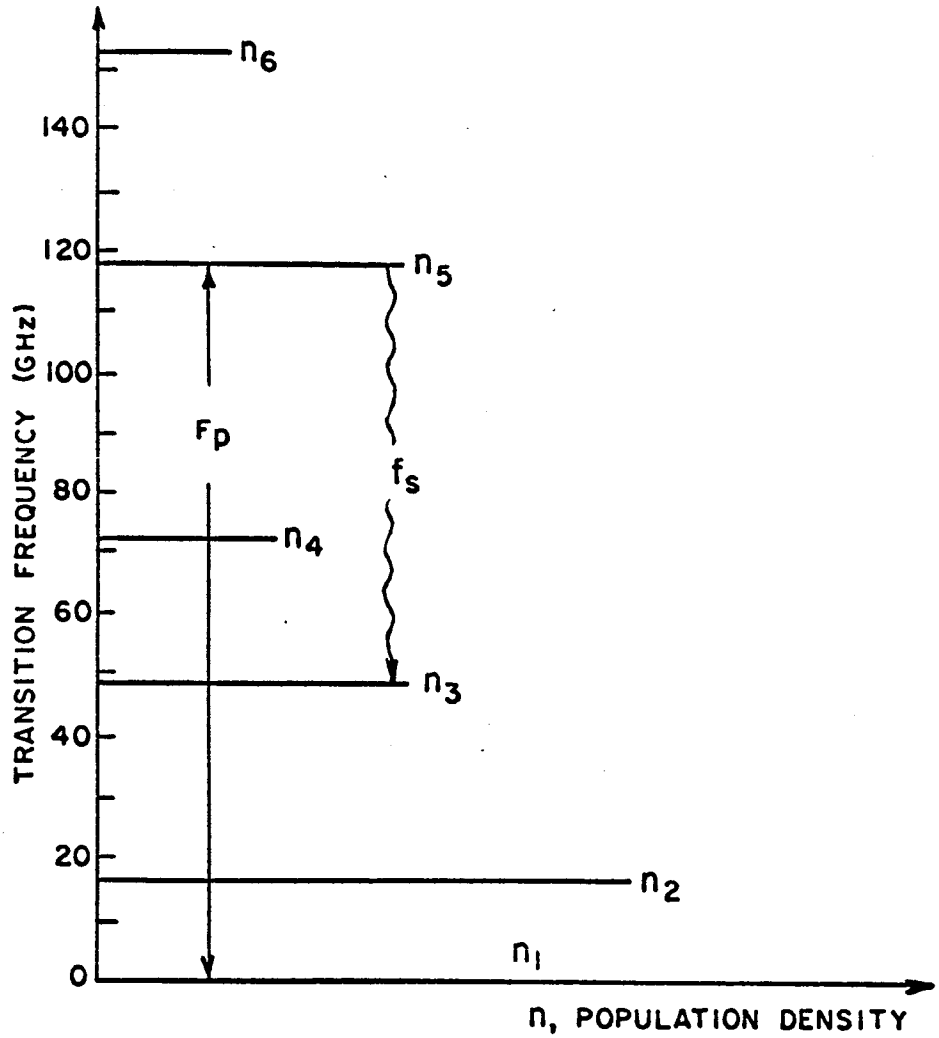

Figure 5.7 Iron-Doped Rutile Maser with f_p = 118 GHz and f_s = 70 GHz

In another instance a signal frequency of 101.05 GHz and a pump frequency of only 70.80 GHz (H = 6.735 Kg) was obtained using Fe^{+3} doped rutile. A pumping configuration has been found which gives a signal frequency of 150 GHz with a pump frequency of 91.05 GHz (H = 6.4 Kg).

Investigation of solid state masers with signal frequency higher than the pump frequency is clearly of great interest to generate submillimeter radiation starting from strong millimeter sources. Work along these lines is also being done at Johns Hopkins University. The requirements on proper combination of electron relaxation times in the different energy levels, however, in this scheme are very critical.

5.8.3.14 Submillimeter Solid-State Masers

The major obstacle in building a submillimeter maser is that of finding an active material which has a reasonable population inversion ratio of at least 10. It also must have a resonance absorption greater than

$$Q_{abs} = 10^3 = \frac{2\pi\sqrt{\epsilon}}{K_{st}\lambda}$$

where K_{st} is the resonance absorption coefficient. Any material not having an electric dipole transition will not make a good submillimeter maser material. Measurements by Rowntree and Chang[77] of the optical constants of $CaWO_4$ and MgO in the wavelength range 100μ to 1 millimeter show that MgO is a good transmitter, especially when cooled to 90°K or below.

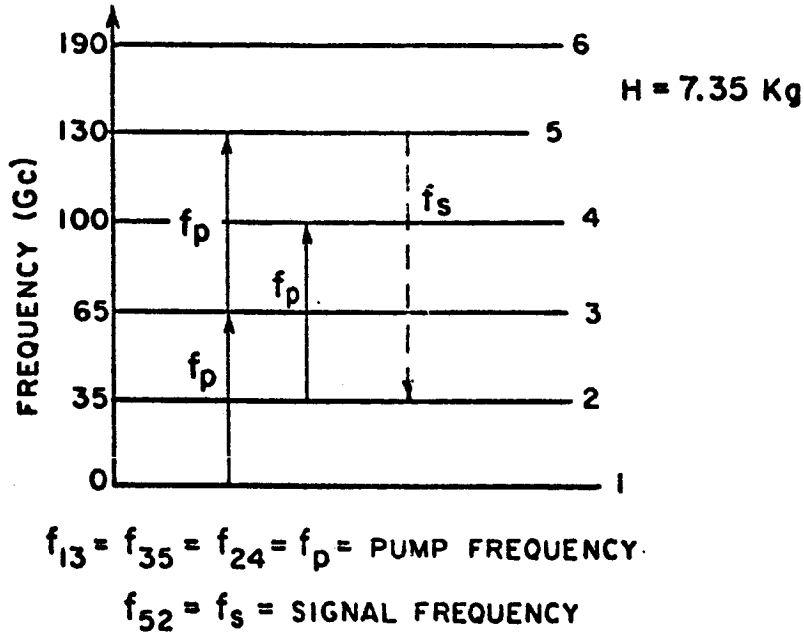

Figure 5.8 Iron Doped Rutile Cavity Maser with a Signal Frequency Larger than the Pump Frequency

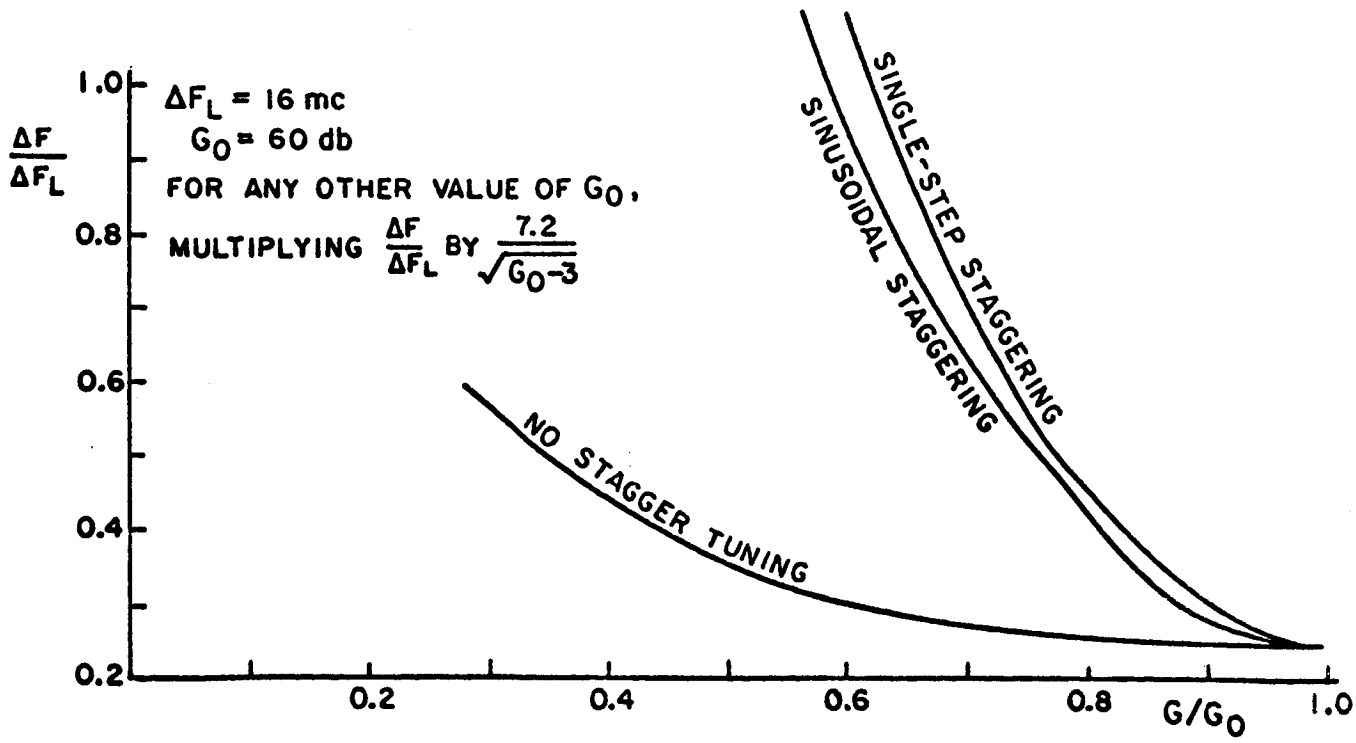

Figure 5.9 Curves of Instantaneous Bandwidth versus Electron Gain

5.8.3.15 Conclusions

A solid state traveling wave maser is mainly applicable in the area of radio and radar astronomy. Table 5-II gives the radiometer figure of merit, which is defined as the ratio of the square root of the bandwidth to the total noise temperature, of various receiving systems.[45] The maser's usefulness is apparent. A very important feature of a traveling wave maser is the possibility of increasing its instantaneous bandwidth by artifically broadening or altering the magnetic resonance line shape. The center frequency of the resonance line can be shifted in discrete sections of the maser structure by varying the magnetic field discretely along the maser's length. This is illustrated in Fig. 5.9 for the case of a maser using chromium-doped rutile as the active material (where the paramagnetic resonance linewidth, ΔF_L = 16 MHz).[46]

Another very important feature is the ease of obtaining nonreciprocal forward gain and nonreciprocal reverse isolation provided a suitable ferrite material can be found at the desired operating frequency. This will cause the amplifier to be unconditionally stable against any combination of input and output mismatches. Because of the problem of finding an adequate reverse isolator material, no traveling wave maser amplifiers have been built above 36 GHz.

Table 5-II

Radiometer Figure of Merit for Various Receiving Systems

Receiver	System Noise Temp. °K	(MHz)	Figure of Merit
A) Superheterodyne Receiver, 7 dB NF	1200	10	2.6
B) Existing Medium-Bandwidth TWT, 6 dB NF	1000	1000	32
C) Existing Cavity Maser System	60	10	53
D) Possible Future TWT, 3 dB NF	300	2000	149
E) Existing Traveling-Wave Maser System	18	25	268

5.8.4 Amplification in Gases

5.8.4.1 MM Wave Amplification by Resonance Saturation in Gases

The response of resonant media to a millimeter wave radiation spectrum consisting of a strong Fourier component at the resonance frequency and weak sidebands is considered.[28] The absorption of the sidebands will depend on the amplitude and phase of the strong component if:

a) the latter appreciably changes the equilibrium population distribution, and

b) the frequency difference between the strong component and the sidebands is not greater than the power-broadened linewidth.

With a strong saturating component, attenuation of the latter and amplification of the sidebands have been obtained at 3.7 millimeters in Fe^{+3} doped TiO_2, first at 3.5 millimeters and later at 1.2 millimeters in the molecular gas $HC^{12}N^{15}$. In the latter case 20 dB of gain was obtained.[29]

In a communication scheme the saturating frequency component may be a local oscillator and the weak sidebands the incoming signal. Use of the Stark effect can make this amplifier tunable. A further advantage of this scheme is its operation at room temperature.

5.8.4.2 The He-Ne Laser Amplifier[22]

a) This is a typical traveling wave amplifier at the characteristic wavelength of 1.15μ where an amplification of 20/1 is obtained by letting the signal enter the rectangular cross-sectioned laser tube and then leave it after 36 traversals of the active length of the He-Ne gas column, during which amplification is achieved by stimulated emission buildup; typically, a 1 mW signal is amplified to 20 mW. Although this device operates in a range of frequencies outside of our immediate range of interest the possibility of a similar technique in the 100μ range should not be overlooked.

b) Submillimeter Maser Amplifier

Amplification by a factor of 2 at 0.377 millimeter has very recently been obtained by passing a signal from a pulsed maser through a discharge in CN.[43]

5.9 SOME NONLINEAR PHENOMENA IN THE MILLIMETER-SUBMILLIMETER RANGE OF FREQUENCIES

5.9.1 General Remarks

The following paragraphs will describe schemes of amplification and generation where a "causal" excitation at a frequency f produces

"effects" at frequencies 2f, 3f, etc. This will occur when the effect expressed as a Taylor series contains second, third and higher order terms.

This kind of nonlinearity can be used for the generation of harmonics, and mixing of two signals for modulation and demodulation purposes.

5.9.2 Hot Electron Devices

The name "hot electron" is given to those electrons of a semiconducting or metallic crystal which, in response to an applied electric field, acquire energies more than the thermal energy of 3/2 kT within a mean free path.

5.9.2.1 Hot Electron Diodes

This is simply a rebaptism of the long known metal-semiconductor rectifying element. The charge carriers which are responsible for the operation of these devices have to gain enough energy to be able to jump over the Schottky barrier, and are consequently "heated." The interest in these devices as far as high frequencies are concerned is due to the fact that the carriers involved are majority carriers and therefore the performance of the device is frequency limited only by the scattering time or the dielectric relaxation time, whichever is lower. With these limits metal semiconductor structures should be able to operate up to frequencies of a few thousand GHz, if other features of the devices such as stray capacitances, etc. do not limit their operation.

Metal point contact rectifiers with both silicon and GaAs have been used for generating up to the 6th harmonic of 70 GHZ.[69] To the best of our knowledge no experimental high frequency limit has been found for these devices.

Another interesting hot electron device is the "Microwave Detector and Mixer"[27] reported by the General Telephone and Electronics Labs., Inc. In this device a point contact is made on either a high resistivity germanium or silicon epitaxial wafer. The contact is nonrectifying; however, when the microwave power is applied to it very large power densities are created under the point "heating up" the majority carriers. A unidirectional thermoelectric voltage is created between the point contact and the base "cool" electrode, which follows the power density variation up to frequencies as high as the reciprocal of the dielectric relaxation time ($\approx$ 100 GHz). The device has been used successfully experimentally at 70 GHz (see also paragraph 9.4.2).

It is clear that the "heating" process in this latter type of device is basically and entirely different from the "heating" process in Schottky barrier type diodes. An easy way of determining whether a given diode is operating as a Schottky barrier diode or a "thermoelectric" detector consists in observing the polarity of the dc voltage developed across the diode. Thus, assuming the diode consists of a small area metallic contact on an n-type semiconductor, the Schottky

barrier rectification mechanism develops a negative voltage at the electrode with respect to the semiconductor, while the thermoelectric detection mechanism develops a positive voltage at the electrode with respect to the semiconductor.

5.9.2.2 Hot Electron Transistors

These are recently developed semiconductor-metal-semiconductor structures which essentially constitute two back-to-back Schottky barriers. C. R. Crowell and S. M. Sze of the Bell Telephone Labs discussed these devices at the Solid States Devices Research Conference (Princeton, July, 1965). Many difficulties have to be overcome in order to make these devices practically useful (such as replacing the emitter semiconductor point contact on the metal by a directly grown, semiconductor single crystal, on the metallic base electrode); however, since the charge carriers of importance in the operation of these devices are majority "hot carriers" very good high frequency performance is expected.

5.9.3 Photoelectric Effects

5.9.3.1 Principle of Operation

The photoelectric effect is intrinsically a "square law" device. Indeed, it is known that the photoelectric current is directly proportional to the number of carriers n excited from the valence band to the conduction band; but n is proportional to the number of photons absorbed, that is, to the absorbed power P_{abs} from the incident electromagnetic radiation. Thus, the photoelectric current I_{ph} is proportional to P_{abs} or E^2 (the square of the electromagnetic radiation electric field). It

would, therefore, seem that the photoelectric effect is an ideal means of mixing two signals of optical frequencies; the difference frequency can easily be made to lie in the submillimeter region (see Sec. 5.2.2.2.4). The basic reason for the failure of such a mixing process is, however, that I_{ph} in all practical cases is proportional to the integral of E^2 over an interval of time τ, i.e.

$$I_{ph} \propto \int_{T_o}^{T_o + \tau} E^2 \, dt$$

It is clear that if τ is comparable to the period of the difference frequency signal, the latter will be averaged to zero. The basic objective of a photoelectric mixing scheme should, therefore, be the reduction of τ to as small a value as possible. The value of τ is determined by two main factors:

a) the lifetime of the photoelectrically generated excess carriers, and

b) the transit time of these carriers in the space charge region.

The application of this principle to photoelectrically generated carriers in a vacuum has recently been demonstrated.[49] Two ruby laser beams of controllable difference frequency were directed at the sensitive surface at definite but almost grazing angles. Outputs at frequencies as high as 40 GHz were observed. However, the values of τ due to electron transit time severely limit the output frequency. It is very unlikely that the vacuum technique would be of value at higher frequencies.

A similar technique which is not photoelectric in nature, mixes two neodynium laser beams in a quartz crystal.[53] The efficiency was extremly low, however, producing 5×10^{-7} watts at 100 μm for 1 kW input. The operation depends on the birefringent effect in crystals. In another version the nonlinear electro-optic effect in cadmium sulfide was used to beat the output of a neodynium laser with the laser stimulated Stokes-Raman emission to produce radiation at 944 μm.[54] The calculated output power was 1.5 watts. Recently, "high speed" photoelectric heterojunctions were developed, as described below, which have better response by several orders of magnitude.

5.9.3.2 A High Speed Heterojunction Photodetector

It consists essentially of a GaAs→GaAsP junction. A detailed description of this device in given in Ref. 24.

It is found that as the As atoms of the GaAs semiconductor are replaced by P atoms, the forbidden energy gap increased from 1.4 eV up to 2.2 eV for GaP. An epitaxially grown junction as shown in Fig. 5.10 is thus constructed.

The first interesting feature of such a structure is that when the photon $h\nu$, emitted from a GaAs diode injection laser, is incident on the upper face of the device, the p^+ layer of $GaAs_xP_{1-x}$ which has a large energy gap is completely transparent to $h\nu$, consequently the radiation is absorbed almost entirely within the space charge region. The latter can be made very narrow (1μ in Ref. 24). With the saturated

velocity of the photoexcited carriers, which is close to 10^7 cm/sec, the response time of such a device is of the order of 10^{-11} sec ($\approx$ 100 GHz). Efforts at mixing two GaAs diode laser emitted optical signals in this photodevice were successful in producing energy at the difference frequency of 39.4 GHz in a waveguide. With the possible pressure tuning of semiconductor diode lasers and the possibility of improving further the speed of these photocells, a continuously variable frequency signal in the millimeter range seems to be rather easily obtainable from this scheme.

5.9.3.3 High Speed Point-Contact Photodiodes

The structure of these diodes[31] is as shown in Fig. 5.11(a) and (b); the photodiode here is a point contact structure where the semiconductor is made of an epitaxial (relatively high conductivity) layer of Ge or Si of about 2 microns, grown on a low resistivity substrate. These diodes are "laser formed" as opposed to the usual "pulse formed" point contacts; an ohmic metal-semiconductor contact is believed to result from this process. It is clear that the structure of these diodes, together with the direction of photoexcitation, determines the very short transit time of photocarriers (see 5.9.3.1) in the thin (1 μ thick) semiconductor layer under the point contact where the electric field is also very high. Detection of 3 GHz modulation signal carried by an amplitude modulated laser beam is reported in Ref. 31. It appears that very short response time, with a probable limit of about 10^3 GHz, can be achieved by careful

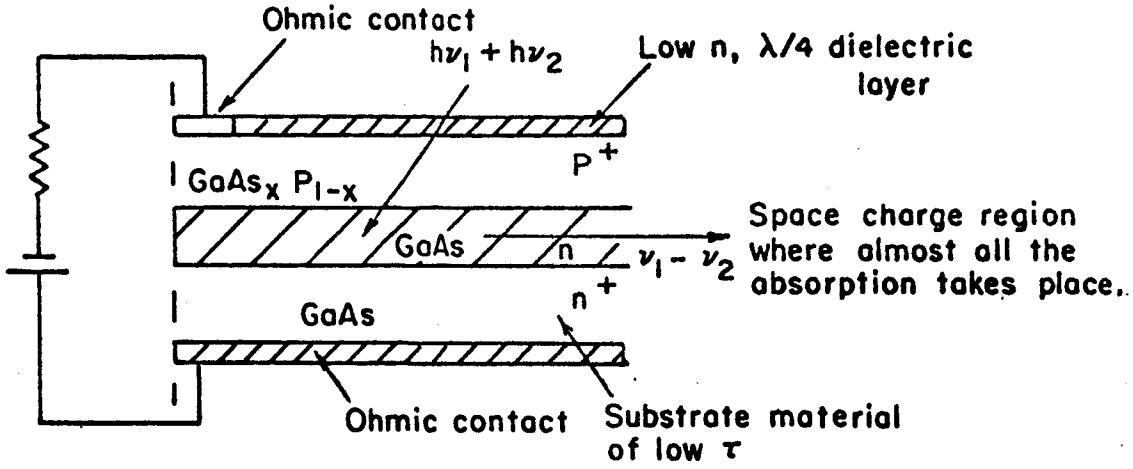

Figure 5.10 Heterojunction for Photoelectric Mixing

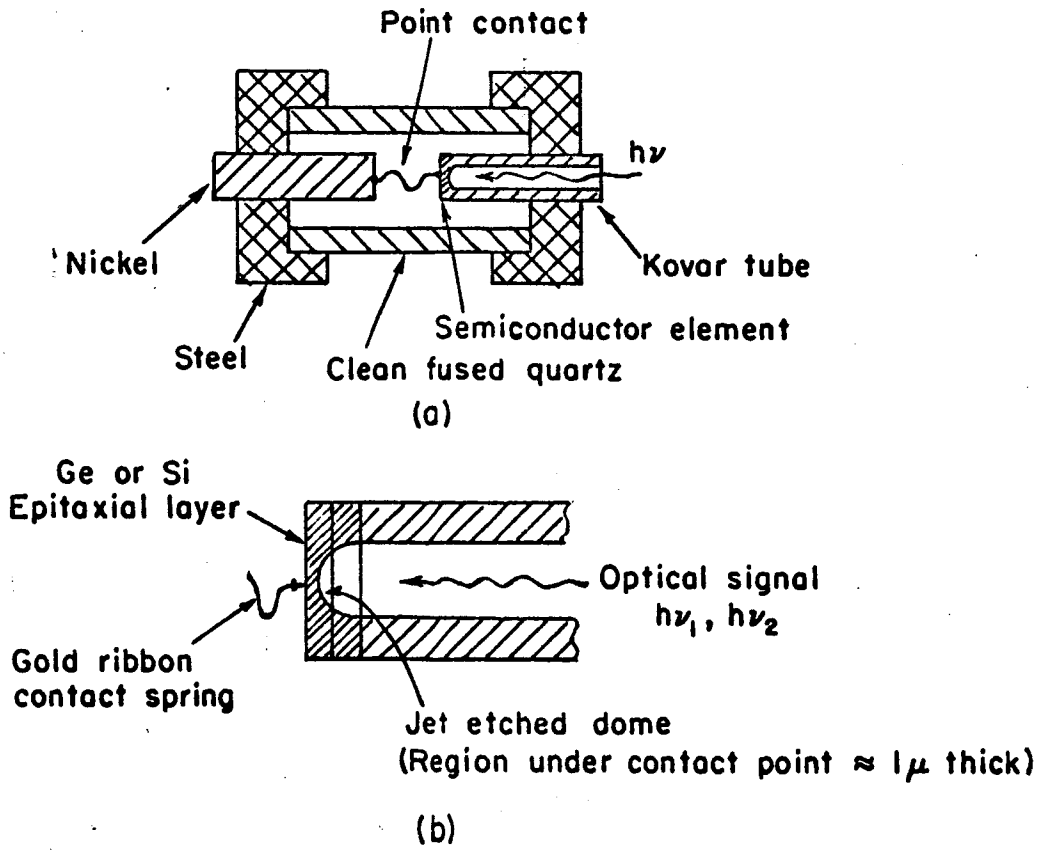

Figure 5.11 High Speed Point Contact Photodiode

variations of this type of structure; it would then be possible to use this element both as a detector for submillimeter frequencies and as a generator, resulting from the mixing of two laser beams.

5.9.4 GAS PLASMA GENERATION

The generation of harmonics in a gas discharge is an effect that has been studied experimentally and, to a limited extent, theoretically. In one technique, breakdown is established across a gap either by direct voltage or by the fundamental frequency power. With 14.7 watts applied at 34 GHz, 440 milliwatts (-15.2 dB) of second harmonic power was obtained. The effect is believed due to the oscillation of electrons in the non-uniform field of the electrodes. The nonlinearity is reactive and therefore, theoretically, conversion efficiency should be 100%, waveguide losses accounting for the overall conversion loss.

No estimates of the upper frequency limit of this technique have been made, but a careful investigation seems warranted to determine if the factors involved can be properly controlled, and to establish theoretical limitations.

Another similar type of harmonic generator described first by Froome[78] provides narrow-band coherent radiation at a number of frequencies in the 200-1000 GHz range. Operation of this device consists of coupling approximately 5 watts of 35 GHz signal to an arc maintained between platinum electrodes in an argon plus 6% hydrogen environment at 2000 lbs/sq. in. Power densities of the applied signal in the arc

approach 1 mW/cm^3 or field strengths of the order of 3 kV/cm. The high field intensities and the strong nonlinear nature of the arc are responsible for the harmonic generation. Typical performance of commercially available units is given in the table below.

Harmonic	Frequency [GHz]	Measured Output [μW]	Conversion Loss [dB]
6	210	100	47
12	420	1	67
20	700	0.01	87
29	1015	0.001	97

5.10 THE JOSEPHSON EFFECT

Recently, more interest has been concentrated on the phenomenon of superconducting tunneling otherwise known as the Josephson effect. The device consists essentially of a sandwich of a very thin insulating oxide layer (about 10 Å in thickness) between two superconducting metal strips. The metal could be Al, Pb, or Sn.

When the oxide layer is relatively thick, the I-V characteristic of the device shows a very strong nonlinearity in the form of a 90° kink at a voltage V corresponding to the superconducting energy gap $\Delta(T)$ of Cooper pairs such that

$$eV = 2\Delta(T)$$

Under these conditions the Cooper pairs of the two superconducting strips are not correlated to each other.

However, when the oxide thickness is reduced to below 10 Å the Cooper pairs of the two metal strips become strongly coupled and a dc Josephson tunneling supercurrent flows through the device at V=0. When this current reaches a certain maximum value the device switches to an operation mode similar to that with a thick oxide layer.

In addition to the direct supercurrent, Josephson had also predicted that an alternating supercurrent should be present when the junction is biased at a finite voltage V, the frequency ν of this current being

$$\nu = \frac{2eV}{h}$$

corresponding to 483.6 MHz per microvolt of applied voltage. It is, of course, this ac effect which is of interest to us. A comprehensive article dealing with this effect is "Josephson Type Superconducting Tunnel Junctions as Generators of Microwave and Submillimeter Wave Radiation," by D. N. Langenberg, et al.[70]

The AC Josephson effect was only recently directly observed; the observation by D. N. Langenberg et al was made on a Sn-Sn Oxide-Sn structure at 1.2°K at 9 GHz. The measured output power was of the order of 10^{-12} watt; however, it is believed that most of the power is not extracted from the device because of a mismatch of the order of 10^{-5}. An efficiency close to 100% is believed to be inherent to the device which should then provide signals of the order of 10^{-6} watts.

The upper frequency limit of this device is determined by photon absorption. Sufficiently high energy photons will break up superconducting pairs into ordinary electrons: the upper frequency limit, ν_{max}, is given by the following relation:

$$h\nu_{max} = 2\Delta(T)$$

ν_{max} is about 350 GHz for Sn, 650 GHz for Pb and 800-1000 GHz for Pb-Bi alloys.

The advantages of this device appear to be

a) voltage-tunable frequency output

b) minimal power supply requirement

On the other hand, liquid helium temperatures are necessary. This device, besides being a source of energy, can be used as a detector or harmonic generator because of its very strong I-V characteristic nonlinearity.

5.11 CONCLUSIONS

In this chapter some of the latest efforts in generating millimeter-submillimeter radiation using different quantum-electronic phenomena have been described. Although not all the attempts toward this goal are presented here, an effort was made to cover all schemes which looked promising from the point of view of practical application. We can conclude on the basis of this study that, since the review of generation schemes is now basically completed, efforts should be concentrated on the improvement and refinement of a large number of promising schemes herein described.

5.12 REFERENCES TO CHAPTER V

1. W. Culshaw, "The Fabry-Perot Interferometer at Millimeter Wave Length," Proc. Phys. Soc., B, vol. 66, pp. 597-608, July 1953.

2. W. Culshaw, "Reflectors for a Microwave Fabry-Perot Interferometer," PGMTT, 1958.

3. A. Yariv and J. Gordon, "The Laser," Proc. IEEE, 51:4, January 1963.

4. R. J. Phelan, A. R. Calawa, R. H. Rediker, "Infrared InSb Laser Diode in High Magnetic Fields," Appl. Phys. Letters, vol. 3, No. 9, Nov. 1963.

5. C. H. Townes and A. L. Schawlow, MICROWAVE SPECTROSCOPY, McGraw-Hill Book Co., Inc., New York 1955.

6. F. S. Barnes, "Masers and Millimeter Waves," Proceedings of the IRE, vol. 51, No. 1, Jan. 1963, pp. 115-119.

7. S. M. Bergmann, "Submillimeter Wave Maser," J. Appl. Phys., vol. 31, pp. 275-276, February 1960.

8. A. Crocker, H. A. Gebbie, et al., "Stimulated Emission in the Far Infra-Red," Nature, vol. 201, p. 250, January 18, 1964.

9. H. A. Gebbie, et al., "Stimulated Emission Source at 0.34 Millimeter Wavelength," Nature, vol. 202, p. 685, May 16, 1964.

10. Bell Telephone Record, February 1965, John Rodda and Louis Enloe.

11. D. Marcuse, "Stimulated Emission of Bremsstrahlung," Bell System Technical Journal, pp. 1557-1571, vol. 41, 1962.

12. J. B. Gunn, "Instabilities of Current in III-V Semiconductors," IBM J. Res. and Dev., pp. 141-159, April 1964.

13. B. W. Hakki, "C. W. Microwave Oscillations in GaAs," International Solid State Circuits Conference, February 18, 1965, Session V, THAM 5:1.

14. R. D. Larrabee and W. A Hicinbothem, "Observations of Microwave Emission from Indium Antimonide," International Conference on the Physics of Semiconductors, Paris, France, 1964.

15. H. Kroemer, "Negative Effective Maser in Semiconductors," Progress in Semiconductors, 4, pp. 2-34, 1960.

16. L. E. S. Mathias and A. Crocker, "Stimulated Emission in the Far Infrared from Water Vapour and Deuterium Oxide Discharges," Physics Letters, 13, 35 (1964).

17. L. E. S. Mathias, A. Crocker and M. S. Wills, "Laser Oscillation at Submillimeter W velengths from Pulsed Gas Discharges in Compounds of Hydrogen, Carbon and Nitrogen," SERL, Technical Journal, Vol. 15.

18. L. N. Large and H. Hill, Applied Optics, Vol. 4, p. 625, May 1965.

19. P. A. Sturrock, "Action Transfer and Frequency-Shift Relations in the Nonlinear Theory of Waves and Oscillations," Technical Note, Contract AF 49(638)-415, Project No. 4750, ML Report 625, Sept. 1959.

20. "Development of a Low-Noise Millimeter-Wave Parametric Amplifier," Contract DA 36-039-AMC-02365(E), Reports 1 to 5.

21. P. Penfield, Jr., "Maximum Cutoff Frequency of Varactor Diodes," Proceedings of IEEE, April 1965, p. 422-423.

22. L. E. S. Mathias, N. H. Rock, "A Helium-Neon Laser Amplifier," Applied Optics, Jan. 1965.

23. F. R. Arams, B. J. Peyton, "Eight Millimeter Traveling-Wave Maser and Maser-Radiometer System," Proc. of IEEE Jan. 1965, p. 12-23.

24. W. J. Moroney, Technical Report No. AFAL-TR-64-270, prepared under contract AF 33(657)-10925 by Microwave Associates, Inc., Burlington, Mass., AD 609625.

25. Special issue of the IEEE, PGED January, 1966, on the Gunn effect and devices using the Avalanche effect.

26. W. T. Read, Jr., "A Proposed High-Frequency Negative Resistance Diode," The Bell System Technical Journal, Vol. 37, 1958, p. 401.

27. R. I. Harrison, J. Zucker, "Microwave Detection and Mixing Using the Thermoelectric Effect of Hot Carriers in Semiconductors," J.A.P.L., Nov. 1, 1963, Vol. 3, No. 9.

28. B. Senitzky, G. Gould, "Millimeter-Wave Amplification by Resonance Saturation," TRG, Syosset, N. Y. Final report, Contract AF 30 (602)-2744, Dec. 1963.

29. Electronic News, June 13, 1966.

30. D. Marcuse, "A Further Discussion of Stimulated Emission of Bremsstrahlung," B.S.T.J., Vol. XLII, No. 2, p. 426; March, 1963.

31. M. DiDomenico, Jr. W. M. Sharpless, J. J. McNicol, "High Speed Photodetection in Germanium and Silicon Point-Contact Photodiodes." Applied Optics, Vol. 4, pp. 677-682, June, 1965.

32. L. C. Morris, D. J. Miller, "Traveling-Wave Masers Employing Iron-Doped Rutile," Proc. of the IEEE, vol. 52, no. 4, April, 1964.

33. H. Genitsen, S. Harrison, H. Lewis, "Chromium-doped Titanium as a Maser Material," J. Appl. Phys., vol. 31, no. 9, p. 1566, Sept. 1960.

34. Haddad and Rowe, "X-Band Ladder-Line Traveling Wave Maser," IRE Trans. on M.T. and T., vol. MTT-10, p. 3, January, 1962.

35. E. Ammann, "A Broadband Solid State Microwave Maser Operating at 77°K," IEEE Trans. on M.T. and T., vol. MTT-13, no. 2, p. 186, March, 1965.

36. G. Friedman, A. Nagy, "Iron Sapphire Maser with No Magnetic Field," Proc. of IEEE, p. 362, February, 1963.

37. W. Hughes, C. Kremenek, W. Richards, "Development of Millimeter and Submillimeter Maser Devices," Contract No. AF 33(657)10472, February, 1965.

38. E. Schimitschek, E. Schwartz, W. Turnbull, "Four-level Ku-band Maser," Proc. of IEEE, p. 364, February, 1963.

39. S. Foner, L. R. Momo, "CW Millimeter Wave Maser Using Fe^{+3} in TiO_2," Journal of Applied Physics, vol. 32, no. 4, April, 1960.

40. D. Carter, "A CW Solid State, Push-Pull Maser in the 5 to 6 Millimeter Wavelength Region," Journal of Applied Physics, vol. 32, no. 12, December, 1961.

41. W. Hughes, C. Kremeneck, "70 Gc Maser," Proc. of IEEE, p. 856, May, 1963.

42. W. Hughes, "Maser Operation at 96 Gc with Pump at 65 Gc," Proc. of IRE, vol. 50, No. 7, p. 1691, July, 1962.

43. H. A. Gebbie, "Submillimeter Maser Amplification and Continuous Wave Emission", Nature 2, July, 1966, p. 62.

44. H. Kroemer, "Nonlinear Space-Charge Domain Dynamics in a Semiconductor with Negative Differential Mobility," IEEE Transactions on ED, Vol. 13, No. 1.

45. P. Das, P. W. Staecker, "Upper Frequency Limit for Gunn Oscillations Imposed by Carrier Energy-Relaxation Time." Electronics Letters, July, 1966, Vol. 2, No. 7, p. 258.

46. R. A. Giblin, "Improvement in Efficiency of a Gunn-Effect Oscillator with Change of Geometry," Electronics Letters, July, 1966, Vol. 2, No. 7, p. 236.

47. B. Lax, CYCLOTRON RESONANCE MASER, in "Advances in Quantum Electronics," (J. R. Singer, ed.) Columbia University Press, New York, 1961.

48. R. L. Bell and R. T. Rogers, Final Report, "Extremely High Frequency Maser Amplifier Study Program," Contract AF 33(657)-9192, May, 1965.

49. J. C. Bass and J. A. Jones, "Observation of Microwave Beats in a Parallel-Plate Transmission-Line Photomixer," Electronic Letters, Jan., 1966, pp. 25-26.

50. C. A. Burrus, "Millimeter Wave Oscillations from Avalanching p-n Junctions in Silicon," Proc. IEEE, Sept., 1965, pp. 1256-1257.

51. G. M. Zverev, A. M. Prokhorov and Shevchevko, "Generation of Millimeter Waves in Optically Pumped Ruby," Proc. of 3rd Conference on Quantum Electronics, Paris, 1963, p. 963.

52. H. Hsu and F. K. Tittel, "Optical Pumping of Microwave Masers," Proc. IEEE, Jan., 1963, pp. 185-189.

53. F. Zernike, "Generation of Coherent Far Infrared Difference Frequencies," 1966 Quantum Electronics Conference, Phoenix, Arizona.

54. M. D. Martin and E. L. Thomas, "Infrared Difference Frequency Generation," 1966 Quantum Electronics Conference, Phoenix, Arizona.

55. D. C. Hanson, J. E. King, J. E. Rowe and C. Yeh, "Solid-State Microwave Research," Int. Sc. Rep. No. 3, 1 Apr.-1 July 1964, Univ. of Michigan, AD 447 667.

56. A. E. Siegman, "MICROWAVE SOLID-STATE MASERS," McGraw-Hill Book Co., 1964, p. 247.

57. Paper by J. M. Besson at the Solid State Device Research Conference in Princeton, June, 1965, and by I. Melngailis, A. J. Strauss and J. O. Dimmock at the SSDRC in Evanston, Ill., June 1966.

58. R. Bowers, et al, Phys. Rev. Lett. 7 (1961).

59. A. Libchaber and R. Veilex, Phys. Rev. 127, 274 (1961).

60. G. A. Williams and G. E. Smith, IBM J. Res. Rev. 8, 276 (1964).

61. R. Bowers and M. C. Steele, Proc. IEEE 52, 1105, (1964).

62. R. D. Larrabee and W. A. Hicinbothem, "Observations of Microwave Emission from Radium Antimonide", International Conference on the Physics of semiconductors, Paris, France, 1964.

63. S. Kakikana and L. Buckmiller, "Two-stream Instabilities in Solids as Millimeter to IR Sources." International Electron Devices Meeting, October, 1966, Washington, D. C.

64. L. S. Bowman, C. A. Burrus, and H. J. Muller, "Fundamental Oscillation of Avalanching Solicon p-n Junction Diodes in the 70 to 140 Gc Range." Solid State Device Research Conference, June, 1966, Evanston, Ill.

65. Packard, "Millimeter Wave Semiconductor Diode Detector, Mixers and Frequency Multipliers," in Proc. IEEE, April, 1966.

66. C. A. Burrus, "Formed-point Contact Varactor Diodes Utilizing a Thin Epitaxial Gallium Arsenide Layer," Proc. IEEE (Correspondence) Vol. 51, pp. 1777-1778, December, 1963.

67. L. E. Dickens, "Millimeter Wave Diodes for Harmonic Power Generation," NASA Contract No. NASw-1000, and U. S. Army Electronics Command, Ft. Monmouth, under Contract No. DA 36-039 AMC-02347(E).

68. Jeffery Frey, "Study of Millimeter Bulk Semiconductor Effects," Quarterly Report No. 2, 1st October to 31 December 1965, Contract No. NAS 12-24, Mathias-Johnson.

69. F. L. Wentworth, J. W. Dozier and J. D. Rodgens, "Millimeter Wave Harmonic Generators Mixers and Detectors," Microwave Journal, June, 1964, Volume VII, No. 6, p. 69-75.

70. D. N. Langenberg, D. J. Scalapino, and B. N. Taylor, "Josephson Type Superconducting Tunnel Junctions as Generators of Microwave and Submillimeter Wave Radiation," Proc. of IEEE, Vol. 54, April, 1966, 560-575.

71. W. C. Chang and R. F. Rowntree. International Conference of Quantrum Electronics. Proc. of 1963 conference in Paris, pp. 677-684.

72. "Laser Action in Optically Pumped CN, " M. A. Pollack, pp. 230-2, Appl. Phy. Letters, 15 Sept. 1966.

73. G. T. Flesher, W. M. Muller, "Submillimeter Gas Laser", Proc. of IEEE, April, 1966, pp. 543-546.

74. H. Steffen, P. Schwaller, J. F. Moser and F. K. Kneubuhl, "Mechanism of the Submillimeter Laser Emissions from the CN Radical." Phys. Letters, Vol. 23, No. 5, 31 October 1966.

75. G. N. Chantry, H. A. Gebbie and J. E. Chamberlain, Nature 205 (1965) 377.

76. H. P. Broida, K. M. Evenson and T. T. Kikuchi, J. Appl. Phys. 36 (1965) 3355.

77. W. C. Chang, R. F. Rowntree, International Conference on Quantum Electronics, Proc. of 1963 Conf. in Paris, pp. 677-684.

78. K. D. Froome, "Microwave Harmonic Generator Capable of Frequencies in Excess of 600 GHz," Nature, Vol. 193, March, 1962, p. 1169.

Chapter VI

MODULATION

6.1 INTRODUCTION

Methods employed in the modulation of millimeter and submillimeter wavelengths are relatively few. The majority of these methods are extensions of techniques used in either the microwave or the optical regions of the spectrum. These methods can be divided into two general categories:

1. Internal modulation methods by which an output characteristic of a millimeter or submillimeter wave source is controlled by some internal mechanism of the source itself.

2. External modulation methods by which a characteristic of the output of a millimeter or submillimeter beam is controlled by inserting an electrically or magnetically activated "modulator" in its path.

In order to utilize fully the relatively wide bandwidths available with millimeter and submillimeter wave sources, the modulation methods used should be sufficiently fast. Other properties desirable in modulators at these wavelengths are small power requirements and simple operation. Also, small size and low weight become desirable where space applications are concerned.

6.2 INTERNAL MODULATION METHODS

Both frequency and amplitude modulation of rectilinear beam interaction devices* (klystrons, laddertrons, O-type carcinotrons), and

---

* These devices employ straight electron beams. Magnetic fields are used purely for beam confinement.

some crossed field devices such as the M-type carcinotron, are possible. In reflex klystrons, modulation is normally obtained by variation of the reflector voltage. O-type carcinotrons can be tuned over a frequency range of approximately 7% of the center frequency by varying the beam voltage. The laddertron, which is a tunable single cavity multigap klystron, has features that enable frequency modulation with the control electrode voltage. Typically, modulation sensitivities of 0.2 MHz/V to 0.4 MHz/V, respectively, are attainable by varying either the resonator voltage alone or the control electrode voltage.

The limitation of internal modulation techniques is the inability to perform frequency modulation without also affecting the output power. This can be overcome by the use of equalizers and complex feedback techniques.

6.3 EXTERNAL MODULATION

The operation of these modulators is based on one of the following effects:

1. change in the absorption properties of a semiconductor
2. diode switching
3. Faraday effect
4. electromechanical displacement

In the following sections a survey of these methods, their properties and potential, is presented.

6.3.1 Free Carrier Absorption Modulators

The phenomenon of free carrier absorption of radiation in semiconductors has been studied by a number of workers.[1,2] The absorption in

the submillimeter wavelength range can be attributed to the interaction of the incident radiation with the free carriers in the semiconductor.[2] This effect has been utilized in infrared modulators[3] by injecting carriers into an n-type germanium bar through which the infrared beam is transmitted. The frequency response of this type of modulator is determined by the lifetime of the injected (minority) carriers. Typically, n-type germanium with a minority carrier lifetime of a few microseconds is used for this type of modulator. Hence, the modulation rate is restricted to frequencies less than one magahertz.

Amplitude modulation of infrared and submillimeter wave radiation using free carrier absorption in either forward or backward biased p-n junction diodes has been the subject of numerous recent articles.[3-8] Forward biased junctions do not have a very wide frequency response and require large driving powers. The backward biased version of this modulator, proposed by Renton[6], seems to be potentially capable of overcoming these limitation.[7] At the present time, insertion loss and harmonic distortion seem to limit the modulation index of this modulator to low values.

In the absorption type modulators described above, the phenomenon of minority carrier injection into semiconductors or p-n junctions is utilized. The converse effect of carrier extraction[9] can also serve as the basis of similar modulators.

A novel modulator that employs both of these phenomena has been described by Gunn and Hogarth.[10] The combination effect employed is referred to as "magnetic rectification." Here, the number of free

carriers in a thin rectangular slab of long lifetime germanium is varied by driving them to surfaces of either high (surface treated by abrasion) or low (etched surface) surface recombination velocity. An external magnetic field is applied parallel to these surfaces and current is passed through ohmic contacts on the narrow sides of the slab. The entire structure is placed in a waveguide as shown in Fig. 6.1. The slab is normally introduced in the waveguide at an angle $\phi \simeq 30^{\circ}$ to reduce reflections. Attenuation changes as large as 15 dB are attainable with n-type, 40 ohm-cm, 0.006 inch thick germanium. The response time was also of the order of a few microseconds.

The effect of high electric fields on the absorption of n-type germanium at millimeter wavelengths (8 millimeter) observed by Arthur, et al[11] can serve as a basis for a pulse modulator with a theoretical rise time of the order of 10^{-12} sec. The effect is due to the saturation of electron drift velocity in germanium in the presence of high electric fields as low as 10 V/cm. A typical modulator arrangement utilizing this effect would consist of a thin slab of germanium of suitable resistivity ($\sim$ 5 ohm-cm) inserted longitudinally in a waveguide through slots cut in the center of the upper and lower walls. The variation of attenuation with applied electric field is not linear; therefore, this effect is most applicable in pulse modulation.

A significant result of Arthur's work is that the change in attenuation in dB caused by electric fields less than 500 V/cm is proportional to the observed signal amplitude. The fast time constant of

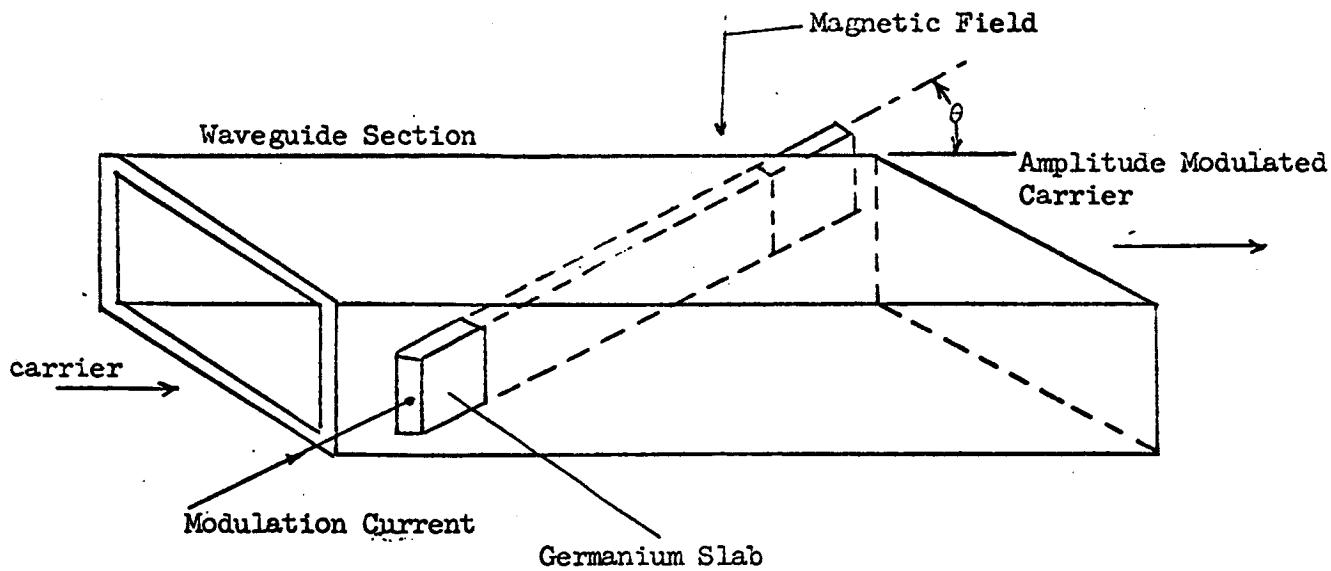

Figure 6.1 Magnetic Rectifier Modulator

this effect, added to its simplicity and low power consumption, recommends further investigation of its applicability to shorter millimeter wavelengths.

Another absorption type modulator developed is the P-I-N modulator. The main part of this modulator consists of a P-I-N germanium structure introduced into a waveguide in such a fashion that the heavily doped p and n regions are outside the guide, the intrinsic part of the structure alone being exposed to the field in the waveguide. This part behaves as a nearly insulating dielectric. When a forward voltage is applied to contacts on the n and p regions, electrons and holes are injected into the intrinsic region where they absorb microwave power, thus causing an attenuation of the power transmitted down the waveguide. Absorption variation of 11 dB was reported[12] with a variation of 15 mA in the dc current flowing through the structure. The maximum power consumption was of the order of 10 mW. The insertion loss of this modulator is of the order of a few dB. The maximum modulation frequency applied between the contacts is determined by the average lifetime of an electron-hole pair in the intrinsic region. The response of the modulator is practically independent of modulation frequency only up to 5 kHz and drops by 3 dB at 50 kHz.

At the cost of higher insertion loss the length of the active region of the modulator can be made longer. This enables, for example, modulation of the response of the entire bandwidth of a 70 GHz klystron. The device was successfully used also at 120 GHz.

It has also been shown[13,14,15] that modulators using two or more P-I-N diodes properly spaced as shunt elements along the gap of a ridged waveguide can provide broadband operation up to a carrier frequency of 18 GHz.

Experimental investigations[16] of the feasibility of extending the operation of these modulators to 40 GHz shows that this can be accomplished by reducing the dimensions of the diodes and using encapsulated versions in a ridged waveguide arrangement. A minimum on/off ratio of 10 dB with an insertion loss less than 2 dB can be obtained over a 1.5 to 1 band of frequencies, 26-40 GHz.

This P-I-N modulator has advantages similar to the point contact diode modulator, (discussed next), i.e.,it is a small device with small power consumption. It, furthermore, has the advantage of not requiring an isolator or a circulator as in the case of the point contact diode modulator because its operation depends on the change in absorption rather than in reflection. The P-I-N modulator has the disadvantage of a relatively slow response.

6.3.2 The Point Contact Diode Modulator

Microwave switching techniques using semiconductors have been discussed and investigated by a number of workers.[24-27] Successful operation of a germanium point contact diode modulator operating at 35 GHz was reported by Cave, et al.[17] in 1959. The principle of operation of this device is its capacitance variation with bias. Low resistivity n-type germanium (1-10 ohm-cm) was used. By placing the diode in a waveguide section and applying an appropriate bias, the diode

can be made to represent either a low or high impedance, thereby reflecting the incident power. These diodes have the advantages of withstanding overloading without damage and can typically modulate several hundred milliwatts of carrier power with a response time of less than 3×10^{-9} sec. Waveguide pulse modulators incorporating this diode have a typical insertion loss of 2 dB. There is no reason why such a modulator could not be made to perform an equivalent task at wavelengths shorter than 8 millimeters.

6.3.3 Ferrite Modulators

The magnetic properties of ferrites are essentially identical to those of ferromagnetic metals.[18] Their resistivities, however, are extremely high (10^6 to 10^8 ohm-cm compared to 10^{-5} for iron). Due to this unique property microwaves can easily penetrate a substantial length of ferrite. Consequently, strong interaction occurs between the wave and the spinning electrons which are responsible for the magnetic properties of the ferrite. As a result of this interaction a non-reciprocal effect known as Faraday rotation is manifested. This effect has been utilized in the construction of microwave phase shifters, isolators, and amplitude modulators. Ferrite modulators are usually capable of handling larger powers than, for example, crystal diode modulators. The signal frequency is normally applied to a magnetizing coil surrounding a ferrite rod placed normally in a circular waveguide section with transitions to rectangular waveguide on both ends. The Faraday effect

consists of the rotation of the plane of the polarization experienced by a linearly polarized carrier wave incident on one edge of the rod. The angle of rotation Ø depends on a longitudinal magnetizing field supplied by the modulating signal.

Faraday modulators operating at x-band were designed and constructed by Morris[19] who achieved a first-order sideband conversion efficiency of the order of 15 to 20 dB for modulating frequencies in the lower end of the megacycle spectrum (~ 10 MHz). The insertion loss was of the order of 0.5 dB. Usual x-band ferrite materials were found to be unsatisfactory due to overheating. Nickel ferrite compositions with excess magnesia and magnesium-manganese ferrite R-1 were used to overcome this problem.

Broadband absorption type ferrite modulators for high speed switching and amplitude modulation have been constructed for the higher microwave frequencies.[20] These absorption type amplitude modulators use a longitudinally magnetized ferrite rod split along its length and centrally located inside a standard rectangular waveguide. A thin resistive film inserted in the ferrite slot, which is aligned perpendicular to the input RF electric field, is used to attenuate the perpendicular mode generated in the waveguide. The degree of absorption is controlled by the magnitude of the magnetizing field. Modulation with frequencies up to 100 kHz and switching times of less than 1μsec. were obtained at x-band. The insertion loss is small, of the order of 0.5 dB.

Eventual development of Faraday modulators in the millimeter and submillimeter wavelengths, where the available bandwidths are in the megacycle range, depends upon finding suitable ferrite materials that could handle modulation frequencies of that order without appreciable overheating. Hexagonal crystal materials such as cobalt-barium, magnesium-barium, and nickel ferrites, described by Jonker,[21] et al., exhibit low losses and should be suitable for signal frequencies in the 100 GHz range. Their practicality, however, is yet to be investigated.

The high power requirements and the bulkiness of ferrite modulators, together with their limited modulation frequency capability, somewhat curtail their extension to millimeter and submillimeter wavelengths.

6.3.4 Electromechanical Modulator

Electrically controlled mechanical displacements are of interest for certain microwave and millimeter-wave devices. In ferroceramic materials such as solid solutions of barium zirconate and barium stannate in barium titanate, small electrical displacements can be produced by either electrostriction or the reverse piezoelectric effect. A change in linear dimension of 0.05% can be obtained in these materials by application of fields up to 10 kV/cm.[22] The magnitude of the deformation is proportional to the square of the applied electric field and the direction of expansion is in the direction of the field. Electrically controlled slot attenuators using a plate of ferroceramic material fitted in a waveguide, such that a small air gap is left between the

upper guide wall and the upper edge of the plate, have been constructed using this principle. One can envision a similar arrangement of such an element for the purpose of amplitude modulation of a millimeter-wave CW signal.

The small and accurately controlled displacements are consistent with the small size waveguides at such wavelengths.

Amplitude modulators employing this phenomenon have been constructed and tested at f = 9.4 GHz.[23] Modulation factors of 50 to 60% were achieved. The disadvantage of the required high voltages can be overcome by using a number of electrodes embedded in the ferroceramic slab. The modulator is simple in design, and its power consumption is very small since the slab is a capacitive load. Time constants of the order of 10^{-6} sec allowing modulation with frequencies up to 10^{6} cps are apparently attainable.

6.4 CONCLUSIONS AND RECOMMENDATIONS

The survey of the current state of the art of millimeter and submillimeter wave modulation indicates that:

1. The field of modulation is open for developments which could be accomplished by either extension of microwave or optical techniques (see "Selected References" at end of chapter) to this frequency range, or by development of new methods specifically suitable for millimeter and submillimeter wavelengths, such as modulators that utilize rotational interaction between radiation at those wavelengths and matter. Both of these courses are strongly dependent on finding materials with suitable properties. Specifically, the following are recommended:

a) The principle involved in the dependence of millimeter wave absorption coefficient in germanium on the externally applied electric field[11] should be used in the construction of pulse modulators theoretically capable of providing response times of the order of 10^{-12} sec. The power requirements of these modulators should be modest.

b) Small electrically controlled mechanical displacements possible in barium zirconate and barium titanate should enable amplitude modulation at millimeter and submillimeter wavelengths. The small accurately controlled displacements possible are consistent with waveguide dimensions at these wavelengths. Time constants of the order of 10^{-6} sec. are predicted.[23] The small power requirements and compactness of such modulators make their development attractive.

c) The utilization of the well known Faraday rotation effect in ferrites in the construction of short millimeter wavelength and submillimeter wavelength modulators is mainly a materials problem. It is worthwhile to investigate the potential of material such as those identified by Jonker et al.[21] for modulation frequencies up to 100 MHz.

2. All the external modulation methods discussed are suitable for pulse or amplitude modulation. Very little work on other types of external modulation has been uncovered. Some work on phase modulation of a 70 GHz carrier using a reversed biased GaAs point-contact varactor is being conducted by Harrison et al.[28] who achieved a phase shift of an

excess of 100° with no appreciable amplitude variation. These phase modulators exhibit a high insertion loss of about 10 dB. Attempts to reduce this insertion loss are underway.[28] In view of the scarcity of frequency and phase modulation techniques, it seems that basic investigation of this area is quite urgent.

6.5 REFERENCES TO CHAPTER VI

1. M. Becker and Y. Y. Fan, Phys. Rev., vol. 76, p. 1530, 1949, vol. 78, 1951.

2. A. F. Gibson, Proc. Phys. Soc., vol. B65, p. 378, 1952, also vol. B66, p. 588, 1953μ

3. A. F. Gibson, "Germanium modulator for infrared communications," Electronics, vol. 27, pp. 155-157, Oct. 1954.

4. K. Lehovec, "New photoelectric devices utilizing carrier injection," Proc. IRE, vol. 40, pp. 1407-1409, 1952.

5. R. B. McQuistan and J. W. Shultz, "Modulation of infrared by free carrier absorption," J. App. Phys., vol. 35, pp. 1243-1248, 1964.

6. C. A. Renton, "Amplitude modulation of light by reverse-biased p-n junction," Proc. IEEE, (Correspondence), vol. 52, pp. 93-94, 1964.

7. S. Deb and P. K. Chaudhuri, "Amplitude modulation of infrared and submm wave radiation by reverse-biased junction diodes," Proc. IEEE, (Correspondence), vol. 53, pp. 81-82, January, 1965.

8. B. Seraphin and D. A. Orton, "Field effect light modulation in Ge," J. App. Phys., vol. 34, pp. 1743-1748, 1963.

9. R. C. Prim, Bell System Tech. J., vol. 32, p. 665, 1953.

10. J. B. Gunn, and C. A. Hogarth, "A novel microwave attenuator using germanium," Journal of Applied Physics, vol. 26, No. 3, pp. 353-354, March, 1955.

11. J. B. Arthur, A. F. Gibson, and J. W. Granville, "The effect of high electric fields on the absorption of germanium," Journal of Electronics, Ser. 1 V. 2, pp. 145-153, Sept. 1965.

12. F. C. de Ronde, H. J. G. Meyer, and O. W. Memelink, "The P-I-N modulator, an electrically controlled attenuator for mm and submm waves," IRE Transactions, MTT-V. 8, No. 3, pp. 325-327, May, 1960.

13. T. H. B. Baker, "Junction-diode microwave modulators," IEEE Conference on Components for Microwave Circuits, Sept. 1962, Conference Digest, p. 40.

14. N. A. D. Pavey, "Broad-band P-I-N diode switches for (8-16) Gc/s range." Proc. of Symp. on Microwave Applications of Semiconductors, London, June 1965. Paper No. 6 (I.R.E. .Conference Proceedings, No. 5).

15. J. K. Hunton and A. G. Ryals, "Microwave variable attenuators and modulators using P-I-N diodes." Trans. I.R.E. on M.T.T., MTT-10, pp. 262-273, July 1962.

16. L. J. T. Hinton and L. F. Burry," P-I-N diode modulators for the K and Q frequency bands," The Radio and Electronics Engineer, pp. 22-26. Jan. 1966.

17. K. J. S. Cave, W. Neu, and A. C. Sim, "A diode modulator for millimeter waves," Proceedings of IEE, vol. 106, Part B supplement, No. 16, pp. 759-761, May, 1959.

18. A. G. Fox, S. E. Miller, and M. T. Weiss, "Behavior and application of ferrites in the microwave region," Bell System Tech. Journal, vol. 34, pp. 5-103, Jan., 1955.

19. A. Langley Morris, "Microwave ferrite modulators for high signal frequencies," Journal of the British IRE, vol. 19, No. 2, pp. 117-129, February, 1959.

20. F. Reggia, "A new broad-band absorption modulator for rapid switching of microwaves," IRE, Trans. on Microwave Theory and Techniques, pp. 343-349, July, 1961.

21. G. H. Jonker, H. P. J. Wijn, and P. B. Braun, "A new class of oxide ferromagnetic materials with hexagonal crystal structure," Proc. Inst. Elect. Eng., vol. 104, part B., supplement s, pp. 249-254, 1957.

22. M. M. Nekrasov and Yu. M. Poplavko, "Possible use of electrostriction in waveguide techniques," Radio Engineering and Electronic Physics, vol. 9, Feb., 1964, pp. 276-278 (English edition).

23. Yu M. Poplavka, Radiotecknika i Electronika, 1962, vol. 7, no. 8, p. 1453.

24. M. A. Armistead, E. G. Spencer, and R. D. Hatcher, "Microwave semiconductor switch," Proc. of the Inst. of Radio Engineers, vol. 44, p. 1875, 1956.

25. R. V. Graver, E. G. Spencer, and R. C. LeCraw, "High-speed microwave switching in semiconductors," J. of App. Phys., vol. 28, p. 1336, 1957.

26. M. R. Millet, "Microwave switching by crystal diodes," Inst. of Radio Engineers Transactions on Microwave Theory and Techniques, p. 284, July, 1958.

27. R. V. Graver, E. G. Spencer, and M. A. Harper, "Microwave semiconductor switching techniques," Trans. of the IRE, p. 378, Oct. 1958.

28. R. Harrison, et al, "Semiconductor microwave amplitude and phase modulator," Contract No. DA36-039 AMC-00284(E), General Telephone and Electronics Laboratories, Inc., Bayside, New York, Report No. 5, May 16-Aug. 15, 1964.

6.6 SELECTED REFERENCES ON OPTICAL MODULATION

1. Frora Andrea and Paul Handler, "Shift of optical absorption edge by an electric field: modulation of light in the space-charge region of a Ge p-n junction," Applied Physics Letters, vol. 5, No. 1, pp. 11-13, 1 July 1964.

2. R. C. Eden and P. D. Coleman, "Proposal for microwave modulation of light employing the shift of optical absorption edge with applied electric field," Proceedings of IEEE, vol. 51, No. 12, pp. 1776-1777, December, 1963.

3. C. F. Buhrer, D. Baird, and E. M. Conwell, "Optical frequency shifting by electro-optic effect," Applied Physics Letters, vol. 1, No. 2, pp. 46-49, 1 October 1962.

4. G. H. Thiess, "Method for detecting microwave modulated light," Proceedings of IEEE, vol. 51, No. 6, p. 950, June 1963.

5. S. E. Harris, B. J. McMurtry, and A. E. Siegman, "Modulation and direct demodulation of coherent and incoherent light at a microwave frequency," Applied Physics Letters, vol. 1, No. 2, pp. 37-39, 1 October 1962.

6. E. J. Schiel and J. J. Bolmarcich, "Direct modulation of a He-Ne gas laser," Proceedings of the IEEE, vol. 51, No. 6, pp. 940-941, June, 1963.

7. R. M. White and C. E. Enderby, "Electro-optical modulators employing 'intermittent ineraction,'" Proceedings of the IEEE, vol. 51, No. 1, p. 214, January, 1963.

8. R. Michael Zilberstein, "A proposal for a magnetically controlled light beam modulator and shutter," Proceedings of IEEE, vol. 52, No. 12, pp. 1751-1752, December, 1964.

9. I. P. Kaminow, "Splitting of fabry-perot rings by microwave modulation of light," Applied Physics Letters, vol. 2, No. 2, pp. 41-42, 15 January 1963.

10. S. E. Harris, "Conversion of FM light to AM using birefringent crystals," Applied Physics Letters, vol. 2, No. 3, pp. 47-49, 1 February 1963.

11. S. F. Sun, "Magnetoresistance of InSb at a microwave frequency," Journal of Applied Physics, vol. 35, No. 1, pp. 211-214, January, 1964.

12. S. F. Sun, "Application of magnetoresistance in InSb to mixer in microwave range," Solid State Electronics, vol. 7, No. 5, pp. 373-377, May, 1964.

13. R. Targ, "Optical helerodyne detection of microwave modulated light," Proceedings of the IEEE, vol. 52, No. 3, pp. 303-304, March, 1964.

14. K. Husimi and T. Inamura, "Pulse-time modulation and frequency modulation using the step recovery diode," Proceedings of the IEEE, vol. 52, No. 1, p. 76, January, 1964.

15. W. W. Buehman and M. Laikin, "Traveling-wave phase modulation," Proceedings of the IEEE, vol. 52, No. 9, pp. 1054-1055, Sept. 1964.

16. G. K. Ujhelyi and S. T. Ribeiro, "An electro-optical light intensity modulator," Proceedings of the IEEE, vol. 52, No. 7, p. 845, July, 1964.

17. R. Michael Zilberstein, "A proposal for a magnetically controlled light beam modulator and shutter," Proceedings of the IEEE, vol. 52, no. 12, pp. 1751-1752, December, 1964.

18. G. Racette, "Absorption edge modulator utilizing a P-N junction," Proceedings of the IEEE, vol. 52, No. 6, p. 716, June, 1964.

19. M. Samuel Stone, "A microwave electro-optic modulator which overcomes transit time limitation," Proceedings of the IEEE, vol. 52, No. 4, pp. 409-410, April, 1964.

20. C. E. Enderby,"Wideband optical modulator," Proceedings of the IEEE, vol. 52, No. 8, pp. 981-982, August, 1964.

21. A. Inaba, "Microwave photomixing of optical maser outputs with a PIN-junction photodiode," Proceedings of the IEEE, vol. 50, No. 8, pp. 1823-1924, August, 1962.

22. W. Eckhardt and F. Steizer, "Microwave-carrier modulation-demodulation amplifiers and logic circuit," Proceedings of the IEEE, vol. 50, No. 2, pp. 148-162, February, 1962.

23. J. Helszajn, "Coupled-wave description of the absorption-type ferrite modulator," British, The Journal of the IRE, vol. 29, No. 2, pp. 129-132, February, 1965.

24. Frank Reggia, "A new broad-band absorption modulator for rapid switching of microwave power," IRE Trans. on Microwave Theory and Techniques, MTT-9, No. 4, pp. 343-349, July, 1961.

25. A. G. Fox, S. E. Miller and M. T. Weiss, "Behavior and applications of ferrites in the microwave region," Bell System Tech. J. vol. 34, No. 1, pp. 5-103, January, 1955.

26. C. L. Hogan, "The ferromagnetic Faraday effect at microwave frequencies and its applications," Bell System Tech. Journal, vol. 31, No. 1, pp. 1-31, January, 1952.

27. A. F. Gibson, "Inject absorption in germanium," Proc. of Phys. Soc. (London) vol. B66, pp. 588-596, July, 1953.

28. A. Uhlir, Jr., "The potential of semiconductor diodes in high-frequency communications," Proceedings of IRE, vol. 46, No. 6, pp. 1099-1115, June, 1958.

Chapter VII

TRANSMISSION LINES AND COMPONENTS

7.0 INTRODUCTION

In this section we discuss the problems and state of the art of millimeter/submillimeter wave transmission lines and components. This topic is important because any system utilizing signals of these wavelengths will require at least some parts of the system to be built of such "hardware." A number of excellent survey articles exist, and it is not the intent to duplicate what appears in them[1,2,4,5,6], but rather to supplement them with additional information.

As the size of waveguides is reduced as one goes higher in frequency, one may expect increasing attenuations. In addition there is a demand for tighter and tighter tolerances as the dimensions are reduced. Consequently, departure from the conventional rectangular waveguide is indicated, but this introduces many new problems of components, excitation, etc. One approach is to utilize optical techniques, and this dichotomy of viewpoint is reflected in numerous places in this report. A recent article by Karbowiak[3] studies the optical waveguide, and many of the comments therein may find application in the present frequency range of interest. Figure 7.1 from that reference shows a comparison of range of applicability of various type waveguides throughout the spectrum.

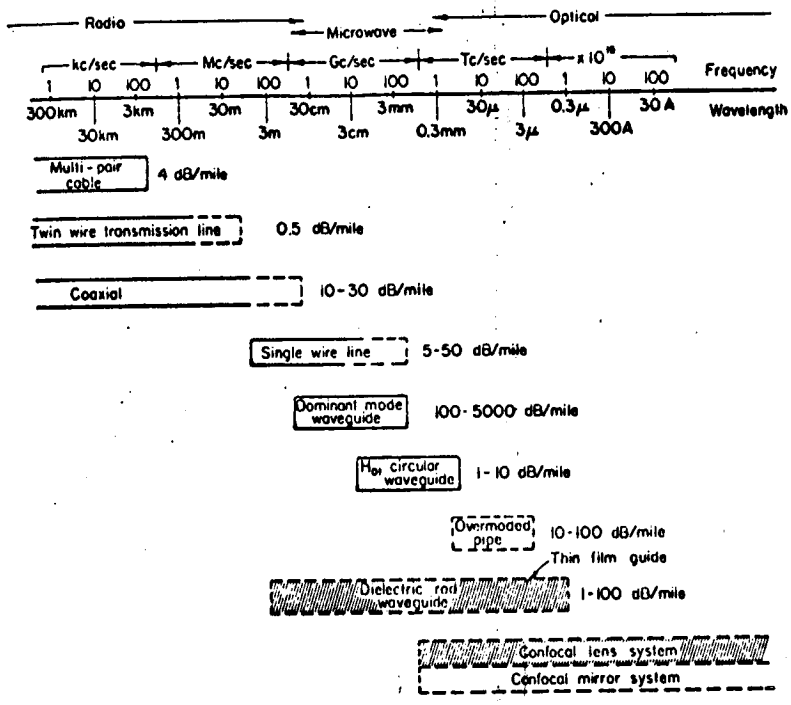

Figure 7.1 Comparison of Guides

7.1 OBJECTIVES AND REQUIREMENTS

7.1.1 Attenuation[1,2]

Ideally for transmission of electromagnetic energy one would like to achieve zero attenuation per unit length. Unfortunately, this cannot be realized anywhere in the spectrum though very low attenuation values can be obtained in the conventional microwave range. While values of less than 1 dB per 100 feet (0.0328 dB/meter) would be desirable--as is obtainable at S-or C-band--attenuation of the order of several dB per hundred feet would be a significant improvement over what can presently be achieved with the hollow metallic waveguide in the millimeter and sub-millimeter region.

In general, with increasing frequency the attenuation increases very rapidly, due to the increasing importance of surface finish when imperfections are an appreciable part of a wavelength. Imperfect surfaces can make the effective conductivity of the metallic surface many times less than its theoretical value. In addition, both surface and cross-section variations affect the propagation constant and consequently the impedance match at any point. Thus, considerable attenuation can occur due to reflection loss.

7.1.2 Impedance

In microwave systems impedance is significant when discussing matching, power transfer, breakdown, and attenuation. It is obvious that a matched system is one in which the impedances of two contiguous elements are matched in an appropriate way. Such a system exhibits zero

reflection coefficient (unity VSWR). Under the matched condition the power transfer is a maximum. Generally speaking, high impedance systems* (in terms of voltage/current) have lower attenuation losses due to conductor dissipation than low impedance systems.

In conventional rectangular waveguides the transverse wave impedance for the dominant mode is a function of frequency and of the order of 500 Ohms. Since the attenuation of conventional waveguides becomes very high indeed at very short wavelengths, it would seem that this could be counteracted by increasing the impedance. Unfortunately this method has its limitations, for as the waveguide dimensions are changed to alter the impedance, so also is the mode separation. A point is reached where the dominant mode is no longer the TE_{10}, but perhaps the TE_{01}. At any rate the possibility of degenerate modes or multiple modes exists when the dimensions are changed significantly away from the standard 2 X 1 ratio in conventional use.

It might be stated more generally that a waveguiding system for the millimeter and submillimeter regions needs to have impedance characteristics compatible with the components and generators with which it is to work.

---

* It is noted that the term "impedance" in waveguide systems can be a source of great confusion. It is possible to change the effective terminal or circuit impedance of a waveguide without affecting its transverse wave impedance.

7.1.3 Mechanical Requirements

Waveguiding systems must have the capability of transmitting both from point to point and around obstacles with minimum loss and mismatch. Consequently, an ideal guiding system should either be flexible or else be utilizable with twists, bends, and other components to accomplish the desired purpose.

The quality of a bend or twist in conventional waveguides is frequently specified by stating the VSWR that results when that component is inserted between a perfectly matched load and a slotted section. Residual VSWR's of the order of 1.1 in the millimeter region are considered to be typical. In the lower microwave frequencies a corresponding typical value might be 1.01.

The use of one of the various types of flexible waveguide also is an approach to the mechanical problem. At the lower microwave frequencies the residual VSWR in these is of the order of 1.05 or so, but as the frequency is raised it becomes more and more difficult to maintain a matched system and, in addition, the attenuation goes up very rapidly.

7.1.4 Power Levels and Voltage Breakdown

In waveguide systems the breakdown of the waveguide normally limits the power handling capability. In hollow waveguide used in high power radar applications, either complete evacuation or else operation with pressurized dry gas is preferable to operation with a normal atmosphere. Without some such precaution the breakdown becomes dependent upon the relative humidity and the barometric pressure. The dielectrically

loaded waveguide is also used to reduce the breakdown likelihood which lowers the impedance and simultaneously substitutes a medium of greater dielectric strength for air.

Whether or not breakdown will be a limiting factor in the submillimeter region depends upon the techniques ultimately utilized for transmission. While present generated power levels above 300 GHz are very small, it is noted that appropriate dimensions for conventional rectangular waveguides in this range are also minute. The power handling capacity of air-filled conventional waveguides varies greatly, but for all sizes the allowable power density is nearly a constant [average allowable power density PD_a = .65 to .7 megawatts/sq. in. (10.07 - 10.84 megawatts/sq. meter)]. By evacuating or pressurizing with a suitable gas, the allowable power density will be changed. In the former situation the allowable power density will first decrease drastically as the pressure is reduced until a minimum occurs of $PD_a \approx .03$ in the region of 2-5 Torr pressure. With further reduction of pressure the breakdown potential and hence allowable power density rises sharply.

With other types of waveguides, such as will be described in the forthcoming sections, other power handling and breakdown conditions will prevail. Very little work has been done on this subject for other than rectangular, circular, and ridged waveguides.

7.1.5 Mechanical Tolerances

All hollow waveguide systems operating in a single mode are highly dependent upon holding fixed dimensions. It has been already pointed out that in the region of very short wavelengths surface imperfections

become an appreciable fraction of a wavelength and cause difficulties. In a similar way the tolerances on mechanical dimensions in general become very critical at the higher frequencies. Even at X-band a mechanical tolerance of 0.001 inch (2.54×10^{-5} meters) is usual; at 100 GHz and above, tolerances of the order of 0.0001 inch (2.54×10^{-6} meters) to 0.00005 inch (1.27×10^{-6} meters) are obtainable.

7.2 CHARACTERISTICS OF VARIOUS TRANSMISSION SYSTEMS

7.2.1 Hollow Metallic Waveguides

Metallic waveguides can be used in a number of ways for the transmission of microwave energy: single mode propagation in rectangular or circular waveguides, and multimode propagation in rectangular or circular waveguides. There exist other possibilities mainly of academic interest only.

7.2.1.1 Rectangular Waveguides in the Dominant Mode

Transmission in rectangular waveguides has reached a high stage of development. Commercially available waveguides span the range from UHF to 325 GHz. Table 7-I, adapted from Harvey,[6] shows the principal characteristics for reference purposes. Unfortunately, the extension of these techniques to still higher frequencies is virtually impossible. Not only is the attenuation expected to be inordinately high, but required tolerance also makes the fabrication extremely difficult.

Figure 7.2 shows the familiar plot of attenuation vs frequency for common varieties of rectangular waveguide operating in the dominant TE_{10} mode. The increasing attenuation with small size is clearly shown.

TABLE 7.I*

Technical Data for Standard Rectangular Guides

Mil Type (typical)+	British R.C.S.C. type	American E.I.A. type	Inside dimensions, in. Width	Inside dimensions, in. Depth	TE_{01} cut-off, GHz	Operating range GHz	Attenuation, dB/100 ft	Power rating, kW
RG-201/U	WG 1	WR 1800	18.000	9.000	0.327	0.41-0.61	0.0334	115,000
RG-202/U	WG 2	WR 1500	15,000	7.500	0.393	0.51-0.75	0.0438	85,000
RG-203/U	WG 3	WR 1150	11.500	5.750	0.517	0.61-0.96	0.0614	45,000
RG-204/U	WG 4	WR 975	9.750	4.875	0.605	0.75-1.12	0.0807	33,000
RG-205/U	WG 5	WR 770	7.700	3.850	0.765	0.96-1.45	0.120	21,500
RG-69/U	WG 6	WR 650	6.500	3.250	0.908	1.12-1.70	0.154	14,800
	WG 7	WR 510	5.100	2.550	1.154	1.45-2.20	0.222	9,300
RG-104/U	WG 8	WR 430	4.300	2.150	1.375	1.70-2-60	0.286	6,500
RG-112/U	WG 9A	WR 340	3.400	1.700	1.737	2.20-3.30	0.450	4,200
RG-48/U	WG 10	WR 284	2.840	1.340	2.080	2.00-3.95	0.555	2,800
	WG 11A	WR 229	2.290	1.145	2.579	3.30-4.90	0.750	2,000
RG-49/U	WG 12	WR 187	1.872	0.872	3.155	3.95-5.85	1.047	1,200
	WG 13	WR 159	1.590	0.795	3.710	4.90-7.05	1.259	900
RG-50/U	WG 14	WR 137	1.372	0.622	4.285	5.85-8.20	1.700	620
RG-51/U	WG 15	WR 112	1.122	0.497	5.260	7.05-10.0	2.338	420
RG-52/U	WG 16	WR 90	0.900	0.400	6.56	8.20-12.4	3.24	250
	WG 17	WR 75	0.750	0.375	7.87	10.0-15.0	3.92	205
RG-91/U	WG 18	WR 62	0.622	0.311	9.49	12.4-18.0	5.21	145
	WG 19	WR 51	0.510	0.255	11.57	15.0-22.0	7.00	95
RG-53/U	WG 20	WR 42	0.420	0.170	14.08	18.0-26.5	10.9	52
	WG 21	WR 34	0.340	0.170	17.37	22.0-33.0	12.8	43
RG-96/U	WG 22	WR 28	0.280	0.140	21.10	26.5-40.0	17.3	28
RG-97/U	WG 23	WR 22	0.224	0.112	26.35	33.0-50.0	24.0	18
	WG 24	WR 19	0.188	0.094	31.4	40.0-60.0	31.3	14
RG-98/U	WG 25	WR 15	0.148	0.074	39.9	50.0-75.0	44.7	8
RG-99/U	WG 26	WR 12	0.122	0.061	48.4	60.0-90.0	59.7	5
	WG 27	WR 10	0.100	0.050	59.0	75.0-110	80.7	3.8
RG-138/U	WG 28	WR 8	0.0800	0.0400	73.8	90.0-140	113	2.3
RG-136/U	WG 29		0.0650	0.0325	90.9	110-170	154	1.5
RG-135/U	WG 30	WR 5	0.0510	0.0255	115.8	140-220	225	0.90
RG-137/U	WG 31		0.0430	0.0215	137.5	170-260	286	0.65
RG-139/U	WG 32		0.0340	0.0170	173.3	220-325	405	0.42

The power ratings are calculated at 1.5 f_c and assume a breakdown field of 30 kV/cm with a power safety factor of four; for any other frequency the values quoted must be multiplied by $1.34 \left\{1-f_c/f)^2\right\}^{1/2}$. The attenuation coefficients are calculated at 1.5 f_c for pure copper; for any other frequency the values should be multipled by $0.421 \left\{ (f/f_c)^2 + 1\right\} (f/f_c)^{-1/2} \left\{(f/f_c)^2 - 1\right\}^{-1/2}$. Further correction is required for other materials and for surface roughness.

* From Harvey, A.F., Microwave Engineering, Academic Press, New York, 1963.
\+ Military type numbers vary according to conductor material.

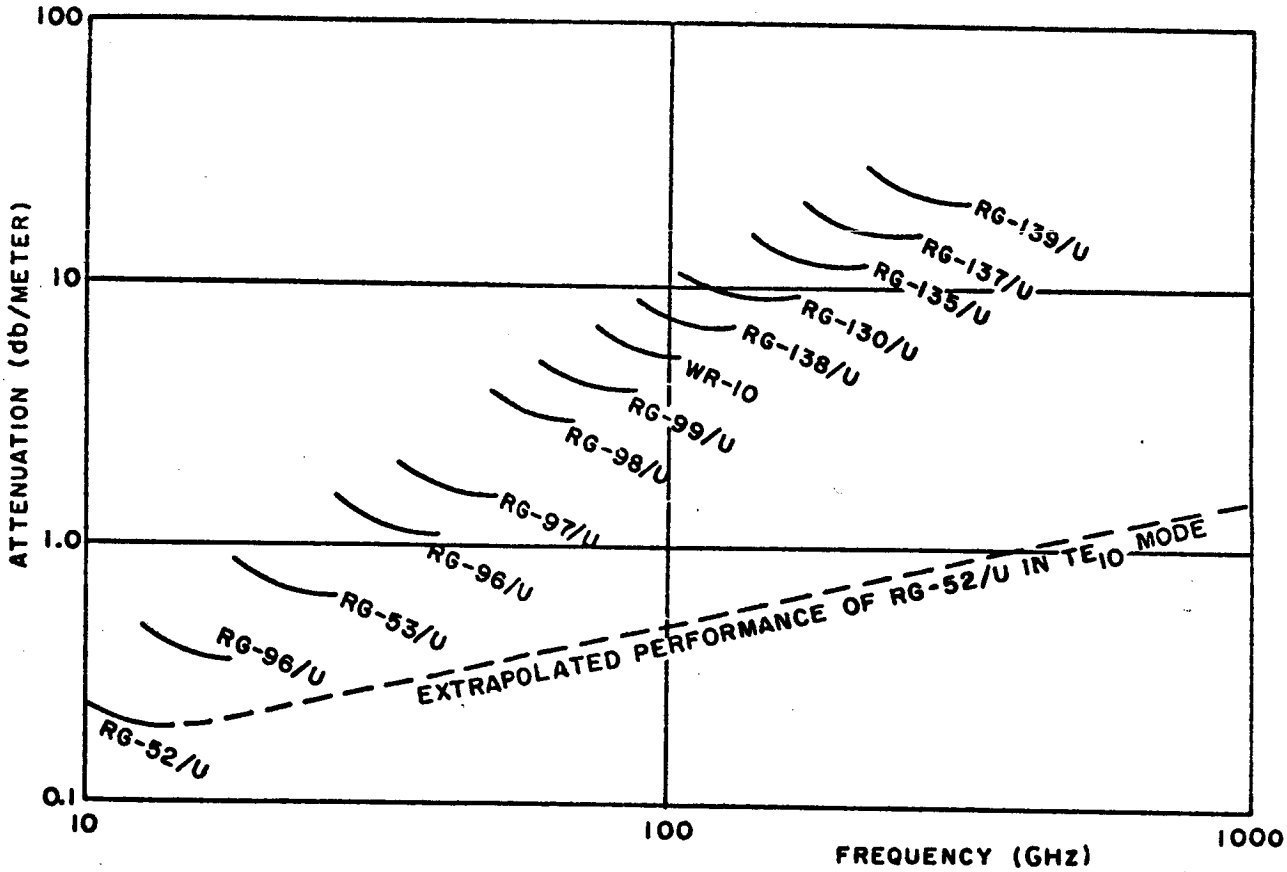

Figure 7.2 Attenuation vs Frequency for Standard Rectangular Waveguide Demonstrating the Expected Improvement of Overmoded Operation

7.2.1.2 Overmoded Rectangular Waveguide[7-11]

Recent work at Airborne Instrument Laboratories has shown the suitability of using rectangular waveguides in the TE_{10} mode but in a condition far above cutoff. If precautions are taken in exciting such a system, the TE_{10} mode alone may be launched. Then, because of the fact that the guide is very large compared to what would normally be used, the wall current density is reduced and hence the attenuation. As a matter of fact, in its central region the waveguide behaves nearly as a region of free space and the TE_{10} mode is almost like a TEM wave in field configuration and velocity. Ray optics may then conveniently be applied in the design of components.

It is reasonable to utilize a waveguide 10 times oversize for this type of operation. One can see from Fig. 7.2 that the attenuation at 10 times the normal frequency has not increased unreasonably.

This general statement holds for all rectangular waveguide sizes, since the shapes of their attenuation characteristics are similar.

The AIL investigators feel that the real potential of such oversize waveguides, however, lies in its applicability for design of various millimeter wave components such as filters, hybrids, directional couplers, etc. While their work has been confined to 330 GHz and below, there is no fundamental reason why the technique should not be usable somewhat higher in frequency. The frequency limit will be dictated by the increasing attenuation even of the overmoded waveguide and by the required mechanical tolerances.

7.2.1.3 Round Waveguide[12-16]

Certain modes in round waveguide have less attenuation than the TE_{10} mode in the rectangular waveguide as can be seen in Fig. 7.3 The TE_{01} circular waveguide mode is particularly attractive since it shows the characteristic of continuously decreasing attenuation with increasing frequency. This has been the subject of considerable investigation as a possibility for long distance waveguide transmission. The drawback is evident also in Fig. 7.3 where it can be seen that other modes can exist in the same frequency range as does the TE_{01} mode. One could argue that the low attenuation of the desired modes with respect to the others should make possible the transmission at the desired one only since it is known that the condition of least attenuation leads to a mode-stable condition. Unfortunately, imperfections in the waveguide, especially over long distances, will lead to local generation of the unwanted modes which will then be dissipated in wall losses. This means that the net attenuation of the desired mode will be higher than indicated and will not continuously decrease with frequency. Indeed, this continuous mode conversion loss due to imperfections will become increasingly bad as the frequency is raised, because all such imperfections will then be appreciable in terms of a wavelength.

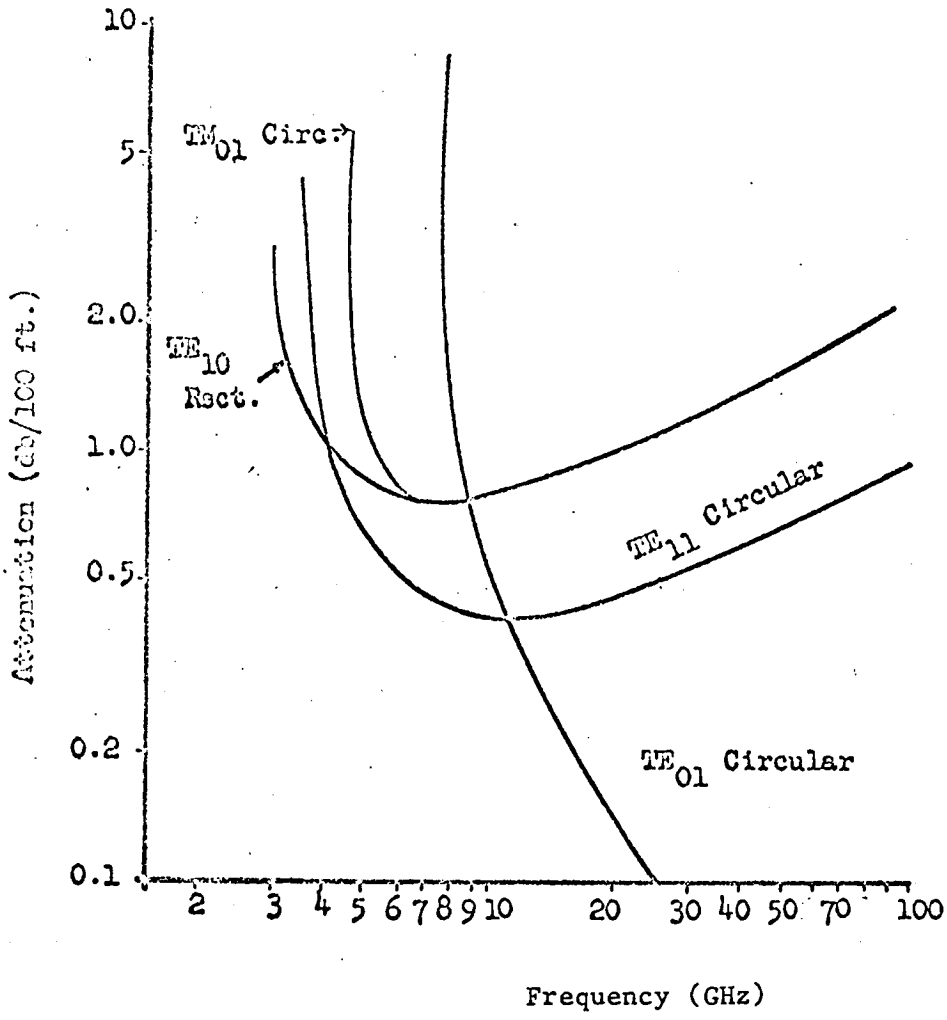

Figure 7.3 Comparison of Attenuation in 2" x 1" Rectangular Waveguide with that of 2" dia. Circular Waveguide. Material - copper.

The low attenuation of circular modes exhibited in Fig. 7.3 is raised substantially as the frequency is increased, particularly if the pipe diameter is also reduced in order to control the number of modes. Table 7.II shows some attenuation values extracted from a paper by Bertan.[4]

Table 7.II

Attenuation of millimeter waveguide, f = 140 - 220 GHz

TE_{10} in RG-135/U waveguide of inside dimension .0510 × .0255 inches (.001295 ×.000648 meters)	α = 317-201 dB/100' (10.4-6.6 dB/M)
TE_{01} in circular waveguide of .156 inches dia. (.00396 meter)	α = 19.8-8.4 dB/100' (.65-.275 dB/M)
TE_{11} in circular waveguide of .141 inches dia. (.00258 meters)	α = 22.1-23.8 dB/100' (.725-.78 dB/M)

To enhance the support of the TE_{01} mode only, a lossy lining (e.g. polypropylene film) is frequently added to the circular guide. The effect of this procedure is to reduce mode conversion by imperfections, which in turn reduces the attenuation. By this means the effects of unwanted bends and sag are minimized and the need for additional mode filters is eliminated. Table 7-III shows a comparison, given by Unger,[12] of the mode attenuation for three types of comparable waveguide at 55.5 GHz. It can be seen that the lined waveguide has a substantial amount of unwanted-mode attenuation compared to the hollow copper waveguide, though this attenuation is not as low as in the helical waveguide discussed in the next section.

Table 7-III

Mode Attenuation for Three Types of Waveguide

Mode \ Guide	Copper Pipe with lossy lining $\epsilon_r^* = 2 - j1$	Copper Pipe	Helix Waveguide
TE_{11}	α = .401 dB/ft. (1.32 dB/m)	α = .0072 dB/ft. (.0236 dB/m)	α = 1.13 dB/ft. (3.7 dB/m)
TM_{11}	α = .95 dB/ft. (3.12 dB/m)	α = .0172 dB/ft. (.0564 dB/m)	α - 11.3 dB/ft. (3.7 dB/m)
TE_{12}	α = .0359 dB/ft. (.118 dB/m)	α = .0012 dB/ft. (.00394 dB/m)	α = 1.13 dB/ft. (3.7 dB/m)

Figure 7.4 shows the effect of changing the size of the pipe diameter for a circular waveguide. With a reasonable sized pipe, lined to prevent unwanted modes, very low values of attenuation can be secured in the millimeter-wave region. Barlow[14] has reported 2.5-3 dB of attenuation over a 300 foot (91.5 meters) run at 28-40 GHz. Conklin[15] has reported similar results in the 50-60 GHz range. It is expected that reasonable values of attenuation can be secured at higher frequency also.

Considerable progress has been made at various laboratories towards solving the problem of bends. By utilizing a carefully-engineered corrugated section of somewhat reduced cross-sectional diameter, Barlow[14] has achieved transmission around bends with negligible phase distortion and mode conversion at 28-40 GHz.

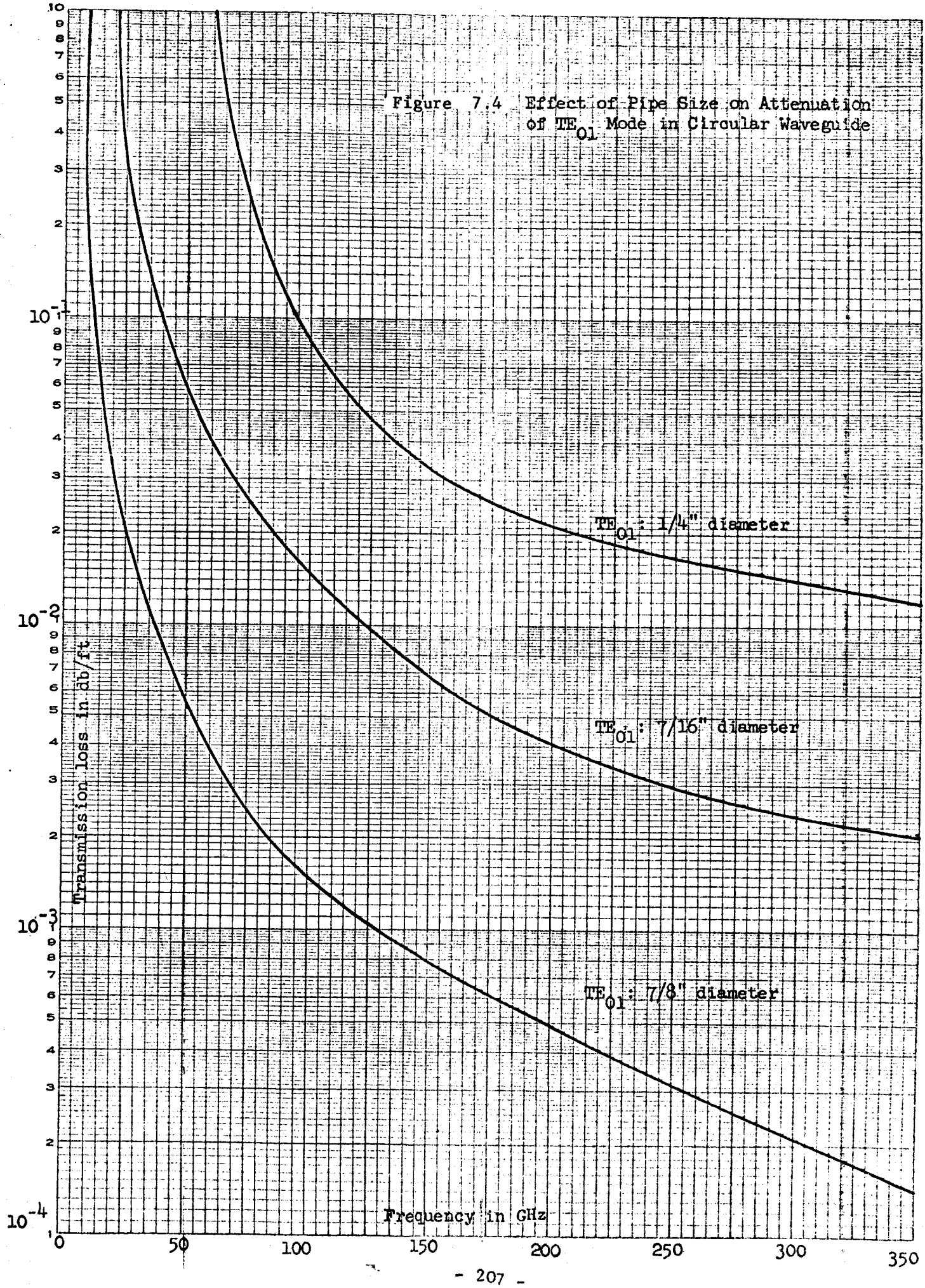

Figure 7.4 Effect of Pipe Size on Attenuation of TE_{01} Mode in Circular Waveguide

Components in the usual sense, such as directional couplers, filters, etc. are not generally available for this waveguide, but it is felt by some investigators that they can be developed if and when needed.

Using a circular waveguide in the TE_{01} mode above 300 GHz poses an interesting possibility. If size is not reduced, then a number of other TE_{on} modes can exist besides the TE_{01}. The use of a lossy lining will discriminate against these.* The extent of this discrimination must be carefully evaluated, as well as practical tolerances with which the dielectric coating can be applied.

7.2.2 Helical Waveguide[17-26]

"Helical waveguide" refers to a structure consisting of a tightly wound wire helix combined with a lossy dielectric medium all mounted within a rigid conducting pipe, as shown in Fig. 7.5. The helix is made of Formex insulated wire. There is thus no longitudinal conductivity to support modes that demand it. A slightly perturbed TE_{01} mode, however, can propagate with no difficulty. The lossy layers tend to absorb any energy that escapes the central propagating region through imperfections in the helix. Such a waveguide has been carried to a high stage of development both here (Bell Telephone Laboratories) and in Great Britain (Marconi). It has been tested extensively in the 50-120 GHz region, and an attenuation as low as 2 to 2-1/2 dB/mile (1.24 - 1.55 dB/km) has been achieved experimentally. Some investigators feel that the helix transmission line is ready for application to long distance transmission in

---

* Private communication with H. M. Barlow

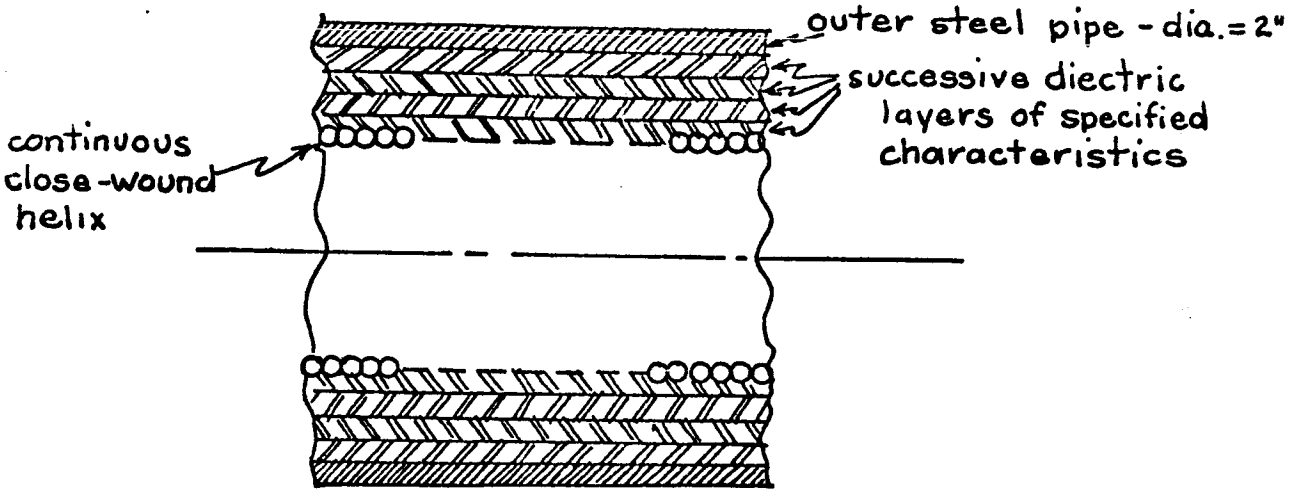

adapted from: M.H. Cuffin, MARCONI REVIEW, XXVIII, No.156, p.7.

Figure 7.5 Construction of Helical Waveguide

this frequency region as soon as there is sufficient demand. The comments previously made with respect to auxiliary components for circular waveguides certainly also apply here. Thus, it is felt that more research will be needed when such components are required.

Since the mode of transmission in both lined circular and helical waveguide is TE_{01}, it might be expected that the respective performances would be very close. It is noted, however, that in the preceding section, an attenuation of 2.5 to 3 dB per 300 feet at 28 to 40 GHz was reported for Barlow's circular waveguide; whereas in the previous paragraph 2 to 2-1/2 dB per mile at 50 to 120 GHz was reported for the Bell Telephone helix waveguide. This apparent wide discrepancy may come about because of factors not reported in the references. Thus, it is to be expected from theory that a lossy-lined circular waveguide will be considerably better than indicated here, but probably never as good as the helix waveguide. The reason for this latter statement is as follows. In the lined circular waveguide the dissipative region is common to all modes. Though the amount of electric field of the TE_{01} mode that penetrates this region is small, nevertheless it is finite, and some dissipation will occur. In the helical waveguide, to the contrary, the TE_{01} mode is unaffected by the outer layer of dissipative dielectric since it occurs beyond the effective guide boundary (the helix). Hence, the TE_{01} mode virtually has no loss mechanism present.

Helical waveguides can be scaled upward in frequency. The various difficulties mentioned in the previous section with respect to other TE_{on} modes are present here also. Reducing the size increases the fabrication problems considerably, and it is expected that a limit exists beyond which fabrication at still smaller diameters becomes physically impossible. It is intuitively felt that due to the greater complexity of the structure, this limit will be lower in frequency than a corresponding limit for circular waveguides.

7.2.3 Dielectric Rods and Tubes[27-29]

Electromagnetic waves can also propagate along a cylinder of low loss dielectric. Above 20 GHz such waveguides have attractive features. Theoretical analysis reveals that for the lowest mode no cutoff exists. At lower frequencies, however, most of the energy travels on the outside of the dielectric cylinder, which allows the possibility of sustaining absorption losses due to nearby objects and supports. As the frequency is raised higher, more of the energy travels within the dielectric. TE, TM, and hybrid modes exist, and the HE_{11} mode in particular is attractive because of its low loss and ease of launching.

Fig. 7.6 shows the attenuation vs frequency for a two inch (.0508m) diameter polystyrene rod waveguide. This size was picked in order to compare its performance with that of previous figures. However, such a comparison does not display the dielectric rod characteristics favorably, for as the rod is made smaller, the losses decrease at a given frequency. Furthermore, a two inch diameter rod is not only unrealistic

Figure 7.6 Attenuation vs Frequency for a Polystyrene Cylindrical Waveguide of 2" diameter

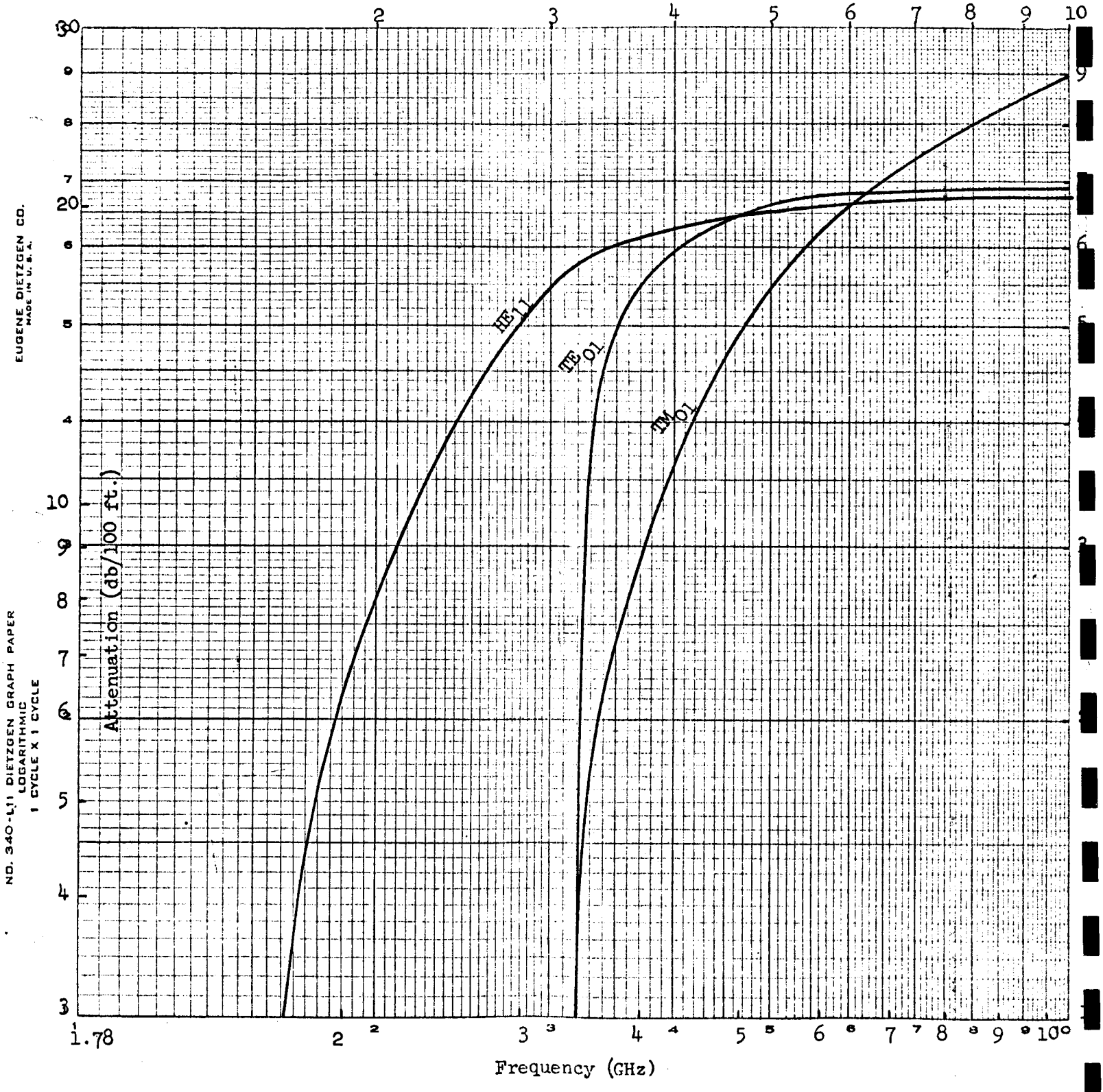

from an attenuation viewpoint, but also from a manufacturing and cost viewpoint as well. For rods whose diameter is a fraction of a wavelength in diameter, attenuation of less than 1 dB/100 ft. (.0328 dB/m) can be obtained in the millimeter wave region.

A drawback of the dielectric rod waveguide is the problem posed by supports and bends. Since in all cases some of the energy propagates outside of the dielectric, any support will provide a new boundary condition to be met which will result in either a reflection or absorption of energy. Bends cause radiation of energy with attendant increase in attenuation along the line.

The extension of the use of dielectric rods upwards in frequency leads to the concept of fiber optics. Here, bundles of dielectric rods, each many wavelengths in diameter, are used to transmit light with low attenuation. However, the situation differs from the simple case described above in that each fiber has a coating with a different refractive index. Besides this, the fibers are so big as to support literally hundreds of modes. The coating enhances the trapping of energy within each fiber. This technique has been examined in great detail at Wheeler Laboratories for use in the optical range, and an optimum combination of dielectric constants for achieving single mode transmission has been found.[54] Experimental verification of theoretical predictions has been accomplished and component development and applications are under way in both circular and rectangular cross-sectional geometry. Such techniques should be applicable to submillimetric waves. The cladding has been found to have a beneficial effect in reducing losses through radiation

in bends, and it is possible that further work could substantially reduce existing losses. A combination of these techniques would suggest the use of a single dual dielectric rod or filament as a guide for submillimeter wavelength energy. The choice of a suitable outer dielectric might well reduce the tendency to radiate from sags and gradual bends.

7.2.4 Dielectric Coated Wires[30-32]

The so-called surface wave transmission line has found some application at lower frequencies such as VHF and UHF as a transmission medium of low attenuation and cost. It has a rising attenuation characteristic with frequency and it also has the same drawbacks as the dielectric rod waveguide mentioned above. Figure 7.7 shows a typical characteristic. Generally, at millimeter and submillimeter wavelengths it is not expected that this type of transmission would have much application. Kikuchi and Yamashita[28] performed experiments at 50 GHz which seem to bear out this conclusion, although they carefully avoid any such pronouncement.

7.2.5 Dielectric Image Lines[33,34,35]

If a dielectric cylinder is split and mounted on a good conducting base plate; it can be regarded as a waveguiding system consisting of the half-cylinder of dielectric plus its image operating in the "dipole" mode. Such a line has been proposed to solve the support problem associated with the dielectric rod waveguide. While the additional image plate introduces extra losses, the attractive features tend to offset this. For one thing the launching problem is made simpler, and the line is less sensitive to mode conversion. It has been shown

Figure 7.7 Attenuation vs Frequency for a Surface Wave (Goubau) type Transmission Line. Copper 0.129" dia. coated with 0.001" Dielectric with $\epsilon' = 3$

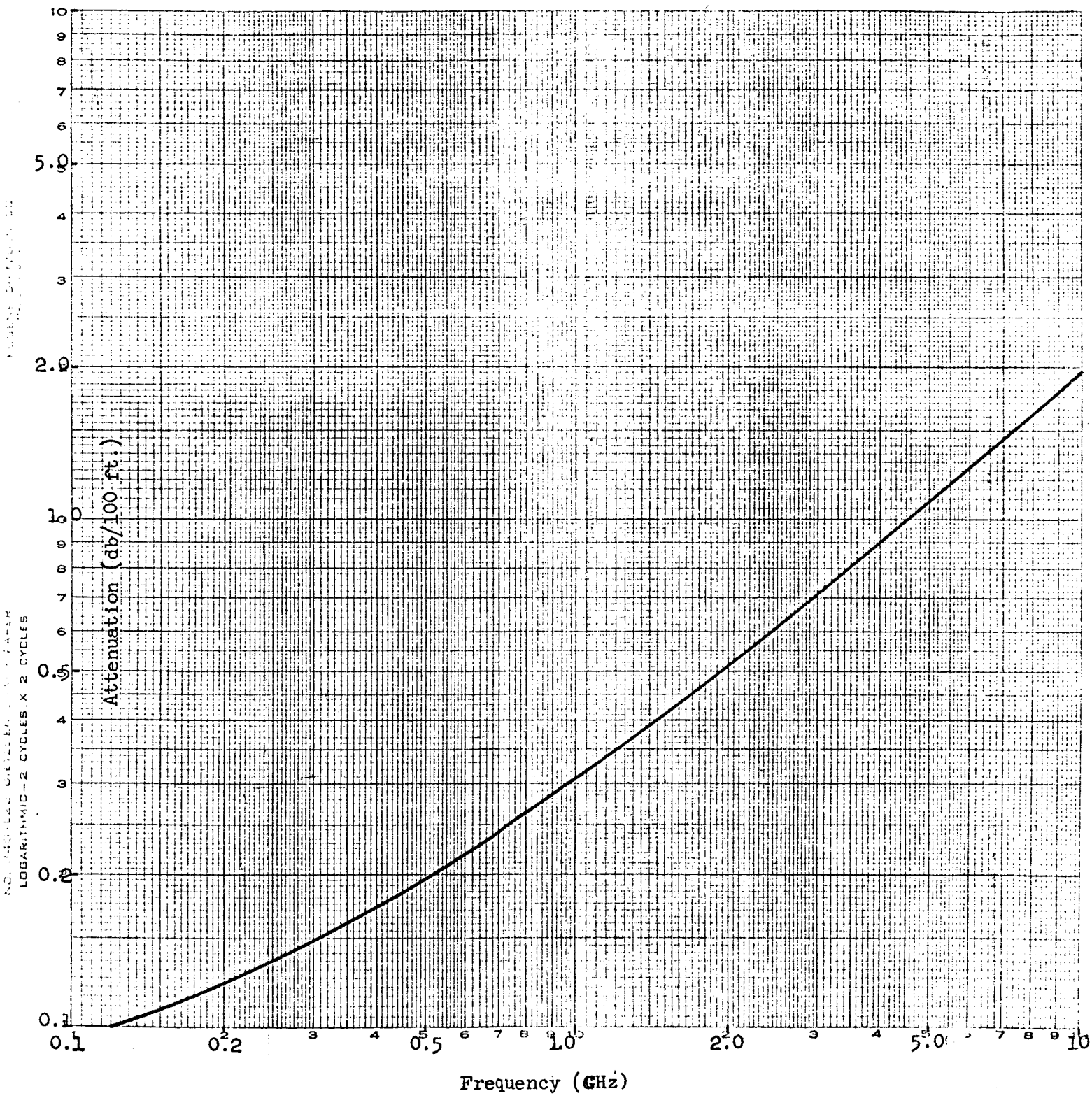

also that it is quite insensitive to changes of shape as well as twists and bends. Consequently, some of the dimensional demands necessary for other waveguiding systems can be relaxed here. These properties make the dielectric image line attractive for millimeter and submillimeter wavelengths. While a great deal of developmental work has been done on this line and components for it, it is not known whether any commercial or military standards yet exist for it. It is believed that such a line could be useful for some purposes in the 300-3000 GHz region.

7.2.6 H-Lines[36,37,38,39]

The H-line consists of a dielectric slab sandwiched between two conducting planes. It may be regarded either as a variant of the dielectric image line or as a derivative of the dielectrically loaded rectangular waveguide. In the latter a slab is usually placed in the center of the waveguide in order to reduce the waveguide impedance and correspondingly the electric field, thus lessening the tendency of breakdown. If one imagines now that the walls are displaced to infinity, an H guide results. Clearly, for sufficiently large dielectric constants most of the energy will travel in the dielectric in preference to the surrounding air. For any dielectric constant, however, some of the energy still will propagate outside the dielectric region. The modes are hybrid in nature, and the losses are largely dictated by the dielectric losses. If low loss tangent material is used, the properties of this line are similar to those of dielectric waveguide and dielectric image line.

Figure 7.8 shows attenuation vs frequency for the H-guide. If the curve for the lower loss tangent material is considered, it can be seen that the resultant total attenuation is substantially below that of a rectangular waveguide operating in the same frequency range. However, it is noted that the attenuation changes markedly as the loss tangent goes up.

The advantages of the H-line as compared with the other types mentioned are that it can be integrated with a conventional rectangular waveguide for purposes of excitation and transition and that it is shielded on two sides instead of one. As in the case of the dielectric image line, it is relatively insensitive to variations of geometry and cross section.

A research group at the University of Sheffield (England) has been investigating what is called the laminated, or double-slab, H-line in which two slabs are placed in close proximity between the parallel metallic plates. This was originally reported by Tischer[39] who claimed that multiple slabs should lead to even lower losses than the single slab variety and, hence, lower attenuation. The group has been conducting a theoretical analysis of the field distribution in the region between the slabs. Major difficulties are encountered in practice in launching the required waves. Extension to higher frequencies should be possible, but is dependent upon the availability of suitable dielectrics.

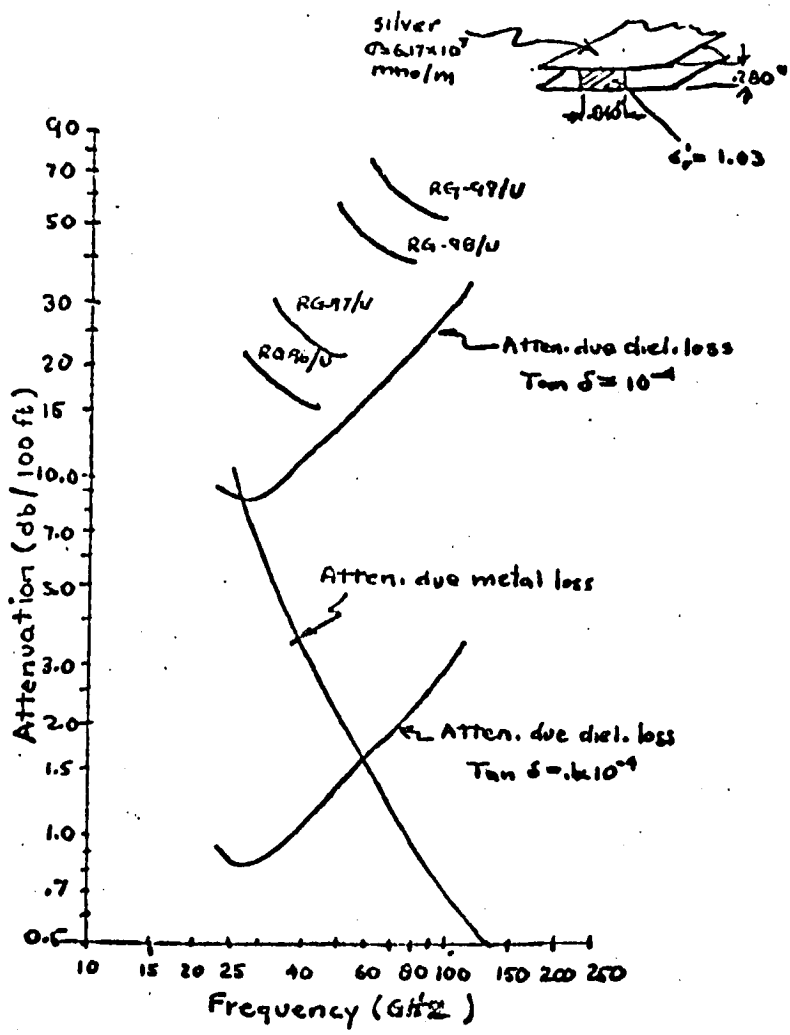

Figure 7.8 . Theoretical Attenuation vs Frequency for H-Guide with Comparisons to Some Standard Rectangular Waveguides

(From: J.W.E. Griemsmann and L. Birenbaum: "A Low-Loss H-Guide for Millimeter Waves," Proc. of Symp. on MM Waves," P.I.B., New York 1959.)

7.2.7 The Groove Waveguide[37,40]

A variant of the H-line proposed by Tischer (see Fig. 7.9) is the groove guide consisting of two parallel conducting plates distorted by a groove. This construction confines more of the field to the groove region with a lower loss due to reduced longitudinal currents. The figure shows that very attractive attenuation values can be obtained.

Other members of this dielectric-metallic family exist with somewhat similar properties.[41]

7.2.8 Beam Waveguides[42-45]

In the past several years the use of a series of lenses and/or mirrors has been considered as a means of transmitting millimeter and submillimeter energy from one point to another. The concept is to collimate or focus the energy with a suitable device, and then at a properly chosen point refocus with another similar device. Thus metallic and dielectric losses are avoided, and the only loss in an idealized system is that associated with the fact that 100% of the energy can never be captured by the second device (and succeeding devices). This statement must be modified, however, when the energy passes through an atmosphere in going from one collimating device to another. Atmospheric absorption can be considerable in the optical, infrared, submillimeter, and millimeter regions of the spectrum. To avoid this problem the system may be enclosed in a suitable chosen evacuated hollow tube, and a second outside pipe can provide further support and thermal isolation. An experimental optical system of this type, 1 km in length, exists at Fort Monmouth. A loss of 1 dB has been mentioned as the attenuation of the 1 km length,

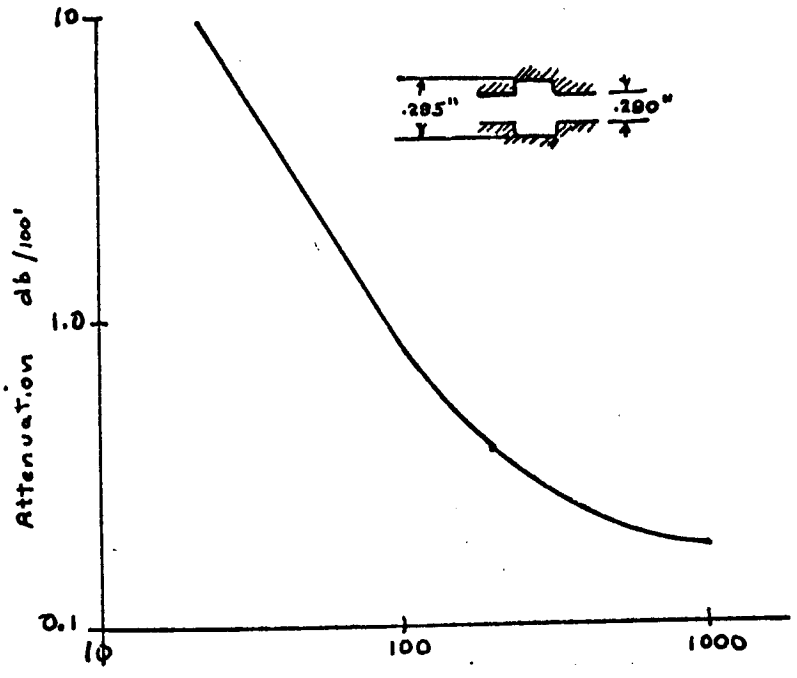

Adapted from: J.W.E. Griemsmann,"Oversized Waveguides," Microwaves, 2, Dec. 1963, pp. 20-31.

Figure 7.9 Approximate Attenuation Characteristic of Groove Waveguide

and half of this is estimated as occurring in the terminal transitions. The drawback of the beam waveguide in this embodiment is that the lenses, for proper operation, are expensive. Furthermore, if one contemplates the use of beam waveguides at lower frequencies, such as at millimeter or submillimeter wavelengths, the size of the required lenses, assuming that they can be made at all, will be large. Karbowiak[3] states that at millimetric wavelengths lenses could be several cm in diameter for a lens spacing of less than 10 meters. Thus for long runs many lenses would be needed and a pipe at least several inches in diameter (including a double wall system for thermal isolation and strength) would be required. An additional point is that no materials are transparent over the whole spectrum. Many of the common refractory materials suitable for lenses in optical systems are unusable in the frequency range in question. Much more materials research is needed to insure that suitable lenses can be made.

To offset this, beam waveguides of the aperture type are under investigation. In this variant the diffraction effect is obtained by means of repeated apertures in the system. Theoretically the loss in such a system can be as low as in the lens case. Practically, one must evaluate the behavior of the aperture boundary material as compared with the behavior of the lens material.

A third type of beam waveguide consists of a zig-zag beam path bounding from confocal mirror to confocal mirror. Again the losses are due to diffraction and dissipation. Work underway at the University of Illinois is concerned with measurements made at the mirror surfaces.

Bands can be engineered for beam waveguide without undue difficulty, but require more frequent spacing of the diffraction devices with the increased attendant loss.

Recent work at Bell Telephone Laboratories has been concerned with replacing the dielectric lens in an optical-beam waveguide with a so-called gas lens. In this device cool, axially flowing gas enters a region surrounded by a wall at a higher temperature. A temperature gradient, and therefore a density gradient, is set up in the gas which makes the index of refraction change in a determinable way. By proper design, excellent focusing properties can be achieved, and the interface problem, such as exists with dielectric lenses, can be eliminated. Current work is concerned with two-gas lenses for further control of the range of such lenses. While this work has been directed toward the optical and infrared region of the spectrum, it should have application in the submillimeter region as well. It is the feeling among a number of workers in the ultramicrowave field that waveguide concepts should be abandoned at these extremely high frequencies in favor of optical techniques. The dividing line in frequency, where such a transition should occur, is very ill-defined, however.

7.3 TRANSMISSION LINE AND WAVEGUIDE COMPONENTS

7.3.1 General Comments

Each of the waveguiding systems mentioned above has varying degrees of adaptability to component design. It is not the intention

here to go into detail about components suitable for each system. Rather we shall discuss the general requirements and relate them to some specific systems, where appropriate.

7.3.2 Mode Launchers

In all of the transmission systems discussed above (with the possible exception of optical fibers) mode purity is a requirement. This may be accomplished by two means: (1) efficient mode launching, and (2) mode suppression. In the former case, the objective is to convert 100% of the energy into the desired mode. In the latter case the objective is to compensate for the generation of unwanted modes by either a poorly designed mode launcher or imperfections in the transmission system.

Theoretically, a suitably disposed array of electric and magnetic dipoles can be used to generate any desired mode. At the lower frequencies, probes and loops are utilized to accomplish this. In normal waveguide practice suitable apertures are used to accomplish the same purpose. In the submillimeter region such methods lose their effectiveness because of the mechanical tolerances required.

Another approach is to use a tapered transition in which a mode distribution in a conventional waveguide is distorted gradually to give the field pattern required. Wide band high efficiency performance with such mode transducers can be achieved, and the method has been used with most of the transmission systems discussed.

A third method of mode launching is to provide a means for directly coupling the energy out of the active region of the generating device into the transmission medium. This is the technique used with

klystrons, magnetrons, etc. The difficulty that occurs as the frequency is raised is that the interaction region of the device becomes more confined and difficult to reach with a suitable waveguide. Furthermore, the "natural" mode pattern in the active region may not be the one desired in the transmission medium.

In laser type devices this technique is realized by using a Fabry-Perot resonator, which not only is necessary for lasing action, but also provides a "window" for coupling. However, mode purity is somewhat of a problem. Goubau reports* that results on his beam waveguide for infrared were not as good as expected due to the lack of mode purity.

While mode launching is an important part of any transmission system, the difficulties of designing a suitable mode launcher for submillimeter wavelength energy, assuming it can be coupled out of a source, are not as great as those of engineering other components.

7.3.3 Mode Suppressors

Two types of mode suppressors are in use. The first of these makes use of the cutoff properties of some waveguides. Of those discussed above, the hollow metallic types have cutoff frequencies. Some of the other types have cutoff frequencies for some modes, but not for others. Hence, the utilization of cutoff to suppress modes depends greatly upon the particular system under consideration. Careful analysis will usually reveal whether this property can be exploited.

---

* Private communication

The second type of mode suppressor is dissipative, in which suitable absorbing material is placed in the waveguide in such a way as to severly attenuate some particular field distribution but not others. The circular TE_{01} waveguide is an example of the use of such mode suppression.

Mode suppression is a problem common to all frequency ranges. In the submillimeter region it becomes more difficult because of the small physical dimensions.

7.3.4 Tuners and Transformers

Impedance mismatches in wave transmission systems can be removed by appropriate impedance transforming devices. In rectangular waveguides these take the form of double stub tuners, slide screw tuners, E-H tuners, quarterwave or multisection transformers, or tapered sections. These do not all have their counterparts in other waveguide systems, at least at this time. One of the reasons why so much can be done with the rectangular guide system is that one is working with a medium in which only one mode (the dominant one) propagates. Also, one has a convenient medium in which to place movable plungers (contacting or non-contacting).

In waveguides such as the dielectric rod, H-guide, etc., all adjustable tuning operations comparable to tuning screws would probably have to be accomplished on the outside of the dielectric medium. Since only a fraction of the energy travels on the outside of the dielectric, it is suspected that such devices would not be of great effectiveness, except in producing loss. On the other hand there is no reason why variable index of refraction materials, and variable cross-sections

could not be used to achieve some degree of impedance transformation. Also, the use of branch guides of fixed length is a possibility; however, there are problems associated with joining such branches to the main line. It is suspected that dielectric welding would have to be used to provide an effective joint.

In the case of beam waveguides, impedance mismatches occur at the various repeated collimating devices. Lenses can be coated or grooved to provide effective matches at their surfaces. The gas lens is well-matched because of a varying index of refraction. Suitable design can reduce mismatch effects in aperture and confocal mirror types of waveguides. Hence, it is not expected that other types of matching devices, equivalent to stubs or tuners, would be needed with beam waveguides.

7.3.5 Loads

The load problem in wave transmission is that of contriving a means of dissipating all or part of the energy that is being transmitted through the system. Loads are useful in providing a means for disposing of power in the testing of generators, and in giving controlled conditions of match or mismatch for the purpose of various tests. The techniques used in rectangular waveguides can also be used with modifications in other waveguide systems. In rectangular waveguides a lossy medium is inserted into the guide with a shape chosen to minimize the reflection coefficient at any one point.

If the dissipative region is long enough, nearly all of the energy will be absorbed and a negligible amount will be reflected from the end of the section.

In a similar way one might taper a dielectric rod, H-guide, or dielectric image line into a lossy medium. Such a medium might only be another dielectric with a significantly higher loss tangent.

In the case of helical and circular waveguides, loads also take the form of tapered blocks of dissipative material placed in the region in which the fields act.

Another technique for providing a load used by some investigators of new transmission systems is that of radiating the energy of the system. Hinden and Taub* used the technique in their work with overmoded rectangular waveguides. However, in most of the systems discussed, this approach is more difficult because of the lack of knowledge about what constitutes an efficient radiator. The problem is akin to that of mode launching, except the transducing in this case is between the system and free space.

In the beam waveguide at optical or infrared wavelength, suitable loads still consist of suitable absorbing materials appropriately placed in the beam.

In the submillimeter region the most difficult task in engineering suitable absorptive loads will be in knowing the properties of

---

* Private communication.

materials. In addition, the design of partially reflecting loads (standard mismatches) will be a challenge in those transmission systems that can support more than one mode because of the likelihood of mode conversion taking place.

7.3.6 Attenuators

The design of an absorbing attenuator is more difficult than that of load design because it is necessary to provide two transition regions (i.e., transition into and transition out of the attenuating region). In the microwave region this usually causes considerable frequency dependence. In the submillimeter region this will continue to be a difficult design problem. In addition, mode conversion will be a matter of serious concern in systems which can support several modes, as noted in the last section. Finally the matter of calibration of attenuators will not easily be resolved until other components and instruments are forthcoming.

In turning to optical techniques, by contrast, attenuators can be easily designed by using coupled prisms. In the work of Hinden and Taub they showed that such techniques can be applied in the millimeter wavelength region. Essentially, what is done is to provide a totally reflecting prism in a suitable waveguiding system. In the back region of such a prism the fields are evanescent in nature. A second inverted prism brought up to the first one will now couple energy from the evanescent field and make it available at greatly attenuated levels, to a suitable waveguiding system. Schineller[51] has worked out the details

for making a variable attenuator for the optical region using this concept. It would seem possible thus that the technique would be useful in some waveguide systems in the submillimeter range.

7.3.7 Slotted Sections, Impedance Meters, and Directional Couplers

In order to determine mismatch in a conventional microwave system a slotted section is employed. Generally these are ineffective in overmoded or multimode systems. They are also impractical in systems involving solid media or structures in which coupling to the fields cannot easily be accomplished with a probe or loop. Hence, conventional slotted line measurements must probably be dispensed with at submillimeter wavelengths.

On the other hand, impedance match can also be measured with a reflectometer. In essence this is a dual directional coupler in which samples of the forward-traveling and backward-traveling waves are compared. Directional couplers can be conceived for all of the transmission systems described. In the structures having an external field, such as dielectric rod waveguides, etc., it is possible to directly couple a second similar, and proximate, guide. This class of problem has been fairly well studied theoretically, and practical results for some waveguide systems are available.[48,49,50]

For most systems, however, directional couplers based upon beam splitting millimeter wave "mirrors" should be possible. In this concept the energy impinges upon an inclined partially transmitting plane mirror. A fraction of the impinging energy is deflected off into a suitable branch waveguide. Energy traveling in the opposite direction

is deflected into a guide positioned 180° from this. By adjusting the transmission coefficient of the mirror, the coupling factor can be adjusted over wide ranges. Such techniques have been used by Hinden and Taub and are known to workers in the laser field. It is likely, therefore, that this method would be of considerable utility in the submillimeter region.

7.3.8 Hybrid Structures

It would be expected, since the directional coupler is a form of hybrid structure, that other types of hybrids would be possible in the quasi-optical range. Certainly no difficulty is foreseen in most systems with hybrids based on prisms or mirrors as discussed above. Hybrid rings (rat races) are possible theoretically in systems allowing bends, but since their behavior is very dependent upon differential path lengths, the very short wavelengths may make their realization impractical.

Whether or not hybrids equivalent to magic tees exist in all of the various waveguide systems described is a matter for some further study.

7.3.9 Resonant Structures

All of the transmission media described can be made into resonators. However, all are not equally useful or practical. In general, resonators composed of an open-guiding structure between reflecting plates will be subject to radiation unless the end plates are very large. Higher Q can be secured theoretically from completely closed structures. Low-loss modes must be chosen however. In the case of overmoded

structures difficulty may be encountered because of mode conversion by imperfections in the "shorted" ends, a tendency that increases with increasing frequency. Micro-finishes and extremely accurate alignment are needed to avoid this difficulty.

In the beam waveguide the resonator may take the form of partially transmitting reflectors appropriately shaped to confine the energy. The coating provides a means for excitation without mode destruction.

7.3.10 Ferrite and Antiferrimagnetic Devices

Suitable ferrite materials are needed for waveguide components, for possible use as modulators, for amplifiers, and for providing reverse isolation in traveling wave masers. The latter application for the millimeter and submillimeter wave regions requires a resonance isolator which has a very high saturation magnetization $\left[4\pi m_s > 5 \text{ kilogauss (kG)}\right]$. For instance, a 35 GHz maser incorporated a nickel zinc ferrite having a magnetization of 5 kG at 4.2° K. This material's maximum saturation magnetization[55] value of 7 kG is obtained with a concentration of $x = 0.3$ in the chemical formula $Ni_{1-x}Zn_xFe_2O_4$. Therefore, according to the boundaries of Kittel's ferrite resonance curves[57] this ferrite could be used for a higher frequency maser.

Among other ferrimagnetic materials which look promising are barium ferrites. The large uniaxial anisotrophy and "built-in" biasing field of 17 kG makes them suitable for building resonance isolators for operation in the 50-70 GHz range. Planar anisotrophy obtained with

a simultaneous $Co^{2+}Ir^{4+}$ substitution in barium ferrite is expected to give internal fields of the order of 100 kG. This will allow operation above 100 GHz using a reasonably low applied magnetic field.

Some rare-earth iron garnets have a large value of spin angular momentum which leads to a large low temperature magnetization. These materials with their room temperature and liquid helium temperature values of magnetization are listed in Table 7.IV.

TABLE 7.IV

SATURATION MAGNETIZATION ($4\pi m_s$) OF RARE EARTH IRON GARNETS

Garnet	$4\pi m_s$	
	$T = 4.2^{\circ}K.$	$T = 300^{\circ}K.$
GdIG	> 7000 Gauss	0 Gauss
Mixed GdEr	6500 "	800 "
Mixed NdGd	7500 "	500 "
TbIG	7500 "	200 "
DyIG	8000 "	300 "
HoIG	6800 "	800 "
ErIG	5800 "	1000 "

These materials should be investigated for possible use in reverse isolators in millimeter traveling wave masers and also for cryogenically operated waveguide components (circulator, isolator, phase shifter). For ferrite applications at higher temperatures, the materials in Table 7.V are suggested for investigation.

TABLE 7.V

SATURATION MAGNETIZATION OF MAGNESIUM AND MANGANESE FERRITES

Ferrite	$4\pi m_s$ (gauss)		Typical Linewidth ΔH (gauss)
	$4.2^{\circ}K.$	$300^{\circ}K.$	
1. Magnesium-Zinc (x=0.5) ($Mg_xZn_{1-x}Fe_2O_4$)	7000	4100	
2. Manganese ($MnFe_2O_4$)	7000	5000	200
3. Manganese-Zinc $Mn_{1-x}Zn_xFe_2O_4$	10,000 (x=0.4) > 7000 for all x	6000	300

These materials have the highest magnetization over a broad temperature range ($0\text{-}300^{\circ}K$) known to this date.

In the submillimeter wave region, a great variety of absorptions and resonances have been observed using iron garnets. A transparency "window" exists in the range $1 > \lambda > 0.1$ mm. Transmission through crystals of YbIG, ErIG, HoIG, SmIG, and GdIG has been investigated by Tinkham and Sievers.[55]

Antiferromagnetic materials[56] hold the most promise for devices operating above 100 GH_z. Their high internal fields cause them to have natural resonant frequencies in the millimeter and submillimeter wavelength regions. Since the normal modes are circularly polarized and the

resonance can be tuned by an external dc magnetic field, these materials can readily be used as resonance isolators or phase shifters. The two best materials found to this date are Cr_2O_3 and MnF_2. Experimental results obtained with Cr_2O_3 as a resonance isolator in a rectangular waveguide are shown below:

frequency = 140 GHz

α_r (reverse loss) = 10 dB

α_ϵ (forward loss) = 1 dB

applied dc magnetic field = 10 kG (1 T)

bath temperature = $77^{\circ}K$

linewidth = 1.5 kG (.15 T)

By adding impurities of Al to Cr_2O_3, operation near 1.3 millimeters is possible. Therefore, it should be possible to "tailor-make" materials for given frequency ranges by adding impurities to various antiferromagnetics.

7.3.11 Commercially Available Components in the Millimeter Wavelength Region

In the range where rectangular waveguide is applicable, most of the usual devices familiar in the microwave range are available from at least one, and sometimes a number of, manufacturers.

A survey of current catalogs reveals that the following items are available in the bands between 26.5 and 220 GHz:

A. Ferrite Devices

1. isolators, broad band
2. isolators, narrow band (to 140 GHz)
3. switches and variable attenuators (to 140 GHz)
4. modulator (to 140 GHz)
5. phase shifter (to 140 GHz)
6. 4-port circulator (to 140 GHz)
7. Y-circulator (to 110 GHz)

B. Rectangular Waveguide Components

1. rotary vane attenuator
2. fixed attenuator
3. level sitting attenuator
4. phase shifter
5. 3 and 4-port manual switch
6. cavity frequency meter
7. directional coupler
8. termination
9. moving load (to 110 GHz)
10. sliding short
11. fixed short
12. hybrid ring
13. short slot hybrid (to 170 GHz)
14. E/H tuner
15. hybrid tee
16. E-plane tee
17. H-plane tee
18. E-and H-plane bends
19. twists
20. tapered waveguide adapters
21. slotted sections (to 110 GHz)
22. other standing wave detectors (90 to 220 GHz)
23. harmonic generator or mixer
24. tunable detector mount
25. fixed detector mount (to 170 GHz)
26. parabolic antennas with feed
27. dielectric lens
28. feed and standard gain horns
29. elliptical reflector antenna (to 75 GHz)
30. linearly polarized feed
31. circularly polarized feed (to 90 GHz)
32. Cassegrain antenna
33. conical horn
34. conical horn lens

C. TE_{01} Circular Waveguide

1. standing wave detector (to 110 GHz)
2. variable attenuator (to 110 GHz)
3. mode transducer
4. directional coupler(to 110 GHz)
5. mode filter
6. rotary joint
7. 90° bend
8. termination

7.4 CONCLUSIONS AND RECOMMENDATIONS

Various transmission systems for millimeter/submillimeter waves have been described and compared on the basis of attenuation and a few other characteristics. As far as is known, no exhaustive comparative study has ever been made. Such a study might be worthwhile, since the present literature does not present a unified view of the various systems.

Of high interest for many waveguide applications are the various overmoded systems, e.g., helical waveguide, lined circular waveguide, and oversize rectangular guide. For the frequencies of interest the latter two would appear most promising, and further research and development on them should be encouraged. It is suggested that a circular waveguide with an oxide inner coating be investigated as a practical substitute for a thermoplastic-lined tube for sizes where the latter would be impractical to fabricate.

Continued research on new systems should be encouraged, particularly in view of the need for finding ways of coupling energy out of some of the new generating devices.

Beam waveguides are far from being realized in the millimeter/submillimeter range. The drawback of size for lens systems is not obviated by resorting to other diffraction devices, and in all systems enclosure and evacuation are needed, but then, so are they for any hollow waveguiding system in this part of the spectrum. Lenses for this region of interest are in a highly unsatisfactory state of development due to inadequacies of commonly used refracting materials. Despite these points, it is felt that the beam waveguide offers many of the same attractive characteristics as do oversized or overmoded waveguide systems; namely, the application of optical principles to component design and very low attenuation. Research and development in this area should certainly be continued.

Components for all systems can be designed either by the extrapolation of techniques used with the rectangular waveguide or by the application of optical principles. This has not been done for many of the unusual waveguide systems as yet, but should be pursued for them.

Ferrite device research has the dual problem of achieving high performance in the frequency range of interest and adaptation to the various waveguide configurations discussed above.

Continued research on several promising materials such as barium ferrites, rare-earth iron garnets, certain magnesium and manganese ferrites, and various antiferrimagnetic materials is required if suitable devices operable without external cooling are to be developed. In addition, work must continue on the development of suitable material configurations for use in some of the unusual waveguide systems mentioned here.

7.5 REFERENCES TO CHAPTER VII

1. P. D. Coleman, "State of the art: Background and research developments-millimeter and submillimeter waves," IEEE Trans., MTT-11, Sept., 1963, p. 271.

2. J. W. Dees and A. P. Sheppard, "Components, performance and cost of millimeter-wave systems," MICROWAVES 2, July, 1963., pp. 18-27.

3. A. E. Karbowiak, "Optical waveguides," Advances in Microwaves, V. 1, ed. L. Young, Academic Press, New York, 1966, pp. 75-113.

4. L. L. Bertan, "Considerations in the design of two-millimeter wave components," Fourth Annual Joint Military-Industrial Electronic Test Equipment Symposium, Armour Research Foundation, Chicago, Ill., 1961.

5. H. J. Moody, et al, THE RADIO SPECTRUM FROM 10 Gc to 300 Gc in AEROSPACE COMMUNICATIONS, ASD-TR-61-589, Vol. III, Contract AF 33(616)-7868, RCA Victor Company, Ltd., Montreal, Canada, July, 1962. (AD 294341).

6. A. F. Harvey, MICROWAVE ENGINEERING, Academic Press, New York, 1963.

7. H. J. Hinden and J. J. Taub, "Oversize waveguide directional coupler," AIL Monograph, Airborne Instruments Laboratory, Deer Park, New York, 1962.

8. H. J. Hinden and J. J. Taub, "Components for the spectrum gap," AIL Monograph, Airborne Instruments Laboratory, Deer Park, New York, 1963.

9. J. J. Taub, et al, "Submillimeter components using oversize quasi-optical waveguide," IEEE Trans, MTT-11, Sept. 1963, p. 338.

10. J. J. Taub, et al, "Quasioptical waveguide filters," AIL Monograph, Airborne Instruments Laboratory, Deer Park, New York, 1964.

11. J. J. Taub, et al, "Millimeter and submillimeter component development," Quarterly repts. 1, 2, 3, and 4, Contract AF 30(602)-3343, 1963.

12. H. G. Unger, "Round waveguide with lossy lining," Proc. on mm Waves, P.I.B., 1959, pp. 535-591.

13. H. G. Unger, "Lined waveguide", BSTJ, 41, 1962, p. 745.

14. H. M. Barlow, et al, "Practical low-loss waveguide for long distance communications," I.E.E. Electronics Letters, 26 March 1965.

15. G. E. Conklin, "Observed 50 to 60 GHz attenuation for the circular electric wave in dielectrically-coated cylindrical waveguide bends," BSTJ, XLV, May-June, 1966, pp. 723-732.

16. A. J. Simmons, "TE_{01} mode components in the 3 mm region," IEEE Trans. MTT-11, Sept. 1963, p. 324.

17. S. E. Miller, "Waveguide as a communications medium," BSTJ, 33, Nov. 1954, pp. 1209-1266.

18. J. J. Morgan, "Theory of curved circular waveguide containing an inhomogeneous dielectric," BSTJ, 30, Sept. 1957, pp. 1209-1251.

19. H. G. Unger, "Helix waveguide theory and application," BSTJ, 37, Nov. 1958, pp. 1599-1647.

20. H. E. Rowe and W. D. Warters, "Transmission in multimode waveguide with random imperfections," BSTJ, 41, May, 1962, pp. 1031-1170.

21. W. H. Steier, "The attenuation of the holmdel helix waveguide in the 100-RS kMc band," BSTJ, 44, May-June, 1965, pp. 899-906.

22. M. H. Cufflen, "The H_{01} mode and the helix waveguide," the Marconi Rev., 28, No. 156, 1965, pp. 1-21.

23. J. A. Berry, "Measurement of H_{01} mode loss at θ band in helix waveguide," Marconi Rev., 28, No. 156, 1965, pp. 22-26.

24. R. A. Waldron and D. J. Rowe, "Normal modes of helix waveguide," Marconi Rev., 28, No. 156, 1965, pp. 29-64.

25. D. J. Bowe and R. A. Waldron, "Coupling between modes in helix waveguide," Marconi Rev., 28, No. 156, 1965, pp. 65-88.

26. Young, Unger, et al, Proc. IEE, 106, pt. B., Supplement No. 13, Sept. 1959, (four papers).

27. P. J. B. Clarricoats, "Propagation along unbounded and bounded dielectric rods," Pts. 1 and 2, Proc. IEE, 108C, 1961, pp. 170 and 177.

28. H. Kikuchi and E. Yamashita, "Theory of dielectric waveguides and some experiments at 50 kMc/s" Proc. Symp. Millimeter Waves, PIB, 1959.

29. M. T. Weiss and E. M. Gyongy, "Low loss dielectric waveguides," IRE Trans. MTT-2, Sept. 1954, pp. 38-44.

30. G. Goubau, "Designing surface wave transmission lines," ELECTRONICS, 27, April 1954, pp. 180-184.

31. G. Goubau, "Surface waves and their application to transmission lines," J.A.P., 21, 1950, p. 1119.

32. G. Goubau, "Single conductor surface wave transmission lines," Proc. IRE, 39, 1951, p. 619.

33. D. D. King, "Properties of dielectric image lines," IRE Trans. MTT-3, pp. 75-81, March, 1955.

34. D. D. King, "Circuit components in dielectric image lines," IRE Trans, pp. 35-37, December, 1955.

35. D. D. King and S. P. Schlesinger, "Losses in dielectric image lines," IRE Trans., MTT-5, Jan., 1957, pp. 31-35.

36. L. Berenbaum and J. Gremsmann, "A low-loss H-guide for millimeter wavelengths," PIB Sym. on mm Waves, 9, April, 1959, pp. 543-562.

37. J. W. E. Griemsmann, "Oversized waveguides," MICROWAVES, 2, Dec., 1963, pp. 20-33.

38. F. J. Tischer, "The H-guide - a waveguide for microwaves," IRE Conv. Rec., 4, pt. 5, 1956, pp. 44-47.

39. F. J. Tischer, "Properties of the H-guide at microwave and millimeter wave regions," Proc. IEE, pt. B, Sup. 13, 1959, pp. 47-57.

40. F. J. Tischer, "The groove guide, a low-loss waveguide for millimeter waves," IEE Trans., MTT-11, Sept., 1963, p. 291.

41. M. Cohn, "TE modes of the dielectric loaded trough line," IRE Trans., MTT-8, July, 1960, p. 449.

42. G. Goubau and F. Schwening, "On the guided propagation of electromagnetic wave beams," Trans. IRE, AP-9, May, 1961, p. 248.

43. G. Goubau and J. R. Christian, "Some aspects of beam waveguides for long distance transmission at optical frequencies," IEEE Trans., MTT-12, March, 1964, pp. 212-220.

44. J. B. Beyer and E. H. Scheibe, "Loss measurements of the beam waveguide," IEEE Trans., MTT-11, Jan., 1963, p. 18.

45. S. E. Miller, "Alternating gradient focussing and related properties of conventional convergent lens focussing," BSTJ, July, 1964, pp. 1741-1758.

46. J. E. Degenford, et al, "The reflecting beam waveguide," IEEE Trans., MTT-12, July, 1964, pp. 445-453.

47. D. W. Berreman, et al, "Gas Lenses," Monograph 4865, Bell Telephone System Technical Publication, 1964, (Group of papers reprinted from BSTJ, 43, July, 1964, pts. 1 and 2, pp. 1469-1479, and pp. 1727-1825).

48. A. A. Meyerhoff, "Interaction between surface wave transmission lines," Proc. IRE, 40, pp. 1061-1065, Sept. 1952.

49. P. P. Lombardini, R. F. Schwartz, and P. J. Kelly, "Multi output directional coupler, final report," Contract AF 309635)-2801, Jan., 1956, Moore School of Electrical Engineering, University of Pennsylvania.

50. W. H. Louisell, COUPLED MODE AND PARAMETRIC ELECTRONICS, John Wiley and Sons, New York, 1960.

51. E. Ronald Schineller, "Variable optical prism attenuator with multiwavelength spacing," Report 1220P, Wheeler Labs, Smithtown, New Jersey, 5 June 1964 (Presented at Symposium on Quasi-Optics, P.I.B., June 8-10, 1964).

52. Rodrigue, "Magnetic materials for millimeter wave applications," IEEE, Trans. on MTT, MTT-11, Sept., 1963, pp. 351-356.

53. Barnes, "Broad-band isolators and variable attenuators for millimeter wavelengths," IRE Trans. on MTT, MTT-9, Nov., 1961, pp. 519-523.

54. E. R. Schineller, et al., "Development of Microscopic waveguide and waveguide components for optical system," Report 1247, Contract NASw 888, Wheeler Labs., Great Neck, N. Y., 28 Nov. 1964.

55. A. S. Boxer, J. F. Allan, R. F. Rauchmiller, "Properties of Ferromagnetic materials for microwave applications," Contract No. AF 33 (657)-8439, Bell Telephone Labs., pp. 74, 145, 176, 196, 201, 286, 308, 342, 381, 466, July, 1964.

56. G. Heller, J. Stickler, J. Thaxter, "Antiferromagnetic materials for millimeter and submillimeter devices," Journal of Applied Physics, Vol. 32, No. 3, p. 3075, March, 1961.

57. MICROWAVE ENGINEERS HANDBOOK AND BUYERS GUIDE, Horizon House, pp. 201, 1965.

Chapter VIII

PROPAGATION

8.1 INTRODUCTION

The propagation of electromagnetic waves in the millimeter region is characterized by a selective interaction of these waves with matter. In this sense, the difference between the propagation of ordinary radio waves and the propagation of ultramicrowaves involves the transition from classical to quantum concepts. In vacuum, both classical and photon theory lead to the same concept of an electromagnetic beam whose structure is essentially dictated by the amount of coherence.[1] In the presence of matter, however, the way in which the electromagnetic energy of the beam is exchanged may differ sharply according to wavelength. For example, consider a microwave beam propagating through rain. At 10 GHz the diffusion of the beam may be explained by the classical theory of the statistical scattering from rain droplets. Around 22 GHz, however, the first lines of the rotational band of the H_2O molecule enter into the picture of the absorption process, and the quantum theory has to be invoked. In general, as the frequency increases, the energy of the photon penetrates more and more into the realm of the binding energies of the molecular structure, and the probability of the occurrence of a resonant interaction with matter becomes very large. Therefore, in the band of ultramicrowaves, diffusion, dispersion and attenuation of the beam passing through matter are essentially the effect of a selective interaction.

In view of these considerations, the study of ultramicrowave propagation requires the specification of many physical and chemical characteristics of the medium, as well as of the wave: pressure, density distribution, kinetic status, molecular composition, wave polarization and frequency may all be important parameters. As a consequence, the topic of propagation is difficult to deal with in a general form. From a physical viewpoint, the topic may be subdivided into (a) propagation in rarefied gases, (b) pressure broadening, (c) effect of density inhomogeneity and turbulence, (d) propagation in liquids and solids, and (e) diffusive scattering from small objects like rain or dust particles. From the viewpoint of the utilization of ultramicrowaves for space purposes, the topic may be better subdivided into (a) propagation in the earth's atmosphere, (b) propagation in outer space in the presence of meteors or planetary dust, and (c) absorption in other planetary atmospheres.

An excellent survey of the literature on centimeter and millimeter wave propagation has already been presented.[2] The present work represents essentially an effort to update that work.

8.2 SUMMARY OF UNDERLYING THEORY

8.2.1 Spectra of Rarefied Gases

When an electromagnetic wave travels in a gas, its oscillating field will interact with the dipole moment of the molecules of the gas. If the pressure of the gas is sufficiently low so that each molecule may be considered independently, absorption

of energy from the field will occur every time the photon energy $\hbar\omega$ of the wave equals a possible transition of the energy spectrum of the molecule. Most of the interactions observed in the ultra-microwave region are produced by transitions in the rotational energy of the gas molecules.

The energy spectrum of the rotational energy of a molecule varies according to the complexity of the molecular structure. In the simple case of a diatomic molecule, all masses are concentrated along one line and the moment of inertia is unique. In this case the allowed energy levels are

$$E_J = \frac{\hbar^2}{2I} J(J + 1) \tag{8.1}$$

where I is the moment of inertia about an axis perpendicular to the interatomic axis, and J is the quantum number of the total angular momentum. From the selection rule for a transition in the rotational energy, it follows that the frequency of absorption is

$$\omega_{JJ'} = \frac{\hbar}{I} (J + 1) \tag{8.2}$$

The same expression is also valid for any linear polyatomic molecule. Thus, the rotational spectra to be expected from diatomic or linear molecules consist of a series of nearly equally spaced lines, the frequency separation being approximately $\hbar/2\pi I$. A more accurate analysis of the mechanical problem shows

that the line spacing is slightly altered by centrifugal distortion, and the lines may be split by the effect of interaction with the vibrational energy levels (ℓ type doubling). Finally, each line may have a hyperfine structure due to the possible interaction between the electric or magnetic moment of the molecule and the magnetic dipole or the electric quadrupole of the nucleus.

In terms of increasing complexity, diatomic and linear molecules are followed by symmetric-top molecules. In these molecules one can distinguish the moment of inertia along the main symmetry axis and the moment of inertia about either of the two perpendicular axes, I_b. The rotational moment is complex, since, while the molecule rotates about its main axis of symmetry, this axis precesses about the direction of total angular momentum. However, only changes of the precessional energy cause interaction with the field, because the electric moment of the molecule lies along the main axis. Thus, to a first approximation, the frequencies of resonance are

$$\omega_{JJ'} \simeq \frac{1/K}{I_b} (J + 1) \qquad (8.3)$$

and the spectrum again consists of nearly equally spaced lines. The main effect of the centrifugal distortion is to remove the degeneracy of different K states (K is the component of angular momentum resolved along the main axis) and to split the line into (J + 1) components.

Finally, the most complex cases belong to the asymmetric-top molecules. Owing to the lack of symmetry in their geometrical structure, the derivation of the rotational energy levels of these molecules becomes very difficult. In general, one may observe that the asymmetry removes the degeneracy of the various K levels (analogous to the centrifugal distortion in the symmetric-top case) and that the effect of centrifugal distortion is here very large.

Other phenomena affect the microwave absorption spectrum to a considerable extent. An example is inversion, which occurs in any non-planar molecule but has a spectacular importance only in the case of ammonia. It consists of a splitting of the ground state related to the two energy levels corresponding to the two possible conditions of equilibrium with respect to the center of mass. According to the simplest theory, only one absorption line is expected,but due to centrifugal distortion a series of lines, corresponding to the different rotational states, are obtained (66 lines observed between 16.7 GHz and 39.9 GHz in $N^{14}H_3$).

There is a long list of substances whose ultramicrowave spectra have been, at least partially, experimentally investigated in the gaseous state. The list includes 36 diatomic and 14 linear molecules, for which spectral tables have been theoretically computed.[3,4] There are also 106 symmetric-top molecules, 34 inorganic and 137 organic asymmetric-top molecules. For most of these molecules the theory is only partially elaborated.[5] A

rather complete list of references related to these molecules is given by Stark and Favero.[6,7]

8.2.2 Pressure Broadening

Knowledge of the locations of the resonances of the interacting molecules is not enough to predict the behavior of the propagating wave in a gas mixture like air. In fact, a pure monochromatic absorption line only belongs to a truly isolated, undisturbed and stationary molecular system. Practically, the spectral lines are widened by various types of unavoidable disturbances, such as thermal agitation (Doppler broadening) and interaction between molecules. The most important broadening of the absorption lines arises from collisions between molecules, and is known as pressure broadening. A rather complete description of pressure broadening may be obtained assuming random interruptions of harmonic oscillators, followed by a Boltzmann distribution of their energies after collision.[8]

Accordingly, the spectrum of absorption results

$$\alpha(\omega) = S_o \sum_i S_{ij} f(\omega_{ij}, \omega) \tag{8.4}$$

where

$$S_o = \frac{\pi \mu^2 N}{3hcQ(T)} \tag{8.5}$$

with

μ^2 equal to P_E^2/ϵ_o for molecules having an electric dipole moment of P_E, and equal to P_μ^2/μ_o for molecules having a magnetic dipole moment P_M; h is Planck's constant, c the velocity of light, Q(T) the rotation partition function, N the number density of the absorbing molecule and

$$S_{ij} = \left\{ \exp\left(-\frac{\hbar\,\omega_j}{KT}\right) - \exp\left(-\frac{\hbar\,\omega_i}{KT}\right) \right\} g_j \left|\mu_{ij}\right|^2 \omega_{ij} \qquad (8.6)$$

with

$\hbar\,\omega_j$ the energy at level j th; $\hbar\,\omega_i$ the energy at level i th; T the absolute temperature, g_j the statistical weight of level j th; $\left|\mu_{ij}\right|^2$ the square of the direction cosine matrix element of the $j \to i$ transition; ω_{ij} the frequency of the $j \to i$ transition; and finally $f(\omega_{ij},\omega)$ is the line-shape factor. According to the Van Vleck-Weisskopf theory,[9, 10, 11] the shape factor is given by

$$f(\omega_{ij},\omega) = \frac{2\omega\,\Delta\omega_{ij}}{\omega_{ij}} \left\{ \frac{1}{(\omega-\omega_{ij})^2 + \Delta\omega_{ij}^{\,2}} + \frac{1}{(\omega+\omega_{ij})^2 + \Delta\omega_{ij}^{\,2}} \right\} \qquad (8.7)$$

where $\Delta\omega_{ij}$ is the spectral width of the line at one-half of its maximum intensity. For a gas mixture it is approximately

$$\Delta\omega_{ij} = \sum_S \beta_{S_{ij}} P_S \qquad (8.8)$$

where, $\beta_{S_{ij}}$ is a factor which characterizes the broadening efficiency of the collision phenomenon between the absorbing gas and the s th component of the mixture, and P_S is the partial pressure of that component. The sum of eq. (8.4) is extended to all rotational levels according to the selection rules.

It follows from the previous expressions that the maximum of absorption at each resonance remains considerably independent of the pressure, while the wings of the absorption lines are approximately proportional to gas pressure. At a particular frequency the absorption is influenced by lines located at considerable frequency separation on each side, so that it is necessary to include these contributions to arrive at a sufficiently accurate absorption coefficient.

8.3 CONSTITUENTS OF THE EARTH'S ATMOSPHERE

The earth's atmosphere up to an altitude of about 90 km is essentially a mixture of N_2, O_2 and Ar in the following percentages: N_2 = 78.08%, O_2 = 20.95%, Ar = 0.93% (see Table 8.I). In the troposphere another important constituent of air is H_2O, whose percentage may change from 0 to about 2%. The presence of H_2O is generally evaluated in terms of the so-called humidity. Absolute humidity is defined as the quantity w of water vapor in air, in grams per cubic meter. It can be computed from observation of the relative humidity and temperature by knowing the weight w_o of the saturated aqueous vapor, which is obtainable from

Table 8.I Atmospheric Gases at Sea Level

(Ref: Handbook of Chemistry and Physics, 44th ed., p. 2582)

Natural Gas	Content (by Volume) %	Content Parts/10^6
N_2	78.084 ± 0.004	---
O_2	20.946 ± 0.002	---
A	0.934 ± 0.001	---
CO_2	0.033 ± 0.001	---
Ne	1.8×10^{-3}	18.18 ± 0.04
He	5.24×10^{-4}	5.24 ± 0.004
CH_4	---	2.0
Kr	1.0×10^{-4}	1.14 ± 0.01
H_2	5.0×10^{-5}	0.5
N_2O	---	0.5 ± 0.1
Xe	8.0×10^{-6}	0.087 ± 0.001
O_3	1.0×10^{-6}	---
H_2O Vapor	0 to 2	---
Man Made Gases		
SO_2	variable	---
CO	"	---
Hydro-Carbon	"	---

standard tables (e.g. Handbook of Chemistry and Physics, 44th ed., page 2582) since,

$$\text{relative humidity} = w/w_o \ (\%)$$

All other constituents of air (Ne, He, Kr, Xe, CH_4, N_2O, O_3) are below .01% in the lower atmosphere.

Because of the essential lack of dipolar moment of the nitrogen molecule, propagation through air is primarily controlled by the absorption of oxygen and water vapor.

8.3.1 Oxygen

Oxygen in its ground electronic state is coupled to the electromagnetic field by a magnetic moment, which results from the unpaired spins of two electrons. The millimeter spectrum of O_2 derives primarily from transitions for which the selection rule is that the electron spin alignment with respect to the total angular momentum changes by one unit, i.e., $(K, J = K + 1) \rightleftarrows (K, J = K)$ or $(K, J = K) \rightleftarrows (K, J = K - 1)$. These transitions are usually denoted by the symbol N^+ and N^-, respectively. The frequencies of these transitions was determined by Muzishima and Hill,[12] and the experimental spectrum has been used by Tinkham and Strandberg[13] to obtain the best fit to five parameters of the O_2 molecule. The transition frequencies are shown in Table 8.II.

Transitions in which the selection rule is $\Delta K=2$ are also possible in O_2,[14] but in this case the line intensity is very weak. The lines which have been observed in a pipe 180 meters long and filled with O_2 pressurized at 1.75 atmospheres are listed in Table 8.III.[15]

Table 8.II Transition Frequencies for Oxygen

N	(+)MHz	(-)MHz
1	56 264.7	118 750.7
3	58 446.9	62 486.7
5	59 591.5	60 306.1
7	60 435.5	59 164.0
9	61 151.3	58.323.6
11	61 800.9	57 612.1
13	62 411.9	56 967.8
15	62 998.5	56 363.1
17	63 568.7	55 783.6
19	64 127.6	55 221.5
21	64 678.2	54 671.6
23	65 222.7	54 671.9
25	65 762.6	53 597.3

Table 8.III Lines Observed in Oxygen at 1.75 Atmospheres Pressure

Transition	Frequency (GHz)
(K=1, J=2) → (K=3, J=2)	426
(K=1, J=2) → (K=3, J=3)	486
(K=3, J=4) → (K=5, J=4)	774
(K=3, J=4) → (K=5, J=5)	834
(K=5, J=6) → (K=7, J=6)	1,122
(K-5, J=6) → (K=7, J=7)	1,177
(K=7, J=8) → (K=9, J=8)	1,468
(K=7, J=8) → (K=9, J=9)	1,526

The absorption appears stronger in transitions where $\Delta J=0$. Attempts to correlate these observations with the absorption spectrum of solar radiation passing through the atmosphere have not been successful.

8.3.2 Water Vapor

The water vapor molecule possesses a permanent electric moment, and consequently exhibits a pure rotational spectrum. Structurally, the molecule may be represented as an isosceles triangle with an apex angel of about 104.5°. Because none of the three moments of inertia are equal, this molecule belongs to the class of asymmetric rotors. The permanent electric moment lies along the axis of the middle moment of inertia. According to the theory, the eigenvalues of the energy levels are roots of a Hamiltonian equation involving all three moments of inertia. The states are designated by the symbols J_T, where J is the total momentum of the system, and T is an integer ranging from +J to -J, which denotes the ordering of the levels within a J group. Each level is also provided with a symbol, (++), (+-), (-+) and (--) which characterizes the symmetry of the nuclear spins in the state. The selection rules are $\Delta J = \pm 1$ or 0, and the transition may only occur between the symmetry class $(++) \rightleftarrows (--)$, or $(+-) \rightleftarrows (-+)$. The antisymmetric levels have three times the statistical weights of the symmetric ones. A table of rotational energy levels of the water vapor molecule may be obtained from infrared data.[16,17] Because of the small

separations involved, the resonances in the submillimeter region cannot be predicted with great precision. The submillimeter spectrum has not yet been fully investigated. A list of all the transitions of the rotational spectrum of H_2O for frequencies below 3,000 GHz are included in Figs. 8.8-8.17.

The terrestrial atmosphere is stratified and approximately obeys the altitude-pressure relationship

$$P = P_0 \exp\left(-\frac{h}{H(h)}\right) \tag{8.9}$$

where $H(h) = \frac{kT}{2M}$ is the isothermal "scale height," P_0 the pressure at sea level, g the earth's gravitational acceleration, and M the air molecular mass. Therefore, the characteristics of radio wave absorption in air will vary radically with altitude. At high altitudes the humidity is very low, and the propagation is primarily controlled by the absorption of oxygen. Below 30 km of altitude, pressure broadening blends together the 25 spectral lines of O_2 located around 60 GHz. At low altitudes the water vapor spectrum enters into the picture with 131 lines spread between 20 GHz and 3,000 GHz. Because of the pressure broadening, all these lines blend together to form a continuum of absorption as the result of the overlapping of all the skirts of many lines.

At the time of Van Vleck's papers (1947), no propagation test had been made through the actual atmosphere in the millimeter wavelength region, and only a very few quantitative data were available in the centimeter region. However, accumulation of

measurements have shown that the attenuation of millimeter wavelengths in the skirts of the oxygen and water vapor lines is inadequately described by the theoretical values of Van Vleck. While Schulze and Tolbert[18] do not purport any justification for a significant alteration of the theory, Zhevakin and Naumov[19] strongly feel that the current prediction of the form of the spectral lines in air requires a more elaborate solution of the statistical problem of molecular collisions.

Before entering further in this topic, it is proper to point out the staggering experimental difficulties which are involved in measurements of attenuation of ultramicrowaves in air. Measurements can be made in the laboratory, or by direct transmission along a given atmospheric path. In the latter case, the general procedure for making the tests is to observe the signal level over a number of days and plot the signal strength as a function of water vapor content in the atmosphere. The slope of this line provides the water vapor losses, and the ordinate provides the oxygen loss. Small and large scale inhomogeneities exist in the water vapor content. However, a reliable measurement of the variation of the path loss with water vapor concentration is obtained by determining the humidity at both ends of the path, and averaging a large number of data. Other disturbances are due to refraction and precipitations along the path.

8.4 EFFECTS OF ATMOSPHERIC OXYGEN

Laboratory experiments are generally performed on small samples of pure or mixed gases. Laboratory testing is limited by the fact that the attenuation can only be measured accurately in the immediate vicinity of a resonance because the skirts of the absorption lines present a loss percentage too small to be measurable in a short path. (The University of Texas cell is 500 feet long.)

Many tests have been performed in the laboratory on oxygen, either pure or in a mixture with nitrogen at various gas pressures.[20,29]

An important parameter measured in these tests is the line width $\Delta\omega_{ij}$. At atmospheric pressure the 25 spectral lines around 60 GHz broaden enough so that they nearly form one single line. Various estimates have been made to obtain one broadening parameter which best fits all observations. The line broadening parameter for O_2 has been determined to be nearly independent of rotational quantum number, and given by[30]

$$\Delta\omega = 2\pi \beta_1 P \left[0.21 + 0.78\, \beta_2\right] \left[\frac{300}{T}\right]^{0.85} \qquad (8.10)$$

where β_1 and β_2 are two constants and p is the pressure in Torr.

For pure O_2 the factor in the brackets is equal to unity. For air, this factor consists of the mole fraction of O_2 in air (.21) plus the mole fraction of N_2(.78) multiplied by β_2 which specifies the relative efficiency of N_2 - O_2 collisions to the O_2 - O_2 collisions in pressure broadening. The parameters β_1 and β_2 are

determined empirically. Best compromise values result in $\beta_1 = 1.95$ MHz and $.21 \leq \beta_2 \leq .37$. Using a standard model of atmosphere (e.g. the ARDC model*), pressure can be related to altitude by eq. (8.5).

Typical laboratory data on dry air at various pressures are shown in Figs. 8.1 and 8.2.

A comparison of these results with measurements of open path propagation at frequencies in the vicinity of the oxygen absorption lines[31-34] shows that the agreement between the two sets of measurements is poor. Straiton and Tolbert[35-36] report the line broadening parameters at atmospheric pressure shown in Table 8.IV.

Table 8.IV Comparison of Experimental Data on Line Broadening

O_2 band	Laboratory $\left(\frac{\Delta\omega}{2\pi}\right)$ MHz	Atmospheric Path $\left(\frac{\Delta\omega}{2\pi}\right)$ MHz
60 GHz	1,490	600
120 GHz	3,600	1,500

Among the causes invoked to explain the differences shown in the table are the presence in the atmospheric path of H_2O and other polar molecules, and of a continuous non-resonant Debye absorption.

In addition to attenuation, oxygen gives rise to emission of radiation. For radiometric purposes it is customary to measure the molecular emission in terms of an equivalent radiation temperature T which would be measured with a narrow-beam antenna looking through

* Airforce Geophysics Research Directorate, Bedford, Mass.

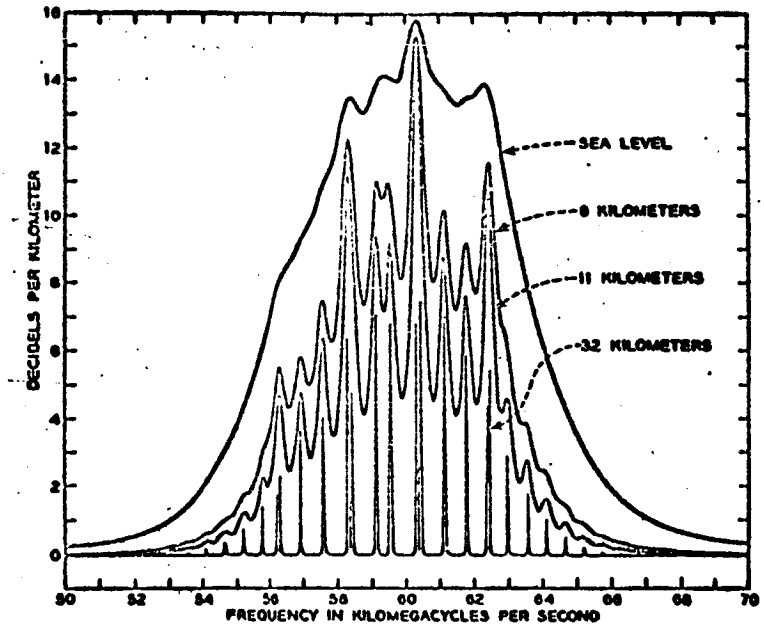

Figure 8.1 Intensity and Shape of the Oxygen Absorption Spectrum between 50 and 70 Gc as a Function of Altitude (taken from Ref. 2).

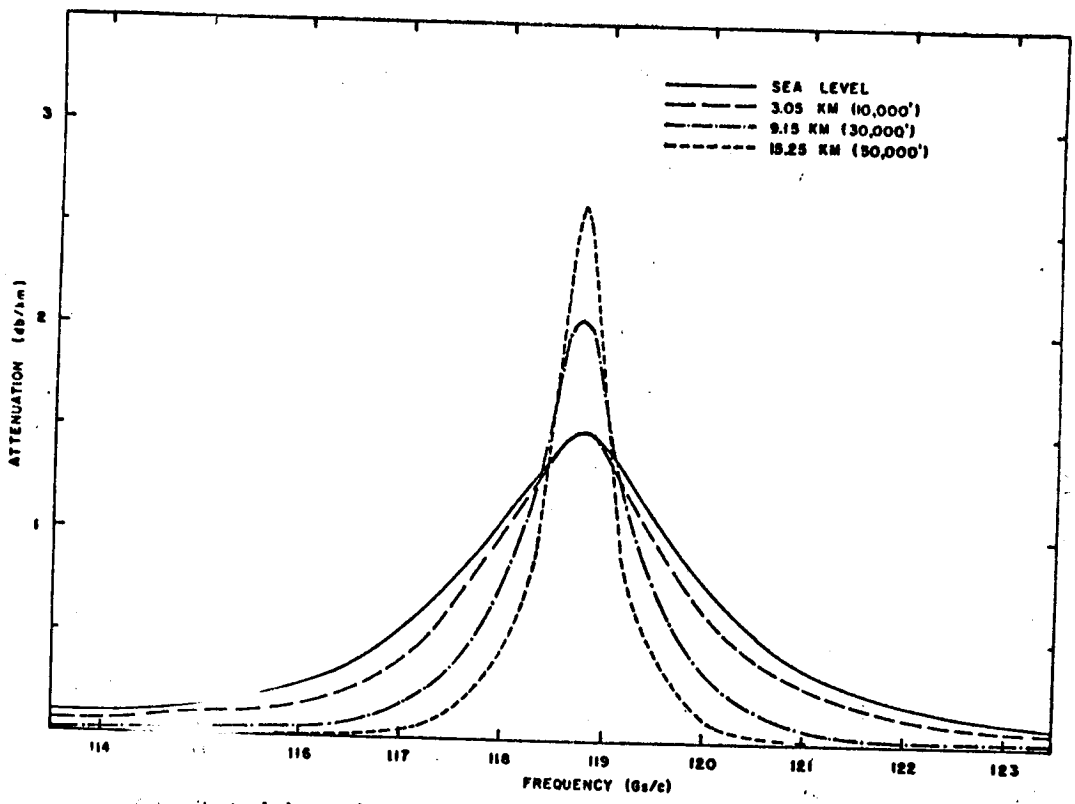

Intensity and shape of the oxygen absorption spectrum between 114 and 123 Gc/s as a function of altitude.

Figure 8.2 (Taken from Ref. 30)

the atmosphere. If the average radiation temperature of a source beyond the atmosphere is T_s, and if the zenith angle of this source is θ, the effect of the atmosphere may be described[30] in terms of the zenith opacity τ_0 and the radiation T_0 as

$$T = T_0 \exp(-\tau_0 \sec\theta) + T_0(\theta) \tag{8.11}$$

The contribution $T_0(\theta)$ to the antenna temperature may be obtained in terms of the atmospheric temperature distribution by means of the integral

$$T_0(\theta) = \int_h^\infty \alpha(\omega, T, p)\, T \exp(-\tau) \sec\theta \, dh \tag{8.12}$$

where $\alpha(\omega, T, p)$ is the attenuation coefficient and h_o the antenna height.

The opacity τ of the atmosphere is a function of the height h above sea level and the angle θ of the line of observation, and is given by

$$\tau = \int_h^\infty \alpha(\omega, T, p) \sec\theta dr = \tau_0 \sec\theta \tag{8.13}$$

The result of computations of (8.13) and (8.12) based upon the ARDC model atmosphere are shown in Fig. 8.3. Measurements of the emission of the atmospheric oxygen at an altutude of about 30 km have been successfully performed using a radiometer carried by a balloon.[37,38]

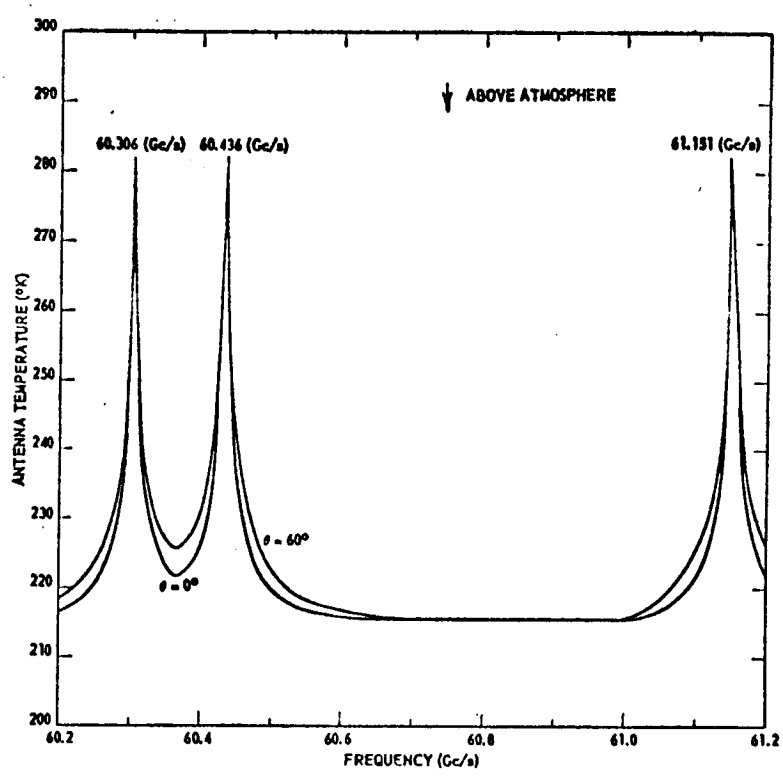

.-Computed antenna temperatures for observation of the earth's atmosphere from altitudes above 50 km. The frequency range includes three oxygen absorption lines. Curves are shown for antennas directed vertically downward ($\theta = 0°$) and directed obliquely downward ($\theta = 60°$).

Figure 8.3 (from Ref.30)

8.5 EFFECTS OF WATER VAPOR

Unlike oxygen, the water vapor concentration in air varies with time, and may be inhomogeneous along atmospheric layers of constant pressure. This renders the evaluation of experimental measurements of the water vapor spectrum an essentially difficult task. The difficulty not only exists in extended atmospheric paths, but also in the laboratory, because it is hard to keep the water concentration constant in a cell long enough to allow reliable measurements of attenuation.

In the laboratory, the absorption was observed essentially by two techniques: either a long cell[33,35] or a cavity, for which the phenomenon of resonance effectively multiplies the length of the path.[53,54] In these tests a gas mixture of H_2O and N_2 was also used, in order to obtain a water vapor spectrum at normal pressure, not perturbed by the absorption lines of O_2. The absence of oxygen does not modify the results noticeably, since nitrogen constitutes 78% of standard air, and also the spectral broadening is mainly controlled by $N_2 \rightleftarrows H_2O$ collisions; the efficiency of the collision phenomena in broadening the spectral lines of H_2O being expressed by the following ratios:[39]

$$(H_2O \leftrightarrows N_2) \ : \ (H_2O \leftrightarrows O_2) \ : \ (H_2O \rightleftarrows H_2O) = 1 : .3 : 5$$

A considerable amount of data has also been gathered on attenuation of millimeter radio links over atmospheric paths of different

lengths, at various water vapor densities (averaged along the path and assumed constant during the test).[40-44] Measurements have also been taken using the sun as the source of radiation.[45-51] Both types of measurements have shown a high degree of correlation between the amount of precipitable water observed along the path and the signal attenuation. In the case of solar radiation, an estimate of the total precipitable water was obtained by measuring humidity on the ground and making reasonable assumptions of the vertical distribution of water vapor.[52] Data have been selected from each group of measurements and plotted in Fig. 8.4. In order to make the data comparable, they have been reduced to the same reference of 1 gr./m^3 of precipitable water, under the simplified assumption that the relationship between this quantity and the measured loss is linear.

Finally, the theoretical prediction of the attenuation is particularly difficult, because most of the absorbing spectrum of H_2O lies in the infrared, so that the absorption in the millimeter region is essentially due to the overlapping skirts of many (871) resonant lines, including those in the near infrared. The correct use of the Van Vleck formula requires a knowledge of the broadening parameters of a large number of these lines. To consider the same half-widths for every line seems a poor assumption.

The existence of all these problems is reflected in the scarcity of available data. The two H_2O spectral lines which have been well studied experimentally lie below 200 GHz.

In order to produce an agreement between experimental data and theory, two width parameters have been defined, namely, a width parameter measured in the proximity of the line center, $\Delta\omega_c$, and a width parameter measured on the wing of the line, $\Delta\omega_w$. Frenkel and Valkenburg[53,54] report the following data:

Table 8.V Bandwidths of Water Vapor Lines

H_2O band	$\frac{\Delta\omega_c}{2\pi}$ (MHz/Torr)	$\frac{\Delta\omega_w}{2\pi}$ (MHz/Torr)
22 GHz	3.6 (Ref. 55)	18 (Ref. 55) 7-11 (Ref. 33, 35)
183 GHz	3.8 (Ref. 54) 4.4 (Ref. 53)	19 (Ref. 54) 23 (Ref. 53)

As for oxygen, water vapor in the atmosphere is responsible for the emission of radiation. The observation of this radiation from the ground gives, at least in principle, an interesting tool for the investigation of the vertical distribution of water vapor in the atmosphere.[56] A receiver suitable for this kind of observation has been built recently at M.I.T.[57]

In concluding these considerations of the effect of water vapor on the propagation of ultramicrowaves, it must be noted that there are still many questions left open. Straiton and Tolbert[58,59] pointed out many discrepancies between the theory and experimental data in the limited band (20 GHz-140 GHz) investigated. Recently, Zhevakin and Naunov[60,61] have sharply attacked Van Vleck's theory,

attributing to it the lack of correspondence between theory and experiment. The attenuation formula they propose is based upon a more elaborate statistical distribution of collisions[62] and uses, instead of the spectral line function (8.5), the expression

$$f(\omega,\omega_{ij}) = \frac{4\omega_{ij}^{2}}{(\omega_{ij}^{2} - \omega^{2})^{2} + 4\omega^{2}(\Delta\omega_{ij})^{2}}$$

A comparison between the two theories is shown in Fig. 8.5.

Introducing now the solid curve of Fig. 8.5 into Fig. 8.4, it is apparent that agreement between the experimental data and theory is again only fair. However, the effectiveness of either theory can only be judged after a further region of the spectrum has been investigated experimentally.

8.6 REMARKS ON PROPAGATION IN THE EARTH's ATMOSPHERE

On the basis of considerations made in the previous sections, it is clear that, apart from two confined oxygen bands (around 60 and 120 GHz), the greatest obstacle to the propagation of ultra-microwaves in the earth's atmosphere is due to the presence of water, either in the liquid state (precipitation or aerosol), or in the vapor state.

From meteorological data on surface temperature, relative humidity, and rainfall rates of four sites in the United States (Boston, Mass.; Washington, D.C.; Austin, Texas; and Los Angeles, Calif.), the Raytheon Company[63] has evaluated the average total

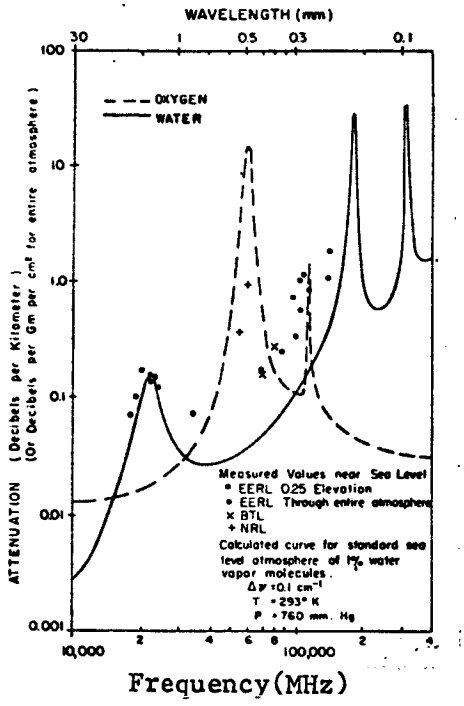

Figure 8.4 Measured Values Near Sea Level (see Ref. 52)

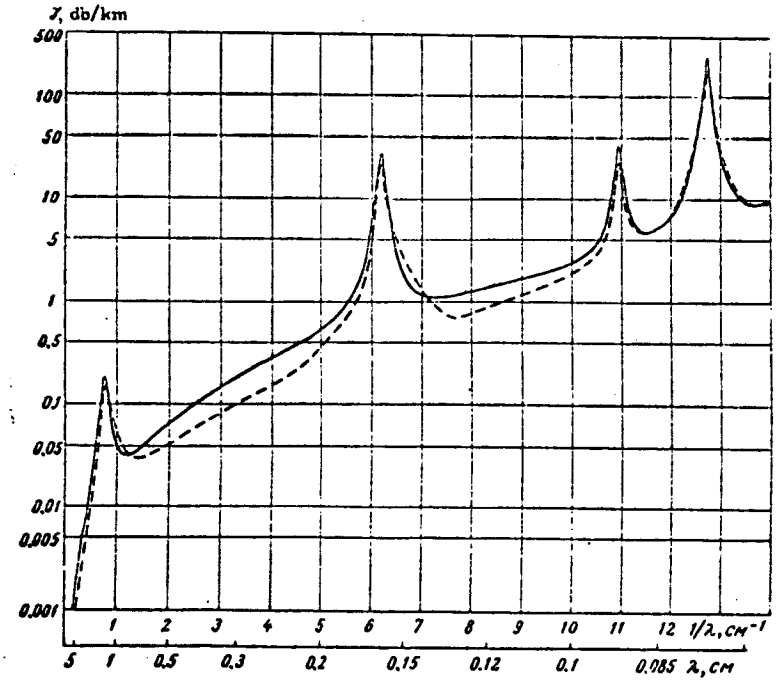

Figure 8.5 A Comparison of the Water Vapor Absorption Coefficient Computed by Zhevakin and Naumov (see Ref. 59), (solid Curve) with the data of Van Vleck (dotted line). In both cases T = 293°K, P = 760 mm Hg, absolute humidity $\rho = 7.5$ g/m^3.

atmospheric loss for the frequencies 16, 35, 70 and 94 GHz. These results are shown in Fig. 8.6 for clear, cloudy and rainy weather respectively. In the same figure are also plotted the expected losses due to O_2 and H_2O separately (dashed lines). The trend of the total absorption versus frequency is plotted as a solid line.

A general picture of the absorption characteristics of water vapor at normal temperature and pressure (T - 293°K, p=760 Torr) for frequencies below 3,000 GHz is presented in Figs. 8.8 to 8.17. These figures refer to water vapor concentration of 1 gr/m^3, which corresponds to a relative humidity of approximately 6%. In the figures, the solid curve represents the theoretical absorption as computed in ref. 60. Whenever possible, experimental data have been introduced. For frequencies above 300 GHz, these data are scarse. Only a certain number of absorption resonances have been accurately measured, and the level of attenuation has been determined for just seven "windows." These last measurements show that the experimental attenuation exceeds the theoretical by at least 5%. All possible transitions of the water vapor rotational spectrum in the band are also indicated in the figures.

For interpretation of the figures, the following observations are in order.

Attenuation coefficient: The attenuation coefficient written in the ordinates of the figures corresponds to the condition of 1 gr/m^3. This implies a relative humidity of about 6%. The

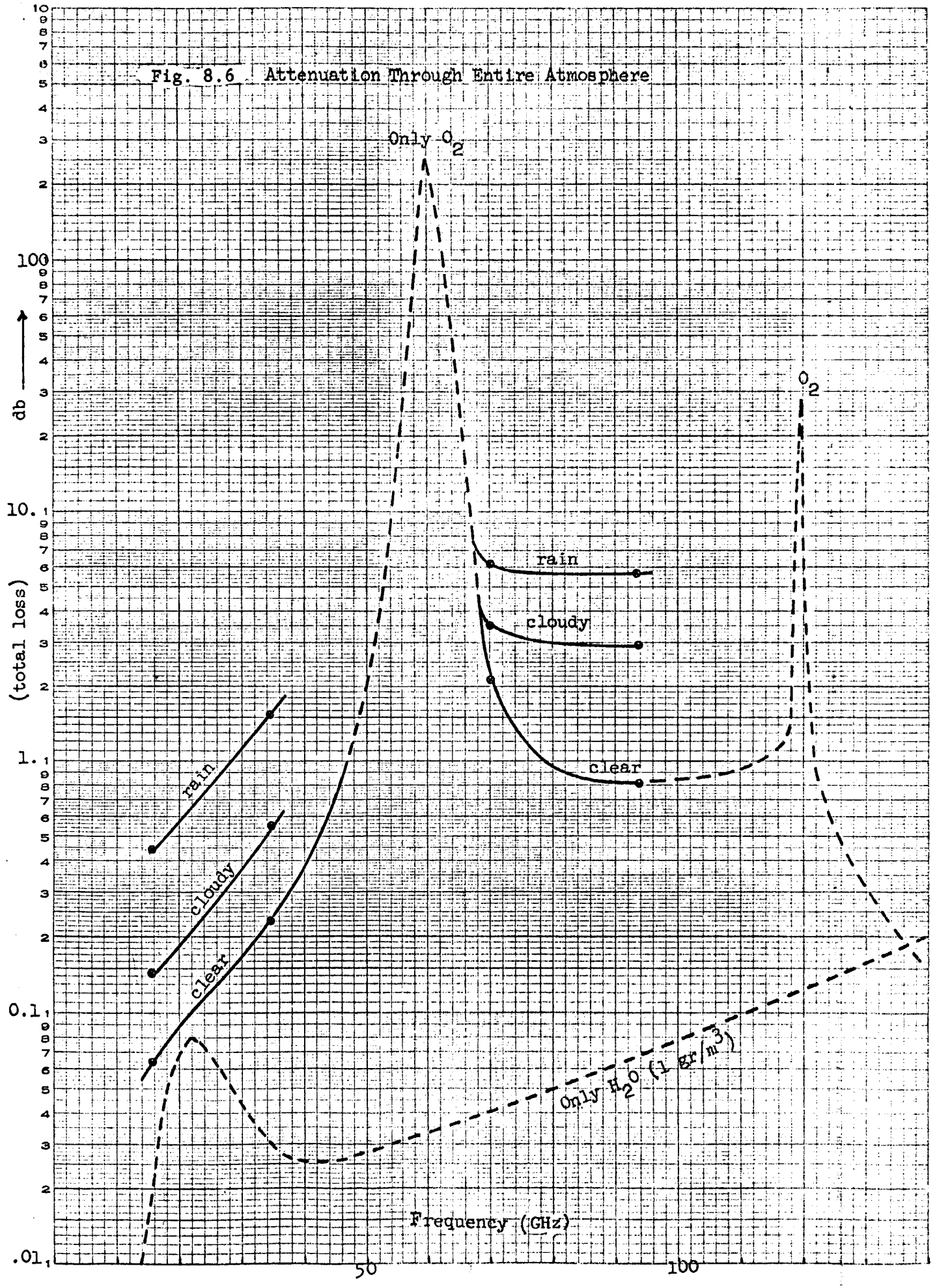

Fig. 8.6 Attenuation Through Entire Atmosphere

EUGENE DIETZGEN CO.
MADE IN U. S. A.
NO. 340-L510 DIETZGEN GRAPH PAPER
SEMI-LOGARITHMIC
5 CYCLES X 10 DIVISIONS PER INCH

MILLIMETER
DIETZGEN CO.
MADE IN U. S. A.

Figure 8-7 Relation between Saturated Precipitable Water and Temperature at Sea Level (p = 760 Torr)

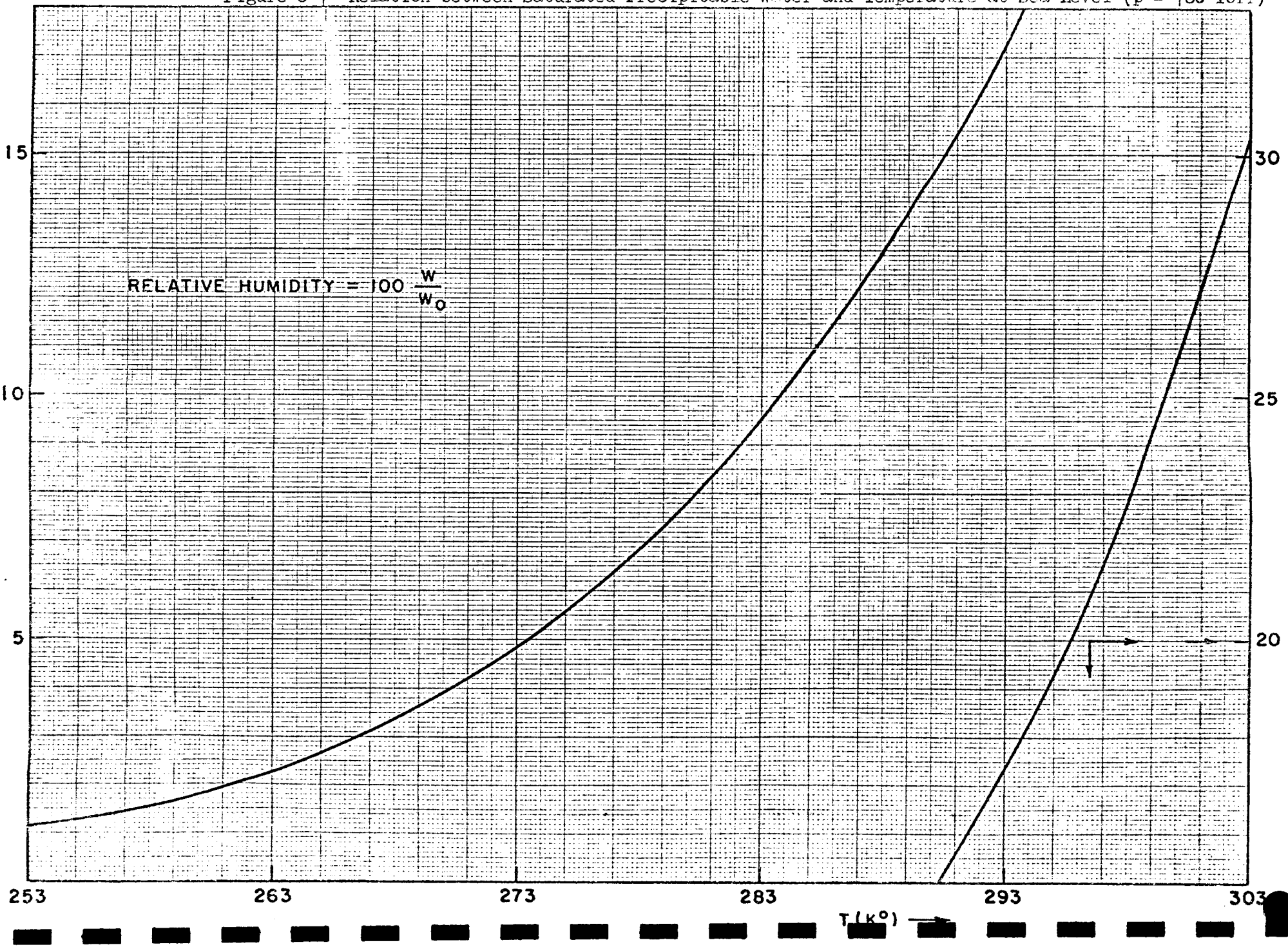

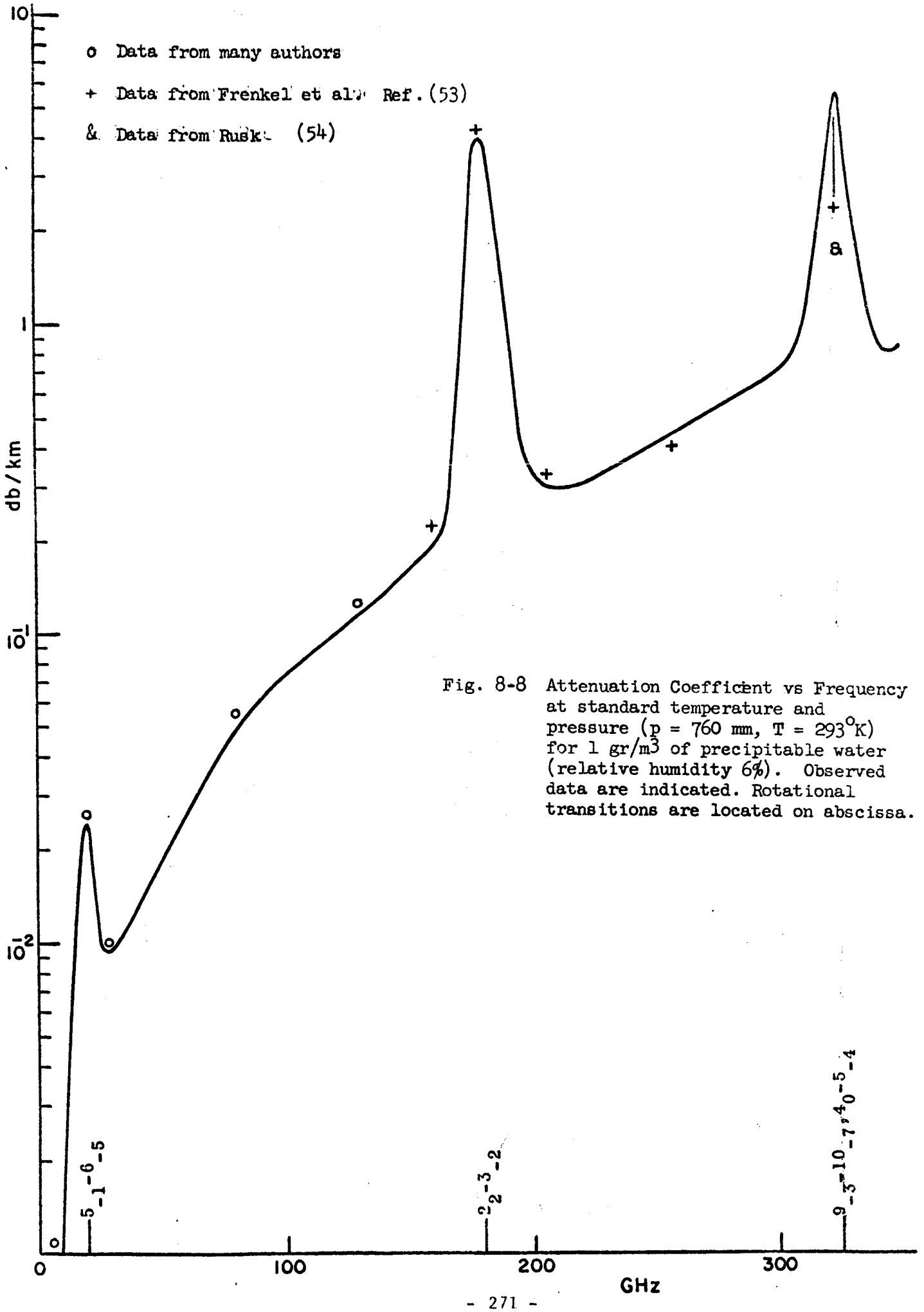

Fig. 8-8 Attenuation Coefficient vs Frequency at standard temperature and pressure (p = 760 mm, T = 293°K) for 1 gr/m^3 of precipitable water (relative humidity 6%). Observed data are indicated. Rotational transitions are located on abscissa.

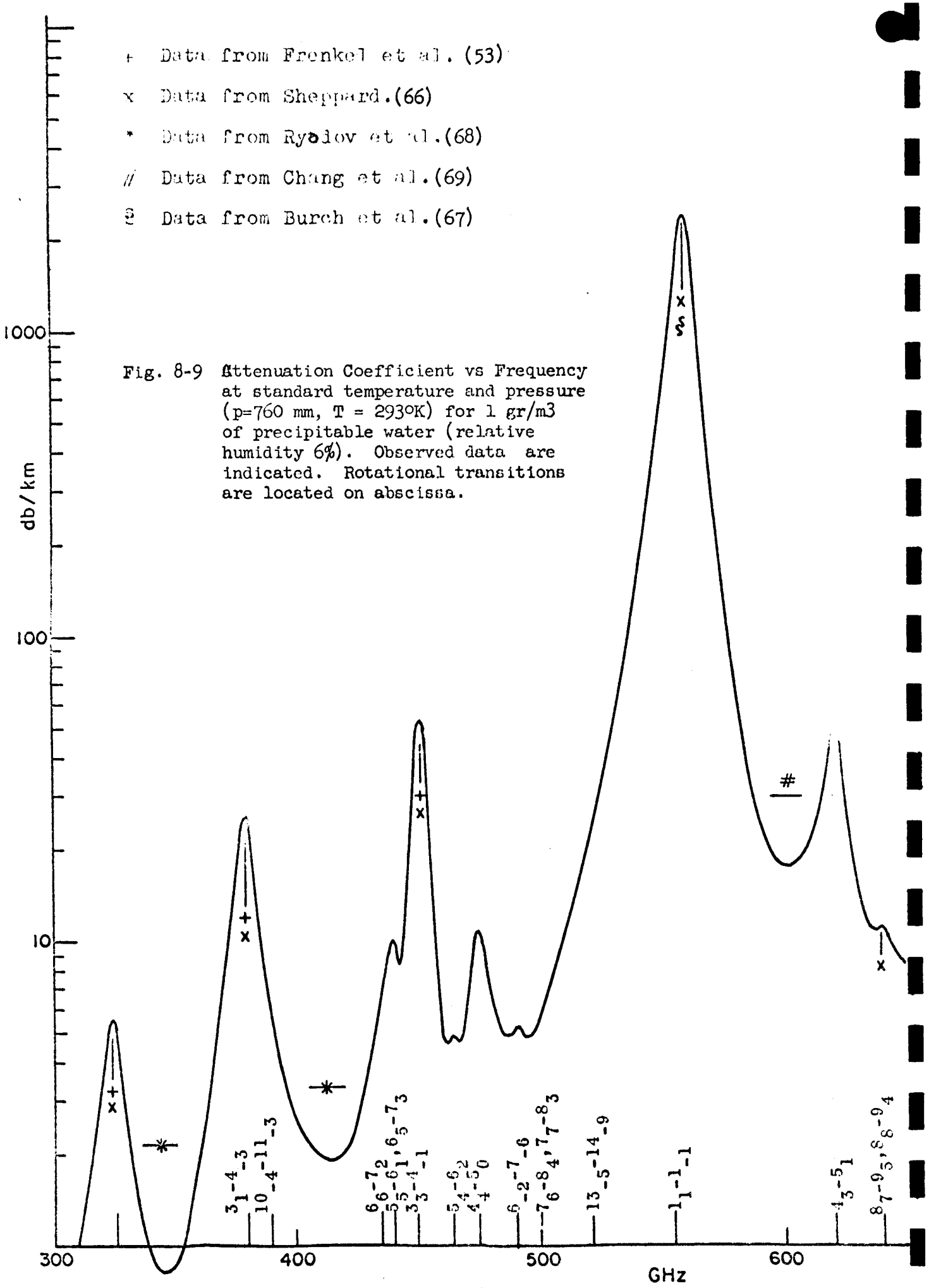

Fig. 8-9 Attenuation Coefficient vs Frequency at standard temperature and pressure (p=760 mm, T = 293°K) for 1 gr/m3 of precipitable water (relative humidity 6%). Observed data are indicated. Rotational transitions are located on abscissa.

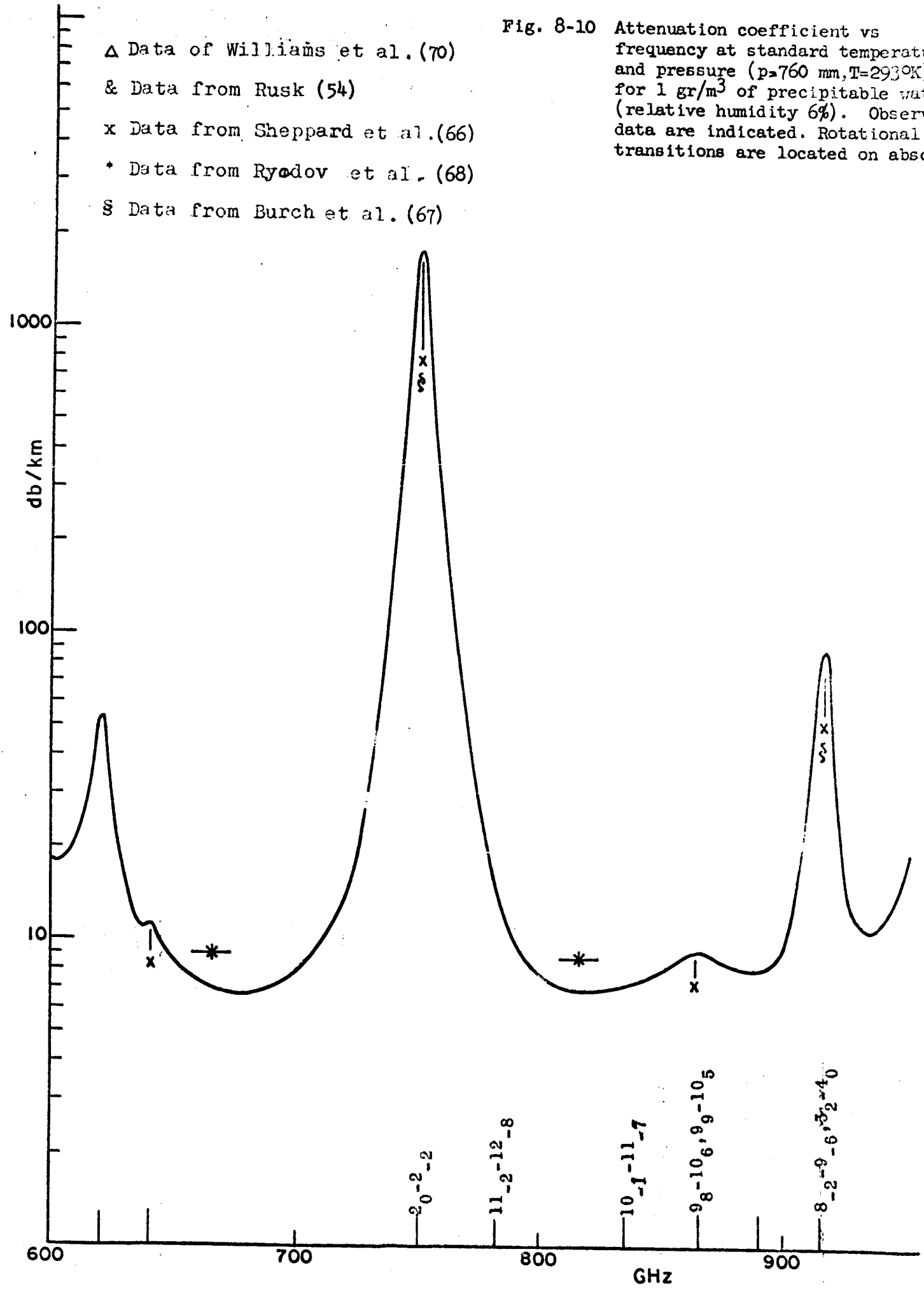

Fig. 8-10 Attenuation coefficient vs frequency at standard temperature and pressure (p=760 mm, T=293°K) for 1 gr/m^3 of precipitable water (relative humidity 6%). Observed data are indicated. Rotational transitions are located on abscissa

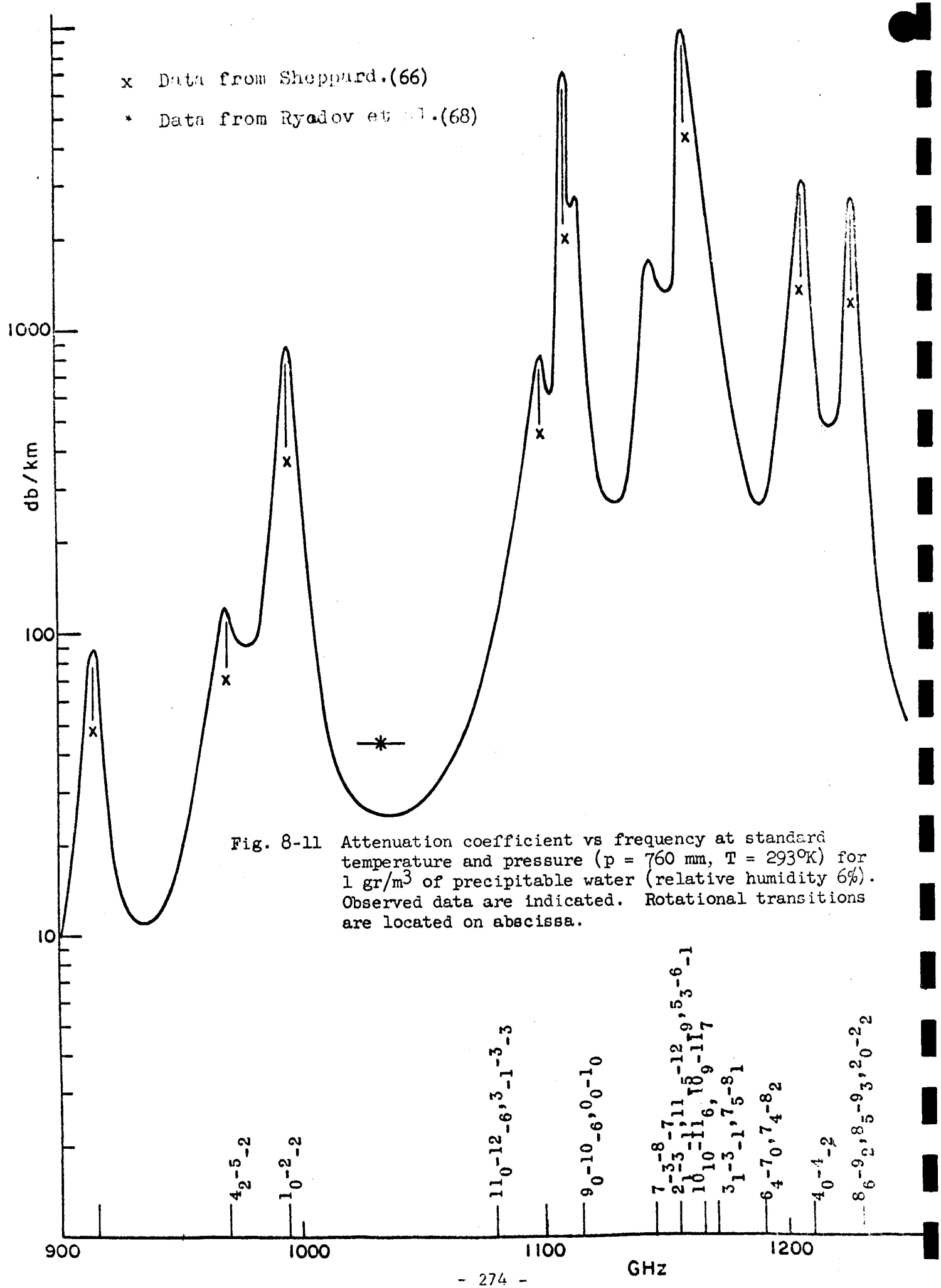

Fig. 8-11 Attenuation coefficient vs frequency at standard temperature and pressure (p = 760 mm, T = 293°K) for 1 gr/m^3 of precipitable water (relative humidity 6%). Observed data are indicated. Rotational transitions are located on abscissa.

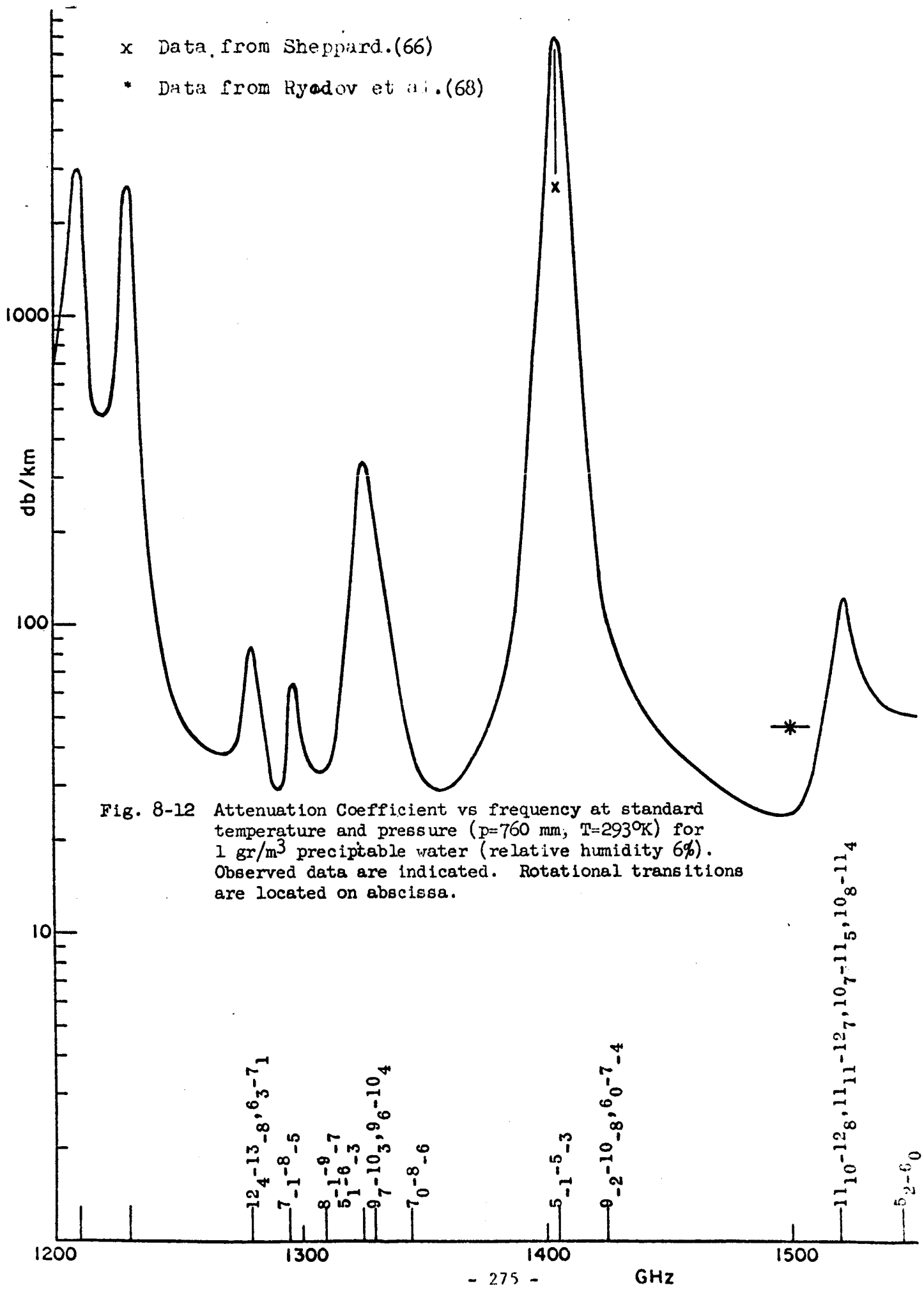

Fig. 8-12 Attenuation Coefficient vs frequency at standard temperature and pressure (p=760 mm, T=293°K) for 1 gr/m^3 precipitable water (relative humidity 6%). Observed data are indicated. Rotational transitions are located on abscissa.

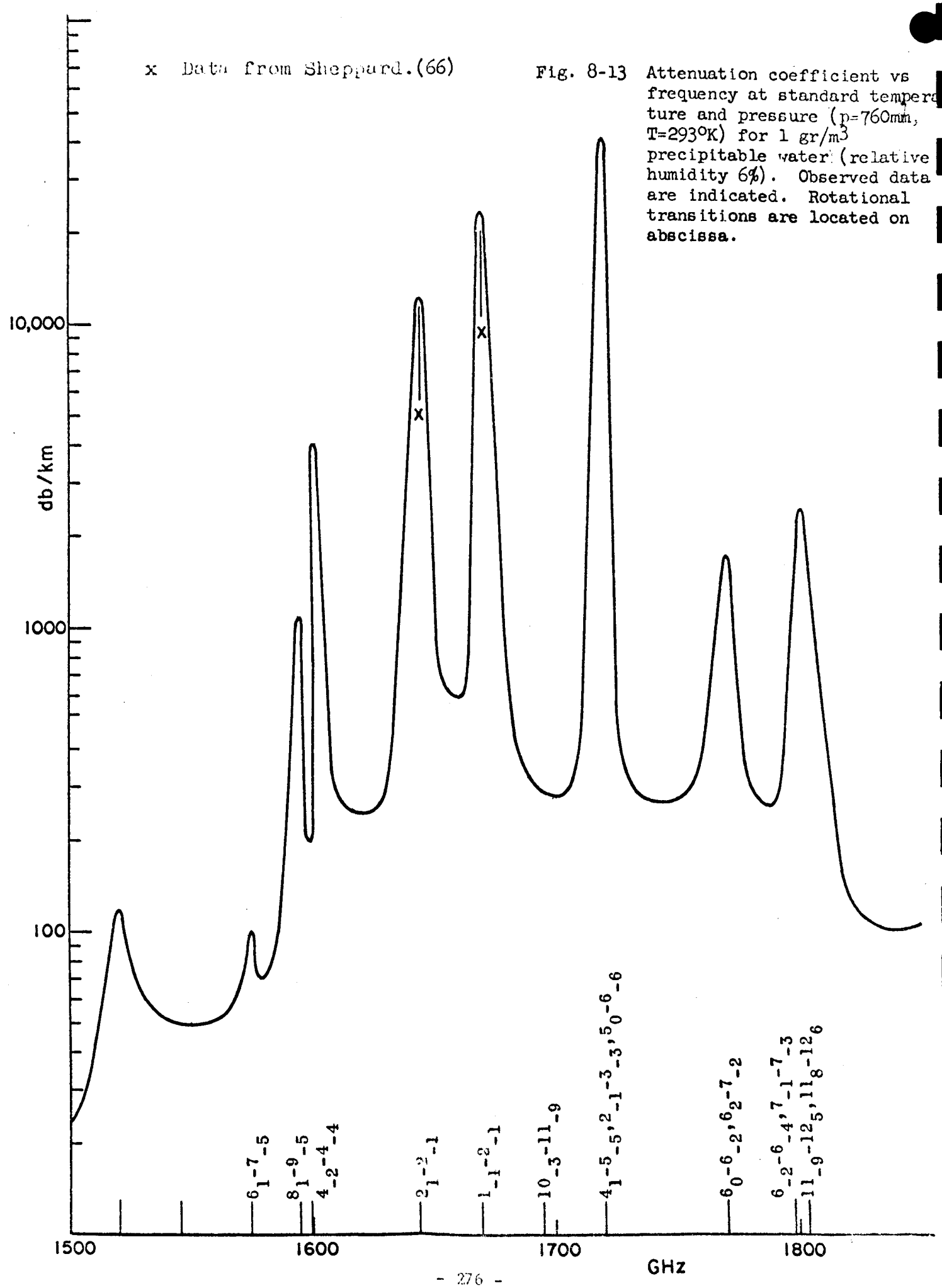

Fig. 8-13 Attenuation coefficient vs frequency at standard temperature and pressure ($p=760mm$, $T=293^{o}K$) for 1 gr/m^3 precipitable water (relative humidity 6%). Observed data are indicated. Rotational transitions are located on abscissa.

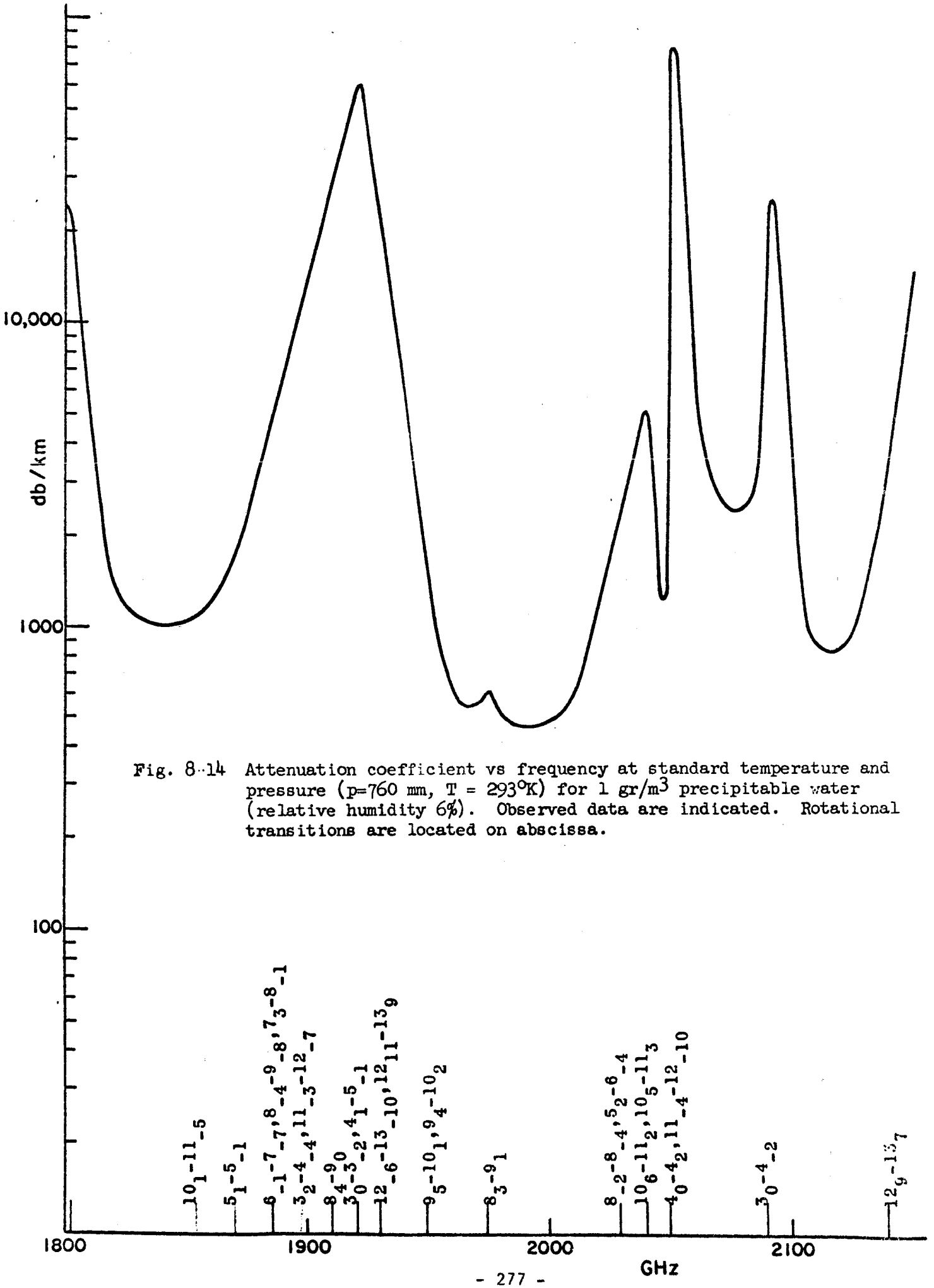

Fig. 8-14 Attenuation coefficient vs frequency at standard temperature and pressure (p=760 mm, T = 293°K) for 1 gr/m^3 precipitable water (relative humidity 6%). Observed data are indicated. Rotational transitions are located on abscissa.

Fig. 8-15 Attenuation coefficient vs frequency at standard temperature and pressure ($p = 760$ mm, $T = 293^{o}K$) for 1 gr/m^3 precipitable water (relative humidity 6%). Observed data are indicated. Rotational transitions are located on abscissa.

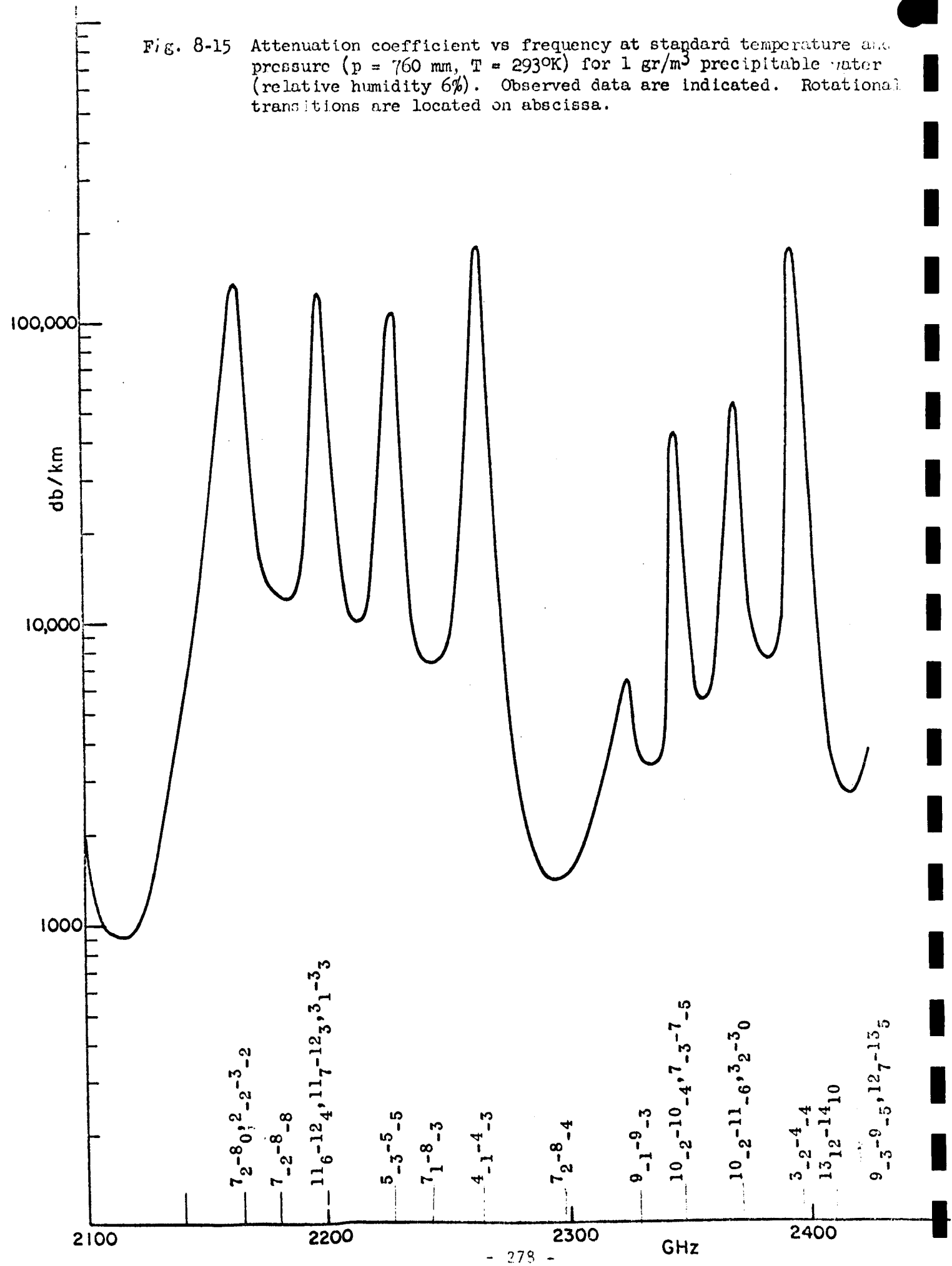

Fig. 8-16 Attenuation coefficient vs frequency at standard temperature and pressure (p=760 mm, T = 293°K) for 1 gr/m^3 precipitable water (relative humidity 6%). Observed data are indicated. Rotational transitions are located on abscissa.

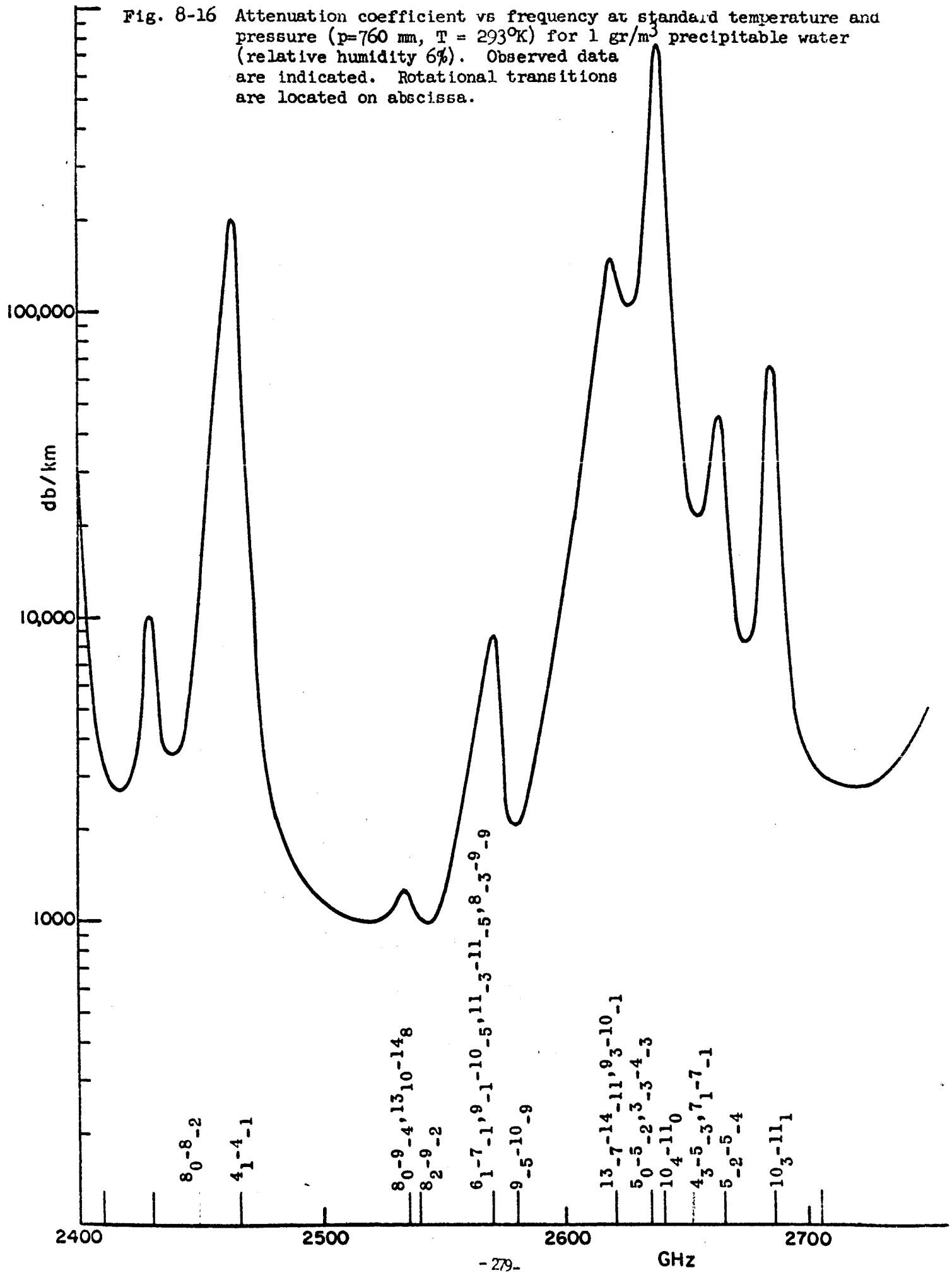

Fig. 8-17 Attenuation coefficient vs frequency at standard temperature and pressure (p=760 mm, T = 293°K) for 1 gr/m^3 precipitable water (relative humidity 6%). Observed data are indicated. Rotational transitions are located on abscissa.

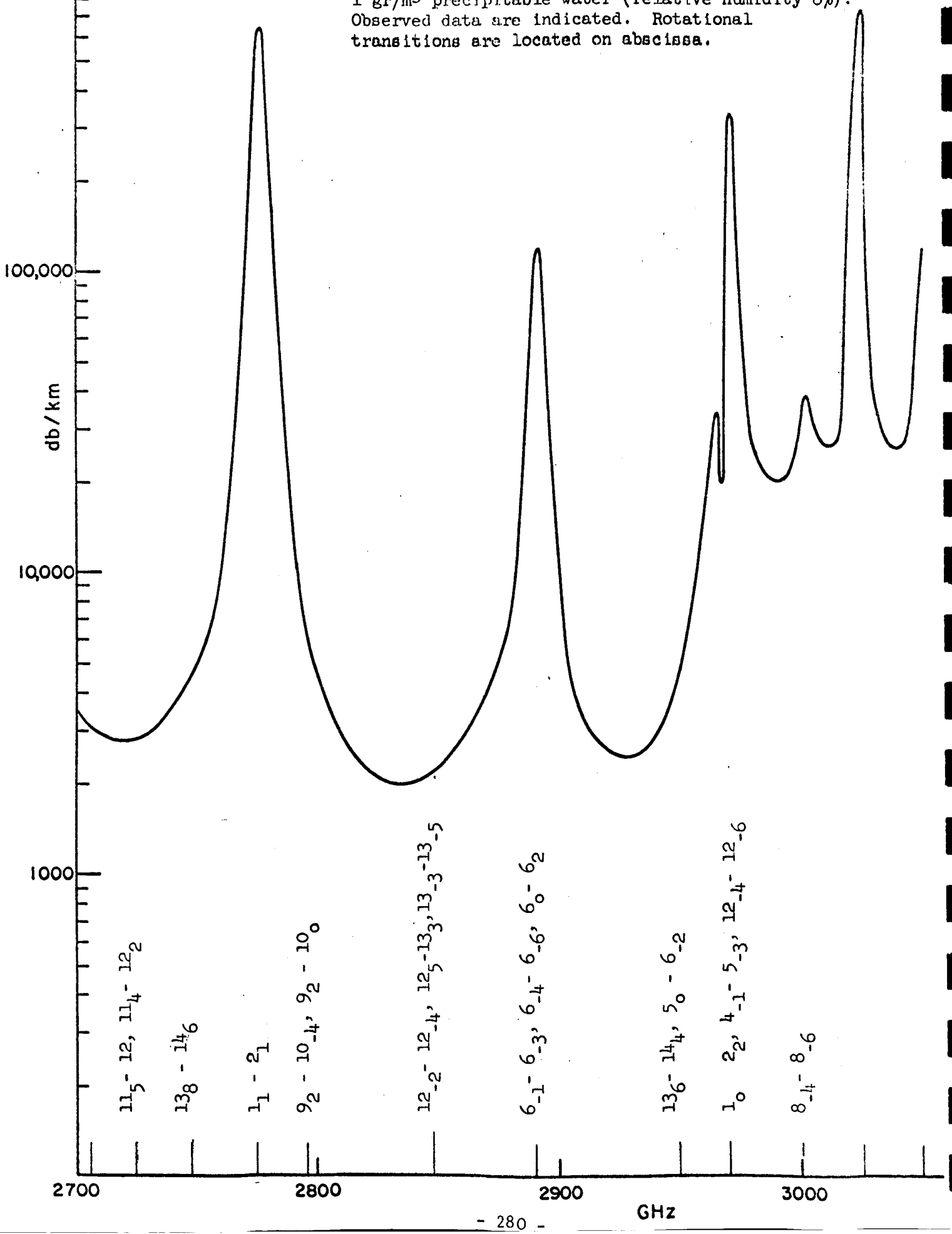

relation between saturated precipitable water, temperature and relative humidity at sea level is presented in Fig. 8.7. A relative humidity of 56% at standard temperature and pressure ($T=293^{\circ}K$, $p=760$ Torr) is considered normal: this corresponds to 10 gr/m^3 of precipitable water. At sea level a change in relative humidity may be accounted for by multiplying the data of the figures by the actual number of gr/m^3 of precipitable water, as obtained from Fig. 8.7, on the basis of the temperature and relative humidity existing along the considered path.

At other altitudes the attenuation coefficient in the "valleys" of the attenuation curve may be estimated by multiplying the data of the figures by the number of gr/m^3 of humidity existing at that altitude. For a standard atmosphere, an accepted formula (see, for example, A W. Straiton, Progress in Radio Science[84]), for the computation of the humidity at any altitude h is,

$$\delta \ gr/m^3 = 10 \exp(-.5 \ h_{km})$$

<u>Total attenuation across the atmosphere</u>: The total attenuation existing in a path which spans from one altitude to another may be arrived at by subdividing the difference in altitudes into a sufficient number of layers of uniform water vapor concentration, and summing up the partial attenuations due to the contributions of each layer computed with the method described in the previous section.[64]

For a standard atmosphere, the integrated effect for a vertical path spanning from a given altitude h to the limit of the atmosphere may be computed with the formula

$$\alpha_{db} = \alpha\ 20 \exp(-\ .5\ h_{km} \sec \theta)$$

where α is the attenuation coefficient of the figures and θ is the slant angle measured from the vertical.

Aside from water and oxygen absorption, the millimeter and submillimeter waves are not expected to suffer noticeable loss from other gaseous components of the atmosphere. Ozone and carbon dioxide, which are largely responsible for the infrared atmospheric absorption, have practically no part in the attenuation of ultra-microwaves. Ozone has many resonant lines between 0.787 and 2,652 GHz[65] and a maximum absorption in the 237 to 250 GHz band. However, the total attenuation for the crossing of the zenith of the ozonosphere (located between 20 and 30 km of altitude, and corresponding to a 3 mm thick layer at atmospheric pressure) is below 0.4 dB. As far as CO_2 is concerned, its molecule has neither an electric nor a magnetic dipole and its spectrum, due to rotational-vibrational levels, does not extend out of the infrared in the lower frequency band.

8.7 EFFECTS OF ATMOSPHERIC PRECIPITATION ON PROPAGATION

The theory of the phenomenology of attenuation by precipitation of condensed water was presented by H. Goldstein in 1951.[71]

This theory, which is essentially based on a classical work of Ryde and Ryde[72] is well summarized by the R. C. A. report.[2] In humid air, the condensation nuclei, ranging in size from 5×10^{-3} to 5×10^{-2} micron, may grow into water droplets. In haze they are from 10^{-1} to 5×10^{-1} micron in size; in fog and clouds they are typically from 10 to 30 micron, with a condensed water content seldom exceeding 1 gr/m^3. These dimensions are much smaller than the wave length for frequencies below 3,000 GHz. When drops are small with respect to the wavelength, the Rayleigh approximation holds: the scattering cross-section is proportional to

$$\left(\frac{a^{3/2}}{\lambda}\right)^4,$$

and the absorption cross section is proportional to

$$\left(\frac{a^3}{\lambda}\right)$$

where a is the droplet radius and λ the wavelength. Consequently, for ultramicrowave, the primary loss mechanism in fog or clouds is absorption, which is directly proportional to the total water mass per unit volume. It is found that attenuation from liquid water in clouds is much larger than from ice clouds, and that in both cases the losses are mainly due to absorption. The attenuation in dB/km is given by the formula

$$\alpha = .44\ M/\lambda^2$$

with λ in centimeters, and M indicating the liquid water content in gr/m^3. (See note on page 286.)

In the case of rain, the drop diameter may reach 5 mm, so that the Rayleigh approximation may not hold, but the Mie scattering solution is required. When the drop's diameter is much larger that the wavelength, the loss depends only on the scattering cross-section density of the particles. This leads to a decrease of loss passing from millimeter waves to submillimeter waves. In Fig. 8.18 the theoretical and observed values of attenuation due to rain are presented for a range of rainfall rates.

Recently a very informative resume has been published, which compares theoretical and experimental attenuation due to rainfall at frequencies up to 100 GHz.[73] It appears from Medhurst's work that, while the theoretical predictions of rainfall attenuation are in qualitative agreement with measurements, the quantitative agreement is not always satisfactory. In particular, the maximum of the theoretical attenuation lies well below the measured maximum. This discrepancy, which appears to increase with frequency, may in part be attributed to the experimental difficulties in measuring rain, but seems also to require a refinement in the theory of the structure of the rain itself. Supporting evidence indicated that precipitation is not uniform, but may tend to contain clusters of several closely spaced drops. An effort to understand the effect of rain irregularities is being made.[74,75]

The radar measurement of rainfall is based upon the following assumed relationship between radar reflectivity of rain, Z, and the drop diameter, D

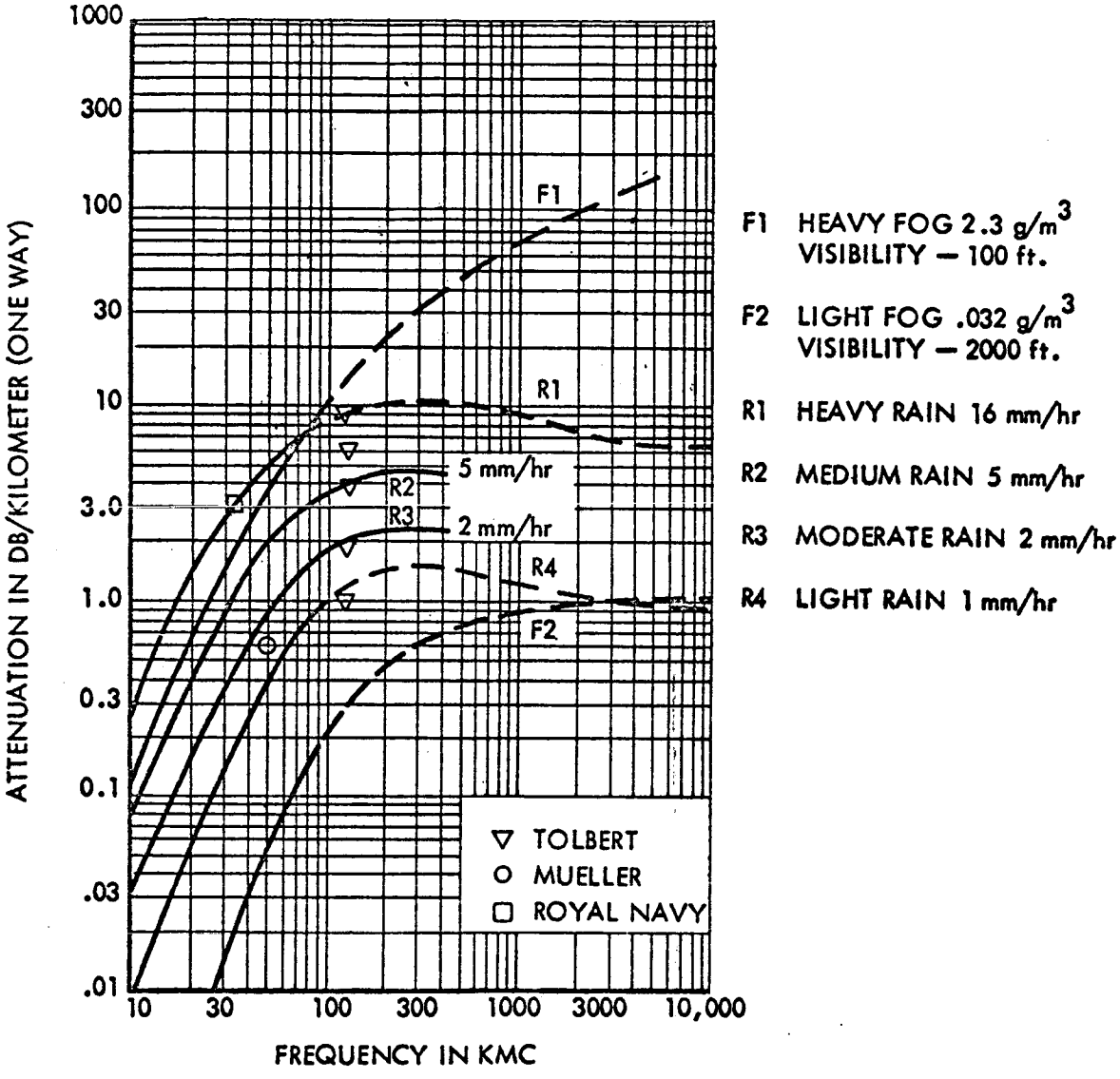

Figure 8.18 Theoretical and Measured Values of Attenuation by Rain and Fog

$$Z = \sum_n a_n D_n^6 \qquad (8.14)$$

where a_n is a dimensional constant, and the sum is extended to all drop sizes.* The rainfall rate is then determined, knowing the drop size distribution, by the empirical relation

$$Z = B R^{\beta} \qquad (8.15)$$

where the constants B and β are characteristics of the kind of rainfall. Examples of various kinds of Z/R relationships are shown in Fig. 8.19.

The attenuation constants for various kinds of rain are shown in Fig. 8.20. The type of rain for each situation is indicated in the figure by the parameters B^{-1} and β^{-1}, respectively. For millimeter waves, formula (8.14), which is based on the Rayleigh scattering approximation, is not satisfied for all raindrops. When the ratio of rain drop diameter to wavelength increases above .1, scattering and attenuation increase sharply.[76]

Snow properties are under test,[77] as well as an attempt to understand the effect of rain on the transparency of radomes.[78,79]

In conclusion, the effect of precipitation on ultra-microwave propagation is under study, but much remains to be done. In particular, a comparative study of the attenuation effects of the various types of water condensations (rain, snow, hail, fog and clouds) with respect to frequency is needed.

---

* It is approximately (Ref. 7) $Z = 0.48\ M^6$.

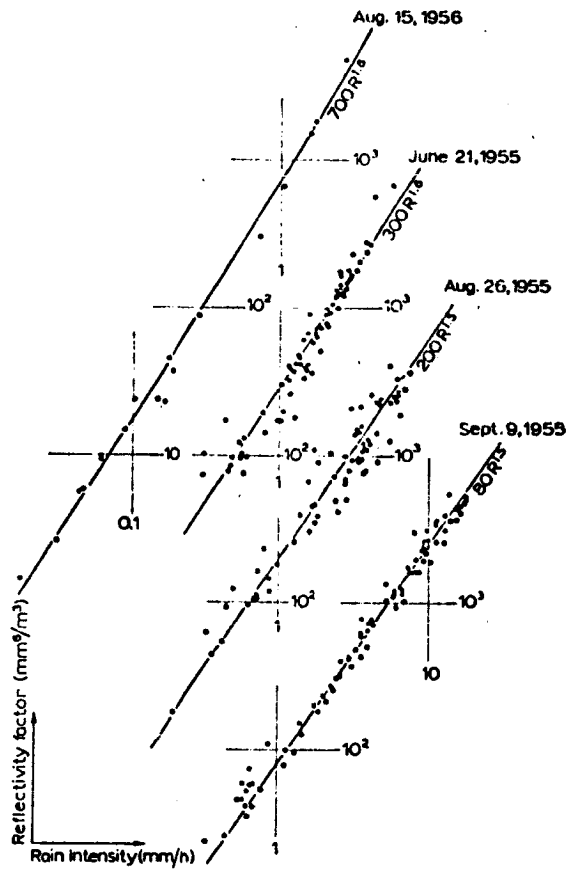

Figure 8.19 Examples Showing the Wide Variation of Z/R Relationships obtained in Various Synoptic Situations

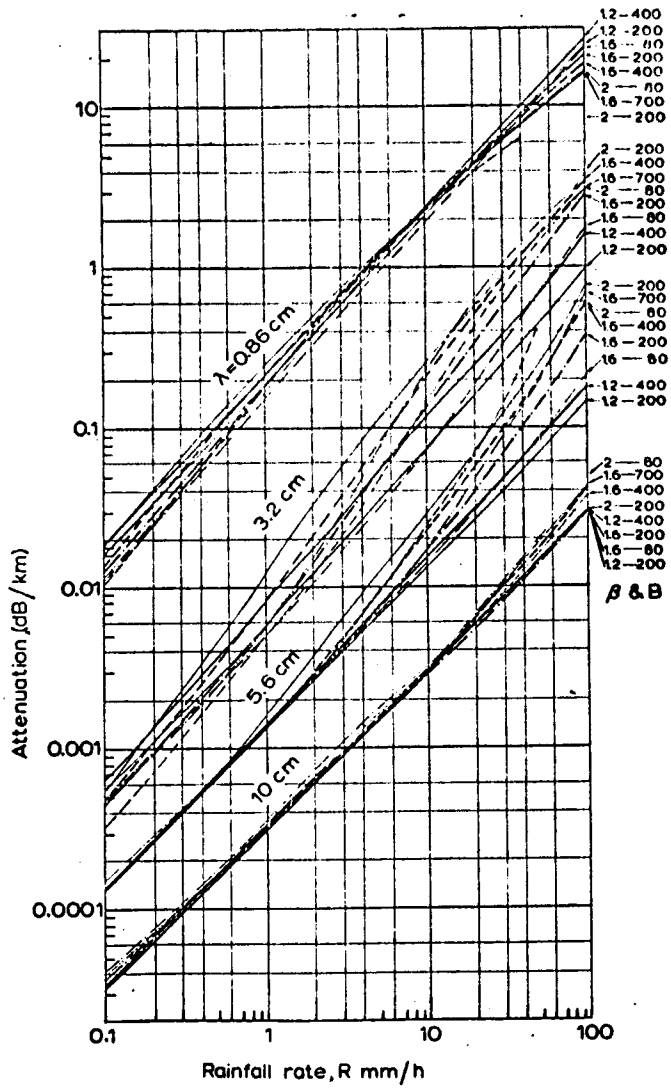

Figure 8.20 Attenuation Constants for Various Kinds of Rain

8.8 TROPOSPHERIC SCINTILLATION

The concept of tropospheric refractivity is thoroughly developed in Kerr's book.[71] In particular, described therein is the effect of a turbulent boundary upon refractivity. The study of the origin and distribution of turbulence in the troposphere is being very actively investigated.[80] However, the effect of tropospheric turbulence on the propagation of ultramicrowaves is not yet well understood, particularly the relation between turbulence dimensions and wavelength. While it has been proposed to establish a relation between propagation and the specific conditions of turbulence,[81] there is a general tendency to lump together all the effects of turbulent refractivity, especially at the highest frequencies, in one statistical factor of signal deterioration due to turbulence. As a matter of fact, the propagation of an electromagnetic beam through a turbulent atmosphere is characterized by fluctuations of the received signal which can be related to: (a) a change in the angle of the arrival of the beam, which displaces the focal point in the receiving antenna (quivering); (b) distortion of wavefront on the incoming beam, which produces in the receiving antenna a defocusing effect similar to that caused by geometrical errors of the reflector (illumination dancing); (c) changes in the overall beam intensity (spatial focusing and attenuation). The importance of these effects increases with the beam concentration, and therefore, with frequency. Particular attention has been given to these phenomena at optical frequencies.[82,83]

In the radio spectrum the data available (see, for example, H. B. Janes, M. C. Thompson, "Errors Induced by the Atmosphere in Microwave Range Measurements," Radio Science, Vol. 68D, No. 11, Nov. 1964, pp. 1229) have been exhaustively discussed in ref. 6 (pp. 3.14 to 3.30) for application to satellite-to-ground communication at 100 GHz.

Continuation of these studies on the effect of tropospheric turbulence on the propagation of ultramicrowaves is highly recommended.

8.9 SUMMARY AND REVIEW OF RECOMMENDATIONS

Atmospheric absorption in the 150 to 3,000 GHz band is essentially due to water vapor. The theoretical absorption coefficient at standard temperature and pressure is shown in Figs. 8.8 to 8.17. Only a limited part of this spectrum has been measured experimentally. The observed data generally exceed the theory by a small but significant percentage. Local variability of humidity makes the integrated water vapor absorption through the lower atmosphere a highly changeable factor. However, at relatively low altitudes the vertical crossing of the whole atmosphere occurs with negligible losses: at the altitude of 10 km, for example, the average vertical atmospheric attenuation for frequencies below 1,000 GHz is less than 1 dB.

Water vapor emission can be detected, and contributes to increasing the apparent antenna temperature. Fog and clouds cause absorption losses which linearly increase with frequency. Losses due to rain tend to be constant in the frequency range of interest,

and proportional to rainfall density. A comparative study of the attenuation effects of the various types of precipitation has not yet been made at these frequencies.

Consideration should, therefore, be given to the following studies:

1) Elaboration of a computational program for obtaining the theoretical attenuation of a given atmospheric path, using as parameters, frequency, altitudes of the path terminals, and humidity versus altitude curve. This program should be kept up to date by introducing new experimental data of frequency and linewidth of water vapor absorption lines as soon as they become available.

2) Laboratory exploration of water vapor absorption of submillimeter waves in order to obtain further experimental data of attenuation and linewidth of more lines of the absorption spectrum.

3) Systematic studies of submillimeter wave propagation on actual paths, and in the presence of various types of precipitation.

4) Statistical investigation of beam coherence on actual paths.

8.10 REFERENCES TO CHAPTER VIII

1. R. J. Glauber, "Optical Coherence and Photon Statistics," pp. 63-186, Quantum Optics and Electronics Les Houches, 1964; Gordon and Breach, New York, 1965.

2. M. P. Bachynski, A. Evans, A. G. Wacker, "The Radio Spectrum from 10 Gc to 300 Gc in Aerospace Communications," Vol. IV--Absorption in Planetary Atmospheres and Sources of Noise, ASD-TR-61-589, August 1962, RCA Victor Co., Ltd., Montreal, Canada.

3. P. F. Wacker, M. Mizushima, J. D. Petersen, J. R. Ballard, Diatomic Molecules, Vol. I.

4. P. F. Wacker, M. R. Pratto, "Line strengths of asymmetric rotors," Vol. II, NBS Monograph 70, December 1964.

5. C. H. Townes, A. L. Shawlow, Microwave Spectroscopy, McGraw-Hill, New York, 1955.

6. B. Stark, "Bibliography in Microwave Spectroscopy, 1945-62," University of Freiburg, West Germany, July 1963.

7. P. Favero, "Microwave Gas Spectroscopy Bibliography 1954-62," National Research Council of Italy, University of Padus, Italy, 1963.

8. J. M. Stone, Radiation and Optics, McGraw-Hill, New York, 1963, p. 252-254

9. J. H. Van Vleck, and V. F. Weisskopf, "On the shape of collision-broadened lines," Rev. Mod.Phys., Vol. 17, April-July 1945, p. 227.

10. J. H. Van Vleck, "The absorption of microwaves by oxygen," Physical Review, Vol. 71, April 1947, p. 413.

11. Van Vleck, J. H., "The absorption of microwaves by uncondensed water vapor," Physical Review, Vol. 71, April 1947, p. 425.

12. M. Mizushima and R. M. Hill, "Microwave spectroscopy of O_2," Physical Review, Vol. 93, 1954, p. 745.

13. M. Tinkham and M. W. P. Strandberg, "Theory of the fine structure of the molecular oxygen ground state," Physical Review, Vol. 97, 1955, p. 937.

14. R. W. Zimmerer, M. Mizushima, "Precise measurement of the microwave absorption frequencies of the oxygen molecule and the velocity of light," Physical Review, Vol. 121, No. 1, Jan. 1, 1961, p. 152.

15. H. A. Gebbie, W. J. Burroughs, J. A. Robb, G. R. Bird, "Observation of the magnetic dipole rotation spectrum of oxygen," Nature, Vol. 212, No. 5057, 1 Oct. 1966, p. 66.

16. D. M. Dennison, "The infrared spectra of polyatomic molecules," Review of Modern Physics, Vol. 12, No. 3, July 1940, p. 175.

17. W. S. Benedict and E. K. Plyler, "Absorption spectra of water and carbon dioxide in the region of 2.7 microns," Journal of Research, NBS, vol. 46, No. 3, March 1951, p. 257.

18. A. E. Schulze, C. W. Tolbert, "The shape, intensity, and pressure broadening of the 2.53 millimeter wavelength oxygen absorption line," Nature, 200 (4908), Nov. 1963, p. 747.

19. S. A. Zhevakin, A. P. Naumov, "Absorption of centimeter and millimeter radio waves by atmospheric water vapor," Radio Engineering and Electron Physics (trans.), Vol. 9, No. 8, Aug. 1964, p. 1097.

20. E. R. Beringer, "The absorption of one-half centimeter electromagnetic waves in oxygen," Physical Review, Vol. 70, July 1946, p. 53.

21. H. R. L. Lamont, "Atmospheric absorption of microwaves," Physical Review, Vol. 74, August 1948, p. 353.

22. M. W. P. Strandberg, C. Y. Meng, I. G. Ingersoll, "The microwave spectrum of oxygen," Physical Review, Vol. 75, May 1949, p. 1525.

23. J. H. Burkhalter, R. S. Anderson, W. Smith, W. Gordy, "Fine structure of microwave absorption of oxygen," Physical Review, Vol. 79, August 1950, p. 651.

24. R. S. Anderson, C. M. Johnson, W. Gordy, "Resonant absorption of oxygen at 2.5 millimeters wavelength," Physical Review, Vol. 83, 1951, p. 1061.

25. R. M. Hill, W. Gordy, "Temperature dependence of the line breadth of oxygen," Physical Review, Vol. 91, July 1953, p. 222.

26. J. O. Artman, J. P. Gordon, "Absorption of microwaves by oxygen inthe millimeter region," Physical Review, Vol. 96, Dec. 1954, p. 1237.

27. C. W. Tolbert, J. H. Douglas, C. O. Britt, "Measured Absorption of Millimeter Wavelengths by Oxygen at Partial Atmospheric Pressures," E.E. Research Lab., Univ. of Texas, Austin, Report No. 100, May 15, 1958.

28. E. H. Young, Jr., "The Static and Dynamic Temperature Characteristics of the Oxygen Line at 2.5 Millimeter Wavelength," Quarterly Engineering Report No. 7, Univ. of Texas, Austin, Nov. 1963, Jan. 1964, (AD 428 845).

29. C. W. Tolbert, L. C. Krause, A. W. Straiton, "Attenuation of the earth's atmosphere between the frequencies of 100 and 140 gigacycles per second," Journal Geophysical Research, Vol. 69, No. 7, April 1964, p. 1349.

30. M. L. Meeks, "Atmospheric emission and opacity at millimeter wavelengths due to oxygen," Journal of Geophysical Research, Vol. 66, Nov. 1961, p. 3749.

31. C. W. Tolbert, C. O. Britt, J. H. Douglas, "Radio Propagation Measurements in the 100 to 118 kMc Spectrum," Rept. No. 107, University of Texas, Austin, April 1959.

32. K. M. Decker, R. C. Dodson, "Propagation Measurements in the 5 Millimeter Region," Report No. 5385, Naval Research Lab., Oct. 1959.

33. C. W. Tolbert, A. W. Straiton, J. H. Douglas, "Studies of 2.15 mm Propagation at an Elevation of 4 km/s and the Millimeter Absorption Spectrum," Report No. 104, Univ. of Texas, Austin, Nov. 1958.

34. C. W. Tolbert, L. C. Krause, A. W. Straiton, "Attenuation of the earth's atmosphere between the frequency of 100 and 140 gigacycles per second," Journal Geophysical Research, Vol. 69, April 1964, p. 1349.

35. A. W. Straiton, C. W. Tolbert, "Anomalies in the absorption of radio waves by atmospheric gases," Proc. IRE, Vol. 48, No. 5, May 1960, p. 898.

36. C. W. Tolbert, A. W. Straiton, "An analysis of recent measurements of the atmospheric absorption of millimeter radio waves," Proc. IRE, Vol. 49, No. 2, Feb. 1961, p. 649.

37. W. B. Lenoir, "Five Millimeter Radiative Transfer in the Upper Atmosphere," Quarterly Progress Report No. 77, M.I.T., April 1965.

38. A. H. Barrett, J. W. Kuiper, W. B. Lenoir, "Observations of microwave emission by molecular oxygen in the terrestrial atmosphere," Journ. Geophys. Rsch., Vol. 71, No. 20, Oct. 15, 1966, p. 4723.

39. W. S. Benedict, L. D. Kaplan, "Calculations of the line widths in the H_2O-N_2 Collisions," Jour. of Chem. Phys., Vol. 30, No. 2, 1959, p. 388.

40. Millimeter Wave Research - Final Report, Bell Telephone Laboratories, New York, ONR Contract 687, (00) Rept. No. 24261-15, May 1955.

41. A. B. Crawford, D. C. Hogg, "Measurement of atmospheric attenuation at millimeter wavelengths," Bell System Technical Journal, Vol. 35, 1956, p. 907.

42. W. E. Petterson, "Absorption of Microwaves of Millimeter Wavelength by Atmospheric Water Vapor," Master's Thesis, Univ. of Texas, Austin, June 1957.

43. C. W. Tolbert, A. W. Straiton, J. H. Douglas, "Studies of 2.15 mm Propagation at an Elevation of 4 km and the Millimeter Spectrum," E.E. Rsch. Lab, Univ. of Texas, Austin, Rept. No. 104, Nov. 1958.

44. E. Wolf, R. Kopeck, A. Mondlock, "Millimeter wavelength atmospheric absorption," Proc. of Inst. of Radio Engineers, Vol. 50, No. 4, Pt. 1, 1962, p. 478.

45. R. H. Dicke, R. Berlinger, R. L. Kykl, A. B. Vane, "Atmospheric absorption measurements with a microwave radiometer," Physical Review, Vol. 70, Sept. 1946, p. 340.

46. H. H. Theissing, P. J. Kaplan, "Atmospheric attenuation of solar millimeter wave radiation," Journal of Applied Physics, Vol. 27, No. 5, 1956, p. 538.

47. H. A. Gebbie, "Detection of submillimeter solar radiation," Physical Review, Vol. 107, No. 4, 1957, p. 1194.

48. C. W. Tolbert, W. W. Bahn, L. C. Krause, "Solar Emission and Atmospheric Attenuation of 2.15 mm Wavelength Radiation," E.E. Rsch. Lab., Univ. of Texas, Austin, Rept. 5-54, July 15, 1960.

49. C. W. Tolbert, B. C. Krause, W. W. Bahn, "Solar Emission and Atmospheric Attenuation Between the Frequencies of 100 and 114 KMc/s," E.E. Rsch. Lab., Univ. of Texas, Austin, Rept. No. 6-39, Oct. 20, 1960.

50. S. I. Averkov, et al., Astronomical Station for Observations in the Far Infrared Region of the Spectrum, Astronom. Zh, Vol. 41, No. 3, 1964, p. 541.

51. V. Y. Ryadov, N. F. Furashov, G. A. Sharanov, "Measurement of atmospheric transparency to .87 mm waves," Radio Engineering and Electron Physics (trans.) vol. 9, No. 6, 1964, p. 989.

52. E. W. Barrett, L. R. Herndon, H. J. Carter, "Some measurements of the distribution of water vapor in the stratosphere," Tellus, Vol. 2, 1950, p. 302.

53. L. Frenkel, E. P. Valkenburg, "Propagation of Millimeter and Submillimeter Waves," Rept. OR 6607, July 1965, Martin Marietta Co., Orlando, Fla.

54. J. R. Rusk, "Line breadth study of the 1.64 mm absorption in water vapor," J. Chemical Physics, Vol. 42, No. 2, 15 Jan. 1965, p. 493.

55. G. E. Becker, S. H. Autler, "Water vapor absorption of electromagnetic radiation in the centimeter wavelength region," Phys. Revies, Vol. 70, 1946, p. 300, Sept. 1-15, No. 5 and 6.

56. A. H. Barrett, V. K. Chung, "A method for the determination of high altitude water vapor abundance from ground based microwave observations," Jour. of Geophys. Rsch., Vol. 69, No. 11, Oct. 1962, p. 4259.

57. D. H. Staelin, "The Microwave Spectrum of Venus," M.I.T., Ph.D. Dissertation, Jan. 11, 1965.

58. A. W. Straiton, C. W. Tolbert, "Anomalies in the absorption of radio waves by atmospheric gases," Proc. of IRE, Vol. 48, May 1960, p. 898.

59. A. W. Straiton, C. W. Tolbert, "An analysis of recent measurements of the atmospheric absorption of millimeter radio waves," (corres.) Proc. of IRE, Vol. 49, March 1961, p. 650.

60. S. A. Zhevakin, A. P. Naumov, "Absorption coefficient of electromagnetic waves by water vapor in the range 2 cm to 10 microns," Izvestiya Vuzov, (Radiofizika) Vol. 6, No. 4, 1963, p. 674.

61. S. A. Zhevakin, A. P. Naumov, "Absorption of electromagnetic radiation by water vapor at wavelengths 10 microns to 2 cm in the upper atmosphere," Geomagnetism i Aeronom, Vol. 3, No. 4, 1963, p. 666.

62. P. W. Anderson, "Pressure broadening in the microwave and infrared regions," Phys. Review, Vol. 76, No. 5, 1 Sept. 1949, p. 647.

63. The Raytheon Co., First Quarterly Rept. for Millimeter Communication Propagation Program, 1 Nov. 1964--1 Feb. 1965, Rept.No. FR 65-40, Sudbury, Mass.

64. R. F. Calfee, D. M. Gates, "Calculated slant path absorption and distribution of atmospheric water vapor," Applied Optics, Vol. 5, No. 2, Feb. 1966, p. 287.

65. E. K. Gora, "The rotational spectrum of ozone," Journal of Molecular Spectroscopy, Vol. 3, Feb. 1959, p. 78.

66. K. H. Breeden, W. K. Rivers, A. P. Sheppard, "High Resolution Interference Spectrometer Measurements of Submillimeter Atmospheric Water Vapor Absorption," URSI 1966 Spring Meeting.

67. D. E. Burch, E. Reisman, "Absorption of H_2O in the 340 Micron Window," Optical Society of America, Wash., D. C. Meeting, March 18, 1966.

68. V. Y. Ryadov, G. A. Sharonov, "Experimental investigation on the earth atmosphere transparency for submillimeter waves," Radiotecnika i Electronika, Vol. XI, No. 6, 1966, p. 1037.

69. S. Y. Chang, J. D. Lester, "Radiometric measurement of atmospheric absorption at 600 Gc/s," Proc. IEEE, Vol. 54, No. 4, April 1966, p. 459.

70. R. A. Williams, W. S. C. Chang, "Observations of solar radiation from 50 microns to 1 mm," Proc. IEEE, Vol. 54, No. 4, April 1966, p. 462.

71. D. E. Kerr (ed), "Propagation of Short Radio Waves," M.I.T., Radiation Lab. Series, Vol. 13, pp. 671-692.

72. J. W. Ryde, and D. Ryde, "Attenuation of Centimeter and Millimeter Waves by Rain, Hail, Fog and Clouds," G.E.C. Report No. 8670, May, 1945.

73. R. G. Medhurst, "Rainfall attenuation at cm waves: comparison of theory and measurement," IEEE Trans. A and P., Vol. AP-13, No. 4, July 1965, p. 550.

74. T. Oguchi, "Attenuation of e.m. waves due to rain with distorted raindrops,"Jour. of Radio Rsch. Lab., Vol. 11, 1964, p. 19.

75. K. Funakawa, "Measurement of the total cross-section of water drops at a 5 mm wavelength," IEEE Trans. Ant. and Prop., AP-13, No. 5, 1965, p. 829.

76. I. Imai, "Application of radar to precipitation physics and synoptic meterology in Japan," Progress in Radio Science, Vol. 4, p. 240, 1963.

77. J. W. Battles, D. E. Crane, "Millimeter Wave Attenuation through Snow," Naval Ordnance Lab., Navsepts Report 8816, 15 July 1965, AD 618 674.

78. B. C. Blevis, "Losses due to rain on radomes and antenna reflecting surfaces," IEEE Trans. A and P, Vol. AP-13, No. 1, Jan. 1965, p. 175.

79. J. Ruze, "More on wet radomes," IEEE A and P, Vol. AP-13, No. 5, Sept. 1965, p. 823.

80. J. L. Lumley, H. A. Panofsky, "The Structure of Atmospheric Turbulence," Interscience Publication, 1964.

81. D. T. Gjessing, "Determination of isotropy properties of the tropospheric permittivity and wind velocity fields by radio propagation methods," Jour. Geophysical Res., Vol. 69, No. 4, Feb. 1964, p. 569.

82. P. Beckmann, "Signal degeneration in laser beams propagated through a turbulent atmosphere," Radio Science, Vol. 69D, No. 4, April 1965, p. 629.

83. A. Consortini, L. Ronchi, A. M. Scheggi, G. Toraldo di Francia, "Influence of the atmospheric turbulence on the space coherence of a laser beam," Alta Frequenza, Vol. 32, No. 11, Nov. 1963, pp. 790.

84. F. DuCastel, "Radio and Troposphere," Vol. II, Progress in Radio Science, 1960-1963, Elsevier Pub. Co., Amsterdam, 1965, p. 279.

Chapter IX

DETECTION

9.1 INTRODUCTION

Since the publication of an extensive survey of millimeter detectors about 4 years ago,[1] considerable progress in the field of millimeter and submillimeter wave detection has been achieved. Better understanding of the underlying physical principles led to improvement of the operation of a number of detectors and also to the development of new detection schemes. Detectors with considerably superior sensitivity and time response compared to thermal detectors exist today practically over the entire range of mm and submm wavelengths (10--0.1) mm. Many of these detectors are, however, still confined to laboratory use and require further development to render them suitable for practical applications.

The aim of this chapter is therefore to

a) update the information of the referenced report

b) formulate criteria for choosing a mm or submm wave detector to perform a specific task

c) point out areas of further development.

The existing state of the art allows the following classification of mm and submm detectors

a) Thermal

b) Photoelectric

c) Semiconductor diode detectors and mixers

d) Bulk semiconductor mixers

e) Others

We shall discuss first each of these categories separately, emphasizing recent developments. This is followed by an overall evaluation and comparison of the various devices discussed using detectivity/sensitivity, time response, simplicity of operation, and scope of application as criteria. Areas and devices with respect to which further development is required are also indicated.

9.2 THERMAL DETECTORS

In principle, any temperature sensitive phenomenon can be utilized as the basis for a thermal detector. In thermocouples, the observed phenomenon is the electromotive force which exists across the junction of two dissimilar materials. For bolometers and thermistors, the observed phenomenon is a resistivity change with temperature, whereas for pneumatic detectors (Golay cell)[2] the observed quantity is a minute mechanical displacement caused by a change in the pressure of a contained volume of gas subjected to the radiation. Two characteristics of thermal detectors are the frequency independence of performance and the long time constant. Because of their relatively slow response time, ranging from about 10 msec for Golay cells and carbon bolometers to about 1 sec for the superconducting tin bolometers, thermal detectors are unsuitable for communication purposes, but they can be useful for measurements of power and energy. However, it has been pointed out that large errors may occur when thermal detectors are used at millimeter wavelengths due to power dissipation in the leads caused by the skin effect.[3]

A thermal detector consists basically of two components, of which one is the receiver which absorbs radiation and the other is the temperature

sensor. However, in many present-day devices, the sensing element often plays the receiver role also. The function of the receiver is to act as an absorbing medium such that, when an amount of radiant energy ΔQ is absorbed, the receiver temperature will change by an amount $\Delta T = \frac{\Delta Q}{C}$, where C is the thermal capacity of the receiver in units of joule/degree. The function of the temperature sensor is to sense the temperature change ΔT. Any temperature sensitive parameter could be used in principle to detect a ΔT. Thermal detectors intended for operation at microwave frequencies, such as thin wire barretters, resistive film bolometers, semiconductor thermistors, and Golay cells are well known.[2,3,4] The Golay cell and a number of specially developed bolometers suitable for use at mm and submm or infrared wavelengths will be described next.

9.2.1 The Golay Cell[2]

This is a thermopneumatic detector in which the incident radiation is absorbed by a thin foil blackened receiver comprising one wall of a gas filled chamber. The expansion of the gas deflects a thin flexible membrane whose deflection is measured by an electro-optical system. Appropriate window material is used at various wavelengths of the spectrum. Crystal quartz and diamond usually are used in the submm region. The Golay cell has a response essentially independent of wavelength. However, at wavelengths longer than 5 mm (when the dimension of the cell becomes comparable to wavelength), a slight dependence on wavelength appears.

Golay cells with noise equivalent power (NEP) (for definition of NEP see section 9.6) of about 4×10^{-10}W are available commercially with a time constant of about 15 msec. The major sources of noise in the cell are the Brownian motion of gas molecules and mechanical vibration.

The Golay cell has the advantages of operating at room temperature, and has an easily measurable and reliable response which is practically independent of wavelength. Its disadvantages are relatively slow response, inferior detectivity (see section 9.6 for definition of detectivity) to that of cooled detectors, and a small amount of microphonics. Despite these disadvantages, the broad spectral response and reliable operation of the Golay cell make it extremely useful as a standard of comparison for other types of detectors. In a recent development, fiber optics were employed by Grove[5] to detect the deflection in the diaphram of a Golay cell. The composite device was complicated and apparently plagued by a long time constant.

A general analysis of the sensitivity of the Golay cell has been given recently by Schuman.[6] Due to its intricate mechanical and optical structure, the Golay detector is not suited for applications where vibrations exist.

9.2.2 Special Bolometers

The factors affecting the operation of a bolometer can best be understood by considering the general equations of its responsivity R and time constant τ,[4,7] for $\omega\tau < 1$, where ω is the angular frequency of the chopped radiation

$$R = \frac{\alpha}{G-\alpha P} V \qquad (9.1)$$

$$\tau = \frac{C}{G-\alpha P} \qquad (9.2)$$

Here, C is the thermal capacity of the receiving element and G is the thermal conductance between the bolometer and its constant temperature heat sink surroundings, α is the temperature resistance coefficient, V is the biasing voltage applied to the bolometer and P is the electrical power dissipated in it.

The equations above show that in order to obtain high responsivity, α must be large and G small. But a small G implies a large τ. Therefore, in order to keep τ small, C must be made small; that is, the receiver element must be made as light as possible while maintaining efficient absorption of the incident radiation.

In addition to reducing thermal fluctuations, cooling of a bolometer reduces the thermal capacity considerably and by suitable choice of materials (semiconductors or superconductors) a large value of α can be achieved. As a consequence of these considerations, the following special cooled bolometers have been designed and operated.

9.2.2.1 Superconducting Bolometers

The operation of a superconducting bolometer is based on the fact that superconductors have a high resistance coefficient in the neighborhood of the temperature at which they change from their normal to their superconducting state[4, 8]. Andrews et al [9] and Fuson[10] used niobium nitride in the first superconducting bolometers. More recently, Martin and Bloor[11] developed a submm superconducting bolometer using tin.

The sensitivity of this detector was about three orders of magnitude greater than a Golay cell. An NEP $\simeq 3 \times 10^{-13}$ watt for 1 cps bandwidth with a time constant of 1.25 sec was obtained. As is pointed out by Putley,[111] better performance of this bolometer is conceivable since the above NEP was obtained with unblackened receiver and with an amplifier whose noise was about 30 times that of the detector. The disadvantages of this detector are delicate construction, the requirement of precise temperature control to within 10^{-5} °K at 3.7 °K and a long time constant which, however, can be reduced to about 1 msec by sacrificing sensitivity. Lead and tin are widely used in superconducting bolometers.[12]

9.2.2.2 Carbon Bolometers

It is well known that certain types of commercial carbon resistors possess a very large temperature coefficient below 20 °K. This effect was utilized by Clement and Quinnell in constructing a carbon resistance thermometer,[13] and by Boyle and Rodgers[14] in making a useful bolometer. This detector is characterized by an NEP of about one order of magnitude better than the Golay cell, i.e., 3×10^{-11} W for 1 cps bandwidth with a time constant of about 1 msec. The resistance of a typical element is about 100 kilohms. Since this detector requires cooling (below the He-λ point of 2.17 °K) many workers prefer to use the required cryostat with a faster type of detector such as the germanium bolometer described next, or one of the InSb photoconductive detectors described on subsequent pages.

9.2.2.3 The Germanium Bolometer

It has been shown by Esterman and others[107] that certain impurity concentrations in germanium gave resistance-temperature characteristics of low temperatures that can be useful in the construction of bolometers. This principle was utilized by Low[15,16] in the development of a high sensitivity and a relatively fast response bolometer. The detector consists of a sample slab (4 by 4 by 0.12) mm^3 of gallium-doped germanium placed in an evacuated and cooled chamber with suitable windows to admit the measured radiation. The sample is fastened to the walls of the chamber by conducting electric leads which determine also the thermal conductance between the sample and the walls which are maintained at a constant temperature. The incident radiant energy is absorbed by the free carriers in the sample. Since these carriers are tightly coupled to the lattice, they quickly raise the temperature of the sample and change its resistance. Low originally reported an NEP of 5×10^{-13}W and a time constant of 0.4 msec for a detector operating at 2.15 ^{o}K. The resistance of the detector was 1.2×10^{4} ohms.

More recently, Low was able to achieve[17] an NEP = $4\ 10^{-14}$W with a $(1.2 \times 1.0 \times 0.36)$ mm^3 germanium bolometer cooled to 2.0 ^{o}K at 1.2 mm wavelength. This indicates an order of magnitude of improvement in the NEP previously reported. The germanium bolometer is relatively simple to construct and seems to be the most sensitive and fastest of all the cooled bolometers in use now for wavelengths above 3.5 microns. Its high sensitivity added to its broad spectral response makes it particularly suitable for applications in the fields of radiometry,

spectrophotometry in addition to astronomical and atmospheric observations.[17] Operation at temperatures lower than $2^{o}K$ could result in higher sensitivities in certain low background applications such as for IR and millimeter wave radiometry.

9.2.2.4 The Pyroelectric Bolometer

A study of the performance of thermal detectors will show the thermistor bolometer to be particularly suited to spacecraft instrumentation. This choice is based on its relatively low NEP, adequate time constant, commercial availability in various sizes, ambient temperature operation, reasonable electrical impedance, which simplifies associated circuitry, and considerable ruggedness to withstand launching forces. As is well known, thermistor bolometers have been successfully used in the Mercury capsule horizon sensors, in the radiometer on board the Tiros meteorological satellites, and the two channel IR radiometer in the Mariner II spacecraft. A drawback of the thermistor is the relatively high power dissipation (typically about 2.5×10^{-3} W) and the negative temperature coefficient which could result in a runaway situation and eventual self-destruction of the thermistor.[18] This drawback prompted researchers to look for devices of equal performance but free of these drawbacks. This led to the eventual development of the pyroelectric detector.[18,19,20,21,22]

The pyroelectric detector has been used in the optical region;[23,24,25] however, since the pyroelectric effect is basically a thermal effect, this type of detector is theoretically applicable to any wavelength. Experimental investigation of the operations of this detector at room

temperature, at mm and submm wavelengths has been conducted by Steir.[26] The detector utilizes a sample of polarizable ferroelectric material such as a single crystal triglecine sulfate (TGS) or single crystal $BaTiO_3$ placed between electrodes connected to a load resistor. The incident radiation heats the sample thus causing a pyroelectric current

$$I = KW \left(\frac{d\ P_s}{dT}\right)\left(\frac{dT}{dt}\right) \tag{9.3}$$

to flow in the external circuit. Here W is the incident power, P_s is the saturation polarization, T is the temperature and K is constant dependent on the heat capacity of the sample and the load resistor.

Since the pyroelectric current, I, is dependent on the time rate of change of temperature rather than on absolute temperature change, the response of this detector is relatively fast. Response time of the order of 30 μsec has been measured in the lower mm regions. Typical voltage sensitivities in $\frac{mV}{mW}$ of this detector, when connected to a cascade amplifier, are 7.15 for TGS measured at both 8.15 mm and 4.1 mm, and 0.67 for $BaTiO_3$ measured at 8.15 mm. Current sensitivities of the detector alone are about 1.79 10^{-4} μA/mW for TGS at both 8.15 and 4.1 mm wavelength, and 1.81 10^{-5} μA/mW for $BaTiO_3$ at 8.15 mm. The response time for the TGS and $BaTiO_3$ detector is 30 μsec respectively, with a minimum detectable signal ($S/N \simeq 1$ db) of 8 μW for TGS and 87 μW for $BaTiO_3$. Measurements performed at 2.14 mm optical and infrared wavelengths with the TGS detector showed a detector plus amplifier sensitivity of about one-half that of a conventional crystal detector. Maximum sensitivity of these detectors is obtained at the Curie point as predicted by

equation (9.3). Preliminary studies of these noise characteristics show an increase in noise near the Curie temperature.

9.2.2.5 The Ferroelectric Bolometer

This type of bolometer utilizes the large dependence of the dielectric constant in ferroelectric materials on temperature in the vicinity of the Curie point. The change in temperature can be produced by the absorption of electromagnetic radiation. Ferroelectric materials have a high dissipation factor at mm wavelength. This bolometer has been constructed[27] with the aim of absolute power measurement at mm wavelengths (70 to 308) GHz. The operation of this detector can be made practically frequency independent by proper matching techniques and the effect of ambient temperature fluctuations can be eliminated through the use of temperature compensated bridge connections.

Both the absorption of EM radiation and the sensitivity ($\Delta C/\Delta T$) (C - capacitance, T - temperature) are greater below the Curie temperature than above it, therefore ferroelectric materials with high Curie temperatures are preferable, since both the effect of ambient temperature fluctuation and absorbed humidity are reduced. Materials suitable for use in this bolometer are composed of various ratios of $PbTiO_3$ and $SrTiO_3$. Power sensitivities ($\Delta C/\Delta P$) of the order of 2.5 pf/mW have been measured[27] at 66, 70, 73, and 93 GHz. The bolometer was tested at 310 GHz showing a 1 pf/mW power sensitivity. Even though the validity of this figure is questionable due to inaccuracies in the measurement, it demonstrates that the bolometer operates at 1 mm and perhaps at shorter wavelengths. The response time of ferroelectric bolometers is very long;

for example,

$$t_{50\%} = 20 \text{ sec, and } t_{90\%} = 180 \text{ sec}$$

Its frequency independence, however, can make it a useful device for absolute power measurement and calibration purposes of various mm wave components. Stabilization and compensation with regard to ambient temperature fluctuations can probably be achieved in the device. Accurate evaluation of its operation at submm wavelengths is required.

9.3 PHOTOELECTRIC DETECTORS

Photoelectric detectors encompass all those detectors whereby absorption of photons results in a corresponding change in some inherent electrical property. Photoelectric detectors can be used for communications purposes since they have reasonably short response times. In the following, photoelectric detectors are divided into groups depending on the electrical quantity which is changed by the absorbed radiation.

9.3.1 Photoconductive Detectors

Photoconductive detectors function on the principle that absorbed photons cause a corresponding change in electrical conductivity. Of primary importance is the selection of a suitable material such that high sensitivity and fast response can be attained. The difficulty in detecting electromagnetic radiation in the millimeter wavelength range is that the corresponding photon energy is low (1.2×10^{-3} ev for $\lambda = 1$ mm), requiring the use of materials whose activation energy between the bound and free (conductive) state of the electron is smaller or equal

to the incident photon energy. Because of such small activation energies, it is necessary to resort to cooling in order to minimize thermal lattice vibrations which are capable of exciting electrons into the conduction band.

Five essentially different mechanisms which have been exploited in the construction of millimeter and submillimeter photoconductive detectors are as follows.

9.3.1.1 Impurity Activated Germanium

Impurity elements from IIIA and VA columns of the periodic table, such as indium or antimony, which have an activation energy of about 0.01 ev have been used as activators. They are susceptible to photo-ionization up to wavelengths of 0.12 mm. An antimony-activated germanium detector has been studied by Fray and Oliver.[28] Bratt and Giggey[29] studied antimony and indium activated germanium, while indium boron and gallium activated germanium detectors were studied by Shenker,[30] who achieved a peak detectivity of $\sim 1.25\ 10^{11}$(cm-cps$^{1/2}$/watt) at 0.1 mm with boron-activated germanium and peak detectivity of $3.1\ 10^{11}$ (cm-cps$^{1/2}$/watt) with gallium-activated germanium at λ - 0.104 mm. Best results seem to be obtainable with p-type elements. The time constant of boron-doped germanium detectors investigated by Shenker was of the order of 8.7×10^{-9} sec at low electric fields and increases to more than 5×10^{-7} sec at fields close to breakdown fields. Copper, gold, mercury, indium and cadmium activated germanium detectors are available commercially.* A list of such detectors is given in Table 9.1. Representative spectral responses of the Raytheon QKN-1009 (Cu: Ge)

* Raytheon Co. Special Microwave Devices Operation, 130 Second Ave., Waltham, Mass.

and the QKN-1179 (In: Ge) detectors covering the 2-100 μ range are shown in Fig. 9.11. Improvements in the operation of impurity-activated germanium detectors may be possible through the use of neutral dopants, such as zinc which appears to hold some promise.[30] Material preparation techniques are expected to contribute some improvements also.

9.3.1.2 Impurity Activated Indium Antimonide

To obtain photoconductivity at longer wavelengths (lower photon energies) indium antimonide has been found to be a suitable material in which impurity ionization energies of the order of 6×10^{-4} ev can be attained. With this low ionization energy, the detection capabilities of this material extend to wavelengths of 2 mm.[31] Because of the large radius of the ground state of an electron of an impurity atom in indium antimonide, it is possible for bound electrons to "hop" to adjacent impurity conduction and is dominant in impurity-activated indium antimonide even at very low temperatures. By applying a magnetic field to the sample, impurity conduction can be sufficiently reduced so that impurity ionization can be observed.[32]

The first indium antimonide detector was successfully constructed and tested by Putley[33,34,112] who reported a peak detectivity of 2×10^{11} (cm-cps$^{1/2}$/watt) at a wavelength of 1.5 mm. This detector is sensitive down to about 0.1 mm where the detectivity is 3×10^{10} (cm-cps$^{1/2}$/watt). Optimum sensitivity was obtained at 1.5°K and 5-6 kG magnetic field strength. Putley observed in his work a small photosignal even in the absence of a magnetic field; also sufficient photosignals were observed

Type	Sensitive Element	Spectral Response μ	Window Material	Time Constant (μ sec)	Typical Detectivity D^* (cm-cps$^{1/2}$ W)	Operating Temp. °K	Responsivity V/W
QKN902	Cu:Ge	2-15	Ba F_2	< 1	1.0×10^{10}	< 17	10^4
QKN1009	Cu:Ge	2-30	KRS-5	< 1	1.0×10^{10}	< 17	10^4
QKN1207	Cu:Ge	2-15	Ba F_2	< 1	1.0×10^{10}	< 17	10^4
QKN1208	Cu:Ge	2-30	KRS-5	< 1	1.0×10^{10}	< 17	10^4
QKN748	Au:Ge	2-9	Si[2]	< 1	2.0×10^9	65-78	5×10^3
QKN884	Au:Ge	2-9	Si[2]	< 1	2.0×10^9	65-78	5×10^3
QKN1003	Au:Ge	2-9	Ba F_2	< 1	2.0×10^9	65-78	5×10^3
QKN1004	Au:Ge	2-9	Ba F_2	< 1	2.0×10^9	65-78	5×10^3
QKN1204	Au:Ge	2-9	Ba F_2	< 1	2.0×10^9	65-78	5×10^3
QKN1205	Au:Ge	2-9	Ba F_2	< 1	2.0×10^9	65-78	5×10^3
QKN1005	Hg:Ge	2-15	Ba F_2	< 1	8.0×10^9	< 35	10^4
QKN1006	Hg:Ge	2-15	Ba F_2	< 1	8.0×10^9	< 35	10^4
QKN1206	Hg:Ge	2-15	Ba F_2	< 1	8.0×10^9	< 35	10^4
QKN1227	Hg:Ge	2-15	Ba F_2	< 1	8.0×10^9	< 35	10^4
QKN961	Cd:Ge	2-15	Ba F_2	< 1	8.0×10^9	< 25	10^4
QKN1007	Cd:Ge	2-25	KRS-5	< 1	8.0×10^9	< 25	10^4
QKN1008	Cd:Ge	2-25	KRS-5	< 1	8.0×10^9	< 25	10^4
QKN1179	P-type In:Ge	2-150	KRS-5	< 1	$2.8\ 10^9$	4.2	--

1 Detectivity, D^*. Values given for D^* must be qualified by test conditions normally given as specified black body temperature °K, chopping frequency in cps, and bandwidth in cps. In this case, 500°K, 900 and 1 respectively.

2 Antireflective coated

Table 9.1 Specifications of Impurity Doped Germanium Photoconductive Detectors (Raytheon)

up to wavelengths as long as 8 mm in the presence of magnetic fields. Since the magnetically induced impurity ionization energy was 6×10^{-4}ev (a wavelength limit of 2 mm), no response was expected above $\lambda = 2$ mm. These observations were interpreted to be due to a free carrier absorption mechanism to be discussed next.

9.3.1.3 Free Carrier Absorption Detector (Free Electron Bolometer)

Upon absorbing a long wavelength photon, a free carrier can make a transition to a higher energy state in the conduction band, in which state it may have a different mobility which brings about the observed change in conductivity. The expected magnitude of this effect[35,36] in high purity indium antimonide was found by Rollin[35] to be sufficiently large to render the phenomenon useful.

Assuming the limiting noise to be Johnson noise, an expected minimum detectable power of $4 \times 10^{-14} (\Delta f)^{1/2}$ watts was calculated by Rollin. Experimental verification[37] of these predictions suggests that at higher magnetic fields (> 10 kG) photoconductivity of InSb in the millimeter wave region is due to an increase in the free-carrier concentration rather than an increase in the free-carrier mobility as is the case in the free-electron bolometer detector. The free-carrier absorption mechanism in InSb is the principle of operation of the Raytheon QKN-1304 photoconductive detector. This detector is marketed with its cryogenic system and is capable of achieving a maximum detectivity of 3.7×10^{11} (cm-cps$^{1/2}$/watt) in the absence of any magnetic field. The specifications and spectral response of this detector are given in Table 9.2 and Fig. 9.11.

Type	Sensitive Element	Spectral Response (mm)	Window Material	Time Constant μsec	Typical Detectivity D* (cm-cps$^{1/2}$/watt)	Operating Temperature °K
QKN1304	n-type InSb	.15 - 10	Crystaline quartz and cooled Polyethelene filter	< 1	D*(4mm,1000,1) and 300°K background $4 \cdot 8\ 10^{10}$	4.2°K (liquid helium)

+ D* (λ, 1000, 1) is greater than 10^8 (cm-cps$^{1/2}$/watt)

Table 9.2 Specification of Raytheon InSb Photoconductive Detector.

9.3.1.4 Narrow-Band Tunable Millimeter and Submillimeter Detectors

The first tunable narrow-band mm wave detector was built and tested by Godwin and Jones.[38] The mechanism responsible for detection is cyclotron resonance, which increases the free carrier absorption coefficient at a particular wavelength,

$$\lambda_c = \frac{2\pi c}{\omega_c} \tag{9.4}$$

where

$$\omega_c = \frac{eB}{m^* c} \tag{9.5}$$

is the cyclotron frequency. Here B is the magnetic field induction, m* is the effective carrier mass, e and c having their usual meaning.

Quantum theory predicts the quantization of cyclotron orbits, i.e., orbits of only discrete energy levels and radii are possible. The allowable energy levels are given by

$$E_n = \hbar\omega_c(n + 1/2) \quad n = 0, 1, 2 --- \tag{9.6}$$

In a semiconductor when $\omega_c > 1/T$ (where T is the mean time between collisions), this quantization is possible, and well defined allowable energy levels (Landau splitting) will occur in the conduction band.

At low temperatures, the majority of free carriers occupy the lowest Landau levels. Upon absorption of radiation of energy equal to $\hbar\omega_c$, which is the transition energy of the next higher Landau level, these carriers will make a transition, and, provided the carrier mobility is different in this higher level, photoconductivity will be observed. The absorption occurs over a narrow band centered about λ_c. By adjusting the magnetic field one can see from eqs. 9.4 and 9.5 that the wavelength λ_c of maximum absorption can be altered.

A maximum detectivity of 10^{10} (cm-cps$^{1/2}$/watt) was obtained by Goodwin and Jones[38] with n-type germanium at a temperature of 4.2°K and wavelength of 8.8 mm. Resolution of about 0.05 λ_c was attainable.

Cyclotron resonance of bound carriers in n-type indium antimonide served as the basis of a tunable detector developed by Brown, Kimmet, and Roberts[39] who obtained tunability from 0.06-0.2 mm by varying the magnetic field from 7 to 25 kG at an operating temperature of 4.2°K. The resolution of 0.1 λ_c and the detectivity ranged approximately from 3×10^{11} to 6×10^{11} (cm-cps$^{1/2}$/watt).

9.3.1.5 <u>The Superconductive Detector</u>

The superconductive detector proposed by Burstein, Langenbert, and Taylor,[40, 41] at the University of Pennsylvania, utilizes the Josephson

effect[42] as a principle of operation. It consists of a superconductor-metal oxide-superconductor sandwich. With proper bias, electrons excited by incident radiation into the conduction band of one superconductor tunnel through the potential barrier into the second superconductor producing a current in the external circuit. The expected signal-to-noise ratio for this detector was computed by the authors, who show that when the generation-recombination noise is the dominant noise source of the detector, the expected signal to noise ratio is about 100 times smaller than for impurity-doped germanium photodetectors. In order to obtain reasonable sensitivities with such detectors, one may need to use temperatures below $1^{\circ}K$ and produce multilayer structures with composite thickness of the order of 100 A°. This type of detector looks promising enough to justify further development. A well-run fabrication process is expected to have a 50% yield of good junctions.

The nonlinear properties of the Josephson junction[43,44,45,46,47] can be utilized in the construction of a combined local oscillator-mixer in a superheterodyne receiving scheme. The junction would be biased in this case to generate oscillations at frequency $f_s \pm f_{if}$ where f_s is the signal frequency coupled into the junction and f_{if} is a convenient IF frequency. The combined local oscillator-mixer configuration is obviously attractive. However, any advantages of sensitivity and noise of this coherent detector over bolometric detectors remains to be seen.[43] Its low operation temperature and low impedance suggest low noise performance.

9.3.2 Photoemissive Detectors and Photodiodes

The use of electron emission from photocathodes in vacuum in detecting near infrared radiation has been a well-established art for some time now. The principle of detection depends upon the ability of an incident photon to transfer its energy to an electron near the photocathode surface. If the acquired energy of the electron is greater than the work function of the photocathode material, the electron will be emitted. Since the photon energy at submillimeter wavelengths is so small, a material with an extremely small work function is required. At the present time, no detectors of this type in the submillimeter range are known.

It might prove to be worthwhile to give some attention to the phenomenon of tunneling of electrons into vacuum from tunnel cathodes.[48] The point in question here is whether the effect of mm wave radiation on the tunnel current, by virtue of internal photo-emission, is sufficient to render the mechanism useful.

It is possible that better understanding of surface phenomena could result in uncovering photoemissive surfaces capable of functioning farther in the IF than what is possible today.

9.4 SEMICONDUCTOR DIODE DETECTORS AND MIXERS

Extending the operation of diode detectors so widely used in the microwave region to mm and submm wavelengths is very attractive for the following reasons:

1. Diodes can be employed in the construction of highly sensitive and broadband mm and submm wave video and superhetrodyne detection systems

which are the backbone of high resolution radars, sensitive radiometers, large capacity communication links and spectroscopic studies.

2. Unlike photoconductive detectors, which require cumbersome cryogenic systems for their operation, diode detectors operate at room temperatures.

3. No external magnetic field is required as is the case in the majority of mm and submm photoconductive detectors.

4. The response time is short.

9.4.1 Point Contact Diode Detectors*

The well-known equivalent circuit of a semiconductor point contact diode, Fig. 9.1, has been shown by Bauer, et al [49] to hold down to wavelengths of about 0.5 mm (600 GHz). Below wavelengths of 1 cm, degradation occurs in the performance of diode detectors due to the shunting effect of the barrier capacitance C_b and the losses in the spreading resistance R_s.

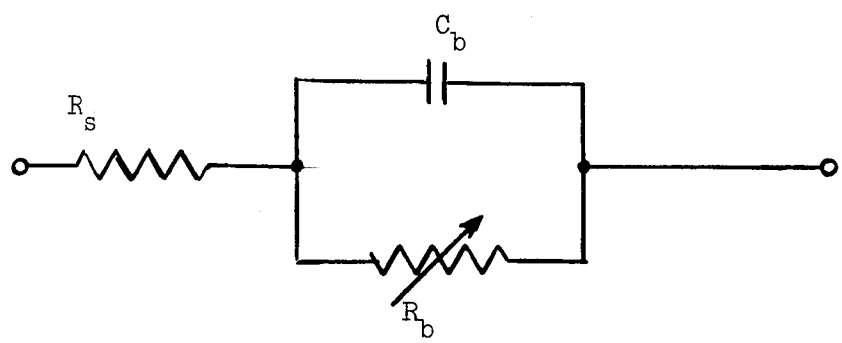

Fig. 9.1 Equivalent Circuit for a Semiconductor Point Contact Diode.

---

* Since the whisker in the majority of mm and submm diodes is welded to the semiconductor by passing a current through the contact, forming thus an alloyed junction, these diodes are frequently referred to in the literature as "Alloyed Junction Diodes."

In video detection it is necessary to reduce the diode parasitics C_b and R_s to a minimum. When the diode is used as a mixer, the conversion loss and diode noise temperature determine the quality of the diode. Both of these quantities are dependent on the diode parameters shown in Fig. 9.1. Point contact diodes were used in 1954 by King and Gordy as video detectors down to wavelengths of 0.5 mm.[53] However, since these workers were concerned with spectroscopy, where relative absorption is important, no efforts were made to evaluate the sensitivity of these early submm detectors. King and Gordy minimized the parasitic effects mentioned above by bringing the whisker point, usually formed by electrolytic etching, and the semiconductor crystal into contact in the waveguide itself with the aid of differential drive mechanisms. Naturally, such an arrangement is not rugged and a trial and error approach for making the correct rectifying contact between whisker and semiconductor was necessary. The present day state of the art of mm and submm wave point-contact detectors stems from the combination of the Gordy detector principle with:

a) special contact forming techniques with the aid of high precision differential mechanisms and capacitor discharge to weld the whisker to the semiconductor, thus providing a more rugged contact

b) advanced semiconductor technology and use of intermetallic semiconductors such as indium-antimonide, which has far higher carrier mobility than germanium and silicon, and, therefore, better performance at higher frequencies, and

c) low loss electroformed waveguide components which are used to increase mount efficiency.

The integral diode-waveguide structure is often hermetically sealed in an inert gas such as dry nitrogen to reduce environmental effects on the contact, and one mil mica windows are used to seal the waveguide ports (see Fig. 9.13). Development of the original King and Gordy millimeter wave detector[54] made at Electronics Comm., Inc. (now Advanced Technology Corp., Timonium, Maryland) resulted in measured sensitivities of the order of 10^{-11} watt at 140 GHz for a signal-to-noise ratio of unity (the amplifier used in this measurement had a bandwidth of 4 cps). Analysis indicates that the higher the conductance of the crystal material used in point contact detectors, the shorter is the wavelength at which the operation of the detector begins to deteriorate.[55] Optimum crystal materials and detector mount configurations for low noise mm detectors (240 ± 20 GHz) were investigated by Valkenberg.[55] Out of 15 semiconductor materials investigated, three exceed a sensitivity of 10^{-10}W for signal-to-noise ratio of unity and post detection bandwidth of 1 cps. A crystal mount similar to the one used by King and Gordy was used. The three crystal materials are all p-type, and the values of the maximum sensitivity achieved with each are given in Table 9.3.

Material	Sensitivity (watts)
silicon	2×10^{-11}
lead selenide	2×10^{-11}
bismuth telluride	6.32×10^{-11}

Table 9.3 Sensitivities of Point Contact Diodes

The whiskers used had a diameter of 0.001" and were mostly tungsten, although phosphor bronze was also used with the softer crystal materials tested. The results of this development program indicated that further improvement in sensitivity could be achieved by:

1. using epitaxial layer crystals
2. using thin film techniques
3. growing semiconductor whiskers which can be run in on metal posts to form the point contact diode
4. using ultrasonics to weld the whisker to the crystal instead of the capacitance discharge method.

Millimeter and submillimeter video detection, superheterodyne detection, and harmonic generation are the areas where the point contact diode finds its major application. The first two areas are within the scope of this chapter and shall be discussed next.

9.4.1.1 Video Detection

Video detection is a term applied to applications of crystal diodes used for direct amplitude demodulation of a received signal.

Since these are essentially low level rectifiers, it is required that the diode operating point be as close as possible to the forward knee of the I-V characteristics of the particular diode. Naturally, a diode can be biased to such an operating point. However, since the 1/f diode noise is directly proportional to the dc bias current, this approach will result in an increase in the diode noise figure. Furthermore, signal loss through the biasing circuit will result in reduced sensitivity. It is for this reason that diodes most

suitable for video detection are those that do not require any biasing since they possess an I-V characteristic with a forward knee very close to the origin. Both Ge and GaAs backward diodes (tunnel diodes with very low peak current in which the normally reverse tunneling current provides the forward conduction current) and p-type point contact silicon diodes are particularly suitable for use in video detectors, since their forward conduction begins at low voltages.[56] It is customary to differentiate between voltage video detectors (high load impedance across the diode) and current video detectors (low load impedance). Normally, higher sensitivities are achieved with voltage video detectors, and better time response of the order of nanoseconds with current video detectors. Video detectors have been successfully employed in the detection of incoherent radiation at 3000 GHz (0.1 mm).[57] Measurements of the output voltage and current versus input power for various video detectors has been performed by Barrus[56] at mm wavelengths. These results (see Fig. 9.2 and 9.3) indicate that the p-type Ge hot carrier diode has the best performance among the voltage video detectors due to its good sensitivity and inherent resistance to burnout (see section 9.4.2).

On the other hand, n-type Ge backward diodes seem to be particularly suited for video current detection due to their good low level sensitivity and low 1/f noise. Silicon-tungsten junction video detectors have been fabricated commercially for operation up to 420 GHz.[49] The tangential sensitivity of these detectors is theoretically inversely proportional to the square of frequency. Measured tangential sensitivity of about -52 dbm (video bandwidth = 1 MHz) has been achieved at 94 GHz.

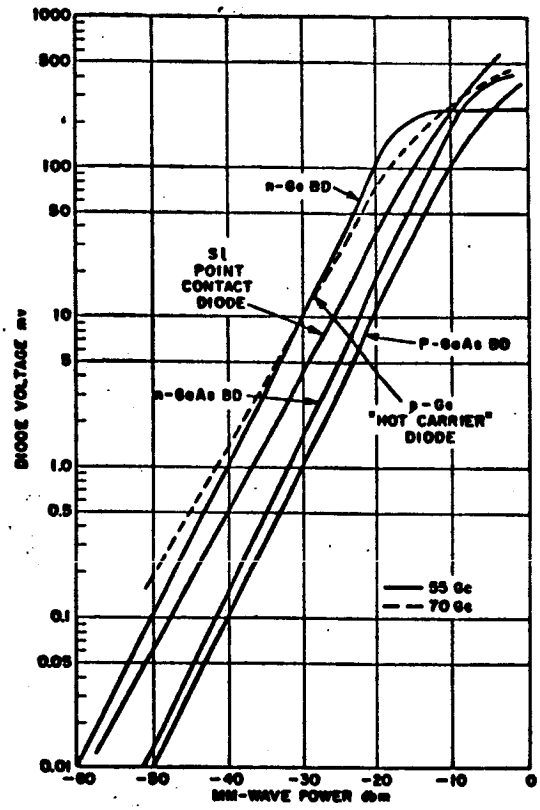

Fig. 9.2

Measured output voltage vs input microwave power for several point-contact diodes acting as video voltage detectors. The diode load was 10 megohms. (From Ref. 56)

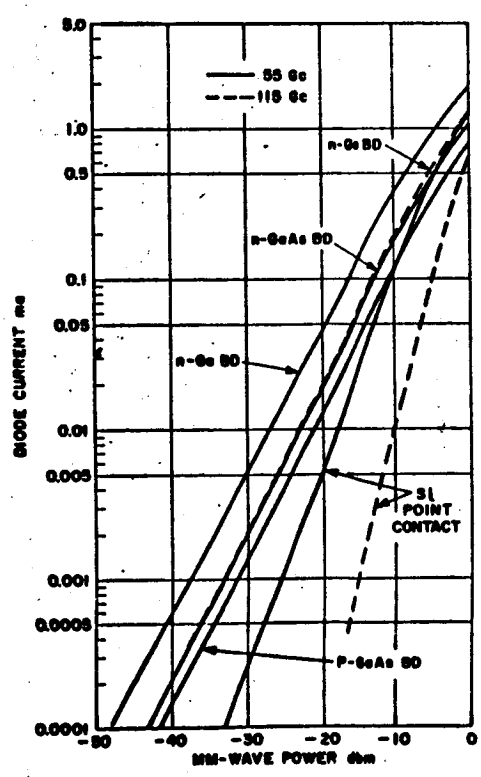

Fig. 9.3

Measured diode current vs input microwave power for several point-contact diodes acting as video current detectors. The diode load was 50 ohms. (From Ref. 56)

This is about 11 db better than the tangential sensitivity of an appropriately biased identical detector employing GaAs as the semiconductor.[49]

Typical values of noise equivalent power (NEP) for these detectors of 1.6×10^{-12} and 5×10^{-12} have been measured by Bauer[49] at 140 GHz (~ 2 mm) and 280 GHz (~ 1 mm) respectively. These results are comparable to the NEP of the Putley photoconductive detector.[33,34] Furthermore, the results indicate significant improvement on the first detailed measurements of the NEP of video point contact receivers that were conducted by Meredith and Warner[50] in 1963, who reported an NEP of 2.5×10^{-11}W and 4×10^{-9}W at 2 mm and 1 mm respectively for a GEC VX 3352 germanium rectifier.

Tunnel diodes have been successfully employed in detection and mixing at microwave frequencies. At mm and submm wavelength the operation of a tunnel diode is curtailed by the junction capacitance of the diode. Although difficult, the reduction of this capacitance is feasible. A specially fabricated tunnel diode with reduced junction capacitance, integrated with waveguide sections, has yielded encouraging results as a 55 GHz detector and mixer.[73] The material used was gallium antimonide with an impurity concentration of about $10^{18}/cm^3$ and a resistivity of 0.001-0.0025 ohm/cm. The diode was formed by passing a current pulse between the semiconductor and a zinc wire. The output voltage of such a diode is about 15-22 db higher than an IN53 diode at 55 GHz. The fabrication of tunnel diodes operable in the submm wavelength is dependent on attaining low junction capacitance and low series resistance. This seems to be possible with present day technology.

Video detectors can be incorporated with solid state broadband preamplifiers and video post detector amplifiers in the construction of compact and sensitive mm and submm receivers and radiometers that operate at room temperature and have low dc power requirements.

9.4.1.2 Superheterodyne Detection

In the last two years a good many advances have been made in the area of mm and submm wave superheterodyne detection, which have been stimulated by:

a) the desire to extend the well-known advantages of superheterodyne receivers to the mm and submm wavelength range

b) pressing demands for more sensitive detection schemes in the fields of astronomy, spectroscopy, radar, atmospheric propagation studies and space communication

c) the gradual availability of mixers and other components, such as waveguides and local oscillator sources necessary for the construction of mm and submm wavelength receivers.

A major obstacle encountered in the construction of superheterodyne receivers in this wavelength range is local oscillator noise suppression. At longer wavelengths, L.O. noise suppression is achieved normally by balanced mixing which requires the use of diode mixers with identical RF and IF characteristics. At shorter wavelengths, construction of balanced mixers becomes increasingly more difficult. However, with the repeatability of mixer performance available currently,[49] balanced mixing is now feasible through the mm wavelength region. In the submm wave region other methods of L.O. noise suppression have been used.

Since, in addition to L.O. noise, excess IF noise is usually generated in the crystal mixer, and since a portion of this shows the familiar 1/f frequency dependence, it has been recognized[58,59] that an alternative method of noise suppression is to construct receivers with higher intermediate frequencies. This has the additional advantage of providing wider bandwidths.

These intermediate frequencies are normally well above the frequency range where the diode 1/f noise is appreciable, allowing dc biasing of the diode to reduce the conversion loss. Typical dependence of mixer diode noise ratio on L.O. power and on intermediate frequency is shown in Fig. 9.4, which indicates that an intermediate frequency of about 2 GHz and L.O. power between +3 dbm to +7 dbm results in a minimum crystal noise ratio, and therefore, in a minimum conversion loss at the frequency considered (94 GHz). Typical dependence of conversion loss on bias and L.O. power are shown in Figs. 9.5, 9.6, and 9.7 for both fundamental and harmonic mixers. The conversion loss of these mixers at various frequencies is shown in Figs. 9.8 and 9.9.

The sensitivity of a superheterodyne receiver is usually described in terms of the absolute noise temperature[62,63]

$$T_R = (F_c - 1)\, T_o + L_c\, (F_{IF} - 1)\, T_o \qquad (9.6)^*$$

---

* Equation (9.6) is for an image blocked receiver. The corresponding equation for a double band receiver of noise figure F_c is

$$T_R = (F_c - 2)\, T_o + L_c (F_{IF} - 1)\, T_o$$

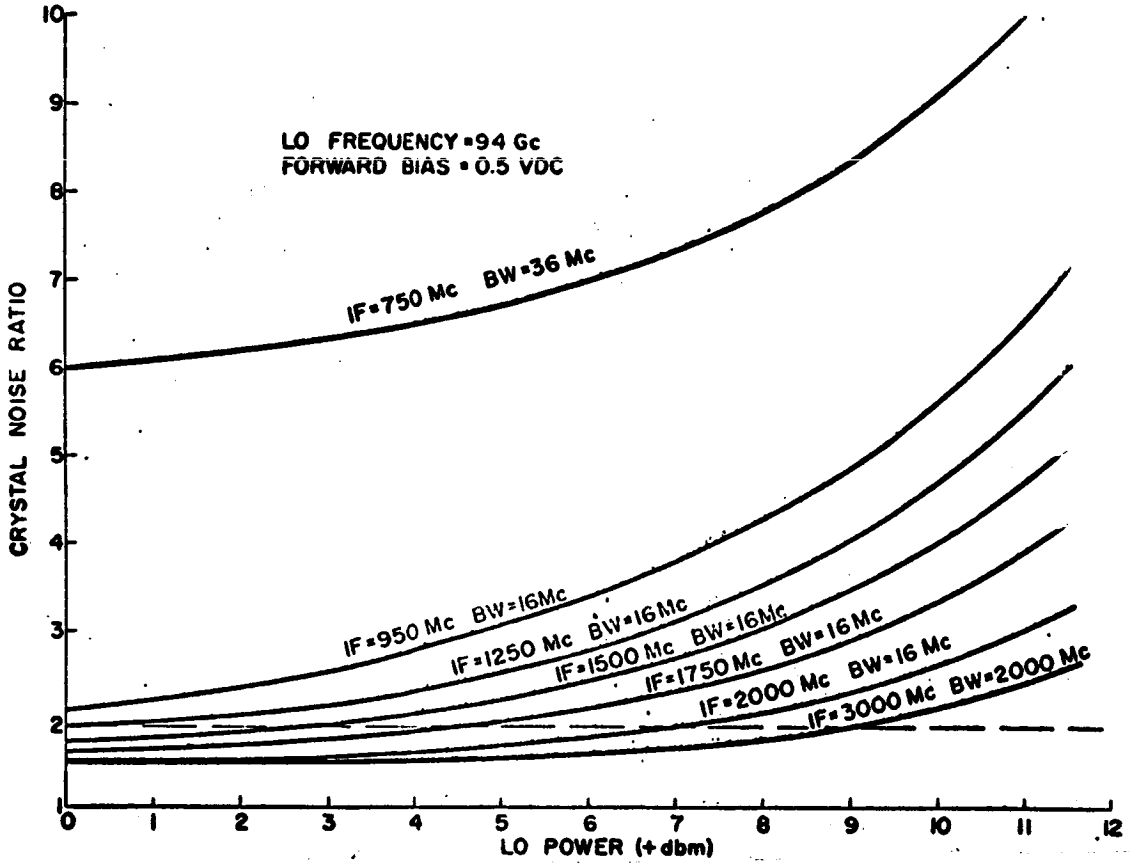

Fig. 9.4 Crystal Noise Ratio (including L.O. Noise) vs L.O. Power (Ref. 53)

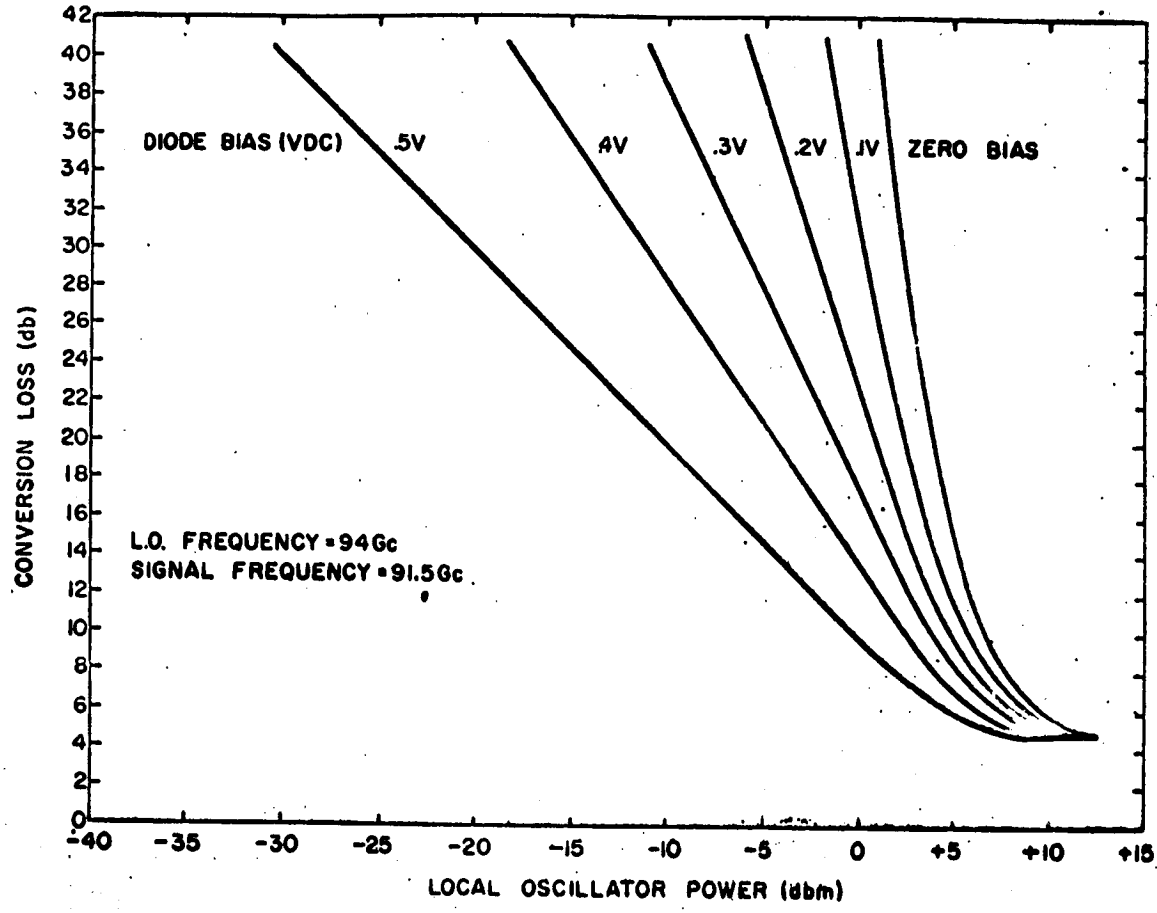

Fig. 9.5 Conversion Loss vs L.O. Power and Bias for an Exceptional GaAs Phosphor Bronze Diode ($L_{c_{min}}$ = 4.7db) (Ref. 53).

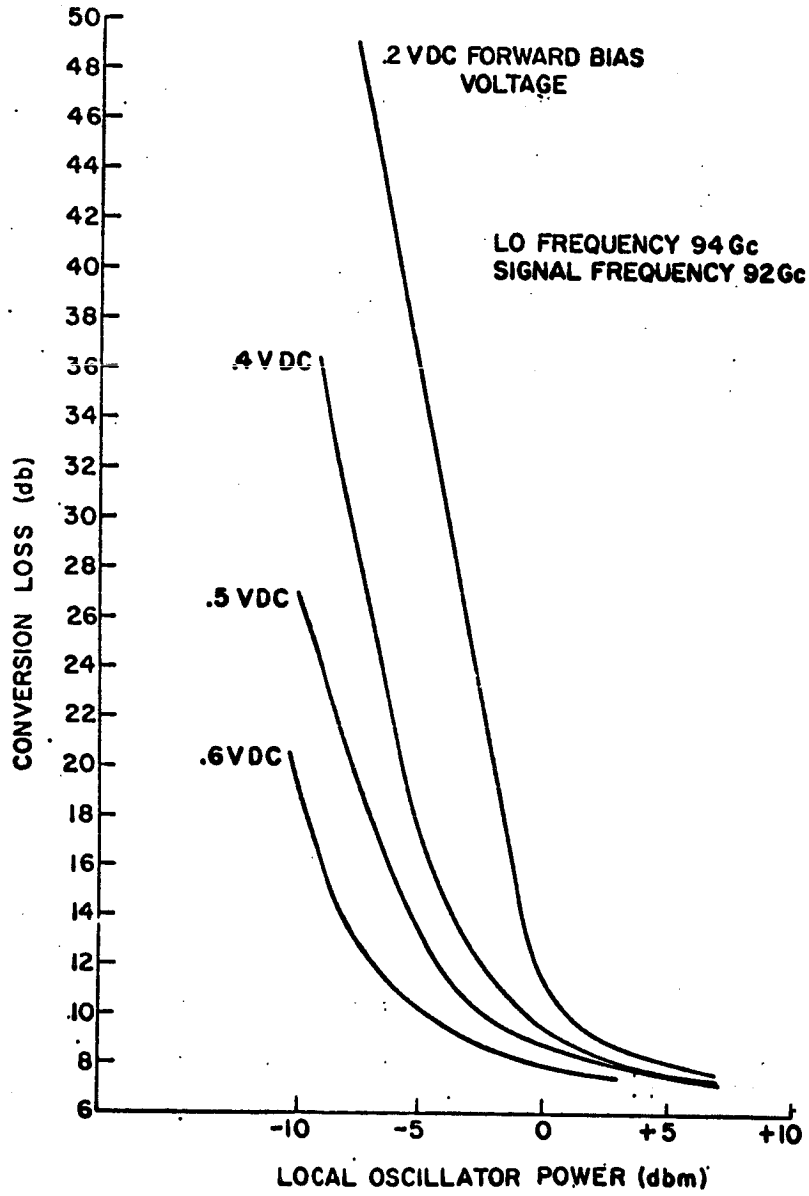

Fig. 9.6 Conversion Loss vs L.O. Power and Bias for Typical GaAs Phosphor Bronze Diode ($L_{c_{min}} \simeq 8$db) (Ref. 53).

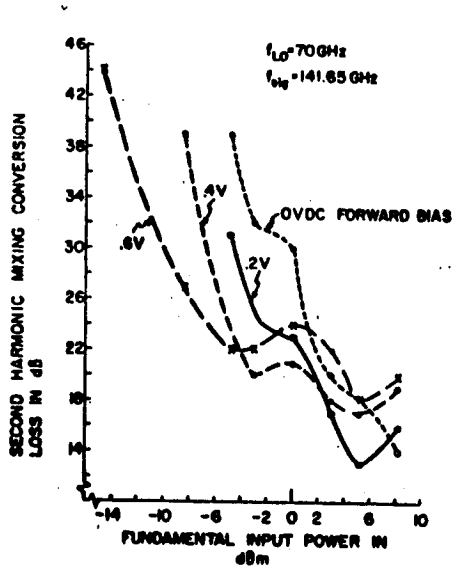

Fig. 9.7

Curves of conversion loss of a typical two-millimeter wavelength second harmonic mixer as a function of loca oscillator power at 70 GHz for different bias voltages.

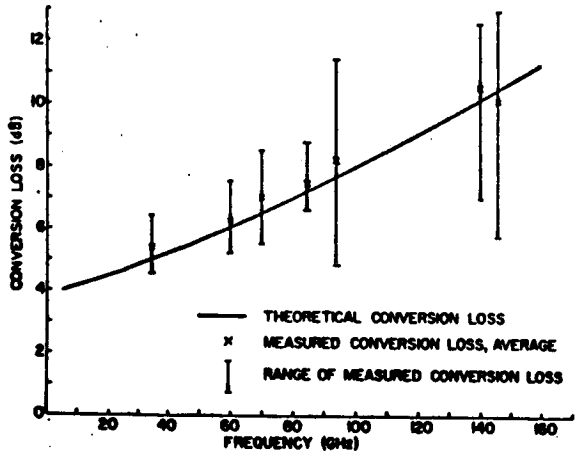

Fig. 9.8

Conversion loss as a function of frequency for fundamental mixing. Measured data obtained with a number of different diode mixers (ref. 49).

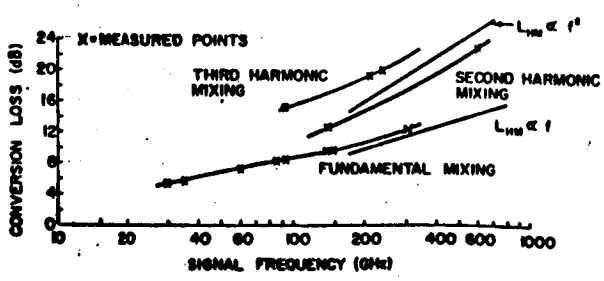

Fig. 9.9

Conversion loss of fundamental and harmonic mixers as a function of frequency. Straight lines have been drawn with slopes in accordance with selected laws and are shown for comparison. (ref. 49).

where

$(F_c - 1)$ = the excess mixer noise figure (image blocked receiver)

L_c = mixer conversion loss

F_c = crystal noise figure = NR L_c where NR is the crystal noise ratio

F_{IF} = IF amplifier noise figure

T_o = the ambient temperature $\simeq 290^oK$

The noise figure of the receiver can be obtained from eq. (9.6) by using the relationship between noise figure and receiver noise temperature

$$F_R = 1 + \frac{T_R}{T_o}$$

Then, from (9.6)

$$\frac{T_R}{T_o} = F_R - 1 = (L_c \, NR - 1) + L_c \, (F_{IF} - 1)$$

or

$$F_R = L_c(NR + F_{IF} - 1) \qquad (9.7)$$

Equations 9.6 and 9.7 indicate the major role played by the crystal diode mixer in determining the receiver noise temperature or noise figure. The effect of the mixer enters through the conversion loss L_c the crystal diode noise figure F_c or noise ratio NR. The conversion loss is related to the mixer diode parameters (see Fig. 9.1) and to the signal frequency by[50, 51,52]

$$L_c(\omega) = L_{co}\left(1 + \frac{R_s}{R_b} + \omega^2 C_b^{\,2} R_s R_b\right) \qquad (9.8)$$

in which L_{co} is the conversion loss with zero spreading resistance, i.e. due to the barrier alone.

The minimum conversion loss occurs when $R_b = 1/\omega C_b$ and is given by

$$L_c(\omega)_{min} = L_o(1 + 2\omega R_s C_b) \qquad (9.9)$$

It is well known that R_b and C_b decrease monotonically as the local oscillator power level is increased, while R_s increases with L.O. power. Thus, eqs. 9.8 and 9.9 indicate that in order to minimize the conversion loss at higher frequencies, it is desirable to minimize C_b and provide optimum L.O. power if available. In the case of point contact diodes, this optimum power can be greater than the burnout value. In this sense, one can see the advantage of electrically rugged diodes, such as the hot carrier diode that will be discussed later in this section.

The parasitic quantities R_s and C_b can normally be determined from a knowledge of the semiconductor barrier height, the dielectric constant, the carrier density, the resistivity and from the radius of the welded contact between the whisker and the semiconductor.

Using the results of microscopic measurements of the radius of several whisker points, values of R_s and C_b were calculated by Bauer[60] for a GaAs diode. Typical values are $R_s = 18\ \Omega$, $C_b \simeq .01$ pF, for a GaAs diode whose R_b was shown to be 167 Ω and whose $L_{c_{min}}$ was shown to be 3.8 db. Using these values of diode parameters in eq. 9.7, a conversion

loss of 4.65 db was calculated for a frequency of 94 GHz. This figure agrees well with the best measured conversion loss of a 94 GHz mixer diode reported.[60]

The crystal diode noise ratio (the normalized crystal noise temperature $t_c = \frac{T_c}{T_o}$) is determined by the series resistance $R_s + R_b$ of Fig. 9.1. The crystal noise is generally dependent on the L.O. power level and is comprised of a complicated combination of thermal noise in the spreading resistor, shot noise in barrier resistor and 1/f semiconductor noise. Typical values of mm and submm crystal mixer conversion loss and noise ratio are given in Tables 9.5 and 9.6. Table 9.4 shows conversion loss and noise ratio in the (50-600) GHz frequency range with various crystal diodes and includes the characteristics of the superheterodyne receivers in which these mixers were combined. The receiver noise figure and the noise equivalent power were computed using eq. 9.7. Wherever assumed values of F_{if} (the IF amplifier noise figure) were used, these values were chosen to represent amplifiers commercially available at the various intermediate frequencies.

Superheterodyne receivers are widely* used as Dicke-type radiometers[61] for the measurement of thermal radiation at mm and submm wavelengths. In this application the performance of the receiver (radiometer) is specified by means of the minimum discernible rms temperature change.

$$\Delta T \simeq k \frac{T_{AR}}{(\beta\tau)^{1/2}} \qquad (9.10)$$

* Incoherent detectors such as Low's germanium bolometer are also used in radiometers.

DIODE	Signal Frequency	IF	Beating Osc. Power	dc Bias	IF Impedance	Conversion Loss L_c, min.	Diode Noise Ratio	IF Amplifier Noise Figure (dB)	Receiver Noise Figure (dB)	Noise Equivalent Power for 1 Hz Bandwidth (W)
Conv. p-Si (tapped)	55.5 GHz	60 MHz/s	1 mW	0 V	260Ω	6.4 dB	1.6 times	2[h]	12	6×10^{-20}
	58	11 GHz/s	1	0		8	---	--	--	----
	115	60 MHz/s	0.6	—[a]		11.1	---	--	--	----
Conv. n-GaAs (formed)	55.5	60 MHz/s	1	~0.5	325	5.6	2.1	2[h]	11.7	5.6×10^{-20}
	115	60 MHz/s	0.6	—[a]	---	9.9	~2	2[h]	17.5	2.2×10^{-19}
	140[b]	2-4 GHz/s	—[e]	—[c]	~50	15	~2	5[i]	20	4.0×10^{-19}
	225[d]	2-4 GHz/s	—[e]	—[c]	~50	20	~2	5[i]	26	1.6×10^{-18}
	600[b]	2-4 GHz/s	—[e]	—[c]	~50	23-28	~2	--	--	----
Conv. n-Ge (formed)	55.5	60 MHz/s	1	~0.2	300	6.6	2.0	2[h]	12.6	6.22×10^{-20}
	140[b]	408 MHz/s				~10	1.8	9.5[i]	20	4.0×10^{-19}
	140[b]	2 GHz/s				~15		9.6[i]	25	1.26×10^{-18}
n-GaAs (pulse alloyed)	50	70 MHz/s	1	~0.5		4.5				
n-Ge backward	55	70 MHz/s	0.3	0		6.7	~1	2[h]	11.5	5.25×10^{-20}
	58	11 GHz/s	0.3	0		8.3		--	--	----
	115	60 MHz/s	0.6	0		11.5		--	--	----
n-GaAs Tunnel	58	11 GHz/s	0.1	~0.2		0				
n-GaAs Schottky barrier	50	70 MHz/s	3	—[a]		4[g]				
	58	70 MHz/s	3	—[a]		4[g]				
	58	11 GHz/s	2.5	—[c]		6	1.3[f]			
p-Si modified Schottky barrier	70	60 MHz/s	1		300-600	7				

a - Bias for min L_c.

b - 2nd harmonic mixer

c - Bias for min L_c (~ 2 mA diode current)

d - 3rd harmonic mixer

e - Tens of mW at the fundamental

f - N.R. ≈ 1, L_c = 9.5 dB at b.o. power of 0.1 mW

g - At 1 mW b.o. power, L_c = 4.5 dB

h - actual IF noise figure

i - assumed IF noise figure

Table 9.4 Best Measured Conversion Loss Reported for Millimeter-Wave Mixers Using Various "Point-Contact" Diodes[56] and Resulting Receiver Noise Figure and Noise Equivalent Power.

In eq. 9.10, T_{AR} is the radiometer system equivalent noise temperature, given by $T_{AR} = T_R + T_A$ where T_R and T_A are the equivalent noise temperatures of the receiver and the antenna respectively. β is the effective noise bandwidth of the IF amplifier (predetection network), τ is the output integration time constant of the radiometer and k is the radiometer constant dependent on other characteristics of the radiometer[62] and is of the order of unity. (For further information concerning radiometry and factors determining the antenna temperature, see Chapter XI of this report).

Type	Frequency	Conversion Loss (dB)
IN 2792	70	16
IN 2792	140	25
IN 2792 A	70	14
IN 2792 B	70	13

Table 9.5 Conversion Loss of Philco Germanium Mixers

a) Single Ended

Model No.	Waveguide	Frequency Range (GHz)	RF*+ Bandwidth (GHz)	Conversion Loss (dB) Typical	Maximum
M-96	RG-96	26.5--40	6	6.5	8.0
M-97	RG-97	33--50	6	7.0	8.5
M-98	RG-98	50--75	7	7.5	9.0
M-99	RG-99	60--90	8	8.5	10.0
M-10	WR-10	75--110	8	9.5	11.0
M-38	RG-138	90--140	9	10.5	12.0
M-36	RG-136	110--170	10	11.5	13.0

* Fixed Tuned

\+ Tunable units are also available with slightly reduced instantaneous bandwidths.

A nominal 50 ohm IF output impedance is provided when used at recommended microwave intermediate frequencies. (Microwave intermediate frequency outputs are recommended for single ended mixing so that the L.O. noise contribution remains a negligible fraction of the crystal noise ratio, i.e., an over-all NR $\leq$ 2.0). These mixers are designed to provide a very large instantaneous IF bandwidth (0.5-1.0, 1.0-2.0, 2.0-4.0 and 4.0-8.0 GHz) and hence are suitable for such applications as high sensitivity radiometers and as receivers for wide band or extremely short pulse systems.

b) Balanced

Model No.	Waveguide	Frequency Range (GHz)	RF*+ Bandwidth (GHz)	Conversion Loss (dB) Typical	Maximum
M-96H	RG-96	26.5--40	6	6.5	8.0
M-97H	RG-97	33--50	6	7.0	8.5
M-98H	RG-98	50--75	8	7.5	9.0
M-99H	RG-99	60--90	8	8.5	10.0
M-10H	WR-10	75--110	9	9.5	11.0
M-38H	RG-138	90--140	10	10.5	12.0

* Includes RF and IF hybrids

A nominal 50 ohm IF output impedance is provided when used at recommended frequencies. The recommended intermediate frequency will depend to some extent on the signal frequency used, e.g., 60 MHz (min.) for 35 GHz, 100 MHz (min.) for 60 GHz, 200 MHz (min.) for 94 GHz, and 300 MHz (min.) for 140 GHz. Using these intermediate frequencies as the lower band edge of the IF bandwidth, large instantaneous IF bandwidths can be utilized (0.1-0.2, 0.2-0.4, 0.25-0.5, 0.5-1.0, 1-2, 2-4, and 4-8 GHz). IF bandwidths greater than one octave are available on special request.

Table 9.6 Characteristics of ADTEC Millimeter Wave GaAs Mixers

It is worthwhile to point out that coherent detection systems are phase sensitive and have faster response than incoherent detectors. Minimum discernible rms temperature changes ranging between a few tenths of a degree to ten degrees have been achieved in the 35-600 GHz frequency range. The characteristics of the radiometers with which these values of ΔT were accomplished are given in Table 9.7.

Both equations 9.8 and 9.11 indicate the direction of future developments in the area of superheterodyne receivers. Both lower conversion loss and crystal noise ratio, and low noise IF amplification are essential for obtaining a lower receiver noise temperature and, therefore, lower noise figure. Development of solid state sources operating in conjunction with high efficiency varactor harmonic generators[68] and balanced mixers will contribute considerably toward achieving this aim. A comparison of the capabilities of present solid state sources with other "conventional" sources is shown in Fig. 9.10. Wideband low-noise solid-state parametric and tunnel diode amplifiers with octave bandwidths, operating at frequencies in the GHz region, and noise figures of the order of a few db at a gain of tens of dbs are being developed.[16,69] The low IF impedance of present day mm and submm mixers provides good matching to such solid state IF amplifiers. The broad bandwidth provided by these amplifiers is useful in lowering the minimum discernible rms temperature change in radiometers and in providing high capacity communication links. Totally solid state receivers would be particularly suited for use in space vehicles due to their expected lower weight and power requirements, and the ability of solid state components to withstand launching forces.

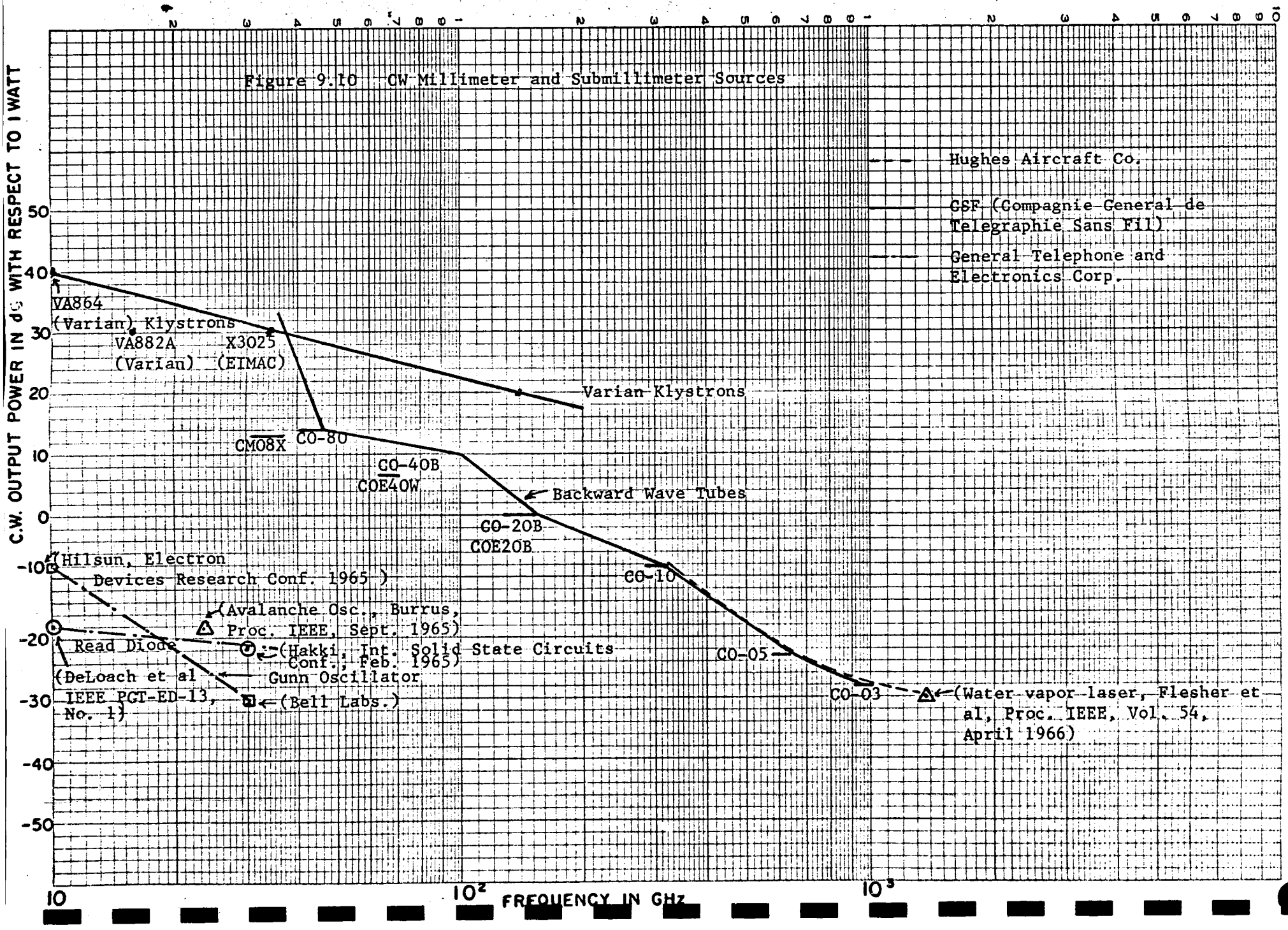

Figure 9.10 CW Millimeter and Submillimeter Sources

Frequency (GHz)	Mixer Type	Local Oscillator	IF Amplifier	Receiver Noise Figure (db)	Integration time (sec)	Minimum discernible rms temp. change(^{o}K)	Remarks	Reference
35	balanced	Klystron	UHF transistorized β_{eff} = 600 MHz	15	1	0.2	All solid state except L.O.	64
94	GaAs fundamental	Klystron	transistorized (200-400)MHz	15	10	~ 0.7	All solid state except L.O.	67
140	GaAs second harmonic	70 GHz Klystron	T.W.T.(2-4)GHz	20	10	0.3	——	58, 59
225	GaAs third harmonic	75 GHz Klystron	T.W.T.(2-4)GHz	26	10	1.0	——	58, 59
600	GaAs second harmonic	300 GHz S.C.F. Carcinotron	T.W.T.(2-4)GHz	33.2	10	11	——	65, 66

Table 9.7 Characteristics of Millimeter and Submillimeter Receivers Operating as Dicke-type Radiometers.

In the laboratory, small size solid state receivers could be completely cooled, resulting in considerable reduction of the overall noise temperature. Reduced temperatures achievable in space vehicles by radiative cooling could also be used to lower the noise temperature of any receivers on board.

9.4.2 Hot Carrier Diode Detectors

Millimeter wave detection, mixing, and harmonic generation using the thermoelectric effect of hot carriers in semiconductors has been proposed by Harrison and Zucker.[70,71,72] The basic concept in this device consists of the fact that the application of an electric field to a semiconductor causes the free charge carriers to acquire a non-zero momentum, and are displaced from the minimum energy ($\vec{k} = 0$) point in the $\vec{k}$ space by an amount proportional to the applied electric field. If, then, the geometry of the device is such that a strong dissymmetry exists between the two electrodes, such as an ohmic point contact on one side and a plated contact on the other side, a large gradient of electric field will exist between the two electrodes. This will clearly be accompanied by a large gradient of the free carrier temperature, which will result in a rectified thermoelectric voltage similar to the well-known conventional thermoelectric effect. The basic difference in this case, however, is that since the change of temperature affects only the charge carriers and not the crystal lattice, the response is very fast and can follow changes in the square of the electric field up to several hundred GHz.

It has been shown[72] that the ratio of the change in lattice temperature, ΔT_{HL}, to the change in electron temperature, ΔT_e,

$$\frac{\Delta T_{HL}}{\Delta T_e}$$

is of the order of 10^{-5} for Ge and Si. For a device configuration where one of the electrodes is a point contact of radius r_1, the majority carrier density is n, the energy relaxation time is τ_e and the applied RF power is P_{RF}

$$\Delta T_e \approx \frac{P_{RF}\,\tau_e}{3\pi n k r_1^3} \tag{9.11}$$

and the thermoelectric voltage V_{th} is approximately given by

$$V_{th} = \pm\left(\frac{3}{2} - \frac{E_F}{kT_o}\right)\frac{\tau_e\,P_{RF}}{3\pi n\,e\,r_1^3} \tag{9.12}$$

where T_o is the room temperature and E_F is the Fermi energy measured from the conduction band edge.

It should be noted that the rectified thermoelectric voltage is such that the dc potential on the metal point with respect to the bulk is opposite to the sign of the majority carrier. On the contrary, in the case of a Schottky barrier detector, the polarity of the dc potential at the metal point is the same as the sign of the majority carrier.

The thermoelectric EMF will follow the instantaneous power variations if the period of the latter 1/2f is long compared to both τ_e and $\tau_d = \rho_o\epsilon$, where τ_d is the dielectric relaxation time, ρ_o is the resistivity and ϵ is the dielectric constant of the semiconductor.

For practical Ge devices operating at room temperature, $1/\tau_e$ and $1/\tau_d$ are of the order of a few hundred gigacycles.

Hot carrier detection, mixing and harmonic generation have been experimentally obtained up to 210 GHz.[71]

With 70 GHz power input for a p-type 35 ohm-cm germanium hot-carrier microwave detector at room temperature, the typical sensitivity is approximately 10 mV/μW.

The input impedance is found to be independent of the input level for a variation of the latter from 10 μW to 30 mW. This fact enables matching of this detector and, therefore, maximum sensitivity of a range of input level.

The continuous use of a typical hot carrier microwave detector has shown negligible aging effect, indicating good reliability.

By increasing the point contact diameter and/or by reducing the semiconductor resistivity, the linear range (i.e. square law operation range) of the hot carrier Ge detector can be extended up to input power levels of 5 mW.[71] A 2 ohm-cm p-type germanium detector incorporating a relatively blunt tungsten point proved to be essentially square law up to 5 mW input power at 70 GHz,[71] with a responsivity of 30 mV/μV.

An experimental 70 GHz superheterodyne receiver incorporating an InSb hot carrier mixer operated at 77°K was constructed and tested by the above authors. It had a noise figure of approximately 23 db which is 6 db higher than a receiver employing a Schottky barrier mixer at room temperature. Since the minimum detectable signal of the hot carrier diode is inversely proportional to the semiconductor mobility and directly

to its conductivity,[72] the use of InSb with higher mobility and/or lower conductivity is expected to improve the noise figure by about 6 db over figures previously reported. The low IF impedance of hot carrier diode mixers is particularly suitable for matching to low noise solid state IF amplifiers.

In conclusion, the hot carrier diode has some very attractive features such as: (a) frequency independent sensitivity that is high at room temperature and can be further enhanced by cooling, (b) input impedance that is independent of input power level which, therefore, facilitates construction of receivers with wide dynamic range, and (c) the relatively large area under the point contact results in diodes with high resistance to burnout and thus high reliability. This resistance to burnout is particularly useful in the diode as a mm wave mixer where dc biasing and L.O. power level that are required for optimum operation could exceed the power levels of the delicate mm and submm point contact diodes. Hot carrier diodes are available commercially in cartridge form for microwave application. In view of the good qualities of this diode, further efforts towards the extension of its practical use to shorter wavelengths are highly desirable.

9.5 BULK SEMICONDUCTOR DETECTORS

9.5.1 Heterodyne Down Convertors

The idea of heterodyne detection (mixing) in bulk semiconductors was first proposed by Rollin.[35] Such bulk semiconductor mixers would be rugged both electrically and mechanically, have good dynamic range, could be easily matched over large bandwidths and easily incorporated in oversize

waveguides. Mixing is due to the nonlinear character of the "photoconductivity of the second kind"* in the bulk semiconductors such as n-type indium antimonide cooled to liquid helium temperature and immersed in a magnetic field.

Heterodyne mixing in InSb has been reported recently by Arams and coworkers.[74] Surprisingly low conversion losses as low as 12 db (corrected from 18 db measured) have been achieved at 8 mm (30-40 GHz) with n-type indium antimonide at 4.2°K. Both local oscillator output and the signal were made incident on a bulk InSb sample placed in an RG-96/U waveguide. The IF signal was obtained through ohmic contacts on two opposite faces of the sample that are used for dc biasing also. The relaxation time of hot electrons to the lattice restricts the IF frequency. This relaxation time is the order of 10^{-7} sec at liquid helium temperature which allows an IF frequency of about 1.5 MHz. A minimum conversion loss of 18 db was measured at 4.2°K in the presence of 12 kG magnetic field aligned parallel to the dc bias current direction in the sample. Superheterodyne mixing in bulk InSb has been extended recently[115] by Putley to the 1 mm wavelength region. An improvement of about six orders of magnitude over the sensitivity of the InSb video detector has been attained enabling detection of signal power as low as $1.7\ 10^{-18}$ watt.

Post-threshold amplification, oscillation and mixing in bulk GaAs has been demonstrated by Hakki[75] at microwave frequencies. In this significant experiment an n-type GaAs sample 54 microns thick was placed

---

* Raising of the effective temperature of the free electron by RF power absorption. These hot electrons have increased mobility which increases the conductivity of the sample (see ref. 36).

in a cavity at room temperature. The sample was dc biased to oscillate at 3.622 GHz, which was used as a local oscillator. An external signal of 6.114 GHz was injected into the cavity. This signal mixed with the 3.622 GHz in the GaAs sample producing a difference frequency at 2.492 GHz. This difference frequency was amplified by the sample itself by appropriately adjusting the sample bias voltage. A maximum conversion gain of 10 db was achieved.

The practical significance of using the same semiconductor sample as mixer, local oscillator and IF amplifier are obviously clear. They justify determining whether the principle could be extended to higher frequencies by using appropriate semiconductor materials aided by cryogenic temperatures and magnetic fields.

9.5.2 Non-Heterodyne Down Conversion

9.5.2.1 Mm and Submm Wave Detectors

This detection scheme, proposed by Krumm and Haddad,[76] utilizes an appropriate system of quantum energy levels to down convert mm and submm wave radiation to microwave radiation where sensitive detection schemes are available. Due to its novelty, a brief discussion of the principle of operation of this detector is given next.

Consider the three energy-level system shown below

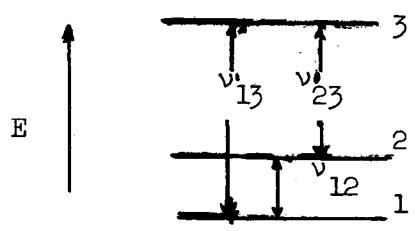

Assume the system is at thermal equilibrium. A local oscillator signal of frequency ν_{12} incident on the system will be absorbed raising some of the population of level 1 to level 2. The amount of power absorbed is proportional to the difference $(n_1 - n_2)$ where n_1 and n_2 are the populations of levels 1 and 2 respectively. If now a signal of frequency ν_{13} is incident on the system, the population difference $(n_1 - n_2)$ will decrease causing a decrease in the L.O. power absorbed. The scheme calls for using an appropriate material in which ν_{12} lies in the microwave region where available sensitive detectors can measure the change in the power absorption, which in turn is indicative of the power absorption at the higher frequency ν_{13}, whose corresponding wavelength lies in the mm and submm wavelength.

Krumm and Haddad show that for optimum relaxation rates between energy levels, the down conversion loss L_{dc} for such a detection scheme is equal to $L_{dc} = \frac{\nu_{12}}{\nu_{13}}$. For signal frequencies of 170 GHz and higher the noise equivalent power of this down converter becomes theoretically better than a superheterodyne down converter. A combination of this proposed down converter with a maser and a superheterodyne receiver would result in much better sensitivities than are presently available with mm and submm wave detectors. The response time of the down converter is greatly dependent on the stimulated transition probability W_{12} between levels 1 and 2. It appears that a larger W_{12} and larger thermal relaxation rate between level 3 and 2 provide shorter rise and decay times. A minimum rise time of 11 ns and decay time of 12 ns have been calculated for a typical system. A host of paramagnetic materials that have been

suggested for maser applications may be employed in this detection scheme. In these materials the energy levels are adjustable by appropriate application of a magnetic field allowing tuning over a finite band of signal frequencies. Possible suitable materials are listed in Table 9.8 with an indication of the frequencies that can be detected.

Material	Signal Frequency Covered GHz
(Rutile) Iron doped titania (F_e^{3+} : TiO_2)	40-120
Iron doped Zinc Tungstate (F_e^{3+} : $ZnWO_4$	up to 220
Vanadium doped sapphire (V^{3+} : Al_2O_3)	around 500
Nickel doped titania (N_i^{3+} : TiO_2)	around 500
Chromium doped cyanite (C_r^{3+} : $SiO_2 . Al_2O_3$	around 2000

Table 9.8 Possible Materials Suitable for Use in the Haddad and Krumm Detector

The possibility of using other media such as gases with appropriate energy levels in this detection scheme eliminate the need of a magnetic field and low temperatures.

9.5.2.2 Reflection Cavity Detector

The use of a reflection cavity containing a small semiconductor slab has been proposed[77] for the purpose of detecting mm and submm radiation. The principle of operation is depicted in the figure below.

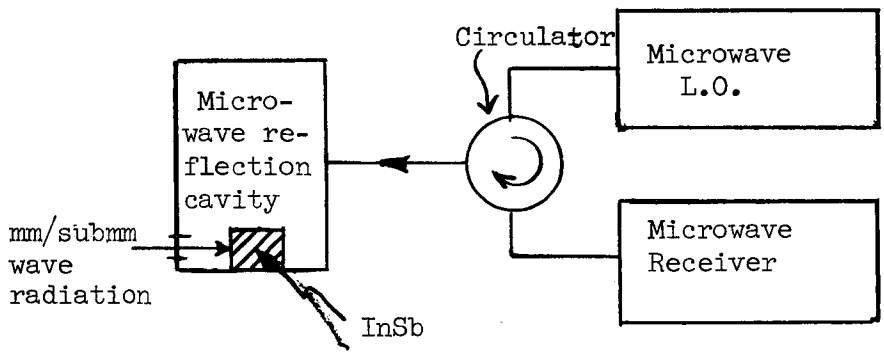

This principle consists of detecting changes in the conductivity of a cooled semiconductor slab caused by the mm wave radiation by measuring the reflection of a microwave signal from the cavity with the aid of easily available sensitive microwave equipment. The semiconductor can be any of the semiconductor materials used in the construction of photo-conductive mm and submm wave detectors, such as impurity activated germanium, or indium antimonide which is used in the Putley detector. This scheme calls for cooling and use of magnetic fields to achieve the required energy levels in the semiconductor. The activation energy of the electron in the semiconductor will be thus smaller or equal to $\frac{hc}{\lambda}$, where λ is the mm or submm radiation wavelength. Notice that the microwave signal will not activate the semiconductor since $\frac{hc}{\lambda_m}$ is much

smaller than the activation energy of the semiconductor (λ_m is the microwave wavelength).

The phenomenon of far infrared absorption in the wavelength range .1-1 mm due to photon-induced hopping of charge carriers between impurity centers in compensated n-type silicon at $2.5^{o}K$[78] could also be utilized as the absorption mechanism of submm wave radiation in the semiconductor inside the cavity. Unlike conventional photoconductive detectors, the semiconductor sample in the proposed reflection cavity detector does not require any dc biasing which normally increases to the overall noise of the detector. The sensitivity of this proposed detector is, therefore, expected to be high.

9.5.2.3 Millimeter Traveling Wave Maser and Maser Materials

The attractive features of masers, such as their low noise figure and rugged nature, makes the extension of their operation to mm and submm wavelengths highly desirable. The main obstacle in doing this is that of materials. Rutile (TiO_2) doped with trivalent chromium ion or trivalent iron ion and iron-doped zinc tungstate are materials that extend the maser operation range up to ~ 100 GHz. These materials are characterized by large dielectric constants. This fact allows the use of small samples which are more adaptable to the necessary cryogenic cooling and superconductive magnets. On the other hand, the high dielectric constant poses problems in matching. Naturally, to facilitate matching, suitable materials with a lower dielectric constant such as iron-doped zinc tungstate could be used. This, however, will increase the size of the structure. An extensive study and search for materials suitable for

mm and submm maser operation is being carried out by Haddad and co-workers.[77] An important recent development in this area is the successful operation of a zero magnetic field, 81 GHz, iron-doped rutile maser by Hughes and Kremenek[79] and Hughes and Deal.[80] These masers still suffer from the matching problem. The maser was made to operate at 4.2°K in a good, stable high-gain mode in excess of 20 db. One of its modes provided useful electronic gain up to temperatures of 15°K. The elimination of the magnetic field in the operation of this maser and maintenance of useful gain at elevated temperature provides two significant developments, in the sense that they bring mm wave masers closer to possible use on board satellites and space vehicles.

Future work in the field of mm and submm masers would include a search for materials that are suitable for maser operation in the mm and submm range that can provide one or more of the following features:

a) zero magnetic field operation

b) operation at elevated temperatures

c) pumping at frequencies less than the signal frequency

d) pumping with laser sources.

9.6 OTHER TYPES OF DETECTORS

Other types of detectors whose operation is extendable to mm and submm wavelengths through appropriate development and modificatipn of their state of the art at microwave frequencies are the following.

9.6.1 Klystron Detectors

The possibility of using reflex klystrons as tunable detectors at frequencies where ordinary microwave crystal diode performance is

relatively poor has been proposed by Whitford.[81] Tangential sensitivities of the order of 40-47 dbm were obtained at 16 GHz. Although no experimental work has been done above this frequency, there is no fundamental reason why a detector of this type could not be made to operate at any frequency where a reflex klystron can be made to operate.

The possibility of achieving amplification and detection simultaneously in a standard 2K25 klystron has recently been demonstrated by Ishii[82] at 9.2 GHz. A noise figure of 10-15 db and more than 20 db gain over a standard crystal detector were obtained. Improved klystron tubes and circuit design would probably reduce the noise figure to 7 db. The prospect of attaining amplification and detection in the same device is certainly attractive enough to justify any attempt to extend the operation of this type of detector to shorter wavelengths.

9.6.2 Plasma Detector

Another type of detector is the plasma microwave detector. In this case electrons of the plasma interact with the incident microwave radiation, which results in a corresponding change in conductivity. The change in conductivity is easily monitored by observing the change in discharge current.[83,84,85] This type of detector has been investigated at centimeter wavelengths, and sensitivities comparable to crystal diodes have been reported.[83] Time constants of the order of milliseconds to microseconds are attainable. Also broadband operation has been observed in the range of 1-5 GHz for a neon glow discharge.[85] Increased sensitivity may be attainable above 10 GHz by using steady magnetic fields, which produces cyclotron resonance absorption of incident

radiation. In the mm wavelength, Severin[86] utilized the cathode fall region of a glow discharge in order to obtain sufficient sensitivity to measure radiation at 2 mm wavelength. Severin predicts that the plasma detector would compare favorably with other detectors at wavelengths shorter than 2 mm. Due to the attractive properties of the plasma detector (mechanical and electrical ruggedness, overload capacity, simplicity and extended frequency range[86]), it seems worthwhile to further investigate its operation at mm and submm wavelength. An apparent drawback of this detector would seem to be the high dc power dissipation required to obtain the plasma. However, with the availability of low work function surfaces, such as Au, Cs, O for use in cathodes of glow discharge tubes, low-voltage glow discharge tubes with considerably lower power dissipation have been developed.[87] They may prove to be quite adaptable for use in plasma EM wave detectors.

9.7 COMPARISON AND EVALUATION OF MILLIMETER AND SUBMILLIMETER WAVE DETECTORS

Several figures of merit used to describe the performance of mm and submm wave detectors[88,89] have been proposed. The most frequently used at present are:

a) Responsivity (R): This quantity denotes the effectiveness of the detector in converting radiant flux incident on it into an electrical signal. The responsivity is given by

$$R = \frac{V_s}{P_{in}} \left[\frac{\text{Volts}}{\text{Watt}}\right] \tag{9.13}$$

where V_s is the output voltage due to an incident radiant flux P_{in}.

The responsivity also provides an idea of the complexity of the post detection amplifier system required.

b) Time constant (sec): This is a measure of the demodulation capability of the detector.

c) Noise Equivalent Power (NEP) in watts: This is the rms value of the sinusoidally modulated radiant flux power incident on the detector that will produce an rms output voltage equivalent to the rms value of the noise voltage of the detector (unity signal-to-noise ratio).

d) Detectivity D* (read D-star): This is a figure of merit particularly useful in specifying the sensitivity of incoherent radiation detectors. The detectivity is given by

$$D^* = \frac{(A\beta)^{1/2}}{NEP} \quad \left[\frac{cm - Hz^{1/2}}{watt}\right] \tag{9.14}$$

where A is sensitive area of the detector and β is the overall bandwidth of the detection system.

Both NEP and D* depend on the conditions under which they are measured. These conditions are:

1) the blackbody temperature in ^{o}K of the radiation source used in the measurement (small dependence)
2) the modulation frequency of the radiant flux incident
3) bandwidth β of the post detector amplifier used
4) the wavelength λ at which the measurement was performed.

It is customary to specify these conditions whenever NEP or D* are quoted. Thus, D* (0.1 mm, 1000, 10) $500^{o}K$ would indicate that the

detectivity was measured at a wavelength λ - 0.1 mm with radiant flux modulated at f_m = 1000 Hz and emanating from a source possessing a black-body temperature of 500°K and post-detector bandwidth of 10 Hz. The spectral dependence of detectivity under the same measurement conditions would be denoted by D* (λ, 1000, 10) 500°K.

Since the performance of cooled incoherent detectors is strongly dependent on the temperature of operation, this temperature should also be specified whenever detectivity or NEP are quoted.

The value of an NEP of a detector is dependent on the noise properties of the detector. Types of noise such as contact noise, external magnetic field, and modulation noise can be eliminated by proper design and fabrication. In photoconductive detectors maximum detectivity is obtained when the generation recombination noise is predominant. Theoretical calculations of the detectivity of an ideal detector, i.e. when the g-r noise is due to the rate of absorption of background radiation (background limited operation) has been made by Bratt and Giggey.[91] The latter two, assuming black body radiation, were able to obtain ideal detectivity curves for various materials. For wideband detectors, these detectivity curves increase linearly with wavelength up to a maximum wavelength λ_m (determined by the material of the detector) and then fall to zero. The locus of all points corresponding to the maximum detectivity in these curves is shown in Fig. 9.11, which also contains the detectivity of an ideal narrow-band detector at 0.11 mm computed by Bratt and Giggey. Against those ideal detectivity curves, Fig. 9.10 shows also the detectivity curves of some of the photoconductive detectors

Figure 9.11 Spectral Response (Detectivity vs Wavelength) of Photoconductive Millimeter and Submillimeter Detectors

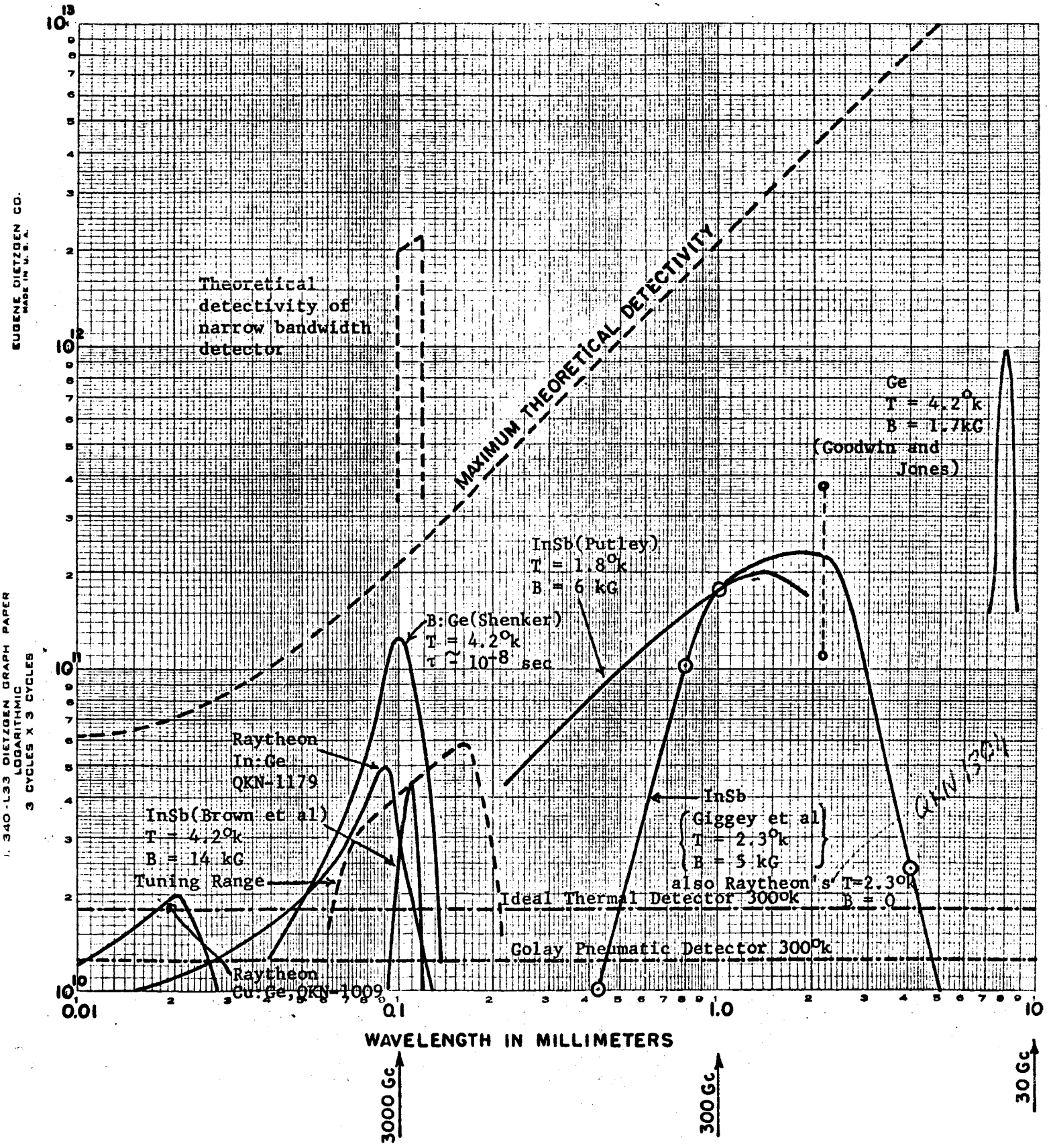

discussed in Section 9.3 of this chapter. The detectivity of an ideal thermal detector and pneumatic detector (Golay cell) operating at room temperature are also included for comparison. It is easily seen that the detectivity of these presently available photoconductive detectors is below the theoretical limits predicted by Bratt and Giggey. This discrepancy between theory and achievement is caused by the post-detector amplifying systems used. It has been suggested[13] that this limitation could be overcome by the development of low noise video amplifiers operating at liquid helium temperature or by using parametric amplifiers.

A list showing the important characteristics of various mm and submm wave detectors is given in Table 9.9. Since the area A (see eq. 9.14) is not meaningful in the case of superheterodyne and video receivers, no value of detectivity is given in Table 9.9 for these detection schemes. As was discussed elsewhere in this chapter, the performance of such receivers is best described by means of the equivalent noise temperature or the noise figure of the system. The noise equivalent power of superheterodyne receivers can be determined from eq. 9.7 and eq. 7 of Appendix 9.I. Given the crystal mixer noise ratio and the IF amplifier noise figure, one can compute the receiver noise figure from eq. 9.7 from which one can determine the NEP using eq 7 of Appendix 9.I. Figures 9.12 and 9.13 give the calculated NEP for superheterodyne receivers employing commercially available mixers for various assumed values of IF amplifier noise figure. The crystal noise ratio is assumed to be NR = 2 in all cases. In Fig. 9.12 also are given the NEP values of actually constructed receivers.

Table 9.9 Characteristics of Millimeter and Submillimeter Radiation Detectors

Detector	Wavelength	Operating Temp. (°K)	Sensitive detector area (cm^2)	N.E.P. for 1 Hz bandwidth (W)	Normalized Detectivity D* (cm-$Hz^{1/2}$/W)	Responsivity R (V/W)	Response time τ (sec)	Remarks	Ref.
Ideal Thermal Detector	flat spectral response	300	1.0	5.5×10^{-11}	1.82×10^{10}	---	---	---	
	$\lambda \geq .1$ mm	1.5	1.0	3.6×10^{-13}	2.78×10^{12}	---	---	Window with .5 steradian assumed	111
	$\lambda = .5$ mm	1.5	1.0	1.8×10^{-14}	5.56×10^{13}	---	---	Filter with 10% bandwidth centered at $\lambda = .5$ mm assumed	
Golay Pneumatic Detector	$\lambda \leq 5$ mm	300	0.015	3×10^{-10}	4×10^{10}	$\sim 10^5$	0.015	available commercially(a)	2
Germanium bolometer (Low detector)	can be designed to operate at least over entire submm band	2.15	0.15	5×10^{-13}	7.75×10^{11}	$\sim 4.5\ 10^3$	$\sim 4 \times 10^{-4}$	available commercially(b) with cryogenic sys.	15 16 17
		2.0	0.012	4×10^{-14}	3.73×10^{12}				
Carbon bolometer	at least entire submm band	2.1	0.2	1×10^{-11}	4.5×10^{10}	2.1×10^4	0.01	---	13
Superconducting bolometer	" " "	3.7	0.06	3×10^{-12}	8.2×10^{10}	---	1.25	---	11
InSb wide-band detector with magnetic field (Putley detector)	$\lambda = 2$ mm	1.5	~ 0.05	1.33×10^{-12}	1.7×10^{11}	$\sim 10^3$	10^{-7}	B = (5-6)kG	33
	$\lambda = 1.5$ mm	1.5	"	1.13×10^{-12}	2×10^{11}	"	2×10^{-7}	see Fig.9.12	34
	---	2.8	0.2	1.0×10^{-12}	2.3×10^{11}	$\sim 10^4$	2.5×10^{-7}		

Continued

Table 9.9 Continued

Detector	Wavelength	Operating Temp. (°K)	Sensitive detector area (cm^2)	N.E.P. for 1 Hz bandwidth (W)	Normalized Detectivity $D^{*1/2}$ ($cm\text{-}Hz^{1/2}/W$)	Responsivity R (V/W)	Response time τ (sec)	Remarks	Ref.
InSb detector without magnetic field (free carrier absorption)	λ =(0.5-8)mm	4.0	0.15	1.0×10^{-12}	3.8×10^{11}	---	3×10^{-7}	available commercially (c) see Figs. 9.1 and 9.11 for spectral resp. (see also Table 9.2)	35
Tuned InSb detector	12% band at (0.06-0.15)mm	4.0	0.25	5×10^{-11}	1×10^{10}	~ 40 at λ=0.1mm	10^{-6}	see Fig. 9.11 for spectral response	39 112
Ge cyclotron resonance detector	λ = 8 mm	4.0	0.02	2×10^{-12}	0.7×10^{11}	~ 10^6	5×10^{-9}	B=1.7 kG see Fig. 9.11	38
Impurity activated Ge detector	Submm band (2μ-100μ). 8 Peak detectivity Figs. are given at 0.1 mm	"	--	---	1.25×10^{11}	---	8.7×10^{-9}	Boron activated available comm.(c)	28 29 30
		"	--	---	3.1×10^{11}	---	"	Gallium activated avail. comm.(c)	
Ideal Superheterodyne receiver	$\lambda \geq 1$ cm	300	--	4×10^{-21}	---	---		---	111
	λ = 1 mm	"	--	2×10^{-19}	---	---	~5×10^{-9}	---	
	λ = 0.1 mm	"	--	2×10^{-18}	---	---			
Superheterodyne receivers	λ = 2 mm	300	--	7×10^{-15}	---	---	~ 10^{-9}	---	50
	λ = 0.5 mm	300	--	~ 10^{-17}	---	---	~ 10^{-9}		108

Table 9.9 Continued

Detector	Wavelength	Operating Temp. (°K)	Sensitive detector area (cm^2)	N.E.P. for 1 Hz bandwidth (W)	Normalized detectivity D^* ($cm\text{-}Hz^{1/2}/W$)	Responsivity R (V/W)	Response time τ (sec)	Remarks	Ref.
Video Receivers	$\lambda = 1$ mm	300	---	5×10^{-12}	----	----	$\sim 10^{-9}$	---	49
	$\lambda \cong 2$ mm			1.6×10^{-12}	----	----			
Meredith and Warner Video Receiver	$\lambda = 2$ mm	300	---	2.5×10^{-11}	----	----	10^{-9}	---	50
	$\lambda = 1$ mm	"	---	4×10^{-9}	----	----	"		

a) The Eppley Laboratory, Inc., Newport, R.I.

b) Texas Instruments, Inc., Apparatus Div., Houston, Texas

c) Raytheon Company Special Microwave Devices Operation, Waltham, Mass.

Figure 9.12 Noise equivalent power of superheterodyne receivers employing available mixers (mixer noise ratio NR = 2 is assumed, IF amplifier noise figure F_{IF} = 1, 2, 4 dB)

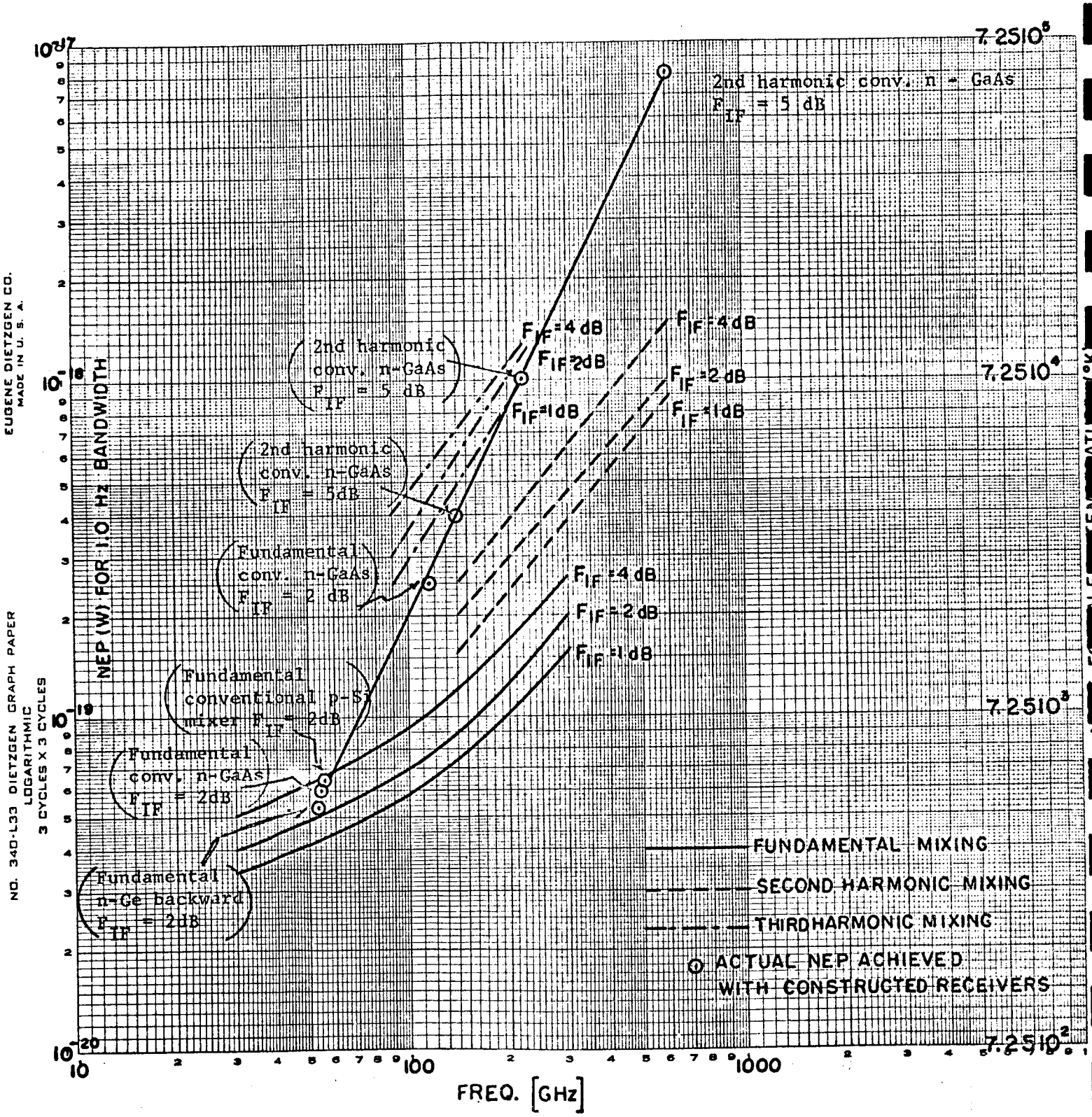

Figure 9.13 Noise equivalent power of superheterodyne receivers employing available mixers (mixer noise ratio NR = 2 is assumed) IF noise figures = 6, 8 and 10.

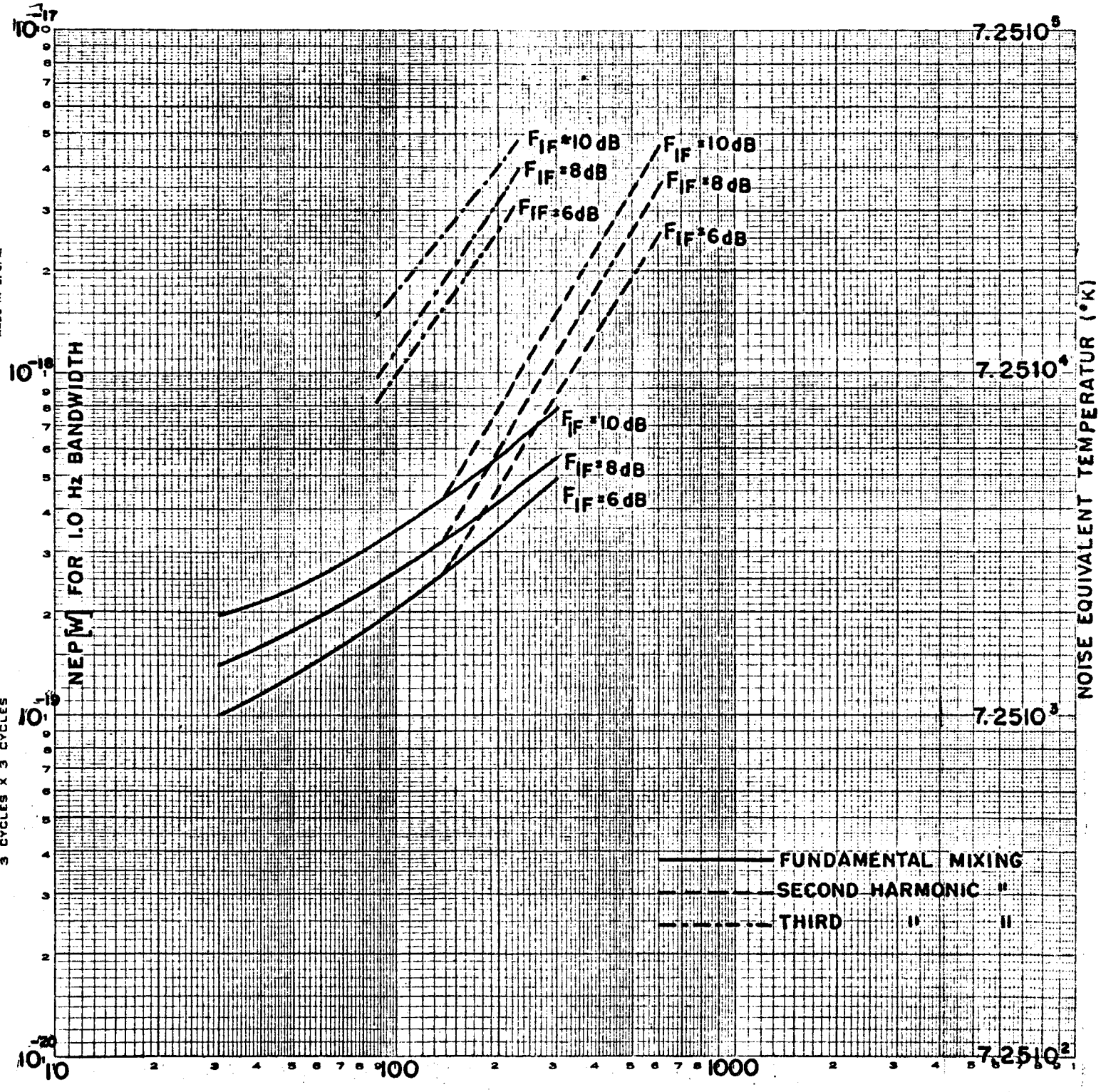

Using the relationship between noise equivalent power and noise equivalent temperature (eq. 12, Appendix 9.I), the values of noise equivalent temperature are calculated for some of the detectors of Table 9.9. The results are given in Table 9.10 for comparison. The superior performance of superheterodyne receivers is quite apparent.

9.8 MILLIMETER AND SUBMILLIMETER DETECTORS, APPLICATIONS AND FUTURE DEVELOPMENT

The same four quantities used in the evaluation of these detectors that were enumerated in Section 9.6 are considered in the choosing of a detector for a particular application.

From Table 9.9 and Fig. 9.11, one can see that in applications where the highest available detectivity is required, the Ge bolometer and helium cooled InSb detectors are suitable. Unless cryogenic systems become practical for space vehicle use, low temperature detectors are confined to use in the ground end of a space communication. At wavelengths shorter than 2 mm, the theoretical detectivity of superheterodyne receivers becomes superior to the cooled InSb detectors. It is for this reason that many efforts have been made and are continued[49,58,59,92-110] to develop submm wave point contact detectors and mixers and to overcome the difficulties in extending the construction of this type of receiver to the submm wavelengths.

Where power measurement is required, one of the bolometric detectors is suitable. In radiometry, both germanium bolometer[16,17] and the crystal diode mixers[58,59] have been used successfully.

When short response time is required, the point contact rectifier used as a video detector or a mixer in a superheterodyne receiver is

Table 9.10 Equivalent Noise Temperature of Various Detectors

Detector	Frequency or Wavelength	NEP for 1 Hz bandsidth (W)	Equivalent Noise Temperature (°K)
Ideal therm. Det.	flat	$5.5\ 10^{-11}$	$4\ 10^{12}$
Golay Pneumatic Cell	$\lambda \leq 5$ mm	3×10^{-10}	$2.17\ 10^{13}$
Germanium bolometer (Low detector)	theoretically entire submm wavelength	$4\ 10^{-14}$ (best achieved)	$2.8\ 10^{9}$
Carbon bolometer	entire submm band	1×10^{-11}	$7.25\ 10^{11}$
Super conducting bolometer	"	$3\ 10^{-12}$	$2.17\ 10^{11}$
InSb wideband detector with magnetic field Putley detector	2m 1.5mm	$1.33\ 10^{-12}$ $1.13\ 10^{-12}$	$\sim.965\ 10^{11} = 9.65\ 10^{10}$ $8.23\ 10^{10}$
InSb detector without magnetic field(free carrier absorption)	$\lambda = (0.5\text{-}8)$mm	1×10^{-12}	$7.25\ 10^{10}$
Tuned InSb detector	12% band at (0.06-0.15)mm	5×10^{-11}	$3.62\ 10^{12}$
Ge Cyclotron resonance detector	$\lambda = 8$ mm	2×10^{-12}	$1.45\ 10^{11}$
Boron activated Ge detector	0.1 mm	1.25×10^{11}	$.9\ 10^{12} = 9\ 10^{11}$
Ideal superheterodyne receiver	30 GHz-(1cm) 300GHz-(1 mm) 3000GHz-(0.1mm)	$4\ 10^{-21}$ $2\ 10^{-18}$ $2\ 10^{-17}$	$2.8\ 10^{2}$ $1.45\ 10^{5}$ $1.45\ 10^{6}$
Superheterodyne Receivers	$\lambda = 2$ mm $\lambda = 05$	$7\ 10^{-15}$ $8\ 10^{-18}$	$5\ 10^{8}$ $5.75\ 10^{5}$
Video Receivers	1 mm 2 mm	5×10^{-12} 1.6×10^{-12}	$3.62\ 10^{11}$ $1.18\ 10^{11}$

the obvious choice. At wavelengths where these are not available, the obvious alternative is one of the InSb cooled detectors or the Ge cyclotron resonance detector.

The development of superheterodyne detection schemes at submm wavelengths seems to be most worthwhile, since this class of detectors is characterized, at least in theory, by:

1) high detectivity

2) short response time which will enable the demodulation of microwave modulated mm and submm signals (The advantages of the wide bandwidth available are evident especially for space applications.)

3) operation at normal temperatures.

A major difficulty in the development of the superheterodyne detection scheme is the requirement of a low noise stable local oscillator with an output frequency nearly equal to the signal frequency, and power considerably higher than that of the received signal. However, with the present day development of mm and submm sources, this disadvantage is becoming merely a technical difficulty.

At the present time, areas in which further work could contribute considerably to the development of sensitive compact, superheterodyne receiving systems at shorter wavelengths are:

1) low noise, low conversion loss crystal mixers

2) low noise solid state sources and efficient harmonic generators for L. O. applications

3) integrated solid state oscillators--mixers and IF amplifiers

4) low noise, high gain, wideband IF amplifiers (parametric and tunnel diode amplifiers).

Homodyne detection schemes have similar advantages to the superheterodyne scheme. Disadvantages are the requirement of a very stable oscillator and phase synchronization between the local oscillator and the carrier.

Finally, one may anticipate the extension of the quantum amplifier concept[113] to the submillimeter range. Although a quantum amplifier is not a detector, it is a photon effect device in which input photons of the carrier frequency are amplified within the device by stimulated emission of radiation which results in a power gain. Values of NEP = $(10^{-19} - 10^{-22})$ W are predicted theoretically. In this respect, it was shown by Strain[114] that the exchange coupled ion pairs in red ruby lasers are applicable to quantum electronic devices (including detectors) in the submillimeter region. Estimates made by Strain show that a laser should be operable in the submillimeter region using optical pumping of the ion pairs in red ruby. Such a laser has not been operable yet. The reason lies probably in the small absorption cross-section of ruby at U and Y bands. This can be verified from knowledge of the spin-lattice relaxation time, which still remains unknown.

APPENDIX 9.I

RELATION BETWEEN NOISE FIGURE, NOISE EQUIVALENT POWER,

AND EFFECTIVE NOISE TEMPERATURE

Consider the definition of the noise factor of a two port network,

$$F = \frac{\left(\frac{S_i}{N_i}\right)}{\left(\frac{S_o}{N_o}\right)} = \frac{\text{available signal to noise ratio at input terminals}}{\text{available signal to noise ratio at output terminals}} \quad (A.9.1)$$

in which S and N refer to signal and noise power respectively and the subscripts "i" and "o" designate the input and output terminals respectively.

Since $S_o = GS_i$ where G is the power gain of the network and $N_i = KT_o\beta$ is the available input noise power*+ (β is the network effective

---

* The power spectrum of Johnson noise generated by a resistor R at temperature T is,

$$P(f) = 4KTR\left(\frac{hf}{KT}\right)\left(e^{\frac{hf}{KT}}-1\right)^{-1}$$

where $h = 6.625\ 10^{-34}$ Joule sec is Planck's constant and f is the frequency. The available power to a network of effective bandwidth β would be, therefore,

$$N_i = KT\beta\left(\frac{hf}{KT}\right)\left(e^{\frac{hf}{KT}} - 1\right)^{-1}$$

For the frequency range ($f \leq 1000$ GHz) of interest in this work, and for $T \simeq T_o$, $\frac{hf}{KT_o} \leq .166$ and $N_i \simeq KT_o\beta$.

\+ For definition of available power, see, for example, Friis, H. T., "Noise Figure of Radio Receivers," Proc. IRE, Vol. 32, pp. 419-422, July, 1944.

bandwidth, $K = 1.38\ 10^{-23} \left[\frac{\text{Joule}}{K^o}\right]$ and $T_o = 290^oK$), eq. A.9.1 can be written in the form,

$$F = \frac{N_o}{GKT_o\beta} \tag{A.9.2}$$

Thus, the total output noise power is

$$N_o = FGKT_o\beta \tag{A.9.3}$$

This output noise power is the sum of the output noise power $N_iG = GKT_o\beta$ due to the input termination and the output noise power N_n generated in the network, i.e.

$$N_o = GKT_o\beta + N_n \tag{A.9.4}$$

Therefore,

$$N_n = N_o - GKT_o\beta = (F - 1)\ GKT_o\beta \tag{A.9.5}$$

The equivalent signal power at the input terminals that will produce an output signal power equal to N_n is called the noise equivalent power NEP. Thus

$$NEP = \frac{N_n}{G} = (F - 1)\ KT_o\beta\ \left[\text{Watts}\right] \tag{A.9.6}$$

It is customary to specify the NEP of networks and transducers for β - 1 Hz. Then

$$NEP = 4 \times 10^{-21}\ (F - 1) \quad \left[\text{Watts}\right] \tag{A.9.7}$$

The relation between noise figure and effective noise temperature of a network is shown next.

From eqs. A.9.2 and A.9.4

$$F = 1 + \frac{N_n}{GKT_o\beta} \qquad (A.9.8)$$

It is customary to represent the noise contribution N_n of the network in terms of an "effective noise temperature", T_e, of the input termination that will produce the same amount of noise power, N_n, at the output of the equivalent noise free network. According to this convention,

$$N_n = GKT_e\beta \qquad (A.9.9)$$

which upon substitution in eq. A.9.7 provides

$$F = 1 + \frac{T_e}{T_o} \qquad (A.9.10)$$

or

$$T_e = T_o(F - 1) \qquad (A.9.11)$$

The relation between T_e in ^oK and the noise figure in db is shown in Fig. A.9.1.

Care must be exercised in the use of expressions A.9.6 and A.9.11 when the two-port network is a superheterodyne receiver. These equations are applicable provided one always uses the noise figure of the image blocked receiver.

Combining eqs. A.9.6 and A.9.11, one can obtain a relation between the noise equivalent power and the effective noise temperature:

$$NEP = KT_e\beta \text{ Watts } (\beta = 1 \text{ Hz}) \qquad (A.9.12)$$

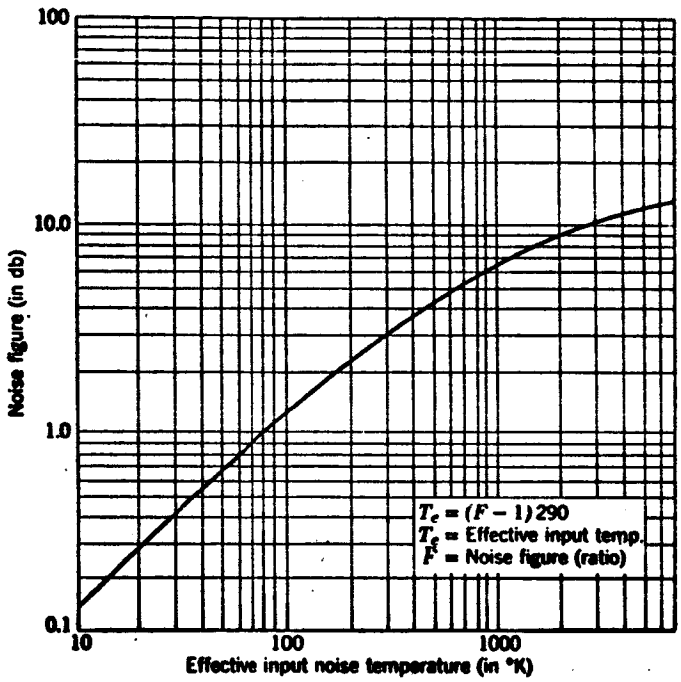

Fig. A.9.1 Relation between Noise Figure in db and Effective Noise Temperature

9.9 References to Chapter IX

1. "The Radio Spectrum from 10 Gc to 300 Gc in Aerospace Communications," RCA Report No. 6-400-6, RCA Research Labs., Montreal, Canada.

2. M. J. E., Golay, "A pneumatic infrared detector," Rev. Scientific Inst., vol. 18, pp. 357-362, 1947.

3. J. A. Lane, "Measurement of power at wavelengths of 3 cm by thermistors and bolometers," Proc. IEEE, vol. 120B, p. 189, Nov. 1955.

4. R. A. Smith, F. E. Jones and R. P. Chasmar, The Detection and Measurement of Infrared Radiation, Oxford University Press, 1957, Chapt. III.

5. R. F. Grove, "The Pneumatic Energy Detector with Remote Optics," Randolph-Macon College, Dept. of Physics, Final Tech. Report, Contract N 178-7904, Nov. 15, 1963.

6. Mark Schuman, "Sensitivity of a selective pneumatic detector," App. Optics, vol. 4, no. 11, p. 1442-1445, Nov. 1965.

7. R. C. Jones, "The general theory of bolometer performance," J. Opt. Soc. Am., vol. 43, pp. 1-14, Jan. 1953.

8. J. A. Hulbert, and G. O. Jones, "The superconducting bolometer as a detector of thermal radiation from low temperature sources," Proc. Phys. Soc., vol. 68B, p. 810, 1955.

9. D. R. Andrews, R. M. Milton and W. F. DeSorbo, "A fast superconducting bolometer," J. Opt. Soc. Am., vol. 36, pp. 518-524, Sept. 1946.

10. N. Fuson,"The infrared sensitivity of super-conducting bolometers," J. Opt. Soc. Am., vol. 38, pp. 845-853, Oct. 1948.

11. D. H. Martin, and D. Bloor, "The application of superconductivity to the detection of radiant energy," Cryogenics, vol. 1, pp. 159-165, March 1961.

12. B. Laleviac, "Criteria for the choice of a superconducting bolometer," J. Appl. Physics, vol. 31, p. 1234, July 1960.

13. J. R. Clement and E. H. Quinnell, "The low temperature characteristics of carbon-composition thermometers," Rev. Sci. Instr., vol. 23, pp. 213-216, May 1952.

14. W. S. Boyle, and K. F. Rodgers, "Performance characteristics of a new low-temperature bolometer," J. Opt. Soc. Am., vol. 49, pp. 66-69, January 1959.

15. F. J. Low, "Low-temperature germanium bolometer," J. Opt. Soc. Am., vol. 51, pp. 1300-1304, Nov. 1961.

16. F. J. Low, "Thermal detection radiometry at short millimeter wavelengths," Proc. IEEE, vol. 54, pp. 477-484, April 1966.

17. F. J. Low, "Performance of thermal detection radiometers at 1.2 mm," Proc. IEEE, vol. 53, p. 516 (correspondence), May 1965.

18. H. C. Ingaro, D. H. Menzel and F. J. Kahn, "Ferroelectric Bolometer for Space Research," (ASTIA D 65-14376) Division of Engineering and Applied Physics, Harvard Univ., Cambridge, Mass.

19. W. D. Brennan, "Uncooled IR Detectors for the Ten Micron Region," Report No. ARF-1208-12A, Feb. 25, 1963, Armour Research Foundation.

20. J. Cooper, "Minimum detectable power of pyroelectric thermal receiver," Rev. Sci. Instr., vol. 33, p. 92, 1962.

21. R. A. Hanel, "Dielectric bolometers, a new type of thermal radiation detector," J.O.S.A., vol. 51, p. 220, 1961.

22. H. C. Ingaro and D. H. D. Menzel,
    1) "Instrumentation for observation of planets in the far IR," Memoires Soc. R. Sc. Liege, Cinquiemeserie, Tome VII.
    2) "Study of IR Instrumentation for Thermal Photography of the Moon," Semiannual Status Report, No. 2, NASA Grant NSG-64060, Harvard University, July to Dec. 1960.
    3) "IR Work at Harvard College Observatory," Informal IR Astronomy Symposium, Nov. 11, 1961, Lab. of Astrophysics and Physical Meteorology, The Johns Hopkins University, Baltimore, Md.

23. T. A. Perls, T. J. Diesel and W. I. Doborov, "Primary pyroelectricity in barium titanate ceramics," J. Appl. Phys., vol. 29, pp. 1297-1302, Sept. 1958.

24. A. G. Chynoweth, "Dynamic method for measuring the pyroelectric effect with special reference to barium titanate," J. Appl. Phys., vol. 27, pp. 78-84, Jan. 1956.

25. M. Sil'vestrova, "Concerning Light Detectors Utilizing the Pyroelectric Effect," Izv Adak Nauk UZ SSR Ser. Fiz. Mat. Nawk, vol. 24, pp. 1213-1215, 1960.

26. W. H. Steier, "Pyroelectric effect detector for submm wavelength," Proc. of the IEEE, Vol. , p. 1114, Aug. 1963.

27. M. Cohn, et al., "Techniques for Superheterodyne Receivers Above 100 Gigacycles," Final Report, Contract NASw-662, Electronic Communications, Inc., Timonium, Md.

28. S. J. Fray, and J. F. C. Oliver, "Photoconductive detector of radiation of wavelength greater than 50 μ," J. Scientific Instruments, vol. 36, p. 195, 1959.

29. P. R. Bratt, "Photoconductive detectors and components for long wavelength infrared radiation (50-150) microns," Proc. IRIS(1963); also, Final Report, "Long Wavelength Infrared Detector Research and Components Measurement," Contract No. AF 33 (616)-7983, Raytheon Co., Research Division, Aug. 1962.

30. R. F. Wallis and H. Shenker, "Detector Investigation for 8-15 and 100-4000 Micron Region," NRL Memorandum Report No. 1493, Jan. 1964, and No. 1550, July 1964.

31. J. Besson, et al., "Le detecteur a antimoniure d'indium dans la band de 0.1 a 10 mm," L'Onde Electrique, vol. 45, pp. 107-115, Jan. 1965.

32. R. J. Sladek, "Magnetically induced impurity banding in n-InSb," J. Phys. Chem. Solids, vol. 5, p. 157 (1958).

33. E. H. Putley, "Impurity photoconductivity in N-type InSb,: Proc. Physical Society, vol. 76, p. 802, Nov. 1960, see also: Photoconductivity, edited by H. Levenstein, Pergamon Press, Inc., New York, p. 241, 1962, and paper T2-03 by E. H. Putley, "International Conference of Semiconductor Physics," Paris, 1964. Also, "Impurity Photoconductivity in N-type InSb," J. Phys. Chem. Solids, vol. 22, pp. 241-247, Dec. 1961.

34. G. F. Giggey, P. P. Debye and P. R. Bratt, "Photoelectric Millimeter Wave Detector," Final Report, AD 608 710, Oct. 1964.

35. B. V. Rollin, "Detection of millimeter and submillimeter wave radiation by free carrier absorption in a semiconductor," Proc. Phys. Soc., London, vol. 77, p. 1102, May 1961.

36. S. M. Kogan, "Photoconductivity theory based on variation of carrier mobility," Soviet Physics--Solid State, vol. 4, p. 1386, 1963.

37. H. Shenker, "Millimeter wave photoconductivity in InSb at a high magnetic field," Applied Phys. Letters No. 9, Nov. 1964, pp. 183-84.

38. D. W. Godwin, and R. W. Jones, "Far infrared and microwave detector," J. Appl. Phys., vol. 32, p. 2056, Oct. 1961.

39. M.S. Brown, M. F. Kimmet, and V. Roberts, "Tunable infrared photodetectors," Proc. IRIS, 1962.

40. E. Burstein, et al., "Quantum Detection of Microwaves and Submillimeter Wave Radiation Based on Electron Tunneling in Superconductors," Advances in Quantum Electronics, ed. by J. R. Singer, Columbia University Press, New York 1961, pp. 481-495.

41. E. Burstein, et al., "Superconductors as quantum detectors for microwave and submillimeter wave radiation," Physical Review Letters, vol. 6, p. 92, Feb. 1961.

42. B. D. Josephson, "Possible new effects in superconductive tunnelling," Phys. Letters, vol. 1, pp. 251-253, July 1962.

43. D. N. Langenberg, et al., "Josephson-type superconducting tunnel junctions as generators of microwaves and submillimeter wave radiation," Proc. IEEE, vol. 54, pp. 560-575, April 1966.

44. A. H. Dayam and R. J. Martin, "Quantum interaction of microwave radiation with tunnelling between superconductors," Phys. Rev. Letters, Vol. 8, pp. 246-248, March 1962.

45. S. Shapiro, "Josephson currents in superconducting tunnelling: the effect of microwaves and other observations," Phys. Rev. Letters, vol. 11, pp. 80-82, July 1963.

46. S. Shapiro, et al., "Effect of microwaves on Josephson currents in superconducting tunnelling," Rev. Mod. Phys., vol. 36, pp. 223-225, July, 1962.

47. I. Giaever, "Detection of the ac Josephson effect," Phys. Rev. Letters, vol. 14, pp. 904-906, May 1965.

48. Julius Cohen, "Tunnel emission into vacuum II," Appl. Phys. Letters, vol. 1, pp. 61-62, Nov. 1962.

49. R. J. Bauer, el al., "Millimeter wave semiconductor diode detectors, mixers and frequency multipliers," Proc. IEEE, vol. 54, pp. 595-605, April 1966.

50. R. Meredith and R. L. Warner, "Superhetrodyne Radiometers for Use at 70 Gc/sec and 140 Gc/sec," Presented at IRE Orlando Millimeter and Submillimeter Conf. Orlando, Florida, Jan. 1963. See also, Proc. IEEE (London) vol. III, pp. 241-256, Feb. 1964.

51. W. M. Sharpless, "Wafer-type millimeter wave rectifiers," Bell Syst. Tech. Journal, vol. 35, pp. 1385-1402, 1956.

52. G. C. Messenger, and C. T. McCoy, "Theory and operation of crystal diodes as mixer, Proc. IRE, vol. 45, pp. 1269-1283, Sept. 1957.

53. W. C. King and W. Gordy, "One to two millimeter wave spectroscopy, experimental methods and results for OCS, CH_3F, and H_2O," Phys. Rev., Vol. 93, no. 3, pp. 407-412, Feb. 1, 1954.

54. F. L. Wentworth, J. W. Dozier and J. D. Rodgers, "Millimeter wave harmonic generators, mixers and detectors," The Microwave Journal, pp. 69-75, June 1964.

55. E. Valkenberg, "Low-temperature germanium bolometer," J. Opt. Soc. Am., vol. 51, pp. 1300-1304, Nov. 1961.

56. C. A. Barrus, "Millimeter-wave point-contact and junction diodes," Proc. IEEE, vol. 54, pp. 575-587, April 1966.

57. V. H. Happ, et al., "Ker kristalldetector als empfanger thermischer strahlung im bebiet von (100-1000) μ wellenlange," Z. Naturfrosh, vol. 12A, pp. 522-524, 1957.

58. M. Cohn, et al., R. F. Packard (ed.), "Techniques for Superheterodyne Receivers above 100 Gigacycles," Final Report, NASA Contract NASw-259, May 1963, Electronic Communications, Inc., Timonium, Md.

59. M. Cohn, R. F. Packard, J. W. Dozier, J. D. Rogers and A. F. Eikenberg, "Techniques for Superheterodyne Receivers above 100 Gigacycles," Final Report, 14 April 1964, Contract NASw-662, Electronic Communications, Inc.

60. R. J. Bauer, "A Low Noise Figure 94 GHz Gallium Arsenide Mixer Diode," Presented at the 1965 Microwave Symposium, Clearwater, Florida (to be published).

61. R. H. Dicke, "The measurement of thermal radiation at microwave frequencies," Rev. Sci. Inst., vol. 17, pp. 268-275, July 1946.

62. C. T. McCoy, "Present and future capabilities of microwave crystal receivers," Proc. IRE, vol. 46, pp. 61-66, Jan. 1958.

63. P. D. Strum, "Considerations in high-sensitivity microwave radiometry," Proc. IRE, vol. 46, pp. 43-53, Jan. 1958.

64. P. R. Jordan and H. G. Pascalar, "The radiometric performance of a solid state 35 Gc receiver," Proc. IEEE, (correspondence) pp. 1655-1656, Oct. 1965.

65. R. F. Packard, "A superhetrodyne 600 Gc radiometer receiver," 1965 IEEE Microwave Theory and Techniques Symposium Digest, pp. 211-215.

66. S. Y. Chang, and J. D. Lester, "Radiometric measurement of atmospheric absorption at 600 Gc/s," Proc. IEEE, vol. 54, pp. 459-461, April 1966.

67. J. J. Kirwan and C. J. Abronson, "An integrated mixer-IF receiver at 94 GHz," Proc. IEEE, vol. 54, pp. 809-810, May 1966.

68. L. E. Kickens, "Millimeter Wave Diodes for Harmonic Power Generation," Internal Report, Advanced Technology Corp., Timonium, Md. (to be published).

69. J. H. Leopoff, "Octave bandwidth tunnel diode amplifiers," IEEE Trans. of M.T.T., vol. MTT 12, Jan. 1964.

70. R. I. Harrison, and J. Zucker, "Microwave detection and mixing using the thermoelectric effect of hot carriers in semiconductors," J. Appl. Phys. (letters) vol. 3, Nov. 1, 1963.

71. R. E. Harrison, et al., "Nonlinear Semiconductors at Millimeter Frequencies," General Telephone and Electronics Labs., Inc., Bayside, New York, Seventh Quarterly Report, March 1965. Contract DA 36-039 AMC - 02300(E)

72. R. I. Harrison and J. Zucker, "Hot-carrier microwave detector," Proc. IEEE, vol. 54, pp. 588-595, April 1966.

73. K. K. N. Chang, Parametric and Tunnel Diodes, (Chapt. 6) Prentice Hall, 1964.

74. S. Arams, et al., "Millimeter mixing and detection in bulk InSb," Proc. IEEE, vol. 54, pp. 612-622, April 1966.

75. B. W. Hakki, "GaAs post-threshold microwave amplifier mixer and oscillator," Proc. IEEE, (letters) vol. 54, pp. 299-300, Feb. 1966.

76. C. F. Krumm and G. I. Haddad, "Millimeter and submillimeter wave quantum detectors," Proc. IEEE, vol. 54, pp. 627-632, April 1966

77. G. I. Haddad, Private Communications.

78. R. C. Millward and L. J. Neuringer, "Far-infrared absorption in N-type silicon due to photon-induced hopping," Phys. Rev. Letters, vol. 5, p. 664-667, Oct. 1965.

79. W. E. Hughes and C. R. Kremenek, "An 81-GHz zero field maser," Proc. IEEE, Vol. 54, pp. 623-627, April 1966.

80. W. E. Hughes and R. E. Deal, "Zero field millimeter maser," Proc. IEEE (correspondence) vol. 52, July 1964.

81. B. G. Whitford, "The reflex klystron as a microwave detector," IRE Transactions on Electron Devices, March 1961, pp. 131-134.

82. T. K. Ishii, "Electronics News," MM Wave Labs., Marquet University, Nov. 1, 1965.

83. A. D. White, "Microwave Detection with Gas Tubes," Final Report, ASTIA AD 25 525, Contract DA 36-039-SC-1552, April 1952, Oct. 1953.

84. T. G. Williams, "A Microwave Phototube," ASTIA, AD 161 547, Washington University, 1958.

85. N. Farhat, "Plasma microwave energy detector," Proc. IEEE, p. 424, Jan. 1963.

86. P. J. W. Severin, "The Interaction of Microwaves with the Cathode Fall and Negative Glow in a Glow Discharge," Supplement, 1965, No. 2, p. 73, Philips Research Reports.

87. R. F. Hall and B. J. Stocker, "A low-voltage glow discharge tube," The Electronic and Radio Engineer, vol. 28, no. 5, Nov. 1964.

88. R. C. Jones, "Phenomenological description of the response and detecting ability of radiation detectors," Proc. IRE, vol. 47, Sept. 1959, pp. 1495-1502.

89. R. R. Potter, et al., "The measurement and interpretation of photodetector parameters," Proc. IRE, vol. 47, Sept. 1959, pp. 1503-1507.

90. P. Bratt, et al., "Germanium and Indium Antimonide Infrared Detectors," Final Report, Contract No. AF 33(616)-3859, Syracuse University Research Inst., Feb. 1960 (Chapt. 3).

91. P. R. Bratt, and G. F. Giggey, "Photoelectric Millimeter Wave Detectors," ASTIA Document AD 427 092, Dec. 1963.

92. Murray D. Sirkis, et al., "Study and Investigation of Millimeter and Submillimeter Wave Receiver Techniques," Third Quarterly Report, 31 Nov. 1963, Contract AF 30(602) 3046, Illinois University AD 433 121.

93. L. A. Hoffman, H. J. Wintroub, and C. J. Carter, "Electronics Research Program: Investigation of Millimeter-Wave Modulation and Signal Processing Techniques," Semiannual Technical Report, 1 July--31 Dec. 1963, Contract AF 04(695) 269, Aerospace Corp. AD 446 429.

94. R. J. Bauer, "Diode, Millimeter Wave Type Mixer (3.2 mm)," Fourth Quarterly Progress Report," 1 March--31 May 1964, Contract DA 36-039 AMC-02347(E), AD 447 083, Advanced Technology Corp.

95. P. R. Bratt, and G. F. Giggey, "Photoelectric Millimeter Wave Detector," Dec. 1963, Contract AF 30(602) 3015 (RADC TDR 63-502), Raytheon Co., Spencer Labs.

96. R. W. Wilmarth and R. J. Kenyon, "Development of Electronically Tunable Converters in the Millimeter Wave Range," Bimonthly Report No. 4, 16 Jan.--16 March 1964, NASA Contract NASw 690, ITT Corp. Electron Tube Div., Easton, Pa.

97. Harrison J. Merrill (ed), "Light and Heat Sensing," Sixth Agard Avionics Panel Meeting, Paris, July 1962, "Advisory Group for Aeronautical Research and Development," Paris (France), Oxford, New York, Pergamon, 1963.

98. "Study and Investigation of Millimeter and Submillimeter Wave Receiver Techniques," Quarterly Report 1, Mar. 1--May 21, 1963, Illinois University, Urbana, Contract AF 30(602) 3046.

99. "Study and Investigation of Millimeter and Submillimeter Wave Receiver Techniques," Quarterly Report No. 2, Illinois Univ., Contract AF 30(602) 3046, AD 425 356.

100. M. D. Sirkis, et al., "Study and Investigation of Millimeter and Submillimeter Wave Receiver Techniques," Quarterly Report No. 3, 1 Sept.--30 Nov. 1962, Contract AF 30(602)2456, AD 298 725, Illinois University.

101. Clyde H. Brunquell, "Low Noise Millimeter Detector," Final Report, Contract AF 30(602) 2651, 7 Jan. 1963, Microwave Associates, Inc., Burlington, Mass., AD 403 139.

102. T. E. Tice, "Receiver Techniques and Detectors for Use at Millimeter and Submillimeter Wavelengths," Semiannual Report, 1 Sept. 1962--28 Feb. 1963, Grant NsG - 74 - 60, Ohio State Univer Research Foun.

103. James E. Degenford, "Study and Investigation of Millimeter and Submillimeter Wave Receiver Techniques," Fifth Quarterly Report, 1 Mar.--Sept. 30, 1964, Contract AF 30(602) 3046, AD 611 536, Illinois Univ.

104. "Receiver Techniques and Detectors for Use at Millimeter and Submillimeter Wavelengths," Annual Summary Report, 1 Mar. 1962--31 Aug. 1963, NASA Grant NsG - 74-60, Ohio State Univ. Research Foundation.

105. "Receiver Techniques and Detectors for Use at Millimeter and Submillimeter Wavelengths," Semiannual Report, 1 Sept. 1963--29 Feb. 1964, NsG-74-60, Ohio State Univ. Research Foundation.

106. Paul D. Coleman, et al., "Study and Investigation of Millimeter and Submillimeter Wave Receiver Techniques," Final Report, Mar. 1, 1961--Feb. 28, 1963, Contract AF 30(602) 2456, Illinois Univ. Electrical Engineering Research Lab.

107. I. Esterman, "Semiconductors as low temperature thermometers," Phys Rev., vol. 78, p. 83, April 1950.

108. R. F. Packard, (ed), "Techniques for Superheterodyne Receivers above 100 Gigacycles," Electronic Communications, Inc., Feb. 1964 also, "A Superheterodyne Gc Radiometer Receiver," 1965 IEEE M.T.T. Symp. Dig., pp. 211-15.

109. "Study and Investigation of Millimeter and Submillimeter Wave Receiver Techniques," Fourth Quarterly Report, 1 Dec. 1963--29 Feb. 1964, Contract AF 30(602) 3046, Illinois Univ., Urbana, Electrical Engineering Research Labs.

110. R. F. Wallis, H. Shenker, "Detector Investigation for 8-15 and 100-4000 Microns Regions," Semiannual Technical Summary, 30 June 1964, ARPA Order 269-62; Proj. Defender, AD 444 084, Naval Research Lab., Wash., D. C., Solid State Div.

111. E. H. Putley, "The detection of submm radiation," Proc.IEEE, vol. 51, pp. 1412-1423, Nov. 1963.

112. E. H. Putley, "Indium antimonide submillimeter photoconductive detectors," App. Optics, vol. 4, pp. 649-657, June 1965.

113. F. Arms, and M. Wang, "Infrared laser preamplifier system," (correspondence), Proc. IEEE, vol. 53, March 1965, p. 329.

114. R. J. Strain, "Submillimeter Wave Quantum Electronics Using Ion Pairs in Ruby," Ph.D. Dissertation, University of Illinois Se Laser/ Maser International, vol. no. 1, April 1964, Pacific Impex Co., Vancouver, B. C., p. 49.

115. E. H. Putley, "The use of an InSb detector at 1 mm," Proc. IEEE, Vol. 54, pp.1096-1098, Aug. 1966.

Chapter X

ANTENNAS

10.0 INTRODUCTION

Antennas for use in the 100 to 3000 GHz (3 to 0.1 millimeter) portion of the spectrum will probably follow the design practices of the region below 100 GHz. It is not anticipated that research on antennas will be required as a consequence of the use of this frequency band. Research may be required for other reasons.

The literature on antennas is rather vast and most of it is not directed specifically to the millimeter wave region. A few references (1 to 11) are of direct concern however and, in addition, include excellent bibliographies. Reviews of this literature, as well as studies of millimeter wave applications, show that all antenna varieties presently known may be exploited. The trend is toward designs based on geometric optics since the antenna dimensions are usually large compared to the wavelength. The choice of a particular antenna type is largely a function of the application, available materials and precision of manufacture.

This chapter will briefly review the antenna types that may be used as well as the limitations on their performance. Particular attention will be directed to the antenna feed system since it appears to be a critical element in this frequency range at this time.

10.1 ANTENNA APPLICATIONS

It is assumed that applications made of the millimeter wave region will follow the example of other portions of the electromagnetic spectrum. This assumption is justified by presently known applications, among which are: point-to-point communications, radar (particularly for close-in surveillance such as harbor docking or airport surface control), radar and radio astronomy and radiometry. Some limited industrial applications have been made mostly using radiometry techniques to detect hot boxes on railroad cars or for intruder control. Industrial process control has had little emphasis largely because of a lack of information on the electrical properties of materials in this frequency range.

Table 10.I is a convenient summary of antenna performance parameters as affected by the application. There is no presently known limitation on polarization; thus, its selection is a matter of convenience. Beam shapes, on the other hand, are directly affected by the application.

The communications circuits of satellite links or probes and point-to-point relay require pencil beams to give optimum system performance and considerable freedom from interference.

Broadcast applications usually require quasi-omnidirectional patterns to maximize the number of subscribers to be served with a specified grade of service. For satellite broadcasting, a fan or conical beam of medium gain will probably be used to avoid steerable antennas at the receiving site.

TABLE 10-I - ANTENNA PERFORMANCE REQUIREMENTS

APPLICATION	ANTENNA				
	Pattern	Polarization	Gain g, (dB)	Beamwidth Ⓗ degrees	Pointing Accuracy °
1. Satellite Link or Probe	Pencil Beam	any	10 to 40 dB or more	60 to 2 or less	6 to .2 or better
2. Point to Point Relay a. On Earth b. Earth to Satellite to Earth c. Satellite to Satellite	Pencil Beam	any	a. 50 to 120 b. 50 to 120 c. 50 to 160	5.8×10^{-1} to 1.8×10^{-4} 5.8×10^{-1} to 1.8×10^{-6}	5.8×10^{-2} to 1.8×10^{-7}
3. Broadcast a. Earth Trans. b. Sat. Trans.	omnidir. wide or fan beam	any	a. 3 to 40 b. 1 to 10	100 to 1.8 180 to 60	10 to .18
4. Navigation	omnidir. or fan beam	any	3 to 50	100 to .58	10 to .058
5. Radar a. Search b. Track.	csc^2 Pencil Beam	any	40 to 120	1.8 to 1.8×10^{-4}	.18 to 1.8×10^{-5}
6. Radio Ast. a. Passive b. Active	Pencil Beam	any	50 to 160 or greater	.58 to 1.8×10^{-6}	.058 to 1.8×10^{-7}
7. Radiometry Industrial	any	any	unknown	unknown	unknown

Search radars and navigation equipment will probably require fan beams or beams having a cosecant squared shape to maximize coverage. Tracking radars require small-beam-width antennas (preferably pencil beams) to get high resolution.

The range of antenna gains given is the highest that can be used for each case. The gain is affected by the application, the properties of the propagation medium and the pointing accuracy of the antenna as discussed in section 10.2.8. The pointing accuracy requirement may dictate a study to determine where in a system the maximum antenna gain may be used with the least penalty in power or weight requirements.

Since large diameter-to-wavelength ratios with antenna apertures of reasonable size are possible in the mm and submm region (D/λ ranging from 10^5 to at least 10), mechanical steering is probably adequate for most applications. For sophisticated radars requiring high speed scanning, electronically scanned antennas, such as phased arrays, have been developed up to about 75 GHz.[11] These antennas can, in principle, be developed for any part of the electromagnetic spectrum. The present limit of 75 GHz is imposed by the available ferrites. Research in materials is required if electrically operated phase shifters are to be used in the submm region.

10.2 LIMITATIONS ON ANTENNA GAIN

The principal factors affecting the performance of large aperture antennas are:

1. antenna diameter, D
2. amplitude distribution (taper factor), η
3. illumination factor or spillover, α
4. aperture block, β
5. focal ratio, f/D
6. surface defects γ
7. type of mounting and coverage
8. drive and tracking system
9. the propagation medium

Most of the above factors are strongly interrelated and, therefore, an antenna design is of necessity a compromise. Let us consider each of them separately.

10.2.1 Antenna Gain and Beamwidth

Most large aerospace and radio astronomy antennas are circular apertures. For such apertures, the gain G and the half-power beamwidth Ⓗ are given by:

$$G = k\,G_o = k\left(\frac{\pi D}{\lambda}\right)^2, \text{ numeric} \qquad (10.1)$$

and

$$Ⓗ = 58.45\,\frac{\lambda}{D}, \text{ degrees} \qquad (10.2)$$

$$= 1.84 \times 10^2\, G^{-1/2}, \text{ degrees for } k=1 \qquad (10.3)$$

where

λ = wavelength in meters

D = aperture diameter in same units as λ

k = aperture efficiency

$\approx$ 0.4 to 0.7 for well-designed antennas

Equations 10.1 and 10.3 are plotted in Figs. 10.1 and 10.2. Typical large antennas are included in Fig. 10.1. From this figure, it can be seen that apertures as large as 305 meters have been successfully built. The largest known aperture, in terms of D/λ, is however the Hale telescope ($D/\lambda \doteq 10^7$). The limitations on diameter will be discussed in Section 10.2.6.

10.2.2 Amplitude Distribution Factor η

The gain and patterns of an antenna are controlled by the amplitude and phase distribution across the aperture. For many antennas the phase distribution is uniform and only the amplitude distribution, η, is of interest. η, in a sense, is a measure of how efficiently an aperture is used. The highest gain and highest side lobe levels are obtained for aperture distributions that are uniform in amplitude and phase ($\eta = 1$). Side lobe levels must be reduced, however, to avoid interference and to get lower antenna temperatures. This is accomplished by tapering the excitation across the aperture. A power law distribution is quite common for circular parabolic apertures (see Table 10.II). From the table the improvement in side lobe levels and resulting antenna gain reduction and beam broadening can be seen. For most antenna applications, a parabolic distribution (p=1) with an edge taper

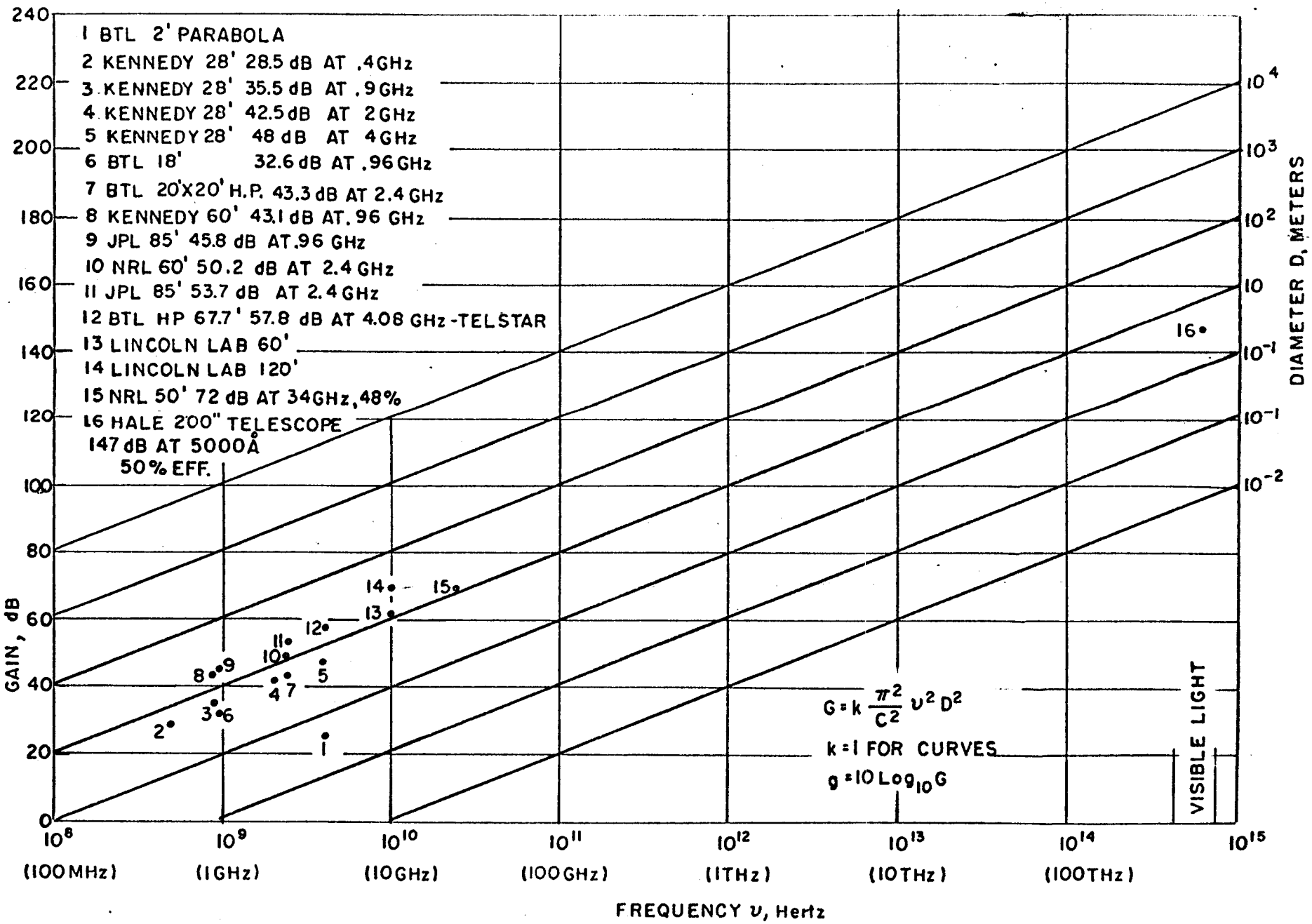

FIG. 10.1 ANTENNA GAIN VERSUS FREQUENCY FOR UNIFORMLY ILLUMINATED CIRCULAR APERTURE

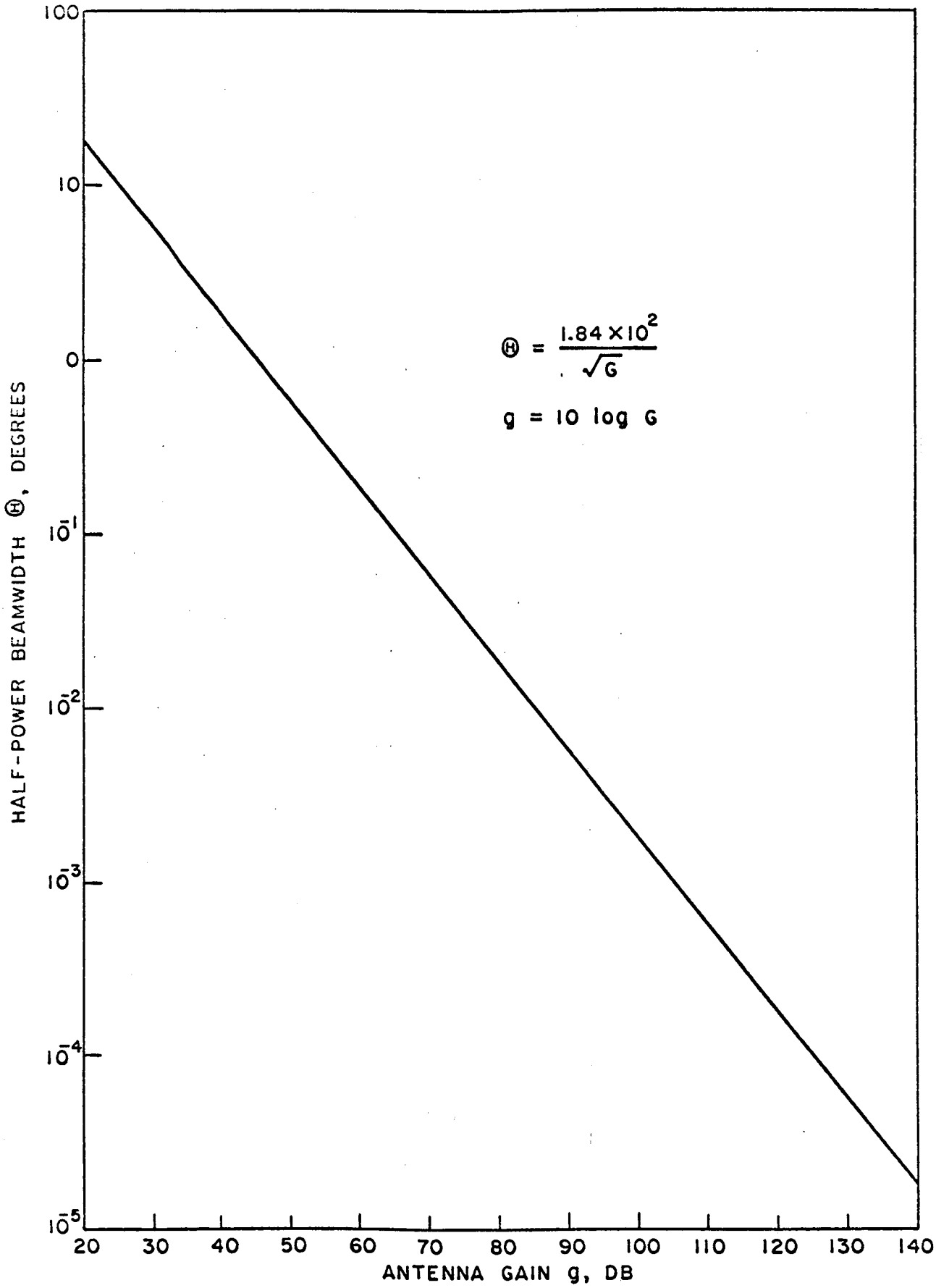

FIG. 10.2 GAIN VS. HALF-POWER BEAMWIDTH

TABLE 10-II - CHARACTERISTICS OF A CIRCULAR APERTURE

p	η (numeric)	Ⓗ Half-Power Beamwidth (radians)	θ Position of First nul (radians)	First Side Lobe Level (dB below peak gain)
0	1.00	1.02 λ/D	$\sin^{-1} \frac{1.22\lambda}{D}$	17.6
1	0.75	1.27 λ/D	$\sin^{-1}$ 1.63 λ/D	24.6
2	0.56	1.47 λ/D	$\sin^{-1}$ 2.03 λ/D	30.6
3	0.44	1.65 λ/D	$\sin^{-1}$ 2.42 λ/D	
4	0.36	1.81 λ/D	$\sin^{-1}$ 2.79 λ/D	

Distribution over aperture: $\left[1 - \left(\frac{2r}{D}\right)^2\right]^p$

Where: D = aperture diameter

(from ref. 17)

is quite adequate. For this case, an expression for η is:

$$\eta = \frac{1}{1 + \frac{1}{3}\left(\frac{1-a}{1+a}\right)^2} \qquad \text{(ref. 5)} \qquad (10.4)$$

where

a = fractional edge taper, numeric

= ratio of field at edge to field at center of aperture

The aperture efficiency as a function of edge taper, from eq. 10.4, is given in Table 10.III.

10.2.3 Illumination Factor or Spillover α

Some energy will spill over the edge of a reflecting aperture because of the feed design. This spillover power results in a reduction in antenna efficiency and an increase in antenna temperature as well as an increase in far side and back lobes. The spillover factor α is a measure of this loss. α and η both modify the maximum gain of the aperture, and design procedures should maximize the product of α and η. Values of α as a function of edge taper (a) are given in Table 10.IV for a parabolic distribution across the aperture. The effect of the product of α and η on antenna gain is shown in Fig. 10.3. Spillover loss is absent in horn-parabola and horn-lens antennas.

TABLE 10-III

Aperture Efficiency η as a Function of Edge Taper a for a Parabolic Aperture Distribution

Edge Taper (decilogs)	Fractional Edge Taper (a)	Aperture Efficiency	
		η	loss in dB
0	1.000	1.000	0.0
1	0.892	0.998	0.009
2	0.795	0.995	0.02
3	0.707	0.991	0.04
4	0.631	0.984	0.07
5	0.563	0.975	0.11
6	0.510	0.965	0.15
7	0.446	0.954	0.20
8	0.398	0.940	0.27
9	0.355	0.930	0.31
10	0.316	0.918	0.37
12	0.251	0.894	0.49
15	0.178	0.860	0.65
20	0.100	0.817	0.88
25	0.006	0.751	1.24
∞	0.0	0.750	1.25

$$\eta = \frac{1}{1 + \frac{1}{3}\left(\frac{1-a}{1+a}\right)^2}$$ for a parabolic distribution

(from ref. 5)

TABLE 10.IV

Illumination Factor and Loss as a Function of Edge Taper

Fractional Edge Taper (a)	Edge Taper (decilogs)	Illumination Efficiency	
		Factor(α)	Loss(dB)
0.398	8	0.71	1.49
0.316	10	0.75	1.25
0.251	12	0.79	1.02
0.178	15	0.81	0.91
0.100	20	0.83	0.81
0.006	25	0.84	0.75
0.0	∞	0.85	0.71

(From Ref. 5)

10.2.4 Aperture Block β

Aperture block is a physical blocking of the aperture caused by the feed and its support structure. The block factor β is not proportional to the percentage of physical aperture blocked. It is given by:

$$\beta = 20 \log \left[1 - \frac{B}{A}\right]\left[1 - \frac{1-a}{1+a}\ \frac{B}{A}\right] \qquad (10.5)$$

for an aperture having a parabolic distribution where:

A = area of the unblocked aperture

B = area of the blocking aperture

The reduction in antenna gain due to aperture block β as a function of edge taper (a) is shown in Fig. 10.4. Aperture block is essentially absent in the horn-parabola and horn-lens antennas.

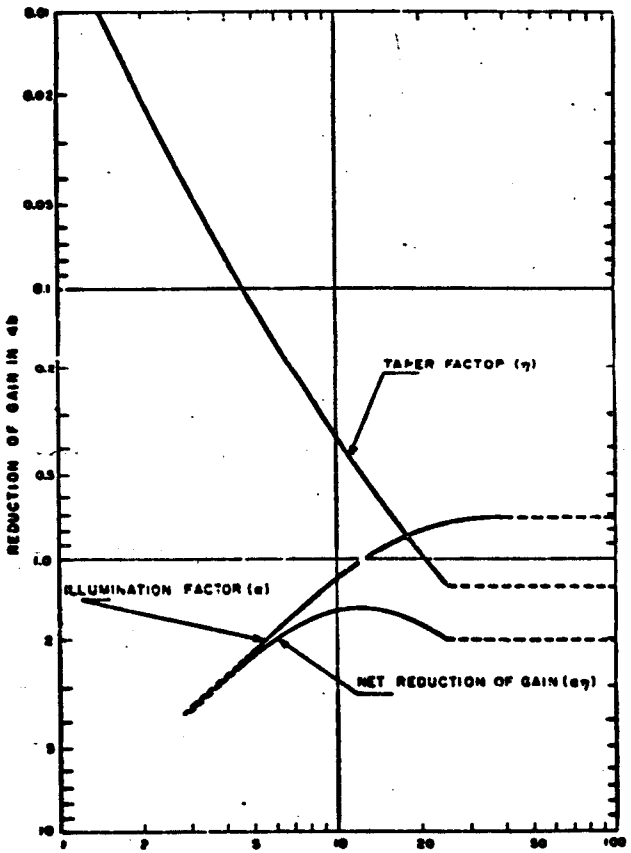

Fig. 10.3 Taper Factor, Illumination Factor, and Net Reduction of Gain in Decibels

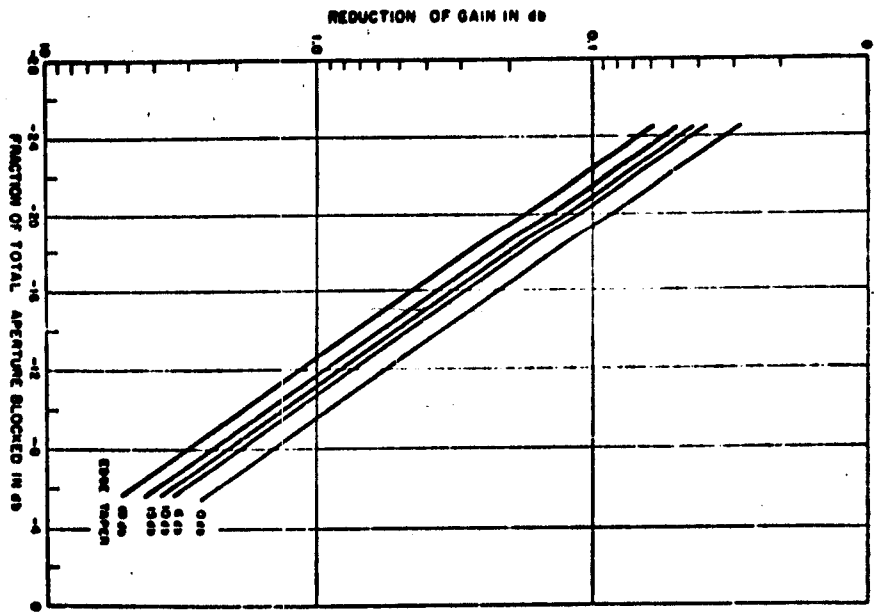

Fig. 10.4 Reduction of Gain Due to Aperture Block

10.2.5 Focal Ratio f/D

The focal ratio f/D is the ratio of the parabola focal length to aperture diameter. If the ratio is small, that is, a deep reflector is used, the feed support will be mechanically strong resulting in a more precise feed positioning. If the aperture is used efficiently, the side lobe level will be small because of reduced spillover. There will be, however, serious coma for feeds off axis and higher loss due to cross-polarization than for large f/D.

The larger the value of f/D, on the other hand, the greater the mechanical support difficulty and the higher the side lobe levels. There will be a reduction in phase error loss, however, due to axial displacement in the source. The practical limits on f/D are then about:

$$0.25 < f/D < 0.5$$

The horn-parabola and the horn-lens antennas do not have the above limitations.

10.2.6 Surface Defects γ

The loss in antenna gain γ due to surface defects is made up of three factors:

a) irregular phase errors

b) symmetrical phase errors

c) astigmatic (bi-symmetrical) phase errors

Surface defects are usually mechanical in nature and constitute a limitation on increase in antenna size. On the other hand, taper factor, illumination factor, and aperture block can be independent of aperture size.

The effects of surface defects on antenna gain have been conveniently summarized by Ruze[6]. The loss in gain is given by γ where:

$$\gamma = \exp - (4\pi\epsilon/\lambda)^2 \tag{10.6}$$

ϵ = effective reflector surface tolerance in same units as λ. The total gain of an aperture is then, combining eqs. 10.1, 10.4, 10.5, and 10.6:

$$\begin{aligned} G &= \eta\alpha\beta\gamma\, G_o \\ &= \eta\alpha\beta\, (\pi \frac{D}{\lambda})^2 \; e^{-(4\pi\, \epsilon/\lambda)^2} \end{aligned} \tag{10.7}$$

The gain G_o, for a perfect aperture, is given in Fig. 10.1. The gain reduction caused by η, α and β is given in Tables 10.II, 10.III, 10.IV and Figs. 10.3 and 10.4. The antenna gain as a function of diameter, frequency and tolerance ϵ in wavelengths is given in Fig. 10.5. A conversion formula for tolerance ϵ in terms of λ and ν is given by:

$$\epsilon = \frac{\lambda}{b} = \frac{c}{b\nu} \tag{10.8}$$

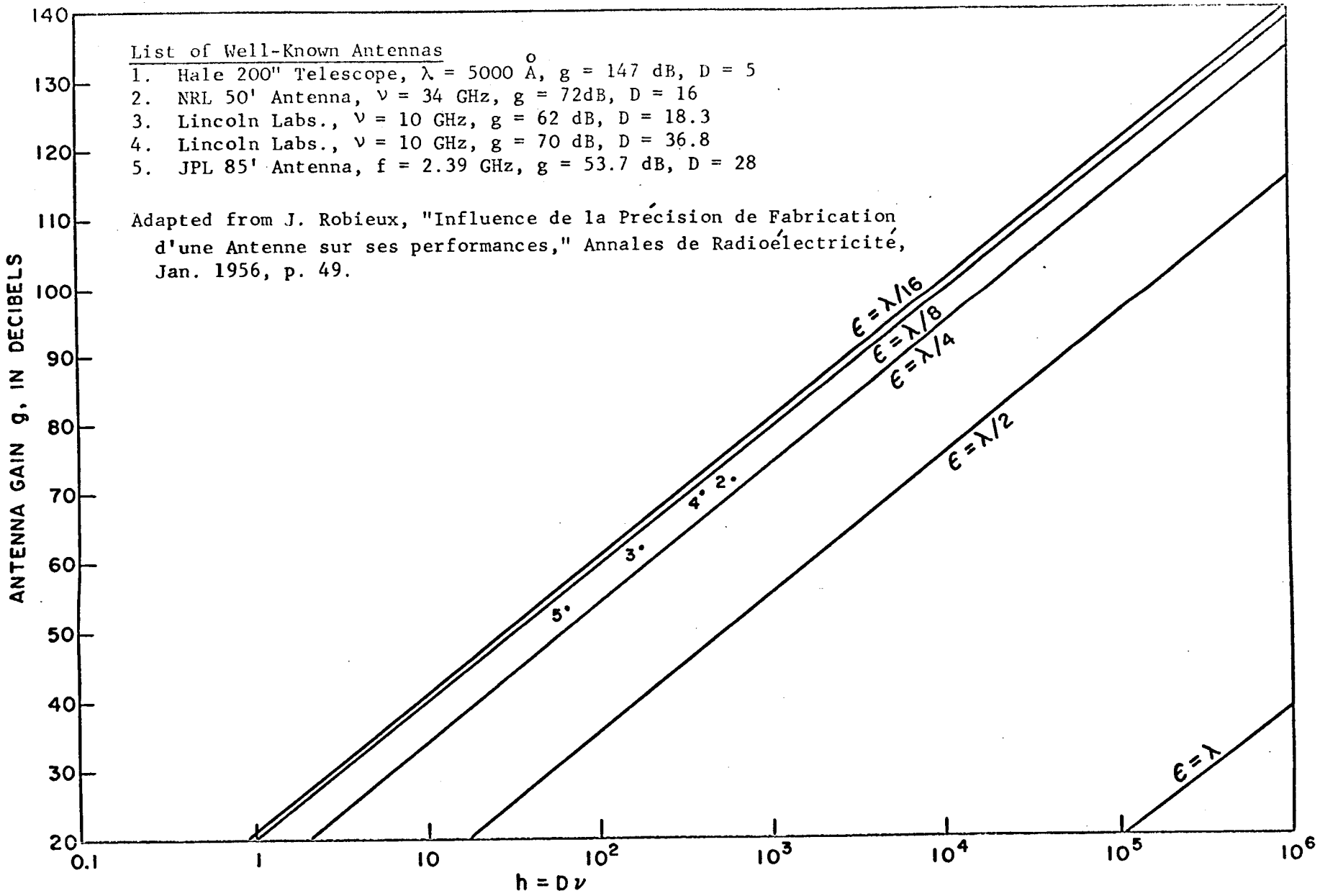

D = ANTENNA APERTURE IN METERS
ν = FREQUENCY IN GIGAHERTZ, λ = FREE SPACE WAVELENGTH, METERS
ϵ = PRECISION LENGTH (TOLERANCE) GUARANTEED WITH 99 % PROBABILITY

FIG. 10.5 ANTENNA GAIN AS A FUNCTION OF $h = D\nu$ AND TOLERANCE UNDER UNIFORM ILLUMINATION AND 100 % EFFICIENCY ($h = 3 \times 10^6$, $G = 147$)

where

b = a number from 1 to about 100

c = velocity of light in meters

ν = frequency in Hertz.

Equation 10.8 is plotted in Fig. 10.6 for the frequently used values of b.

From Fig. 10.5, it can be seen that for a given frequency and antenna diameter, the loss in gain caused by surface tolerance is large for tolerances greater than $\lambda/8$ and the gain reduction in going from $\lambda/16$ to $\lambda/8$ is a little over one decibel. Optical reflector telescopes are routinely figured to $\lambda/8$ to $\lambda/10$. The Hale telescope (200 inch) is figured to $\lambda/10$.[13-14] A few optical telescopes use tolerances as fine as $\lambda/50$.[17] These telescopes are alleged to have improved clarity of images but the gain improvement in going from $\lambda/10$ to $\lambda/50$ is less than one decibel. Radio telescopes and point-to-point microwave relay antennas are routinely constructed to tolerances of $\lambda/16$ to $\lambda/32$.

It should be noted that the maximum gain of an aperture as a function of surface tolerance occurs when $\lambda_m = 4\pi\epsilon$, where a tolerance loss of 4.3 dB with respect to a perfect reflector is incurred. This maximum gain is given by:

$$G_{max} \approx k/43 \left(\frac{D}{\epsilon}\right)^2 \qquad (10.9)$$

where

$$k = \eta\alpha\beta$$

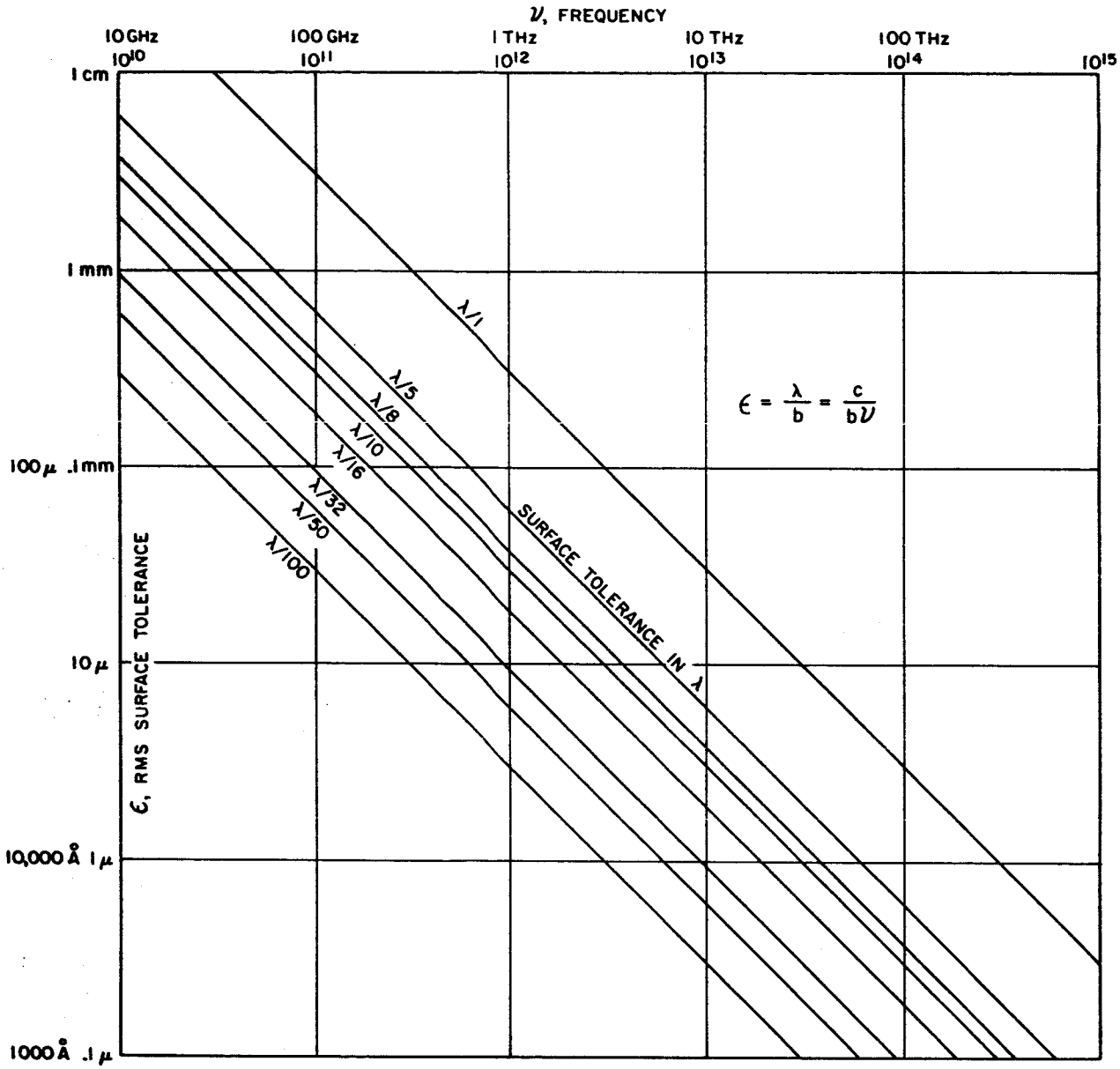

FIG. 10.6 SURFACE TOLERANCE IN WAVELENGTHS VS. RMS TOLERANCE AND FREQUENCY.

G_{max} is proportional to the square of the precision of manufacture (D/ϵ). The maximum gain of an aperture as a function of diameter, frequency and tolerance is shown in Fig. 10.7.

The precision with which large aperture antennas have been built is shown in Fig. 10.8. These data were obtained from references 3 and 4 and numerous other sources. By comparison, the precision of the 200 inch Hale telescope at $\lambda = 5600$ Å is $\lambda/10$ or 0.056 μ, that is, many orders of magnitude better than the best antenna of equivalent aperture (5.08 meters). Thus, it appears that our technology is capable of more precise manufacture and that cost and materials are the only obstacles to the use of this precision. The precision of a number of well-known large aperture antennas is shown in Table 10.V.

10.2.7. Type of Mounting and Coverage

The type of antenna mount used is largely a matter of convenience and cost. It poses no special problems for millimeter antennas. The equatorial mount is probably the simplest for apertures up to perhaps 30 meters in diameter. The azimuth-elevation mount is suitable for all antenna sizes and can give complete coverage in the hemisphere above the ground. On space vehicles, other types of mounts may be convenient.

10.2.8 Drive and Tracking System

The only item of concern here for millimeter and higher frequency antennas is that of pointing accuracy. Antenna pointing

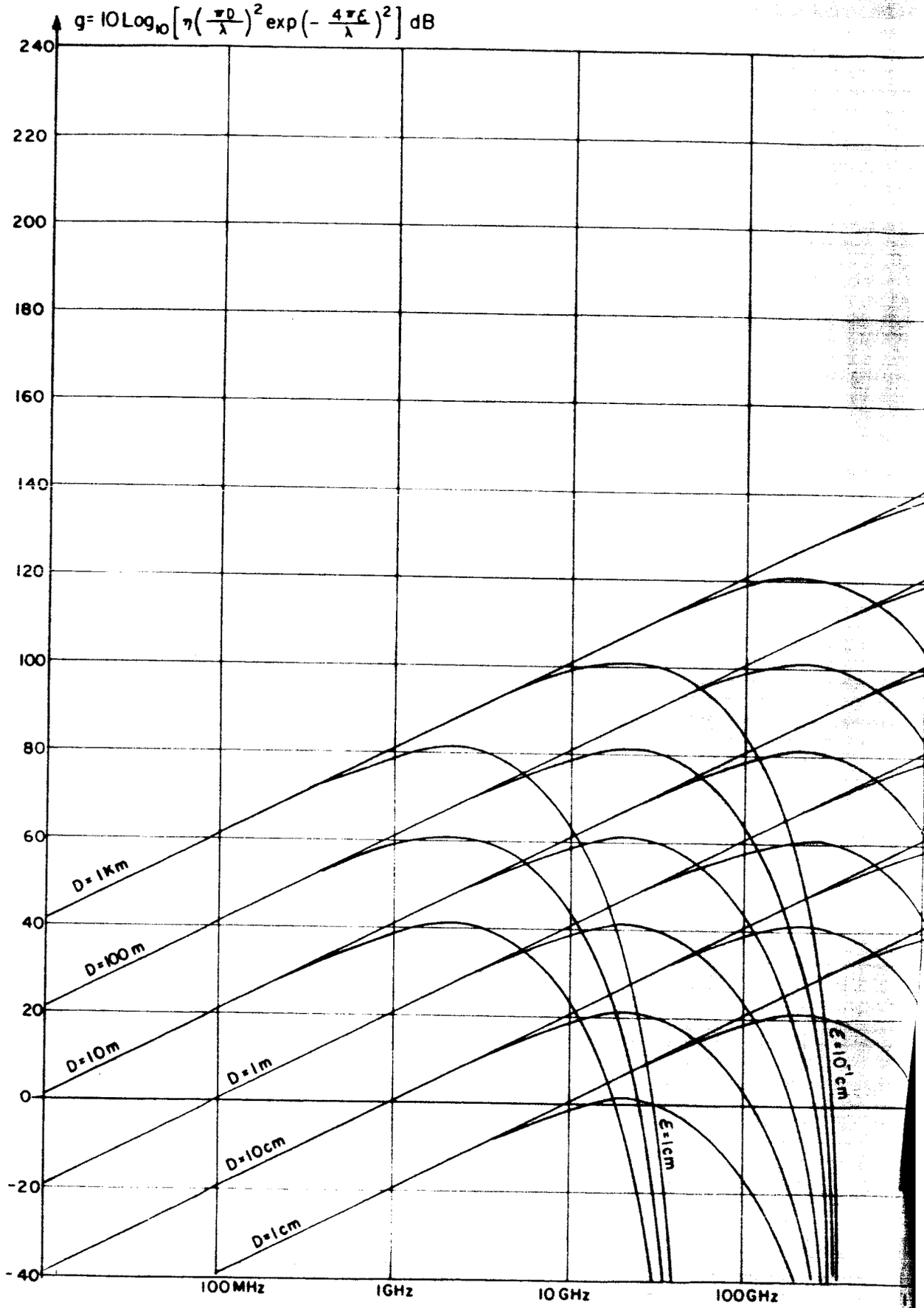
$g = 10 \mathrm{Log}_{10}\left[\eta\left(\frac{\pi D}{\lambda}\right)^2 \exp\left(-\frac{4\pi\varepsilon}{\lambda}\right)^2\right]$ dB
240
220
200
180
160
140
120
100
80
60
40
20
0
-20
-40
D=1Km
D=100m
D=10m
D=1m
D=10cm
D=1cm
ε=10⁻¹cm
ε=1cm
100MHz
1GHz
10GHz
100GHz

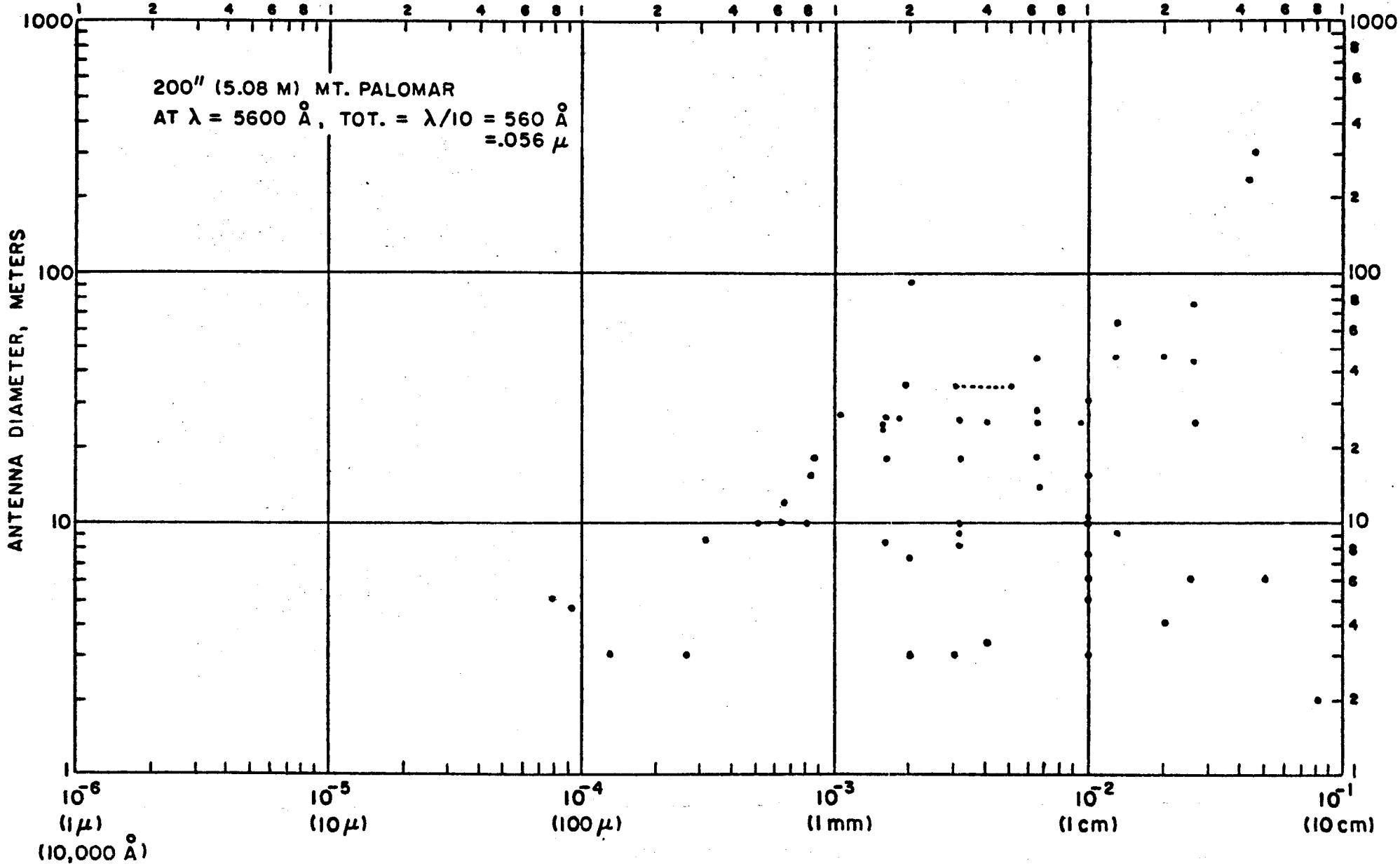

FIG. 10.8 SURFACE TOLERANCE, METERS

TABLE 10.V - PRECISION OF REPRESENTATIVE LARGE APERTURE ANTENNAS

	Diameter D		RMS Tolerance ϵ		D/ϵ	ν	Ⓗ
Antenna	Feet	Meters	Inches	Meters	$\times 10^5$ Numeric	GHz	Minutes
Arecibo	1000	305	1.8	4.57×10^{-2}	6.66	0.434	8
Jodrell-Bank	250	76.3	1.2	3.05×10^{-2}	2.5	0.65	26
Stanford	150	45.8	0.55	1.4×10^{-2}	3.27	1.42	20
Greenbank	300	91.5	0.47	1.2×10^{-2}	7.66	1.66	8.5
Parkes-CSIRO	210	64	0.14	3.56×10^{-3}	18	5.6	3.5
*CAMROC	400	122	0.13	3.3×10^{-3}	37	6.0	1.71
Michigan	85	26.9	0.043	1.1×10^{-3}	23.6	18	2.75
Lebedev	72	22	0.025	6.35×10^{-4}	34.5	31	1.9
Haystack	120	36.6	0.040	1.02×10^{-3}	36	20	1.8
**Haystack	120	36.6	0.025	6.35×10^{-4}	58	32.4	1.1
Aerospace	15	4.57	1.8×10^{-3}	4.57×10^{-5}	100	434	0.54
Hale-200"	16.7	5.08	2×10^{-6}	5.08×10^{-8}	10^5	3.9×10^5	5.34×10^{-4}

* Ref. 15

** Rerigging, Ref. 15

ν - frequency at which antenna gain loss due to surface tolerance ϵ is 3 dB

Ⓗ - Half power beamwidth at frequency ν

accuracy inposes an additional constraint on the realizable gain of the antenna, particularly if it is mounted on a spacecraft. The loss due to pointing accuracy is shown in Fig. 10.9, and is given in terms of the ratio of the angle δ from antenna boresite to the half-power beamwdith (H). If the degradation of gain is to be held to 0.12 dB, then the antenna half-power beamwidth must be 10 times the pointing accuracy of the antenna structure. Pointing accuracy is a severe problem for millimeter and higher frequency antennas since such antennas are capable of high gain and small beamwidths for apertures of reasonable size. Pointing accuracy that has been achieved by representative antennas is shown in Table 10.VI.

10.2.9 The Propagation Medium

The performance of an antenna or an optical telescope is affected by the atmosphere in which it is immersed. The magnitude of the effect is a function of the length of the path through the atmosphere as well as the nature of the atmosphere and its constituents. The antenna parameters affected are: half-power beamwidth, resolution, gain, temperature and apparent position of the source.

The natural gaseous constitutents of the earth's atmosphere are given in Chapter VIII. In addition, many man-made gases such as SO_2, NO, N_2O_3 and the hydrocarbons are present, particularly in industrial areas. These gases result in absorption of electromagnetic energy in certain calculable frequency bands (see Chapter VIII).

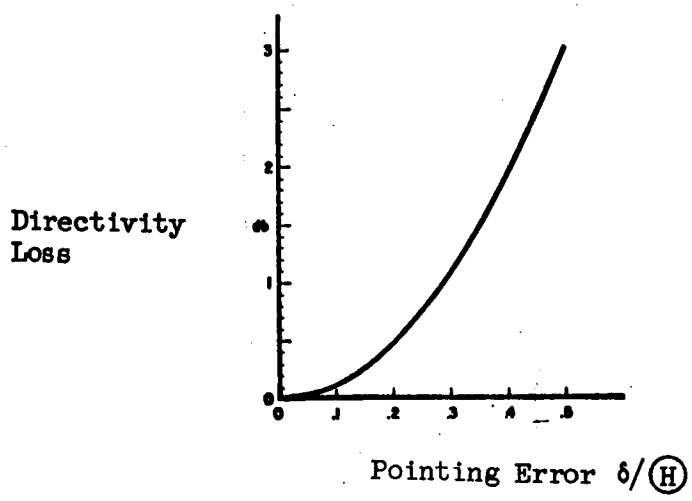

Fig. 10.9 Loss Due to Pointing Error

(from Ref. 16)

TABLE 10-VI--POINTING ACCURACY OF LARGE ANTENNAS

Antenna	Diameter D Meters	Half-Power Beamwidth Ⓗ Minutes	Pointing Accuracy δ, Minutes	Ⓗ/δ
Arecibo	305	10	± 2	5
Jodrell-Bank	76.3	15 x 20	± 12	1.5
Stanford	45.8	20	± 6	3
Greenbank	91.5	10	± 2	5
Parkes-CSIRO	64	15	± 1	15
CAMROC	122	1.71	± 0.25	7
Michigan	26.9	6	± 1	6
Lebedev	22	1.9	± 1	1.9
Haystack	36.6	1.8	± 0.3	6
Aerospace	4.57	2.8	± 0.33	8.4
Hall-200"	5.08	5.34×10^{-4}	--	--

Water vapor may both absorb and scatter electromagnetic energy as well as modify atmospheric refractivity.

Dust of all particle sizes is also present in the atmosphere. The range of sizes is shown in Table10.VII.Substantial scattering occurs when the wavelength of the radiation is smaller than the particle size. Scattered radiation contributes to the antenna temperature and in optical telescopes results in loss of definition.

Table 10.VII Atmospheric Particle Sizes

Particle	Particle size Microns
Dust	150 to 1
Clouds	100 to 40
Wet Fog	30 to 40
Fumes	1 to 0.3
Smoke	< 0.3
Cigarette Smoke	0.1
Condensation Nuclei	0.1
Gas Molecule	10^{-4} (1 Å)

Atmospheric inhomogeneities having dimensions of the order of 15 centimeters are believed to be responsible for optical limitations in telescopes.[13] It has been stated that a telescopic aperture of 7 to 10 centimeters will yield clearly defined star images, but the images wander around in a circle having a diameter of two arc seconds. If the telescope aperture is increased to 1.5 meters, all the stars are enlarged and blurred but steady,

and the diameter of the smallest is about two arc seconds. In other words, the large aperture has integrated the wandering of the star image. Shuddering of the star image is of the order of one arc second for average "seeing," 10 arc seconds exceptionally and 20 arc seconds for bad seeing with the rate of shuddering about 5 to 100 oscillations/sec. The amplitude of the fluctuations varies inversely with the diameter of the antenna.

There thus seems to be general agreement among astronomers that under the best seeing conditions, the earth's atmosphere sets a limit of 1/2 arc second on resolution and this limit is more or less independent of frequency.[12] In a series of photographs in reference 12, the quality of the image is shown as a function of resolution. At one arc second resolution, the images are equivalent to good still-life photographs. At 34 arc minutes resolution, the image is a blob or disc. At one arc minute resolution, the image begins to resemble a photograph. This resolution is beyond all presently available radio-telescopes.

A resolution of 1/2 arc second corresponds to $D/\lambda = 4.2 \times 10^5$, thus setting a fundamental limit on the maximum usable aperture from the standpoint of "image" clarity. The maximum aperture for a few wavelengths is shown below.

λ	D, meters
Visible Light 5000 Å (5×10^{-7}m)	0.21 m
0.1 mm (10^{-4} m)	42 m
1 mm (10^{-3}m)	420 m
10 mm (10^{-2}m)	4.2 km

It can thus be seen that this criterion on aperture size, except for the infrared and visible region, is unlikely to impose a limitation for some time to come. It should be mentioned that the nature of the disturbance causing atmospheric turbulence is unknown. It is believed to be a wind phenomena at altitudes of the order of two kilometers.

10.3 FRESNEL REGION PHENOMENA

A frequently quoted criterion for the separation distance between the Fresnel and far field regions of an antenna is:

$$d \geq \frac{2D^2}{\lambda} \qquad (10.10)$$

where:

d is the distance from the aperture in meters.

In the far field, the antenna beam pattern is well formed and it and the gain are independent of the distance from the aperture. In the Fresnel region, both gain and beam shape are a complex function of the distance from the aperture. As D/λ becomes large, the far field distance becomes large, and for a few known large aperture antennas it may extend through the earth's atmosphere.

This poses some interesting questions since the effect of atmospheric disturbances is not the same in the Fresnel and Fraunhofer regions. This point and antenna focusing deserve further study.

10.4 ANTENNA TEMPERATURE (see also p. 441)

An antenna has an equivalent temperature T_a because its pattern views a surrounding space having a temperature $T(\theta\phi)$. The antenna temperature is given by (see Chapter XI):

$$T_a = \frac{\int_s T(\theta,\phi)\, G(\theta,\phi)\, ds}{\int_s G(\theta,\phi)\, ds} \qquad (10.11)$$

where

$$\int_s G(\theta,\phi)\, ds = 4\pi$$

ds = the solid angle given by $\sin\theta\, d\theta\, d\phi$

$G(\theta,\phi)$ = the antenna gain in the direction θ,ϕ

$T(\theta,\phi)$ = the source temperature in the direction θ,ϕ

The greatest contribution to the integral comes from the earth's temperature of $290^{\circ}K$ when the antenna is oriented skyward. The antenna temperature will vary with antenna orientation since its side and back lobes will see different temperature distributions in general.

Antenna side and back lobes must be reduced, to lower antenna temperature as well as to avoid interference. The reduction can be accomplished by using a more favorable aperture distribution

and taper and by reducing aperture block and spillover losses. A new development in antenna design may accomplish side and back lobe reduction without a significant increase in cost. The portion of the aperture needed for defining the beam is made to the necessary precision since it receives the maximum power levels. The outer portions of the aperture having lower power levels, because of the chosen aperture illumination and taper, may be made less precise. In fact, an outer ring or shroud added to an existing antenna of given design and illumination will significantly reduce side and back lobes.[20] Some development work may be necessary to determine the required tolerances.

10.5 ANTENNA TYPES

Antenna types that may be used in the millimeter and submillimeter region are: dipoles, slots, horns, lenses, reflectors, leaky wave devices, arrays and gratings.

10.5.1 Dipoles and Slots

Dipoles and slots for the millimeter and submillimeter region are difficult to manufacture by conventional means. Photoengraving techniques are quite satisfactory however.

Two additional difficulties are present: low power handling ability because of voltage breakdown problems and feed problems, and losses associated with the transmission line between generator or detector and dipole or slot may be of interest in systems for this frequency region. Dipoles and slots may find applications in array antennas (section 10.5.6).

10.5.2 Horns

Horns can be used throughout the region of interest. Precision manufacture and power handling capabilities are not a problem. With proper tapers and exact flare angles all types of illumination may be produced. Horns will be free of shadowing and spillover losses.

10.5.3 Lenses

There are two types of lens antennas, namely: dielectric and metal. The dielectric lens is difficult to manufacture and there is a dearth of suitable materials. There are no insurmountable problems with the metal lens. Metal-dielectric lens types may be used if suitable dielectric materials are available. Losses may be higher in dielectric lens types than in metal lens types. Lens may also be used to correct horn antennas, thus giving the hybrid horn-lens antenna. These antennas are more or less free of shadowing and spillover losses.

10.5.4 Reflectors

Reflectors may be used without frequency limitations if suitable reflecting surfaces are available. Manufacturing difficulties and surface precision are not a problem. The main difficulties are in the feed system which usually results in shadowing and spillover losses. Except for the Cassegrain structure, feed line losses may also be high.

The horn-reflector antenna is free of all of the above-mentioned losses but is much more expensive to manufacture and mount.

10.5.5 Leaky Wave Antennas

Leaky wave structures are usually arrays of slots in a waveguide. Many waveguides may be arranged in parallel to form a square or rectangular array. This device suffers primarily from mechanical tolerances and power loss in the waveguides. It is unlikely to have much utility in the 3 mm to 0.1 mm wavelength region.

10.5.6 Arrays

Array antennas can in principle be designed and constructed for any portion of the frequency spectrum. With electronic phase shift techniques, considerable freedom is available for high speed beam shifting and beam forming without the complications of a mechanically orientatable system.

Arrays of individual radiators such as dipoles or slots may be expected to be difficult to construct unless photo-etching techniques are used. In addition, the individual radiators have low power handling capability or high transmission line losses associated with their feed system. This method would show promise if the generator or detector and the radiating element could be made one and the same. Simple solid state devices such as discussed in Chapter V may be applicable, but development of phase control methods is required.

Arrays of horns, reflectors or lenses may be expected to be more promising. Arrays using horns have been exploited at about 70 GHz.[11] In one system two phase shifting techniques are used. Each horn has a block of ferrite in its aperture and its beam may be shifted electronically. Ferrite phase shifters are also used in the feed line to each horn radiator. Success of such a system in the mm and submm region will depend on the development of ferrites or other phase shifting materials suitable for use in overmoded waveguides.

10.5.7 Gratings

Gratings and corrugated surfaces should be very useful in the mm and submm region. They are not difficult to construct to the required accuracy if suitable materials are available. They may be used in combination with horn radiators.

10.6 CONCLUSIONS

A survey of the antenna literature shows that there are no insurmountable problems and that additional research is needed only in the areas of materials, Fresnel region phenomena and the effects of atmospheric inhomogeneities. Aperture size does not appear to be limited by manufacturing methods or precision. It is unlikely that individual radiators, such as dipoles or slots or arrays of such radiators, will prove useful unless the radiator and the generator or detector can be combined.

10.7 REFERENCES TO CHAPTER X

1. C. J. Sletten, Modern Antennas for Space Communications, AFCRL-63-51, Feb. 1963, AD-403987

2. E. E. Altshuler, Earth-To-Space Communications at Millimeter Wavelengths, AFCRL-65-566, August 1965, AD-621942

3. A. R. Giddis, Reflector Antennas for Radio and Radar Astronomy, WDL-TR-1500, Aug. 1961 revised (Philco Corp.) also IRE Trans., vol. AP-9, pp. 579-580, Nov. 1961.

4. A. R. Giddis, Present and Future Development of Radio Telescopes, WDL-TR-E313-1, March 1963, AD-410288.

5. B. M. Hadfield, J. B. Suomala, P. L. Konop, The Peak Gain and and System Performance of a Large Paraboloidal Antenna, ESD-TDR-64-132, Nov. 1964, AD-608832

6. John Ruze, "Antenna tolerance theory--a review," Proc. IEEE, Vol. 54, No. 4, April 1966, pp. 633-640.

7. A. F. Kay, "Millimeter wave antennas," Proc. IEE, vol. 54, No. 4, April 1966, pp. 641-47.

8. J. M. Cotton, Research Study into the Near Earth Application of Millimeter Radio Waves as Applied to Certain Battlefield Problems, March 1965, AD-465280.

9. R. C. Fisher, H. S. Hoard, "Radio Telescope for Millimeter Wavelengths," AIAA paper no. 64-423, June 29-July 2, 1964, Washington, D.C.

10. E. Jacobs, H. E. King, 2.8-minute Beamwidth, Millimeter-Wave Antenna—Measurements and Evaluation, SSD-TDR-64-285, March 1965, AD 460716.

11. T. R. Schiller, et al, Electronically Steerable Array, April 1966, AD 633495

12. G. B. Kistiakowsky, Ground-Based Astronomy, A Ten Year Program, National Academy of Sciences--National Research Council, Wash., D.C., 1964, Library of Congress 64-62266, Pub. no. 1234.

13. J. B. Sidgwick, Ameteur Astronomer's Handbook, Faber and Faber, Ltd., London 1955.

14. G. P. Kuiper, B. M. Middlehurst, Stars and Stellar Systems, Vol. 1, Telescopes, Univ. of Chicago Press, 1960.

15. J. B. Brinton, Jr.,"A 500-foot dish for radio astronomy," Mcirowaves, V. 5, No. 12, Dec. 1966, pp. 10-12.

16. W. T. Patton, and A. B. Glenn, Component Problems in a Microwave Deep-Space Communication System, RCA Missile and Surface Wave Radar Div., Moorestown, N. J., 11 Technical Papers, 1966, pp. 9-13.

17. S. Silver, Microwave Antenna Theory and Design, MIT Radiation Laborabory Series, V. 12, Boston Technical Litohgraphers, 1963.

18. W. A. Miller, "A solar observatory on Long Island," Applied Optics, Vol. 2, No. 1, Jan. 1963, pp. 93-103.

19. R. C. Weast, et al., Handbook of Chemistry and Physics, 45th Ed. 1964-65, The Chemical Rubber Co.

20. O. M. Salati, and H. Kritikos, Unpublished research at the University of Pennsylvania.

Chapter XI

ENVIRONMENTAL CONSIDERATIONS

11.1 INTRODUCTION

In this chapter we are only concerned with providing an adequate description of the sources of energy in the millimeter and submillimeter frequency ranges arising from natural causes. There are, of course, many attributes of the physical environment which are of serious concern in the design of an electronic system, such as temperature, gravitational force, meteorite impact, etc. However, these effects are not of unique interest in the millimeter wavelength region although they are of concern.

The effects of planetary atmospheres are of concern. That of the earth has been extensively discussed in Chapter VIII. That of other planets is discussed in this chapter.

Since many of the environmental sources are thermal in origin, the subject of radiometry is central to the discussions of this chapter. An extensive discussion of definitions pertinent to the subject, and of techniques, is given in an appendix to this chapter, and should be read first by those unfamiliar with the subject.

11.2 TERRESTRIAL RADIOMETRY

Radiometric observation of the earth's surface reveals a fine distribution of the apparent temperature. This is caused by the different reflecting and emitting characteristics of the various terrestial objects. The reflectivity δ of an object is the ratio of the amount of

energy reflected by it to that of a perfect reflector of the same area, and similarly the emissivity ϵ is the ratio of the apparent radiation of an object to that of an equivalent black body at the same temperature. These two quantities are related as follows:

$$\delta + \epsilon = 1 \tag{11.1}$$

A good emitter is a good absorber and a bad reflector, and vice versa. However, a distinction should be made between physical and radiometric temperature. Observing the earth at infrared frequencies, one generally sees hot bodies against a cold background. On the contrary, when observing at ultramicrowaves, cold bodies contrast against a warm background. Rough surfaces appear warmer than metallic and liquid surfaces, which reflect the cooler sky above.[1-2]

Table 11.I
Typical Emissivities of Various Terrains Observed at Different Zenithal Angles for 35 GHz[10]

	horizontal polarization			vertical polarization		
type	10°	30°	50°	10°	30°	50°
earth	.86	.95	.99	.87	.99	.99
10 cm. long grass	.96	.99	1.	.88	1.	1.
marsh weeds	.93	.99	1.	-	-	-
bay water	.38	.36	.45	-	-	-
sheet metal	.40	.27	.25	.36	.25	.25

The observed ocean temperature changes with the degree of surface roughness. The temperature depends on the thermometric temperature of the water, the atmospheric conditions of the reflected sky, and the zenithal angle, and varies with the polarization.[3] Figure 11.1 shows the effect of the water temperature on the apparent temperature for a horizontally polarized radiation. Figure 11.2 plots the horizontally polarized temperature at a wind speed of 6 m/sec for 94 GHz. It has been found[4] that the vertically polarized radiation is much less affected by the wind, and for 19 GHz, at zenithal angle of 50°, is almost independent of the state of the sea. These facts demonstrate the possibility of the radiometric detection of the ocean's surface conditions.

Similarly, it is possible to make radiometric measurements of partially frozen water, because of the noticeable difference in the emissions of ice and water at a given angle of incidence. The simultaneous utilization of two radiometers at different frequencies may enable an observer to locate otherwise undetectable areas of ice in water and permit the measurement of its thickness.[5]

Systematic measurements of the radiometric characteristics of a selected set of material surfaces, for example various types of soil, vegetation, etc., under rigorously controlled conditions, are being conducted at Space General, Inc., El Monte, California.[4] A list of these measurements and the equipment utilized is shown in the attached Table 11-II.

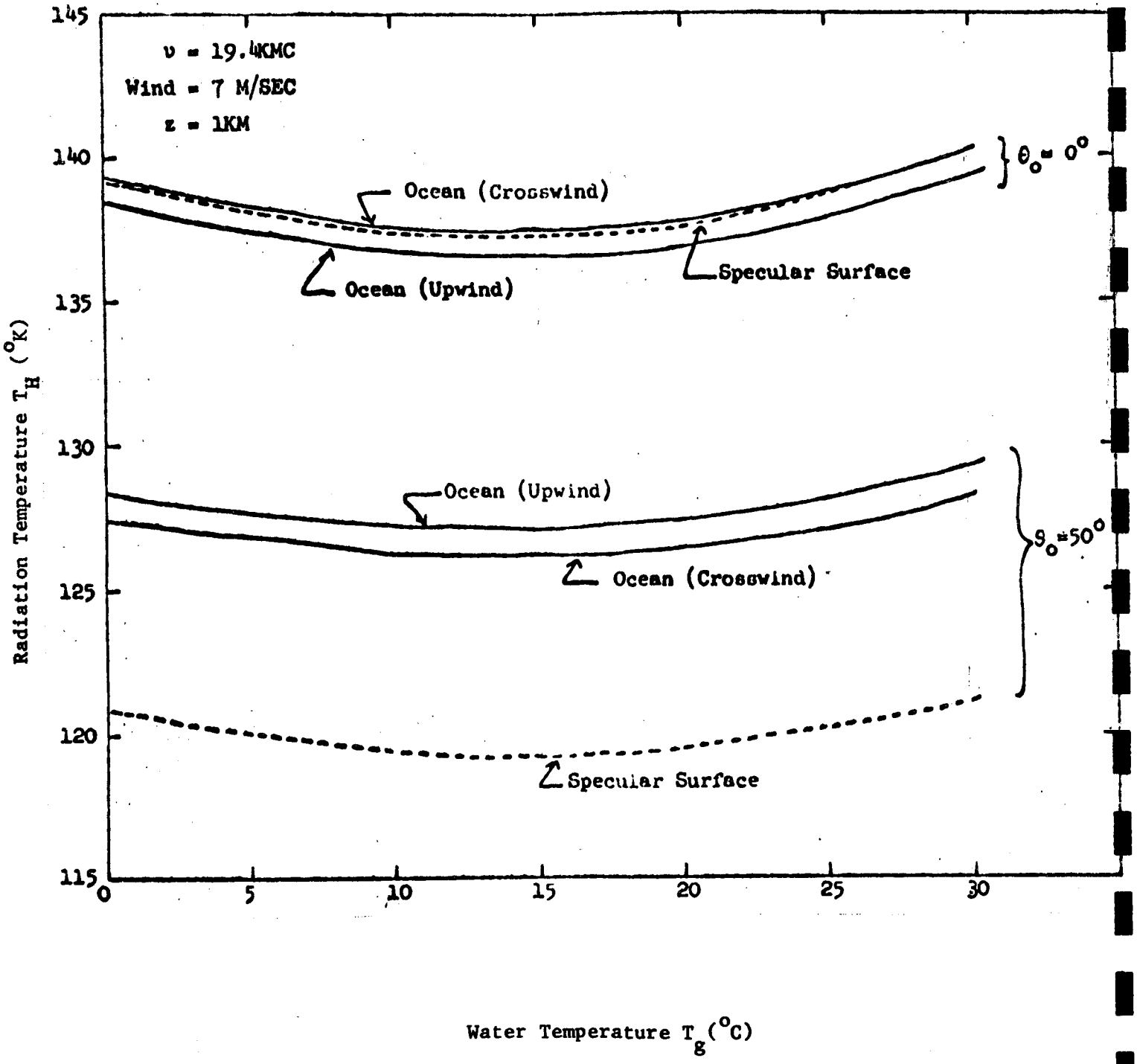

Figure 11.1 Temperature of Horizontally Polarized Radiation as a Function of Water Temperature

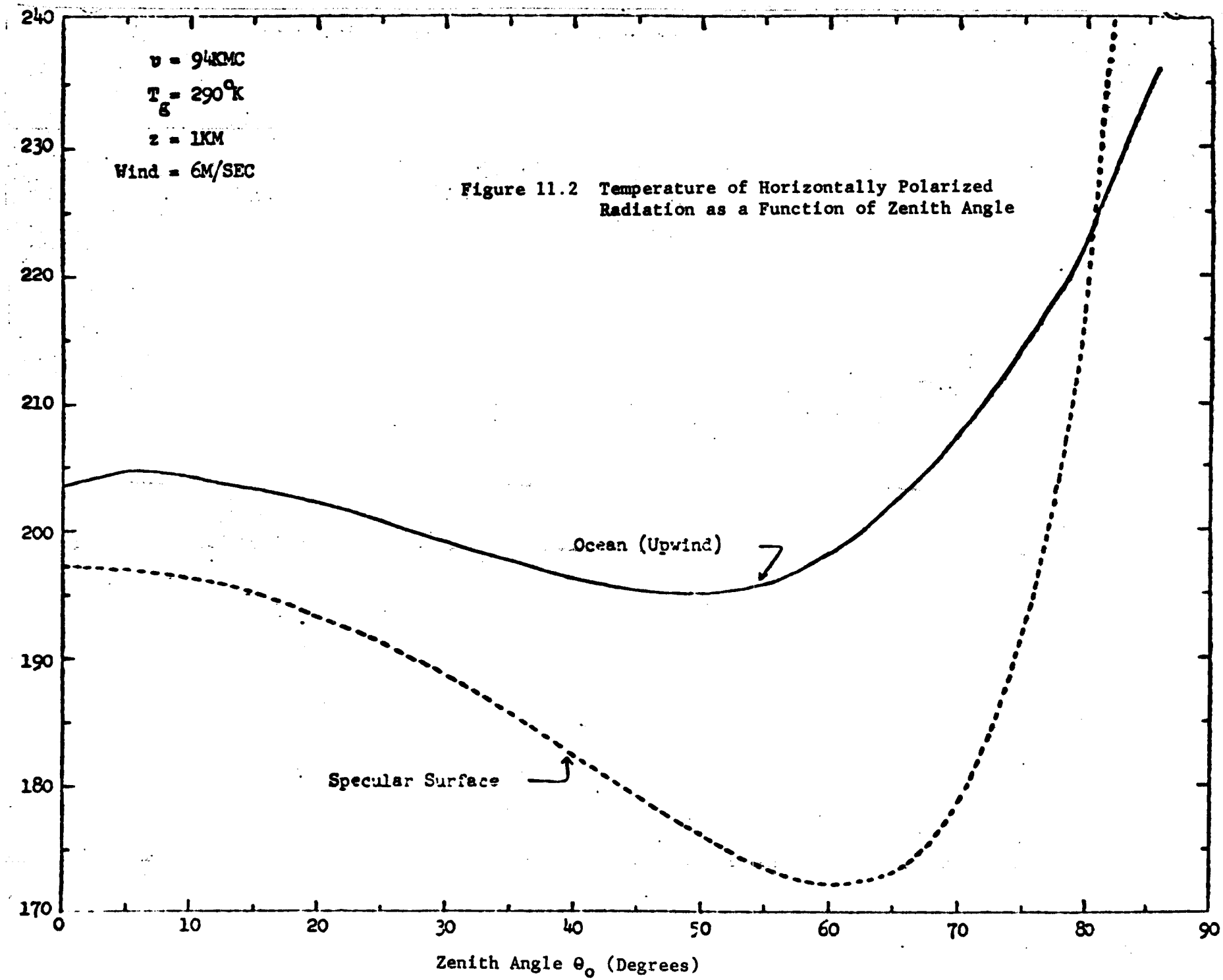

Figure 11.2 Temperature of Horizontally Polarized Radiation as a Function of Zenith Angle

Table 11-II

Radiometric Equipment Developed by Space-General

	Instrumentation					Measurements				
Frequency	Operational Application	ΔT/cps	Achievable Today ΔT/cps	Calibration System & AGC	Device Development	Reflectivity Models	Sky Temperature & Weather	Terrain Emissivity	Multilayer Terrain & Hydrological	Target Reflectivity
0.6 - 1.0 Gc (Tunable)	Flight Unit	0.4°	Transistor TRF 0.4°	Cold Load & Gain Stability References	AGC Circuit, Reference		Fair Weather Only	Several Typical Terrains	Discern Water Tables	
12 - 15 Gc	Field Instrument	< 1°	Tunnel Diode 0.5°	Hot Load Reference	Reference, Load	Flat Plate, Cone, & Complex Shapes	All Weather Fair to Rain	Maps & Several Typical Terrains	Snow & Ice Over Terrain & Water	Flying Aircraft, Rocket & Plasma Plume
17 - 19 Gc	(1) Field (1) Flight Test Instrument	< 1° < 1°	Tunnel Diode < 0.5°	Hot & Cold Load Reference	Reference, Load RF Amplifier	Flat Plate, Cone, & Complex Shapes	All Weather Fair to Rain	Complete Maps of 38 Target Areas 287 Flights	Ice Thickness, Penetrability Through Terrain Material	Cars, Trucks, Other Vehicles
34 - 37 Gc	(2) Field Instruments	1°	Superhet Bw 400 mc 0.2°	Hot Load Reference	Mixer/IF Amp Matching Structure	Flat Plate	All Weather Fair to Rain	Typical Terrains: Natural, Disturbed, Buried Objects	Snow & Ice Over Terrain & Water	Aircraft, Rocket & Plasma Plume
35 Gc (Tunable)	Solid State Light Weight Field Instrument	0.2°	400 mc IF Bandwidth	Hot and Cold Load	Mixer/IF Amp Servo Controlled Calibration to 20,000°K		Sun, Moon			Plasma Applications & Atmospheric Studies
68 - 71 Gc	Laboratory Instrument	2.5°		Noise Tube Reference		Metal Plates	Fair & Cloudy Weather	Several Typical Terrains		
92 - 96 Gc	(2) Field Instruments	3° 0.5°	Superhet Bw 400 mc 0.5°	Noise Tube Reference	Single-End GaAs Mixer & VHF Amp Structure	Metal Plates	All Weather Fair to Rain	Maps of Several Typical Terrains	Snow & Ice Layering, Terrain & Water	Cars, Trucks Buildings
94, 144, 250 Gc	Prototype Lab/Field Instruments	Cryogenic Direct Detector < 5°		Reflected Cold Surface Reference	Detector & Tunable Filter		Preliminary Sun Only			

The apparent earth temperature observed through air includes the effects of thermal absorption and radiation from the atmospheric gases, and, in addition, possible scattering from fog and rain.

The apparent radiometric temperature of a calm sea, as observed above, may be expressed by the formula

$$T_a = T_v \epsilon_v (1 - \epsilon_w) L_v + L_v^2 (1 - \epsilon_w) T_s + T_w \epsilon_w L_v + T_v \epsilon_v$$

where the subscripts v and w refer to water vapor and sea water, respectively; L is the absorption loss and T_s is the sky temperature. In Figs. 11-3 and 11-4 the sky temperature distribution at 35 GHz is shown as a function of the zenithal angle.[6]

The sky temperature has been computed[7] at frequencies of 30, 70, 90, 140, and 250 GHz for a variety of conditions, as listed below:

Humidity	Extent of Cloud	Extent of Rain
25%	0	0
50%	0	0
100%	0	0
100% up to 1.17 km	1.17 km	1.17 km
100%	1.17 km	1.17 km
100% up to 2.33 km	1.83 km	1.83 km
100%	1.83 km	1.83 km
100%	7 km	4 km

The difference in apparent temperature between the frequency of the first water vapor resonance (22.2 GHz) and a non-absorbed frequency (for

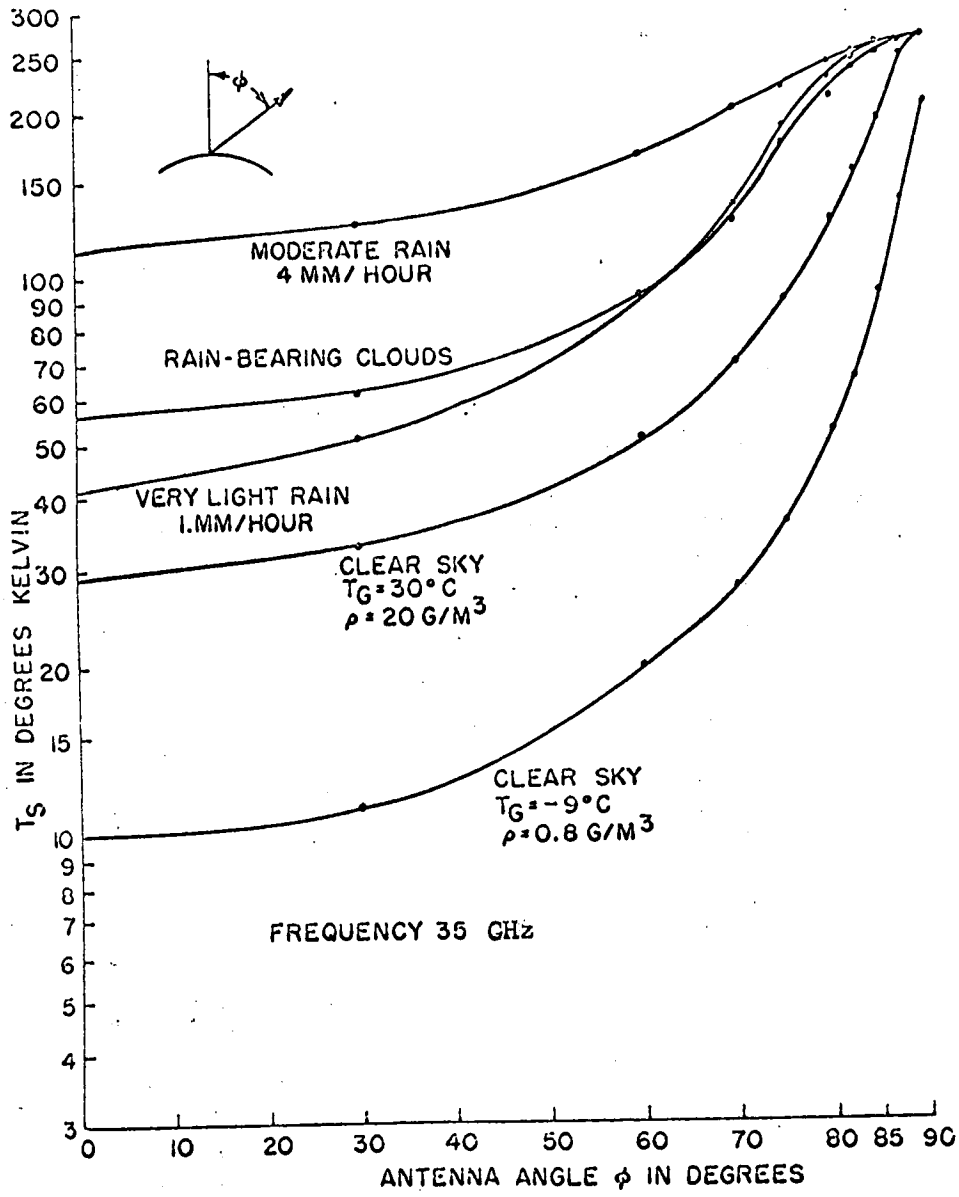

Figure 11.3 Sky Temperature Profiles at 35 GHz

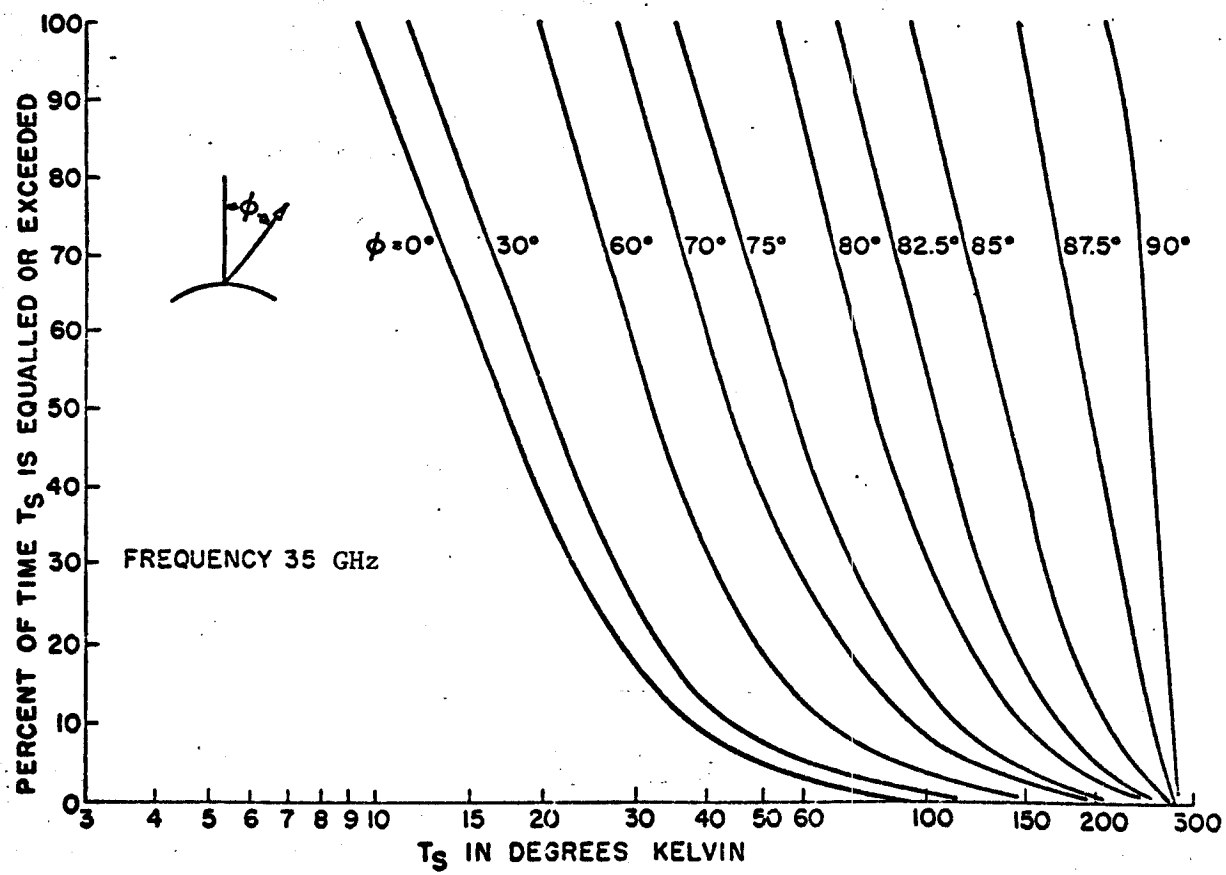

Figure 11.4 Sky Temperature Distributions at 35 GHz

example, 35 GHz) offers a method for measuring water vapor concentrations in the atmosphere. A map showing these differences should give the total water vapor distribution over the earth.[8]

Analogously, measurements of the emission from atmospheric oxygen in air could give sufficient information about the gross temperature structure of the terrestrial atmosphere below 40 km.[9]

11.3 PROPAGATION CONSIDERATIONS

Above an altitude of about 10 km, the atmospheric density is low enough so that pressure broadening is no longer the controlling factor in molecular absorption. The absorption of ultramicrowaves therefore becomes sharply frequency dependent, and will change with altitude as the chemical composition of the atmosphere changes. Because of the narrow bandwidth of the absorption lines, the medium can be considered absorption-free for all practical communication problems. However, the absorption lines may be used for the purpose of studying the composition of the upper atmosphere. The detection of O_2 and H_2O has been previously discussed, and a proposal for sounding by this method the high altitude water vapor content using a satellite has appeared in the literature.[10]

A similar method could be used to resolve the controversial problem of the presence of the NO radical in the D zone.[11] Actually, the NO absorption spectrum has a favorable cluster of lines located around 250 GHz.[12]

11.3.1 Re-entry Plasma

High speed bodies entering the atmosphere undergo a shock-wave regime which creates around them the so-called re-entry plasma. The

electron density distribution associated with a re-entering body has a complicated dependence upon initial velocity, mass and shape, and vertical angle of approach. For typical conditions, this distribution may be evaluated by the use of computers. When the initial velocity is sufficiently large, the maximum electron density created at the front of the re-entering body becomes such that its critical frequency involves millimeter and submillimeter waves. In Fig. 11-5 the theoretical stagnation electron plasma is plotted as the function of free stream velocity for various altitudes, assuming verticle re-entry, and neglecting lift effects.[13] It appears that ultramicrowave may be useful to assure constant communications during the re-entry phase of space crafts.

11.3.2 Interplanetary Dust

Various concentrations and forms of dust particles are known to exist in the interplanetary space. According to the phenomenology through which it is revealed, this dust is usually subdivided into meteoric dust, noctilucent cloud, zodiacal dust, and cometary dust.[14-18]

The effect of this dust on interplanetary ultramicrowave communication is expected to be totally negligible. However, it would be interesting to establish whether the scattering produced by these particles is observable. Evidence exists indicating that using laser light echoes may be obtained from meteoric dust located at about 100 km above the earth.[20] According to the mechanism of reflection suggested in the above-mentioned paper, the echoes are due to a selective concentration of particles of optimum size (about .1 micron) to give maximum

Figure 11.5 Critical frequency of re-entry plasma as the function of free stream velocity assuming vertical re-entry and neglecting lift effects.

Parameter - altitude

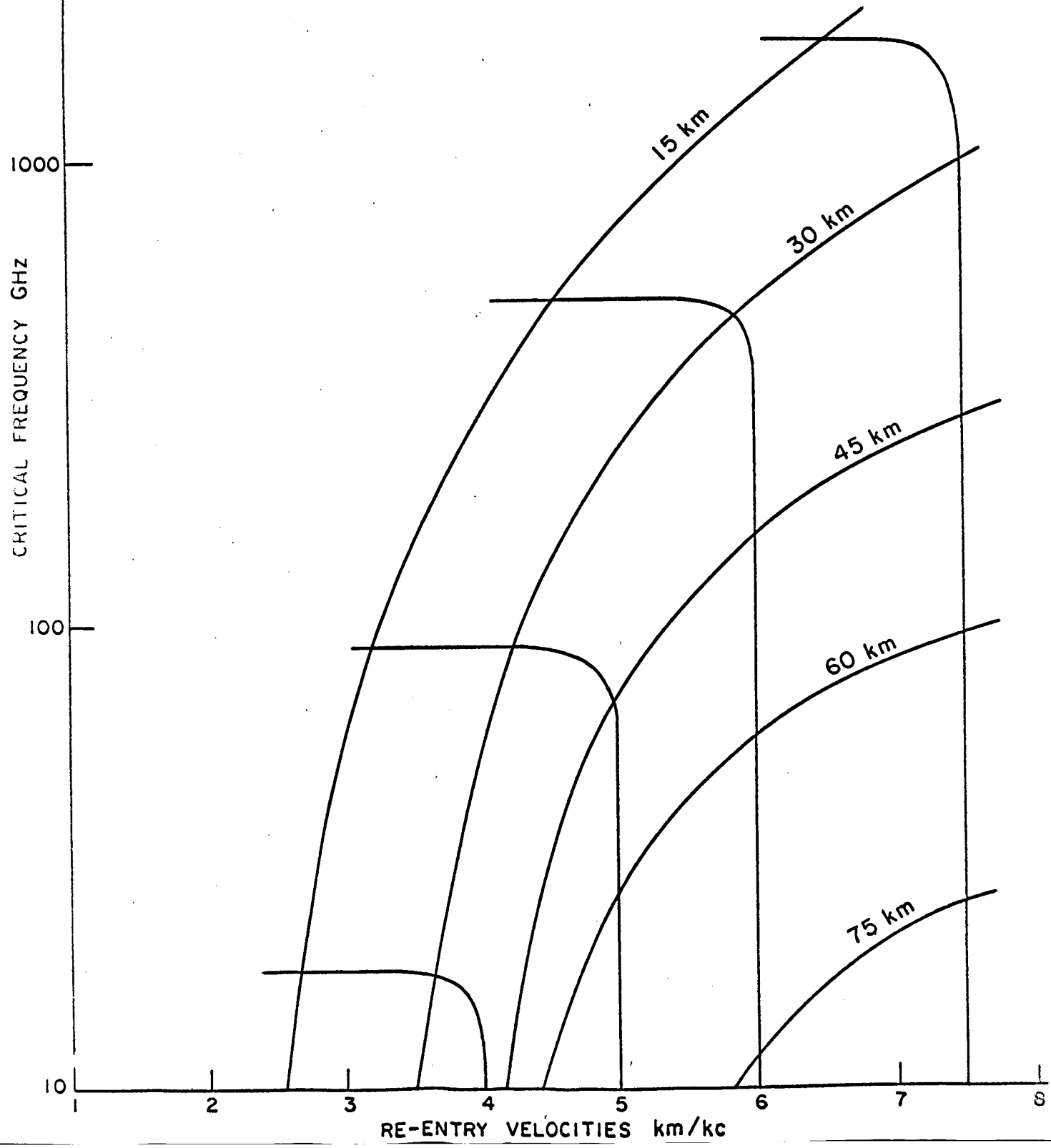

backward scattering at the wavelength used (.7 micron). Since the size of cosmic dust particles varies uniformly from a fraction of a micron to several hundred microns,[21] it is conceivable that the use of radar at various frequencies in the submillimeter band may selectively detect the presence of particles of different sizes. Furthermore, there are planetary space regions of zero gravity, in which particles at rest are in equilibrium.[22] Six of such regions are known to exist in the earth-moon gravitational system. These regions may be loci of concentration of particles of similar size, and therefore may be particularly effective scatterers of radio waves at selective frequencies.

11.3.3 Interplanetary Plasma

It has been established[23] that the plasma emanating from the solar corona extends well beyond the orbit of the earth. Radio waves passing through this plasma may thus be subjected to intensity fluctuations, and other refractive effects. However, it seems quite unlikely that millimeter and submillimeter waves, in view of their frequency so well above the cutoff of the interplanetary plasma, will be affected by it. Accurate measurements[24] of 0.184 GHz emission of the radio star α Tauri, at various angles with regard to the sun, have demonstrated that no detectable (within 5%) attenuation occurs at this frequency for a propagation path of the order of 300 million kilometers.

11.4 EXTRA-TERRESTRIAL RADIOMETRY

11.4.1 Solar Radiometry

The atmospherically attenuated solar spectrum in the ultra-microwave range has been studied by Averkov, et al.,[25] using a grating spectrometer, and by Gaitskell[26] using a Fabry-Perot interferometer. In order to obtain an estimate of the absorption coefficient of atmospheric water vapor, a series of spectra were recorded at different solar elevations.[27] Bands of relatively high atmospheric transparency have been noticed, centered at the frequencies of 307, 340, 405, and 670 GHz. The relative intensities observed at these frequencies were consistent with the attenuations expected from water vapor absorption.[28]

The relative intensity of solar emissions in the radio frequency band is shown in Fig. 11-6.[29] The 100-3,000 GHz frequency band appears to be covered by the thermal emission of the quiet sun, and by the type IV solar burst. This type of burst is associated with large solar flares, and generally lasts from about ten minutes to several hours. The origin of the phenomenon[30] seems to be associated with synchrotron radiation from accelerated electrons of exponential rigidity. The magnetic field necessary to produce the observed spectrum is below 500 gauss, and the number of electrons involved is of the order of the number of protons accelerated in a large flare. Observations of the spectrum extent give a measure of the maximum energy in the flare. Calling γ the ratio of the

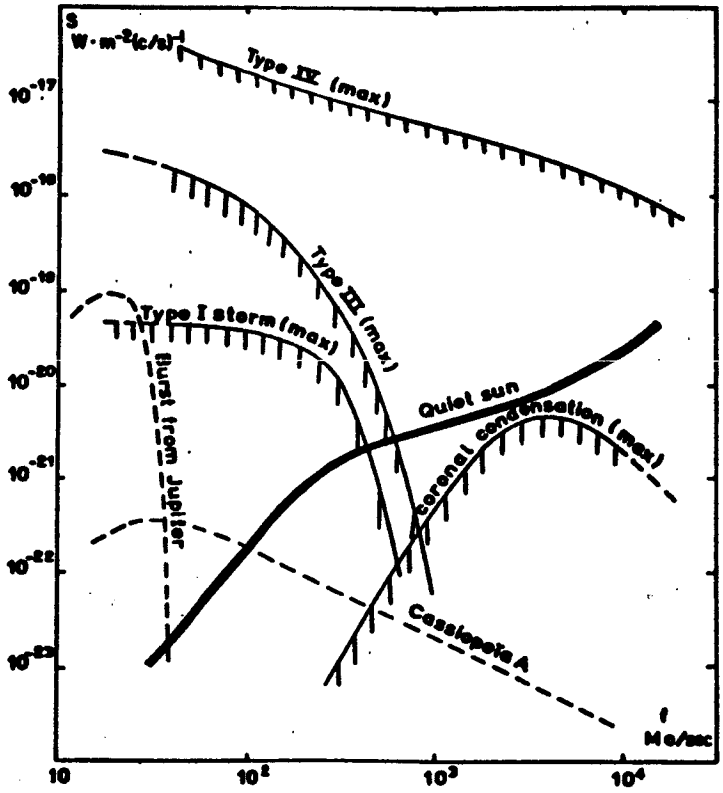

Figure 11.6

Relative intensities of the different solar emissions as a function of frequency. For solar activity only maximum values are given. The values for coronal condensations correspond to the emission of only one intense center of activity. For comparison the intensities of Jupiter's emissions and of the radio source Cassiopeia A are also plotted.

electron energy to their rest energy, the highest frequency of the radiated spectrum is given by the formula

$$\nu_{m(\text{Hertz})} = 2\ 10^6\ \gamma^2\ B_{(\text{gauss})}$$

For electrons of 50 MeV, and B = 500 gauss, it is ν_m = 1,000 GHz.

The sun shows blackbody temperatures of 5,800°K at 300 GHz[1] and 6,400°K at 94 GHz.[31]

Detection of changes in the chromospheric temperature may be related with solar flare activity.[32-34]

During a total eclipse, the residual thermal flux which originates from the annular ring of the outer radius, 1.5 times that of the optical sun, was measured to be 52% of the solar flux.[35]

11.4.2 Moon Radiometry

Radio observations of the moon are summarized in Table 11-III. At 94 GHz the lunar temperature observed is, T = 208 ± 21°K.[36]

Millimeter radiometry may make important contributions to the study of the moon's structure. Observations at the near infrared (8-14 micron) have shown[37] that "hot spots" exist in the Tycho and Copernicus craters. Longer wavelengths, being more penetrating, may give more information on the detailed distribution of the surface temperature of the moon.[38]

11.4.3 Planetary Radiometry

Only a small fraction of planetary radiation is due to reflected and scattered solar radiation. The most important contribution of the observed planetary radiation in the ultramicrowave region is the effect

Table 11-III

Radio Observations of the Moon
(T_e represents the radio brightness temperature at the center of the disk, T_d is the radio brightness averaged over the disk.)

Wave length (cm)	*Apparent black-body temperature* (°K)	*Uncertainty*	*Observer*
0.4	$T_d = 230 + 73 \cos(\omega t - 24°)$	.....	Kislyakov
0.43	$T_e = 170$ to 290	25 per cent	Coates
0.75	$T_d = 125$ to 175	.....	Mitchell and Whitehurst
0.80	$T_e = 197 - 32 \cos[\omega t - 40(\pm 5)°]$	10 per cent	Salmonovich
0.86	$T_e = 150$ (single observation)	40 per cent	Hagen
0.86	$T_e = 145$ to 225	.....	Gibson
1.25	$T_d = 270$ (single observation)	.....	Dicke and Beringer
1.25	$T_e = 249 - 52 \cos(\omega t - 45°)$	5 per cent	Piddington and Minnett
1.63	$T_e = 224 - 36 \cos(\omega t - 40°)$	±10–15 per cent	Zelinskaya, Troitskii, and Fedoseev
2.20	$T_e = 200$ (constant to ±10 °K)	5 per cent	Grebenkemper
3.15	$T_e = 195 - 12(+5) \cos[\omega t - 44(\pm 15°)]$	±25 °K	Mayer, McCullough, and Sloanaker
3.20	$T_d = 183$ (constant to ±9 °K)	±13 °K	Zelinskaya and Troitskii
3.20	$T_d = 170$ (constant to ±12 °K)	±20 per cent	Troitskii, Zelinskaya
3.20	$T_d = 133$ (constant to ±10 °K)	±20 °K	Kaidenovsky, Turusbekov, and Khaikin

of the thermal energy of the planet itself. This energy comes, actually, from the sun via visible and near infrared radiation, and is re-emitted by the planet as the thermal radiation of a black-body heated to a characteristic temperature, T_p. The radiation emitted from the planet may not be uniform because of the spatial variations of the thermal properties of its surface or of the atmosphere around it.

A list of planetary and satellite equivalent temperatures for the rotating (equatorial) or the non-rotating (polar) cases, are listed below.[39]

Planet or Satellite	Mean Distance A.U.	Diameter (Mega-meter)	$T_{rotating}$ °K	$T_{non\text{-}rotating}$ °K
Mercury	0.39	2.4	471	561
Venus	.72	6.2	230	273
Mars	1.52	3.4	219	260
Jupiter	5.20	71.4	88	105
Saturn	9.55	60.4	64	76
Uranus	19.2	23.8	33	39
Neptune	30.1	22.3	32	38
Pluto	39.5	7.2	43	51
Jupiter iii	5.2	2.47	107	129
Jupiter iv	5.2	2.34	115	137
Titan	9.55	2.5	88	104
Ceres	2.77	0.37	168	200
Pallas	2.77	0.24	167	199

Note: A.U. (astronomical unit) is the geometrical mean distance of the earth from the sun, and is 1.49 10^5 megameter.

The terrestrial atmosphere is a factor which limits the radiometer's performance on the earth by giving sky radiation background and absorption. The minimum detectable temperature T_d of an extended body (as the moon) is a quantity of considerable interest. During an average night the sky delivers a radiation of approximately 5×10^{-9} watt. Correspondingly, the expected statistical fluctuation is 10^{-14} watt.[40]

Ultramicrowave observations of planetary spectra, possibly performed with high flying aircraft or satellites, would permit the identification of atmospheric gases in the planet, the measurement of their relative abundance, and the determination of the atmospheric structures.[41] The possible gaseous components of planetary atmospheres having molecular spectral lines in the radio-frequency band are tabulated below. The planets Venus, Earth, Mars, Jupiter, Uranus and Neptune are indicated by their initials: upper case letters indicate compounds already found; lower case are compounds of probable existence.

Gas	Planet
O_2	v,m,E
OH	E
O_3	v,m,E
H_2O	V,M,E
H_2S	j,s
SO_2	E
NO	E
NO_2	v,m
N_2O	v,m
NH_3	J,S,E
CO	v,E,m
CH_2O	E
CH_4	v,E,m,J,S,U,N

Radar astronomy at millimeter waves is still in its first steps[42] but promises interesting new contributions when sensitivity improvement of at least 30 dB will be obtained.

11.4.4 Venus Radiometry

The ultramicrowave radiometric study of Venus could reveal information of this planet which is hidden from optical vision.

A number of observations of Venus were made, starting in 1956, at each conjunction. The most significant result of these observations was the discovery that the emission of Venus at millimeter wavelength (37.5 and 75 GHz) corresponds to a black-body temperature of about 400°K, while at 1.4 GHz the deduced temperature is 600°K.[43]

Mariner II carried two microwave radiometers, one at 1.6 and one at 2.2 GHz, in close proximity to the planet. The measured temperatures were 460°K and 400°K for the limb scans, and 570°K for the center.[44]

The temperatures of Venus observed from the ground at various ultramicrowave frequencies were[45] (see Fig. 11-7):

Observed Temperature °K	Frequency GHz
375 ± 17	35
330 ± 9	70
300 ± 4	94

The microwave spectrum of Venus, measured around the 5_{-1} - 6_{-5} transition of the water vapor molecule, has shown no water vapor resonance.[46-47] Further work along these lines is suggested.

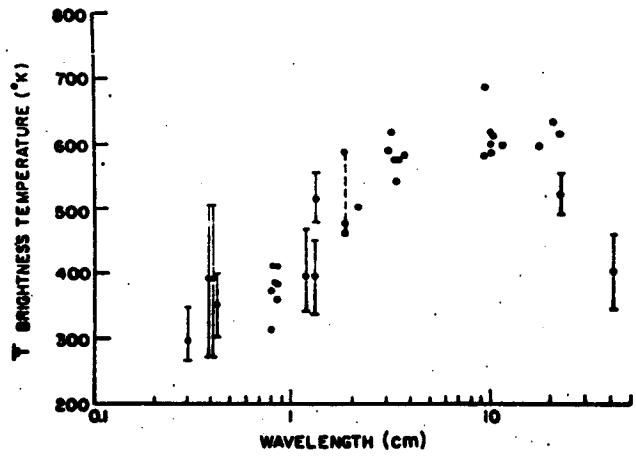

Figure 11.7 The microwave spectrum of Venus

(Error bars are omitted where the points cluster closely together, but those shown are generally typical.)

11.4.5 Stellar and Nebular Radio Sources

A list of stellar and nebular sources up to a frequency of about 10 GHz is currently available.[48] Only a limited number of observations have been performed above that frequency.

Portions of the radio spectra of Taurus A and Orion A are shown in Fig. 11-8.[49-50] To justify the observed spectra of these nebulae a model is required having two separate emissions; one at lower frequencies from the dense regions, and the other at ultramicrowave frequencies due to denser conglomerations.

In general, the radio spectra of nearly all radio objects suggests a great conformity in the radiation mechanism, namely the synchrotron radiation connected with the motion of relativistic charges having exponential rigidity.[51] Therefore, the detailed observation of the radio-frequency stellar spectrum, possibly from a station located outside of the earth's atmosphere, could give a notion of the energy involved in the emission of stellar radio objects.[52-53]

11.4.6 Interstellar Space

Interstellar space contains gases and cosmic dust, with a concentration which varies from place to place. The origin of this matter is attributed to "sputtering" from hot celestial bodies, and fragments of exploded stars.[54] The average concentration of interstellar hydrogen, near the galactic plane, is 5×10^5 m^{-3}, mainly in a non-ionized state. Helium has also been detected in a concentration of about 20% smaller. Other elements, atoms, molecules, and free radicals, show a concentration ranging from 10^3 m^{-3} to 1 m^{-3}. In addition, dust

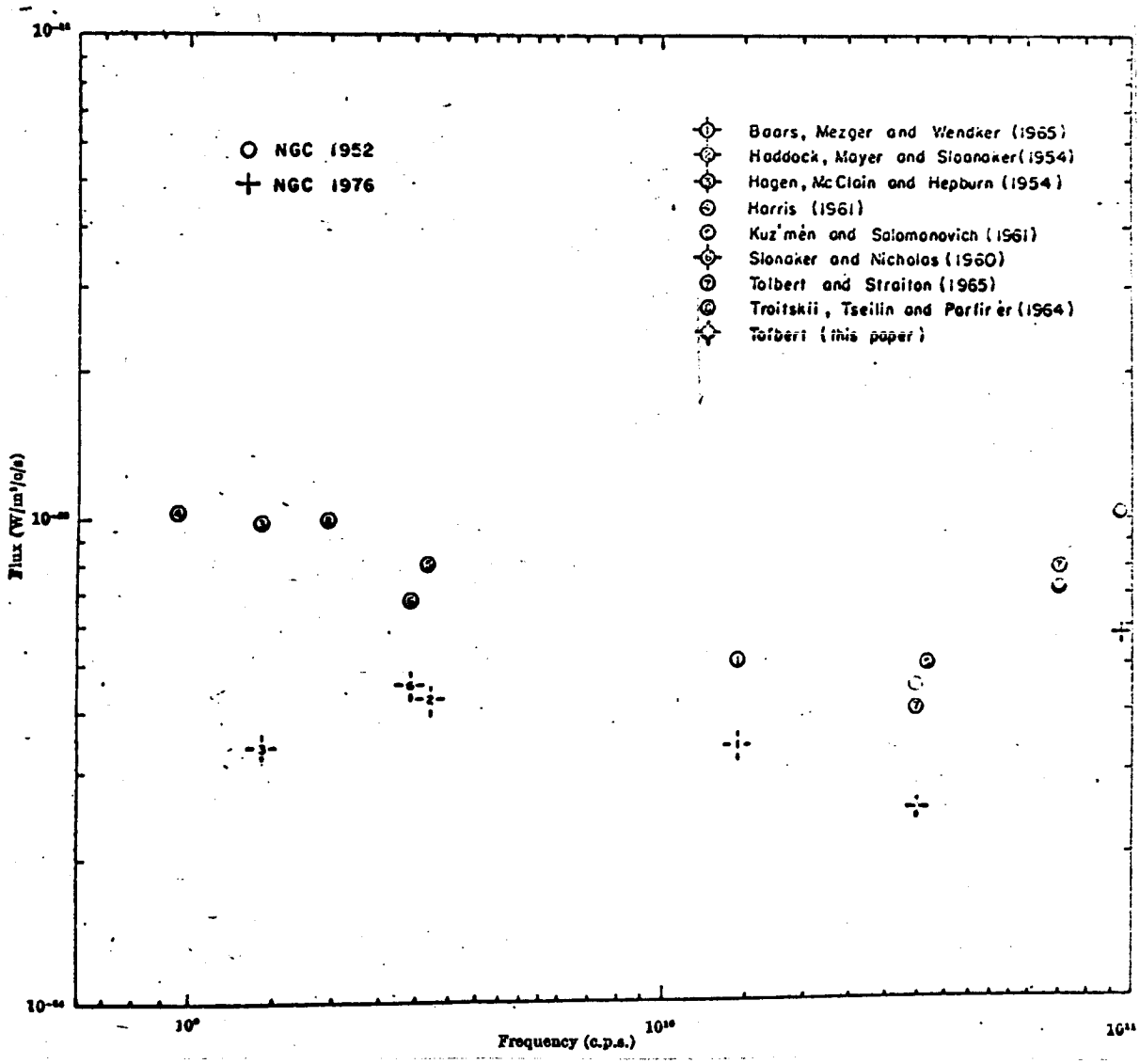

Figure 11.8 Flux of the Orion Nebula and flux of the Crab Nebula as functions of frequency

particles exist with an entire mass which does not exceed 1% of the mass of interstellar hydrogen. They may be aligned by intergalactic magnetic fields, and give rise to polarization of stellar light. Furthermore, dust particles play a catalystic role in the formation of interstellar molecules.[55]

The interaction of stellar radiation with interstellar radiation and interstellar matter during its lengthy path through it is revealed by both emission and absorption effects. Since 1945, when Van de Hulst[56] predicted the detectability of the "spin-flip" of the atomic hydrogen line at 1.4 GHz, a huge amount of observation data have been accumulated on interstellar microwave emission. More recently, the recombination emission of ionized hydrogen and helium have been detected.[57-58] These emissions occur at frequencies given approximately by the Rydberg formula

$$\nu_{N,N'} = 3.3\ 10^6 (1/N'^2 - 1/N^2) \text{ GHz}$$

where N' and N are two principal quantum numbers. The intensity of these lines decreases with increasing ΔN so that only $\Delta N = 1,2$ and 3 are generally considered. Note that the ultramicrowave spectrum is covered by quantum numbers larger than about 15. The detection of these lines from the earth's surface is hampered by atmospheric and ionospheric absorption, but the complete spectrum should be observable from a satellite-borne receiver.

Also absorption[59] and emission[60-61] of the radical OH was observed. The spectrum in this case is due to the transitions associated with doubling and splitting of rotational levels (around 1.67 GHz). This mechanism of emission has been associated with a maser effect.[62]

Many other constituents of the interstellar medium are liable to be active sources of emission and/or absorption in the ultramicrowave band. Evidence exists on the excitation of the free radicals CN and CH^+.[63] There is no doubt that promising results are expected from the extended application of ultramicrowave radiometers in this type of research.

A practical datum of considerable importance is the level of the background noise of space in the millimeter and submillimeter band. Dicke, et al[64] have suggested that radiation emitted during a contracted stage of the universe may still exist in the form of black-body emission at about $3^{o}K$. The experimental evidence which has been collected up to the present is in surprising agreement with this theory. The measured values are:

frequency GHz	temperature ^{o}K
4.1	3.5 ± 1.0 (Ref. 65)
9.4	3.0 ± 0.5 (Ref. 66)
114.5	$2.7 \div 3.4$ (Ref. 67)

11.5 SUMMARY AND RECOMMENDATIONS

A radiometer located on the earth's surface is subject to radiation coming from both the ground and the warm atmosphere, and can only detect objects whose brightness temperature is above a certain threshold. For an extended object in a limpid dark sky this threshold is about $70^{o}K$ in the ultramicrowave band.

Terrestrial radiometry offers promising uses for ground and air detection, and for oceanographic, geological and meteorological research.

Extraterrestrial radiometry represents a new astronomical tool as yet unexploited. In particular, it appears useful for solar flare forecasting, planetary atmospheric and surface study, and the detection of interstellar matter.

It is recommended that:

1) Emphasis be given to the extension of the superheterodyne radiometer in the submillimeter region. Submillimeter masers could provide stable and low noise local oscillators, and no upper limit has yet been set for the usable frequency of point contact mixers.

2) An evaluation be made of the use of ultramicrowave emission or absorption spectrometry above 100 GHz to study gases of terrestrial and planetary atmospheres.

3) Air-or-satellite-borne ultramicrowave radiometers be extensively used for a detailed study of the earth's surface.

4) An evaluation be made of the feasibility of the possible use of aircraft, balloon or satellite borne ultramicrowave radiometers for astronomical observations.

5) Further attention be given to ground-based astronomical observations (particularly at high altitudes).

APPENDIX XI.A

FUNDAMENTALS OF RADIOMETRY

11.A.1 Thermal Sources

All bodies which are not at zero temperature radiate electromagnetic energy. A good radiator is also a good absorber of radiation. An object which absorbs all radiation incident upon it is called a "black body". Black-body radiation is a function of temperature and wavelength only. The ideal black body is well approximated by a small hole opened in a hollow box having isothermal walls. Inside the box the radiation moves in all directions and at all polarizations. In terms of the wall temperature, T, the brightness, i.e., power density flowing out of the hole into a unit solid angle, per unit bandwidth, is given by Planck's law

$$\left(\frac{\partial S}{\partial \nu}\right)_T = \frac{2h\nu^3}{c^2}\left(\exp\frac{h\nu}{kT} - 1\right)^{-1} \left[\frac{\text{watts}}{\text{m}^2\ \text{Hz rad}^2}\right] \qquad \text{(A-1)}$$

where h is Planck's constant ($6.62\ 10^{-34}$ joule sec), ν the frequency, and k is Boltzmann's constant ($1.38\ 10^{-23}\ \frac{\text{joule}}{^{o}\text{K}}$).

Integrating (A-1) over all frequencies, the total radiant flux of the hole results

$$S = \frac{2(kT)^4}{c^2h^3}\int_0^\infty x^3\left(\exp x - 1\right)^{-1} dx = \sigma T^4 \left[\frac{\text{watts}}{\text{m}^2\ \text{rad}^2}\right] \qquad \text{(A-2)}$$

where $\sigma = 2(\pi^5/15)\ k^4/c^2h^3 = 5.67\ 10^{-8}\ \text{watts/m}^2\ {}^{o}\text{K}^4$ (A-3)

is Stefan's constant.[68]

Maximizing (A-1) one gets Wien's displacement law

$$\nu_{max} = 2.77\ k\ T/h = 5.8\ 10^{10}\ T \qquad \text{(A-4)}$$

which relates the temperature of the black body with the frequency of maximum radiance emittance.

From (A-1), (A-2), and (A-4), it appears that the whole ultra-microwave band is well covered by black-body thermal emission at temperatures starting from about $4^{o}K$. For a non-perfect black body the thermal emission depends upon the physical characteristics of the radiating surface. These characteristics are generally expressed[69-70] in terms of an equivalent brightness temperature T_B, which is a function of both angle and frequency. The receiving antenna plays an important role in the definition of the brightness temperature. It has been pointed out by Dicke[71] that the effective antenna temperature is related to the temperature of the bodies with which the antenna exchanges radiation in the frequency band under consideration, not that of the surface of the antenna itself.

11.A.2 Antenna Temperature

If the antenna is completely enclosed by an isothermal surface at temperature T_A, it behaves like the previously mentioned "hole", and the total power absorbed by its matched load is given by,

$$P_A = \frac{1}{2} \int_{\Delta\nu} \int_{4\pi} \left(\frac{\partial S}{\partial \nu}\right)_{T_A} A(\Omega)\, d\Omega\, d\nu \tag{A-5}$$

where, $A(\Omega)$ is the effective aperture of the antenna in the direction of the incident rays, $\Delta\nu$ is the antenna bandwidth, and the factor 1/2 accounts for the assumption of unpolarized radiation.

Since the definition of antenna aperture implies[72]

$$G(\Omega) = \frac{4\pi\, S(\hat{\Omega})}{\int_{4\pi} S(\Omega)\, d\Omega} = \frac{4\pi\, A(\Omega)}{\lambda^2} \tag{A-6}$$

where $G(\Omega)$ is the antenna gain in the direction of the rays, (A-5) may also be written, introducing (A-6) and (A-1),

$$P_A = \frac{1}{4\pi} \int_{\Delta\nu} \int_{4\pi} \frac{h\nu\, G(\Omega)}{\exp\left(\frac{h\nu}{kT_A}\right) - 1}\, d\Omega d\nu \tag{A-7}$$

and, for $kT_A \gg h\nu$ (Rayleigh-Jeans approximation)

$$P_A \approx \frac{kT_A \Delta\nu}{4\pi} \int_{4\pi} G(\Omega) d\Omega = kT_A \Delta\nu \tag{A-8}$$

which is formally identical to the expression of the Nyquist noise. Incidentally, if the antenna is connected to a load, the maximum value of noise power transferred to this load is

$$P_T = kT_A \Delta\nu \tag{A-9}$$

and occurs when the load is matched to the antenna.

In general, however, the radiating source has a limited extension, so that the antenna cannot be considered completely enclosed by an

isothermal surface. In this case, it is assumed that expression (A-5) is still valid, but now the brightness temperature, $T_B(\Omega,\nu)$, is considered to be a function of both angle and frequency.[79]

Thus, the antenna temperature is defined by

$$T_A = \frac{1}{4\pi\ k\Delta\nu}\int_{\Delta\nu}\int_{4\pi}\frac{h\nu\ G(\Omega)}{\exp\left(\frac{h\nu}{kT_B}\right)-1}\ d\Omega\ d\nu \qquad \text{(A-10)}$$

In the realm of the Rayleigh-Jeans approximation and for practical situations when T_B is essentially constant over the antenna bandwidth, Eq. (A-10) becomes

$$T_A = \frac{1}{4\pi}\int_{4\pi} T_B(\Omega)\ d\Omega \qquad \text{(A-11)}$$

In practice, the brightness temperature T_B of a radiating body is obtained by measuring the total antenna temperature, using (A-9) and (A-10) in the presence and absence of the source.

When the antenna beamwidth and the solid angle of the radiation source are such that the gain function subtending the source is constant and approximately equal to the maximum directive gain G_o, the effective antenna temperature may be expressed in terms of the brightness temperature distributions $T_{B\ source}$, $T_{B\ sky}$ and $T_{B\ earth}$ of the source, the sky and the portion of the earth viewed by the antenna minor lobes,

$$T_{AS} = \frac{1}{4\pi}\ G_o\Omega\ T_{B\ source} + \frac{1}{4\pi}\int_{sky} G(\Omega)\ T_{B\ sky}(\Omega)\ d\Omega + \frac{1}{4\pi}\int_{earth} G(\Omega)\ T_{B\ earth}(\Omega)\ d\Omega$$

$$= T_{source} + T_{sky} + T_{earth} \qquad \text{(A-12)}$$

where T_{AS} is the effective antenna temperature in the presence of radiation coming from the ground, which has a brightness temperature of about 290°K. In the case of antennas with a reflector this radiation enters directly into the feed horn, usually along paths close to the edge of the reflector and is called "spillover" radiation. All radiation received from directions other than the main beam, which also includes the spillover radiation is called, collectively, "minor-lobe radiation." The noise contribution of this minor-lobe radiation from the earth depends critically on the type of antenna and its feed system and may vary from as low as a few degrees to as high as an appreciable fraction of 300°K.

At shorter microwave wavelengths and at millimeter and submillimeter wavelengths, where antennas have good resolution, the gain function is not always necessarily constant over the solid angle subtending the sources.

In this case, Eq. (A-12) must be rewritten as

$$T_{AS} = \frac{1}{4\pi}\int_{source} G(\Omega)\, T_{B\ source}(\Omega)\, d\Omega + \frac{1}{4\pi}\int_{sky} G(\Omega)\, T_{B\ sky}(\Omega)\, d\Omega$$

$$+ \frac{1}{4\pi}\int_{earth} G(\Omega)\, T_{B\ earth}(\Omega)\, d\Omega$$

$$= T_{source} + T_{sky} + T_{earth} \qquad \text{(A-13)}$$

The effective antenna temperature in the absence of the radiation source is only determined by the second and third terms in (A-13) only.

At millimeter and submillimeter wavelengths, where water vapor and oxygen resonance absorption create a lossy atmosphere, the observed

antenna temperature in the realm of the R-J approximation may be expressd then as

$$T_{AS}' = \left(1 - \frac{1}{L_o}\right) T_{at} + \frac{1}{L_o} (T_{source} + T_{sky}) + T_{earth} \qquad \text{(A-14)}$$

where T_{at} is the average temperature of the atmosphere and L_o is the loss factor of propagation,

$$L_o = \exp\left(\int_{h_o}^{\infty} \alpha (h) \sec \theta \, dh\right) \qquad \text{(A-15)}$$

with $\alpha(h)$ the attenuation coefficient of the atmosphere, h_o is the observation height and θ the angle at which the wavepath is inclined with respect to the zenith.

The above formulas are used to calculate data such as given in certain figures of Chapter II.

If α_1 and α_2 denote the fractional absorption coefficients of the antenna and the connecting waveguide which are assumed to be at the ambient temperature T_o, then the effective antenna temperature T_{AR} at the receiver terminals will be,

$$T_{AR} = (1 - \alpha_2) \left[(1 - \alpha_1) T_A + \alpha_1 T_o\right] + \alpha_2 T_o \qquad \text{(A-16)}$$

$$T_{AR} = (1 - \alpha_1) (1 - \alpha_2) T_A + \alpha_1 (1 - \alpha_2) T_o + \alpha_2 T_o \qquad \text{(A-17)}$$

Thus, $(1 - \alpha_1) (1 - \alpha_2) T_A$ is proportional to the noise power which reaches the receiver due to the effective antenna temperature. $\alpha_1(1 - \alpha_2)T_o$ is proportional to the noise power reaching the receiver that is emitted by the ohmic losses of the antenna. $\alpha_2 T_o$ is proportional

to the noise power reaching the receiver emitted by the ohmic resistance of the waveguide. When α_1 and α_2 are negligible $T_{AR} \simeq T_A$.

11.A.3 Application of Radiometers

The purpose of a radiometer is to detect radiation in a given frequency region and from this to determine the equivalent black body temperature of the source. The important parameters of a radiometer are:

1) the receiver sensitivity

2) the antenna spatial resolution.

The sensitivity of a radiometer can be specified either in terms of the minimum power change, or in terms of the minimum equivalent black body temperature change which it is able to detect. The relation between these two quantities may be obtained from (A-7), i.e.

$$\frac{\Delta P}{\Delta T} = \frac{1}{4\pi} \int_{\Delta\nu} \int_{4\pi} \frac{h^2 \nu^2 G(\Omega) \exp\left(\frac{h\nu}{kT}\right)}{kT^2 \left[\exp\left(\frac{h\nu}{kT}\right) - 1\right]^2} \, d\Omega d\nu = k\beta\Delta\nu \qquad \text{(A-17)}$$

Note that when $h\nu \ll kT$, and the beamwidth of the antenna is smaller than the angular dimension of the source, then

$$\beta \rightarrow 1 \qquad \text{(A-18)}$$

According to the technique used, ultramicrowave radiometers have been distinguished[73] as coherent or incoherent radiometers. A coherent radiometer is a generalization of a device known as the Dicke radiometer and makes use of a superheterodyne receiver (utilizing "coherent" detection) such as shown in Fig. A.1. At present, in radiometers below 100 GHz

the local oscillator operates at its fundamental frequency; above 100 GHz harmonic mixing is used.[74]

The minimum detectable power of Dicke's radiometer may be expressed by[75-76]

$$\Delta P_m = \alpha \frac{F - 1}{\sqrt{B\tau}} N_o + \Delta N \qquad \text{(A-19)}$$

where N_o is the ambient noise power

F is the total noise figure of the receiver

B is the IF bandwidth

τ is the integration time after detection

α is the noise factor of detector

ΔN is the difference of noise power commuting from the reference source to the background.

If ΔN is set equal to zero and the following equivalents are used

$$\Delta P_m = kB\Delta T$$

$$\alpha(F-1)N_o = kBT_{AR}$$

one obtains Eq. 2.10 of Chapter II, i.e.

$$\Delta T = \frac{T_{AR}}{\sqrt{B\tau}} \qquad \text{(A-20)}$$

The values of (A-19) and (A-20) are usually minimized by making B and τ as large as possible. The spatial resolution sensitivity of the coherent radiometer is dictated by diffraction.

11.A.4 Radiometer Characteristics

Table A-I presents a list of state-of-the-art sensitivity obtained by microwave radiometers. These are capable of detecting changes

TABLE A-I

STATE OF THE ART RADIOMETERS

Coherent

Frequency GHZ	L.O	mixer	B MHz	τ sec	F db	ΔT_o K	ΔP watt	Ref.
19	Klystron (fundamental)	tunnel-diode	500	1	7.5	1.10^{-1}	$7.\ 10^{-16}$	77
35	solid state (fundamental)	balanced crystal	500	1	16	3.10^{-1}	$2\ 10^{-15}$	2
70	Klystron (fundamental)	crystal	800	10	18	3.10^{-1}	$3.5\ 10^{-15}$	2
94	Klystron (2 harmonic)	crystal	500	1	20	2°	$1.4\ 10^{-14}$	77
140	Klystron (2 harmonic	crystal	1,500	10	26	2°	$3x\ 10^{-14}$	2
225	Klystron (3 harmonic)	crystal	1,500	10	30	5°	10^{-14}	2
600	Carcinotron (2 harmonic)	crystal	1,500	10	33	11°	$2.3\ 10^{-13}$	78

Incoherent

Frequency GHZ	Detector	Antenna Gain Efficiency	B MHz	sec		ΔT	ΔP	Ref.
850	Low type	$6.4\ 10^{-3}$	66,000	5		0.2	$1.6\ 10^{-11}$	27
850	Golay type	$6.4\ 10^{-3}$	66,000	10		23°	$1.6\ 10^{-9}$	27

of effective antenna temperature of ten degrees or less with greater than 95% certainty when using an effective video bandwidth of one cycle (or an observation and integration time of one second).

Above 100 GHz, where the lack of oscillators and point contact detectors hampers the construction of microwave radiometers, far-infrared radiometers may be used by the extension of techniques commonly employed in the infrared.

A diagram of a typical far-infrared radiometer is sketched in Fig. A-2. The input frequency selector, called a monochromator, generally consists of a diffraction of echelette grating, combined with a transparency filter (i.e., black polyethylene, crystal quartz, etc.) which eliminates the higher order diffraction pattern. (This is the reason why this type of radiometer is also referred to as a quasi-coherent radiometer).

It may appear that in the far-infrared radiometer the simplest signal modulation would be a rotating chopper placed along the path of radiation. However, in this case the noise compensation, which is easily performed in the Dicke radiometer, becomes a difficult task. The modulation therefore requires, in addition, the provision of an interferometric device such as a movable reflector (Michelson) or a lamellar grating with variable groove depth (see Fig. A-3). Two typical interferometric modulators, one aperiodic and the other periodic, are shown in Fig. A-4b and Fig. A-4a, respectively. The aperiodic interferometer requires a video amplifier and a digital computer, while the periodic interferometer is simpler at equal sensitivity. In both cases the minimum detectable power may be expressed by Eq. A-12.[79] In this case, however, the noise power

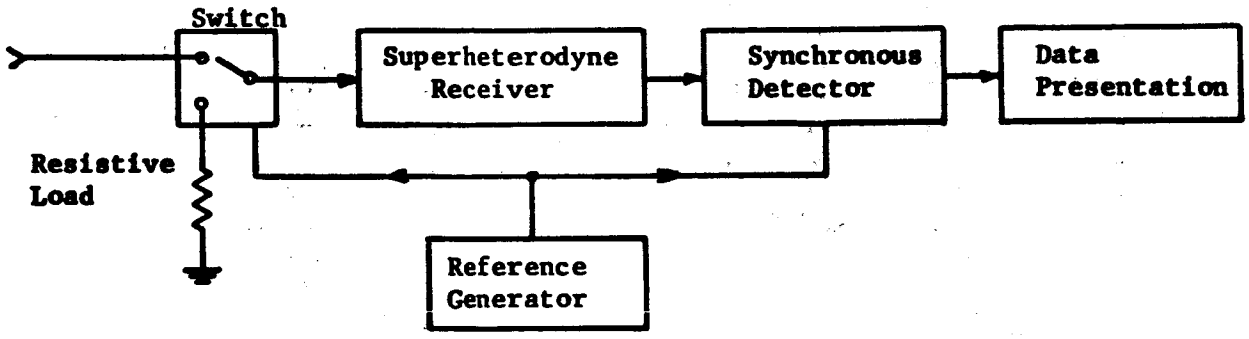

Figure A.1 Microwave Radiometer

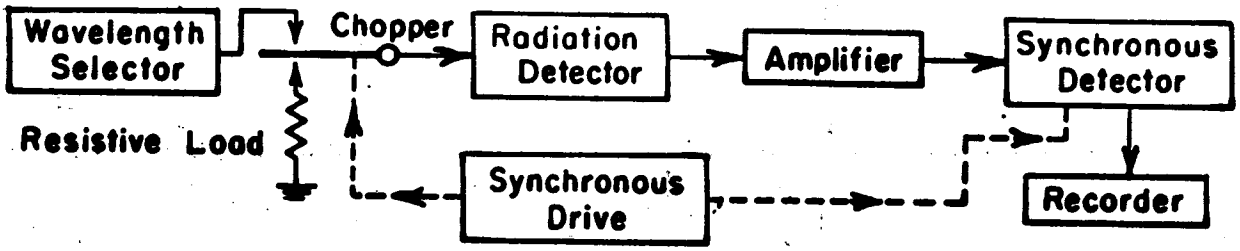

Figure A.2 Far-Infrared Radiometer

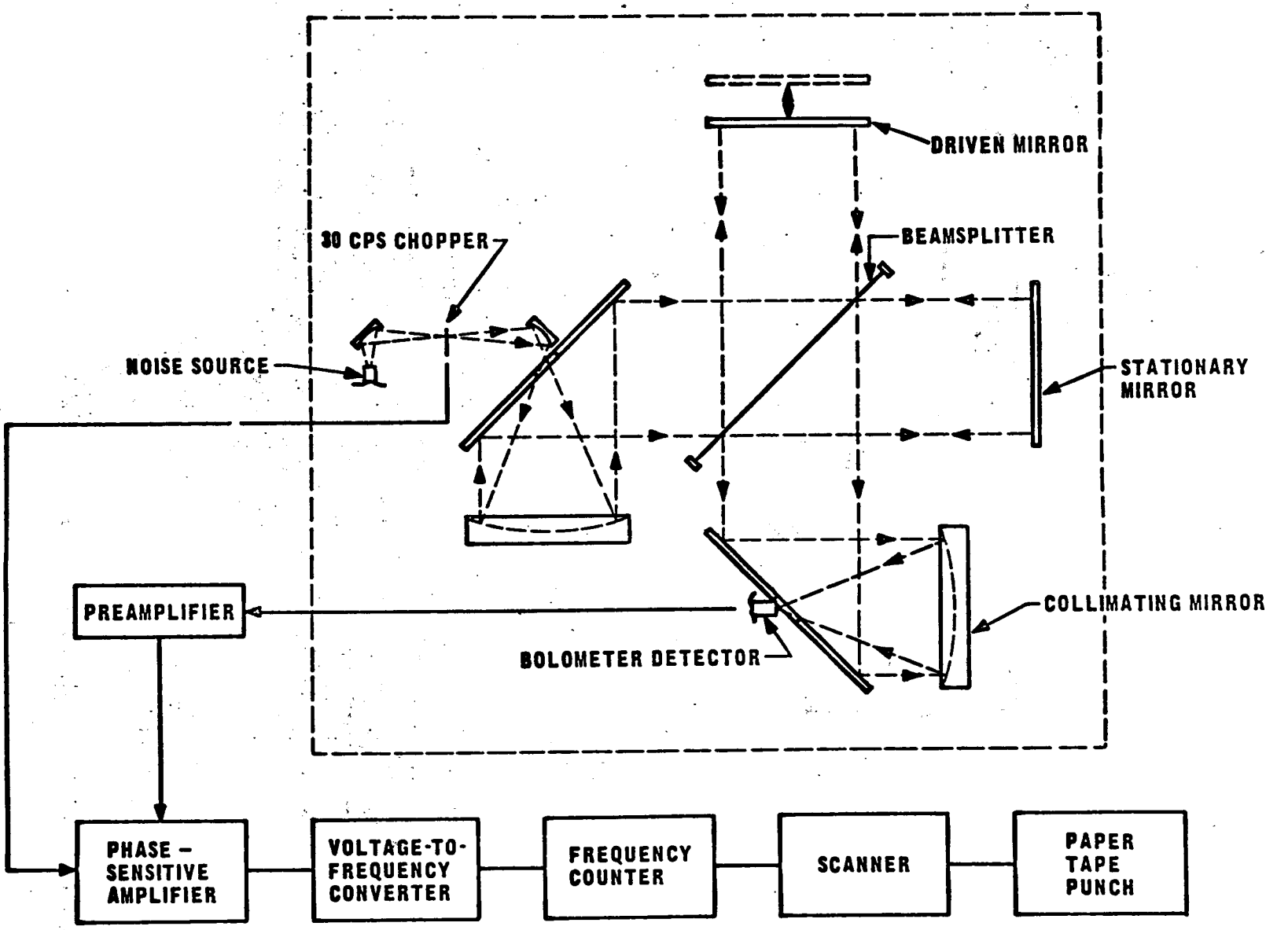

Figure A.3 Schematic of Spectrometer and Block Diagram of Output and Data Recording Equipment

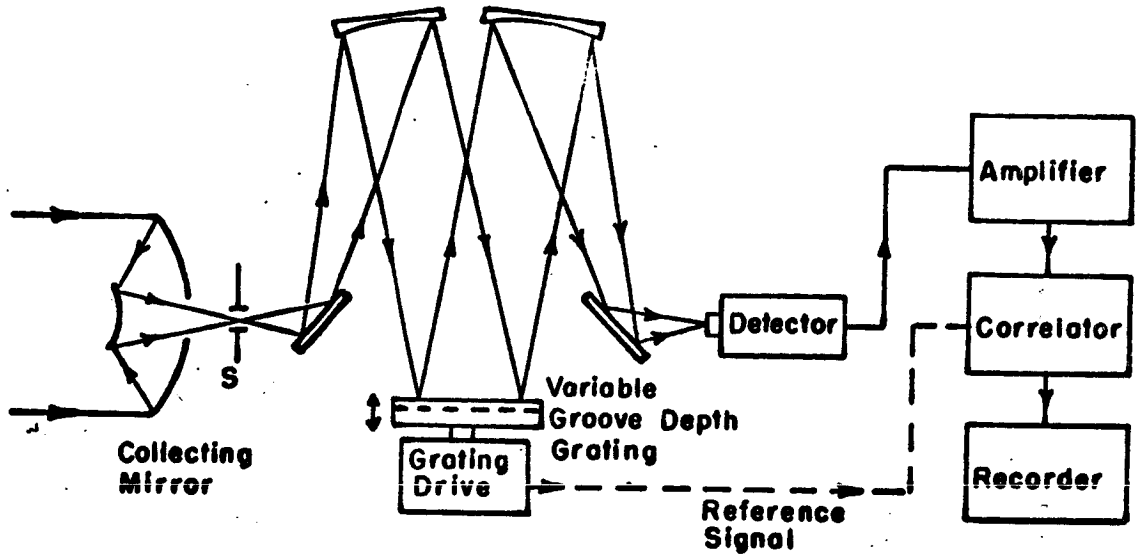

Figure A.4a Lamellar grating type of an interferometric radiometer

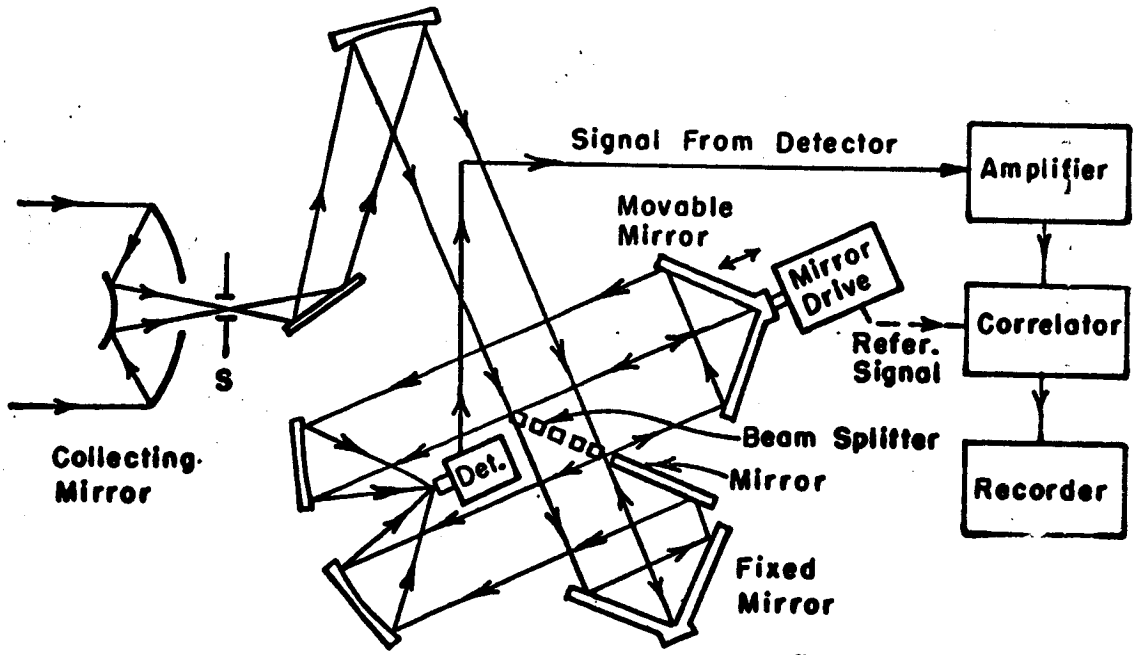

Figure A.4b Michelson type of interferometric radiometer using corner mirrors to eliminate light loss

level at the detector input is related to the total noise power spectral density, and the integration time is inversely proportional to the spectral pass-band. In the aperiodic case the minimum detectable power is optimized by slowing down the scan velocity, and in the periodic case by lengthening the integration time.

In the incoherent radiometer the detector is generally thermal (superconductive thin film bolometer, gallium-doped germanium bolometer, Golay cell) or photoconductive (indium-antimonide detector) as discussed in Chapter IX. These detectors receive the radiating energy directly on their surface, which has a finite area. This differentiates them from point contact detectors used in coherent radiometers, where the detector is a part of a lumped circuit. In the far-infrared radiometer, instead, the detector must be participating in some way toward the pick-up function of the antenna. Because of the finite area of the detector, the gain of the antenna beam is limited by phenomena of geometrical optics rather than by diffraction.

In this case it has been shown[70] that if the beamwidth of the antenna is smaller than the angular dimension of the source, the incoherent radiometer is more sensitive to temperature change than the coherent radiometer, for the same sensitivity to changes of received power.

REFERENCES TO CHAPTER XI

1. M. M. Rosenthal, "Millimeter radiometry applied to navigation," Technical News Bulletin, General Precision Aerospace, Vol. 8, No. 3, 1965, p. 18.

2. K. A. Richer, D. A. Bauerle, "Near-earth millimeter wave radiometer measurements," Ballistic Research Laboratories, Aberdeen Proving Ground, Maryland, Report No. 1267, December, 1964, ASTIA A65-12018.

3. W. H. Conway, A. Mardon, "Microwave radiometers for ocean and weather measurements," Proceedings of the 1964 Oceanographic Conference, Woods Hole, Mass.

4. A. Stogryn, "The apparent temperature of the sea at microwave frequencies," Space General Company, El Monte, California, March 2, 1966.

5, H. G. Pascolar, R. T. Sakamoto, "Microwave radiometer measurements of ice and water," Third Symposium on Remote Sensing of the Environment, Institute of Science and Technology, University of Michigan, Ann Arbor, Mich., October, 1964.

6. K. N. Wulfsberg, "Apparent sky temperatures at millimeter-wave frequencies," Microwave Physics Laboratory, Air Force Cambridge Research Laboratory, Hanscom Field, Mass. Technical Report 64-590, July, 1964.

7. A. P. Stogryn, "Effect of scattering by precipitation on apparent sky temperature in the microwave region," Space General Company, El Monte, California, Technical Report No. 613 TM-1, 25 Sept. 1964.

8. E. J. Dutton, R. R. Beam, "The Bi-exponential nature of tropospheric gaseous absorption of radio waves," Radio Science, Vol. 69, No. 6, June, 1965, p. 885.

9. E. R. Westwater, "Ground-based passive probing using the microwave spectrum of oxygen," Radio Science, Vol. 69D, No. 9, September, 1965, p. 1201.

10. E. C. May, A. B. Kahle, "On the satellite determination of high altitude water vapor," Journal of Geophysical Research, Vol. 69, No. 19, October, 1964, pp. 4141.

11. N. Nicolet, "Nitrogen oxides in the chemosphere," Journal of Geophysical Research, Vol. 70, No. 3, February, 1965, pp. 679.

12. J. J. Gallagher, C. M. Johnson, "Uncoupling effects in the microwave spectrum of nitric oxide," Physical Review, Vol. 103, No. 6, September, 1956, pp. 1727.

13. J. J. Martin, "Atmospheric re-entry," Prentice Hall, Inc., Eaglewood Cliffs, N. J., 1966, pp. 20 and 25.

14. T. A. Mutch, "Volcanic ashes compared with paleozoic salts containing extra-terrestrial spherules," Journal of Geophysical Research, Vol. 69, No. 22, November, 1964, pp. 4735.

15. R. K. Soberman, C. L. Henenway, "Meteoric dust in the upper atmosphere," Journal of Geophysical Research, Vol. 7, No. 19, October, 1965, p. 4943.

16. R. D. Southworth, "The size distribution of the zodiacal particles," Annals of the New York Academy of Sciences, Vol. 119, November, 1964, pp. 54.

17. W. L. Webb, "Morphology of noctilucent clouds," Journal of Geophysical Research, Vol. 70, No. 18, Sept. 1965, pp. 4463.

18. P. W. Hodge, F. W. Wright, C. C. Lanway, "Studies of particles of extra-terrestrial origin," Journal of Geophysical Research, Vol. 69, No. 14, July, 1964, pp. 2919.

19. G. S. Hawkins, "Interplanetary debris near the earth," Annual Review of Astronomy and Astrophysics, Vol. 2, 1964, pp. 149.

20. G. Colombo, G. Fiocco, "Optical radar results and meteoric fragmentations," Smithsonian Institution Astrophysical Observatory Special Report 139, October, 1963.

21. T. Laevastu, O. Mellis, "Size and mass distribution of cosmic dust," Journal of Geophysical Research, Vol. 66, No. 8, August, 1961, pp. 2507.

22. G. Colombo, I. I. Shapiro, D. A. Lautman, "The earth's dust belt," Journal of Geophysical Research, Vol. 71, No. 23, December 1, 1966, p. 5695.

23. C. W. Snyder, M. Neugebauer, "Interplanetary solar-wind measurements by Mariner II," Proceedings of the Fourth International Space Science Symposium, Warsaw, June 4-10, 1963, North Holland, Pub. Co., Amsterdam, 1964, p. 89.

24. O. L. Yanovler, A. I. Yefimov, K. M. Shvachkin, "Attenuation of radio waves in the interplanetary space and in the space about the sun," Soviet Radio Engineering and Electro-physics, Nov. 4, 1966, p. 528.

25. S. I. Averkov, V. I. Ryadov, V. Y. and N. I. Furashov, "Astronomical station for far-infrared observations," Soviet Astronomical Journal, Vol. 8, 1964, p. 422.

26. J. N. Gaitskell, A. E. Gear, "Solar and lunar observations at submillimeter wavelengths," Icarus, Vol. 5, No. 3, May, 1966, p. 237.

27. J. A. Bastin, A. E. Gear, G. O. Jones, H. J. T. Smith, P. J. Wright, "Spectroscopy at extreme infrared wavelengths," Proc. Roy. Soc. (London), Vol. A278, 1964, p. 543.

28. R. A. Williams, W. S. C. Chang, "Observation of solar radiation from 50 microns to 1 mm," Proc. IEEE, Vol. 54, No. 4, April, 1966, p. 462.

29. A. Boischot, J. F. Denisse, "Solar radio astronomy," Advances in Electronics and Electron Physics, Vol. 20, 1964, Academic Press, N. Y., p. 147.

30. W. A. Stein, E. P. Ney, "Continuum electromagnetic radiation from solar flares," Journal of Geophysical Research, vol. 68, No. 1, 1 Jan. 1963, p. 65.

31. R. J. Coates, "Solar observations at millimeter wavelengths," Proc. IEEE, Vol. 54, No. 4, April 1966, p. 471.

32. P. M. Kallegahan, "Solar observations at a wavelength of 8.6 millimeters," North East Electronics Research and Engineering Meeting, November, 1966.

33. W. T. Sullivan, III, "Solar observations at millimeter wavelengths," NEREM, November, 1966.

34. R. J. Coates, "Spectra of millimeter wavelength solar bursts," NEREM, November, 1966.

35. C. W. Tolbert, L. C. Krause, A. W. Straiton, "Solar radiation at the 3.2 mm during the July 20, 1963, eclipse," Astrophysical Journal, Vol. 140, No. 1, July, 1964, p. 306.

36. F. J. Low, A. W. Davidson, "Lunar observations at a wavelength of 1 millimeter," Astrophysical Journal, Vol. 142, No. 1, July, 1965, p. 1279.

37. B. C. Murray, L. R. Wildey, "Stellar and planetary observations 10 microns," Astrophysical Journal, Vol. 137, No. 1, January, 1963, p. 692.

38. V. L. Lynn, M. D. Sohigian, E. A. Crocker, "Radar observations of the moon at a wavelength of 8.6 millimeters," Journal Geophysical Research, Vol. 69, No. 4, Feb. 15, 1964, p. 781.

39. U. F. Weaver, S. Silver, "Planetary research in the millimeter and infrared region of the spectrum," U.R.S.I. General Assembly, XIV, Vol. 8, Space Radio Science, Tokyo, Japan, Sept. 15-20, 1963, p. 71.

40. N. I. Ananov, A. Y. Basharinov, K. P. Kirdjashev, B. G. Kutuza, "Fluctuations of the radiofrequency radiation of a cloudy atmosphere in the millimeter wavelength region," Radiotekhnika i Elektronika, (Eng. Ed.), No. 11, Nov. 1965, p. 1658.

41. A. H. Barrett, "Passive radio observations of Venus, Saturn, Mercury, Mars and Uranus," Radio Science, Vol. 69D, No. 12, December, 1965, p. 1565.

42. J. W. Meyer, "Radar astronomy at millimeter and submillimeter wavelengths," Proc. IEEE, Vol. 54, No. 4, April, 1966, p. 484.

43. C. H. Mayer, "Introductory review of the radio emission of the planets," Space Research, Vol. III, North Holland, New York, 1963.

44. A. H. Barrett, A. E. Lilley, "Mariner 2 microwave observations of Venus," Sky and Telescope, Vol. XXV, No. 4, April, 1963, p. 192.

45. C. W. Tolbert, A. W. Straiton, "35 GHz/s and 94 GHz/s cytherean radiation," Nature, Vol. 204, No. 4965, 26 Dec. 1964, p. 1242.

46. D. H. Staelin, E. C. Reifenstein, "K-band observations of Venus and Jupiter during 1966," NEREM, November, 1966.

47. D. H. Staelin, et al, "Spectral observations of Venus near 1 centimeter wavelength," Astrophysical Journal, April, 1966, p. 352.

48. W. E. Howard, S. P. Maran, "General catalogue of discrete radio sources," Astrophysical Journal, Supplement Series, N. 93, Vol. X, March, 1965.

49. C. W. Tolbert, "Millimeter wavelength spectra of the crab and orion nebulae," Nature, Vol. 206, No. 4991, 26 June 1965, p. 1304.

50. C. W. Tolbert, A. W. Straiton, "An investigation of tau A and S.G.R. a millimeter wavelength radiation," Office of Aerospace Research, Air Force Cambridge Research Laboratory, Bedford, Mass., Report β6-61, 28 August 1964.

51. W. L. Ginzburg, S. I. Syrovatskii, "Cosmic Magnetobremsstrahlung (Synchrotron Radiation)" Annual Review of Astronomy and Astrophysics, Vol. 3, Annual Reviews, Inc., Palo Alto, Calif., 1965, p. 297.

52. J. W. M. Baars, P. G. Mezger, H. Wendner, "The spectra of the strongest non-thermal radio sources in the centimer-wavelength range," Astrophysical Journal, Vol. 142, No. 1, July 1, 1965, p. 122.

53. G. Neugebauer, D. E. Martz, R. B. Leighton, "Observations on extremely cool stars," Astrophysical Journal, Vol. 142, No. 1, July 1, 1965, p. 399.

54. N. H. Dieter, W. M. Goss, "Recent work on interstellar medium," Reviews of Modern Physics, Vol. 38, No. 2, April, 1966, p. 256.

55. T. P. Stecher, D. A. Williams, "Interstellar molecular formation," Astrophysical Journal, Oct. 1966, p. 88.

56. H. C. Van de Hulst, "Radiowaves from space," Ned. Tijdschr. Naturk., Vol. 11, 1946, p. 210.

57. A. E. Lilley, P. Palmer, H. Penfield, B. Zuckermann, "Radio astronomical detection of helium," Nature, Vol. 211, No. 5045, 9 July 1966, p. 174.

58. A. E. Lilley, D. H. Menzel, H. Penfield, B. Zuckermann, "Detection of h. emission lines," Nature, Vol. 209, No. 5022, 29 Jan. 1966.

59. A. H. Barrett, "The detection of the OH and other molecule lines in the radio spectrum of the interstellar medium," IEEE Trans. on Antennas and Propagation, Vol. A.P.12, No. 7, Dec. 1964, p. 822.

60. N. H. Dieter, H. Weaver, "The interstellar hydroxyl radio emission," Sky and Telescope, Vol. XXXI, No. 3, March, 1966, p. 132.

61. D. D. Cudabauk, "Diameter and portion of three sources of 18 cm OH emission," Phys. Review Letters, 22 August 1966, p. 452.

62. M. M. Litvak, A. L. McWhorter, M. L. Meeks, H. J. Zeiger, "Maser model for interstellar OH microwave emission," Phys. Review Letters, Vol. 17, 10 Oct. 1966, p. 821.

63. G. H. Hebig, "The diffuse interstellar bands I. A possible identification of λ 4430," Astrophysical Journal, Vol. 137, 1963. p. 200.

64. R. H. Dicke, P. J. E. Peebles, P. G. Roll, D. T. Wilkenson, "Cosmic black body radiation," Astrophysical Journal, Vol. 142, No. 1, July 1, 1965, p. 414.

65. A. A. Penzias, R. W. Wilson, "A measurement of excess antenna temperature at 4080 MHz/s," Astrophysical Journal, Vol. 142, No. 1, July 1, 1965, p. 419.

66. P. G. Roll, D. T. Wilkinson, "Cosmic background radiation at 3.2 cm," Phys. Review Letters, Vol. 16, No. 10, 7 March 1966, p. 405.

67. B. G. Field, J. L. Hitchcock, "Cosmic black body radiation at $\lambda = 2.6$ mm," Phys. Review Letters, Vol. 16, No. 18, 2 May 1966, p. 819.

68. J. Stefan, "On the relation between heat radiation and temperature," Fortschritt. Physik, 1879, p. 660.

69. T. P. Merritt, F. F. Hall, "Black body radiation," Proc. IRE, Vol. 47, No. 9, Sept. 1959, p. 1435.

70. R. A. Williams, W. S. C. Chang, "An analysis of the interferometric submillimeter radiometer," Ohio State University Research Foundation Report 1093-9-23, July, 1962, p. 4.

71. R. H. Dicke, "The measurement of thermal radiation at microwave frequencies," Review of Scientific Instruments, Vol. 17, No. 7, July, 1946, p. 268.

72. C. T. Tai, "On the definition of the effective aperture of antennas," IRE Antenna and Propagation Transactions, Vol. A. P. 9, No. 2, March, 1961, p. 224.

73. F. J. Low, "Thermal detection radiometer at short millimeter wavelengths," Proceedings of the IEEE, Vol. 54, No. 4, April, 1966, p. 477.

74. R. S. Ohl, P. P. Budenstein, C. A. Burrus, "Improved diode for the harmonic generation of millimeter and submillimeter waves," Review of Scientific Instruments, Vol. 30, September, 1959, p. 765.

75. P. D. Strum, "Considerations in high-sensitivity microwave radiometry," Proceedings, I.R.E., Vol. 46, No. 1, January, 1958, p. 43.

76. F. D. Drake, H. I. Ewen, "A broadband microwave source comparison radiometer for advanced research in radio astronomy," Proceedings I.R.E., Vol. 46, No. 1, January, 1958, p. 53.

77. Space General Report SGC, p. 6332, 1966.

78. S. V. Chang, J. D. Lester, "Radiometric measurements of atmospheric absorption at 600 Gc/s", Proceedings of the IEEE, Vol. 54, No. 4, April, 1966, p. 459.

79. R. A. Williams, W. S. C. Chang, "Radiometry in the submillimeter region using the interferometric modulator," IEEE Trans. on microwave theory and techniques, Vol. MTT-11, No. 6, November, 1963, p. 513.

Chapter XII

MILLIMETER AND SUBMILLIMETER WAVE MEASUREMENTS

12.1 INTRODUCTION

As one goes up in frequency from the microwave region, the applicable techniques for measurement change. Most of the standard rectangular waveguide components are available up through 220 GHz; however, the cost is high, and the precision and performance are limited. Complete measuring systems for determining attenuation, phase shift, etc. are also available. In the less conventional waveguiding systems such as dielectric image, V-lines, overmoded circular and rectangular waveguides, etc., standardized components are, in general, not available. Consequently, to use such waveguides the investigator must devise and fabricate his own components. This places a limitation on what he can do with such lines without a very large peripheral effort.

The millimeter wave region mainly utilizes techniques extended upward in frequency from the microwave region. Scaled versions of klystrons and magnetrons are available to provide signal power; rectangular waveguide and corresponding components are utilized and crystal mixers and detectors still function adequately for some purposes.

At the submillimeter wavelengths, however, one appears to be reaching the limit to which conventional microwave techniques can be pushed, as pointed out elsewhere in this report. Here one also encounters the extension of optical and infrared techniques downward in frequency. Hence in this region the use of ray optics in analyses often

is preferred to the solution of Maxwell's equations. In the laboratory, gratings, prisms, quarter-wave plates, and other tools of optics take the place of their waveguide equivalents. At the same time, one finds quantum generators and detectors being considered for application. Thus in the millimeter and submillimeter range are found a fusion of techniques derived from the spectral regions on either side.

12.2 QUANTITIES TO BE MEASURED

The fundamental quantities which must be measured are, as in the microwave region, power and frequency (or wavelength). Other quantities of possible interest are impedance, phase, reflection coefficient, transmission coefficient, polarization, etc.

12.3 LIMITATIONS OF EXISTING TECHNIQUES IN GENERAL

We may characterize radio frequency measurement systems as active or passive techniques, according to whether the signal source is a part, or is not a part of the measuring system. In active systems the necessity of having a source may pose a serious limitation in the millimeter/submillimeter region because of restricted outputs available with respect to source and frequency and with respect to cost. The dollars-per-milliwatt figure assumes very high values above 100 GHz. Table 12.I lists the availability of sources in the millimeter/submillimeter region of the spectrum.

The increasing difficulty of using conventional waveguides at the higher frequencies has already been mentioned. The principal feature which degrades their utility is the high value of attenuation attained. For example, rectangular waveguide for the 220-325 MHz range typically

TABLE 12.I

Availability of Laboratory Sources for

Millimeter and Submillimeter Wave Measurements

	Frequency in GHz								
	26.5-40	33-50	50-75	60-90	90-140	110-170	140-220	220-325	>325
Reflex Klystrons	x	x	x	x	x	x			
Floating Drift Klystrons	x	x	x	x					
Magnetrons	x	x	x	x					
BWO	x	x	x	x	x	x	x	x	
Lasers									x
Harmonic Gen	x	x	x	x	x	x	x	x	
Packaged Sig Gen	x	x	x						
Packaged Oscillators	x	x	x						
Packaged Sweep Gen	x	x	x						
Random Noise Gen	x	x	x	x	x	x			

has a theoretical attenuation of 4.05 dB per foot for pure copper. It is well known that actual waveguides seldom behave as well as theoretically predicted. Oxidation, dirt, oil films, surface imperfections, and misalignment can cause significant degradation of calculated values. The high attenuation decreases the overall sensitivity of a detection system and may significantly restrict the flexibility of the experimental arrangement.

Most of the alternates to rectangular waveguide that have been proposed for the super-high frequencies have been evolved to provide a lower attenuation value. Unfortunately, in attaining improved performance

in this area, they have in general lost the convenient geometry that led to useful waveguide components. Consequently, waveguide systems for measurement in the millimeter/submillimeter region leave much to be desired, even in those ranges where standard guides exist.

If one turns to overmoded waveguide (circular or rectangular) or to beam waveguide, the attenuation problem diminishes greatly in so far as wall losses are concerned; however, the design of components becomes more complex. Furthermore, at submillimeter frequencies atmospheric attenuation can be important. If the guiding system is enclosed, it can be evacuated or filled with inert gas. This adds complication to the system.

12.4 OBJECTIVES IN MEASUREMENT

Any method of measurement has the following attributes which influence its suitability for a particular application:

1. accuracy
2. calibratability
3. stability
4. utilizability
5. ease of construction
6. ruggedness
7. cost

Definitions of these are available from textbooks on electrical measurement. The foregoing paragraphs have indicated that accuracy, stability, ease of construction, and cost are of great concern in the millimeter/submillimeter range.

12.5 POWER MEASUREMENT

12.5.1 Calorimetry[1-25]

A standard method of power and energy measurement adaptable to all frequency ranges is calorimetry. In this method the energy to be measured is converted to heat, and the temperature rise of a calorimetric substance is measured. Commonly the latter is a liquid such as water or oil. However, there are many embodiments of the technique, some of which are "dry".

In the so-called static, liquid calorimeter, the energy to be measured is introduced and converted to heat in a region essentially surrounded by liquid. The latter is usually stirred so as to insure good heat transfer to it from the heat source. The temperature rise is almost exponential for a sustained input level. The energy components involved are given by

$$k\,\Delta U = M\,C_t\,\Delta T + \text{losses}$$

where k is the conversion factor from the input units (typically Joules) to kilogram calories ($k = 2.3889 \times 10^{-4}$ kg.-cal./Joule), ΔU is the energy input in Joules, M is the mass in kg., C_t is the specific heat in kg. cal./kg./$^{\circ}$C, and ΔT is the temperature rise in $^{\circ}$C. The losses must be evaluated by supplementary measurement and analysis and, in the equation shown, are expressed in kilogram calories.

To apply static calorimetry to power measurement it is necessary to accurately know the time interval during which power is applied. Thus we have

$$\Delta U = \int_{o}^{\Delta t} P \, dt$$

and

$$P_{av} = \frac{\Delta U}{\Delta t}$$

To remove the inaccuracies arising from the uncertainty in the values of M, C_t, and Δt, a comparison technique is usually used in which accurately known dc power is dissipated in the same or an identical structure within the calorimetric medium to achieve the same temperature rise as with the unknown power. This, of course, introduces a new error, but by careful design such substitution error can be made small.

Calorimetry modified in this way, and with other refinements, is considered a standard method for the measurement of microwave power and provides the basis for calibration at several frequencies by the National Bureau of Standards. The accuracy achieved by N. B. S. is of the order of 1%.

The dry calorimeter is more attractive to the ordinary laboratory. Here, the temperature rise of the dissipative element structure is directly measured by thermocouples attached to it. DC calibration can be used. Dry calorimeters are available commercially up to 220 GHz[23] and normally have overall accuracies of about 5%. Fundamentally there is no reason why dry calorimetry could not be used up into the

submillimeter region. However, the accuracy obtainable would be less because of increasing difficulty in maintaining matched conditions and because of increasing coupling losses.

The mismatch error arises from the fraction of incident power not converted to heat. The fraction of power not so converted is given by the square of the magnitude of the voltage reflection coefficient. The termination efficiency can thus be given very closely by

$$\eta = 1 - |\Gamma|^2 = \frac{4S}{(S + 1)^2}$$

where Γ is the reflection coefficient and S is the VSWR. A plot of this is shown in Fig. 12.1.

In addition to the above effect, one has to contend with the fact that some of the net input power will be dissipated in portions of the structure other than the region desired. As the frequency is raised, and conventional waveguide attenuation goes up, this effect becomes increasingly important, and it is a factor to be reckoned with in bolometry as well as calorimetry. The resulting error is termed the mount efficiency error. Clearly these factors will play important roles in power measurement in the millimeter/submillimeter wave region. Nevertheless, the validity of calorimetry as a basic technique is not destroyed.

12.5.2 Bolometry[26-39]

In bolometry the resistance change of a temperature-sensitive element is used as a measure of the heat causing the change. Commonly, substituted dc or low frequency power in the same unit is used as part

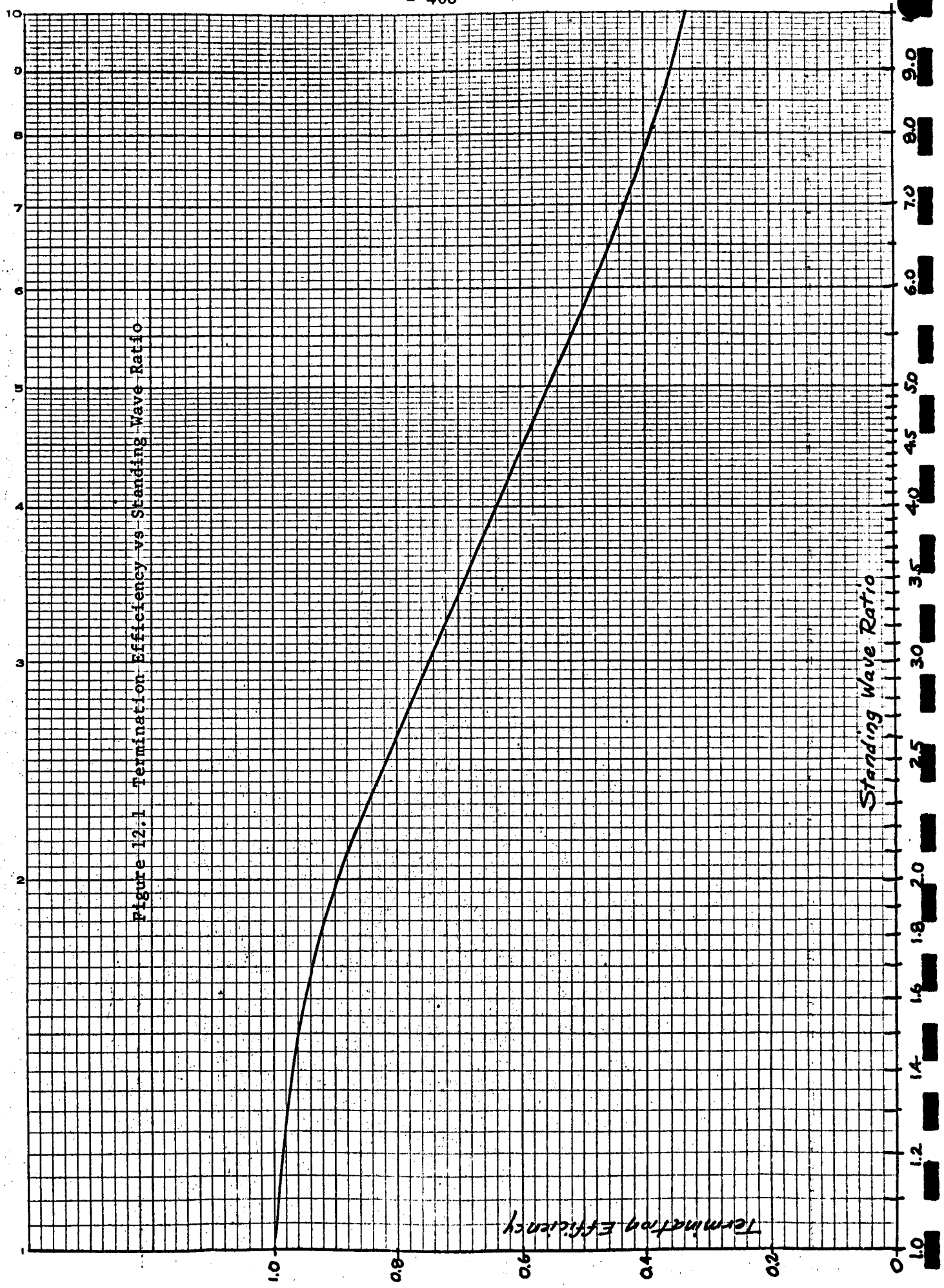

Figure 12.1 Termination Efficiency vs Standing Wave Ratio

EUGENE DIETZGEN
MADE IN U.S.A.
NO. 359-L110 DIETZGEN GRAPH PAPER
SEMI-LOGARITHMIC
1 CYCLE X 10 DIVISIONS PER INCH

of the measuring scheme. Generally the substitution and mount efficiency errors of bolometric devices are high relative to calorimeters. However, bolometer mounts can be calibrated against calorimetric standards to give high overall accuracies. Barretter or thermistor mounts are commercially available for frequencies up to 220 GHz. Figures 12.2 and 12.3 show minimum claimed mount efficiencies and typical mount efficiencies for several commercially available mounts. There are several other manufacturers making equipment in this range. The data given, however, are typical of all.

The choice of barretter or semiconducting thermistor at these frequencies is often dictated by what is available. If both types are available, the choice must be based upon the nature of the measurement to be made and the accuracy desired. Table 12.II shows a comparison of approximate characteristics taken from various sources.

TABLE 12.II

Comparison of Approximate Characteristics of Barretters and Semiconducting Thermistors

	Sensitivity Radio (ohms/mW)	Time Constant (msec)	drift (pts/^{o}C)	Max.Pwr. (mW)	Min.Det. Pwr.(W)
Barretter	4-120	0.1 - 0.5	1.5×10^{-3}	10-25	10^{-8}-10^{-9}
Thermistor	25-35	1000	1.8×10^{-2}	400	10^{-7}

At the frequencies under consideration here there is a considerable fabrication problem associated with whatever type of waveguide is used. In the small size waveguides this is caused by the tiny dimensions of the sensitive elements, whether they be of the barretter or of the

FIG. 12.2 MININUM CLAIMED EFFICIENCY OF THERMISTOR MOUNTS AS A FUNCTION OF FREQUENCY.

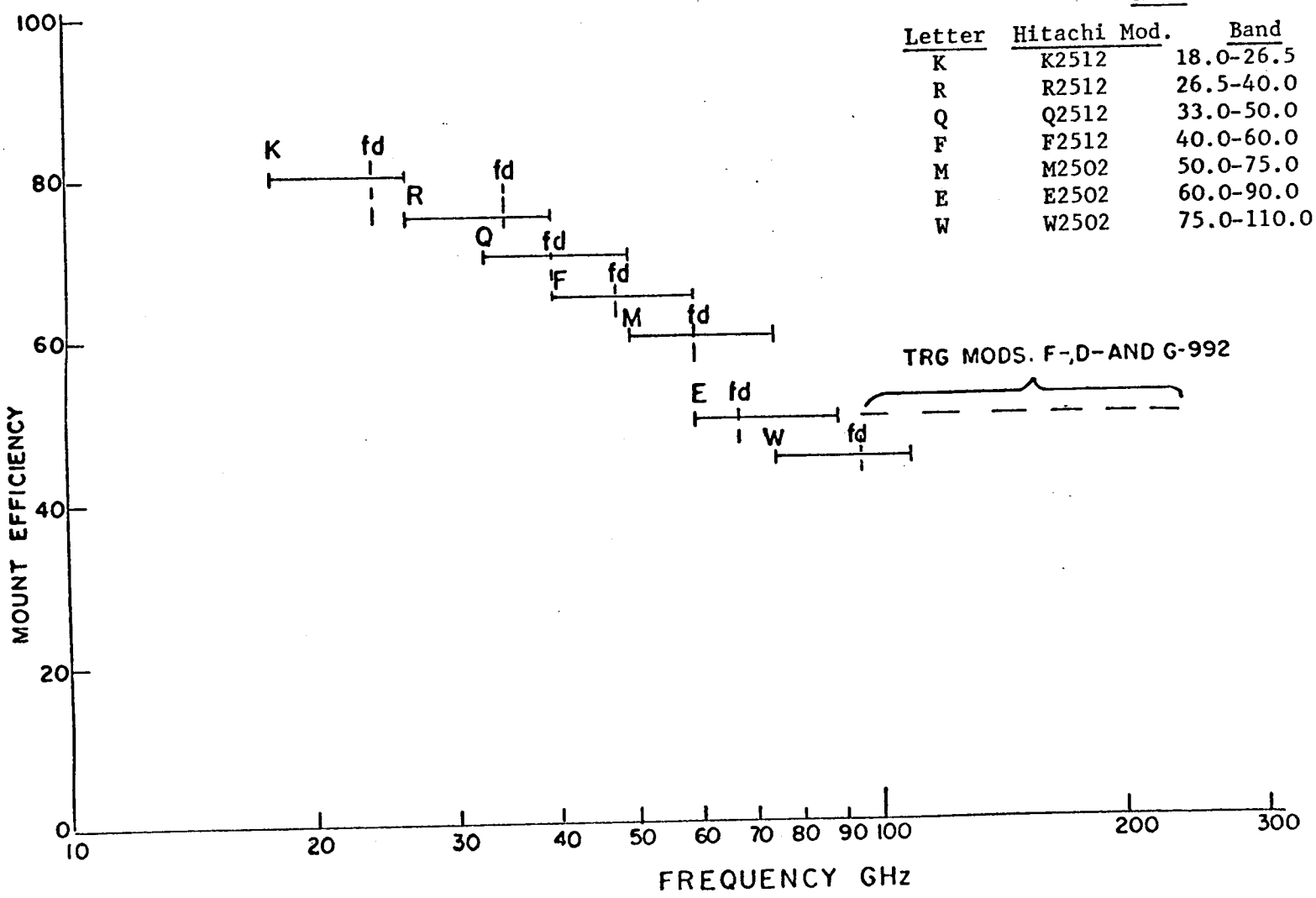

NOTE

Letter	Hitachi Mod.	Band	Design Freq.
K	K2512	18.0-26.5	24.0
R	R2512	26.5-40.0	35.0
Q	Q2512	33.0-50.0	40.0
F	F2512	40.0-60.0	48.0
M	M2502	50.0-75.0	60.0
E	E2502	60.0-90.0	68.0
W	W2502	75.0-110.0	96.0

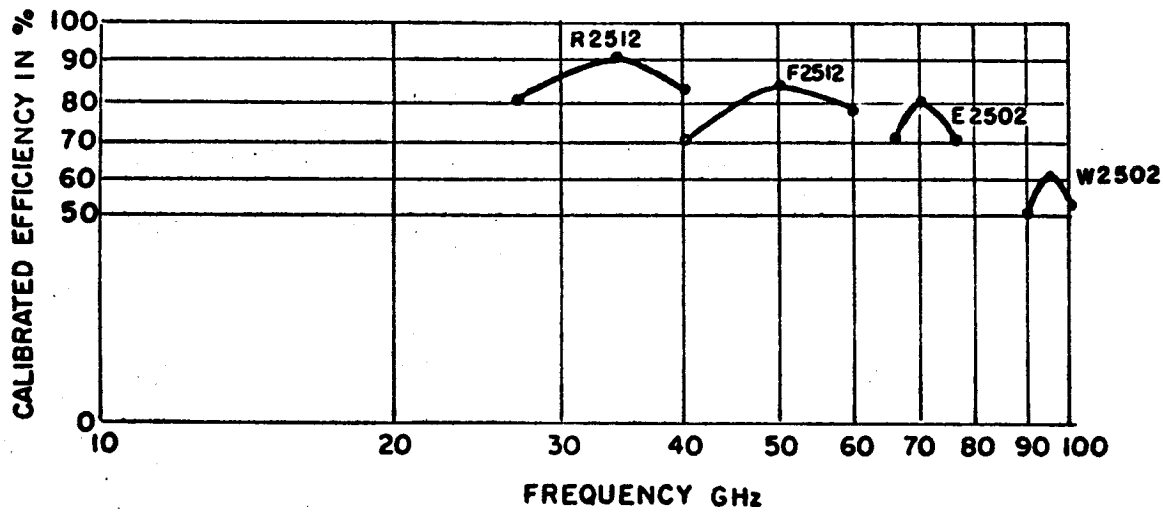

(FROM HITACHI 1966 CATALOG)

FIG. 12.3 TYPICAL DATA OF BOLOMETER MOUNT EFFICIENCY

semiconductor type. In overmoded waveguides the problem is to design a bolometer which will absorb all of the incident energy in all modes present without generating additional modes. There is also some evidence that despite the tiny size, skin effect plays a role in the behavior of both types.

The above remarks have been primarily directed at thin-wire and semiconductor bead bolometers. Another type that has been applied in the microwave range, and which holds some promise for the higher frequencies as well is the thin film bolometer.[40-41] A vacuum deposited thin film of platinum, nichrome, or other suitable material on a non-conducting substrate is mounted in the waveguide and forms the dissipative element. Typically, heavier deposits of gold provide the means of connecting to the external circuit. Thin film bolometers have been applied, at least experimentally, up to about 75 GHz. It appears that they might provide a usable technique for use in overmoded waveguides where the use of a thin-wire element might be disadvantageous due to mode conversion problems. Other thin film devices utilizing thermoelectric elements have also shown promise in the microwave region up to 35 GHz and probably can be used at higher frequencies.[42-45]

12.5.3 Force and Torque Methods[47-62]

The familiar radiometer, in which vanes blackened on alternate sides are suspended so that they can rotate in a region of reduced gas pressure, was invented by Sir William Crookes and forms the basis of a serious radiation measuring instrument in the ultraviolet through the far infrared region of the spectrum. By using a single vane suspended by a

quartz fiber and an optical beam from an attached mirror, extremely minute intensities have been measured, such as those of individual stars.[46]

Vane deflecting instruments of a different type have been developed in the microwave region and form the basis for a commercially available watt-meter for use at x-band.[47-50] In yet another type of instrument the interaction of the electromagnetic field with a suspended rod in a resonant cavity excites torsional oscillations, the amplitude of which is proportional to the exciting power. The technique has been applied to milliwatt levels of power measurement up to about 35 GHz.[24,25,55,56,60]

In the Acs power meter[61,62] incoming power is dissipated in an absorbing vane so mounted as to activate the motion of air by natural convection. The convective air flow is then detected and related to the incoming power. The principle has been applied to a commercially available x-band power meter in Hungary.

Little has been reported on the extension of any of these techniques to the millimeter/submillimeter region of the spectrum. It is very possible that force-torque methods could be used to provide an accurate instrument of reasonable sensitivity in this region.

12.5.4 Radiometers as Power Measuring Instruments

Radiometers are described in detail elsewhere in this report, hence, we shall not treat them in detail here. However it should be pointed out that besides providing means for making temperature and noise measurements on distant bodies, these instruments can be used for minute power measurements in the laboratory.

12.6 FREQUENCY AND WAVELENGTH MEASUREMENT

12.6.1 Resonant Structures

The familiar technique of using resonant cavities continues to be useful as the frequency is raised. Cavity wavemeters are commercially available up to 220 GHz. Above this frequency the technique can be used with increasing mechanical difficulties and with decreasing Q-values.

There is no reason, however, why enclosed cavities are always needed. In the optical and infrared regions of the spectrum open resonating structures are familiar. Actually, workers in these fields speak of interference patterns, but these are, in our parlance, standing wave patterns. In the simplest of such structures which has been adapted to the millimeter wave region, two large, flat, reflecting plates are aligned parallel to one another. Energy is introduced into the system usually through an aperture in one of the plates. The plates are large enough and the spacing far enough that the energy can bounce back and forth between the plates in essentially a TEM wave. A probe completes the system. When the spacing is adjusted so that resonance occurs, the probe can be used to measure the standing wavelength.

In such a cavity the Q is determined by the end plate dissipation and by the loss of energy from the open sides of the structure (diffraction loss). For the lowest order resonance this is given by $\alpha_D = 0.2\left(\frac{a^2}{b\lambda}\right)^{-1.4}$ where the reflecting plates are a by a in dimensions, the separation is b, and λ is the wavelength. If the plates are large, the latter loss can be small, and substantial Q-values can be obtained.

Optical interferometers have been adapted to the millimeter wave region. The principles are well presented in standard optical texts[63] and the adaptation summarized by Harvey[64], Brown[65], and Tremblay and Boiven[66]. Essentially, the idea is to provide interference between two (or more) rays in such a way that adjustment of an element of the interferometer and the corresponding shift in the interference pattern can be used to deduce the wavelength. It can be seen therefore that the idea is very similar to that of the parallel plate resonator with probe. Besides their use in determining wavelength, interferometers can be used to determine the velocity of propagation and the transmission properties of materials.

In making the transition from the optical region to the millimeter/submillimeter region, difficulty is encountered due to the different relative aperture sizes and path lengths. Diffraction effects, however, can be minimized by judicious choice of dimensions.

Hartshorn and Saxon[67] reviewed Culshaw's work[68] on adapting the Michelson interferometer to millimeter wavelengths, and Culshaw republished a fairly detailed account in 1961[69]. The description of the technique has appeared in nearly every survey paper of millimeter wave techniques published, and hence, will not be repeated again here. Culshaw used the Michelson technique at 12.5 millimeter wavelength. There seems to be no limitation in using it throughout the millimeter/submillimeter region. Though correction for diffraction effects should be made, even without such corrections, accuracies of the order of 2 or 3 parts in 10^4 are obtainable.

Culshaw also adapted the Fabry-Perot interferometer to the millimeter wavelength region[69,70]. This, too, has been adequately described in various survey papers and will not be described in detail here. Like the Michelson structure it can be used to measure wavelength, velocity of propagation and material properties.

Brown[65] lists two advantages of the Fabry-Perot system over the Michaelson structure:

"1. The response of the receiver as a function of reflector separation is a series of peaked curves, compared with the sinusoidal variation of receiver output with reflector position for the Michelson. The very sharp response facilitates the accurate determination of the separation between adjacent peaks...This suggests that the sharpness of the Fabry-Perot response may be expressed as an equivalent Q factor, and Culshaw has shown that for his instrument the value is 60,000.

"2. The Fabry-Perot is less sensitive to diffraction effects. This can most easily be seen with the help of the plane wave spectrum idea. The transmitting antenna radiates around the axis of the instrument and in the resonant position only the wave in the axial direction has the correct phase relation between the components arising from multiple reflections. The plane waves off-axis are thus 'filtered out' in the same kind of wave as those traveling very long distances between a transmitter and a receiver. This conclusion is strictly true only for a monochromatic beam and a detailed theoretical analysis is needed to determine the limitations imposed by frequency variations in the radiated signal."

The Fabry-Perot technique has been used at 50 GHz, 75 GHz, and even higher in frequency. However, there are increasing difficulties in maintaining the required flatness in the plates. Also in certain regions of the spectrum the problem might be to find materials which were suitable for reflectors.

Other types of interferometers have been devised, but for the most part these have had as their objective the investigation of material properties rather than the measurement of wavelength.

12.6.2 Spectroscopic Techniques

In optics the measurement of wavelength is often accomplished by refracting the beam under investigation through a prism or grating system in such a way that the displacement of the final beam from a certain reference will give a measure of the wavelength. The references available are the known characteristic lines of emission (or absorption) of the elements. The same techniques can be used in principle in the millimeter/submillimeter region of the spectrum, where the characteristic lines are those of molecules. Many of these have been identified, although our knowledge of them is far from complete.

12.7 MATERIALS MEASUREMENTS

12.7.1 Interferometer Techniques

The Culshaw adaptation of the Michelson interferometer has been used to measure the properties of dielectrics[68,69]. The measurement of dielectric constant is accomplished by the insertion of a sample sheet in

some well-defined position, preferably in the fixed arm. From the shift in the minima the complex dielectric constant can be deduced. As in the case of wavelength measurement, the results must be corrected for diffraction errors.

The Fabry-Perot arrangement is sometimes preferred for material measurement. If an unknown dielectric material without excessive loss is placed between the reflecting plates, a change in the shape of the resonance curve, and hence the Q, will result. From this may be deduced the properties of the material. In many cases such a technique is easier than the usual waveguide or cavity methods of determining dielectric constant.

The Froome interferometer has been applied to the study of the properties of matter in the millimeter/submillimeter region[71]. The instrument consists of three fixed mirrors, a movable standing wave detector, an adjustable attenuator-beamsplitter, and a stable radiation source, as shown in Fig. 12.4. The beam splitter directs two beams along different paths to produce a standing wave pattern in the detector arm. The detector can detect the maxima and minima of this pattern which should be cosinusoidal in form. The detector uses a magic T as shown in Fig. 12.5. Arms 1 and 2 are fitted with horns, arm 3 has a termination connected, and arm 4 has a crystal detector mounted.

By introducing a slab of unknown dielectric into arm 1 and readjusting the prism and detector for minimum output, it is possible to

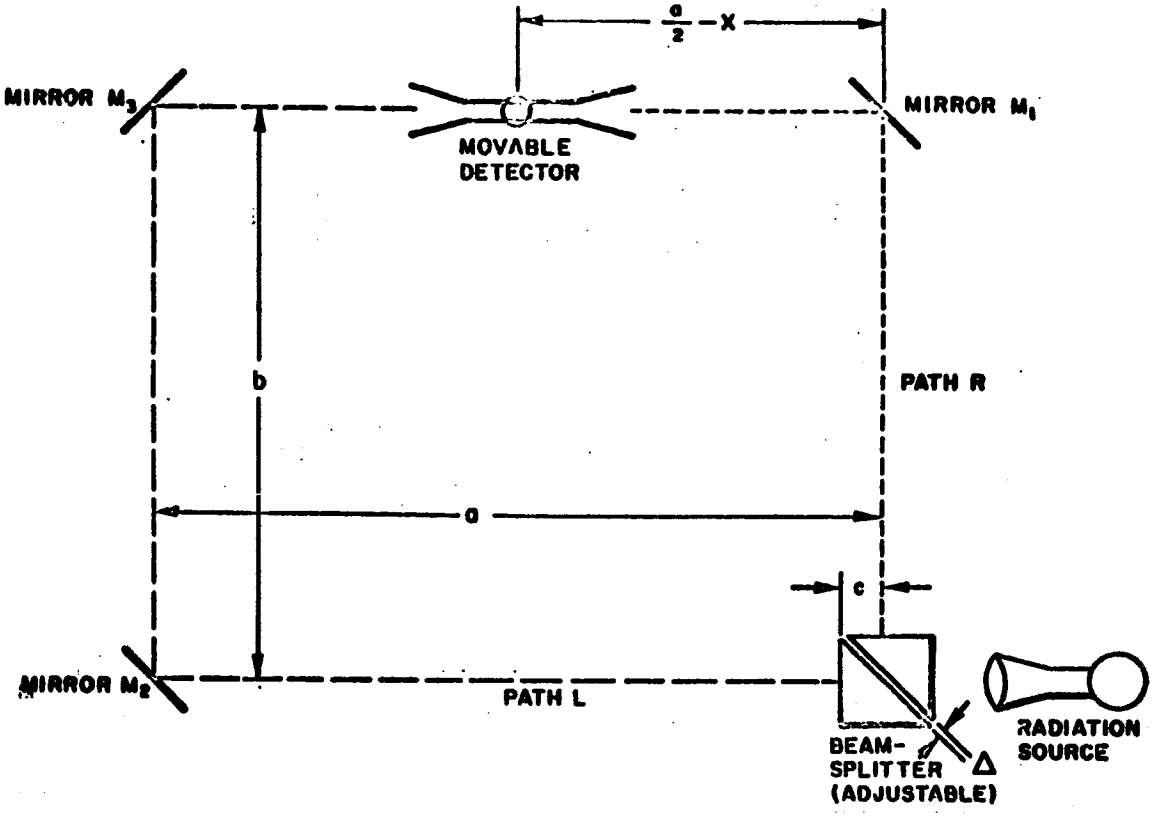

Figure 12.4 Arrangement of Interferometer Components

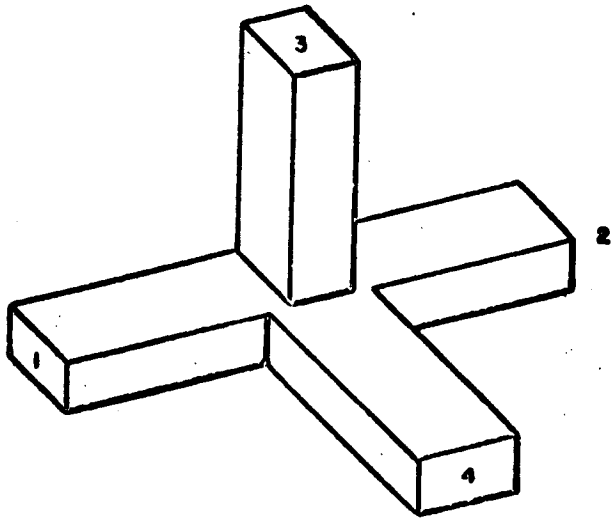

Figure 12.5 Magic T Arm Numbers

determine the transmission coefficient and all of the related quantities. The algebraic manipulations are involved, but the technique has the advantage that no part of the interferometer needs special calibration. The tests reported were for 35 GHz but it was planned to extend them to 75 GHz.

Interferometers of yet other types have been devised. A Michelson type instrument attributed to Froome[65] replaces one path in air with a waveguide medium, and substitutes a magic T for the beam splitter. The possibility of using a calibrated attenuator in the waveguide arm gave the ability to equalize amplitudes and obtain very sharp minima. Two other types due to Jamin and Boltzmann have also received attention for millimeter-wave work.[65] Details on these are not necessary here. Suffice it to say in concluding that interferometric techniques have proved of interest and continue to hold promise for the investigation of materials at the frequencies in question. Their great advantage over some other techniques is simplicity, and there is no doubt that they will continue to be used, particularly in the unexploited regions of the spectrum. To our knowledge no such instruments are commercially available.

12.7.2 Spectrometers

The spectrometer is sometimes defined as an instrument for determining the index of refraction. In essence it is a spectroscope in which the prism is replaced by a refracting sample whose properties are to be determined. In the millimeter embodiment of this device, adapted as so many other optical instruments to those frequencies by

Culshaw[69], two horns are mounted respectively to illuminate a sample and pick up the refracted energy as shown in Fig. 12.6. The sample itself need not be the conventional triangular shaped prism, but of any regular shape. It is interesting to note that the same arrangement can also be used to obtain reflection and diffraction patterns of arrays of objects, or bistatic cross-section data. When the source is monochromatic, a simple application of Snell's law will enable the index of refraction to be determined. For lossy materials a more involved analysis may have to be undertaken to determine the complex index. The provision for making measurements with either parallel or perpendicular polarization allows this additional information to be secured. Although such instruments have been built at several millimeter-wave frequencies, they are custom made devices. However, their simplicity and relatively low cost makes them attractive for laboratory instruments.

12.7.3 Spectrophotometer

With this class of instrument the absorption of materials as a function of frequency is obtained. Measurement of the absorption gives both qualitative and quantitative information about the molecular system involved. At each wavelength it measures the ratios of transmitted to incident radiation.

The Beckman IR-11 is representative of this type of instrument, shown in Fig. 12.7 The beam from a far-infrared incoherent source is focused by a concave mirror and either passes through the sample under test or is reflected into an alternate (reference) path by a chopper, C_1. This disc, half mirrored and half open, rotates at 11 hertz. The

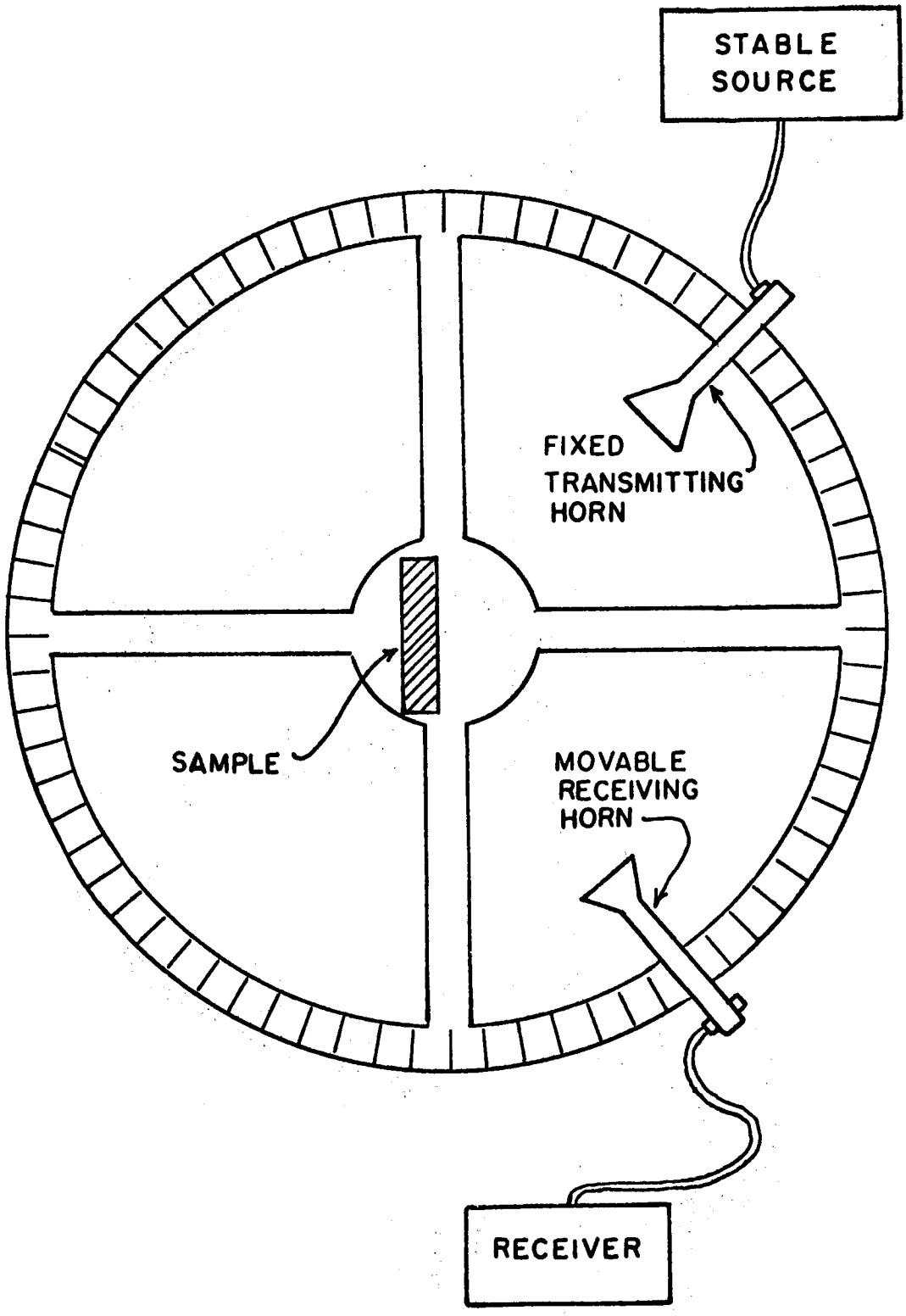

FIG. 12.6 MILLIMETER SPECTROMETER

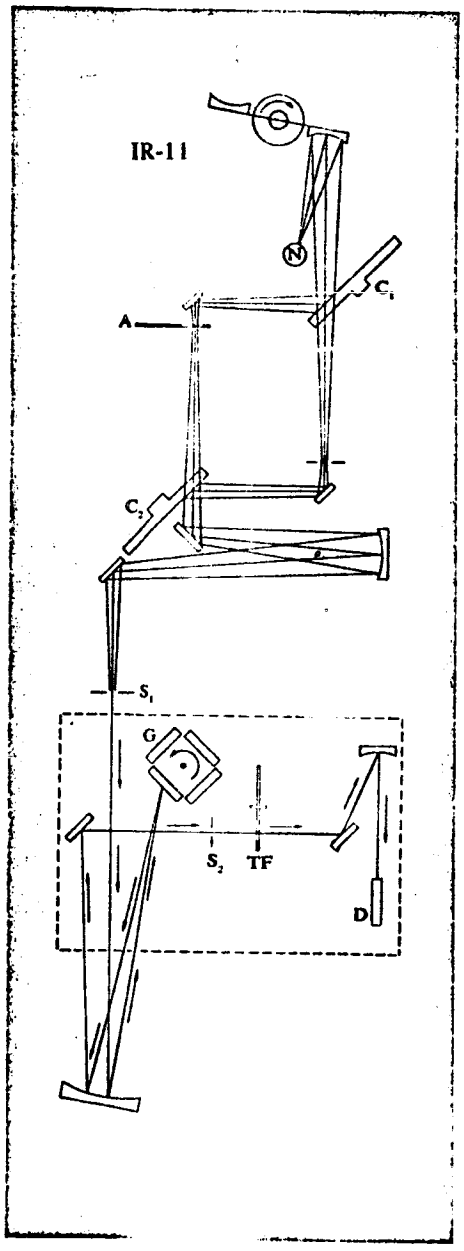

Figure 12.7 Far-Infrared Spectrophotometer

reference path has a variable attenuator, A. The sample beam after passing through the material under test is directed through a slit onto a flat mirror and thence to a second chopper, C_2, where it is combined with the reference beam. The composite beam now passes through a slit, S_1, into a monochromator consisting of various mirrors and four sequentially rotating gratings, G_1, which provide the needed scan. Each individual grating covers a portion of the range. The dispersed beam now passes through the final slit, S_2, a transmission filter for eliminating unwanted components, and onto a detector, D, which in the case being described is a Golay cell. The detector output positions the attenuator, A, to make the reference path and the sample path equal in intensity. The attenuator position is linked to a pen on a strip recorded so that a recorded transmission spectrum is obtained.

While a particular make of spectrophotometer has been described for illustrative purposes, there are other manufacturers. In general the operation is the same. The principles of this instrument could be carried into the millimeter/submillimeter region provided suitable sources were available. The use of a swept coherent source, if available, could probably yield more precise information than the currently used method. This might be a fruitful field for further endeavor.

12.8 CONCLUSIONS

A variety of techniques exist for measurements in the millimeter/submillimeter region. Conventional waveguide techniques can be adapted with varying degrees of success to all frequencies where waveguide exists.

Techniques developed for optical and infrared use can be adapted to lower frequencies and have been used in research laboratories down to about 35 GHz. Further development of measurement methods for laboratory purposes above 100 GHz should prove of considerable value in advancing the field. Of particular interest are the measurement of power, frequency (wavelength), attenuation and phase shift (refractive properties). These latter are of particular interest in the measurement of materials. It is not always clear what accuracy can be obtained in the cited methods, and often one has no theoretical reason for choosing one method over another. Considerably more work needs to be done in this area.

12.9 REFERENCES TO CHAPTER XII

1. Joint Service Review and Recommendations on Radio Frequency Power Measurements, Report No. REMC/26/FR, Ministry of Aviation Radio and Electronics Measurements Committee, September, 1961 (AD 271 703).

2. MICROWAVE MEASUREMENTS FOR CALIBRATION LABORATORIES, (2nd Ed.), Applic. Note 38, Hewlett-Packard Co., Palo Alto, Calif., June, 1962.

3. MICROWAVE POWER MEASUREMENT, Applic. Note 64, Hewlett-Packard Co., Palo Alto, Calif., 1965.

4. "Product Survey: Microwave calorimeters," Microwaves 2, September, 1963.

5. Levin W. Landsowne, "Report on revision of calibration procedures for microwave test equipment," Report No. DPS-896, Aberdeen Proving Ground, Maryland, April 1963, (AD 400 356).

6. A. C. Macpherson and D. M. Kerns, "A microwave microcalorimeter," Rev. Sci. Instr., 26, January, 1955, pp. 27-33.

7. M. Sucher and H. J. Carlin, "Broad-band calorimeters for the measurement of low and medium level microwave power: I - Analysis and design," IRE Trans., MTT-6, April, 1958, pp. 188-194.

8. A. V. James and L. O. Sweet, "Broad-band calorimeters for the measurement of microwave power: II - construction and performance," IRE Trans., MIT-6, April, 1958, pp. 195-202.

9. H. J. Sharpless, "A colorimeter for power measurements at millimeter wavelengths," IRE Trans., MIT-2, September, 1954, pp. 45-47.

10. C. J. Carter, "Calorimeter-type power meters," Engineering Report, Contract W 33-038-ac-15162, Ohio State Univ. Research Foundation, Columbus, Ohio, August, 1953, (AD 26 873).

11. L. D. Strom, "A calorimeter for microwave and low level power measurements," 1955 AERONAUT. ELECTRONICS DIGEST, IRE, Dayton, Chapter, May, 1955, pp. 158-159.

12. E. W. Ernst and J. H. Schusse, "Conduction calorimetric power meter," Tech. Rept. No. 3, Contract W-33-0380-ac-014538, Elect. Eng. Rsch. Lab., University of Illinois, Urbana, Ill., April, 1951.

13. R. G. Fellers, "Measurement techniques at millimeter wavelengths," PROC. SYMP. ON MOD. ADV. IN MICROWAVE TECH., New York, N.Y., June, 1955, pp. 355-367.

14. A. V. James, A SENSITIVE MILLIMETER CALORIMETRIC POWER METER, M.E.E. Thesis, Polytechnic Institute of Brooklyn, Brooklyn, N.Y., April, 1956.

15. A. V. James, "Broadband, rugged calorimetric power meters," First Quart. Rept. R-414.3-55, PIB-346.3, April, 1955.

16. G. F. Engen, "A refined x-band microwave microcalorimeter," Jour. Rsch., NBS, 63C, July-Sept. 1959, pp. 77-82.

17. L. B. Turner, "Balanced calorimeters for 3000 and 10,000 Mc/s with tapered water loads for H_{01} rectangular pipes," Jour. IEEE, 93, Pt. III-A, 1946, p. 1467.

18. T. Jaeger and M. V. Schneider, "Ein breitbandiges microwellen kalorimeter fur hohe leistungen," Arch. Elektr. Ubertr., 13, 1959, pp. 21-25.

19. P. A. Hudson and C. M. Allred, "A dry static calorimeter for RF power measurement," Trans. IRE, 1-7, December, 1958, pp. 292-296.

20. W. I. Brodskii and V. I. Pronenko, "Microcalorimeters for measuring super-high-frequency power in the 3 cm range," Imerital'naya Tekhnika, 5 (R.A.E. Trans. No. 807), 1957, p. 685.

21. I. R. Neilson, "A flow calorimeter for radio frequency power measurements in the ten-centimeter microwave region," M.S. Thesis, Stanford Univ. Stanford, Calif., 1948.

22. W. A. Penton and I. Overton, "A balanced water-flow calorimeter for centimeter wavelengths," Jour. Sci. Tech. (New Zealand), 29, Sec. B, 1948, p. 215.

23. Calorimeter for Centimeter and Millimeter Waves, PRD Reports, 5, April-Oct. 1956, pp. 87-93.

24. R. F. Schwartz, et al, "Development of microwave power standards for 3 Gc/s coaxial line and 33 Gc/s waveguide," Final Report on Tasks C and D, Contract No. DA 36-034-ORD-3693-RD, Institute for Cooperative Research, Univ. of Pa., 30 November 1963.

25. R. F. Schwartz, et al, "Development of power measurement standards," Final Report on Task C, Contract DA 36-034-ORD-3693A, Institute for Cooperative Research, Univ. of Pa. 31 Oct. 1964 (Moore School Report 65-14).

26. E. L. Ginzton, MICROWAVE MEASUREMENTS, McGraw-Hill Book Co., New York, 1957.

27. H. J. Carlin and M. Sucher, "Accuracy of bolometric power measurements," Proc. IRE, 40, Sept. 1952, p. 1042.

28. D. M. Kerns, "Determination of efficiency of microwave bolometer mounts from impedance data," Jour. Rsch., NBS, 42, 1949, p. 579.

29. M. Sucher and H. J. Carlin, "The operation of bolometers under pulsed power conditions," IRE Trans. MIT-3, July, 1955, pp. 45-52.

30. J. A. Lane, "The measurement of power at a wavelength of 3 cm by thermistors and bolometers," Proc. IEEE, 102B, November, 1955, pp. 819-825.

31. M. Sucher, "A comparison of microwave power measurement techniques," Proc. Symp. on Mod. Adv. Microw. Tech., New York, N. Y., June 1955, pp. 309-323.

32. J. A. Lane, "Measurements of efficiency of bolometer and thermistor mounts by impedance methods," Proc. IEEE, 104B, September, 1957, pp. 485-486.

33. H. J. Carlin, "Broadband bolometric measurement of microwave power," Radio and TV News, Engrng. Ed., July, 1949.

34. B. Bleaney, "Radio-frequency power measurements by bolometer lamps at centimeter wavelengths," Jour. IEEE., 93, Pt. III-A, 1946, pp. 1378-82.

35. G. F. Engen, "Status report on microcalorimetric technique for evaluation of bolometric mounts," Rep. on Comm. I, URSI, 12th Gen Assem., Boulder, Colo., August 8, 1957.

36. R. F. Desch and Roy E. Larson, "A low-level microwave power measurement technique employed in the electronic calibration center," NBS Report 7202, U. S. Dept. of Commerce, Nat. Bur. of Stds., Boulder, Colo., Sept. 28, 1961.

37. G. F. Engen, "A bolometer mount efficiency measurement technique," JOUR. of RSCH. NAT. BUR. STDS., C Engineering and Instrumentation, 65C, April-June 1961, pp. 113-124.

38. R. F. Desch and R. E. Larson, "Bolometric microwave power calibration techniques at the National Bureau of Standards," IEEE TRANS. ON INST INSTR. AND MEAS., I-12, June, 1963, pp. 29-33.

39. A. F. Harvey, MICROWAVE ENGINEERING, Academic Press, London, 1963, pp. 146-150.

40. J. A. Lane, "Transverse film bolometers for the measurement of power in rectangular waveguides," Proc. IEE, 105B, p. 77, 1958.

41. J. A. Lane and D. M. Evans, "The design and performance of transverse film bolometers in rectangular waveguides," Proc. IEEE, 108-B, 1961, p. 133.

42. P.Y.C. Tsao, "An investigation of errors of a thin film device for precise microwave power measurements," Technical Memorandum 6134-2, Contract DA 36-034-ORD-3693RD, The Institute for Cooperative Research, University of Pennsylvania, Phila., Pa., December, 1964, (Moore School Report No. 65-15).

43. S. Hopfer, N. H. Riderman, and L. A. Nadler, "The properties of thermoelectric elements as microwave power detectors," 1962 IRE CONVENTION RECORD, Part 3, pp. 77-84.

44. J. A. Lane, "Resistive film calorimeters for microwave power measurement," Trans. IRE, MIT-7, p. 177, 1959.

45. I. Lemco and B. Rogal, "Resistive-film milliwattmeters for the frequency bands 8.2-12.4 Gc/s, 12.4-18 Gc/s, and 26.5-40 Gc/s," Proc. IEE, 107-B, 1960, p. 427.

46. R. S. Clay, "Radiometry," ENCYCLOPAEDIA BRITANNICA, 1951 ed., Vol. 18, Encyclopaedia Britannica Inc., Chicago, Ill., 1951, pp. 900-901.

47. N. Carrara and P. Lombardini, "Radiation pressure of centimeter waves," Nature, 163, 1949, p. 171.

48. A. L. Cullen, "Absolute measurement of microwave power at microwave frequencies," Nature, 163, 1949, p. 403.

49. A. L. Cullen, "Absolute measurement of microwave power by radiation pressure," Nature, 165, 1950, p. 726.

50. A. L. Cullen, "Absolute measurement of microwave power in terms of mechanical forces," Nature, 167, 1951, p. 812.

51. A. L. Cullen, B. Rogel, and S. Okamura, "A wide-band double-vane torque-operated wattmeter for 3 cm microwaves," IRE Trans., MIT-6, 1958, p. 135.

52. A. L. Cullen, "A general method for the absolute measurement of microwave power," Jour. IEE, 99, Pt. IV, 1952, pp. 112-120.

53. A. L. Cullen, "The measurement of microwave power by radiation pressure, Engineering, vol. 172, 1951, p. 377.

54. A. L. Cullen, "Absolute power measurement at microwave frequencies," Proc. IEE, vol. 99, 1952, p. 100.

55. A. L. Cullen and H. A. French, "An instrument for absolute measurement of low-level microwave power in the 3 cm band," Proc. IEE, vol. 104C, 1957, p. 456.

56. A. L. Cullen, "A microwave vibration milliwattmeter," Nature, vol. 170, 1952, p. 1121.

57. A. L. Cullen and I. M. Stephenson, "A torque-operated wattmeter for 3 cm microwaves," Proc. IEE, Monograph No. 22M, 99-IV, July, 1952, p. 294.

58. S. Okamura and S. Kansaki, "Double-vane torque-operated wattmeter for 7 kMc/s," Jour. Rad. Rsch. Labs., 5, 1958, pp. 157-163.

59. R. A. Bailey, "A resonant-cavity torque operated wattmeter for microwave power," Proc. IEE, 102C, 1955, p. 59.

60. S. E. Diamessis and W. Boerner, "Refinement of 'Vibration milliwattmeter' techniques and their extension to 33 kMc," Technical Memorandum 6134-1, Contract DA 36-034-ORD-3693RD, The Institute for Cooperative Research, University of Pennsylvania, Phila., Pa. 31 October 1964, (Moore School Report No. 65-08).

61. E. Acs, "A proposed method of microwave power measurement," Proc. IEE, 109B, pp. 744-745, 1962.

62. "Microwave power meter type TKI V 1045-200," Brochure of the Research Institute for Telecommunications, Budapest, Hungary, 196(?).

63. M. Born and E. Wolf, PRINCIPLES OF OPTICS, Macmillan Co., New York, 1959, Chapter VII.

64. A. E. Harvey, MICROWAVE ENGINEERING, Academic Press, London, 1963, pp. 607-611.

65. J. Brown, "Microwave optics", ADVANCES IN ELECTRONICS AND ELECTRONIC PHYSICS, Vol. X, Academic Press, New York, 1958, pp. 107-151.

66. R. Tremblay and A. Boiven, "Concepts and techniques of microwave optics," Applied Optics, 5, Feb. 1966, pp. 249-278.

67. L. Hartshorn and J. A. Saxon, "Dispersion and absorption of waves," Handbuch der Physik, Springer-Verlag, Berlin, 1958, pp. 703-705.

68. W. Culshaw, "The Michelson interferometer at millimeter wavelengths," Proc. Phys. Soc., 63B, 1950, p. 393.

69. W. Culshaw, "Millimeter wave techniques," Advances in Electronics and Electron Physics, Vol. 15, Academic Press, New York, 1961, pp. 197-263.

70. W. Culshaw, "The Fabry-Perot Interferometer at millimeter wavelengths," Proc. Phys. Soc., 66B, 1953, p. 859.

71. J. W. Battles and D. E. Crane, "Millimeter Interferometer," Navweps Report 8201, Research Dept., Naval Ordinance Lab. Corona, Corona, Calif., 1 Aug. 1964 (AD 603544).

Chapter XIII

ELECTROMAGNETIC RADIATION HAZARDS

13.1 DEFINITION OF HAZARDS

The hazards of exposure to electromagnetic radiation are historically the result of experimental observations. The hazards have been observed for biological materials, flammable materials, electroexplosive devices and components, and materials in general. The danger of exposure has been observed at all parts of the frequency spectrum from essentially zero to 10^{25} Hertz. In some cases, the resulting damage is not permanent; that is, the object or device recovers completely when radiation is removed. In other cases, the damage is permanent. Furthermore, the permissible dose rate may be a threshold or it may be cumulative. Thus, one can see that there are many aspects to electromagnetic radiation hazards. For convenience, these aspects are described separately in the sections which follow for biological materials, flammable materials, electroexplosive devices and components or structural materials. The treatment is primarily documentary since, except for scientific reasons, no further research is recommended.

13.2 BIOLOGICAL HAZARDS

13.2.1 Nature of Hazard

Damage to living tissues result from physical and chemical changes that occur when electromagnetic energy is absorbed by these

tissues. Depending on frequency and the nature of the tissue, the absorption may be at the tissue surface, deep in the tissue, or the tissue may be semi-transparent.

The nature of the hazard depends on the frequency of the incident radiation. There is a natural dividing line in the frequency spectrum at about 2000 Å (1.5×10^{15} hertz). Below this wavelength, the radiation ionizes living tissues and other materials and the effects of exposure are cumulative. Above this wavelength (lower frequencies), the effects of radiation exposure are primarily thermal and are non-cumulative.

13.2.2 Thermal Effects

Below 1.5×10^{15} hertz (above 2000 Å), the presently known harmful effects of excessive amounts of radiation are associated with the average power of the absorbed radiation, are thermal in nature, and are observed as either a general rise in total body temperature or as a selective temperature rise of sensitive parts of the body such as testes or the eyes.[1,2,3,10] The only known non-thermal effects are associated with field strength values considerably higher than currently available (in fact, higher than one can launch without spark-over in air). While these effects are still under study, they are not considered serious at this time[4]. Radiation in this region is detected by the senses and gives rise to the sensation of heat. The nerves of the eye, however, are not very sensitive to heat and thus eye damage may occur without warning.

It is assumed in the case of total body irradiation that a fever corresponding to a temperature rise greater than $1^{\circ}C$ is intolerable. Eye cataracts are produced when the eye temperature elevation is of the order of $10^{\circ}C$.[5] It thus appears that body temperature rise is the more serious problem for total body irradiation and tolerance dose levels should be based on it.

Based on considerations of the amount of heat that the body can dissipate, it appears that if total body absorption of electromagnetic energy is assumed, the tolerance dose is a power density of 0.01 watt/cm^2 for periods of 0.1 hour or more and should not exceed the above mentioned body temperature rise of $1^{\circ}C$. For intermittent exposure, the tolerance dose is an energy density of 1 milliwatt-hour/cm^2 for periods up to 0.1 hour.[6,36] This guide applies whether the radiation is continuous or intermittent. The tolerance dosages are the dividing line between noticeable and unnoticeable biological effects and as such do not have built-in safety factors.

Exposure to electromagnetic radiation is but one of several sources of thermal input to the body. Body temperature rise also depends on other thermal inputs such as metabolism, physical labor and high ambient temperature as well as on heat dissipation capability which depends on clothing, humidity and air circulation. Persons suffering from circulatory and certain other ailments are also more vulnerable.

The above tolerance guide assumes total body absorption of the incident radiation. It is known that details of anatomy and the frequency of the radiation affect the precentage of absorbed radiation. In order to interpret the permissible dosage in terms of free field power density, the absorption properties of mankind must be known. This is formulated in terms of the relative absorption cross-section S, which is defined as the ratio of the power absorbed by a body from the incident field to the power falling on the shadow cross-section of the body. Relative absorption cross-section has been determined theoretically and experimentally in terms of a size parameter α, for simple spheres, cylinders and concentric spheres having complex dielectric properties similar to biological materials. α is defined as the ratio of the circumference of the sphere or cylinder cross-section to the wavelength of the incident radiation. Experimentally, human body relative absorption cross-section has been determined by means of phantoms and expressed as a function of α. From anthropometric data for human adults, considered as equivalent cylinders or spheres, it has been found that α lies in the range of $1 < \alpha < 34$ with most of the values much greater than one. The corresponding relative absorption cross-section S for these values of α over the frequency range of 400 MHz to 10 GHz is of the order of 50% to 60%, regardless of incident polarization except for the case of TM waves with α less than one (the extreme case of a small man or average

woman exposed to microwave fields at 300 MHz). In the latter case, for waves polarized parallel to the axis of the subject (TM waves), S may be between 60 and 80%. This is for man considered as an equivalent homogeneous (infinite) cylinder.[7,8]

Since the shape of man may be considered to be effectively between that of an infinite cylinder and a sphere, one might expect that the appropriate values of relative absorption cross-section should lie between those for a cylinder and those for a sphere for a given α. In addition, since in the case of the concentric sphere model it has been shown for $\alpha > 2$ that values of S are somewhat higher than for a single sphere, one would expect higher values of S for a concentric cylinder model than for a single cylinder model and these values should be between those for the concentric sphere model and a double layer slab model.

Thus, on the assumption that adult man may be represented by concentric truncated cylinders, one may expect values of S in the range of 50 to 125%.

Schwan and Li[2] have shown for a 3-layered plane slab made up of skin, muscle and fat that the influence of skin thickness is quite frequency-dependent. Above 3 GHz, for instance, normal values of skin thickness reduce relative absorption cross-section to one half of the value obtained for a two-layer plane slab model without skin. At 900 MHz, however, there may be a small reduction or increase in S depending on the thickness of the fat layer. Because of previously

shown similarities between the double layer plane slab and the concentric sphere model, it may be assumed that the above-mentioned effects of skin will also apply to a three concentric sphere model.

The experimental work on homogeneous doll phantoms has given values of S of 50 to 60% in the frequency range of 300 MHz to 10 GHz. It is now reasonable to believe that a 3-layered phantom, which would more closely resemble man, would have given higher values perhaps in the region of 50 to 125% which has been previously predicted theoretically.

It thus can be concluded that adult man will absorb 50 to 125% of the incident energy in the frequency range of biological interest (300 MHz to 10 GHz), and particular values in this range will depend on frequency, thickness of skin and subcutaneous fat. Above 10 GHz, absorption is predominantly in the skin and is usually associated with the sensation of heat. The exact amount of energy absorbed or reflected is not presently known for the frequency region of 100 GHz through 30 THz. However, no serious hazard is believed to exist since the skin sensation of heat gives adequate warning of exposure and at worst one gets a skin burn similar to sunburn.

13.2.3 Ionizing Effects

Presently known high power generators of millimeter and sub-millimeter waves use voltages in excess of 10,000 volts and consequently x-radiation from these devices may be expected. For laser type devices, one may expect incidental radiation in the visible light or higher frequency region. Consequently the effects of ionizing radiation must be briefly mentioned.

Above 1.5×10^{15} hertz (below 2000 Å), one has the regions of the spectrum known as ultraviolet rays, gamma rays, X-rays and cosmic rays, or fast neutrons. This is the region of ionizing radiation (photon energies in excess of 3 electron volts). The material which follows has been reproduced with additions from reference 9, which is a convenient summary of extensive material in references 11 through 24.

Damage to living tissues results from the physical and chemical changes that occur when energetic particles or photons dissipate energy in body tissue. Harmful results can occur either through brief, severe exposures that cause extensive tissue damage, or as the result of constant exposure to low-level radiation of sufficient intensity to destroy tissue cells faster than the body can replace them. It is important to note that these radiations are not detected by the senses and that symptoms of radiation sickness may not appear for hours or days after even severe exposures. It is therefore extremely important to monitor carefully all radiations to which personnel may be exposed and to adhere closely to established radioisotope handling procedures and radiation tolerance limits.

Hazardous radiations occur commonly in work involving the use of radioactive and fissionable materials, nuclear reactors, X-ray generators and high-energy particle accelerators, as well as magnetrons, klystrons, TWT and other high vacuum tubes operating at voltages above eight kilovolts. Radioisotopes emit energetic γ rays, β and α particles. High-energy accelerators can produce intense primary beams of protons, electrons, deuterons, α particles (and X-rays and neutrons as secondary radiations when the beams are allowed to strike matter). The fissioning

materials of nuclear reactors produce enormous amounts of all radiations, particularly neutrons, as well as large volumes of radioactive waste materials. Radiation intensities encountered range from those of small microcurie radioactive wastes that must be removed periodically from nuclear reactors to those of high voltage particle accelerators and cosmic rays.

13.2.4 Protective Measures

For the frequency region in which thermal effects are dominant, (below 1.5×10^{15} Hertz) tolerable dose rates have been established. It is sufficient to surround the source of radiation with an enclosure which prevents access to other than authorized persons. The enclosure should be posted with the standard microwave radiation hazard symbol shown in reference 36. A new hazard, laser light, has appeared recently. Little is known about it except for its potential for producing severe eye damage. This is not presently a hazard in the millimeter and sub-millimeter region but it may become one when these waves are obtained as a result of mixing of optical or infrared lasers. A warning sign has been designed for lasers but is unofficial (see Microwaves and Laser Technology). For persons who must have access to regions having hazardous microwave fields, protective clothing has been developed by the U.S. Air Force (RADC) and the U.S. Navy (BuShips).

For the frequency region above 1.5×10^{15} Hertz, ionizing effects are dominant and the effects are cumulative. The tolerable dose rates are known and it is sufficient to surround the source of radiation with lead shields or shields of other suitable materials.

The radiation region should be posted with the well-known ionizing radiation symbol. Persons who must have access to posted regions must wear radiation badges to determine the amount of exposure and should in addition be protected by suitable shielding aprons, gloves and other garments.

13.3 FLAMMABLE MATERIALS

13.3.1 Nature of Hazards

Flammable materials, typically aviation fuels and diesel and heating fuels, may be ignited if the proper conditions exist. These conditions are: the proper air-fuel ratio, the amount of energy required for ignition and the proper physical circumstances to allow an absorbed or induced field to initiate a current or a spark having the proper energy.

The above materials have been ignited by corona currents, lightning discharges, frictional charge resulting from the motion of the fuel through a hose, orifice, filter, or nozzle, and induced voltages from radio transmitters. Ignition has occurred on aircraft and on naval refueling operations.

Ignition phenomena appear to be more or less independent of frequency. There is extremely little documentation, however. It is sufficient to note that ignition has occurred from a single capacitor discharge or transient spike as well as from X-band radiation causing an arc-over. Some arc-overs observed have been sufficiently intense at S-band to destroy a fiberglass radome. Additional research may be required for the frequency region above 100 GHz.

13.3.2 Permissible Field Strength

Laboratory studies of the effects of corona currents and sparkovers on the ignition of various fuels is given in ref. 25. Figure 13.1, reprinted from this reference, shows the minimum corona currents required for ignition of various aircraft fuels. A minimum current of about 190 microamperes is required for Ramjet fuel, while most of the others require about 220 microamperes. The minimum ignition currents occurred approximately in the middle of the flammability range. Currents of this order of magnitude are known to occur on modern aircraft as the result of accidental discharges caused by high power radar and communications equipment.

An investigation of sparkover to ignite aviation gasoline was also reported in ref. 25. Figure 13.2 gives a curve of minimum capacitance vs voltage to ignite the fuel. This curve is representative of energy on the order of 0.64 to 0.88 millijoule, which compares favorably with the figure of one millijoule reported by other researchers. Ignition current-time variation also has an effect. Figure 13.3 gives a plot of minimum current vs time duration for capacitor discharge ignition of aviation gasoline.

From the above, it can be seen that for ignition of aviation fuels, corona currents must exceed 180 microamperes; capacitor discharge spikes or sparks must exceed one millijoule of energy, and have durations greater than one microsecond.

The translation of data such as this to ignition of fuels on a missile, aircraft, or naval vessel by electromagnetic waves is somewhat more difficult since resonant structures and gaps are required to

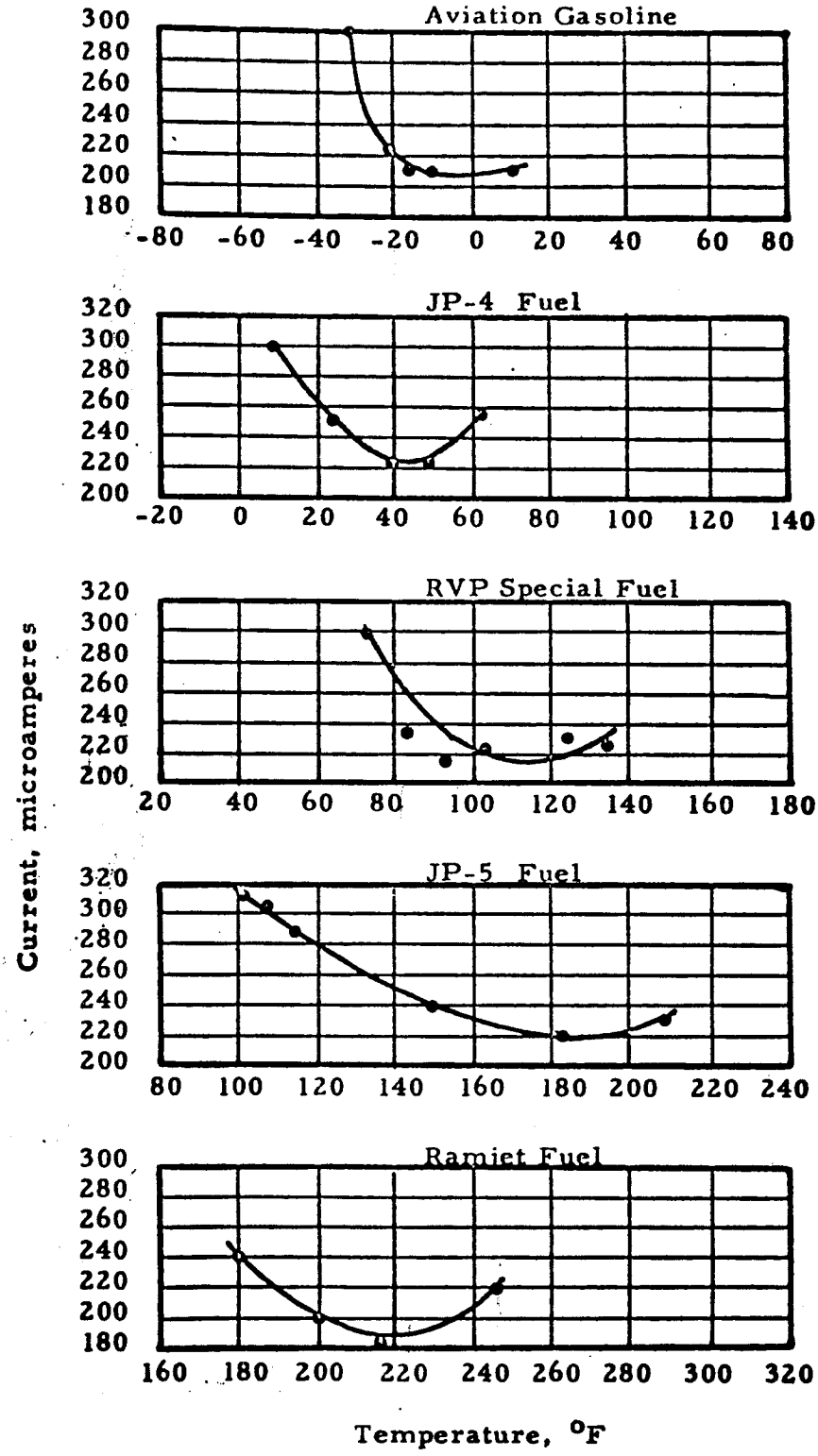

Figure 13.1 Minimum corona currents required for ignition of various aircraft fuels

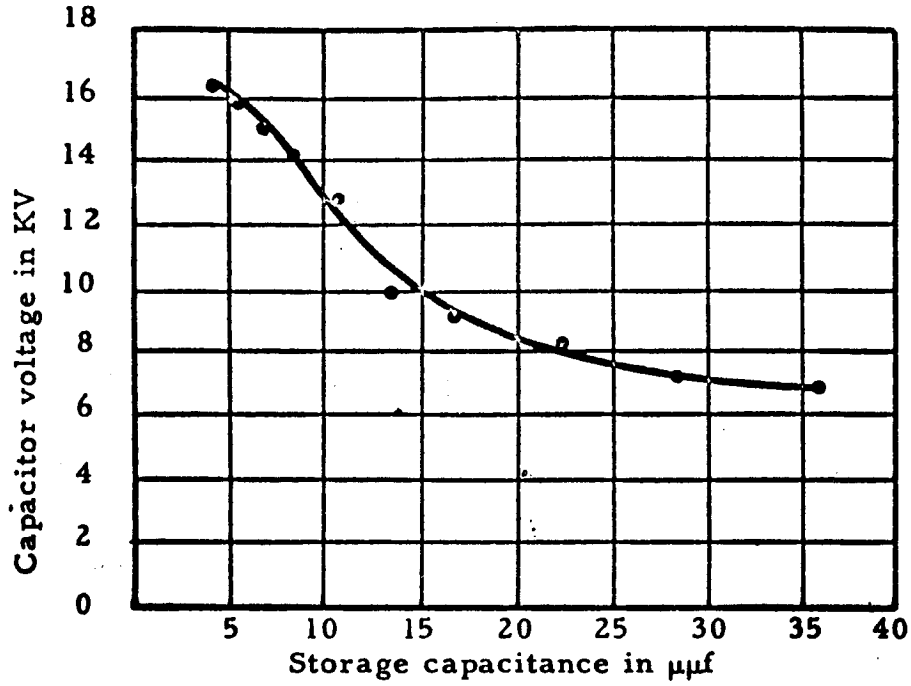

Figure 13.2 Curve of minimum capacity vs voltage required for spark ignition of aviation gasoline

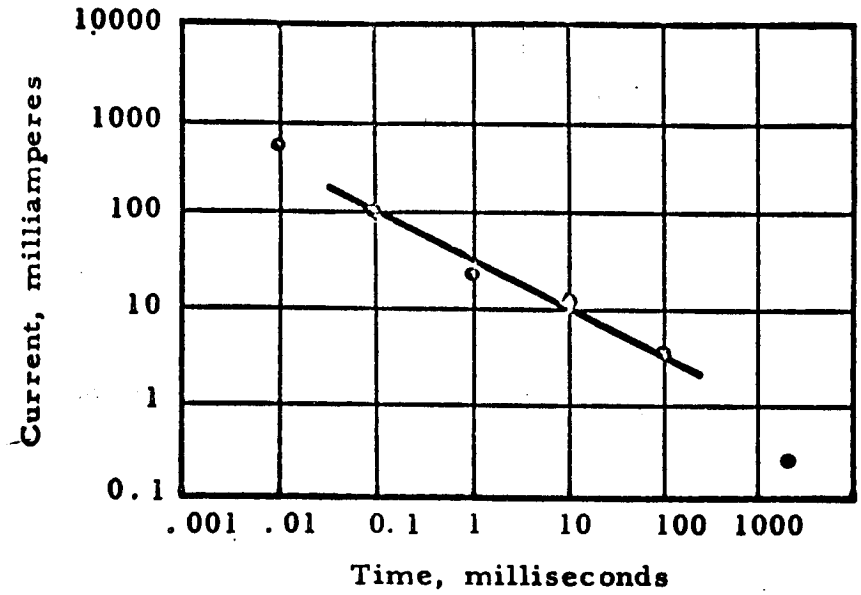

Figure 13.3 Plot of minimum current vs time duration for capacitor discharge ignition of aviation gasoline 100/130 grade

pick up and discharge the energy. Research reported in reference 25 shows that for an air-fuel mixture which can be ignited by sparks having the above required minimum energy, no ignition occurs in fields of average power density less than 25 mW/cm^2. The U.S. Air Force has established a limit of 5 $watts/cm^2$ peak power density for refueling operations near transmitting antennas. Depending on duty cycle, this is about 3.5 to 10 mW/cm^2 average power density.

Hazards in refueling in an electromagnetic field are considered far greater than hazards to a missile or aircraft transiting a radio or radar beam. Thus, it seems that the limit of 10 mW/cm^2 used for a long term biological hazard is also safe for refueling operations and radio or radar beam transits.

13.3.3 Protective Measures

If the fuels were slightly conductive, much of the hazards of refueling operations would be reduced. In reference 27, it is reported that turbine fuels have conductivities of 0.2 to 5 C.U. (conducting units: 1 C.U. = 10^{-12} pico mho/meter). Turbine fuels having conductivities above 50 C.U. have never been ignited. Addition of an additive, Shell ASA-3 in concentrations of 0.5 to 1 part per million to the fuel will raise the fuel conductivity to 50 to 300 C.U. without apparent deleterious effects on engine performance.

Most refueling problems on naval vessels stem from the use of grounding wires in the refueling hoses.[28] These wires were used to prevent static charge build-up due to fuel motion. The wires break

in service and thus constitute arcing points when refueling near transmitting antennas. With the use of fuel additives, these grounding wires may be eliminated and this source of trouble may vanish.

Proper design of vents on fuel tanks and enclosures may also prevent the ignition of vapors by corona, lightning discharges and induced voltages from transmitting antennas.

13.4 ELECTROEXPLOSIVE DEVICES

13.4.1 Nature of Hazard

Electroexplosive devices (EED) are electrochemical prime movers. A small chemical explosive charge, contained in a small capsule, is detonated by the heat from an electrical resistance wire filament embedded in the charge, the energy of a spark between electrodes embedded in the charge or electromechanically. These are one shot devices that have been usefully employed for igniting rockets, separating the stages of a missile, explosive bolts, opening or closing valves, as detonators for dynamite, etc.

The EED's are designed to operate or fire above a certain energy or voltage level and not to fire below it. There are over 15,000 different types of devices, each having somewhat different characteristics. Some are shielded. The wiring normally used for detonating the EED frequently acts like an antenna, thus picking up energy from electromagnetic fields. Thus premature firing of the device may result.

13.4.2 Permissible Field Strength

It has been found that slight changes in the arrangement of wiring or in orientation of a missile with respect to the field may

produce large variations in the amount of energy delivered to the EED. Thus the nature of the hazard is quite complex. Electroexplosive devices have been studied in considerable detail [29] and their sensitivities are known up to about 10 GHz. The sensitivity data on EED's is only available in classified reports. There is no reason to believe, however, that there is a frequency limitation on the devices themselves.

EED's with wire bridges have functioning times of a few milliseconds and ignition may occur after a time which is long compared to normal radar pulse durations. Thus average power is an adequate criterion.[30]

Devices with conducting mix or carbon bridges have functioning times of the order of radar pulse durations and thus peak power is a proper criterion.[30]

Reference 30 gives a theoretical calculation of power received by an EED from an electromagnetic field. This paper assumes a very simple model for the wiring and thus may not be appropriate for other cases. Reference 31 gives experimental data for an anti-personnel mine (an overall evaluation of the complete mine). It is our opinion, based on the present state of the art, that this is the only reasonable way to determine susceptibility. This means that every device employing an EED must be tested over the complete frequency range of interest.

13.4.3 Protective Measures

The best way of protecting equipment using EED's is to suppress the EED itself or to design it such that it only responds to the

design triggering stimulus. Reference 32 describes filters for EED's that attenuate stray electromagnetic fields. The use of filters plus shielded cases for the EED's may well eliminate the problem.

On the other hand, the EED's may be designed to use materials that function only at a critical frequency and thus automatically make them independent of their environment except at the control frequency. This is an approach that has not as yet been investigated.

13.5 COMPONENTS

13.5.1 Nature of Hazard

There are three areas of hazards to components, namely: thermal effects, photo/phonon effects and effects due to ionizing radiation, either primary or secondary.

Thermal effects on components are relatively well known. They may arise from any of the above-mentioned effects as well as from mechanical action. Most materials deteriorate in high thermal ambients. This is particularly true of dielectrics and semiconductors. While the effects of millimeter wave energy on materials has not been studied extensively, there is little reason to believe that any new mechanisms exist. It is our belief that the effects are the same as those of lower frequency radiation.

Photo/phonon effects may be expected when intense laser or maser beams irradiate materials and components. There is extremely little information on this subject in general, and essentially nothing on photo/phonon effects on millimeter components. This is an area which may require considerable study.

The effects of ionizing radiation on materials and components is extremely well documented. The best summary of this work may be found in reference 32. This reference includes the environment as well as the effects on materials. References 34 and 35 provide specific information on specific components.

As far as millimeter wave components are concerned, there is essentially no documentation of the effects of microwave, thermal, photo/phonon and nuclear radiation. Most presently known millimeter components are extrapolations of components used in other regions of the electromagnetic spectrum. It is reasonable to believe, as far as radiation effects are concerned, that these components will behave essentially the same as their prototypes. This is probably true for vacuum tubes, silicon diodes, and tunnel diodes. There is no information on Gunn effect diodes, Read diodes and the Josephson effect or on the behavior of masers and lasers in the millimeter region when exposed to the above mentioned environments.

13.6 CONCLUSIONS AND RECOMMENDATIONS

13.6.1 Biological Hazards

It is presently believed that biological hazards of millimeter waves are probably of the same nature as those caused by microwave and thermal radiation. Further studies of these phenomena would be warranted only for scientific reasons to improve our detailed knowledge and to provide further documentation for the above conclusion.

13.6.2 Flamable Materials and Electroexplosive Devices

The effects of millimeter waves on flamable materials and electroexplosive devices are believed to be the same as in other regions of the electromagnetic spectrum. Further research is warranted only for documentation of this statement.

13.6.3 Components

The effect of millimeter waves on most components is probably the same as the effects of microwaves and thus further study is not essential.

The effects of ionizing radiation on millimeter components such as vacuum tubes, silicon diodes and tunnel diodes can be extrapolated from their lower frequency prototypes. Gunn effect devices, Read diodes, Josephson effect devices, masers and lasers must be studied since little is known concerning their behavior in an ionizing environment.

13.7 REFERENCES TO CHAPTER XIII

1. H. P. Schwan, E. L. Carstensen, K. Li, "Heating of fat-muscle layers by electromagnetic and ultrasonic diathermy," Paper 53-206, AIEE Summer General Meeting, Atlantic City, 15-19 June 1953.

2. H. P. Schwan, K. Li, "Hazards due to total body irradiation by radar," Proc. IRE, V. 44, No. 11, pp. 1572-1581, November 1956.

3. H. P. Schwan, K. Li, "Capacity and conductivity of body tissues at ultrahigh frequencies," Proc. IRE, V. 41, No. 12, December 1953.

4. M. Saito, D. Sher, H. P. Schwan, "RF field-induced forces on microscopic particles," Proc. 4th Intl. Conf. on Medical Electronics, New York, July 1961

5. D. B. Williams, J. P. Monahan, W. J. Nicholson, J. J. Aldrich, "Biologic effects studies on microwave radiation; time and power thresholds for the production of lens opacities by 12.3 cm microwaves," IRE Trans., PGME-4, Feb. 1956, pp. 17-22.

6. Standard, Safety Level and/or Tolerances with Respect to Personnel, ASA Committee C-95, 20 May 1964.

7. A. Anne, M. Saito, O. M. Salati, H. P. Schwan, "Penetration and thermal dissipation of microwaves in tissues," Final Report Contract AF30(602)2344, RADC-TDR-62-244, 14 June 1962.

8. O. M. Salati, A. Anne, H. P. Schwan, "Radio frequency radiation hazards," Electronic Industries, Nov. 1962.

9. Reference Data for Radio Engineers, 4th ed., ITT Corp. New York, 1956, pp. 913-919.

10. Additional References on Microwave Radiation Damage:
    a. W. W. Mumford, "Some technical aspects of microwave radiation hazards," Bell Telephone System Monograph 3865.

    b. Handbook--Radio Frequency Radiation Hazards, USAF T.O. 31-1-80, 2 Jan. 1959.

    c. Biological Effects of Radio Frequency Radiation--Bibliography, RADC-TR-60-205, 1960.

    d. Proceeding of Tri-Service Conference on Biological Hazards of Microwave Radiation, ARDC-TR-58-51, Astia AD 115603, 15-16 July 1957.

e. Proc. 2nd Annual Tri-Service Conference on Biological Effects of Microwave Energy ARDC-TR-58-54, Astia AD-121477, Sept. 1958.

f. Proc. 3rd Annual Tri-Service Conference on Biological Effects of Microwave Radiating Equipment, RADC-TR-59-140, August 1959.

g. Proc. 4th Annual Tri-Service Conference on the Biological Effects of Microwave Radiation, Vol. 1, The Plenum Press, 1961.

11. Handbooks of the National Bureau of Standards available by purchase from Superintendent of Documents, U. S. Government Printing Office, Washington 25, D. C.

23 - Radium Protection: 1938.
41 - Medical X-ray Protection up to Two Million Volts: 1949.
42 - Safe Handling of Radioactive Isotopes: 1949.
47 - Recommendations of the International Commission on Radiological Protection and of the International Commission on Radiological Units: 1950.
48 - Control and Removal of Radioactive Contamination in Laboratories: 1951.
50 - X-ray Protection Design: 1952.
51 - Radiological Monitoring Methods and Instruments: 1952.
52 - Maximum Permissible Amounts of Radioisotopes in the Human Body and Maximum Permissible Concentrations in Air and Water: 1953.
54 - Protection Against Radiations from Radium, Cobalt-60, and Cesium-137: 1954.
57 - Photographic Dosimetry of X- and γ Rays: 1954.
59 - Permissible Dose from External Sources of Ionizing Radiation: 1954.

12. R. D. Evans, FUNDAMENTALS OF RADIOACTIVITY AND ITS INSTRUMENTATION, Advances in Biological and Medical Physics, Vol. 1, Academic Press, Inc.; New York, N. Y., 1948.

13. "Tabulation of available data relative to radiation biology," Report 1019-1ER-17, NEPA Project, U.S. Atomic Energy Commission, Oak Ridge, Tenn.: 1949.

14. "Guide for selection of equipment for radioactivity laboratories," Nucleonics, Vol. 7, p. R-1, November, 1950.

15. O. Glasser, Ed.: MEDICAL PHYSICS, II, Year Book Publishers, Inc.; Chicago, Ill.: 1950.

16. R. E. Zirkle, Ed., BIOLOGICAL EFFECTS OF EXTERNAL BETA RADIATION, McGraw-Hill Book Co., Inc.; New York, 1951.

17. A. Haddaw, Ed., BIOLOGICAL HAZARDS OF ATOMIC ENERGY, Clarendon Press, Oxford, England, 1952.

18. J. R. Bradford, ed., RADIOISOTOPES IN INDUSTRY, Reinhold Publishing Corp., New York, 1953.

19. F. G. Spear, RADIATION AND LIVING CELLS, John Wiley and Sons, Inc., New York, 1953.

20. "General handbook for radiation monitoring," Report LA 1835, Los Alamos Scientific Lab., Los Alamos, N.M., Sept. 1954.

21. H. A. Blair, Ed., BIOLOGICAL EFFECTS OF EXTERNAL RADIATION, McGraw Hill Book Co., Inc., New York, 1954.

22. L. D. Marinelli, "Radiation dosimetry and protection," Annual Review of Nuclear Science, Vol. 3, Annual Reviews, Inc., Stanford, Cal., 1954.

23. R. E. Zirkie, Ed., BIOLOGICAL EFFECTS OF EXTERNAL X- AND γ RADIATION, PART 1, McGraw-Hill Book Co., Inc., New York, 1954.

24. C. L. Comar, RADIOISOTOPES IN BIOLOGY AND AGRICULTURE, McGraw-Hill Book Company, Inc., New York, 1955.

25. M. M. Newman, J. D. Robb, "Investigation of minimum corona type currents for ignition of aircraft fuel vapors," NASA, Technical Note TN-D-440, June 1960.

26. J. J. Kulik, "Microwave radiation hazard to aircraft transiting radio and radar beams," FAA Report RD-64-1, December 1963.

27. M. L. Yaffee, "Airlines trying anti-static fuel additive," Aviation Week and Space Technology, 30 Nov. 1964.

28. Private correspondence.

29. R. G. Amicone, "Sensitivity determination of electroexplosive devices for reliable circuit designs," IEEE Trans. Appl. and Ind. V.83, No. 2, May 1964, pp. 143-147.

30. D. Georgevich, "Theoretical calculation of RF energy received from a transmitter by an electroexplosive device and computation of safe separation distances," Picatinny Arsenal, TM 1326, Oct. 1964, AD 450567.

31.. R. G. Satz, "M18A1 anti-personnel mine RF susceptibility test report," Picatinny Arsenal, TR 71-63.

32. S. M. Adelman, Sr., "Detonators that tune out stray R-F," Electronics, V. 38, No. 11, 31 May 1965, pp. 76-80.

33. H. H. Lind Olesen, "Designing against space radiation," Part 1, Electronics, V. 37, No. 32, Dec. 28, 1964, pp. 61-71; Part 2, Electronics, V. 38, No. 1, 11 Jan. 1965, pp. 70-76.

34. H. L. Hughes, R. R. Giroux, "Space radiation affects MOS FET'S," Electronics, V. 39, No. 32, 28 Jan. 1964, pp. 58-60.

35. A.S.T.M., "Radiation effects in electronics," A.S.T.M. Special Technical Publication, No. 384, 1965, Lib. of Cong., No. 65-18216.

36. United States of America Standards Institute, U.S.A. standards:

    a. Safety Level of Electromagnetic Radiation with Respect to Personnel, C95.1-1966.

    b. Radio Frequency Radiation Hazard Warning Symbol, C95.2-1966.

Chapter XIV

RADIO INTERFERENCE

14.0 INTRODUCTION

In this chapter we are concerned with those aspects of electromagnetic compatibility of concern in aerospace technology related to the millimeter and submillimeter portions of the spectrum. In general, it is convenient to define two aspects of electromagnetic compatibility: intrasystem compatibility and intersystem compatibility. The first, intrasystem compatibility, is concerned with mutual interference problems in a local or restricted area such as, for example, within a satellite or within the confines of a ground station. In its usual connotation, it is concerned only with the operational aspects of a single system. However, it is sometimes difficult to separate one system from another, since in many respects an operational satellite may really consist of a number of subsystems which are connected together to form the complete system on the satellite, and it is in this sense that the term "intrasystem" is used.

Much work has been done on the intrasystem problem in connection with satellites which have already been launched, and in connection with their tracking and communicating ground stations. It has been generally concerned with wavelengths falling outside of the millimeter and submillimeter range. At the present state of the art, it is considered extremely unlikely that there will be interaction between parts of a given satellite or ground station at the millimeter and submillimeter ranges for two reasons: (1) except for thermal noise components, and harmonics of transmitters, these wavelengths do not arise in a spurious manner as far as is known, i.e.,

they must be intentionally generated, and (2) the number of applications for devices in the millimeter and submillimeter range are not likely to be so numerous that mutual interference within a given satellite or given terminal location cannot be adequately taken care of by careful but straightforward design.

Accordingly, the rest of this chapter is concerned only with the intersystem compatibility problem. For the time being, it is extremely unlikely that interference will actually be experienced in this portion of the spectrum, except for the possibility that there may be background levels of radiation, such as are emitted from the sun, which conceivably could interfere with a satellite system. Source material on this subject in the frequency range of interest is quite limited, hence there are only a few specific listings in the references of this chapter. For reference purposes, however, it should be mentioned that as a subject of investigation, interference in satellite systems has come under serious scrutiny recently in the activities of CCIR. The work reported includes no specific considerations at frequencies above 10 GHz. However, many of the documents which have been presented are general in treatment, so that they may be considered to assist with analysis of effects at millimeter and submillimeter frequencies. The documents which are part of the record of Study Group IV (Space Systems and Radioastronomy) of the XI Plenary Assembly of CCIR, held in Oslo in 1966, are included under ref. 1 of this chapter. Each document contains a rather extensive list of references to source material.

In section 14.2, quantitative methods of analysis of situations which might develop in the future are discussed in some detail.

14.1 CHARACTERISTICS OF COMPONENTS

In evaluating any given electromagnetic compatibility situation, the following properties of components should be taken into consideration.

a) Generators operating at frequencies below the range of interest may have substantial output at harmonic or spurious frequencies in the range of interest. Output levels may be of the order of one milliwatt or higher at the 30th harmonic.

b) Since space systems will be required to operate at low levels, thermal radiation from a planetary surface or atmosphere or non-thermal radiation from the sun or planets may be significant as interference sources.

c) Most, but not all, of the available generation techniques will produce spurious outputs due to intermodulation. The solid-state maser is an exception to this.

d) Filter techniques appear to be available and can probably be adequately designed for specific applications.[2]

e) Some design work is required to optimize antennas in this range with respect to lower effective noise temperature and reduced sidelobes.

f) Shielding techniques provide effective means of control because of the relatively small size of components.

g) New techniques for performing many of the necessary electronic functions are under investigation. Such techniques will require

careful evaluation from the electromagnetic compatibility point of view.[3]

h) In relatively unsophisticated receivers which may be used on satellites, strong out-of-band transmitters (e.g., earth-based or satellite-borne radar) may block the receiver unless it is adequately filtered.

14.2 INTERSYSTEM COMPATIBILITY

The following general classifications shall be used for discussion purposes:

1) ground-station to ground-station
2) ground-station to satellite or aircraft
3) satellite to ground
4) satellite to satellite
5) cosmic to satellite or ground-station

14.2.1 Ground-Station to Ground Station

Interference in the millimeter and submillimeter portions of the spectrum is extremely unlikely because of the low power levels that can be expected and because of the high directivities with which such frequencies would likely be radiated. One consideration of importance, however, that could be grouped in this class concerns the launching phase. In this case, as the satellite rises off the ground it could come within line of sight of a source of millimeter radiation while it is at relatively low altitudes. This, in turn, would interfere with ground station operations. Such is likely to be the case only if the site transmitting the millimeter or submillimeter radiation is in relatively close geographical proximity to the launching station. By careful control of

frequency allocations, and by keeping accurate records of research organizations which might be engaged in the use of this portion of the spectrum, such situations can be controlled without difficulty. Special consideration should be given to the fact that receivers of this type may have relatively low spurious frequency rejection characteristics, and at some time in the future when the use of this portion of the spectrum becomes more extensive, it will be necessary to provide formal control methods. Meanwhile, it is considered that no special measures need be taken for protection of this frequency range.

14.2.2 Ground to Satellite

Satellites in orbit at distances of the order of 100 miles or so have direct line of sight to rather extensive areas of the earth's surface. Furthermore, because of physical limitations, they may contain relatively unsophisticated equipment. Satellites are therefore likely to be vulnerable to radiation in this portion of the spectrum, especially if the radiation is being used for studies of the atmosphere or lunar or planetary surfaces by means of an active device.[4] It is recommended that some group be charged with responsibility for keeping records of the uses of these frequencies so that when missions are designed which will utilize them in the near future, information will be available that can be used for the purpose of evaluating the possibility of mutual interference. In frequencies below 10 GHz, there is considerable activity in tabulating frequencies in use and the location of transmitters. In the millimeter and submillimeter regions the maintenance of such records is a simple matter because of the low density of sources.

14.2.3 Satellite to Ground

Reports have been received from the ground stations of the Satellite Tracking and Data Acquisition Network of interference due to the simultaneous appearance of satellites over ground installations.[5] Though the bands available for this work are parceled out with a view to avoiding such interference, the number of satellites aloft is such that frequency sharing has become necessary. For instance, there are now about 30 satellites in orbit which require about 45 frequency assignments in the 136-137 MHz band. Current plans are for nearly 80 satellites with a need for about 120 frequency assignments in the band. Though not all the transmitters require much bandwidth, an average channel bandwidth of about 30 KHz is indicated. There are therefore only 33 clear channels in the 1 MHz allocation, and frequency sharing is a consequence. At one site at Rosman, North Carolina, there were, during 1965, about 25 encounters involving satellite to ground interference. Of these, 9 incidents were recorded involving co-channel interference. It is revealing that the congestion is such that an even greater number of adjacent-channel interference situations have arisen.

Studies are currently underway to devise means for reducing the number of interference encounters. In addition to devising ways for reducing the equipment susceptibility, especially in regard to adjacent channel effects, advantageous frequency assignment techniques are being developed. The latter make use of the known or expected orbital parameters, the parameters of the communications systems involved, the traffic handling capabilities of the ground stations, and satellite priorities.

From these an assignment procedure can be worked out on the basis of maximum information transfer from satellite to ground.

At some time in the future it is conceivable that this type of interference can be expected in the millimeter and submillimeter range. In order to control this situation, it is advisable to keep a record of transmitters which are in use. Furthermore, consideration should be given in the design of equipment at any give time to the possibilities of mutual interference. It is likely that it will be rather difficult to generally suppress the response of this equipment to spurious radiations. However, one can benefit from the high directivities that can be obtained, and a system tradeoff study would appear to be in order at such time as the situation appears to get critical.

14.2.4 Satellite to Satellite Interference

It seems extremely unlikely that one satellite will interfere with another in this frequency range. In the first place, the power radiated is likely to be small, and in the second place, the distance of separation will be large. On the other hand, it is likely that in some cases antennas of low directivity will be used. In such a case incompatible situations could be produced, but they must be evaluated at the time when such techniques appear to become more extensively used than at present.

14.2.5 Cosmic to Satellite and Ground Station Interference

This case can be of considerable concern. Studies are now going on to determine whether or not there is any substantial radiation in the millimeter and submillimeter region which is of cosmic origin. For surface installations, much of the spectrum is shut off because of the attenuation of the earth's atmosphere. The primary source of cosmic

interference is likely to be the sun, because of its high temperature. Levels of solar radiation at critical frequencies are given in Chapter X.

14.3 CONCLUSIONS

The limited use being made of millimeter and submillimeter waves and the expected limited use in the near future indicatesthat no special steps should be taken at this time in the area of electromagnetic compatibility.

As soon as frequent use of such wavelengths is made, records of such use should be carefully kept. If the use becomes extensive, serious interference problems may be created because of the potentially poor spurious response characteristics of equipment and the limited number of useful frequencies.

14.4 REFERENCES TO CHAPTER XIV

1. Documents from the XI Plenary Assembly of CCIR pertinent to space systems electromagnetic compatibility:

Document No.	Title
IV/1002E	Radioastronomy; Characteristics and factors affecting frequency sharing with other services (Ques. 244(IV)).
IV/1003-E	Factors Affecting the Possibility of Frequency Sharing Between Radar Astronomy and Other Services, (Ques. 236(IV) and 245(IV)).
IV/1007-E	Line Frequencies of Bands of Interest to Radio-Astronomy and Related Sciences, in the 30 to 300 Gc/s Range Arising from Natural Phenomena (Ques. 244(IV)).
IV/1010-E	Radiation Diagrams of Antennae at Communication Satellite Earth Stations, for Use in Interference Studies (Ques. 234(IV)).

Document No.	Title
IV/1013-E	Protection of Frequencies Used for Radio-Astronomical Measurements.
IV/1014-E	Communication-Satellite Systems and Line-of-Sight Radio-Relay Systems Sharing the Same Frequency Bands; Criteria for the selection of preferred reference frequencies for communication-satellite systems (Ques. 234(IV) and Study Programme 235A(IV)).
IV/1016-E	Interference and Other Special Considerations for Telecommunication Links for the Manned and Unmanned Spacecraft in the Space Research Service (Study Programme 235B(IV)).
IV/1017-E	Maintenance Telemetering, Tracking and Telecommand for Developmental and Operational Satellites; Frequency Sharing between earth-satellite telemetering or telecommand links and terrestrial services.
IV/1018-E	Feasibility of Frequency Sharing Between the Radionavigation-Satellite Service and Terrestrial Services
IV/1019-E	Feasibility of Frequency Sharing Between Communications-Satellite Systems and Terrestrial Radio Services; Site selection criteria for earth stations in the communication-satellite service.
IV/1022-E	Determination of Co-ordination Distance (Study Programme 235F(IV)).
IV/1025-E	Draft Modifications to Report L.2.g(IV)--Frequency Sharing Between Communication Satellite Systems and Terrestrial Services (Ques. 235(IV)).
IV/1026-E	Feasibility of Frequency Sharing Between Communication-Satellite Systems and Terrestrial Radio Services; maximum power in any 4 kc/s--band which may need to be radiated in the horizontal plane by active communication-satellite earth stations (Study Programme 235F(IV)).

Document No.	Title
IV/1027-E	Estimating Interference Probabilities Between Space Systems and Terrestrial Radio Relay Services; Propagation considerations.
IV/1028-E	Techniques of Calculating Interference Noise in Communication-Satellite Receivers and Terrestrial Radio Relay Receivers, (Ques. 235(IV)).
IV/1029-E	Communication-Satellite Systems and Line-of-Sight Radio-Relay Systems Sharing the Same Frequency Bands; Maximum allowable values of interference in a telephone channel of a communication-satellite system.
IV/1030-E	Communications-Satellite Systems and Line-of-Sight Radio-Relay Systems Sharing the Same Frequency Bands; Maximum allowable values of interference in a telephone channel of a radio-relay system, (Study Programme 235A(IV)).
IV/1031-E	Frequency Selection and Carrier Energy Dispersal for Communication-Satellite Systems (Ques. 235A(IV)).
IV/1032-E	Space Research and Maintenance Telemetering Tracking and Telecommand Systems; Possibilities of sharing and protection criteria.
IV/1034-E	Communication-Satellite Systems and Line-of-Sight Radio-Relay Systems Sharing the Same Frequency Bands; Maximum allowable values of power flux density at the surface of the earth produced by communication satellites, (Ques. 235(IV)).
IV/1035-E	Propagation Factors Affecting Sharing of the Radio Frequency Spectrum and Co-ordination Between Space and Terrestrial Radio Relay Systems.
IV/1037-E	Telecommunication Links for Deep-Space Research; Frequencies, bandwidths and interference criteria, (Ques. 236(IV)).

Document No.	Title
IV/1041-E	Communication-Satellite Systems and Terrestrial Radio Systems Sharing the Same Frequency Bands; Determination of the coordination distance, (Study Programme 235A(IV)).
IV/1042-E	Frequency Sharing Between Active Communication-Satellite System and Terrestrial Radio Services in The Same Frequency Bands (Ques. 235(IV)).

2. J. J. Taub and J. Cohen, "Quasi-Optical Waveguide Filters for Millimeter and Submillimeter Wavelengths, Proc. IEEE, V. 54, No. 4, April, 1966, pp. 647-656.

3. S. Becker, J. W. Aichroth, F. G. Haneman, P. Kalesiak, J. F. Lyons, L. M. Orloff, M. L. Wright, "Final Report on Interference Analysis of New Components and Circuit Techniques," Vol. I and II, RADC-TDR-62-221, May, 1962, Contract AF 30(602)-2384.

4. L. A. Hoffman, K. H. Hurlbut, C. J. Zamites, "Radio Frequency Interference at Orbital Altitudes, Aerospace Corporation, June, 1965, Contract AF 04(695)-269 and AF 04(695)-469.

5. F. Haber and M. Celebiler, "Interference in Satellite Systems," Paper FA 31.4 presented to the 1966 International Communications Conference, Phila., Pa., May 17, 1966 (Summary on pp. 220-221 of Digest.).